MICRO-SEGREGATION IN MULTICOMPONENT STEELS INVOLVING THE PERITECTIC REACTION

by

Andrew Aitken Howe, MA, CEng, MIM

A thesis presented in fulfilment of the requirements
for the degree of Doctor of Philosophy in the
Department of Engineering Materials,
Faculty of Engineering,
The University of Sheffield,
February 1993

PAGINATED BLANK PAGES ARE SCANNED AS FOUND IN ORIGINAL THESIS

NO INFORMATION IS MISSING

ORIGINAL COPY TIGHTLY BOUND

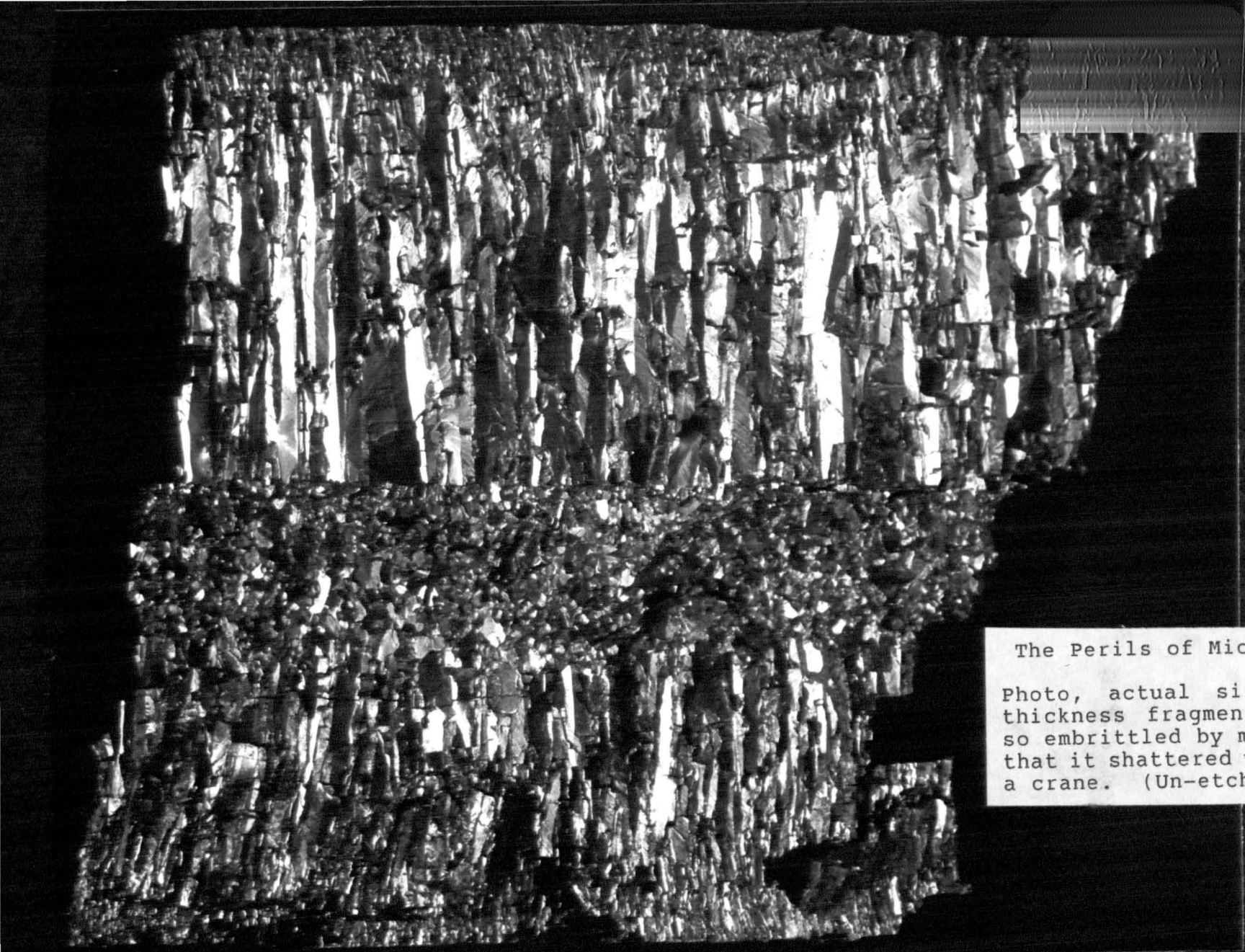

The Perils of Micro-Segregation

Photo, actual size, of through-thickness fragment of cast slab, so embrittled by micro-segregation that it shattered when dropped from a crane. (Un-etched sample)

MICRO-SEGREGATION IN MULTICOMPONENT STEELS

INVOLVING THE PERITECTIC REACTION

by

A. A. Howe, MA, CEng, MIM

*** SUMMARY ***

This thesis concerns the micro-segregation resulting from the casting process. This involves the passage of interfaces which maintain local equilibrium through a volume which was initially already at equilibrium, but which results in a non-equilibrium distribution of alloy elements. The primary feature of this work is the mathematical modelling of this process, extending existing techniques of both analytical and numerical character. The resultant, numerical model can be summarised as follows:

a) Static-grid, Finite-Difference computer model

b) Finite, temperature dependent diffusion employed in solid phases

c) Interfaces allowed to progress smoothly across grid, i.e. not restricted to nodes

d) Controlled by heat extraction or cooling rate. No initial assumptions made such as for growth rate or solidification time

e) Operates either on a static, primary arm basis or coarsening secondary arm basis according to any imposed coarsening law of the form $\lambda = Bt^n$

f) The model can consider planar, cylindrical or spherical representative cells

g) Any reaction path through a peritectic region of the phase diagram can be catered for

h) A novel routine for the solid/solid interface movement allows local equilibrium for all solutes under diffusive control from both adjoining phases while maintaining a numerically agreed growth rate

i) Optional "streamlining" of the program whereby carbon can be considered as being uniformly mixed within a given phase, requiring simultaneous solution of all the equations for both phase interfaces during the peritectic.

j) The required equilibrium data can now be obtained from the National Physical Laboratory by free-energy minimisation calculation.

The emphasis of the work has been on the development of this tool for tackling micro-segregation phenomena, but experimental validation of both the model output and the equilibrium data input has been performed with promising results.

To my wife, Joanna, and children, Katie and Fiona,
for their tolerance

"How many poor scholars have lost their wits, or become dizards, neglecting all worldly affairs and their own health, wealth, being and well being, to gain knowledge!, for which, after all their pains, in the world's esteem they are accounted ridiculous and silly fools, idiots, asses and (as oft they are) rejected, contemned, derided, doting and mad!"

....Robert Burton, 'Anatomy of Melancholy', Part 1, section 2, member 3, sub-section 15.

NOMENCLATURE

The following nomenclature is employed unless locally defined otherwise within the text. Similarly, the choice between any alternatives quoted below will be locally confirmed within the text.

α	Brody-Flemings back-diffusion parameter
β	Parameter (n/2m) modifying back-diffusion term, A
γ	Austenite (fcc)
δ	Ferrite (bcc)
λ	Dendrite arm spacing, m
a	Parameters within Newton-Raphson solution scheme, 1 to 4, and z (p.166)
A	Back-diffusion parameter (alternative local definitions)
A	Re-meshing parameter
B	Dendrite arm coarsening coefficient, ms^{-n}
B	Re-meshing parameter
C	Carbon content, o/bulk, l/liquid, wt.%
C	Re-meshing parameter
C_p	Specific heat capacity, $Jm^{-3}K^{-1}$
D	Diffusivity, m^2/s
E_p	Peritectic equivalent
fs	Fraction solid
f_δ	Fraction ferrite
F	Function
F'	Derivative of function
g	Coefficient in solidus prediction
H	Volumetric latent heat, L/liquid to austenite, δ/austenite to ferrite, Jm^{-3}
k	Partition coefficient
$k_{(x/y)i}$	Partition coefficient of element i at x/y interface
L	Half dendrite arm spacing, m
m	Solvus slope, l/liquidus, (x/y)i/ of element i at x/y interface
m	Exponent in growth and coarsening equations
M	Atomic mass
n	Number denoting dimensional basis, 1/planar, 2/cylindrical, 3/spherical
n	Exponent in arm coarsening equation
N	Number of solutes, i
p	Program parameter for re-meshing operation
P	Program parameter for interface position between nodes
Q	Heat extraction rate, $Jm^{-3}s^{-1}$
r	radial distance solidified, m
r_δ	radial distance through ferrite, m
R	Number of ultimate program node before an interface
R	Atomic mass ratio
S_I	Interfacial surface area, m^2

t	Time, s
T	Temperature, K (unless stated locally to be Celsius)
U	Arm coarsening parameter
V	Arm coarsening parameter
V	Volume, o/representative cell, s/solid
W	Cooling rate (-T), Ks^{-1}
Xn	Nodal spacing, m
Y	Solubility product for MnS (etc.), $Wt.\%^2$
Y	Program parameter for diffusive flux under non-planar geometry
Y	Parameter in solute profile equation
Z	Content of an element, other than carbon if the 'streamlining' option is employed, o/bulk, l/liquid, δ/in ferrite at δ/γ interface

Subscripts:

1	At start of time increment
2	At end of time increment
δ,γ	Phase
c	Carbon
f	Final
i	Solute identifier
I	Interface
new	To be determined
o	Initial/datum
old	Already determined in previous iteration
older	Already determined 2 iterations earlier
p	Peritectic
s	Solid

A dot above a variable signifies its derivative with respect to time, and two dots the second derivative.

CONTENTS

CHAPTER ONE

INTRODUCTION

"To the mischievously idle reader"

> "Whoever you may be, I caution you against rashly defaming the Author of this work, or cavilling in jest against him. Nay, (to be brief), neither tacitly reproach him because of others' censure, nor employ your wit in foolish disapproval, or false accusation."
> ....Robert Burton, 'Anatomy of Melancholy'

1.1) DEFINITIONS, RELEVANCE, AND SCOPE OF WORK

The term, segregation, refers here to the inhomogeneous dispersion of elements present in an alloy. The aspect with which this thesis is concerned is the segregation which results from solidification. Apart from some curious and exotic techniques, all alloys Man produces are liquid at some point in their history, and although it is relatively easy to make a liquid homogeneous, i.e. free from segregation, segregation is liable to develop during the solidification process. Solidification is, indeed, the most important cause of compositional inhomogeneity.

The majority of casting processes result in a dendritic (from the Greek for 'a tree') solidification morphology, i.e. the microscopic interface between the growing solid and diminishing liquid vaguely resembles a forest of branched trees, Figure 1.1. In this context, the term 'segregation' can be split into micro and macro categories; micro-segregation describing the compositional inhomogeneities on the scale of the dendrite branches, or arms, and macro-segregation describing the larger scale compositional

inhomogeneities which may develop. Some authors employ the term meso-segregation for scales only a little larger than that of the dendrite arms.

Although this thesis primarily concerns the micro-segregation resulting from solidification, some consideration is given both to macro-segregation during solidification and to micro-segregation which does not result purely from the solidification process. The basic concepts are fairly general to metallic alloys but the details and examples will usually be specific to steel.

The various forms of segregation resulting from solidification are of great commercial importance to industry in terms of both the liklihood of successfully casting and 'working' (reduction by rolling or forging) the material without cracks and the degree to which the material has to be worked before the required property specification (e.g. mean and scatter in strength and toughness measurements) can be met. The micro-segregation is, of itself, important in this respect, describing the scale and intensity of the compositional variations around the resultant, fully solidified dendritic structure. It is, however, so fundamental to the solidification process that it should not just be considered in these terms.

The micro-segregation phenomenon is intimately related to the growth and morphology of the dendrites, the nature of the solidification phases and precipitation reactions, the ranges of temperature and position within the casting over which solidification occurs (-the so-called 'mushy zone'-) and the fractional solidification within that range. This provides a description of the chemical and physical environment which, in turn, controls the phenomena of macro-segregation and solidification cracking. (A complication for the modeller is that the relationships between all these factors are interactive rather than consecutive.)

At present, a considerable gulf exists between the fundamental, mathematical models of solidification and those employed to address industrial problems [1,2]. Each employ assumptions untenable by the alternative approach. The various, fundamental models are limited to selections of most of the following factors: a) cellular rather than dendritic solidification, b) 'free dendrites' in an undercooled melt, c) application only to low solid fractions, d) single solute species, e) constant partition coefficient and liquidus slope, f) no solid state diffusion, g) single solidification phase, h) no compound precipitation, i) extreme solidification rates, and j) excessive computer usage (one example being 'many hours' on a Cray supercomputer per run [1]). None of these conditions are acceptable for a model, as in the present case, aiming at quantified predictions in industrially significant alloys so some other assumption has to be made. The relevant starting point, at least in the forseeable future, is to assume a simple morphological basis which thereafter enables all the above restrictions to be lifted. This, therefore, is the approach adopted in the present work. (The acceptability of this is discussed in a later section, 'Model versus Reality, Section 2.8.)

1.2) NOVEL COMPONENTS OF WORK

The central feature of this thesis is the extension of a computer model of micro-segregation due to Kirkwood and Ogilvy [3-7]. The original basis and current extensions will obviously be described in detail within the main text but can be outlined as changing a ternary, single solidification phase model with an assumed, constant cooling rate and empirical secondary dendrite arm-coarsening laws specific to certain steels to a general, multicomponent, dual solidification phase (as in the peritectic reaction) model with any assumed rule for heat extraction and a single, generally applicable law describing the arm-coarsening behaviour.

The model is described in detail in Chapters 4 and 5 but comprises finite difference of solid state diffusion coupled with up to two moving interfaces and their associated solute balances, i.e. solute lost from the moving interface must equal the sum of that dispersed into the adjoining phases, Fig.1.2 (Fig.1.2a, solid/liquid, A = B + C + D, Fig.1.2b, solid/solid, $A = B_1 + B_2$). This much is not novel, but the capability of the final program places it at the forefront of such work.

Certain extensions to analytical treatments are also proposed [8] but the emphasis must necessarily lie with the numerical model as the former are more restricted (see Section 2.8).

The associated experimental work comprises verification of both the multicomponent equilibrium data for input to the model (by liquidus measurements at BST Swinden Laboratories and sub-liquidus equilibrium measurements at Sheffield University) and the computed model output of micro-segregation (by CAMECA SX50 electron micro-probe measurements) in laboratory and commercial steel.

The bulk of this work was conducted at BST Swinden Laboratories under an ECSC project [9] proposed and conducted by the author, extending his previous work for British Steel in this field [10-14]. The extended capabilities for calculation of multicomponent equilibria obtained during this project are, of course, reported in this thesis but was performed under sub-contract by the NPL [15-17]. Considerable use was also made from related projects at Sheffield University [18,19].

CHAPTER TWO

THEORY

"How finely we argue upon mistaken facts!"

....Laurence Sterne, 'The Life and Opinions of Tristram Shandy', Vol.IV, Chapter 27

2.1) FUNDAMENTALS OF SOLIDIFICATION

2.1.1) First Things First

The first question to be addressed is why does a liquid elect to solidify at all? Unfortunately, the answer entails Thermodynamics. According to Atkins [20]; "Life's rich pageant is summarized ... by the Laws of Thermodynamics, of which there are four. The first to be discovered was the Second, and the second was the First. The Third is possibly not a law of thermodynamics at all, and the Zeroth, discovered fourth, is an afterthought. That is all there is that is complicated about thermodynamics; the application of the laws is very much simpler." (His reassurance does not, however, reflect the majority opinion.) It is the first two which concern us.

The First Law states that energy can neither be created nor destroyed, although it may be converted from one form to another. This is a very useful Law, although it is demonstrably wrong. The errors, however, only concern the physics of Relativity and Quantum Mechanics whereas Metallurgy largely resides in the Newtonian, common-sense Universe.

This law states a limit within which change occurs but does not state why or how things change. A clue is provided here in the Second Law. To quote Atkins again; "Everyone knows why things change: things tend to get worse (though) Scientists express this differently". Many verbal formulations of the Second Law exist, often in terms of heat engines, but the basis is that isolated systems tend towards maximum entropy (dispersal~disorder). This gives us some idea of the direction of change (the word 'entropy' derived from the Greek for 'to give a direction') and is sometimes called "Time's Arrow".

So, the essence of change is increasing entropy; a time-irreversible process even though all the component, individual events or reactions are time-reversible (Loschmidt's paradox). All very well but, as it stands at the moment, this would imply that solidification simply cannot occur, which would rather detract from the point of this thesis. Solidification obviously results in a dramatic ordering, and consequent decrease in entropy. The pertinent fact, however, is that a solidifying liquid is not an isolated system: it must be losing heat and, hence, pouring disorder into the surrounding world. This is, of course, the latent heat of solidification. In terms of the First Law, this is heat energy being converted to or from 'ordering' energy.

It is the combination of these two laws which lies behind the concepts of use to the case in question. A transfer of energy with the surroundings must be reflected by the change in total energy content of the system. Moreover, at a given temperature, it is much easier to lose energy by spreading chaos than the reverse. Therefore, if a choice of states with different energy contents is available, there will be the tendency for the system to adopt that which has the lowest energy content and is, therefore, the most stable. This may not be an easy process, but as more time elapses, descent down to the lowest energy level becomes more likely.

The direction of change for a 'closed' system of constant mass and composition but able to exchange energy with its surroundings, can therefore be described in terms of the minimisation of this 'energy content'. This is described by the Gibbs Free Energy (at constant pressure):

The term, H, is the enthalpy,('heat content' or 'internal energy' with an additional pressure~volume term which is relatively small for condensed phases), T is the absolute temperature, and S is the entropy. The enthalpy tends to be small in well ordered, strongly bonded structures (the reason for the bonding being to lower the energy). The H term in the Gibbs free energy equation dominates at low temperatures, and strongly bonded structures are therefore favoured. At high temperatures, the TS term dominates, and the more random, high entropy, 'looser' structures are favoured. A solid would therefore be expected to transform to a liquid on heating, and the liquid transform to a solid on cooling, just like egg doesn't.

In practice, there must be a finite free energy in order to provide the driving force for solidification. This means that the actual temperature must be less than the equilibrium melting temperature, Tm. For steel and, indeed, most metallic systems, there is no great kinetic barrier to the high temperature, energetic, single atoms or small atom clusters in the liquid adapting to the relatively simple solid structures, and equilibrium is virtually achieved after very short periods. Once a solid phase starts to appear, however, departure from equilibrium is observed, and is progressive with decreasing temperature for given times. Interfaces, however, between solid and liquid, or one solid form and another, often maintain equilibrium locally (Section 2.6).

The same treatment applies to alloys, but the presence of another atomic species introduces additional terms to both the bonding (and pressure~volume), hence enthalpy, and the entropy. The extra entropy term applies not so much to differences in the structure itself, but the arrangement of distinct species within that structure.

The result of this minimisation of free energy, formulated in terms of both temperature and composition, is outlined in the following section and is the basis of the multicomponent equilibrium calculations sub-contracted to the National Physical Laboratory [9] and described in more detail in Section 2.2.2. Suffice it to say for the present that the minimisation of Gibbs free energy now predicts equilibrium between phases of specific but distinct compositions, although each phase will, itself, be uniform in composition. Indeed, Gibbs defined a phase as being uniform in both physical state and composition, but the definition is more relaxed in use, allowing minor differences in structural parameters as the lattice is strained by varying amounts of solute, and the significant differences in local solute content before equilibrium is achieved are also overlooked. (Diffusion is a process by which these differences are levelled out until equilibrium is achieved, but this will also be dealt with later.)

2.1.2) Solidification Morphology

The simplest way in which a liquid can undergo the transition to solid is by the advance of a plane front. This would be expected of a pure element solidifying away from an infinite, planar heat sink, into a semi-infinite body of liquid at or above the melting point. Under these circumstances, there is no reason for the growing solid to be of a different thickness from one place to another. The removal of latent heat dominates at first, but the 'sensible' heat required to cool the solid becomes progressively more important as the solidified thickness increases. (A temperature gradient has to be maintained or there would be no reason for heat to flow away from the interface and solidification would stop.) This results in a progressive decrease in solidification rate as the solid shell thickens, assuming constant heat transfer conditions at the boundary. Indeed, it can be shown to result in a square root of time dependence on this thickness sometimes called the Ruddle Equation [21].

If by some chance there does happen to be a minor perturbation on the planar surface, the liquid interface is further removed from the heat sink than are the surroundings, and therefore has a relatively slow growth rate, such that the surroundings are encouraged to catch up and even out the interface again. Moreover, if the liquid is above the melting point, a temperature gradient must also exist in the liquid. Under these circumstances, any perturbation is further discouraged by being in the vicinity of a steeper temperature gradient to the hotter liquid. The plane front is therefore stable.

Many analyses of solidification have settled with these assumptions, as in the so-called Stefan Problems. To handle more practically relevant situations, we must first get back to basics.

a) The Atomic Scale

The morphology of the solid/liquid interface at the atomic scale largely depends on the ease with which the basic units, whether atoms or molecules, can be added to the solid substrate. This, in turn, depends on the relative bonding in the liquid and solid, and the degree of ordering required to obtain a suitable match.

Where this process is difficult, attachment of new units is likely to be less so on the 'ragged', high index planes. Unfortunately, this localised, relatively rapid growth tends to wipe out the high index planes, leaving only regular, low index planes exposed to the liquid. The subsequent growth displays obvious crystallinity, and is known as 'faceted growth'.

Because of the difficulty in gaining additional units, a large degree of undercooling is required to drive the process. Furthermore, crystal defects play a prominent role because they provide 'ragged', favourable sites as with the short-lived, high index planes. Some defects are similarly short

lived but others are maintained despite the growth process and can result in markedly different morphologies on the larger scale. (For example, a eutectic containing both rods and plates of one phase could simply reflect the presence of both line and planar defects in the original nuclei.)

Faceted growth can be encountered in solidifying steels with compounds such as cementite or intermetallics, or from solid state reactions. Otherwise, however, there is no real difficulty in transferring metal atoms from the liquid to the solid, and they can pile on any-old-how, resulting in an atomically 'rough' surface. The units are small with no problem of configuration, and the lattice is simple and relatively isotropic. This, more typical morphology is given the imaginative title of 'non-faceted', and will be the basis of most of the subsequent discussion.

b) The Micro Scale

On the micro scale, you can tell an atomically smooth (faceted) interface because it looks angular, and an atomically rough (higgledy-piggledy) one because it looks smooth. At the moment, however, both are growing in an essentially planar manner. The non-faceted mode, exhibited by the simple solidification of metals, needs no great driving force for atom transfer as described above.

Keeping to a pure material for the moment, if a non-equilibrium initial condition of undercooled liquid applies, any perturbation is stabilised by the presence of colder liquid and a totally different morphology results on the micro-scale. Indeed, were it not for surface energy considerations, any perturbation would experience accelerated growth into a cusp disappearing off to infinity [22].

The surface energy is generally low and perturbations are markedly encouraged, but slight anisotropy of the albeit low surface energy with respect to the crystal structure is still sufficient to dominate the subsequent morphology. Therefore, under this supercooled condition where a planar front is unstable, the surface energy limits the extreme curvatures mentioned previously but encourages directions of growth which are on the principal lattice axes, in competition with the otherwise optimum directions for heat flux. With increasing rates of heat extraction and undercooling, the crystallographic 'easy-growth' directions become increasingly prevalent, leading from cells to the classic 'dendritic' morphology (fig 1.1). At present, however, the argument has only explained dendritic growth into undercooled melts.

In alloys, composition as well as temperature fields can stabilise perturbations, such that cellular and dendritic morphologies can be and, indeed, usually are, found under standard casting procedures whereby the bulk liquid is not undercooled. The basis for this is micro-segregation. The expected difference in solubility for the solute between solid and liquid means that (with $k<1$) solute has to be rejected into the liquid as the solid grows. A planar front would produce a diffusion layer of solute in the liquid like a 'bow-wave' in front of a ship (albeit with a semi-permeable hull). This local variation in liquid composition necessarily leads to a corresponding variation in liquidus temperature through this layer. The planar interface must be at the liquidus temperature of the adjacent liquid, but the stability of any perturbations will depend on the relative liquidus and actual temperatures across the diffusion layer (fig.2.1). If the actual temperature profile falls below the liquidus temperature of liquid in the diffusion layer, then that region of liquid is obviously supercooled even though the temperature gradient is positive from the interface. This is known as 'constitutional supercooling' [21]. A reciprocal argument applies with $k>1$ such that dendrite growth could similarly result. (Hillert comments that the big fuss over constitutional supercooling is surprising to one brought up with solid state transformations where the constitutional effects were considered before those of temperature changes [23].)

Constitutional supercooling, therefore, is why the same morphology as encountered with undercooled melts is found with alloys even when the bulk liquid is superheated. The required, solute field is much more localised than the temperature field in an undercooled melt and, consequently, less extreme behaviour may be anticipated, but of essentially the same character.

Assuming steady state planar growth has been established, the effect can be quantified as follows (-according to the original treatment by Chalmers rather than more sophisticated versions like that of Mullins and Sekerka [24,25]). The critical condition is for the actual temperature gradient, G, to equal the gradient in liquidus temperature, which will be the product of the liquidus slope and the concentration gradient in the liquid. The latter can be obtained through the solute balance, equating the loss of solute upon an increment of growth to that which has diffused down the solute gradient in the liquid. (Being steady state, there is no solute gradient in the solid. Compare solute balances in Section 2.5.)

$$Zl(1-k)V = Dl.dZl/dx \qquad (2.2$$

$$dT/dx = m_l .dZl/dx \qquad (2.3$$

The critical condition for a stable planar front is:

$$G > dT/dx \qquad (2.4$$

Combining Equations 2.2-4, and expressing in the standard form with Zo rather than Zl,

$$G/V > m_l .Zo(1-k)/(k.Dl) \qquad (2.5$$

The anticipated morphology has been expressed in terms of this variable as reproduced in Figure 2.2. The greater the right hand side of equation 2.5 exceeds G/V then the more 'non-planar' is the observed morphology.

It must be remembered, however, that this argument applies to the stability of a planar front and does not describe the situation once a cellular or dendritic morphology has developed. Indeed, such morphologies essentially destroy the effect simply because the effect is why they occur: they are a response to it (fig 2.3 [26]). Residual effects in cells promote branching to dendrites, and so on to higher orders of branching until the effect is minimised. Minor solute fields still exist, however, within the dendritic mesh because of the local differences in equilibrium composition (and temperature) resulting from the differences in interfacial curvature. These are not sufficient, however, to promote additional branching: indeed, their nature is such as to discourage it, resulting in coarsening of the side-arms and a net reduction in their number (Section 2.4).

There still appears to be disagreement as to the extent of the diffusion layer ahead of the dendrite tips. It is progressively lessened on changing from planar through cellular to proper, dendritic morphologies but is still considered to be of sufficient extent to promote the growth of equiaxed crystals [27]. Studies with EPMA on interrupted-quench solidification experiments tend to show that such compositional variations are slight [28,29] unless fairly extreme casting conditions are considered. This is also evidenced by the fact that the solidification temperature is very close to the equilibrium liquidus under standard casting conditions.

c) The Macro Scale

The standard macrostructure obtained in either continuous or ingot casting comprises a chill, columnar and equiaxed zone, though all three need not be present in a particular case (fig 2.4).

The chill zone results from the very rapid cooling of the first liquid to hit the mould wall. The high heat extraction encourages the display of the random, crystalline directionallity of the nuclei, as described above, and can achieve a significant but brief undercooling of the liquid, both of which promote a macroscopically isotropic, equiaxed morphology. Competition between adjacent grains as they grow, however, is such that those favoured by orientations close to that of the heat extraction tend to survive and take over. The macrostructure therefore evolves into columnar crystals as a result of the growing dendrite array being essentially competitive: the heat extraction rate is such that crystalline directionality is observed rather than growth directly reflecting the optimum path for heat extraction, but the subsequent territorial disputes with neighbouring grains bring them back into line.

Equiaxed solidification is normally said to require the presence of undercooled liquid; a heat sink is required for solidification and although local constitutional supercooling is sufficient to promote a dendritic morphology it obviously cannot support heat loss into the superheated or even liquidus temperature bulk melt. Moreover, very little additional solidification is required to remove likely degrees of undercooling. To maintain the situation, the heat loss from the liquid to the surrounding, columnar solid must be such as to keep the required undercooling in the bulk melt while the columnar zone, itself, despite the more direct heat sink, fails to grow significantly.

d) The Columnar-to-Equiaxed Transition (CET)

There is an extensive literature on this subject [e.g.30] which is only indirectly related to the present thesis but the following is provided here, which mixes standard theory with opinion.

In the common casting modes for steel (continuous or ingot) all the potential nuclei for equiaxed crystals are produced at an early stage in the process, whether heterogeneous nuclei, or dendrite fragments broken or remelted from the solidification front or showering from the exposed surface. (Generation from the mould wall [31] cannot be important in continuous casting.) Many of these will remelt because the liquid will still be superheated at this stage, but, by doing so, they will reduce the melt down to the liquidus temperature whereupon any remaining nuclei are stable, neither remelting nor growing. Electromagnetic stirring in the continuous casting mould, for example, is therefore effective even though the equiaxed zone does not normally appear for several metres down the strand. (The optimum location for an EMS device will depend upon the operating superheat in the mould; the higher the superheat, the lower the ideal location such that sufficient superheat has already been removed prior to dendrite fragmentation to ensure a significant number of these nuclei survive.)

We now have the situation of a columnar shell containing bulk liquid around the liquidus temperature and which contains stable nuclei. These may well be coarsening but, more importantly, settling through the melt. It seems difficult to accept that these nuclei grow as a result of constitutional supercooling in a melt otherwise at liquidus temperature. It is difficult even to accept that they grow faster than the columnar zone under a maintained, thermal (as opposed to constitutional) supercooling of the bulk liquid under otherwise equivalent conditions. This effect is, however, encouraged because the equiaxed dendrites can grow at a supercooling less than the albeit small supercooling required by the columnar dendrites. Even so, an additional effect would appear to be called for.

One such possibility is the increase in heat extraction rate of the central liquid within the cast section primarily due to the rapidly increasing surface area-to-volume ratio of the residual liquid [32,33]. The author found that a simple, corresponding modification of the rate law involved in the

standard, root-time Ruddle equation for shell thickness generates an analytical shell thickness equation which is in remarkable agreement with computer-based numerical models (Fig. 2.5):

$$d/ds = 1-\sqrt{1-\sqrt{t/ts}} \qquad (2.6$$

or $$d/ds = 1-\sqrt{1-(K/t)/ds} \qquad (2.7$$

where d is the actual shell thickness, ds is half the section thickness, t and ts are the corresponding times, and K is the 'solidification factor', though twice that relevant to the simple, 'root-time growth' Ruddle Equation [21] where the described geometric factors do not apply. (A 'solidification factor' is applied directly to real, finite casts such that under equivalent cooling conditions, ds=K/ts as implied, for example, in the Chvorinov Rule. The presented equation does, indeed, still satisfy this rule for the end of solidification but it is incorrect to apply Chvorinov to intermediate stages, fig 2.6.)

This increase in heat extraction rate will, however, encourage both the columnar and equiaxed crystals to grow. Indeed, some practical measurements on plant indicate that increased heat extraction favours the columnar at the expense of the equiaxed zone [34] although theoreticians usually claim the reverse.

A major possibility is that an important growth mode for the equiaxed crystals is by contact with the columnar solidification front, thereby acquiring a direct heat sink and physically hindering continued columnar growth. In curved-strand continuous casting, for example, the equiaxed zone is commonly centred below the strand axis. At a given stage during solidification, the thermal and constitutional conditions will be the same on both the upper and lower growth fronts but the settling equiaxed nuclei prevent continued columnar growth on the lower front whereas the upper front continues unhindered (Fig 2.7). An in-between stage is the

branched or psuedo-columnar zone where equiaxed nuclei become attached to the growth front but are present in insufficient numbers to halt the overall, columnar morphology.

The author came across some interesting structures in a Bessemer twin wheel cast strip, where it appears that the roll-mould pool contained a low solid fraction slurry which was subsequently frozen in by much finer, rapid columnar growth from the roll surfaces. There was some entrapment of coarse slurry dendrites within the columnar zone, but most of these "gross nuclei" were evidently pushed ahead of the advancing columnars until they were physically filling the middle. This mechanism is probably standard in normal columnar/equiaxed structures, but was made much more evident from the different scales, and hence origins, of the component structures in this case. This is supported by statements that solid nuclei are not inherently "sticky" unless of aligned crystallographic orientation, such that the majority of these gross equiaxed nuclei are pushed ahead of the columnar front rather than incorporated into it.

The CET is therefore seen as a fairly haphazard event depending on the propensity of the population of existing nuclei to obstruct the growing columnars. This is seen as an essentially physical process with solute fields and curvature arguments being entirely secondary.

The influence of columnar or equiaxed solidification on segregation will not be discussed in detail here. Suffice it to say that both are dendritic in standard steel casting processes. Although this is the morphology to be considered in this thesis, the model best applies to "long" dendrites as described in Section 2.8, and will therefore be less appropriate to poorly formed, typically stubby equiaxed dendrites (unless so poorly formed that the spherical morphology option becomes tenable).

Detailed calculations of morphological development are being attempted [35-40] but, as described in the Introduction, are inappropriate to the present work because of the required simplifying assumptions. The adopted alternative approach is to assume a simple morphology which then enables the other simplifications to be pruned or even removed. This aspect, being of obvious importance, is discussed in Section 2.8.

2.2) EQUILIBRIUM PHASE DIAGRAMS

2.2.1) Solidification and the Equilibrium Phase Diagram

It has already been described how a system will tend to the lowest available energy configuration of phases and respective compositions, i.e. equilibrium. In order to understand the basis of phase diagrams, it is therefore necessary to consider the energies which they reflect, as described in various textbooks. The Gibbs curves can also be used to treat meta-stable equilibria; there will be a driving force for change (i.e. an ability to lower the total energy) until true equilibrium is established, but that could take time. Non-equilibrium states such as this are very important in this project regarding delayed transformations, and indeed in the common use of the iron-cementite phase diagram instead of iron-graphite.

There is a slight problem in describing solidification under equilibrium because, at equilibrium, there is no driving force for change and, hence, no solidification. In practical terms, one can consider solidification under a sufficiently slow cooling rate for 'effectively' complete diffusional mixing to have occurred and with local concentration differences stabilised by boundary structures absent or ignored.

In many systems at low concentrations, the liquidus and solidus can be assumed linear, whereupon k=ko, remaining constant during solidification, but this is a convenient simplification much overused even when patently invalidated by the phase diagram.

The partition coefficient concept can be used even when variable, and merely provides information as to the respective compositions. Conservation of solute dictates a relationship between the quantities of each phase:-

$$Ms*Zs+Ml*Zl=Mo*Zo \qquad (2.8$$

where M is the corresponding mass of each phase.

In terms of mass fractions, which must always sum to unity, and employing the partition coefficient:

$$fs*k*Zl+(1-fs)*Zl=Zo,$$

$$Zl=Zo/(1-(1-k)*fs) \qquad (2.9$$

This is one representation of the 'Equilibrium Lever Rule', which will hereafter be addressed merely as 'lever rule'. The use of the word 'lever' stems from a different but totally compatible representation similar to the balancing of a lever:

$$fs*(Zo-Zs)=fl*(Zl-Zo) \qquad (2.10$$

It should be noted that no residual segregation exists after solidification by such equilibrium treatment. The only segregation as such was the composition difference between the solid and liquid phases, but uniform solid of the same, initial composition Zo results.

For a three phase reaction the solute balance is as follows:

$$fa*Zsa+fb*Zsb+fl*Zle=Zo'$$

The equivalent formula to equation 2.9 is:

$$Zl=Zo/(1-(1-ka)fa-(1-kb)fb) \qquad (2.11$$

but this is of little use because the balance of fa and fb will be such that Zl is constant at Ze. A useful equation to be drawn from this solute balance would describe the fraction of one solid phase in terms of the total fraction solid, e.g.:

$$fa=(1-Zo/Ze-(1-kb)fs)/(kb-ka) \qquad (2.12$$

A minimum of two phases reacting is obviously required for solidification. The maximum for a binary system (Gibbs phase rule, constant pressure) is a three-phase reaction, whether eutectic, peritectic, monotectic or metatectic. All these are three-phase reactions where at least one is liquid, with either one phase changing to two (eutectic or metatectic) or two changing to one (peritectic or monotectic, see later). The Gibbs Phase Rule indicates that these reactions are invariant in a binary system; they occur at fixed compositions and temperature.

The metatectic reaction is unusual but deserves mention because it occurs in the iron-sulphur system, which is included within this project. The monotectic, whereby two liquid compositions produce a solid, is not relevant to this project where no miscibility gaps are expected of the liquid.

For purposes of the subsequent argument for ternary systems, the transition from eutectic to peritectic is now described for a binary system.

Consider the schematic peritectic in Figure 2.8a. Depending on the relative distances AB and BL, different phase proportions are involved but it is still a peritectic, until the L point is coincident with the B point. Here, the L point is swapping places with the B point and the reaction is changing from a peritectic to a eutectic. Looking just at an isotherm, or down from above, so to speak (Fig.2.8b), L is between the two solids for a eutectic, but beyond them for a peritectic, although this 'projected' view will lose some information; the peritectic could be a metatectic and, apart from its intrinsic

unlikeliness, the eutectic could be the reverse A+B->L reaction. The isotherm (or, for a binary, the equivalent viewpoint of a projection from above) does not itself contain sufficient information to define the system uniquely, although there is, of course, no difficulty in identifying it from the full, 2D diagram. This is all rather hypothetical and trivial, but, once said, might help in the following, highly confusing discussion of ternary systems.

The phase diagram for a ternary system obviously involves an extra dimension, such that all the relevant information cannot be contained in a 2D sheet of paper. The standard diagram has an equilateral triangle as the composition grid, with temperature as ordinate, or vertical axis. Any point on this grid is of unique composition (hence its suitability and adoption for the purpose), with the amount of component 'a' being read off a line parallel to the side b-c. The proportion of 'a' will equal the ratio of the graphical distance beyond this line to the total length of any radial line from the 'a' corner; any line parallel to b-c is the locus of compositions with a given quantity of 'a'. Similar logic applies to the calculation of phase proportions corresponding to a particular point (i.e. bulk composition) within the three-phase field or "tie-triangle", Fig.2.9, even though it is unlikely to be equilateral as in the full ternary grid.

The three-phase reactions can be defined in pseudo-binary terms of eutectic, peritectic, etc., but the respective compositions and temperatures are not uniquely defined. The compositions will only be unique for a specific temperature, or vice versa. As to which type of three phase reaction it is deserves careful consideration. The three-phase field in the ternary isotherm in Figure 2.10a, for example, could be any such reaction; however closely it is examined, its shape gives no indisputable clue as to which phase(s) are growing at the expense of which other(s). In the binary case, the isotherm through the three-phase reaction could only define it as one of two possibilities. In a ternary, the same tie-triangle can represent all reaction types, and more information is needed to find out which it is.

The projection from above of the three corners of the roving triangle is helpful (Fig.2.10b). On one binary edge there is a eutectic, and there is a peritectic along another (c.f. Fig. 2.8). The traces of the respective solvi are projected onto the diagram, including the case in point of the tie triangle from Figure 2.10a, and two other example tie triangles thrown in for good measure. As with the binary, the peritectic (or metatectic) is usually identified by the liquid trace being beyond the two solids, and between for the eutectic, but 'beyond' is now harder to define with the extra dimension. We need to know both the shape of the tie-triangle and the direction it is travelling in (and, indeed, the change in shape of the tie-triangle as it travels).

Consider Figure 2.11. This represents a tie-triangle at a particular temperature. The surrounding domains describe the nature of the reaction the triangle represents should it move in that direction upon a decrease in temperature. For a mean composition (point X) taken as the 'centre of gravity' of the triangle, if the triangle nudges towards the bottom right, the L point is getting further away from it (hence decreasing in quantity) while both the A and B point are nearing it (hence increasing in quantity). The reaction, therefore, is L->A+B, i.e. a eutectic. The same argument applied to the other directions produces the appropriately labelled domains. The borderlines are when the sense of movement is along one of the triangle's sides. Under this circumstance, the proportion of the phase opposite to that side remains constant (the perpendicular from that point to the plane through the centre of gravity remaining constant), i.e. the phase is in equilibrium but dormant.

Due to the general stability of liquid at higher temperature, one influence is that a eutectic is more probable than a peritectic which, in turn, is more probable than the metatectic, and the final case of the 'inverse eutectic' is highly improbable. A second influence is of the triangle shape; the narrower the angle at point L, the narrower and more unlikely is the domain for a eutectic reaction, and correspondingly more likely is a neighbouring, peritectic reaction. Thus the most likely reaction can be estimated from the shape, but need not be correct.

Even so, we have not tied things down completely. Hillert [23] pointed out that a further effect is that of the changing shape of the tie-triangle as the temperature decreases. He expresses this in terms of algebra, but the point is more readily seen using the old intersection rule for phase proportion. Consider Figure 2.12. For mean composition X, the proportion of A is decreasing, as expected, and a similar construction will show this to be so for B, as well. However, for mean composition Y, the proportion of A is ~in~creasing, and Y is undergoing a peritectic reaction. It is, therefore, possible for the nature of the reaction of a given tie-triangle travelling in a given direction across the ternary diagram with decreasing temperature to depend on exactly where your mean composition is within that tie-triangle.

In one sense, the four-phase reactions allowed in ternaries are less problematic; they are composition and temperature invariant. There are, however, two types of peritectic; one direct extension to incorporate another phase, and another which has properties of both the peritectic and eutectic in that liquid and a solid are both being consumed, but two other solids are being deposited simultaneously. The 'n:m' terminology should help here.

Eutectic (Ternary eutectic,1:3):	L -> A + B + C	
Peritectic (Ternary,2:2):	L + A -> B + C	(2.13
(" 3:1):	L + A + B -> C	

In higher order systems, there will be 'psuedo-ternary' versions of the above which vary in composition/ temperature, and whose nature will depend on the movement and shape change with temperature, and higher order variants of the above invariants. The label, 'peritectic', is probably not worth keeping for these, and the shortest form of any use would be the 'n:m' terminology.

Another feature which is not allowed in binaries concerns the behaviour of partition coefficients. The 'sense'

of the partition coefficient depends on whether it is less than or greater than one, whereupon solidification results in enrichment or denudation of the element in question in the residual liquid. No solute of commercial interest has a partition coefficient greater than one when in dilute quantities in iron but, this project is (i), not restricted to dilute compositions, (ii) not restricted to binaries, but (iii), includes solid:solid partitioning whereupon coefficients greater than one <u>are</u> encountered even in the dilute binaries. Moreover, even in the dilute binaries, the partition coefficient of iron is greater than one.

In order that any point on a phase diagram must have a total of 100% or unit fraction composition, one point cannot have less or more of all elements than another. In a binary, if one partition coefficient, k, is less than one, then the other must be greater than one. In a ternary, however, there is more freedom. Two k's can be determined independently. Two must be in the same sense, and the third in the other.

Consider a point on the ternary grid in Figure 2.13. The lines drawn through the point represent those of the same concentration of one of the three elements in turn. This divides the triangle up into 'sextants' which have been labelled with triplets of 'h' and 'l' indicating that the composition within that sextant is higher or lower than the arbitrary point, in order for elements a, b and c, as apparent from the lines. If a tie line is to be drawn from the chosen liquid point into any sextant, the respective k's will be greater than one for h, and less than one for l.

Having established that, we can now consider two tie-lines from the liquid point, i.e. a three-phase reaction. A triangle can be drawn with the second side in the same, adjacent, two-removed or opposite segments in either direction. In terms of the partition coefficients, this means that none, one, two or three of the k's can change sense (which could be termed a 'partition order' of 0,1,2 or 3).

To explain the implications of this, in the binary systems with which we are more familiar, the k's of a solute element must maintain the same sense for both solid phases in a peritectic (partition order 0), but must be of reversed senses for those of a eutectic (partition order 2). The above point, in combination with the previous description of when is a eutectic not a eutectic, etc., means that this is not so for ternary (or higher order) systems. All things are possible provided that there are two of one sense and one of the other.

The most important case of this in the present study is the Fe–Cr–Ni system, where we not only have the complications of the peritectic–eutectic transition but where, even for the avowed eutectic, it changes from the k's of Ni and Cr being of opposite to the same sense.

A further point to investigate is what happens to the liquidus slopes, and how to split the total temperature change for a small displacement on the diagram into the components due to the individual elements. For a start, one must not consider all the elements, but elect one to be a nominal 'solvent'. This might stike one as odd at first, but remember that one does the same in a binary. In a system A–B the change in temperature from a composition X(A,B) to Y(A+δA,B+δB) is $\delta A.dT/dA$ OR $\delta B.dT/dB$, and NOT the sum of both effects. A and B are not independent variables. In a ternary, there is more choice as one might expect. In figure 2.14a, to get from the one composition (X) to the other (Y), you can consider the change in any two of the three components, and the remaining one is a dependent variable, fully defined by those two moves. There are three ways of doing that: (δA,δC; δB,δC; δB,δC). Each δ can be performed equally validly along two axes, but each pair has to be self consistent for validity insofar as they both consider the same component to be the dummy solvent. Also, each way is reversible; they are commutative translations, although only one version of each is pictured for (relative!) simplicity. With that understood, the third dimension can be considered, i.e. temperature (out of the

page). Each δ must be multiplied by the correct gradient to yield the relevant contribution to the overall temperature change. Two of three routes depicted in Figure 2.14a are represented in this way in Figure 2.14b. In each, one element is the implicit 'solvent' which varies as it is forced to do by virtue of the others but which cannot be held responsible for an additional translation. This same logic applied to the binary case although it was trivial, but moreover, will also apply in higher order systems. The associated temperature changes can now be understood. Generalising these, and extending to multicomponents, the equation is as follows:

$$\delta T = \sum_i \delta X_i \,.\, [dT/dX_i]j \qquad (2.14$$

where]j is defined to mean "for all i's constant apart from that specified and the adopted solvent".

The ideal way out of all this confusion is to let a computer do all the thinking for you, which leads us into the next section.

2.2.2) Methods of Calculation of Equilibrium Phase Diagrams

The equilibrium phase diagram is one way of representing the result of the competition between the various phases as to which has the lowest energy under given conditions (composition, temperature and pressure), as described in the previous section. The diagrams should therefore be consistent with the thermodynamics of the phases and, indeed, calculable therefrom. The thermodynamics are not, however, immediately available as equations, but as specific, experimental values from which equations have to be constructed. The thermodynamics can give leads to the sort of forms such equations should contain but cannot as yet give the full equations from theoretical analysis. Therefore, a lot of 'curve-fitting' is called for; the stock-in trade of the CALPHAD group formed specifically to address these matters [17].

The problem consists essentially of three parts: first, the derivation of basic data in terms of both equilibrium phase diagram measurements and the underlying energetics; second, the optimisation of data from both sources into a consistent whole, and third, derivation of suitable equations for the representation of such data.

This is the regime of the sub-contract to this project given to the National Physical Laboratory, who are part of the SGTE [16] and CALPHAD [17] ventures for cooperative research in this field. As far as the NPL are concerned, the experimental data are gleaned from the literature, and the optimisation is performed by a regression analysis derived for this purpose by Lukas [41].

a) Basics and Terminology

In the following description, equations in terms of temperature and composition will be presented; the effects of pressure are fairly easily included with appropriately placed 'PV' terms in the enthalpies but are not very relevant to the thesis.

Obviously, there are a variety of ways from which the problem could be approached, but the following format has proved flexible and useful, and has been standardised upon for the bulk of such work [42-46].

Dealing with effectively constant pressure, we require representation of the Gibbs function, G; -really a free enthalpy, but commonly referred to as a free energy. The 'energies' with respect to a suitable reference state of the pure components present as a particular phase are termed 'lattice stabilities', and the expressions for these are temperature dependent. The energy of mixing or transforming these pure component phases into multi-component phases is expressed as the simple, proportional mixing of the lattice stabilities, the analytical, ideal mixing entropy term and a

catch-all 'excess free energy' which is the difference between this and the actual value. The bulk of the work has therefore been done before the fitted, catch-all term (a function of both composition and temperature) is introduced.

This format is represented in the following equations.

b) Lattice Stabilities

The lattice stabilities are purely temperature dependent as described above. It is easier to see why the adopted form is so structured if one first accepts that people have found the following equation for the specific heat to be successful [47].

$$Cp = a_2 + a_3 T + a_4 T^2 + a_5 T^{-2} \qquad (2.15$$

The enthalpy and entropy are related to the specific heat in the following manner:

$$\Delta H = \Delta H(To) + \int Cp.dt \qquad (2.16$$

$$\Delta S = \Delta S(To) + \int (Cp/T)dt \qquad (2.17$$

Integration of these temperature dependences, combined with equation 2.15 and the the standard ΔG relation (Section 2.1.1) yields the following form of polynomial for the lattice stability:

$$\Delta G = a_o - a_1 T + a_2 T(1-\ln T) - a_3 T^2/2 - a_4 T^3 - a_5 T^{-1}/2 \qquad (2.18$$

where the extra constants, a_o and a_1, are definable in terms of standard enthalpy and entropy, the temperature, and the constants, a, previously adopted.

Of the various ways of representing these, the most widely used is the Redlich-Kister polynomial [48]:

$$\Delta Ge = x(1-x)(a_0 + a_1(1-2x) + a_2(1-2x)^2 \cdots \quad (2.19$$

or the equivalent, alternative form:

$$\Delta Ge = \Sigma\, a_k . x_1 . x_2 . (x_1 - x_2)^k \quad (2.20$$

Some researchers use simple power series, Legendre or Chebyshev polynomials [45,49,50] but, provided integral powers are used, they are mutually transformable. The above form does, however, stress that the excess term must be zero for the pure components, and successive terms have progressively smaller effects on the resultant 'bulge' curve. The diagram series in Figure 2.15 shows the form of the terms (even powers symmetric about x1=x2=.5, odd powers anti-symmetric) and simple combinations, after Hack [44]. It can be seen that the higher powers influence the shape of the curve progressively closer to the pure element axes, although collapsing to zero at the actual axes.

The above equation is for binary systems, although Margules [51] extended it to multi-component systems over 50 years before Redlich and Kister put their names to the binary form:

$$\Delta G^{\bullet} = \sum_{i=1}^{m-1} \sum_{j=i+1}^{m} \sum_{k=0}^{n} a_k\, x_i x_j (x_i - x_j)^k \quad (2.21$$

where n is the maximum exponent used in any one of the binary systems (otherwise all zero), and m is the number of components.

Partial excess free energies can be derived for this equation [44].

The coefficients, a_{0-k}, are temperature dependent, adopting the same form as the lattice stabilities in this respect.

For a ternary system, the Margules equation is equivalent to weighting the corresponding values from the three binaries in accord with the geometric construction in Figure 2.16. Indeed, Muggianu [52] proposed this procedure. Other geometric constructions for weighting the ternary results from the binaries have been proposed by Toop, Bonnier, Kohler, Colinet and Muggianu [52-56], but the Margules (Muggianu) is the most widely adopted and extendable to higher dimensions, and is the approach employed by the NPL.

The Margules equation does not always adequately represent the excess free energies across a ternary or higher order diagram, and extra, ternary interaction terms, both symmetric ($x_1.x_2.x_3$) and non-symmetric (e.g. $x_1.x_3^2$). Such terms tend to be minimised, however, the better is the description of the binary energies. Higher order interactions are inherently less likely and not simply because of the lack of good experimental data sufficient to justify extra terms. Physical coordinations reflecting such terms are progressively less likely the greater is the number of units (atoms/molecules) involved. Apart from its intuitive logic, this is reflected by the rapidly dwindling number of additional, chemical compounds obtained with additional solute species (over and above those which can be considered as a lower-order compound but with substitution of some elements from one or more sub-lattice).

d) Problems of Computation of Phase Diagrams

The computation procedure requires lattice stability information for all the lattice/phase types present in the whole sytem for each pure component, whether or not a pure component actually exhibits such a phase. Data on, for example, fcc nitrogen are, however, hard to come by, and a lot of

inspired guesswork is required. Such imaginary values can, of course, be checked 'backwards' from real, multi-component results but might not be obtainable directly. Other imaginary values can be obtained by extrapolation from the nearest compositions which do contain such a phase, or, indeed, from hypothetical, first-principle thermodynamics, but there is plenty of room for uncertainty.

Let us presume we now have the optimised source data represented by lattice stabilities, analytical expressions and fitted, weighted, Margules equations. For a specified composition and temperature, we can calculate the Gibbs energy for each phase and see which is the lowest, but the computation is seldom this simple: there are quite likely to be more than one phase present, and the compositions within are likely to be different, provided the average corresponds to the specified, overall composition. Within these limits, therefore, composition is a variable, and it can be seen that the determination of the allowed combination of phases and respective compositions with the lowest energy, i.e. the equilibrium result, is not a trivial exercise.

This, then, is the field covered by the NPL sub-contract to this project, providing multi-component equilibrium information which should optimise the existing, experimental data and fill in the gaps between the data points. The centre of most multi-component systems tends, however, to be a very large gap, and any curve fitting exercise, no matter how sophisticated, must be open for examination in such, uncharted regions (see Scope of Work 1.1).

2.3) DIFFUSION

2.3.1) Fundamentals

The compositions of co-existing phases at equilibrium tend to vary with temperature. One phase will grow at the expense of another and, being of different compositions, solute has to be redistributed and homogeneously mixed in. It is the fact that the mixing process takes time which leads to departure from equilibrium behaviour: conversely, it is this departure which provides the driving force for the mixing process.

Mixing-in will naturally tend to homogenise, maximising the entropy and achieving the minimum free energy equilibrium state. There are two main diffusion mechanisms: one involving missing atoms or vacancies within the array, and the other involving smaller species which can occupy the gaps within even a full array.

Both these mechanisms, i.e. substitutional and interstitial diffusion, can be tackled in the first instance by the same mathematical treatment as in stagnant fluids, despite the absence of a lattice therein, and, moreoever, as thermal diffusion. (Indeed, Fick [57] adopted the equations from Fourier [58].)

Consideration of numbers of atoms in adjacent planes, each with the same probability of jumping, readily reproduces Fick's First Law [57], whereby the diffusive flux across any plane is proportional to the concentration gradient across it, where the constant of proportionality, D, is the diffusion coefficient. (Returning to the case of gases, there is no fixed spacing, L, and a sensible solution requires the probability of a molecule jumping a particular distance in a given time to be proportional to $1/L^2$.)

Now considering a particular plane on the concentration profile, it can readily be seen that the change in its

composition with time will correspond to the imbalance of the flux across the plane. From this argument, this change can be described as:

$$dc/dt=d(D.dc/dx)/dx \qquad (2.22$$

If the diffusion coefficient, D, is a true constant rather than varying with distance or concentration (the temperature remaining constant for this argument), then this can be written in its more standard form, though both would count as Fick's Second Law:

$$dc/dt=D.d^2c/dx^2 \qquad (2.23$$

(The more general form, with no implicit assumptions such as a planar interface, is dc/dt = div(D grad(c)).)

The process of diffusion has been defined in terms of the frequency with which atoms jump from one plane into another. That frequency will be temperature dependent. Indeed, so much so that billions of jumps may be expected every second in a mole of a typical metal near its melting temperature whereas you might have to wait a week or so for a single jump at room temperature [59]. The temperature dependence is described by the Arrhenius equation:-

$$D = Do.e^{-Qa/RT} \qquad (2.24$$

The study of diffusion might seem vaguely manageable with Fick's Laws solved according to whatever initial/ boundary conditions were appropriate to the case in point [e.g. 60] but, unfortunately, this is far from the case.

2.3.2) Unwanted Complications

These are explored in a variety of turgid text books, e.g. [61], and no great detail will be attempted here.

a) Which Diffusion Coefficient?

The diffusion coefficent can be variously defined as tracer, for vanishingly small amounts as in radioactive tracer experiments, exhibiting ideal behaviour, intrinsic, allowing for non-ideality at practical concentrations, and chemical inter-diffusion, allowing for the solute/solvent effects. The latter is the one measured most directly in diffusion couple experiments and, by the same token, of most practical use.

b) Diffusion with Respect to What?

The Matano interface in a diffusion couple is that which has had equal numbers of atoms diffusing across it in both directions. Generally, it is the same as the 'laboratory-fixed' original plane throughout (which will also be the Grube interface where the composition is the average of those in both halves of the couple). The Kirkendall interface is that of the lattice plane of the original interface, which moves in response to a net flux of vacancies unless the intrinsic diffusivities of the species happen to be equal.

The simple D is difficult to apply (relating to the 'Kirkendall interface') and the more sophisticated D is straight forward to apply (relating to the the 'Matano interface').

The maximum inter-diffusion flux occurs at the Matano interface, whereas the maximum intrinsic flux occurs at the Kirkendall interface.

c) Interactions

At the moment, these equations only relate to free atoms or molecules of a single species. If two species are present, but which interact with each other in just the same way as they do with themselves, it is readily seen that the same rule will apply. If they interact differently, it is necessary to state the argument in terms of their 'activities' or, better still, 'chemical potentials', rather than straight concentrations; one complicating factor which was addressed by Darken [62]. Darken also addressed the fact that in a solid lattice, diffusion can no longer be considered simply as the free movement of these atoms through boxes, but through an ordered array of themselves: the movement is no longer nearly so free, and the atoms form their own 'boxes', so complications can be expected.

According to the recorded discussion after Darken's classic paper revising diffusion theory [62], he had a pretty rough reception -"It is obvious that the solution to this problem is to be found in the laboratory and not at the desk". Even the Kirkendall Effect [63] (movement of inert markers placed at the interface of a diffusion couple) which the revised theory explained (markers move in accord with unbalanced diffusive fluxes past them) was dismissed as an artefact of poor experimental procedure. (It appears that Kirkendall's co-author was unfortunate in that his name, Smigelskas, was far too forgetable to share in the 'Effect'.)

At low enough concentrations it can be seen that Fick's laws would be expected to apply again, but deviations are now more likely. Being a different species, the solute is likely to cause some local distortion to the lattice shape and bonding. The distortion will vary with the composition, and direct application of Fick's laws in terms of composition will not be accurate. As mentioned before, use of the laws with chemical potentials rather than concentrations greatly extends their applicability.

d) Multicomponent Systems

Diffusion in binary systems seems complicated enough but, unfortunately, multi-component systems are required by this project. The classic example of how this can complicate everything is Darken's 'up-hill' diffusion of carbon [64]. A diffusion couple constructed of steel with different silicon contents exhibited flow of carbon from the lower carbon half to the higher carbon half; the flux was still down the chemical potential gradient, but this was so affected by silicon that this was in the reverse sense to the composition gradient. This flux would reverse once the silicon differential reduced. In a binary system, a diffusive flux up the concentration gradient is only possible with spinodal decomposition.

The off-diagonal, or cross terms of an element's diffusivity matrix [65] can be used as devices or fudge factors to compensate for using concentration gradients, but a more satisfactory approach is to redefine the flux matrix in terms of mobilities and chemical potential gradients. The diagonal elements are the major, pure component terms and, described by chemical potential gradients rather than concentration gradients, are sufficient to describe Darken's up-hill diffusion. (This is not true in an ideal solution, where cross-terms are required for such an effect [66].) The remaining, generally small, cross-terms imply that the flux of one component is not just affected by the local changes in alloy composition, but also by the chemical potential gradients of other elements. It is readily seen that a flux of vacancies due to other components could affect the diffusion of a given solute but, if vacancies are included as a component, it is not immediately obvious why such an effect should persist. An intuitively attractive idea [67] is that if the chemical potential gradient is described with complete accuracy, then such cross terms should be redundant.

Unfortunately, such accuracy is not yet available, but neither are sufficient experimental data to warrant use of cross-terms in all but a few systems. Determination of the diffusivity matrix for a single composition from a ternary system involves a laborious procedure with two diffusion couples whose diffusion paths intersect at the composition point of interest [67]. Certainly, for the purposes of this thesis with high order alloys, these off-diagonal elements have to be ignored simply because they are unknown, which is a matter of no regret to the author. Therefore, plain concentration gradients are employed here.

2.4) SECONDARY DENDRITE ARM COARSENING

A typical dendrite did not always have the same separation between adjacent secondary arms as is apparent in the fully solidified, etched structure. This was noted a long time ago by Papapetrou [68] in inorganic-salt systems, and leisurely followed up by a couple of Russians [69,70] but it took another Greek over 30 years later (Kattamis [71]) to convince people that it also happened in metals at high temperatures.

Papapetrou referred to it as a process of 'distillation', whereby material would melt off from regions of high curvature and redeposit on regions of low curvature. This involved dissolution of arms which were, themselves, finer than their neighbours or which had narrow roots such that dendrite lobes would 'neck off' (Fig.2.17). (This second mechanism was analysed by Klia [69].) His inorganic solutions had the twin advantages of being transparent and solidifying at ambient temperatures.

Kattamis observed the phenomenon in the ubiquitous Al-4.5%Cu system, both under isothermal holding and continuous cooling. He proposed two possible mechanisms: the necking off, as before, but his dissolution of the finer dendrites was by reducing radius at fixed length. Kahlweit [72] disagreed on the strength of his work with inorganic salt, whereby he observed the finer arms dissolving back from tip to root at fixed radius. He stated that the same should be expected in metallic systems; after all, the curvature at the tip was bound to be higher than that down the sides. This seems correct if his hemispherically-capped cylindrical arms are present, but lobe-like side arms would still be expected to neck off (Fig.2.17). Kirkwood [73] adopted the mechanism of melt-back from the tip at constant radius [74] in his analysis of the coarsening process, although such a feature was not incorporated in his numerical model of micro-segregation, in

which the coarsening process was represented purely by an increasing distance between neighbouring arms ([5], Section 4.2).

Allen and Hunt [75] took another approach. They observed secondary arms marching up primary stem towards the primary arm tip. This apparently suicidal migration into hotter climes was explained by temperature gradient zone melting (TGZM). Consider figure 2.18. The temperature gradient leads to a reverse gradient in liquidus and solidus (assuming $k<1$). The actual establishment of the corresponding liquid concentration gradient, essential for the continuation of the argument, requires a little thought.

Thermal diffusivity is much faster than solute diffusivity, even that of carbon in the liquid. We are dealing with a steady state, rather than equilibrium condition. Heat is continually pouring down the temperature gradient but there is ample supply and removal of heat either side of the system under consideration to maintain this situation. If this is sufficiently stable and long lived (the ideal being a constant gradient), a similarly non-equilibrium, steady state solute gradient can be established in response. If local equilibrium is assumed at the interfaces, we produce the sort of profile as in Figure 2.19.

The 'hot' side of a given secondary arm has solute gradients leading away from it in both the solid and the liquid. It must therefore be losing solute and, the only way it can do so while maintaining local equilibrium is solidify, thereby generating 'free' solute to keep the balance. On the 'cold' side, it will either remelt or solidify depending on the balance of the opposed fluxes in the solid and liquid. Commonly, the higher diffusivity in the liquid will more than compensate for the reduced gradient such that will be a net flux in to the interface, which can only be accommodated by some remelting of that interface.

We must now superimpose continuous cooling; the whole system is gradually slipping backwards down the temperature gradient. On its own, this would result in an increment of solidification with a corresponding increase in residual liquid concentration. The superimposition gives the 'hot' edge even more reason to solidify, but this solidification tendency could still be outweighed by the flux balance at the 'cold' edge.

The hot interface is therefore moving up towards the dendrite tip, whereas the cold interface may or not be, depending on the particular circumstances. In any event, its progression towards the primary tip must be slower than that of the hot interface, even if not negative. So, if the conditions are right for bodily migration of the secondary arms, this will also lead to coarsening of the arm spacings, although this is a relatively subtle and finely balanced mechanism.

As is the case with the ripening mechanisms, this has the effect of reducing the extent of micro-segregation with respect to that with static arms; relatively pure solid is melting back into the residual liquid and diluting it, and the solid at the core of the arm need no longer be the first solid to have appeared. (However, other researchers have concluded that its effect is rather small [76].) In addition, it can result in a non-symmetric 'saw-tooth' composition profile in the solid [77,78].

Lalli [79] extended this analysis to a numerical treatment, confirming Hunt's conclusions on migration distance, showing that the micro-segregation decreases with increasing ratio of migration distance to final arm spacing, and that the coarsening increases with increasing ratio temperature gradient to isotherm velocity.

Kurz [1] points out that these various coarsening mechanisms may be all very well at the later stages of solidification but that, early on, it is a simple case of competitive growth. The arms which get there first stub out the others with their solute bumpers in a purely statistical

manner, as pictured in Figure 1.1. To a large extent, however, this doesn't matter, being restricted to the early stages whereupon the segregation is highly insensitive to what's going on.

Mortensen [80] derived an analytical treatment of the influence of coarsening by ripening on micro-segregation. He employed an imposed coarsening law and a constant cooling rate, and ignored diffusion in the solid. In comparison with experiment he found that coarsening reduced the extent of micro-segregation too much, and concluded that it is incorrect to assume that ripening persisted to the end of solidification. Rather, coalescence takes over towards the end, which would have much less an effect on solute redistribution/ homogenisation. This is discussed further in Sections 2.8.2(d) and 5.6.3(d)

This popular alternative that the important coarsening mechanism at later stages is the zipping-up of particularly close pairs of dendrite arms, is again encouraged by the removal of sharp curvatures [80], Fig 2.19. In this case, the high curvature is now in the opposite sense to that pictured for the ripening mechanisms, with consequent growth, rather than dissolution, of these regions.

Whatever mechanism is operative, it is agreed that the phenomenon significantly reduces the extent of micro-segregation at the later stages of solidification, and is therefore of great importance to the current study.

Following Brody and Flemings [81] the secondary arm spacing is commonly expressed in terms of the local solidification time, t_f, defined as the time elapsing from the start to the end of solidification at a particular point in the alloy, the relationship being of the form:-

$$\lambda_f = Kt_f^n \qquad (2.25$$

where K and n are constants. Other workers use the average cooling rate, W, (defined as positive) during solidification, instead of t_f in an equation of equivalent form.

A common equation for the coarsening during solidification is:

$$\lambda = K'.t^{1/3} \qquad (2.26$$

Kirkwood [18] points out that this should not be confused with the equation for the final arm spacing, as this rule breaks down at high fractions solid. Kirkwood has also devised an analytical model of how a solute affects coarsening according to the mechanism of melt-back from the dendrite tip, and Beaverstock [82] has extended this from a binary to a multicomponent treatment. However, the improvement thus obtained was relatively small on the alloys investigated.

The current program can use a variety of imposed laws, and is described in Chapters 4 and 5.

2.5) SEGREGATION MODELLING

2.5.1) Analytical Treatments of Micro-Segregation

The equilibrium lever rule (Section 2.2.1,Fig.2.20) describes the proportion and respective composition of phases in equilibrium but provides no information regarding the residual composition differences within a phase. These differences result from the inability of the diffusion process (Section 2.3) to equalise the chemical potential within a given time, and the diffusivity is therefore central in determining the extent of residual segregation.

The first attempts to quantify this micro-segregation [83,84] assumed that no diffusion occurred within the solid at all, but maintained complete mixing in the liquid. The resultant solute balance (Fig.2.20) is:-

$$Zl(1-k)\dot{fs} = (1-fs)\dot{Zl} \qquad (2.27$$

Integration of this equation with a constant partition coefficient, k, yields the well-known Scheil equation:

$$Zl = Zo(1-fs)^{(k-1)} \qquad (2.28$$

As it stands, micro-segregation will proceed to infinity with k less than unity unless artificially curtailed at the attainment of a composition corresponding to a minimum on the phase diagram solidus such as a eutectic, or at an arbitrary fraction solid. With k greater than unity, the liquid composition will fall to zero as solidification proceeds, but the only elements exhibiting such behaviour in steel are of limited commercial interest: e.g. Ir, Os, and Pd.

Despite such limitations, this equation has been of considerable use and, before the advent of electron microprobes, there was little incentive to advance the theory because of the lack of experimental data regarding actual microsegregation profiles. The ~~lever rule and~~ Scheil Equation is shown ~~are compared~~ schematically in Fig.2.21.

The next advance was not until 1966, when Brody and Flemings [81] introduced finite diffusivity into the source, solute balance equation, assuming planar growth of an interdendritic volume element:-

$$Zl(1-k)\dot{r} = D(dZ/dr)_I + (r_f - r)\dot{Zl} \qquad (2.29$$

In order to solve this equation, k and D were assumed constant, a growth law was imposed, and the solute gradient in the solid at the interface (which will be modified by back-diffusion in reality) was assumed equal to the change in interfacial composition of the solid as the interface advances, i.e.

$$(dZ/dr)_I \approx dZ_I/dr = k(dZl/dr) \qquad (2.30$$

This latter assumption is only true at the Scheil limit, and leads to progressive errors with increasing diffusivity.

Defining a constant:

$$\alpha = D.t_f/r_f \qquad (2.31$$

equation 2.29 can be integrated with a linear growth law to:-

$$Zl = Zo(1-(fs/(1+\alpha k))^{k-1} \qquad (2.32$$

and with a parabolic growth law to:-

$$Zl = Zo(1-(1-2\alpha k)fs)^{(k-1)/(1-2\alpha k)} \qquad (2.33$$

The planar model could be interpreted either as sheets of primary dendrite arms (Fig.2.22a), or planar secondary arms (Fig. 2.23a), but the latter appeared to give better agreement with experiment.

The break-down at high diffusivity leads to non-conservation of solute, and attainment of the Lever rule with finite diffusivity (at alpha=.5 in equation 2.33).

Clyne and Kurz [85] addressed these difficulties in 1981, employing an alternative treatment corresponding to adulteration of the form of equation 2.29 relevant to the case of equilibrium. At equilibrium, it is undefinable because the back-diffusion term involves the product of infinity and zero, but it must correspond to the following equation:-

$$Zl(1-k)\dot{r} = rk\dot{Zl} + (r_f-r)\dot{Zl} \qquad (2.34$$

Algebraically, their treatment consisted of inserting a constant in front of the back-diffusion component of the equilibrium balance (2.34,Fig.2.20). Calling this constant 'A', their solute balance is therefore:-

$$Zl(1-k)\dot{r} = (r_f -(1-Ak)r)\dot{Zl} \qquad (2.35$$

When A=1, this reduces to the lever balance, and with A=0, it collapses to the Scheil balance. More specifically, however, it should tend to the Brody and Flemings balance at low diffusivity, whereupon, by comparing 2.35 with 2.34, it can be seen that:-

$$A \rightarrow D / r\dot{r} \qquad \text{as} \quad D \rightarrow 0 \qquad (2.36$$

With parabolic growth (i.e. $r = \sqrt{Bt}$) this is constant, and the equation is integrable: indeed, it produces the same equation as (2.33). The present definition of A, however, only applies at low diffusivity, and it must be "rationalised" so as to tend to the correct limit at high diffusivity, i.e. A -> 1. An exponential diffusion field argument coupled with an appropriate spline function led Clyne and Kurz to propose the following definition of A:

$$A = 2[\alpha(1-e^{(-1/\alpha)}) - e^{(-1/2\alpha)}/2] \qquad (2.37$$

This, however, is rather awkward for use as a hand-calculator, analytical estimate, and a suggested alternative [8,10] is the simplest spline between the Brody-Flemings and lever limits, i.e.:

$$A = 2\alpha/(1+2\alpha) \qquad (2.38$$

It can be seen from figure 2.24 that the agreement between these alternative formulations is very good over the complete range of alpha from zero to infinity.

Ohnaka [86] obtained this same term via a different approach. Rather than finding an empirical simplification of the Clyne-Kurz back-diffusion parameter, it was derived as a consequence of assuming a second order polynomial form for the segregation profile across the solid. Moreover, he states that use of use of 4α instead of 2α enables the formula to be applied to a cylindrical morphology.

Additional micro-segregation formulae have been presented, under various assumptions, which are so complicated as to defeat the object of a simple, readily calculable estimate. Fujimura and Brimacombe [87] developed a highly contrived 1D analytical treatment with root-time growth and an assumed, linear relation between fraction solid and composition. One of Ohnaka's expressions involved umpteen algebraic terms [86]. At this level of complexity, a computer is called for, whereupon the inclination would be to use a basic numerical treatment which at least allows for the variation of diffusivity with temperature.

Fredriksson applied analytical equations to the peritectic reaction [88]. Complete mixing was assumed in both the liquid and the ferrite, with the austenite developing according to two, back-to-back Scheil equations into these two phases. In Fe-C alloys, the respective growth rates were coupled so as to keep C in its binary equilibrium. In stainless alloys, the two equations were linked by temperature through Raoult's law for the equilibria. Obviously, this treatment suffers from the same limitations as the Scheil equation.

Cornelissen [89] approached the peritectic reaction with a Clyne-Kurz treatment of finite diffusion. Once the peritectic was encountered, the system was assumed to switch from two-phase ferrite and liquid to two-phase austenite and liquid, thereby still amenable to the standard equation. A hypothetical "bulk" composition was assumed at the change-over such that there was no step change in residual liquid composition. As with the standard Clyne-Kurz treatment, of course, the analysis follows only the change in residual liquid composition, with no regard to the composition profile within the solid, and indeed contains no implied ferrite-austenite interface.

In Section 4.1 it will be demonstrated that a simple extension of the coefficient, A, enables application of the standard equation to (convex) cylindrical and spherical growth, and estimation of the effects of alternative growth laws. Furthermore, an extended micro-segregation equation will be derived which incorporates secondary dendrite arm coarsening.

2.5.2) Numerical Treatments

The first recognised numerical treatment of micro-segregation was that due to Brody and Flemings [81], accompanying their previously described analytical study. A 1D plate morphology was assumed, initially taken as primary arms although a secondary arm basis was later recommended (Fig.2.22,2.23). A standard (Carslaw and Jaeger) finite difference scheme for solid state diffusion was employed.

The interface compositions required as a boundary to the FD scheme were estimated in two ways. First, these were computed simply from the Scheil equation, and second, from the basic solute balance equation but where the same approximation of dC/dr|i=dCi/dri as in the analytical solution was assumed. (This was stated as being unsuitable for systems with significant solid state diffusion.) Linear or parabolic growth laws were also imposed as in the analytical case. The advantages over the analytical expression were therefore limited to inclusion of varying diffusivity and partition coefficient, and derivation of a composition profile across the solid.

Kirkwood and Evans [90] improved upon this in 1968, removing the imposed growth law and interface compositions, which are unnecessary in a numerical treatment. This led to the MISEG program inherited at the start of this PhD, which will be described later.

Kobayashi [91,92] numerically extended the Brody-Flemings analytical equation by allowing the back-diffusion parameter to vary, as solved simultaneously with the heat balance. This was further extended to include the peritectic and convex-hexagonal 'columnar' (2D primary arm basis) solidification. In the former case a variable C* was defined as C_s/k which is continuous at both phase boundaries. This was solved by an undefined FD scheme and the interfacial solute balance, with the boundary movements fixed to nodal positions. The hexagonal treatment was not explained in detail but it yielded very similar (albeit lower) levels of segregation and, moreover, the planar model exhibited better agreement with experiment.

Matsumiya et al. [93,94] have also adopted a 2D primary arm basis of hexagonal form, although, originally, their hexagons were not close-packed. Subsequent solidification of the remaining triangles after impingement of the hexagons led to a kite-shaped basic geometry, Fig. 2.25. The program operates with a set cooling curve; the liquidus of the residual

liquid is calculated, which sets the time and the corresponding growth rate with progressive, integral-node advance of the interface. The solidification phase was determined by an Fe-C-P ternary diagram. The final segregation continued to increase with increasing number of nodal planes although this failure to find a consistent solidus was said to be unimportant because subsequent solid state difusion soon ironed out such differences. This apparently severe, final segregation which is artificially blunted by use of few nodes is consistent with my work on concave solidification morphologies which these final triangles represent.

Liquid phase diffusion is included, and so is the peritectic transformation; by belated change of whole nodes which find themselves having a composition not allowed for that phase according to an analogue of the liquidus, binary-summation equation for the delta/gamma solvus (Ar4). More recently, the same authors have adopted a close-packed hexagon morphology [95], presumably having recognised the drawbacks in concave cells mentioned earlier.

Subramanian [96] addressed the questions of solidification, solid state homogenisation and precipitation of TiN in a multi-component steel. A regular solution model was adopted for the central, Fe-Mn-C equilibria [97] with a largely unexplained FD treatment of diffusion in the solid. It appears that the model is 1D with fixed arm spacings and restricted to fully ferritic solidification, although sub-solidus transformation to austenite is included. The interstitials, C and N, were predicted to show negligible micro-segregation, and the C content had a pronounced effect on the degree of homogenisation of the interstitials due to its influence on the persistance of ferrite, consistent with expectation.

Battle [98] is manfully struggling with a highly involved, invariant imbedding ("Method of Lines") technique for 1D, static arm, binary micro-segregation. He admits to stability problems on anything he has tried other than Fe-Ni,

for which he generates very similar results after massive run-times on a main-frame to those of MISEG (see later) which takes a few minutes on a BBC-B. Very recently, he has also provided a useful review of segregation modelling [76].

Meittinen [99] has developed a simplification of Agren's model (see later) which allows for the peritectic with complete mixing in both the ferrite and the liquid and finite diffusion only in the austenite. Similarly to myself, he uses the Jernkontoret work [100] as a prime source of experimental comparison. He finds the calculated liquidus (from free-energy expressions) to be higher than in practice, which is put down to lack of undercooling in the model. On the same steels, my simple binary summation agrees very well with the measured liquidus values, implying no such problem. Also, the calculated solidus can be lower than experiment, which he puts down to limitations in the model whereas a major effect is the failure of the thermal analysis to detect the ~true~ solidus (Section 6.1) which does, indeed, lie well below apparent measurement (as evidenced by the presence of eutectics which would not exist at the quoted temperatures).

In 1980, Lalli [101] presented a 1D secondary dendrite arm model which incorporated the phenomenon of dendrite arm migration, following on from the analytical work of Allen and Hunt ([75,76] Section 2.4). He modelled two arm spacings with a Murray-Landis [102] moving grid FD diffusion scheme coupled with the Crank-Nicolson [103] technique for the time derivatives. An upwinding technique was employed for mass transport in order to avoid numerical instabilities. Migration was demonstrated to bring the extremes of core and final concentration closer together than with static arms, and to produce 'saw-tooth' concentration profiles.

This work was originally presented as a term paper for Prof. H. D. Brody at the University of Pittsburgh. Prof. Brody informed me about some unpublished work on the effects of dendrite coarsening but this did probably not refer to Lalli's study (albeit published only in a conference proceedings). I understood Prof. Brody to mean that the mystery model considered coarsening by dissolution of the smaller arms (ripening) rather than as a consequence of migration. In any event, the work

to which he referred demonstrated that coarsening only influenced the micro-segregation of slowly diffusing species, consistent with my numerical and, indeed, analytical work.

The source work of Dr. Kirkwood's is detailed in Section 4.2. Roosz and Exner [104,105] have also followed this lead of modifying the solute balance so as to represent arm coarsening. Their program is set up for an Al-Cu-Si ternary, with a large proportion of the project's effort on determining the relevant equilibrium information by experiment. A Crank-Nicolson diffusion scheme is employed in the solid on a 1D secondary arm basis. The three-phase eutectic reaction is included, with 'classical' behaviour whereby further solidification occurs by simultaneous precipitation of both solid phases, with the liquid composition precisely following the equilibrium eutectic valley, and no encroachment into hypo-eutectic solid. Thermal control over the solidification process is imposed from recorded cooling curves of specific experiments which the program is set to mimic and, indeed, for which agreement is found to be good. (After discussions with Dr. Roosz during the Solidification conference at Sheffield [104], he provided a copy of his program and data-set for information.)

Other than this, the 'rival' models appear to have adopted a static secondary arm basis, with either 1D or simple, convex 2D forms. The most important of these is that of John Agren [106-108], although it appears to be commonly overlooked. This work will be considered in more detail.

Agren's model has the traditional, static arm basis but is otherwise very sophisticated. It claims to handle planar, cylindrical or spherical morphologies, and solidification of a single phase or of twin phases as a classical eutectic, peritectic, or the essentially similar 'divorced eutectic'. The required equilibria are calculated within the program from Gibbs energy equations as in Section 2.2.2. Volume changes through phase transformation are allowed.

The Crank-Nicolson FD scheme is employed for solid diffusion. The solidification interface always lies on a node, with linear interpolation for compositional adjustment of the nodes when shifted to match the advance of the interface. Diffusion of a particular solute can be defined to a particular sub-lattice.

The time derivatives required to advance the process are calculated by Gaussian elimination from the last established values, but the new composition:

$$Zl' = Zl + \dot{Zl}.dt \qquad (2.39$$

acts only as a predictor. The equations are re-run with the predictor to generate the new rate of composition increase, whereupon the accepted new compositions are derived as follows:

$$Zl'' = Zl' + 0.5*(Zl' - Zl) \qquad (2.40$$

This corresponds to a second order Taylor series expansion for the new composition with a forward second-difference.

Various little manoeuvres were introduced to help things out. After each iteration, solute conservation was checked by the trapeze rule and, if out, an appropriate adjustment was arbitrarily made to the liquid composition. For cases where drastically different diffusivities were exhibited in a given phase, simplifying assumptions were employed, although some of these appear somewhat dubious.

Agren has not included dendrite arm coarsening and, the present work also has a superior treatment for the solid/solid interface in a multicomponent system, particularly if species of vastly different diffusivity are present, and appears to run more happily judging from Agren's comment about arbitrarily injecting or removing solute from the system if a conservation check reveals a mismatch.

A further development of interest is the COSMOS project. COSMOS is a collaborative project with the Max Planck Institute in Dusseldorf, The Royal Institute of Technology in Stockholm, and Volkswagen. These are involved in the CALPHAD work on phase diagram calculations, and the project is concerned with the extension of this from equilibrium to non-equilibrium conditions (building up from the established models of Hillert$ and Agren). Specifically, they are addressing diffusion controlled reactions in multicomponent steels, with particular reference to steel heat treatment. In principle, there is no reason why it should not be applied to a static-arm solidification, including the peritectic reaction.

The COSMOS model is usually employed isothermally, tackling the growth of an initial, finite (minimum 3 nodes-worth) amount of one phase in another, with the associated changes in composition profile, upon insertion into an annealing furnace. They currently deal with austenite, ferrite and cementite, with the latter two not yet coupled as for pearlite development. It can also run under a prescribed time-temperature function (not by heat extraction, as yet), and they have used it for the direct calculation of ferrite noses in CCT diagrams.

An array of different representative cells is possible on a given run, allowing, say, different microstructural scales across a sample, with solute flux between them if appropriate. Representative cells can be planar, cylindrical, spherical, or spheroid/ellipsoid, with the cell radius being interpreted as the average half spacing between nuclei or centres of islands of one phase in another. All three phases which they currently address can be included in the cell, but the interpretation of this arrangement is problematic; the program employs a peritectic/peritectoid "coating" style arrangement which is not appropriate for the three phases in question.

Full local equilibrium for all solutes is assumed at the interfaces, with full diffusive control by simple, first-order gradients in the FD scheme, albeit by activity rather than straight compositions. As with my program (second order but with straight compositions), a special procedure has to be adopted to ensure that all these conditions are satisfied. The solute balance scheme is in one program module which iterates with the Swedish equivalent of MTDATA (i.e. Thermocalc) to find the one tie line out of the whole range allowed by temperature alone which also allows the solutes to agree on a single growth rate for the phase interface.

They use this program at temperatures lower than for which many expect the full local equilibrium and diffusive control assumptions to be valid. They can get effectively no partitioning between ferrite and austenite of the sluggish substitutional elements, but with evident adjustment of the interstitial elements (i.e. "para-equilibrium" behaviour), but by the passage of a very sharp "bow-wave" of substitutional solutes. There is still equilibrium partitioning at the interface, but no net change in composition in either phase away from this bow-wave spike. Computation at lowish temperatures can predict this spike to be thinner than an atomic spacing, but Professor Inden was not worried about this; its physical interpretation becomes suspect here, but he considers it still perfectly acceptable as a mathematical device. They had had a lot of discussion of this point in the past, and had concluded that it would be forced to give the same response as an alternative model with no such bow-wave and no partitioning of the sluggish elements, but he could not muster the arguments involved "off the cuff". Their approach had the advantage of yielding a continuum up to this limit, rather than a step change with need to resort to a different model.

The program has a modular structure for flexibility, but which makes it all rather long-winded both to set up and to display the results. Their target is user-friendliness, but they have a long way to go yet before the average heat-treatment shop could use the model themselves.

One aspect of interest in the COSMOS run they showed me was how you can get a hiccup in heat-treatment response upon changing heat-treatment temperature, delaying or even temporarily reversing the anticipated transformation. Such behaviour has been noted, for example, by Gordon Allan at BST with residual ferrite dissolution, and qualitatively explained by Colin Haworth (Sheffield University/BST).

2.6) INTERFACE MODELLING

2.6.1) Theory

The high temperature, solid/liquid interface of a typical alloy is relatively simple. The assumption of local equilibrium at the interface for all species is expected to be a good approximation and, indeed, has been demonstrated to be a successful one. It is the common assumption of alloy micro-segregation treatments, although what small departures from equilibrium do exist are essential and cannot be ignored by those concerned with calculating the solidification morphology from scratch. Similarly, a morphology is assumed in order to remove that enormous burden from the calculations (and indeed, from the programmer), as described in the introduction and Section 2.8, and am not concerned with any small inaccuracies anticipated from holding this complete, local equilibrium assumption.

The real problem comes in with solid/solid interfaces. Grain boundary interfaces between regions of the same phase are not the direct concern of this project, but rather the interphase interfaces moving around in the solid during solidification, and, indeed, after completion of solidification, as encountered in the peritectic reaction.

Even if, as in the peritectic, a solid phase transformation occurs at a temperature equally as high as the solidification transformation, it is readily seen that equilibrium would be more difficult to achieve. In the liquid, there is little barrier to the arrangement of atoms and modification of local composition required for the phase change, whereas both aspects are hindered when both phases are solid.

At low temperatures, solid state phase changes can occur by shear transformation, as for example, martensite from austenite. There is no change of composition, even locally, and the lattice merely slips from one arrangement to the other. This is a 'military' transformation with coordinated, cooperative, small movements of atoms. At the temperatures of interest to this project, however, we are concerned with changes between phases which would like to be of dissimilar composition as in equilibrium, even if they cannot quite get there. This is a 'civilian' transformation with independent, long range movement of atoms by diffusion through the lattice. This is, therefore, highly thermally activated as implied before.

Hultgren [109] coined the terms, 'ortho-equilibrium' for transformations as of that from liquid to solid, where proper equilibrium can be achieved by all species, and 'para-equilibrium' where only the relatively fast species are assumed to obey equilibrium. This latter case, with possible support from experimental results, means that a transformation can take place even if only one of the solutes wants it to. If this can be assumed, it makes the computer modelling very simple again; e.g. equilibrium can be assumed at the interface for carbon whereas the slow, substitutional elements just find themselves forced into a new lattice type regardless of how they are arrayed at the interface.

Hillert [110-112] gave local equilibrium a new lease of life by assuming that it was met without needing long-range transport of the slow solutes. Instead, they would array themselves into a 'spike' (or the inverse) like a bow-wave at the interface. This behaviour, however, still implies that the transformation is being forced by the likes of carbon against the will of the others. Moreover, this spike was often predicted to be of similar or even smaller extent than the atomic spacing, whereupon it was maintained as a mathematical device of admittedly troublesome interpretation. The presented results, however, were very impressive. Inden has the same approach in the COSMOS project (Section 2.5), employing full

local equilibrium down to temperatures at which para-equilibrium could be expected. A variant of this involved a hypothetical interface 'phase' as a mathematical device.

An additional complication to consider is that interfaces necessarily have different structures to standard matrices, which will affect their thermodynamic properties.

2.6.2) Mathematical Practice

Complete equilibrium across a two phase binary system is simply represented by the Lever Rule if no special interface composition feature is considered, with straightforward extensions to three phases and so on. In a multicomponent system, it remains simple provided data are known to derive the chemical potentials which must be uniform for each element. If the effect of interface structure on chemical potential is known, then it is also possible to include the phenomenon of different compositions around the interface even at equilibrium.

Equilibrium across one phase and finite diffusion in another is the standard case for building up a micro-segregation model (Fig.1.2). The problem is relatively trivial in a binary, involving the solute balance with knowledge of the relevant equilibria (partition coefficient and liquidus slope) and the driving force for change (cooling rate or heat extraction rate):

$$Zl(1-k)\dot{r} = D(dZ/dr)_I + (r_f - r)\dot{Zl} \qquad (2.41$$

Extension to multicomponents gets a little more complicated but is the natural extension to the above in terms of simultaneously solving a solute balance for each species along with the equilibria and driving force. Additional complications for multi-component systems are determination

of the relevant equilibria to feed into the equations and, indeed, the relevant diffusivities (Section 2.3), but for current purposes these aspects are 'source data problems' outside of the current argument.

The natural extension to volume diffusion control in both phases is as follows:

$$Za(1-k_{a/b})\dot{r} = D(dZa/dr)_I - D(dZb/dr)_I \qquad (2.42$$

Application of this equation for a binary system with local equilibrium and a constant temperature is within the scope of text books. Its extension beyond these restrictions is not trivial, however.

(An alternative, isothermal phase transformation problem is where one phase is a compound of fixed composition, as dealt with, for example, in ref. 113. This, again, avoids the main problems and, moreover, is not all that relevant to the current work where temperature is continually decreasing.)

The problems encountered when trying to extend this formalism beyond a binary concern the shortage of suitable time-derivative variables. There is no immediate provision for introducing either a varying temperature or a correspondingly varying interfacial composition. The solution, as addressed in Chapter 5, is to "float" the solute balance equations in time, rather than have time derivatives explicitly in the equations.

2.7) MACRO-SEGREGATION

The primary target addressed by this thesis is, of course, micro-segregation, but it is only sensible to consider the likely implications from such work for the important problem of macro-segregation. It is therefore appropriate to describe its various forms at this stage.

Macro-segregation arising from dendritic solidification is defined as compositional inhomogeneity on a scale larger than that of the dendrite arm spacings. (Some people employ the term "meso-segregation" for that on a scale only somewhat larger than of the dendrite arms, reserving "macro-segregation" for truly macroscopic phenomena.)

Macro-segregation is not a fundamental feature of dendritic solidification, despite it being taught as such till relatively recently [21]. 'Normal' segregation in ingots was traditionally described as a natural consequence of enriched solute being pushed ahead of the solidification front, as in the Scheil equation. With a planar solidification front, this would, indeed, be a fair first-approximation, but less so with cellular growth and downright misleading with dendritic growth. The more removed is the morphology of the solidification front from planar, the more the enriched liquid is held within that 'mush'. The morphology is a response to constitutional supercooling and, by its nature, virtually removes it. In so doing, it has also essentially removed the solute field ahead of the dendrite tips under the standard range of solidification conditions and, hence, has avoided 'normal' segregation. Indeed, various people have solidified test lumps of steels to study the phenomenon and not found it. So, assuming a well developed dendritic morphology, and apart from the left-over, residual effects of the above solute "bow-wave" argument, why do we get the various types of macro-segregation in dendritic solidification?

The "mushy" zone can be thought of as sponge full of dirty liquid. Unless you hold it very carefully, the liquid will ooze out and, under various ways of squeezing or bending it, the liquid will squirt or gather in certain places, which is one representation of macro-segregation. To take it further, the sponge must be thought of as fragile and, moreover, readily corroded by cooperative flow of the liquid which thereby produces macro-scopic channels to aid further such flow. Another stage on, and our sponge is, itself, contracting as it cools and is thereby producing its own driving force for fluid flow. Further still, the density of the impure liquid tends to vary according to exactly how impure it is, producing buoyancy forces to drive circulation currents around the sponge. Thus armed, we can address all the significant forms of macro-segregation (Fig.2.26), bar two; (one of these is the reverse, i.e. settling of solid nuclei within the liquid, and the other is a local response to sudden changes in growth conditions at the solidification front, as with "white bands" under electro-magnetic stirring of the solidifying strand; indeed, continous and vigorous stirring along the whole strand length can reduce the solidification morphology on the micro-scale to planar, resulting in massive macro-segregation [114], equivalent to the micro-segregation normally confined to the micro-scale by the dendrite arms).

Micro-segregation, therefore, is a central precursor for macro-segregation, and any useful treatment of the latter requires knowledge of the former. In the present work, qualitative implications can be drawn, or simplistic relative susceptibilities derived, but a further major project would be required (and is, indeed, under discussion) to link a sophisticated micro-segregation model with a sophisticated macroscopic treatment.

2.8) MODEL-versus-REALITY

"Let him know his fairy tale accurately, and have perfect joy or awe in the conception of it as if it were real; thus he will always be exercising his power of grasping realities."
-John Ruskin, introduction to "German Popular Stories",1868

2.8.1) FUNDAMENTALS: a homily

A model helps us to understand Reality. It can be a conceptual model to let us picture what is going on, or a mathematical one to help us make quantitative predictions rather than resort to experiments all the time. 'Theory' (from the Greek for 'to see') can be used in either respect but a model is normally a simplification of the full, theoretical understanding currently obtained but one which can be used more easily. A common error is to assume too much Reality in our theories, or that there must be a unique theory for a particular phenomenon.

An obvious, general principle is that the more accurate the conceptual model, the potentially more accurate are the predictions it can yield. However, it is also a mistake to assume all relevant theory should be built in to every model: much is simply not worth the effort of its inclusion. The value of a model should be judged from whether it gives the required information in the relevant context. The purist may try to take models to the very limits of known science but the pragmatist settles on the simplest model which serves the purpose in question. I would class myself as the latter, applying techniques and concepts comfortably removed from the forefronts of knowledge and, therefore, within my capability.

An important limitation to consider is the availability of data; not data as in observations to test theories, but bread-and-butter data with which to feed our models. The theory behind such data is well established; it is simply a question as to whether anyone has actually bothered to perform the experiments required to get them or, if several people have but have obtained very different values. In either case, we do not really know what values to use. There is little point in constructing a highly sophisticated model if it requires data which are simply not available. This largely explains the belated development of micro-segregation theory: why bother to invent something more sophisticated than the Scheil equation until techniques of microanalysis arrived, able to measure what you were predicting? In the present case, there was a severe lack of multicomponent equilibrium data, in particular, hence the incorporation of the sub-contract for their derivation (Section 2.2.2).

Three mathematical approaches are employed in this thesis: 'curve-fitting', analytical models, and numerical models. The 'curve-fitting' type is the "never mind the quality, feel the width" sort of approach where analytical style equations are invented to match known data or boundary conditions. This, obviously, is a poor relation and does arguably not deserve the lable, 'model' at all, but is sometimes all we have. Analytical models have the virtue of preciseness: provided the mathematics are correct, the model is as real as its starting assumptions. (I try to keep to words such as model and mathematics here rather than arithmetic, which is generally considered an obscure ancient art no longer practiced in developed countries.) Some examples of both these can be found in Section 2.5.1. With numerical models, some of that preciseness is lost but you are generally more able to use starting assumptions more akin to those Nature actually uses.

In terms of the current work, the solidifying steel knows precisely what it is doing and how to go about it, and the results of the process are measurable. If the model gives the wrong answers, then the equations are an inadequate analogue

of the real process; whether over-simplified or plain wrong. Mathematics gives exact results in relation to the model (albeit with errors from numerical method) and has the power to give exact results in relation to theory. We can only hope that it can go close enough to Reality to be of use, and all the evidence is that it can go very close indeed. The important limitation then, is the model (including its required, bread-and-butter data).

2.8.2) Conceptual Model

A dendrite is as unique as a fingerprint, but the target of this model is the 'typical' level of micro-segregation expected from the 'average' dendrite, but noting effects which would lead to variability.

a) The Average Dendrite

There are obvious local variations under ostensibly the same solidification conditions and these will affect the local micro-segregation. The differences in morphology between rather than within solidifying grains can also lead to important differences in this segregation. Experimental measurements which adopt the 'scatter-gun' approach (i.e. taking large numbers of measurements at different points of a 'large' specimen, blind to the actual micro-structure) as recommended in some quarters [115,116] mis-represent dendritic profiles which contain subsidiary composition peaks and sum the effects of varying fractions of different morphology and scale. It is therefore wrong to expect an 'average' dendrite to reflect the cumulative segregation plots thus determined. The statistical nature of this summing procedure is, perhaps, reflected by the success in fitting the statistical Weibull function to the 'scatter-gun' cumulative segregation plots [116].

Such plots exhibit 'tails' at both low and high concentrations; that at low concentration being more noticeable by its incompatibility even with the form of segregation profile predicted by models [Fig 2.27a -v- b]. A likely origin lies in the Weibull/scatter-gun approach representing the sum of a whole range of profiles; a few volume percent of material exhibiting the more extreme profile in Fig.2.27b, couples with the rest of the less extreme profile, could sum to something like the scatter-gun profile. Intuitively, this tail should tend to the bulk composition multiplied by the initial partition coefficient, i.e. the local scale and morphology for a very small fraction of the total sample are such that back-diffusion is unable to adjust the original composition. Similarly, other regions will be much more heavily segregated than the model prediction, but although such results are 'real', they should not detract from the model. Rather, the model should be run with different scaling factors numerous times and the results summed with a weighting system reflecting the local scale distribution within the sample, whereupon similarly tailed plots would be generated. Determining the correct, scalar distribution to mirror the observed plots quantitatively would be a significant modelling problem in itself.

Regarding the presence of troughs or subsidiary peaks in segregation profiles resulting from a peritectic reaction, a trough as exhibited by an austenite stabiliser could also give a low concentration tail as seen in scatter-gun profiles, Fig.2.27c. A subsidiary peak, however, as exhibited by ferrite stabilisers, would be re-shuffled into a kink or shoulder on the cumulative plot (Fig.2.27d), which by its definition rises continually in concentration from $f_c=0$ to $f_c=1$.

Butler [116] found some cases where two Weibull functions were required. Such a result could correspond to the loss of information regarding the actual profiles: i.e. such curves would be expected where there is a subsidiary composition peak at the dendrite core as well as at the interdendritic position (Figs.2.27d). An alternative explanation is, however, required for the case in point because the element in question, Mn, should not exhibit twin peaks (such as MnS precipitation producing the observed kink).

The 'average dendrite' approach must use the concept of a particular dendrite, therefore, rather than expect to represent the overall segregation as described above.

b) Limiting Micro-Segregation Behaviour

Historically, there's the lever rule for complete mixing/ diffusion in both liquid and solid (equilibrium), and the Scheil (Gulliver, Pfann) equation for complete mixing in the liquid and absolutely no diffusion in the solid, with the 'real' answer assumed to lie somewhere between these bounds. There are, however, underlying assumptions to be questioned even here.

The pertinent assumptions are 1), local equilibrium at the interface with the bulk liquid, with no curvature (Gibbs-Thompson) modification to that equilibrium, 2), temperature gradient negligible within the representative cell, 3),constant partition coefficients (for the Scheil bound), 4), complete mixing in the interdendritic liquid and 5), lack of interaction between adjacent 'slices' of dendrite of different fractions solid (i.e. the representative cell can be considered in isolation).

These were dealt with by Brody, Bower and Flemings [117] who found the dendrite tip temperature to be within experimental error (2°, and <1°C later quoted for steel [26,28,29]) such that any effects of (1) must be very small. The magnitude of the relative diffusivities implies that thermal fields should be very flat relative to solute fields, and likewise solute fields in the liquid should be very flat relative to those in the solid. A previous model [Howe,12] which included liquid diffusivity [12] showed it to be essentially uniform, as often quoted elsewhere [81,87,98]. (Indeed, even the much slower diffusivity of carbon in the solid can be closely approximated to equilibrium mixing [3,14,118].) The problem arises from extending the Lever or Scheil bounds to actual dendrites.

There is no problem if we consider a sealed element or isothermal 'box' (Fig.2.28) but, in most modelling work, the treatment is applied to a 'slice' through a dendrite at a fraction solid which increases with time, ignoring the changes with distance other than to say that they are what the considered element will represent at a different time. How can you have complete mixing in the liquid transverse to the primary arm growth direction, yet zero mixing parallel to that growth direction?

A large aspect ratio will help, limiting the influence of neighbouring slices. We usually have that, and some people have calculated that that alone will usually suffice for this assumption [87]. If we do allow longitudinal solute transport in the liquid, what comes in must balance what goes out to enable us to keep to the helpful assumptions. How realistic is this?

The pragmatist might say that were it not, the overall solute content would not remain constant so, therefore, it must be right. A trifle circular an argument, perhaps, and it should be remembered that undisturbed steady-state solidification does not result in macro-segregation, implying there is indeed no net transport between 'slices'.

c) Morphology

We had already introduced questions of morphology into the lever and Scheil bounds, but only insofar as they supported the assumptions which they actually employ in their derivation. So, if we accept these limits (that is, infinite and zero solid diffusion), the first problem is to fit finite diffusion between them. This requires input of size and morphology or at least some dimensionless number comprised of such terms. Simple fractions liquid and solid won't do anymore.

My target, as described earlier, is a 'typical' dendrite, only as far as is needed to afford useful results. The simplest morphology is, of course, 1D, and this has been the basis of most modelling work. This can be interpreted either as primary dendrite sheets rather than arms, or, if the bulk of the solidification is assumed to occur on the secondary arms, these are the sheets in questions, on spindley, inconsequential primary arms (Figs. 2.23,2.24,2.26).

Several researchers have employed a 2D, cellular (primary arm) morphology [91-95], either cylindrical or hexagonal (for 'packing'). More complicated and, indeed, realistic morphological models are currently very limited in terms of other factors which can be considered so it is a question of choosing one of a few, simple morphologies.

As mentioned before, the morphology becomes more important the larger is the fraction solid. I have noted that a first order binomial expansion of the Scheil equation, valid for low fractions solid, generates the Lever rule, thereby demonstrating the tolerance of micro segregation models at the early stages of solidification. We are operating between bounds which are so close that secondary assumptions really make no significant difference to the result. So the question can be re-phrased as what shape does the final liquid usually adopt? In actual fact, it will consist of all sorts, but, typically, a film may be adopted, consistent with 1D or 'convex 2D' format (final liquid on external surface of 2D form).

A previous numerical model [Howe,12] was a rather crude finite difference arrangement based on the 'cellular dendrite'-- a grid of primary arms webbed by merged plates of secondary arms, forming square pyramidal pools of interdendritic liquid (Fig.2.29). This 'concave 2D' format (final liquid at axis of 2D form) gave grossly overestimated micro-segregation. It was difficult even to find a credible solidus with a moderate carbon steel. (This was the model which also considered diffusion in the liquid and found it was sufficient for essentially complete mixing as has been assumed.) Comparisons elsewhere between 1D and convex 2D showed far less dramatic an effect [91,92].

The rough effect of different morphologies can be assessed in the following manner. In Section 4.1, a modification is proposed to the Clyne and Kurz [85] equation now in standard use for analytical treatment of micro-segregation, extending it beyond a planar growth morphology. For convex growth where a single distance, r, is sufficient to describe the situation, extension from 1 to 2 or 3D is found to be relatively straight-forward, with segregation moderating with increasing dimension. For concave growth, it appears that segregation should increase markedly with increasing dimension, but this was not directly amenable to an analytical approach (Fig.2.30).

The main distinction appears to be whether the final liquid is present as films (convex growth) or pockets (concave growth). Obviously, the actual case will comprise varying proportions of various morphologies, but, in general, films seem to be the common form, and the 1D case represents the severest such case.

So, a 1D model is not so gross an assumption as it might look. As before, this basis has a distinguished pedigree. It is, however, best applied when secondary dendrite arms are well developed, and the model cell should therefore be based on the secondary dendrite arm spacing, which introduces the problem of arm coarsening.

d) Secondary Dendrite Arm Coarsening

The phenomenon of secondary dendrite arm coarsening is described in Section 2.4, and was first incorporated into a quantitative micro-segregation model by Kirkwood [3]. A full account of its effect on micro-segregation would require a model which follows the actual coarsening mechanism. At the initial stages of solidification the mechanism is one of competitive growth rather than coarsening as such: those which surge ahead and thicken and block out the slower ones [1] Fig.1.1. After this initial period of rapid and drastic pruning of large numbers of branches, traditional ripening processes

take over, but by four possible mechanisms: melting back of arms with greater curvature from the tip, melting back from the sides, necking off at the root, or migration along the primary stem.

Inclusion of these alternative mechanisms would obviously be a very complex modelling problem, and hindered by lack of much of the relevant data. Kirkwood incorporated the phenomenon by simply considering a particular secondary arm whose axis lies a progressively greater distance from that of its nearest neighbour as solidification occurs (Figs. 1.2,2.31). This was achieved by including the extra term in the solute balance, as has been described before. This term is not, however, the full amount of solute involved in the 'new' volume resulting from the expansion of cell size, but the amount exceeding the bulk composition; the rest being provided automatically. This point has a tendency to puzzle people: it does not mean to say that bulk composition liquid from beyond the dendrite tips is magically transported in appropriate volumes to each solidifying increment, but is a necessary result of increasing the size of the volume element under study whilst conserving solute. (This is merely equivalent to the original cell being already populated with bulk composition; any increase in size must be similarly populated, as, perhaps, most readily understood from considering the simplest case of a uniform composition.)

This might well approximate to the net effect on the composition of the residual liquid but does, however, beg the question as to how well it treats the solid. Just adding a term into the liquid to account for the increase in size of the volume element implies that the solid arms are merely moving further apart, intact, rather than undergoing a remelting-type mechanism which could lead to different solute profiles in the solid. A saw-tooth segregation profile can be observed, for example, moving across secondary arms parallel to the primary stem, which presumably results from the migration mechanism. This could well be modellable but does, however, raise the question of what we intend to get from the model. Perhaps we should not bother to target more than just an average profile, translated back into terms of fraction solid. Modelling particular instances like this does, however, have

more merit than a purely academic modelling exercise because its success or failure gives you some indication as to whether you have understood the mechanism correctly.

CHAPTER THREE

EXPERIMENTAL

Einstein to a student, upon learning of the experimental verification of his prediction of the bending of light by the Sun:

"I knew the theory was correct. Did you doubt it? (-Had the experiment proved otherwise-) Then I would have to be sorry for dear God. The theory is correct."

3.1) LIQUIDUS EXPERIMENTS

3.1.1) Background

Accurate predictions of liquidus temperature are of obvious commercial importance to casting, and particularly so for continuous casting. In the present context, however, liquidus measurements have been performed to provide experimental equilibrium data, and check computed equilibrium data, for use in the micro-segregation model. With local equilibrium at the phase interfaces, the solid/liquid interface temperature will be at the liquidus temperature of the residual liquid with which it is in contact.

Previous work [Howe,119-121] (see below) had already addressed the determination of liquidus for the majority of standard steel types. Therefore, the compositions addressed by the current project were selected on two alternative counts: first, to represent the sort of compositions which the interdendritic liquid might obtain late in the solidification of a more normal alloy, and, second, purely for testing the accuracy of the equilibrium liquidus temperatures calculated by the NPL, i.e. significant amounts of a few species.

3.1.2) Theory

Liquidus temperatures are the easiest, relevant, equilibrium value to measure. A steel is likely to commence solidification under normal casting conditions with only a minor supercooling below the equilibrium value (Chap. 2). One major, measurable change accompanying onset of solidification is the release of latent heat and, indeed, the standard method of liquidus determination is by thermal analysis; observation of the time/temperature cooling curves recorded from thermocouples immersed in the liquid sample.

In the absence of solidification, the natural cooling curve would be a smooth, concave slope (i.e. lower cooling rates at lower temperatures) but the necessary dissipation of latent heat reduces the cooling rate at a given rate of heat extraction, producing a convex distortion of the cooling curve. Normally, a significant proportion of the sample solidifies close to the liquidus temperature and this is, therefore, clearly marked. The schematic cooling curves of four compositions from a simple binary system are displayed in figure 3.1. Ternary and higher order alloy systems can exhibit additional 'kinks' as the deposition of successive phases alters the rate of evolution of latent heat. The schematic cooling curve types which can be encountered in the FeCrNi system in addition to those in Fig. 3.1 are displayed in figure 3.2.

The form of the cooling curve can vary with sample size and thermocouple location. At the edge of a large casting, the cooling curve will be similar to the theoretical examples in figures 3.1 and 3.2. Within a casting, the cooling rate can be less than that of natural cooling above the liquidus temperature when latent heat is being produced by solidification in the cooler, outer regions. Nevertheless, even in the centre of large castings, the superheat is dissipated fairly quickly and a plateau is observed on the cooling curves close to the equilibrium liquidus temperature until the growth front of solid has reached the thermocouple (Fig.3.3). Apart from any transient, nucleation-undercooling, the expected growth-undercooling (at least in iron-rich alloys) is typically within a degree [26,28,29,117], and is therefore an acceptable systematic error for present purposes.

In terms of thermal analysis experiments, the 350/400gm liquidus samples employed in the current study can be termed 'large'. This facilitates accurate determination of liquidus temperature because it is manifested as a plateau of considerable duration rather than a brief kink. Furthermore, large samples largely avoid problems of nucleation undercooling (as opposed to the growth undercooling referred to previously) because even if solidification at the surface is delayed (unlikely in the present case with a rough container and air-melting) the subsequent growth will quickly bring the temperature back up to a liquidus plateau as before.

3.1.3) Experimental Procedure

The majority of the experimental melts were produced in the 10Kg 'SS' induction furnace at BST Swinden Laboratories. Other furnaces were used on occasion depending on circumstances. No vacuum or inert gas procedures were adopted, knowing from experience that pick-up of gases (with employment of Si and, occasionally, Al deoxidation) would not be at such a level as to have a significant effect on the recorded temperature. The melting and sampling was performed with assistance of BST technical staff.

The liquidus temperatures were measured by the Land Checkpoint system [122]. Between 350 and 400gm of metal were top-poured from the induction furnace into the disposable Checkpoint ceramic crucibles which were equipped with Pt/Pt-13%Rh thermocouple heads in silica sheaths (Fig.3.4).

The signal from the thermocouple was originally displayed on Kent chart recorder, modified so as to convert the voltages into a linear temperature response, with an electronic 'cold junction', and backed-off so as to give 1400-1550°c full scale range. This was an ex-demonstration model of Land's with a claimed accuracy of +/- 0.5oC for the thermocouples and +/- 1oC for the thermocouple-recorder combination. For the early casts (pre-PhD work, -see later), 1400oC was accepted as a minimum temperature. Later, however, the electronics were modified in order to alter the degree of backing-off and, hence, allow temperature measurements below 1400oC.

Calibration checks consisted of recorder response to a range of calibrated voltages, once at Land [122] and subsequently by the Instruments personnel at BST Swinden Laboratories, prior to major cast runs. Prior to the third set of casts under this PhD project (Nos. 120-133), calibration was performed via monitoring thermocouple readings within a calibrated furnace. During this exercise, major problems were revealed with the admittedly archaic recording equipment. The nominal accuracy was within a degree but one calibration check indicated that the first 19 liquidus results for this thesis might have been susceptible to a random error of up to 15K. The Kent recorder was, therefore, abandoned, and the subsequent casts were monitored with a Thurlby 1905a Intelligent Digital Multimeter with NPL-traceable calibration.

Two determinations were made from each cast, and further measurements were performed if the first pair disagreed by more than 1K. One of the solidified samples from each cast was sectioned and the composition was determined by a combination of X-ray fluorescence and wet chemistry on drillings. Compositions of some of the later casts (Nos. 120-134) were determined from separate 'lollipop' or crucible

samples taken immediately prior to pouring the liquidus samples. Further samples were analysed to test repeatability or in cases where an unexpected variation in measured temperature was noted.

The results of the author's previous work in this field [119,120] were available to this project (designated by one or two digit numbers in the ensuing tables) and, therefore, most of the alloys produced subsequently under this PhD submission bore very little similarity to practical steels, as described at the start of this chapter.

The twin initial targets for experiment and computation into the general multicomponent case were the Fe-C-Si-Mn and Fe-C-Cr-Ni quaternary systems, as reflected in casts 101-108 and 109-119, with variants and combinations thereafter, and addition of Mo, up to cast 162. Also included were some Fe-Cr-Ni steels from another BST/ECSC project, designated as casts 201-222. All the compositions are recorded in Table 3.1, and calculated and experimental liquidus temperatures in Table 3.2. The calculation scheme is described in Table 3.3 for liquidus and solidus, and the results for the sub-set of casts from the previous work for which solidus was assessed are recorded in Table 3.4.

3.1.4) Results of Previous Work

Previous work [Howe,119,120] was summarised in a recent paper in Ironmaking and Steelmaking [121] where the temperature results were combined with those from a Jernkontoret study [100] and compared with those from simple methods of calculation. The total population of alloys were split into 'low alloy and quasi-binary steels' and 'high alloy steels'. The term 'quasi-binary' was used for alloys which had only one solute element present in large amounts. The simple, purely empirical or binary summation techniques for liquidus calculation:-

$$T_{liq} = T_o + \Sigma f(Z_i), \qquad (3.1$$

(T_o datum temperature of 1537oC being the melting point of pure iron)

are likely to be successful for the low alloy steels with minimal interaction effects, and also for quasi-binary alloys. Moreover, the initial solidification phase will either be delta ferrite, or a function of the quasi-binary solute already accounted for in its liquidus depression, i.e. the approach need no expicit consideration of the solidification phase, only the depression from the melting point of delta-iron. (This makes the calculation scheme much more amenable to operation on plant.) Reasonable accuracy should not be expected for high alloy steels, for which more than one element is non-dilute, with such an approach. The compositions are listed in Table 3.1.

The liquidus equations previously derived by Andrews and coworkers [123] are of the binary summation type. Where inadequacies were apparent in their predictions, alternative binary liquidus depressions were taken by Howe [121] from more recent references [124] than those available to Andrews and represented by simple, algebraic expressions. These modified Andrews predictions are compared with experiment in Table 3.2 and Figure 3.5 (designated BS). Also included in the comparison were the predictions according to Wolf (empirically devised primarily for stainless steels) and Kagawa and Okamoto, who specifically addressed the differences expected with ferritic and austenitic solidification. In addition, some consideration was given to estimation of solidus values in the more dilute steels.

In the case of the austenitic stainless steels (for which binary summations are expected to be inadequate) alternative estimates were obtained for comparison by defining the datum temperature, T_o, as the liquidus expected of the Cr

and Ni contents according to the ternary Fe-Cr-Ni liquidus surface [127,128], Figs.3.6 and 3.7. Cr and Ni would then, of course, be excluded from the ensuing summation.

The correlations, and extremes, means, and standard deviations of the differences between calculated and measured temperatures are presented in Table 3.2.

In the 50 quasi-binary steels the current modification to the original work of Andrews has proved superior to both that recommended by Wolf [125] and Kagawa and Okamoto [126]. The largest discrepancies in this work were for the highest carbon (7.4K overestimation) and manganese (10.1K underestimation) steels (Tables 3.2). The Wolf equations seriously underestimated the liquidus of the high manganese or nickel steels (by up to 87K). These are, however, adequate for most of the ferritic and lower alloy austenitic stainless steels for which they were primarily intended. The apparent inferiority of the Kagawa and Okamoto equations may be surprising as only these took explicit account of the change in liquidus slopes according to the nature of the solidifying phase. Two reasons for this could be, first, that their quadratic equations for the dominant carbon effect are not suitable for extrapolation much beyond the relevant ferrite and austenite phase ranges in the iron-carbon binary and, second, there is little difference within the population between the actual solidification phase and that automatically accounted for by the single non-dilute element in the quasi-binary approach. This would not generally be the case when more than one element is non-dilute but, in such cases, the whole approach of summation of binary depressions would be expected to be inappropriate.

Within the population of 37 high alloy (largely Cr-Ni) steels, the predictions of Kagawa and Okamoto were superior to either those of Wolf or the present binary summations. The predictions were not, however, sufficiently reliable for practical purposes with up to 36.5K error, or 79.5K error

should the incorrect solidification phase be assumed. Better results were obtained with either the Rivlin and Raynor [127] or Chuang and Austin Chang [128] ternary based calculations (with subsequent binary depressions for the remaining elements as for the modified Andrews factors). The ternary base due to Chuang and Austin Chang proved marginally superior, with one particular discrepency for Alloy 800 (27K over-estimate, Table 3.2, Figure 3.8).

The best predictions overall from this previous work were thus obtained from the modified Andrews binary depressions in combination with the Chuang and Austin Chang Fe-Cr-Ni ternary where appropriate.

Solidus temperatures were not forthcoming from the present study but a similar exercise was performed on the solidus results as measured in the Jernkontoret study [100] by thermal analysis. Unlike liquidus, this is unlikely to approximate to equilibrium values and is bound to be more problematic. Some attempt to allow for this was made by performing a linear regression of the equilibrium solidus (according to binary summation as before) in conjunction with the cooling rate, $\dot{T}$, leading to the following form:

$$T_{sol} = T_o + \Sigma f(Z_i) - g.\dot{T} \qquad (3.2$$

where the functions f (based on diagrams in ref. 96) are as listed in Table 3.3, and the optimum multiplier, g, was found to be 30. The average sample cooling rate from liquidus to solidus was employed rather than the quoted furnace cooling rates in the Jernkontoret experiments. This exercise was restricted to the most dilute compositions (Nos. 27-42).

A reasonable prediction of solidus is evident for these steels (Table 3.4, Fig.3.9) despite the simplicity of the approach. The equations representing the binary solidus depressions as recorded by Kubachewski [96] gave a slightly higher correlation and lower standard deviation of differences

with measurement than did those according to Andrews and only the former are reported here. An attempt was made to improve the solidus prediction by employing carbon equivalent coefficients for the peritectic such that the dominant effect of carbon would be influenced by the presence of the other elements. This, however, only gave a slight improvement which could not justify the loss of simplicity in calculation.

It should also be pointed out that the solidus temperatures quoted in the Jernkontoret study according to thermal analysis cannot represent the 'effective' non-equilibrium solidus (the temperature for final solidification of matrix material in a typical or average region). For example, eutectics were observed which would not have appeared until temperatures were far below the quoted value. The difficulty lies in the existence of persistent, highly segregated liquid films which are of too low a volume fraction to produce a significant distortion of the cooling curve. Indeed, the Jernkontoret work states that evidence of such liquid films was present on some samples despite the quench temperature being below their quoted solidus. The 'solidus' thus measured by thermal analysis may still be of some value, however, as a guide to the maximum safe temperature for certain operations, although very low ductility is to be expected from a casting down to the true solidus.

3.1.5) Results of Present Work

The experiments were performed in accord with the procedure described above, which unfortunately includes possible (though unlikely) errors of up to 15K in the first 19 casts (i.e. employing the original recorder). These comprised high carbon and FeCrNi alloys. Results from an additional 10 FeCrNi compositions are, however, available from another BST-ECSC project [Allan,129], indeed, using the same (corrected) apparatus. For the purposes of identification during the ensuing assessment of liquidus data, the original

work of mine maintains its original numbering sequence, the current work gains 100 (e.g. the first sample under this thesis is labeled '101', etcetera), and that of Allan, 200.

The first assessment employed the rules for liquidus prediction as derived from the earlier work. Casts for which no satisfactory liquidus plateau was obtained were obviously excluded from the analysis. The remaining casts were then split as 'low alloy and quasi-binary steels', and 'high alloy (FeCrNi) steels', as before, and are indicated as such in Table 3.2. This is, of course, a somewhat arbitrary split.

a) Low Alloy and Quasi-Binary Steels

Comparison of measurement with prediction according to the scheme established from the earlier work produced a correlation coefficient of 0.997, maximum disagreements of -17K to +15K, and a standard deviation of 5.44K (i.e. 95% confidence band of +/-11K).

The largest errors were with the particularly high C,Si,Mn and Mo contents. Those with C and Si were not evidently systematic. The high carbon, i.e. 2.5 to 4%C, errors could have a variety of contributions: the possible random errors of up to 15K identified with the original recorder for casts 101-119; the exotic compositions and lower temperatures encouraging sizeable (but only negative) departures of apparent liquidus from equilibrium liquidus values; and the fact that a given percentage error in prediction of the liquidus depression effect will naturally give larger absolute errors at these low temperatures (down to 1170oC recorded in the present work).

Use of an alternative prediction of the Si effect, which closely approximated to that apparent from MTDATA for such compositions, i.e. $\Delta T_{Si} = Si^2 + 14Si$, produced poorer agreement with results (corr. 0.995,-29.7 to +9.2K,σ 6.55).

The errors in Mn appeared to reflect a lack of account of the change in solvus slope at its peritectic change from δ to γ solidification. This was remedied in close accord with the binary by changing from ΔT_{Mn} = 5Mn to (62.5 + 10Mn)/3 at 12.5% Mn. This only affected few results, but was sufficient to drop the overall standard deviation from 5.44 to 5.21.

Similarly to Si, use of an alternative factor for Mo which was in better agreement with MTDATA, weakened the overall agreement with experiment. Combined use of both the MTDATA-compatible Si and Mo expressions was also counter-productive. It was evident that a relatively steep solvus slope was required at low Mo contents, which grew shallower with increasing Mo content, although this was not evident from either MTDATA or the Kubachewsky binary collation [96]. Adoption of such an empirical expression (ΔT_{Mo} = (19Mo - Mo^2)/3) improved the overall correlation, but two casts were in obvious disagreement. These two (161 a and b) were high in both Mo and C content. The composition was designed to be austenitically solidifying, whereas the Mo expression was still that for ferritic solidification, i.e. it is arguable that it should be excluded from the quasi-binary data set. There are other examples where there is a substantial quantity of an element present in an alloy where the other components are sufficient to cause the alloy to have the 'wrong' solidification phase for that element, e.g. No.46 where 5%Cr is present in a high C, austenitically solidifying alloy, but for which the consequences of such mis-assignment have not been so severe. Removal of the high C-Mo case improved the correlation coefficient to 0.998, scatter -11.7 to +15K, and standard deviation 4.35K (i.e. 95% confidence on prediction of +/-9K).

Liquidus calculations according to MTDATA proved less accurate than by the British Steel (modified Andrews) approach, with a correlation coefficient of 0.985, scatter -43.5 to +21K, and 95% confidence of +/-24K. Differences were noted particularly with high Cr alloys (Types 409 and 430 stainless steels).

The statistics are summarised in Table 3.2. The final predictions and measurements are compared graphically in Figs. 3.10 and 3.11. The resultant expressions for the binary summation approach for liquidus prediction are included in Table 3.3.

b) High Alloy, FeCrNi Steels

The 37 previous, 30 current, and 10 additional results were compared with predictions made from a ternary datum according to the Rivlin and Raynor [127],Fig.3.6, and Chuang and Austin Chang [128],Fig.3.7, FeCrNi representations, from which the relatively minor liquidus depressions of the remaining solutes were subtracted according to their respective binaries, and from MTDATA, Figs. 3.10 and 3.11.

All the approaches yielded typically less accurate predictions than for the low alloy and quasi-binary steels, and MTDATA was particularly poor with Cr/Si combinations. The BS approach with an FeCrNi ternary datum exhibited a correlation coefficient of 0.908, scatter -68 to +10.8oC, 95% confidence =/-26K, whereas the equivalent figures for MTDATA were 0.849, -70 to +45K, and +/-36K.

3.2) EQUILIBRATION EXPERIMENTS

"Tell me, ye learned, shall we for ever be adding so much to the bulk - so little to the stock?"

....Laurence Sterne, "The Life and Opinions of Tristram Shandy", Vol.V, Chapter 1

This aspect of the practical work utilised an equilibration furnace at Sheffield University. The object was, after suitable modification and checking of the equipment, to validate computed equilibrium data as above, the difference being that the experiments would be performed sub-liquidus. This technique had the potential to reduce the albeit small departures from equilibrium expected from the liquidus determinations and, moreover, to allow better measurement of partition coefficients; the composition of the first-formed solid was not measureable under the liquidus experiments because the results were affected by back-diffusion.

3.2.1) Rationale

The basic technique is to soak the specimen at the relevant high temperature until it is a coarse mixture of solid and liquid, with fairly uniform composition within each phase, i.e. until it is essentially equilibrated and coarse enough for ease of subsequent micro-analysis. Thereafter, the specimen must be quenched as quickly as possible in order to retain these compositions although, even so, analyses have to be taken away from the evident original solid-liquid

interfaces. Thus two requirements need to be met: a good heating system with close temperature control and minimum specimen contamination, and a good quenching mechanism/medium.

Induction heating systems tend to have some longitudinal variability (typically 10K/m [130]). Low induction frequencies are better for penetration (i.e. transverse homogeneity) but high (radio) frequencies are better for rapid heating to high temperatures:

$$\delta = (\pi/\Pi\mu f)^{-.5} \qquad (3.3$$

The problem of penetration with radio frequencies can, however, be avoided with use of a susceptor. This is a construction (e.g. a hollow cylinder) which surrounds the specimen, made from material of higher melting point than the specimen and reasonably high resistivity. A common material for this is graphite. The induction coil therefore heats the susceptor, which transmits heat to the specimen via radiation and conduction, thereby benefiting from the fast heating rate from radio frequencies whilst avoiding a problem of transverse temperature gradients due to limited penetration.

Water and oil are the most commonly employed quenching media. Aqueous solutions of salts are particularly good. It has been suggested that salt crystals break the vapour film which otherwise acts as a barrier to reduce the efficiency of heat extraction [131]. Molten metal quenchants, such as lead and tin, are excellent quenchants insofar as they have very high thermal conductivities and are not prone to vapour formation with initial specimen temperatures usually employed. They are, however, much more cumbersome and expensive to employ, needing some heating to keep them molten, and comprising possible health hazzards. For a similar exercise at MIT [132], liquid gallium was employed as quenchant. This requires minimal heating to keep it molten (melting point 29.772°C) but does not vapourise until 2070°C (both aiding quenching efficiency and reducing its health hazzard). It is however, very expensive, and aqueous salt solutions provide an adequate quench rate for most purposes.

It is by no means new to extend the anneal and quench technique into the mushy zone [130,138] for purposes of determining partition coefficients. For example, in the apparatus of Morita, heating was by resistance elements, under an argon atmosphere to prevent oxidation. His alloys were first completely melted and then lowered to the equilibration temperature with solid growing from the melt. The subsequent solid/liquid slurry is then ejected into the quenching medium but, particularly with a dendritic morphology, only very low solid fractions could be ejected. A less viscous slurry might be achieved for a given fraction solid and equilibration time, from heating up to the equilibration temperature rather than cooling from the liquid state. A simplified procedure, adopted in this work, is to eject the slurry still in its crucible, accepting the consequently reduced quench rate.

3.2.2) The Apparatus as Acquired

Its basic construction is represented in Figure 3.12. Heat is generated in a graphite susceptor of 38mm outside diameter and 50mm length by a radio frequency induction heating coil of 62mm internal diameter, 7 turns and 60mm long, supplied from a 450 kHz frequency Inductelec 1EH5 generator of maximum power 5kW. The graphite susceptor sat on a fireclay cylinder/"pedestal" (later replaced by recrystallised alumina) and fireclay brick with a hole drilled through the centre for a thermocouple is placed on top of it.

Samples of length up to 20mm and 12mm diameter can be contained in recrystallised alumina crucibles of 18mm outside diameter, 1.5mm wall thickness, and 26mm depth. The crucible is placed on a graphite seat on top of a recrystallised alumina pedestal, and this assembly was slid into the furnace from the bottom. The pedestal is clamped in position by a lever mechanism attached at the bottom of the furnace tube.

Atmosphere control was provided by passing purified ("five nines") argon through the furnace, entering through the top and leaving through the bottom aluminium plates. The gas is passed through an oil bubbler for visual adjustment of the flow rate so that only a small positive pressure exists in the furnace.

After the equilibration time is reached, the pedestal/crucible assembly is allowed to fall from the furnace rapidly, by pushing down the lever. The quenching conditions are variable in that the crucible and sample may fall together or separately into the brine tank. The height through which the specimen falls before touching the quenching medium is 200mm, and the time taken to cool the specimen is about 2 seconds as judged by cessation of significant bubble generation from the specimen in the brine quench tank.

Temperature measurement is provided by inserting thermocouple wires of 0.2mm diameter Pt-Pt/13%Rh into the specimen in the furnace accommodated in recrystallised alumina sheaths. The twin bore inner sheath serves merely to separate the two wires away from their fused junction. The outer protective sheath is 4mm diameter and about 300mm long, and this is placed into the furnace such that its tip (housing the junction) touches the crucible bottom. The wires are connected to a cold junction maintained at 0°C via copper/constantin compensating cables and from there to a recording instrument, which is a potentiometer/chart recorder in combination. For the narrow temperature range of interest an indication of a limited variation of the voltage with time was required and the potentiometer was used as a millivolt supply to back off the emf and consequently improve the chart recorder's sensitivity (i.e. the chart recorder was only responding to thermocouple voltages above the backed-off datum, rather than the full signal).

The crucible was placed on the assembly such that 10mm of susceptor length existed both above and below it, with a 1.5 mm radial gap between it and the susceptor. Due to the nature of induction heating, the hot zone is not of uniform temperature, especially when the susceptor is of uneven thickness, as, for example, a result of burning by oxygen gas present as an impurity. The temperature attained and distribution would also be susceptible to the flow rate of the protective argon gas.

Temperature gradients of up to 5K/mm were recorded in the specimens, somewhat defeating the objective of an equilibration furnace, particularly with her Fe-Cr-Ni alloys being of rather narrow freezing range. The gradients were first determined by moving the thermocouple sheath about 2mm at a time and holding for twenty minutes at each position, both early in the susceptor's life (20 hours) and when it was due for replacement (exceeds 1.2 Amp to maintain 1400oC as opposed to 0.64 Amp as new). At later times, the gradients were monitored by moving the thermocouple wire within its sheath, and holding until an apparently stable temperature had been reached (e.g. 30-60 seconds).

The equipment was acquired with the main containment tube broken, requiring a complete strip-down and rebuild. Minor dimensional differences necessarily resulted (e.g. the existing spare susceptor was 1mm diameter too big for the new containment tube) but the apparatus was essentially the same as described.

3.2.3) Discussion

The objectives for this practical phase were:-

1 Re-establish use of equipment

2 Streamline data acquisition

3 Test operation of equipment with dummy specimen -
Test attainment and control of temperature
Ascertain non-uniformities of temperature
Ascertain presence/effects of oxygen impurities

4 Modify equipment in response to the above, and re-test

5 Employ equipment on a selection of alloys for the determination of sub-liquidus equilibria

Example thermal histories are presented in Fig.3.13 and temperature gradients/variability during the soak period in Fig.3.14 and Table 3.6. Specimen positioning within the furnace is detailed in Fig.3.15.

This aspect of the experimental work failed to meet expectations. The problems can be catalogued as follows:

a) HT UNIT. Two major failures of the HT unit requiring repair by Inductelec.

b) OXIDATION. Even with use of Hyplas Ar/5%H, significant oxidation was evident, from degradation of the susceptors and scaling of the specimens themselves.

Some of this could occur between quench-out and re-sealing of the furnace, but the susceptor degradation was more

severe at the upper end, away from the opening. The thermocouple insertion is through an O-ring which, with positive pressure of Ar/H (unless negated by the Venturi effect of the gas flow), should prevent air ingress.

c) LONGITUDINAL TEMPERATURE GRADIENT. (c.f. Fig. 3.14) This could have been expected from the inherited susceptor and specimen support arrangements (Fig. 3.15) which placed the specimen at the bottom end of the susceptor. Use of a taller specimen column was prohibited by the quench release mechanism, i.e. unless this assembly were to be re-made as well, the column (which was attached to the hinged furnace bottom-plate) would still not be clear of the furnace tube upon quench-out. Reducing the susceptor support height was also undesirable unless the induction coil height were also changed; indeed, in the original arrangement the susceptor was already towards the bottom end of the coil. A further question was over the contribution of the thermal conductivity of the support ceramics (re-crystallised alumina) to the observed gradients.

The final arrangement (Fig.3.15) employed insulating (fibrous alumina) collars for seating the susceptor and raising it within the coil, and an insulating extension to the specimen support column to raise the specimen to the centre of the susceptor and coil. This extension had to be simply resting between column and graphite plinth to the crucible such that it could tumble out upon quench-out, in view of the restrictions mentioned previously. The end of the upper insulating column was re-shaped such that it rested on the crucible rather than the susceptor, providing a closer top to the specimen cavity for better insulation, and also some force to encourage the specimen downward upon quench-out, as it no longer had the weight of the quench-out mechanism to pull it free of the susceptor.

d) SUSCEPTIBILITY TO DISTURBANCE. Once an equilibrium temperature appeared to have been established, for a given thermocouple insertion depth there could be one or two degrees susceptibility to joggling the thermocouple or the apparatus

in general, not necessarily reversibly. A simple, lateral temperature gradient would have resulted in reversible changes if the thermocouple was returned to the original position. Two thermocouples were employed during the work, and they exhibited no such sensitivity at low temperatures, so it is presumed not to be a poor contact within the thermocouple. A contributory factor could be slight repositioning of the assembled components (particularly contact between crucible and susceptor); for example, a major change was once noted when the whole apparatus was slightly tilted. The Ar/H gas flow could increase such sensitivity by adopting different flow paths around the slightly repositioned assembly. Turning the gas off led to temperature rises of several degrees, but even so, the temperature remained sensitive to disturbances.

It was therefore quite difficult to ascribe a temperature to the specimen to within a couple of degrees.

e) CHOICE OF TEMPERATURES. As the liquidus of the samples was already known from previous experiments (Section 3.1), interest centred on a substantially lower temperatures such that both the partition coefficient and the liquidus of the enriched residual liquid were "new" information. The viable range for most accurate measurements from within the liquidus/solidus interval is severely limited, however, as this requires substantial distances both across the solid globules and intervening quenched liquid for proper micro-analysis; for solid globules within a prior-liquid network matrix this corresponds to quite a low fraction solid and therefore, only minor enrichment and little difference from the liquidus temperature. Furthermore, the low fraction solid range is covered by a relatively narrow temperature interval. The preference in this work was therefore to err towards lower temperatures, where direct measurement of the liquid composition could be difficult, but would hopefully be determined by a mass balance as the composition and volume fraction of the prior solid should be evident. The volume fraction, however, was often not as evident as hoped, and much hampered by the temperature gradients within the specimens.

f) CONCLUSIONS. An equipment redesign is desirable such that the specimen is located within a much longer susceptor and coil. This should play a large part in removing the temperature gradients, coupled with an insulating seat and lid, as adopted during this work. Regarding oxidation, a containment sleeve capable of withstanding vacuum is desirable, combined with use of Ar/H flushing as already adopted. These measures should also reduce the temperature sensitivity to "joggling" as noted in this work, although this is not fully understood. The use of a digital multimeter for thermocouple reading within an induction coil/ susceptor assembly did not appear to be problem. Closer tolerances and avoidance of leaks (and repeated breakdowns) within the existing design would solve a lot of the problems, but a longer equilibration zone is strongly preferred.

From ease of metallographic examination and micro-analysis, it may also be sensible to employ equilibration temperatures only marginally below liquidus.

This part of the practical work was generally disappointing and it proved impossible to glean accurate data from it due to the difficulties described above. The results obtained are detailed in Section 3.4.

3.3) MICROSTRUCTURE

The liquidus temperature and primary solidification phase should reflect the equilibrium values for most of the compositions produced under this practical work. The cooling rate down to liquidus was, however, too rapid for the more exotic compositions and some substantial departures from equilibrium were observed. The information other than temperature can be obtained metallographically, and all casts were examined in this way apart from 149 (which was a wash-heat, nominally iron for "cleaning" the furnace, with little segregate to etch and little doubt that the primary solidification phase must be ferrite) and 133 (which was so effervescent that only a skull of metal was left lining the ceramic cup).

The results are included in Table 3.2 in numerical (chronological) order of the liquidus programme, but are described here in more logical groupings of the Cast-Iron (Figs.3.16-3.19, Nos. 101-8, 122-126), Stainless (Figs.3.20-3.25, Nos.109-119,127-132), and Miscellaneous (Figs.3.26-3.27, Nos.120, 121,135-162) types.

For reference, an Fe-C diagram is presented in Fig.3.16 with carbon in the metastable phase, cementite (Fe_3C). The stable austenite-graphite eutectic occurs at a very similar position but with a notably steeper liquid/graphite solvus. Alternative FeCrNi diagrams are presented in Figs.3.6 and 3.7.

3.3.1) Cast Iron Series

A considerable proportion of the total experiments were of this type, in an attempt to represent the residual liquid at a late stage in the solidification of a more normal alloy. These did, however, show variable departures from equilibrium (evident from comparison with phase diagrams and implicit in the variability between repeat experiments), detracting from the prime object of their production, but still revealing features of interest and relevance.

Samples 101 and 122 are simple Fe-C binaries displaying a typical white iron structure of prior austenite dendrites (essentially pearlitic following transformation upon cooling) within a ledeburite (i.e. prior austenite-cementite eutectic) matrix, Fig.3.17. Sample 122(3.3%C) exhibited a kink in its cooling curve at 12-13° above liquidus prediction by either BS or MTDATA and a further such kink at 1140°, presumably corresponding to the eutectic.

The presence of Si in sample 123(3.1%C,1.5%Si) had stabilised graphite with respect to cementite, yielding prior austenite dendrites in an austenite/graphite eutectic matrix. In the previous sample, the austenite had decomposed to pearlite and cementite upon cooling (and some shear transformation was also evident) whereas in this case, the presence of graphite had denuded the metal to such an extent that it was ferrite. Moreover, ferritic halos were evident around the pearlite/cementite cores of the prior austenite dendrites corresponding to the diffusive loss of carbon from the outer layer of the dendrite, into the graphite, during cooling (Fig.3.18).

In sample 124 (3.15%C, 5.38%Si) the high Si content had stabilised the graphite to such an extent that it was the primary solidification phase, in accord with MTDATA (or, e.g., Angus[134]) prediction. Eutectic cell rosettes were also observed, but the bulk of the material exhibited a non-equilibrium structure whereby the austenite only appeared on the primary graphite at substantial undercooling below the liquidus, whereupon it grew rapidly as spindley austenite

dendrites and subsequently filled out by a fine scale, undercooled eutectic of austenite and secondary graphite (Fig.3.19). All of the austenite had since transformed to ferrite with carbon transfer to the graphite. Indeed, this sample is a rather nice example of the overshooting of equilibrium as in divorced eutectics.

Samples 125 and 126 were of similar C and Si content to Sample 123 but with 0.5 and 2.7%Mn, respectively. The Mn content partially stabilised the pearlite and cementite, with consequently less evidence of ferrite encroachment into the prior austenite dendrites, and areas of ledeburite instead of austenite/graphite eutectic. In some areas, the ledeburite, itself, exhibited a partially dendritic appearance of cementite, suggesting variable composition. Some shear (martensitic) transformation was also evident.

Samples 102-8 were water quenched after the liquidus measurements had been attempted. This resulted in significantly less pearlite and a more acicular martensitic appearance for otherwise similar samples. Light etching laths were apparent across the prior austenite, pearlitic dendrites in Sample 102, and no pearlite was evident in Samples 103,4,7 and 8. Nos. 105 and 106 showed mixed transformation of the dendrites. None exhibited a graphitic eutectic, although the ledeburitic eutectic was often distinctly different from that in an Fe-C binary. It was often highly aligned, but is unlikely to be very cellular in growth morphology because this should be reflected by a variation in temperature whereas the reaction appeared to be temperature invariant (at least on the final pot sample from No.108 where such a measurement was taken), as in the binary. Rather, this might just indicate that the sample was quenched before the eutectic reaction was complete. In Sample 108, the matrix had more the appearance of a second phase rather than a eutectic, but this might be due to the scale and proportion of the residual liquid at this stage hindering its development.

MTDATA successfully predicted primary graphite solidification for Sample 124, and primary austenitic solidification for the others in this series.

3.3.2) FeCrNi Series

The Fe-Cr-Ni system is the most important base ternary in the industry for which large amounts of both solutes are involved, and is therefore attractive not only as a test for multicomponent theory but also as a commercially important target.

This series comprised Samples 109-119 and 127-132, whose ternary compositions (i.e. ignoring the low impurity contents) are reproduced in Fig.3.20. The main object of the metallography was as an aid to the determination of the primary solidification phase which, with its corresponding liquidus temperature, should be a good guide to the equilibrium result. The judged primary phase for each cast is compared with equilibrium prediction by MTDATA, Rivlin and Chuang [15,127,128]. Apart from MTDATA, the primary phase was predicted both from the ternary composition and the full composition expressed as Cr and Ni equivalents [100,135], but no disagreements were noted. The MTDATA predictions proved the most accurate.

The micrographs are discussed with respect to a progression along the peritectic fold -cum- eutectic trough from the FeNi binary to the CrNi binary, rather than in numerical cast order. The MTDATA prediction for Nos.127 and 128 is for austenitic solidification in the region of a peritectic section, whereupon no secondary ferrite solidification is expected. The microstructures are consistent with this, No.127 having subsequently undergone a martensitic transformation upon cooling to room temperature. However, it is still possible that an alternative, partly ferritic mode had occurred but with all the ferrite having transformed in the solid state. No.129 is predicted to have undergone primary austenitic solidification in the vicinity of a eutectic section, with secondary, interdendritic ferrite deposition from the liquid. Vestigial traces of such a second phase were, indeed, apparent in an austenite matrix (Fig.3.21).

The sequence 119,118,116 and 111 lies in the vicinity of the eutectic trough but with substantial increases in alloy content (Fig. 3.22). Rivlin would predict these to be borderline (119,111) or primarily austenitic (118,116) whereas MTDATA successfully predicts that they are all primarily ferritic. No.110 appears to have undergone primary austenitic solidification with secondary, interdendritic ferrite, as expected (Fig. 3.23). The MTDATA prediction for No.109 is similar, but with a considerably lower proportion of primary austenite. However, both primary dendrites of ferrite and austenite were apparent, as were large areas of primary, eutectic solidification (Fig.3.24). This indicates that this composition lies very close to the eutectic trough and that a test cast of a much slower cooling rate would be required to verify the equilibrium mode in this case.

The remaining casts (111-115,117,130-132) all had ferrite as the primary phase with the ferrite proportion in broad agreement with the distance from the eutectic trough. Nos.114 and 131 were essentially fully ferritic on solidification. Such sub-liquidus detail is, of course, predictable from the phase diagram but cannot be verified quantitatively from these experiments with substantial cooling and solidification rates (typically 0.3mm/s dendrite tip advance). Indeed, an examination at Sheffield University [136] of the effect of cooling rate on the borderline between fully ferritic and primary ferritic solidification with some secondary austenite, has shown that it can go either way. This might reflect a balance between increased cooling both supressing second phase nucleation, and increasing micro-segregation such that the residual liquid could reach the eutectic trough composition which was unobtainable under equilibrium.

Solid state ferrite/austenite transformation still on the dendrite morphology (e.g. yielding the common vermicular type of residual ferrite in stainless steels) should be suited to the micro-segregation computer model but the alternative, complicated, subdendrite-arm scale lacey transformation is

beyond the scope of the present work. Work of Beech [136] showed that this transformation grows into the primary ferrite dendritic lobes in a mixed faceted/cellular manner. A further transformation morphology was observed to varying degrees in several of the high alloy compositions in the current work, which does not appear to have been reported before. The appearance is more "woolly" than "lacey", with linear trails and broken swirls with no ready explanation for their appearance (Fig.3.25). A mixed morphology was evident in several specimens, suggesting that there might be a progressive change from lacey to woolly appearance with increasing alloy content, possibly reflecting changes in transformation temperature or extent of the ferrite phase field.

3.3.3) Miscellaneous Samples

The initial solidification phase was seldom clearly apparent from most of the remaining steels (for comparison of primary phase with prediction) although there would be little doubt about the expected mode for most of these compositions. Where modes were suggested by the microstructures, they are included in Table 3.2. Otherwise, detailed reporting of the metallography is probably of little value here and, therefore, only certain items of interest are highlighted.

Fig.3.26 presents a clear example (from Sample 121, 4.9%Si) of the relationship between the as-cast dendritic and grain structures. In Sample 33 (Fig. 3.26b,C-Cr Ni) totally different scales and morphologies existed side by side, and the same body of a given phase could exhibit both dendritic and faceted aspects.

In Sample 153 (0.3%C,0.3%Si,0.1%P), the final interdendritic regions have etched out as dark, linked trails of rounded pits, but there is also a population of an angular, dark-etching phase. This second structure appears to cross the interdendritic features, indicating that it occurred purely in the solid state, and unaffected by the residual, as-cast micro-segregation. This particular morphology was not observed

in any other sample despite various similarities with other compositions as evident from Table 3.1. In Sample 159, however, (1%C, 10%Cr) an acicular, solid-state transformation was evident which was controlled by the as-cast micro-segregation, being present only on the original dendrite cores.

A particularly interesting structure, and of considerable relevance to the behaviour of the computer model, was found in the final sample, No.162 (0.5%C, 10%Mo, Fig.3.27). In addition to the usual interdendritic segregation, pockets or even films of similar segregation appeared to be present within the dendrite arms. A possible mechanism (as suggested in certain tool-steels[4]) is that the encroachment of austenite into the initial ferrite during the peritectic reaction, enriches the content of the ferrite stabilising elements (Mo in this case), and possibly to such an extent that the dendrite cores temporarily remelt. Such an enrichment is predicted by the micro-segregation model (although it contains no routine to allow the remelting to occur), provided that the effect is not lost through degeneration of the austenite-ferrite reaction to a finer scale, as with "lacey" ferrite in stainless steels.

MTDATA successfully predicted the primary solidification phase of most of the alloys for which it was known. It is interesting to note that the use of a peritectic equivalent defined in Section 4.1.5 was equally successful.

3.4) ELECTRON METALLOGRAPHY and MASS SPECTROSCOPY

Selected material from the practical work was submitted to electron probe microananlysis (EPMA) by Cameca SX50 and secondary ion mass spectroscopy (SIMS) by VG-Ionex Simslab, as detailed below. The SIMS is primarily employed for surface analysis, but it is used here as a high resolution, micro-analytical tool. The standard data format thus produced was colour-coded segregation maps, of which certain examples are provided in Figures 3.28 to 3.35.

The data presented in Table 3.7 quote partition coefficients judged by three criteria: a), core/bulk composition (=k under the Scheil condiiton), b), dendrite/matrix composition (=k under lever rule condition), and c), as predicted by MTDATA [15].

3.4.1) Cast Iron Series

An area of Sample 104 (2.88%C,1.45%Si,5.08%Mn) from the liquidus casts was subjected to EPMA, Figure 3.28.

The carbon values by (a) are obviously inappropriate, as its result should closely approximate to the lever rule condition, (b). Excellent agreement was indeed observed with (b) and (c). It must be admitted, however, that the range of values which could be gleaned from the EPMA map was large, the quoted value of 0.37 being middle of the possible range of 0.34 to 0.40. This is because of the limitations of the colour coding of composition, i.e. the intervals being fairly large relative to the composition range encountered. Si suffered more severely from this, and even confirmation that the (b)

value was greater than unity, consistent with prediction, was somewhat subjective. The Mn value was the least affected by back-diffusion, and its results were in tolerable agreement.

This was the first sample analysed for this study, and more sophisticated data handling was available for the subsequent EPMA maps.

3.4.2) FeCrNi Series

EPMA has been performed on areas from samples 109, 119 and 129.

Sample 109 was a 48%Cr 45%Ni alloy (Table 3.1), with different regions displaying primary ferritic solidification, primary austenitic solidification, and primary eutectic solidification (Figs. 3.24,3.29). EPMA revealed that there was no macrosegregation to account for these different modes, indicating that this composition was very delicately balanced, i.e. essentially on the eutectic trough in the ternary diagram (Figures 3.6 and 3.7). Fe,Si,Mn,Cr and Ni concentrations were mapped, but with little segregation detectable of Mn. Si segregation could be identified, but, like Mn, it was only present in small quantities and the emphasis of the work is on Fe, Cr and Ni, for which partition coefficients were estimated from the segregation maps (simplified versions presented in Figure 3.29) and are compared with MTDATA prediction in Table 3.7. Although each of the three solidification modes had a distinct microstructure, the mean compositions of ferrite and austenite were essentially the same.

Reasonable agreement was found between measured and predicted partition coefficients, assuming back diffusion was sufficiently limited to approximate better to the (a) condition (Scheil) than to the (b) condition (Lever Rule).

Sample 119 was a 26.4%Cr 15.4%Ni alloy of primary ferritic solidification, consistent with MTDATA prediction, but which was quenched while there was still a significant proportion of liquid present. Partition coefficients were estimated for the initial ferritic solidification and the ferrite/austenite solid state reaction for comparison with MTDATA as before, although the latter was hampered by the lack of knowledge of the relevant temperature for purposes of the comparison. Reasonable agreement was observed, with the ferrite/liquid result approximating to the (a) condition as before, but approximating to the (b) condition (Lever Rule) for the fine scale transformation within the prior ferrite dendrite.

The quenched, residual liquid solidified austenitically, but on too fine a scale for useful quantification of the partition coefficients, although the sense could be determined, i.e. Cr and Ni both exhibited positive segregation indicative of partition coefficients less than unity, whereas MTDATA prediction suggests that Ni should have a partition coefficient greater than unity for the quenched liquid composition.

Sample 129 was a 20.1%Cr 15%Ni alloy of primary austenitic solidification, consistent with MTDATA prediction. This sample exhibited a standard, single phase solidification microstructure, and Fe,Cr and Ni partition coefficients could only be estimated from the ratios of dendrite spine to bulk compositions, i.e. the (a) condition, for comparison with prediction in Table 3.7. The agreement for Cr was not very good but, moreoever, the actual sense of the partitioning of Ni was incorrect, as noted for the residual liquid within Sample 119 (Table 3.7).

3.4.3) Equilibration Furnace Samples

There were many problems with the equilibration experiments, hindering the attainment of useful equilibrium data for comparison with MTDATA, or indeed the simplified data set used so far in the micro-segregation model. Temperature gradients present were significant compared to the alloy freezing ranges (even though the wider freezing range alloys of those available were selected for the experiments). The quench-out was unreliable such that indeterminate homogenisation often occurred below the soak temperature. This was in part due to reactions between the specimens and the alumina sheathing of the thermocouple (as described later in this sub-section) which itself led to complications in selecting areas for analysis. Furthermore, the CAMECA probe failed to meet its criterion of being able to perform carbon analysis, due to rapid carbon contamination within the vacuum chamber.

The best example of the three alloy types used was submitted to EPMA analysis, and in one case, SIMS (a surface chemistry technique but used here in a microanalytical mode).

a) EF1:

The equilibration sample was far from ideal, exhibiting variable microstructures reflecting the presence of temperature gradients within the specimen, and a region (lower centre) of quite different character which might reflect macro-segregation. Values for Si and Mn partition coefficients are quoted in Table 3.7, on the basis of mean dendrite to mean matrix composition ratios. In both cases these were higher than the MTDATA result, but the possibility of some homogenisation in this sample precludes statements that MTDATA must be wrong. Indeed, slightly better agreement was found for Mn in the liquidus pot sample, No.4, supportive of some homogenisation having taken place.

SIMS qualitatively revealed the as-solidified, interglobular segregation of carbon (and a much finer scale segregation from low temperature, solid state transformation) but the regions of residual liquid prior to quenching were too small in consideration of the rapid diffusion of carbon for any meaningful attempt at quantification.

b) EF8:

Of this series of experiments, this sample was the optimum for determination of equilibrium data. The calibrated composition maps are given in Fig. 3.30. Again, there was variability in the structure and the results have been based on the exclusion of the top-left region of the figures which was a large residual liquid pool, or "embryonic macro-segregate", prior to the successful quench-out. The dendrite and matrix compositions listed in Table 3.7 indicate partition coefficients of 0.67 for manganese and 0.65 for silicon, for which the temperature was around 1486oC and the fraction solid was 0.82 (result as provided by image analysis, excluding the top left region of the figures).

These results can be tested to some extent for self-consistency, as well as against MTDATA predictions. For the quoted mean compositions, the fractions solid which would conserve solute for the quoted dendrite and matrix compositions were 0.61 for Mn and 0.57 for Si, i.e. in good agreement with each other but not so with the evident fraction solid. However, the mean compositions were taken from the whole diagram, including the top left region; the mean composition of the region in question could well be lower, which would lead to higher fractions solid calculated for solute conservation. This point is therefore unclear but it is satisfying that the fractions solid for the two species are in good agreement.

According to MTDATA, the steel should be fully liquid at the specified temperature of 1485/6oC, whereas the binary summation approach yields a liquidus of 1488.5 (1486 from composition determined by chemical analysis). At the quoted fraction solid (around 1478oC) the calculated partition coeffients are 0.66 and 0.75 for Si and Mn, i.e. Si is in excellent agreement (0.65) but the calculated value for Mn is high (c.f. 0.67).

A further area of interest from this sample was the central pool of scale within the thermocouple recess (Fig. 3.31). Some of this was dendritic, indicating it was liquid at the soak temperature, and exhibiting solution. Apart from Fe,Si and Mn, Al was incorporated in these phases, indicating reaction had taken place with the alumina thermocouple sheath. Two areas are evident: on the Al image, yellow (high Al) dendrites in a moderate matrix, and angular red (very high Al, probably hercynite, $FeO.Al_2O_3$) particles in a moderate matrix. Mean compositions were taken from both areas and, albeit with no ZAF correction, were shown to be the same, suggesting that the homogeneous liquid scale solidified locally by two distinct paths, presumably dependent on subtleties of nucleation. Reaction with the thermocouple is addressed further in the next sub-section.

c) EF9:

This sample failed to exit the furnace and has thus been subject to indeterminate homogenisation. However, interesting results were still available. Taking core/bulk composition ratio as a first approximation to the partition coefficient, i.e. assuming no diffusive homogenisation of the core, k_{Mo} is evident as 0.74 whereas the MTDATA prediction is 0.64. (No value for the more rapidly diffusing Si was apparent.) So, all that can be salvaged here is that the experimental value is in line with the calculated one given that some homogenisation took place in the furnace below the soak temperature. The MTDATA liquidus was around 1452oC, i.e. below both the test temperature (1460oC) and the binary summation

liquidus (Taken as 1462oC at the time, although a later modification to the Mo depression equation put it to 1460oC). It is evident from the coarseness of the main structure, and moreover the physical appearance of the treated specimen, that this sample was semi-solid at temperature, inconsistent with the MTDATA liquidus.

The microstructure also contained colonies of fine pearlite, and a grain boundary/interglobular phase. Partitioning is evident at the pearlite/matrix interface, with Mo and Si enriched at the pearlite side and depleted in the matrix side at this interface. Both appear to be slightly enriched in the body of the pearlite, although the major composition effect is restricted to the interface. It is suggested that this sort of profile, typified in Figure 3.32, indicates that the element in question is simply having to try and respond to interface movement driven by another factor. The peak/trough pair or "bow wave" maintains local equilibrium without altering the bulk phase compositions, sc the alteration of phase composition with respect to that particular element cannot be the driving force: it hasn't happened and no energy has been released accordingly. Instead, it may be driven by a more rapidly diffusing element, or perhaps the latent heat associated with the lattice change.

In Figure 3.33, the grain boundary phase is shown to be enriched in Mo, and slightly if at all depleted in Si. This is probably a carbide but carbon could not be mapped on the EPMA machine employed.

This material failed to quench out because the specimen stuck to the thermocouple. EPMA showed the two to be bonded by a slightly iron rich hercynite, evidently a reaction product between the iron oxide and the alumina of the thermocouple. The phase was homogeneous, with no evidence of it having been liquid, unlike that examined in EF8. Any such reaction as alumina had not been anticipated as it is used as standard with molten steel without such problems. However, it is apparently known that such a reaction can occur under reducing conditions, i.e. the use of Hyplas gas in the equilibration furnace probably prompted this difficulty.

3.4.4) Miscellaneous Samples

Further EPMA was performed on a uni-directionally solidified (UDS) slab of plate grade steel. SIMS was performed on Sample 162 (0.5%C 9.7%Mo) from the liquidus cast series.

Segregation maps (512x512um) and normal and cumulative histograms of EPMA composition distribution were produced for Si and Mn contents within the UDS sample (Fig.3.34). Partition coefficient estimation was dubious in these samples because of the long times at high temperatures in their recorded thermal histories resulting from the solidification and subsequent cooling of the 2 tonne slab. Rather, the EPMA was performed for comparison with computation of micro-segregation, as described in Section 6.2. In the present context, however, it should be noted that there is not a universal correlation between the Si and Mn segregation maps. The standard coring pattern is discernible for Mn, but close inspection of Figs 3.34 a and b indicate that the minimum Mn content at the dendrite cores corresponds to a minor peak of Si content. Ratioing of the Mn and Si images, Fig.3.34c, makes this clear: to a first approximation the ratio would be the same across a dendrite spacing solidifying to a single phase, but the core peak of Si reduces this ratio markedly in such regions. This is predicted by the micro-segregation model for ferrite stabilising elements, provided that the austenite/ferrite transformation in the peritectic occurs on the same scale as the original ferrite/liquid transformation.

SIMS investigation was performed on Sample 162 from the liquidus cast series (0.5%C, 9.7%Mo), which had displayed unusual etching behaviour, Figure 3.27. Optical metallography (Section 3.3) had suggested that severe, positive segregation was present within as well as between the dendrite arms. From the micro-segregation model, this would be expected of ferrite stabilisers, and to a much greater extent with Mo than for Si as observed in the UDS sample, above. If the enrichment of Mo at the dendrite cores were sufficient to temporarily remelt this region, then positive segregation of carbon could also be observed there.

It can be seen in Figure 3.35 that Mo is, indeed, highly enriched in pockets or films within the original dendrite arms, as well as between them. Furthermore, some of these regions correspond to positive carbon segregation as well (albeit less intense), indicating that temporary, local remelting had also occurred in some parts of the dendrite cores.

CHAPTER FOUR

SECONDARY MODELS OF MICRO-SEGREGATION

"I could have done it in a much more complicated way", said the Red Queen, immensely proud. ....Lewis Carroll

4.1) EXTENSIONS TO ANALYTICAL TREATMENTS

4.1.1) Dimensional Basis

The solute balance presented in Section 2.5, Equation 2.29, can be generalised for convex (outward) growth forms which are adequately described by a single distance and 'dimension' term, n, i.e. n=1,2 or 3 for 1D(plane), 2D(cylinder) or 3D(sphere). The solute balance has to be expressed in terms of volumes, V, and surface area, S. In the original 1D case, the other dimensions were not required because they were constant and cancelled out of the equation, but the general case should be expressed as follows:

$$Zl(1-k)\dot{V}s = S_I D(\delta Z/\delta r)_I + (Vo-Vs)\dot{Z}l \qquad (4.1$$

The 'processing' of this equation in order to obtain a solution is performed in analogous fashion to that described in Section 2.5. At equilibrium, the back-diffusion term involves the indeterminate product of infinity (D) and zero ($\delta c/\delta r$) and the alternative soluble form is as follows:

$$Zl(1-k)\dot{Vs} = Vs.k\dot{Zl} + (Vo-Vs)\dot{Zl} \qquad (4.2$$

At low diffusivities, the following approximation applies (exact at the Scheil limit of zero solid diffusivity):

$$(\delta Z/\delta r)_I \sim dZ_I/dr_I = k.dZl/dr_I \qquad (4.3$$

Comparing the above three equations, it is evident that Equation 4.2 will be translated to the general solute balance, Equation 4.1, if the equilibrium back-diffusion term is multiplied by a constant 'A' where A is given by:

$$A = S_I D/(Vs.\dot{r}) \qquad (4.4$$

The surface area to volume ratio, S/Vs, contained in the expression, is pq/pqr for a plane (p=length q=width), $p2\pi r/p\pi r^2$ for a cylinder, and $4\pi r^2/(4/3)\pi r^3$ for a sphere, i.e. it simplifies to n/r in each case whereupon:

$$A = nD/r\dot{r} \qquad (4.5$$

Therefore in terms of the Brody-Flemings parameter:-

$$A = 2\alpha n \qquad (4.6$$

Normalising this expression as before, now yields:-

$$A = 2\alpha n/(1+2\alpha n) \qquad (4.7$$

The required solute balance formula is therefore given by:-

$$Zl(1-k)\dot{Vs} = \{AVs.k + (Vo-Vs)\}\dot{Zl} \qquad (4.8$$

This integrates to the standard micro-segregation equation (Equation 2.33) as the influence of dimension is wholly contained in the modification to the back-diffusion parameter, A, i.e.:-

$$Zl = Zo\{1-(1-Ak)fs\}^{(k-1)/(1-Ak)} \qquad (4.9$$

This results in a modest decrease in segregation with increasing dimension, n, for convex, root-time solidification (Fig.4.1 and c.f. Kobayashi [91,92],Fig.4.2).

4.1.2) Growth Law

A similar approach can be used to predict the effect of other growth laws. The term, $r\dot{r}$, is only constant for root-time growth as mentioned previously, but the results of alternative growth laws can be estimated with use of an additional approximation.

Micro-segregation is very insensitive to morphology or growth law at low fractions solid, whereas at high fractions solid the variable, $r\dot{r}$, tends to 2m times that of root-time growth where m is the power representing the alternative growth law. The desired estimate can be obtained by assuming the term was constant at this value throughout solidification. This will generate an under or overestimate of segregation depending on whether m is less or greater than 0.5 but appears to be reasonable in comparison with a simple numerical test program allowing for this variation of $r\dot{r}$. Moreover, use of the resultant modification to A for linear growth produces values for the maximum micro-segregation from the otherwise standard 'root-time' equation which are good approximations to those obtained from the Brody-Flemings [81] linear growth equation (both, indeed, tending to $(\alpha k)^{k-1}$ at low diffusivity). The relevant modification to A for use in Equation 4.9 as before is as follows:-

$$A = 2\alpha\beta/(1+2\alpha\beta) \qquad \text{where } \beta=n/2m \tag{4.10}$$

The form of the variation of maximum segregation with the term, β, is demonstrated in Figure 4.1. The reduction in segregation with increasing dimension, n, is greater with a root-time growth law in terms of fraction solid than of distance. Moreover, the standard equation for root-time planar growth is seen to be directly applicable to linear cylindrical growth ($\beta=1$).

4.1.3 Concave Growth

Concave (inward) growth forms would be expected to lead to very severe micro-segregation (c.f. Fig.2.31) as the effective varying coefficient, A, tends to zero at completion of solidification for all finite solidification times. This is consistent with a previous numerical model of mine which assumed a concave growth morphology (a solidifying grid of secondary dendrite arm sheets on the primary stems, producing inward growth of square cylinders). Dramatic micro-segregation was encountered at the final stage of solidification even for binary Fe-C steels which should approximate closely to equilibrium. The adopted morphology may well be resaonable at intermediate stages of solidification [29] but practical levels of micro-segregation are more consistent with the all-important final liquid existing as sheets or films, i.e. planar or convex growth morphologies. It should be noted, however, that extreme segregation (not liable to terminate until reaching a eutectic such as iron/carbide/phosphide) is predicted for any local region of a casting which does exhibit concave growth, such as small pockets between dendritic grains (Fig.4.3).

4.1.4) Secondary Dendrite Arm Coarsening

In a similar manner to the numerical model (section 4.2, Chapter 5) the generalised solute balance of Equation 4.8 can be extended to incorporate the effect of an imposed coarsening behaviour on the residual liquid concentration:

$$Zl(1-k)\dot{V}s = AVs.kZ\dot{l} + (Vo-Vs)\dot{Z}l + (Zl-Zo)\dot{V}o \qquad (4.11$$

The 'new' volume included in the solute balance by the expansion of the representative cell must inherit the bulk composition and therefore only the difference between liquid and bulk composition in this volume should be included in the solute balance. An analytical solution can be obtained if the arm coarsening law is of the same power as the assumed growth law, i.e.:

$$Vs = Qt^m \qquad (4.12$$

$$Vo = V^* + Pt^m \qquad (4.13$$

for the volumes of the solid and of the representative cell, respectively, where V^* is the assumed volume of the initial liquid cell.

Substituting for tm from (4.12) in (4.13) yields:-

$$Vo = V^* + UVs \qquad (4.14$$

where U=P/Q which is also dVo/dVs, and which under the above assumption is constant. Employing the chain rule on V_o from (4.11) therefore produces the following equation:

$$Zl(1-k)\dot{V}s = AVs.kZ\dot{l} + (Vo-Vs)\dot{Z}l + (Zl-Zo)U\dot{V}s \qquad (4.15$$

Substituting for V_o from (4.14) and collecting like terms, there are now only two variables and their respective differentials, allowing integration of the expression. Subsequent manipulation, substituting fo V^* from Equation 4.14 and employing fs=Vs/Vo, eventually yields the following expression:

$$Zl = Zo\left(\frac{1-k}{1-U-k}\right)\left(\left\{\frac{1-(1-Ak)fs}{1-Ufs}\right\}^{(k+U-1)/(1-U-Ak)}\right)^{\frac{-U}{(1-k)}} \qquad (4.16$$

It can be seen that this reduces to the standard Equation (4.9) for constant arm spacings, i.e. U=0. Furthermore, it reduces to the equilibrium lever rule for high diffusivity (A=1) regardless of any arm coarsening.

If the standard assumptions are made of a one dimensional form with root-time growth, the suggested value for U is 2/3. The micro-segregation calculation is only sensitive to U at the later stages of solidification and this choice of U leads to the same coarsening rate at the end of solidification as apparent from the frequently quoted 1/3 power coarsening law:

$$\lambda = (\lambda_f / t_f^{1/3}).t^{1/3} \qquad (4.17$$

Equation 4.16 can be used to demonstrate that the arm coarsening phenomenon is only important with regard to micro-segregation (in the residual liquid/final solid) for solutes of low diffusivity, such as Mn, Cr and Ni in iron (Fig.4.4). Moreover, the effect is only significant towards the end of solidification (Fig.4.5), which supports its use despite its poor implied dendrite morphology at the beginning of solidification (Figs.2.23,2.24), but its usefulness is diminished, however, by the expected change of coarsening mechanism towards the end of solidification (Section 2.4).

It is difficult to do a direct comparison with the work of Mortensen [80] (Section 2.4) owing to his assumption of a constant cooling rate rather than a standard growth law. One important difference, however, is that under the stated assumptions, Mortensen's equation is a true analytical solution, whereas the present formulation compounds the lack of rigour of the Clyne-Kurz solution with a further assumption of coarsening and growth and sharing the same power law. Mortensen's equation is examined further in Section 5.6.3d.

4.1.5) Simplified Peri/Eu-tectic Equilibrium Data

It is possible to construct a simple analytical representation of a multicomponent equilibrium phase diagram with fully mutually consistent phase field boundaries. Moreover, such data have been employed in the numerical models for the bulk of this project.

This approach employs constant solvus slopes, m_i, and partition coefficients, k_i, (although the micro-segregation computer program is constructed so as to allow them to vary between iterations in response to changing composition and temperature). Apart from the aim that these should be reasonable approximations to the albeit variable real values for each solute, the data must be self-consistent for satisfactory construction of an analytical representation of a phase diagram, and operation of the computer program.

The first criterion is that negative m's must be associated with k's less than unity, and vice versa. If the slope on the phase diagram is negative (e.g. Fig.3.1), the solid phase can only be of lower composition than the liquid. This is much more obvious from looking at a sketched diagram than from text, but is a geometric necessity.

Further requirements for consistency arise when considering a three-phase situation as for the peritectic. Firstly, there must be relationship between the k's for the three types of phase interface. On the actual peritectic, compositions within both solid phases are in equilibrium with the same composition within the liquid. It therefore follows that:

$$k_{a/L} = k_{a/b} . k_{b/L} \qquad (4.18$$

and, if the partition coefficients are constant, this relationship is maintained away from the peritectic.

Secondly, and this is where the real problem comes in, the three phases must agree on the composition and temperature of the peritectic. From the binary summation approach, -a nice "linear" approximation again,- the temperature of the peritectic is given by:

$$T = To_{a/L} + \Sigma\, m_{a/L} Zl$$

or $$T = To_{b/L} + \Sigma\, m_{b/L} Zl$$

or $$T = To_{a/b} + \Sigma\, m_{a/b} Z_a \qquad (Z_a = k_{a/L} Zl)$$

$$(4.19$$

where the To values are the datum temperatures for the respective phase changes in the pure solvent. For a given set of Zl_i on the peritectic, all three equations should generate the same temperature, T.

In effect, these cannot be independent equations. For a simple binary, algebraic manipulation (assisted, perhaps, with regard to figure 4.6) shows that:

$$m_{b/L} = \frac{(To_{b/L} - To_{a/b}) m_{a/L} + (To_{a/L} - To_{b/L}) k_{a/L} m_{a/b}}{(To_{a/L} - To_{a/b})} \qquad (4.20$$

Furthermore, the content of that element in the liquid at the peritectic, Zl_p, is given by:

$$Zl_p = (To_{a/L} - To_{a/b})/(k_{a/L} m_{a/b} - m_{a/L}) \qquad (4.21$$

It transpires that this linearised phase diagram is valid for any number of solutes in a multicomponent system. Provided one of the k's and m's is defined from the other two so as to be consistent for each individual solute, the net result is also self-consistent. A further satisfying by-product from this approach is that one can readily find out where one is with regard to the peritectic with use of a peritectic equivalent:

$$E_p = 1/Z_{Lp}$$

whereupon

$$P = \Sigma E_p Z_L \qquad (4.22$$

is equal to unity at the peritectic, and less than one for a hypo-, and greater for a hyper-, peritectic composition. If a carbon-equivalent is preferred, this is simply given by the carbon content of the liquid at the peritectic (0.53) multiplied by the respective E_p values. Thus, for example, the track of the peritectic in the Fe-Cr-Ni ternary calculated according to this scheme corresponds to a carbon-equivalent of 0.53 even though carbon is not one of its constituents. Example results including Fe-Cr-Ni are presented in Figure 4.7 employing:

$$To_{\delta/L} = 1537°C$$
$$To_{\gamma/L} = 1526°C$$
$$To_{\delta/\gamma} = 1392°C$$

and individual component data as in Table 4.1. The resultant, peritectic equivalents are also presented.

This scheme was adopted for the computer program, "EQUIL", which would compute the equilibrium solidification path of a multicomponent alloy, in terms of both composition and temperature, up until the onset of the peritectic. This program is listed in the Appendix.

4.1.6) Further Thoughts

a) Solid Phase Composition Profiles

For the lever rule, the liquid composition is sufficient to define the solid phase composition, i.e. it uniformly equals that of the final solid to form. Similarly, the Scheil Equation also sets the solid profile because it does not change once it has been set at the solid/liquid interface even though that interface moves on.

For a single solidification phase where back-diffusion is occurring, it seems that it ought to be possible to construct an equation for the monotonically increasing concentration profile across the solid, and various attempts were made to do so.

i) Quadratic Equation.

The three pieces of information required for its construction. First, was a definition of the core composition, by inspection, seeing that it must lie between k and 1, dependent on the back-diffusion term A:

$$Z_{(min)}/Z_o = k^{(1-A)} \qquad \text{or } k+(1-k)A \qquad (4.23$$

Second, was a definition of the final interdendritic composition, equal to that from the last solid definable from the micro-segregation equation),

$$Z_{(max)}/Z_o = k(Ak)^{(k-1)/(1-Ak)} \qquad (4.24$$

Third, was the condition that the solute must be conserved (i.e. as described, its integral between f=0 and 1 must be unity). This was achieved quite readily but the profile was prone to plunge into negative values before shooting back up towards $Z_{o(max)}$. This was not a case of fine-tuning being required, so the approach was abandoned.

ii) Exponential Equation

Employing the minimum and maximum values as above, and rough solute conservation by trial and error on the computer, the most promising approach was of the form:

$$Z = (min)*(max/min)^{fn} \qquad (4.25$$

employing (min) as shorthand for $Z_{(min)}$, and so on, and fn being some function of fraction solid, f. However, it was evident that the curve was not of similar profile to the Scheil equation at low values of A, and it was decided that the Scheil equation ought to be imposedas a limiting condition upon the equation.

iii) Adoption of Micro-Segregation Equation Form

A half-way house between the forms described above and below was to reflect the basic form of the micro-segregation equation as follows:

$$Z = (min)*\{1-(1-(max/min)^{1/y})f\ \}^{y} \qquad (4.26$$

This assumed (min) and (max) were predefined, as above, was flat for the Lever Rule but awkward at the Scheil limit, and necessarily equalled (max) at f=1. Solute was conserved if y was defined from iterative solution of the following:

$$y = (1+y)\{(max/min)^{1/y} -1\}/\{(max/min)^{(1+y)/y}-1\} \qquad (4.27$$

This was compared with profiles from an early, binary program which was also used to set (min) and (max), but the profiles were considerably different (even though credible, i.e. free from spurious troughs) which combined with the failure to tend to the Scheil equation (i.e. y not obliged to tend to k-1 as (max) increases) led to the abandonment of this initially promising appoach.

iv) Adapting the Micro-Segregation equation

Having decided that the formula must tend to the Scheil profile at low A, the approach then turned to alterations of the micro-segregation equation such that: (min) lay between k and 1, (max) was as defined in Equation 4.24, the profile was flat for A=1 and Scheil for A=0, and conserved solute.

To this end, the standard equation (i.e. Equation 2.33):

$$Zl = Zo\{1-(1-Ak)fs\}^{(k-1)/(1-Ak)} \qquad (4.28$$

was altered by: modification to the initial k term by A and f, adoption of an "effective k" throughout, substitution of f by a function of f dependent on A, integration from a modified differential equation where the solute rejection at the interface is a function of A, and simple addition of a back-diffusion term to the micro-segregation equation, being a function of A and that required to bring the Lever Rule profile to the flat profile required across the solid.

A formula was constructed which satisfied all these conditions apart from giving credible profiles. As with the original quadratic attempt, the profiles were not obliged to rise from core to termination. Sometimes, if one satisfies all the boundary conditions, one automatically produce the right answer but, evidently, not necessarily so. From this,

one concludes that the problem is surprisingly tricky, with the micro-segregation equation displaying an unusual combination of characteristics for what looks initially to be a straight-forward piece of algebra.

b) Contraction

Agren [106-8] includes phase-change contraction in his micro-segregation model. A modified Scheil Equation was constructed which included solidification contraction in its source differential equation which displayed a finite cut-off at a fraction solid of unity for a finite contraction. The differences in profile for realistic contractions only affected the final dribble of liquid beyond the range of usefulness of the equation. This obviously diminished the usefulness of such a treatment, but moreover, there were other ways (see below) in which one could consider the contraction to act. Not knowing which it did (or more probably, under which circumstances one was the most important effect), further reduced the drive to include this effect.

If the material is free to contract, the dendrite mesh will simply do so, with a very minor change to the characteristic length for the diffusion calculation, such that one might as well continue to employ the treatment without any contraction term. If the mesh is constrained to some extent, the process will be affected, but the nature and effect of the constraint will depend on the macroscopic events and properties. Making one such assumption would not cover all eventualities. Furthermore, such an effect is likely to lead to macro-segregation, again needing a macroscopic model tailored to the case in hand. As purely micro-segregation is often observed, i.e. with retention of an average bulk composition over a considerable distance, one can infer that such contraction effects often do not happen.

Therefore, it seemed prudent to exclude contraction from the micro-segregation model.

c) Surface Area Density

A lot of importance is attached by some to the Surface Area Density, i.e. the amount of solid/liquid interfacial area per unit volume of mushy zone. This parameter has been examined in terms of the solute balance employed here.

For dummy distances of p (width) and q (thickness), solidified distance r and cell size R, the SAD for dimensions n of 1, 2 and 3 respectively are:

$$pq/pqR,\ p2\pi r/p\pi R^2,\ 4\pi r^2/(4/3)\pi R^3$$

i.e. $$n.r^{n-1}/R^n$$

or $$(n/r).f_s \qquad (4.29$$

Therefore, for a planar morphology, it is constant for a given arm spacing, whereas it increases linearly or quadratically with r for cylinders or spheres, respectively. (In reality, there will be a precipitous fall as r converges on λ, due to impingement.) Attempts to employ this as a variable for solution of the solute balance were not successful because it needed a definite characteristic distance, r.

SAD may well dominate coarsening behaviour or permeability, but it does not appear to be a very useful variable for straight micro-segregation.

4.2.1) "PAR-SEG"

My introduction to work on the theory and computer modelling of micro-segregation came with the brief (from Swinden Labs) to use the element interaction type of approach (as, for example, Morita and Tanaka, [130]) to allow the elements present in a multi-component steel to effect each other's solid/liquid partition coefficient. The segregation behaviour followed differential Lever and Scheil-type rules for the interstitial and substitutional elements (with simple, step change in appropriate coefficients upon attaining the carbon peritectic composition in the liquid), but the continually changing partition coefficients dictated that a numerical procedure was required. The simplified approach of Morita was adopted, from the requirement for equal chemical potential at the interface for local equilibrium, and from which the following form can be obtained:

$$Kx^{M} = Kx_{o}^{M}.\exp(Ex^{x,l}.Nx^{l} + Ex^{y,l}.Ny^{l} \text{ etc.}) \\ *\exp(Ex^{x,s}.Nx^{s} + Ex^{y,s}.Ny^{s} \text{etc.}) \qquad (4.30$$

An equivalent expression can be obtained for weight percentages and the corresponding, "e_x", interaction coefficients.

Major differences in results could be obtained depending on whose element interactions were employed [45,137,138]. Certain preferences were obvious, e.g. for the self-interaction coefficient of Cr the value of Sigworth and Elliott [137] originally adopted was 'small' and negative whereas that required for the observed increase in partition coefficient with increasing Cr is to be 'large' and positive, as indicated by Bodsworth and Bell [138].

This approach was still restricted to essentially dilute steels, and more sophisticated treatments based on the same approach (such as the drastically revised interaction formalism of Pelton and Bale [139] did not seem warranted by the available data. Preliminary discussions with the NPL indicated that superior treatments were available, but these were not taken on immediately due both to the current lack of capability of handling important elements such as Mn, and, indeed, to the quoted costs.

4.2.2) "SQUARE"

The second stage of this work was to incorporate finite diffusion within the solid.

Considering the apparent growth of secondary arms into 'side-plates' well before the completion of solidification [29], Fig.2.30, a square lattice was the adopted morphology in an attempt to improve upon existing approaches with a 1D treatment. The square section, transverse to the growth direction, was of a size set externally in accord with available data for primary arm spacing. Solidification within this frame was set by imposed local solidification times (for example, from results of macro-scopic solidification models) and imposed growth rate. Bearing in mind that root-time growth was commonly deemed appropriate for planar growth [21], the corresponding law for concave growth of a cylinder [31] (Fig.2.5) was:

$$d/ds = 1 - \sqrt{1 - \sqrt{t/ts}} \qquad (4.31$$

or, indeed, a linear simplification thereof. (d is the shell thickness, ds that for complete solidification, and t or ts are the corresponding times.)

The extension of the diffusion calculations was by straight-forward extension of the logic of Fick's laws into 2D. The stability criterion, however, dictated that the calculations would not be stable for carbon for any number of solidification increments with growth occurring by integral nodes, and the adopted resort was to introduce a minimum 6 time steps per distance step.

Apart from accruing considerable run times, the program failed to find a sensible solidus, which would not continue to decrease for successive refinement of the nodal grid, even for plain medium carbon. Eventually, it was realised that this was an artefact of imposing a solidification growth law, rather than granting the dendrites their "free will".

Connections with Sheffield University in this area came from engaging Dr. Kirkwood in discussion as to how best to go about this.

4.2.3) Adoption of Kirkwood-Ogilvy Models

In addition to confirmation that one should not impose a growth law, Kirkwood stressed the importance of the phenomenon of dendrite arm coarsening, and the inaccuracies expected from integral node jumps. Furthermore, just such a model for planar growth of a single solidification-phase binary alloy, "MISEG", was made available (stemming from the work of Kirkwood and Evans [90]) assuming planar growth of secondary dendrite arms.

As this is the forerunner of my present models, it will be described in some detail.

a) Diffusion

The diffusion calculation within MISEG is of the 1D finite difference type, with the Schmidt [140] simplification of the explicit, forward difference scheme. This is the device whereby the new composition at a given node point is the average of the previous, adjacent values if the program operates at the limit of numerical stability (i.e. if the time and distance steps are chosen such that the program operates at the diffusion modulus).

$$Z_{i,t+\delta t} = (Z_{i-1,t} + Z_{i+1,t})/2 \qquad (4.32$$

The diffusivity is temperature dependent, and the time step is altered for each iteration to maintain operation at the modulus with fixed nodal spacings. The nodal grid is static, but growth is not restricted to integral node jumps. The interface is treated by a method due to Crank [60], in terms of concentration gradients at the interface, update of composition of the penultimate node from previous values (P, below, lying between 1 and 2, avoiding division by a very small value if set from the final full node), and update of the node immediately behind the interface by interpolation from the updated, adjacent values. The procedure is the interpolation due to Lagrange [141] which corresponds to a second-order Taylor series expansion or, indeed, the fitting of quadratic equations.

$$dZ/dx = (1/X_n)\{ kZl.(1+2P)/(P(1+P)) - Z_{R-1}(1+P)/P + Z_{R-2}P/(1+P) \} \qquad (4.33$$

$$d^2Z/dx^2 = (2/Xn^2)\{ kZl/(P(1+P)) - Z_{R-1}/P + Z_{R-2}P/(1+P) \} \qquad (4.34$$

b) Secondary Dendrite Arm Coarsening

The effects of this phenomenon are restricted to the residual liquid, i.e. the solidified arm remains unadulterated but finds that its neighbours are gradually moving away, as if on a stretchy primary arm. In terms of the calculation, this involves expansion of the solidification cell at each iteration (in accord with an imposed arm coarsening equation) with appropriate adjustment of the solute balance. The 'new' volume must inherit the bulk composition, so only the difference between the bulk and actual residual liquid composition in that volume is included in the solute balance equation. (This should not be seen as bulk composition liquid magically being transported into place but a necessary result of expanding the

cell size. A more obvious case is of a fully liquid cell of uniform composition which would only remain so on expansion of the representative cell if it inherits the bulk value.)

In comparison with Equation 4.1, it can be seen that this revision leads to the following solute balance:

$$Zl(1-k)\dot{Vs} = S_I D(dZ/dr)_I + (Vo-Vs)\dot{Zl} + (Zl-Zo)\dot{Vo} \qquad (4.35$$

c) Solution Scheme

Kirkwood employed the assumption of a set constant cooling rate in the solidification cell for MISEG. Equation 4.35 can therefore be solved for the growth rate with the solute gradient in the solid determined from the Crank scheme (a), diffusivity, partition coefficient and arm coarsening rate set by their own, appropriate equations, and noting that:

$$dZl/dt = m.T \qquad (4.36$$

Time dependent variables were updated in the simple, 'forward' or linear manner (first order Taylor expansion):

$$P' = P + \dot{P}.dt \qquad (4.37$$

No predictor/corrector type process was employed to ensure that the updated values still suited the gradients which got them there. Indeed, none seemed to be necessary as the computations exhibited pronounced consistency for repeat runs above a modest number of nodes.

With too few nodes, the calculated result can be patently improbable and, moreover, widely different from that with one more or one less node. This will be referred to as **nodal sensitivity. Convergence** will be used here to indicate the stage whereupon the same result is achieved within acceptable accuracy with any increase in number of nodes employed. The distinction is arbitrary but useful.

d) Investigation and Use of "MI-SEG"

The MISEG program was originally set up for Al with a few percent Cu. Data were substituted for Fe-C (partitioning, diffusivity, temperature/composition dependence) with Kirkwood's general analytical equation for arm spacing [73].

$$R = [\ (-16D_L YT/W(1-k)H).\ln(1+Wt/Zo.m)\ ]^{1/3} \qquad (4.38$$

where D_L =diffusion coefficient in the liquid ($2x10^{-8} m^2/s$)

Y =interfacial energy (1 J/m^2)

T =liquidus temperature (K)

H =volumetric heat of fusion ($2x10^9$ J/m^3)

W =cooling rate (K/s)

The resultant calculations showed no meaningful departure from equilibrium and needed lengthy run times, supporting the subsequent use of the Lever Rule for carbon.

A further simplification was noted from inspection of Equation 4.38 in that the final arm spacing could be predicted in advance for an equilibrium solute.

A major aspect of the assessment of this program [Howe,13] was discussing its extension to multi-component systems. Obviously, a multi-component steel will only have the one arm spacing at any time whereas Equation 4.38 is likely to suggest different values for each solute. This problem was addressed in more detail by Beaverstock [82] but, in outline, the argument was as follows.

The terms Y,T,W and H will apply to the overall composition and therefore Equation 4.38 can be re-written in terms of a constant, B (and transcribing the logarithmic term for reasons which will soon be apparent):

$$R = (-B/(1-k)).\ln(Zl/Zo) \qquad (4.39$$

Considering the slowly diffusing species, ln(Zl/Zo) can be approximated by the Scheil equation to (k-1)ln(1-fs) and, therefore, the predicted arm spacing will be the same for all such species:

$$\lambda = [B\ln(1-fs)]^{1/3} \qquad (4.40$$

For a different steel, B will be different and, during solidification, the only variable will be another which is common to all solutes, i.e. the fraction solid, giving arm coarsening behaviour of the form represented in Figure 4.8

This neat trick fails with finite diffusivity. Moreover, for carbon, at least, the diffusivity in the liquid is likely to be higher than for the average solute. Comparative, graphical plots are presented in figure 4.8. The suggestion was made that the actual arm spacing might just be the finest out of those available through calculation, but a more rigorous treatment was desirable.

It was noted that elements with lower partition coefficients favoured coarser spacings. The opposite is sometimes quoted (low k, increased segregation, easier instability, hence finer spacings). In practice, several of the low partition coefficient species would have a strong effect on Y which could dominate and lead to such a refinement.

A further question raised in the [13] was that of the finite difference diffusion scheme. The simplified Schmidt scheme cannot be extended to multi-components unless they all happen to share the same diffusivity.

The ternary model due to Ogilvy [4,5] then became available.

e) Investigation and Use of "TERNARY"

Extension to a ternary system was performed in the following manner. The simplified Schmidt scheme was exchanged for the standard forward difference procedure with a time step set such that the faster diffusing species operated at the modulus (which automatically means that the stability criterion for the other species will also be satisfied). The simplified solution at the core node was maintained, which was correct for the faster solute but introduced an error for the other solute. (This region is not, however, very sensitive to such an error.)

4.2.4) "HI-SEG"

Analysis of the solute balance equations revealed that these could be solved simultaneously for any number of solute species, though not within the framework of the inherited program. Therefore, a new program, "HI-SEG", was written with this capability but otherwise based on the Kirkwood/Ogilvy formulation. Prompted by the results from MISEG and TERNARY for carbon, equilibrium was assumed for the fully interstitial elements, C and N, which drastically reduced the required run times on the computer. This was achieved by reassigning the back diffusion term for these elements in the manner of Section 2.5, i.e.

$$D.dC/dx \rightarrow r.dC/dt \qquad (4.41$$

(Kirkwood has subsequently produced a streamlined version of the TERNARY program with one interstitial element which operates in a similar manner.)

Trial runs of HISEG were continued at this stage for a 13%Cr steel included in a Jernkontoret study [100] where liquidus, solidus, solidification time, final secondary arm spacing and the spacing within a few degrees of liquidus, were measured by thermal analysis for recorded cooling rates and

metallography. Surprisingly, this was the only steel of the 42 in the study which met the current restrictions on the program for single phase solidification with no compound or eutectic precipitation. The program ran to completion with the secondary arm coarsening equation used by Ogilvy [4] for Fe-~1%C-~1.5%Cr but with too fine an arm spacing and consequently underestimated micro-segregation. It is interesting to note that his was a linear coarsening law, which would result in greater solidus depressions at slower cooling rates, as discussed in Section 5.6.3. Attempts to employ various, different coarsening laws which would give closer agreement with the Jernkontoret arm spacing data were unsuccessful as the calculations became unstable.

A check for stability was through the equation:

$$L.\dot{r} > r.\dot{L} \qquad (4.42$$

If this is not satisifed, then the fraction solid within the volume element is decreasing, i.e. remelting is occurring. This check was, indeed, triggered at around 99% solid. Further test runs revealed that HISEG only attained full solidification for certain ranges of composition and cooling rate. These problems persisted despite an extensive 'de-bugging' operation and were even found, on occasion, to occur with a static arm spacing. The primary reason for the program misbehaving was, however, too much increase in arm spacing causing a decrease in solute content in the residual liquid. This was, presumably, a fault in the described conditions under which the program was operating rather than reflecting a physical phenomenon. It was prevented by reducing the proposed increment to the arm spacing (should the stability test of Equation 4.42 be triggered) such that the solute content in the liquid would not be forced to decrease. Although this was hardly satisfactory and could not be considered as a final solution to the problem, it produced encouraging results for the first test case of Fe-13%Cr in combination with a program development to operate with a constant rate of heat extraction rather than rate of cooling.

Assuming the specific heats of the solid and liquid to be the same, the governing equation was as follows:

$$\dot{Q} = H\dot{f} + C_p.\dot{T} \qquad (4.43$$

where $\dot{f} = (\dot{r}/L) = (1/L)\dot{r} - (r/L^2).\dot{L}$

therefore $$\dot{T} = (1/C_p)[\dot{Q} - (H/L)(\dot{r} - f.\dot{L})] \qquad (4.44$$

The central equation to the solution of the full set of equations becomes:

$$(\delta r/\delta t) = [(L-r)(\dot{Q}/C_p) + \dot{L}\{ f(1-f)(H/C_p) + \Sigma m(Zl-Zo) \} + \Sigma mD(dZ/dr)] / \{ (1-f)(H/C_p) + \Sigma mZl(1-k) \} \qquad (4.45$$

where $D(dZ/dr)$ is replaced by $rkdZ_l/dt$ for the interstitials.

The HISEG program was run with a heat extraction rate of $29MJm^{-3}s^{-1}$ equal to the average value for the Jernkontoret [100] test steel J306 (Type 410s stainless) at a furnace cooling rate of 2 K/s. (The average cooling rate of the sample, however, was 0.8125 K/s during solidification.) The steel composition, experimental data and equivalent data generated by the HISEG program are presented in Table 4.2 from which it can be seen that the computed results are remarkably accurate. Good agreement was also obtained with the results from the 0.5K/s furnace cooling rate (actual, average sample cooling rate of 0.286K/s and heat extraction rate of $11MJm^{-3}$) although a different arm coarsening rate had to be employed to match the experimental spacings. (The program was not run for the third experimental case because no final arm spacing was quoted.)

It must be admitted that the high degree of accuracy is partly fortuitous in view of the simplified or somewhat arbitrary data employed.

Additional comparison could be made for the second case ($11 MJm^{-3}s^{-1}$) as the Jernkontoret study reported the development of fraction solid and sample cooling rate with time. Agreement was still reasonable and this is probably as far as this comparison can be taken: the quoted fractions solid were back-calculated from the temperatures and the cooling rates will be affected by surrounding material away from the thermocouple. Also, a constant heat extraction rate as assumed by HISEG is still only an approximation.

4.2.5 "PHASEG"

As the program title implies, the next development was to accommodate more phases in the segregation calculation. The peritectic reaction is the most important, i.e. enabling extension of the calculations to most steels, and the first approach was to assume the steels were still effectively Fe-C binary type. The condition whereupon the peritectic reaction was deemed to start was when a suitable carbon-equivalent of the alloy reached the Fe-C binary value of 0.53% in the residual liquid.

Having failed to find appropriate peritectic carbon equivalents (PCE's) in the literature, attempts were made to derive some statistically [142] from the compositions and ferritic solidification proportions quoted for carbon and low alloy steels in the Jernkontoret guide [100], building up (where possible) from rough values taken from binary phase diagrams. Later, such coefficients were quoted by Kagawa and Okamoto [126] but our values still made much better sense of the Jernkontoret results (Table 4.3). (The author revised these subsequently, to be self-consistent at the peritectic as in Section 4.1, Table 4.1.)

The interstitial elements were assumed to maintain uniform compositions within all three phases during the peritectic. The back-diffusion term required for the solute balance of such an element is presented in Fig. 4.9.

The carbon content was controlled independently, either by assuming it to be constant as in the binary peritectic, or by assuming the carbon equivalent to be constant during the reaction. In the first case, $\dot{C}l$ is zero, and (with the adopted peritectic invariant compositions of 0.09,0.17 and 0.53%) it can be seen that $\dot{f}_{bcc} = -4.5 * \dot{f}_{fcc}$. In the latter case, $\dot{C}i$ depends purely on what the other elements are doing.

Nitrogen (the only other interstitial considered) sometimes objected to this formulation, evidenced by decreasing its concentration in the residual liquid.

The substitutional elements disregarded the progress of the bcc/fcc boundary, exhibiting their austenite diffusivity across the solid as soon as the peritectic reaction began.

Carbon equivalents for the eutectic were taken from the literature on cast-irons [134] (indicating whether an iron was hypo- or hyper- eutectic). Solidification was then deemed to terminate at the corresponding temperature, as in the binary case. This is not, however, thought to be a poor approximation for a multi-component carbon steel because, a) it only effects a very small liquid fraction in even the highest carbon steels of practical significance, and b) thermo-couple experiments indicate that the eutectic, even with appreciable amounts of Si and Mn, does occur at a fairly constant temperature.

The most important 'compound' as such in terms of this work is manganese sulphide. Indeed, most of the carbon and low alloy steels in the Jernkontoret reference used for comparison contained such a precipitate from the liquid, albeit in small quantities towards the end of solidification. It is not, however, adequate to assume that solidification terminates at the temperature at which it first appears, because it does only involve the Mn and S. Consequently, a routine has been introduced to remove Mn and S from the residual liquid in appropriate ratio as it precipitates but which allows this liquid to continue its solidification with decreasing

temperature. A maximum solubility product, Y, in the liquid was employed, and the resultant formulation is given in Section 5.5.4. However, this has not been incorporated into the final version of the microsegregation model.

Two further steels from the Jernkontoret guide [100] were used to test the PHASEG program; one low carbon undergoing the peritectic reaction and one medium carbon, also undergoing the peritectic reaction but terminating with some MnS precipitation and austenite/cementite/phosphide eutectic (Table 4.4). The liquidus and peritectic-start temperatures were predicted with reasonable accuracy and so was the solidus of the low carbon steel, although the predicted value for the medium carbon steel was substantially below that experimentally recorded by thermal analysis. The thermal analysis solidus was, however, inconsistent with the observed presence of eutectic which would only have precipitated at much lower temperatures.

From the three results so far, a reasonable generalisation was postulated. In steels of low overall content of highly segregating species, the calculated solidus (an indicator of the 'net' level of micro-segregation) appears to be in good agreement with that measured by thermal analysis experiments. Agreement is poor, however, if significant amounts of strongly partitioning species such as carbon (despite its high diffusivity) are present, in that the computed results fall substantially below such measurements. The calculated results, however, are believed to reflect a real effect of persistent, highly segregating films of too small a volume fraction to be detected by thermal analysis. Moreover, such an effect is of great importance because it appears to be largely responsible for the total lack of measurable ductility down to temperatures previously described as substantially sub-solidus [143,144].

This model formed the basis of my publication in Applied Scientific Research [6], representing the stage of development prior to the onset of the PhD project. It can be seen that, despite some encouraging results, there was still plenty of room for improvement and hence, scope for my current work.

4.3) DATA FOR USE WITH PROTOTYPE PROGRAMS

4.3.1) Peritectic Equilibrium Data

One complication worth avoiding during the development of the computer programs was the variation in liquidus or δ/γ solvus slopes, m, and partition coefficients, k (according to composition or temperature). Such information was to be provided by the sub-contract (NPL) but, if only for the purposes of getting the micro-segregation model established, constant values are very useful approximations.

These are as described in Section 4.1 and presented in Table 4.1

4.3.2) Hyperperitectic Fe-C-Cr Data

In the course of this work, the variation in equilibrium coefficients in the Fe-C-Cr system was wanted for hyperperitectic (austenitically solidifying) alloys, wherein there was no need to ensure consistency of data among the three phases (Section 6.1). A colleague (Tim Fox) was commissioned to glean composition and temperature data from the work of Rickinson [145] as corrected by Ogilvy [146], Table 4.5, from which he derived the following partition coefficients by statistical analysis:

Range: 0.77-2.33 wt%C, 1.55-6.05 wt%Cr

$$K_C = 0.3 + 0.044[C] + 0.011[Cr] \quad \text{(MTDATA)} \quad r^2=0.623$$

$$K_C = 0.306 + 0.028[C] \quad \text{(OGILVY)} \quad 0.136$$

$$K_{Cr} = 0.906 - 0.076[C] - 0.004[Cr] \quad \text{(MTDATA)} \quad 0.992$$

$$K_{Cr} = 0.867 - 0.089[C] \quad \text{(OGILVY)} \quad 0.912$$

(4.46

The equations fitted to the values calculated according to MTDATA had higher statistical correlation as measured by the r^2 value, but are of course one stage removed from actual data because MTDATA is itself a calculation scheme. Moreover, the MTDATA values gave surprisingly high Cr partition coefficients. Both sets were employed in Section 6.1 but those of Ogilvy gave better agreement with experiment.

In addition to the partition coefficients, the author inspected the liquidus slope data inherent in the data from Table 4.5, again by statistical analysis. The two sources gave quite similar net temperatures but regression indicated that Ogilvy's data were consistent with a POSITIVE solvus slope for Cr, which is unexpected from such relatively lean alloys. The r^2 value was 0.973, with a maximum error of 8.4°. MTDATA, however, gave remarkably strong correlation (r^2 of 0.992 and maximum error of 2.3°) with a logically acceptable and simple equation:

$$T(K) = 1809 - 72[C] - 2.1[Cr] \qquad (4.47$$

and it was decided to adopt this for the runs in question.

4.3.3) Diffusion Data

As discussed in Section 2.8, there are insufficient data to justify use of rigorous mathematical treatments of diffusivity. Simple concentration-driven fluxes are employed in this work: a further restriction on applicability to low alloy compositions. The data employed were those of Fridberg [147] who found that reasonable approximations to solute diffusivity could be obtained by simple employment of factors on the self-diffusivity of iron. (Beaverstock [82] has pointed out that some of these approximations are not as good as he infers, particularly for phosphorus, and he has experienced less problems at solidus with the program when using more accurate diffusivity data for this element.) The data employed in this work are provided in Table 4.6.

CHAPTER FIVE

DEVELOPMENT OF MICRO-SEGREGATION MODEL

> Part of the liquid, rich in metalloids, becomes trapped between the growing branches of the crystallites, and finally solidifies where it has been imprisoned.
> ....F.Osmond and J.E.Stead, "Microscopic Analysis of Metals", Charles Griffen & Co, 2nd ed., 1913

5.1) EXAMINATION OF NODAL SENSITIVITY AND CONVERGENCE

Repeating the useful but somewhat subjective distinction made in Section 4.2.3b, 'nodal sensitivity' is satisfactory when there are sufficient nodes, for a given case, to avoid wide variability and oscillation in computed results between parallel program runs with a slightly different number of nodes, and 'convergence' is achieved when any successive increase in the number of nodes on which the calculation is based leads to no significant difference in the computed result. The latter case is when the ideal result has been obtained according to the numerical scheme, essentially freed of errors due to the finite chopping-up of the modelled system.

The variables adopted as standard in this work to test the nodal sensitivity and convergence of results are the final composition of the interdendritic liquid disappearing at solidus, and the solidus temperature, which is a net function of the final liquid contents of all the solutes present. This is an extreme test-variable. Numerical schemes have enough problems at a boundary such as the solid/liquid interface with a step change in composition, -an example of a 'singularity'. Numerics are really struggling when such a singularity meets a boundary of the modelled system, such as at the solidus. With only a few nodes, convergence can be achieved for almost all of the solidification cell, but many times more nodes may be required even for moderate nodal sensitivity at solidus.

Matsumiya [93-95], for example, acknowledged this problem but avoided it by saying that, during subsequent cooling below solidus, the more extreme the gradients around the final point of solidification, the more quickly they homogenised, such that little difference was apparent at the end of the day. This get-out can only be invoked, however, if there is no great interest in features such as possible compound precipitation from the final enriched liquid, or the temperatures upon which some ductility becomes apparent

The MISEG (Kirkwood) program operating with a constant cooling rate displayed consistency at remarkably few nodes. Major problems first became apparent with the HI-SEG program for multi-component steels under heat extraction-rate control and coarsening arms. The following description relies on a lot of back-tracking, program restructuring, and hindsight.

Calculation of a binary (and single solidification phase) alloy under an assumed constant cooling rate is inherently rather stable. The cooling rate control is only concerned with the enrichment of the single solute as multiplied by its liquidus gradient. For any temperature, there is a simply defined and unique time taken to get there and, moreover, corresponding residual liquid concentration. For the purpose of comparative runs, a test case of a solute characterised in

Table 5.1a with a target of 90-second solidification, was adopted. In Table 5.1b it can be seen that the initial, MISEG, formulation was not nodally sensitive even with only 10 nodes, and achieved convergence from about 40 nodes. (The increase in calculated final liquid composition from 10 to 40 nodes necessarily resulted in an increase in solidification time from the initial target.)

These results were compared with those of binary test programs employing constant (MISEG1) and root-time (MISEG2) heat extraction control, and with PHASEG (with constant heat extraction control, Section 4.2.5) restricted to the binary case in question. MISEG1 was patently sensitive with around 10-12 nodes, and requiring about 60 for convergence. MISEG2 was less sensitive but still needed a similar number of nodes for convergence. PHASEG was successful (and reaching the necessarily same answer as MISEG1) with comparatively few nodes (30) but finer time-steps had been introduced into this program as complete solidification was approached.

Further runs were performed with MISEG2 but with artificial variation of specific heat capacity. It can be seen from Table 5.2a that nodal sensitivity and convergence improve as the specific heat capacity is increased. Indeed, in conjunction with Table 5.2b where the solute diffusivity is varied for zero specific heat, it can be seen that no real stability is achieved under this condition.

The picture becomes clearer in relation to the heat extraction equation:-

$$Q = H.\dot{fs} + C_p.\dot{T} \qquad (5.1$$

An assumed constant cooling rate equates to zero latent heat in this formulation, and nodal sensitivity or convergence become progressively more difficult as the ratio of latent to sensible heat increases, culminating in no stability with no sensible heat (i.e. zero heat capacity or zero liquidus gradient, - a physical instability). This reflects a

progressive relaxation of control over the changes in solute content of the residual liquid; if the latent heat term dominates, a large error in solute content and, hence, temperature, makes limited impact on the governing condition of heat extraction. Furthermore, this relaxation is increased with increasing number of solutes as each exhibits less influence over the already uninfluential temperature change which enters the governing condition. Chromium is a good example of an element liable to misbehave under heat extraction controlled and/or multicomponent solidification on account of its shallow liquidus slope; even with a reasonable specific heat capacity, errors in Cr content will represent only minor errors on temperature and, therefore, very small errors on the governing condition.

This is a recognised problem in FD or FEM modelling; the heat ratio in question is termed the Stefan Number, and it is unfortunate that most solidification problems involved materials, like steel, of low Stefan Number and consequently sensitive numerical behaviour.

One intuitively obvious influence on stability is solidification rate, faster rates requiring more nodes to cope with the correspondingly faster variations, whether by cooling rate or heat extraction rate control.

A further factor identified in the original study was the description of arm coarsening behaviour. If the arms coarsen at too large a rate, the inherited bulk solute in the additional volume can dilute the residual liquid from the previous iteration~cell size so as lead to a reduction in solute content. This usually became apparent towards the end of solidification where the residual liquid volume was small and, therefore, more susceptible to significant dilution. This reduction of one or more solute concentration within the residual liquid upset the interface composition, hence the solute gradient in the solid and solute balance, and hence the solution for the overall growth rate and, thereafter, the behaviour of the other elements present. The response at the time was to get the program to check for any initial overdilution and, if present, arbitrarily restrict the

coarsening rate so as to remove the tendency. This was partially justified by considering that the imposed coarsening law must be wrong for this effect to occur and, therefore, in need of some form of correction.

The primary observation is that any numerical scheme is inherently delicate around discontinuities and converging boundaries. Behaviour at an interface and, especially, upon the disappearance of a particular phase, is bound to be problematic. The primary resort is to throw more and more nodes at the system (the 'Brute Force' finite difference method as described by Fox [148]), although this leads to a lot of unnecessary computation before the system is in a delicate condition which requires the finer nodes. This led to the construction and incorporation of a routine for re-meshing the FD array, such that the bulk of the calculation could be performed with few nodes (e.g. 10) whereas a delicate stage such as solidus could be addressed with many more (e.g. 50). A further action was to use very fine time steps below that required by the diffusion modulus and, indeed, below the value for ostensibly minimised numerical errors in terms of the diffusion calculation, once the system has approached such a condition, e.g. for fractions solid above 0.99.

This was examined further with a prototype version of the SOLVER program, comparing calculations on 6%Ni, static 100μm, for 10,20 and 50 nodes variously re-gridded (Section 5.5.3), with that from 100 nodes. As before, the sensitive test variable of liquid composition at solidus was employed, with the difference between the alternatives and the 11.4721%Ni recorded from using 100 nodes throughout, presented in Table 5.3. It is evident that large improvements can be achieved through regridding to more nodes for the last 0.1 fraction solid, with little extra benefit from regridding at an earlier stage. For example, regridding the "wrong way" from 20 to 10 was only marginally better than from using 10 nodes thoughout, and regridding from 10 to 20 was only marginally worse than from using 20 nodes throughout.

Beaverstock, at Swinden Labs., has extended the stability criteria argument to solute balance equations, which

evidently can be the controlling feature rather then the diffusion modulus [149]. It is expected that such an expression will be incorporated into the SOLVER program.

5.2) EXAMINATION of ALTERNATIVE FINITE DIFFERENCE FORMULATIONS

5.2.1) Moving-Grid Scheme

Prompted by the problems of stability referred to above, an alternative finite difference scheme was tested to see if it was more robust in operation. The chosen scheme was that due to Crank and Gupta [150] where the nodal grid was still of fixed spacing but which moved at the velocity of the interface. The interface, therefore, always resided on a proper node, without having to advance by coarse, integral node jumps. The compositions of the bulk shifted nodes are interpolated from those of the old nodal positions but with updated concentrations by a third order equation set up so as to give the same second derivative as employed in the diffusion calculation.

The Crank-Gupta scheme was modified so as to have a growing number of nodes marching into nodeless liquid, and assigning a value to the concentration at the spine whether or not a nodal plane happens to reside there, enabling the first full node to be diffusively updated. The latter could not be achieved by standard finite difference diffusion because the extra mini-node at the spine would be vanishingly small when a new node had just been created and, therefore, would require vanishingly small time steps for numerical stability.

In terms of the schematic in Figure 5.1, the spinal composition was updated in the following manner:

$$C0' = C0 + (C(N0)-C0)*(D\delta t/\delta x^2)^P \qquad (5.2$$

This formulation had the right properties so as to equal the standard numerical formulation for P=1 and to increase C0 to no more than C(N0) when P tends to zero. A comensurate update has also to be employed for the first node:

$$C(N0)' = C(N0) + (C(N0+1)-C(N0))*(D\delta t/\delta x^2) - (C(N0)-C0)*P*(D\delta t/\delta x^2)^P \qquad (5.3$$

The correct behaviour at the limits does not necessarily imply correct behaviour in between, but it should not be far out and, with the moving grid formulation, this interpolation technique is only applied at a relatively robust location.

Comparative runs with the original MISEG program are recorded in Table 5.4. It can be seen that the moving grid formulation was closer to the high node-number result at low nodes but was relatively less close at intermediate node-numbers. Moreover, for a given number of nodes, extra computation was required of the moving grid procedure; run-time perhaps is a more pertinent factor for assessment of relative merits.

With the target in mind of a twin moving boundary program for the peritectic, the moving grid could not be expected to move so as to keep both interfaces on a nodal plane. Seeing that the non-nodal interface scheme would have to be addressed for at least one interface, and in view of the dubious benefit apparent from test comparison, this alternative scheme was not pursued. The comparison did serve, however, to restore some faith in numerical procedures in that a different technique would give essentially identical results provided that there were enough nodes in the calculation.

5.2.2) Crank-Nicolson Diffusion Treatment

The finite difference scheme employed in these programs has been the standard explicit forward difference procedure. The semi-implicit central difference scheme proposed by Crank and Nicolson [103] (with use of the "TDMA" or "Thomas" algorithm [151]) is generally considered to be superior while still avoiding time consuming predictor-corrector type iterations. Unlike the forward difference scheme, Crank-Nicolson has no limiting diffusion modulus (or Fourier Number) for numerical stability which dictates a maximum time step, although accuracy is still impaired by large time steps.

A Crank-Nicolson scheme has therefore been written and incorporated into a single solidification phase binary test program for comparison with the original procedure. In order to make proper use of the scheme, it should be employed right up to the moving interface rather than curtailed at a full node, thereby requiring modification. The final spacing to the interface is not only different from that between the other concentration points, but it is also changing during the time step for which the Crank-Nicolson operation applies. The calculation for diffusive updating of the node nearest the interface is, therefore, not only lopsided, but gets more lopsided during the iteration (Fig.5.1b).

This was tackled in the following manner. Crank-Nicolson updates the nodal compositions with use of a second derivative for composition with respect to distance which equals the average of that in the initial, known condition and the target, unknown condition at the end of the current time step. Using:

$$\partial Z/\partial t = \partial^2 Z/\partial x^2 = Z'',$$

then:

$$Z''(\text{Crank-nicolson}) = [\ Z''(@\ t) + Z''(@\ t+\delta t)\ ]/2 \qquad (5.4$$

In terms of the second-order Lagrangian interpolation procedure employed in my programs (Sections 4.2.3-5), the second derivative in this region is defined as follows:

$$Z'' = 2(Z_{(R-1)}/(1+P) - Z_{(R)}/P + Z_I/(P(1+P)))/\delta X^2 \qquad (5.5$$

This equation has then to be inserted into the two above with the nodal and interfacial compositions, and parameter, P, for the relevant time. All terms at time t are already known, and the terms δt, Z_I(@ $t+\delta t$) and P(@ $t+\delta t$) are knowable in advance with the standard, forward predictor scheme for the solute balance and interfacial update (at least, for a binary). Employing the Fourier Number, $r=\delta t/\delta X^2$, appropriate manipulation of these equations leads to the following coefficients for the R node in the Crank-Nicolson solution matrix according to the Thomas algorithm:

$$\begin{aligned} a_R &= 1 + r/P(@\ t+\delta t) \\ c_R &= 0 \\ b_R &= -r/(1+P(@\ t+\delta t) \end{aligned} \qquad (5.6$$

(using the notation whereby 'c' are the diagonal elements, 'a' to the left and 'b' to the right).

The appropriate bunching of 'knowns' for the column matrix is as follows:

$$\begin{aligned} v_R = {} & Z_{(R-1)}\, r/(1+P) + Z_R(1-r/P) + Z_I\, r/(P(1+P)) \\ & + Z_I(@\ t+\delta t)\, r/(P(@\ t+\delta t).(1+P(@\ t+\delta t)) \end{aligned}$$

where values refer to the initial time, t, unless otherwise stated.

This procedure was written into a test binary, single solidification phase program for comparison with the previous formulation. As before, the highly sensitive variable of final disappearing liquid composition at 100% solid was used for the test comparisons, illustrative examples of which are presented

in Figure 5.2. It is apparent that the two schemes are in encouragingly close agreement. For the same number of nodes and with the same Fourier number of 0.5, the Crank-Nicolson scheme does appear to be more accurate. (There is a slight anomaly here in the 20-node case which appears to be due to the Crank-Nicolson-based program terminating one iteration too soon; in the other examples, the same number of program loops were noted for equivalent conditions.) However, there did not appear to be any reduction in run time for similar accuracy with the more sophisticated scheme, and, therefore, no real incentive to incorporate such a scheme into the multicomponent or peritectic programs which would be a very tricky operation.

5.2.3) Second-Order Growth Predictor

A further attempt to render the solidification calculation more robust was the use of a second order predictor for the interface position. The standard program construction is such that, for each iteration, a growth rate, $\dot{r}$, is determined so as to satisfy the solute balance equations which are, in turn, coupled with the solid diffusion scheme. The interface is then advanced by an increment equal to the product of the growth rate and the time step. This is a predicted updated value equivalent to a first order Taylor series expansion of interface position, r. The corresponding second order predictor is:

$$r' = r + \dot{r}\delta t + \ddot{r}.\delta t^2/2 \qquad (5.7$$

A standard, central difference determination of the second time derivative of r (i.e. $\ddot{r}$) would require knowledge of the subsequent growth rate, $\dot{r}'$, which has yet to be determined. A backward finite difference approximation was therefore employed which would still be an improvement on the usual, first order prediction:

$$\ddot{r} = (\dot{r} - \dot{r}^{\circ})/\delta t \qquad (5.8$$

where $\dot{r}^{\circ}$ was the growth rate at the previous iteration. Therefore,

$$r' = r + (3\dot{r} - \dot{r}^{\circ})\delta t/2 \qquad (5.9$$

A binary micro-segregation program was constructed to compare computed results with or without the second order component. As before, the test variable was the maximum concentration of solute in the liquid, i.e. at solidus, because it is highly sensitive to the imposed conditions. Computations were repeated with different numbers of nodes and different Fourier numbers for diffusion (the Crank-Nicolson diffusion scheme being employed). For a given number of nodes and Fourier number, the second order predictor did appear to be an improvement (i.e. in closer agreement with the high node and low Fourier number result) but not markedly so. An example plot of maximum liquid concentration versus node number for a Fourier number of 1 is presented in Figure 5.3.

Attempts to update liquid composition also by a second order predictor led to inconsistencies in the solute balance; whether the equation is right or wrong, it helps if it is self consistent. Further thought on how to incorporate this extension without wanting the solute balance to say two things at one time might have led to success, but this was not pursued because of the expectation of limited returns.

Incorporation of the second order growth predictor into a multicomponent program ("PHASEG") gave slightly poorer results. This contrary effect defied explanation in terms of either logic or apparent programming bugs, but, as above, was not pursued as the venture did not appear to promise worthwhile rewards.

After this brief and confusing skirmish, second order predictors were abandoned.

5.2.4) Discretisation

Use of the differential formula, Equation 4.35, resulted in minor departures from the imposed thermal conditions which were particularly evident for operation with a small number of nodes and with rapid arm coarsening. It appeared that these inconsistencies resulted from treating the solute balance as a true differential formula rather than acknowledging that it progressed in finite time steps, with consequent changes in X and L during each iteration. Various methods of approach were tried, the eventual choice being to interpret Equation 4.35 (Figure 1.2) such that term (B) involved only established values, (C) mixed the increased solute into the resultant volume, (D) employed the established liquid concentration (being automatically corrected by the (C) term) and (A) involved the interfacial solute loss according to the established concentrations, between the resultant and established solid volumes. Division of the equation through by the resultant volume, and employing subscripts of 1 and 2 for established and resultant values respectively, gave the following solute balance equation:-

$$Zl_i(1-k)\{fs_2 - r/L_2\} = (1/L_2).D_i(\delta Z_i/\delta r).\delta t + (1-fs_2)\delta Zl_i + (Zl_i - Zo_i)(1-L_1/L_2) \qquad (5.10$$

where fs_2 and δZl_i are unknown.

In conjunction with the heat balance, Equation 4.43, and the local equilibrium condition, fs_2 can be obtained from solution of the following quadratic equation:-

$$-(H/Cp).fs_2^2 + \{(Q/Cp)\delta t + (H/Cp)(1+fs_1) + \Sigma m_i(1-k_i)Zl_i\} - (Q/Cp)\delta t + (H/Cp)fs_1 + \Sigma(m_i D_i/L_2)(\delta Z_i/\delta r)\delta t + (1-k_i)Zl_i/L_2 + (Zl_i - Zo_i)(1-L_1/L_2) \simeq 0 \qquad (5.11$$

Solution for each δZl_i can now be obtained by back-substitution of fs_2 in each solute balance equation.

This treatment gave thermal behaviour fully consistent with the imposed cooling or heat extraction rate, and is used for the two phase solid/liquid subroutine in the final program. This mode of discretisation is also adopted in the three phase peritectic subroutine involving simultaneous solution of both interfaces (Section 5.4).

5.3) EXTENSION TO CYLINDRICAL AND SPHERICAL MORPHOLOGIES

All the models to date have assumed a planar representative cell for the solidification process, i.e. platelike arrays of primary or secondary arms (Figs.2.23,2.24). Despite the extremely complicated nature of actual dendrite morphologies, this appears to be reasonable first approximation (Section 2.8) but it is obviously desirable to make some assessment of the influence of morphology. My original "SQUARE" micro-segregation model was a genuine 2D finite difference scheme which assumed concave solidification of a square mesh of primary arms linked by plates of secondary arms (Fig.2.30 Section 4.2.2). This, and analytical musings discussed in Section 4.1, indicated that such inward growth gave vastly overestimated segregation. Outward growth of non-planar solid nuclei may well, however, be of value and, moreover, radially symmetric forms can be calculated by a modified 1D finite difference scheme. The extensions discussed here are so as to create a single routine for planar (1D, n=1), or convex cylindrical (n=2) and spherical (n=3) growth.

5.3.1) Diffusion Scheme

The diffusive adjustment of composition profile is bound to be affected by dimension, n. Considering finite annular rings and spheres, the diffusing atoms are jumping in and out of volumes of different sizes, with consequently different effects on the local concentrations. Inspection of the finite difference formulae presented by Crank [60] for the three morphologies in question, revealed that a single formula could be obtained which satisfied each case:

$$Z_{(i)} = (D/\delta x_N^2)(Z_{(i-1)}.(1-y_{(i)}) - 2Z_{(i)} + Z_{(i+1)}.(1+y_{(i)})) \quad (5.12$$

where x_N is the node spacing and $y_{(i)} = (n-1)/2i$.

It can be seen that either for n=1 or with i approaching infinity, regardless of dimension, the formulation becomes that of the standard, planar finite difference equation (i.e. $y_i=0$).

5.3.2) Solute Conservation

It is always prudent to check that one's program has neither created nor destroyed matter. Averaging of the nodal compositions for this purpose must also take account of the dimension. By summing a core of half a node's radius, annular shells of nodal thickness, and a final shell of half a node's thickness, the following average was obtained which satisfies all three morphologies:

$$Z' = (Z_{(0)}/2 + n\Sigma\, i^{n-1} Z_{(i)} + nN^{(n-1)} Z_{(N)}/2)/N^n \qquad (5.13$$

where N is the total number of nodes.

5.3.3) Interfacial Solute Balance

The solid/solid interface with control by diffusion in both adjoining phases can be used directly in each morphology. Each term applies over the same interfacial area, which therefore cancels out of the equation. The solid/liquid (or solid/solid with complete mixing in one or both phases) interface, however, needs considerable attention, especially if the arm coarsening feature is to be included.

The solute balance formula should be applied to the relevant volumes undergoing change (Figure 1.2); the standard equation for 1D has already cancelled out the width and breadth but the underlying equation should be considered for extension to higher dimensions, as in the analytical derivations in Section 4.1.

$$Zl(1-k)*\dot{Vs} = S_I D\partial Z/\partial x+(V_o-Vs)\dot{Zl} +\dot{Vo}(Zl-Z_o)$$

(A) (B) (C) (D)

(5.14

where V is volume, S_I is surface area, and subscripts 'o' and 's' denote the current size of the representative cell, and of the solid, respectively. Component (A) is the solute change required by the movement of a partitioning interface, (B) is the solute loss from the interface by diffusion into the bulk solid, (C) is the solute change in the residual liquid, and (D) is that associated with the expansion of the representative unit cell so as to mimic the arm coarsening process. This basic equation can be translated into distances and discretised for finite difference treatment in various ways, all of which should tend to give the same final result within a micro-segregation model, but some of which are simpler to manage, less prone to instability, or achieve a given level of precision, or 'convergence', with a smaller number of nodes. In terms of the part-node parameter P used in this work to free the interface from the fixed grid, the interface and associated terms controlling the solute fluxes are represented in Fig.5.4.

The rate of change of volume is equal to the product of current surface area and the movement of the characteristic distance, or radius, of the axisymmetric morphologies in question. Division of the equation by the surface area therefore changes Vs in (A) to r, and (B) merely becomes $D\partial Z/\partial x$, i.e. the (A) and (B) terms equate to those of the original, 1D formula. For the remaining terms, it should be noted that the surface area of a planar, cylindrical or spherical body relates to the differential with respect to distance of the volume and, in ratio, π or 4π terms cancel out. By inspection, it can be seen that (C) and (D), similarly divided through by S_I, can be represented generally for dimension, n, by:

$$(L^n - X^n)/(nX^{n-1}).\dot{Zl} \quad \text{and} \quad \dot{L}(L/X)^{n-1}.(Zl-Zo)$$

The solute balance for each dimension is thus set up ready for manipulation in accord with the chosen cooling rate control or heat extraction control-based mathematical solution.

5.3.4) Heat Balance

Attention must be paid to dimension because it involves the rate of change of fraction solid:

$$Q = H.\overset{\circ}{fs} + Cp.\overset{\bullet}{T} \qquad (5.15$$

where $fs = d(X/L)^n/dt$ and where both X and L are functions of t,

$$fs = n(X/L)^{n-1}\{\dot{X}/L - X.\dot{L}/L^2\}$$

$$fs = nX^{n-1}\{\dot{X}/L^n - X.\dot{L}/L^{n+1}\} \qquad (5.16$$

5.4) THE PERITECTIC REACTION

5.4.1) The Problem

Complete equilibrium across a two phase binary system is simply represented by the lever rule, with straightforward extensions to three phases and so on. In a multicomponent system, it remains simple provided data are known for the partition coefficients or to derive the chemical potentials which must be uniform for each element.

Equilibrium across one phase and finite diffusion in another is the standard case for building up a micro-segregation model. The problem is relatively trivial in a binary, involving the solute balance with knowledge of the relevant equilibria (partition coefficient and liquidus slope) and the driving force for change (cooling rate or heat extraction rate). Extension to multicomponents gets a little more complicated but is the natural extension to the above in terms of simultaneously solving a solute balance for each species along with the equilibria and driving force. Additional complications for multicomponent systems are determination of the relevant phase equilibria to feed into the equations and, indeed, the relevant diffusivities, but for current purposes these aspects are 'source data problems' outside of the current argument.

The peritectic obviously requires solution at two phase interfaces. Treatment of the solid-solid interface generally requires volume diffusion control in both phases as is described in Figure 1.2b. Application of this equation for a binary system with local equilibrium and a constant temperature is within the scope of text books. Its extension beyond these restrictions is not trivial, however.

(An alternative, isothermal phase transformation problem is where one phase is a compound of fixed composition, as has been addressed by several authors. This again avoids the main problems and, moreover, is not all that relevant to the current work where temperature and composition are continually varying.)

The general form of the equation for the solid/solid interface solute balance, i.e. between two phases of finite diffusivity, is as follows:

$$Z_I(k-1)\dot{r} = Da(\delta Z \delta r)_a - Db(\delta Z/\delta r)_b \qquad (5.17$$

This equates the change in composition from interfacial advance with the net diffusive fluxes in the two phases.

The problems encountered when trying to extend this formalism concern the shortage of suitable time derivative variables. There is no immediate provision for introducing either a varying temperature or a correspondingly varying interfacial composition. Therefore, there are no means of updating these variables in a predictive manner for the next iteration. The equation naturally suits an isothermal binary system, but can be applied to non-isothermal cases by imposing the temperature/ composition adjustments upon the equation which are uniquely defined with binaries. For ternary and higher order systems, even if isothermal, this cannot be done as a range of compositions is available which would satisfy the temperature change, but there is no facility in this formulation whereby any particular set of compositions should be chosen in preference to the others.

Agren [106-108] allowed for this by floating Z_I with the equations describing the equilibria, i.e. defining Z_I in the finite difference expression, Equation 5.17, as the 'new' unknown value. The term, Z_I, however, is also implicit in the gradients, $\delta Z/\delta X$, and the proper requirement must be to define the complete solute balance in terms of new values. This, therefore, was the target of this work. (Simpler models were also generated en-route, with complete diffusion assumed in both liquid and ferrite [7].)

5.4.2) Interfacial Advance with Finite Diffusion in Both Phases

The finite difference formulation central to this work uses the Lagrangian equations to allow the interface to reside at any position, i.e. it is not obliged to reside only in nodal planes with growth only by coarse nodal increments, and uses a second order interpolation for composition gradients and second derivatives. The interface position with respect to the nodal grid is described by a parameter, P, as pictured in Fig. 5.5, whereupon certain terms in Equation 5.17 can be expanded as follows:

$$\dot{r} = X_n(P-Po)/\delta t \qquad (5.18$$

where X_n=nodal spacing and Po=previous value of P.

$$(\delta Z/\delta r)_a = (1/X_n)\{[P/(1+P)].Z_{R-2} - [(1+P)/P].Z_{R-1} + [(1+2P)/P(1+P)].Z_I \qquad (5.19$$

$$(\delta Z/\delta r)_b = (1/X_n)\{-[(3-P)/(4-P)].Z_{R+3} + [(4-P)/(3-P)].Z_{R+2} - [(7-2P)/(3-P)(4-P)].k.Z_I \qquad (5.20$$

where Z=solute content at the node indicated by the subscript, and R=node number just before the interface.

In addition to P, all the Z terms, as described in the previous section, should be considered as the new, unknown values, i.e. solving Equation 5.17 for the new time whereas previous formulations employed the previous known values in the solute balance equations so as to determine the derivatives from which the relevant variables could be updated. The nodal Z values away from the actual interface can be predicted explicitly with knowledge of the surrounding nodal compositions and the time step. (If an implicit scheme is employed, such as Crank-Nicolson [103]), these nodal compositions are not determinable in advance.) Moreover, a net function of the

interfacial compositions, Z_I, of each solute can be calculated according to the local equilibrium conditions, but not the individual Z_I values. We therefore have for N solutes, N unknown values of Z_I, and an unknown value of P (which must be the same for all solute balances), to be solved according to N solute balance equations and one equilibrium equation; an inherently soluble set although the solution is not trivial. Equation 5.17 has to be written in terms of Z_I which appears three times in the equation, as a function of P. All these functions from each solute have then to be inserted into the equilibrium condition. The resultant equation is, not surprisingly, somewhat complicated. Its solution employed the Newton-Raphson procedure, for which the derivative of the resultant equation was determined analytically.

The formulation is not described here because it is contained within the extended peritectic formulation to allow for the option of an interstitial element being of uniform composition within each phase, Section 5.4.5. It is, however, worth describing the behaviour of a two-phase model according to this treatment, in the absence of further such complications.

A computer program has been written which operates by these means for a dual phase situation. A binary test case assumed $D_\alpha = 10^{-5}\exp(-15000/RT)$, $D_\infty = 2D_\alpha$, k=0.6 (i.e. β/α) and m=-20 (for α) with an initial equilibrium profile at 1400°C as pictured in Fig. 5.6. The α phase has the higher equilibrium composition, whereas the β phase has 0.6 of this, but within which the diffusivity is twice as fast. Initially a cooling rate of 1 K/s was imposed. The equilibrium "step profile" for 1400°C was disturbed by the temperature change requiring a change in interfacial composition so as to maintain local equilibrium. With a falling temperature and negative solvus slope, the interfacial composition wishes to rise, pulling a solute profile up with it and causing interface movement so as to maintain the solute balance. The interface movement accelerates as the solute profiles become steeper. After 10 seconds, the imposed cooling rate was reversed and the interface composition was therefore obliged to decrease. The interface

movement, however, continues in the same direction as before, driven by the inherited solute gradients. These gradients are eroded by the falling interface compositions with a consequent deceleration of interface movement. Eventually, the solute gradients and interface movement are reversed. Upon returning to 1400°C, the solute profile is markedly different from the original despite the symmetry of the thermal cycle. Maintaining that temperature, the interface compositions remain constant but the inherited solute gradients still lead to interface movement. This movement decelerates as the gradients diminish, approaching ever more slowly to the original equlibrium condition across the cell (attained to 3 significant figures after holding for 70 seconds).

This behaviour of the program appears rational. Furthermore, this test case was successfully repeated for ternary and quaternary situations. Original profiles of half the amount each of two identical solutes, and a third the amount each of three identical solutes were employed respectively. Logically, the same net result should be observed and, indeed, was observed, which provides confidence that extension to higher order systems did not of itself introduce errors.

Use of an intelligent first guess for P (linear rate of change) enabled the Newton-Raphson iteration scheme to achieve a value correct to 5 significant figures in the first iteration, such that computer run times remained modest.

Very low diffusivites led to pronounced spikes or troughs of composition at the interface in order to maintain local equilibrium (requiring very fine nodal spacings to avoid instabilities). Eventually, of course, local equilibrium at the interface will break down in practice with such low diffusivities, but this is beyond the scope of the formulation. Moreover, local equilibrium should be a fair approximation at the temperatures associated with solidification, as primarily addressed by this project.

5.4.3) Comparison of Formulations

The new formulation described above served to update the interface compositions and position over a given time step such that the result automatically was the unique solution, out of all the unlimited alternatives allowed in a multicomponent system which satisfied the local equilibrium condition, which also satisfied the solute balances. The standard formulation employing previously established compositions and gradients is adequate for a binary system with finite diffusion in both phases; there is a unique equilibrium interfacial composition at a given temperature. Therefore, an obvious validating test for the new procedure was direct comparison of computed results for binary cases. On the thermal cycle described in the previous section, the results were, indeed, essentially identical (as was the case with further, simpler test cases employed).

Extension to multicomponent systems, although beyond the scope of the standard approach for testing, involves no different procedures in the new formulation and it is therefore presumed that its application to such systems is equally valid. Mathematical cross-validation of its behaviour is not possible, however. Kirkaldy [113] quotes a solution for isothermal phase reaction in multicomponent systems, but this is not an acceptable test case because he assumes maintenance of constant interfacial compositions: even in an isothermal case, the concentrations of distinct solutes must change in accordance with the changing solute gradients and interface movement, as with the example in Fig. 5.7.

5.4.4) Incorporation into Peritectic Model

The new routine described above can move a phase interface around with suitable choice of the unique set of compositions which satisfies both the temperature and the interface movement. The target, however, is a model which can cope with and, indeed, automatically assign all the various routes allowed by a peritectic section, Fig.5.8. Further

procedures are needed to cope with the onset of a new phase and the disappearance of an old one, particularly in respect of the formulation as there will be too few nodes on one side of the interface for the treatment described above to operate.

The disappearance of one phase can be handled initially by assigning values to the virtual nodes beyond the boundary of the representative cell. This can be accomplished because the boundary is reflective and the values will be those of the corresponding nodes within the cell. For when there is less than a nodal spacing of one phase left, an additional routine was constructed which assumed that the disappearing phase was of a uniform composition, i.e. equivalent to the solid/liquid routine at solidus. For the peritectic case as follows, this would have involved the construction of a routine of similar complexity to the main solution where both ferrite/austenite and austenite/liquid interfaces have to be solved simultaneously. Instead, it was decided simply to lose the old phase once there was less than a nodal spacing of it left.

5.4.5) Interstitial Streamlining

In the previous section the state of development of the micro-segregation model was already satisfactory insofar as it met the targets of a flexible computer program able to invoke and handle ferritic, austenitic or three phase peritectic solidification as appropriate, for multicomponent alloys with local equilibrium at each phase interface and diffusive control of interface motion. Furthermore, it could consider a planar, cylindrical or spherical morphological cell on a primary (static) or secondary (coarsening) dendrite arm basis, and could go on to consider the subsequent sub-solidus motion of a remaining δ/γ interface, and the continuing adjustments to the micro-segregation profile. Additional targets were identified, however, i.e. incorporation of a δ/γ heat of transformation (previously ignored in comparison with the solid/liquid latent heat) and assumption of complete mixing for the rapid interstitial diffusion of carbon (already found

to be a good approximation in this and other work [5,29,118], and avoiding the orders of magnitude increase in run times required from the previous program with time increments dictated by carbon).

Both these targets required a new central formulation for the peritectic reaction whereby both interfaces were solved simultaneously, i.e. N γ/L and N δ/γ interfacial solute balances for N solutes other than carbon, local equilibrium equations for both interfaces, a single (three-phase Lever Rule) solute balance equation for carbon for the whole cell, and a single heat balance equation incorporating both γ/L and δ/γ heats of transformation. With discretisation performed as before:-

Solute balance, γ/L, i = 1 to N,

$$Zl_{1,i}\left(1 - k_{(\gamma/L)i}\right)\left(fs_2 - \left(Xs_1/L_2\right)^n\right) = \delta t\left(n/Xs_1\right)\left(Xs_1/L_2\right)^n D_{\gamma i} \cdot \frac{\partial Z_{(\gamma/L)i}}{\partial x}$$

$$+ \left(1 - fs_2\right)\left(Zl_{2,i} - Zl_{1,i}\right) + \left(Zl_{1,i} - Zo_i\right)\left(1 - \left(L_1/L_2\right)^n\right) \qquad (5.21$$

where

$$\frac{\partial Z_{(\gamma/L)i}}{\partial x} = \left(Zl_{1,i}\, k_{(\gamma/L)i} \cdot \frac{(1 + 2Ps)}{Ps(1 + Ps)} - Z_{(Rs-1)i} \frac{(1 + Ps)}{Ps} + Z_{(Rs-2)i} \frac{Ps}{(1 + Ps)}\right)/Xn$$

Solute balance, δ/γ, i = 1 to N,

$$Z\delta_{2,i}\left(k_{(\delta/\gamma)i} - 1\right)\left(fs_2 - \left(X\delta_1/L_2\right)^n\right) = \delta t\left(n/X\delta_1\right)\left(X\delta_1/L_2\right)^n \left\{D\delta_i \cdot \frac{\partial Z_{(\delta/\gamma)i}}{\partial x} - D\gamma_i \cdot \frac{\partial Z_{(\gamma/\delta)i}}{\partial x}\right\}$$

where (5.22

$$\frac{\partial Z_{(\delta/\gamma)i}}{\partial x} = \left(Z\delta_{2,i} \cdot \frac{(1 + 2P)}{P(1 + P)} - Z_{(R-1)i} \frac{(1 + P)}{P} + Z_{(R-2)i} \frac{P}{(1 + P)}\right)/Xn$$

and

$$\frac{\partial Z_{(\gamma/\delta)i}}{\partial x} = \left(-k_{(\delta/\gamma)i} Z\delta_{2,i} \cdot \frac{(7 - 2P)}{(3 - P)(4 - P)} + Z_{(R+2)i} \frac{(4 - P)}{(3 - P)} - Z_{(R+3)i} \frac{(3 - P)}{(4 - P)}\right)/Xn$$

Local equilibrium, γ/L,

$$\delta T = m_{(\gamma/L)C} \cdot \left(Cl_2 - Cl_1\right) + \sum m_{(\gamma/L)i}\left(Zl_{2,i} - Zl_{1,i}\right) \qquad (5.23$$

Local equilibrium, δ/γ,

$$\delta T = k_{(\delta/L)C} \cdot m_{(\delta/\gamma)C} \cdot \left(Cl_2 - Cl_1\right) + \sum m_{(\delta/\gamma)i} \left(Z\delta_{2,i} - Z\delta_{1,i}\right) \qquad (5.24$$

Carbon, whole cell,

$$Cl_2 = Co/\left(1 - \left(1 - k_{(\gamma/L)C}\right) fs_2 - \left(k_{(\gamma/L)C} - k_{(\delta/L)C}\right) f\delta_2\right) \qquad (5.25$$

(Note: $C_\gamma = k_{(\gamma/L)C} \cdot Cl$, $C_\delta = k_{(\delta/L)C} \cdot Cl$, uniform within a phase)

Heat balance, whole cell,

$$Q.\delta t = H_L\left(fs_2 - fs_1\right) + H_\delta\left(f\delta_2 - f\delta_1\right) + \delta T\left(Cp_L\left(1 - fs_1\right) + Cp_\gamma\left(fs_1 - f\delta_1\right) + Cp_\delta f\delta_1\right)$$

Required, subsidiary equation, *fraction ferrite*, (5.26

$$f\delta_2 = \left(\left(X\delta_1 + \left(P_2 - P_1\right)Xn\right)/L_2\right)^n \qquad (5.27$$

Thus described, the unknown values at the start of a time increment are fs_2, $Zl_{2,i}$, $f\delta_2$, $Z\delta_{2,i}$ (noting its direct appearance within the governing equation and also within the δZ/δX formulation), P, δT and Cl_2. There are evidently 2N+5 independent equations and 2N+5 unknown variables, whereupon a unique solution should be obtainable. Library routines for the solution of such a complicated set of non-linear non-symmetrical simultaneous equations were not available. Therefore, manual algrebraic manipulation and cross-substitution was performed in order to render down the set to a single equation in terms of a single unknown, to be solved by Newton-Raphson iteration. (Subsequent back substitution could then be peformed in order to generate the other unknown values.) Furthermore, the solution scheme should be devised in such a way that iterative procedures (which obviously extend run times significantly) were not required for the generation of component terms within the final equation. Moreover, multiplication or division throughout by solute specific terms would be avoided, enabling the computer model to operate with or without carbon or other solutes, i.e. with zero-percent of any solute.

The chosen primary variable was P, denoting the position of the δ/γ interface between the nearest nodes of the finite difference scheme. The final equation was Equation 5.26 but with fs_2, $f\delta_2$ and δT expressed as functions of P.

The relevant function for $f\delta_2$ is relatively trivial and has already been provided by Equation 5.27. The function for fs_2 is given by a root of the following quadratic equation:-

$$\left(H_L/Cp\right)fs_2^2 + \left(a_1 + a_2\right)fs_2 - \left(a_1 + a_3\right) = 0 \qquad (5.28$$

where

$$a_1 = \left(H_\delta/Cp\right)f\delta_2 - \left(Q\,\delta t + H_L fs_1 + H_\delta f\delta_1\right)/Cp + \left(1 + a_4\right)a_Z$$

$$a_2 = a_4 \sum m_{(\gamma/L)i}\, Zl_{1,i}\left(1 - k_{(\gamma/L)i}\right) - \left(H_L/Cp\right)$$

$$a_3 = \left(Xs_1/L_2\right)^n\left(a_2 + \left(H_L/Cp\right)\right) + a_4 \sum m_{(\gamma/L)i}\left\{\frac{n}{Xs_1}\left(Xs_1/L_2\right)^n \delta t\, D\gamma_i \frac{\partial Z_{(\gamma/L)i}}{\partial x}\right.$$

$$\left. + \left(Zl_{1,i} - Zo_i\right)\left(1 - \left(L_1/L_2\right)^n\right)\right\}$$

$$a_4 = k_{(\delta/L)C}\, m_{(\delta/\gamma)C}/\left(m_{(\gamma/L)C} - k_{(\delta/L)C}\, m_{(\delta/\gamma)C}\right) \qquad (5.29$$

An additional component, a_Z, is here defined separately as it will also be required later:-

$$a_Z = \sum m_{(\delta/\gamma)i}\left(Z\delta_{2,i} - Z\delta_{1,i}\right) \qquad (5.30$$

where

$$Z\delta_{2,i} = \frac{\frac{n\delta t}{X\delta_1 Xn}\left\{D\delta_i\left(Z_{(R-2)i}\frac{P}{(1+P)} - Z_{(R-1)i}\frac{(1+P)}{P}\right) - D\gamma_i\left(-Z_{(R+3)i}\frac{(3-P)}{(4-P)} + Z_{(R+2)i}\frac{(4-P)}{(3-P)}\right)\right\}}{\left(k_{(\delta/\gamma)i} - 1\right)\left(f\delta_2 - \left(X\delta/L_2\right)^n\right) - \frac{n\delta t}{X\delta_1 Xn}\left\{D\delta_i\frac{(1+2P)}{P(1+P)} + D\gamma_i\, k_{(\delta/\gamma)i}\frac{(7-2P)}{(3-P)(4-P)}\right\}}$$

The remaining function of P (both directly and through other functions of P already defined) for insertion in Equation 5.26 is as follows:

$$\delta T = k_{(\delta/\gamma)C}\, m_{(\delta/\gamma)C} \left\{ Co/\left(1 - \left(1 - k_{(\gamma/L)C}\right) fs_2 - \left(k_{(\gamma/L)C} - k_{(\delta/L)C}\right) f\delta_2\right) - Cl_1 \right\} + a_Z \qquad (5.31$$

The Newton-Raphson iterative scheme for the solution of the overall equation provides successive improvements to previous guesses for the required value of P:-

$$P_{new} = P_{old} - F(P_{old})/F'(P_{old}) \qquad (5.32$$

where F(P) is Equation 5.26 suitably substituted with Equations 5.27-5.31 and rearranged such that it equals zero with the correct P, and F'(P) is the derivative of that function with respect to P. The equation for this derivative was obtained analytically, but will not be reproduced here. (It is, however, obviously contained within the progam listing, Appendix.) The first guess was originally obtained by assuming a linear rate of change of P from the previous two iterations, for which the function F(P) generally converges within 10^{-15} of zero in only 4-6 iterations for each time increment. However, for little effort a second-order first guess can be used which should circumvent one or two iterations, namely:

$$P_{new} = 3*P - P_{old} - P_{older} \qquad (5.33$$

As one might expect, it is not a simple matter to check whether or not this formulation (and its subsequent programming) is right. There are, however, numerous hopeful pointers: the evident convergence of the Newton-Raphson scheme, close agreement between temperatures at the different boundaries, close maintenance of the set heat extraction or cooling rates, conservation of solute, etcetera. Certain more specific tests are also possible. A pure hypo-peritectic Fe-

C binary composition under a prescribed heat extraction rate will automatically exhibit a temperature plateau during the entire peritectic reaction as treated by the current formulation, in accord with theory, with adjustment of phase proportions but not of phase compositions. (The alternative prescribed cooling rate control is not tenable in this case as it would require an instant step change in solid phase proportions at the peritectic temperature, i.e. an impossible case for which the program should be excused failure. Such a scheme could not occur in situations represented by the current unit cell whereby the temperature across the finite cell is assumed to be uniform.)

Alternatively, carbon-free compositions can also be considered and compared with the previous, non-interstitial program, (or indeed steel with carbon present but treated as a finite diffusivity species). Very similar answers are obtained, and tend to exact equivalence with increasing numbers of nodes. In the absence of carbon, there is no direct link between the δ/γ and γ/L interfaces apart from temperature, but the combined formulation presented here is still valid. Also, this absence of a link means that the δ/γ interface should be unaffected by the attainment of solidus, although the program will hand on the solution to a different sub-routine at this stage. Indeed, despite this change to a different solution scheme, the program does show a continuous, smooth variation in δ/γ interface parameters.

The target, of course, is comparison with experiment although this is not a simple matter either. In terms of the computer model this requires proper multicomponent equilibrium data and diffusion data to be supplied. In terms of the experimental comparison this requires appropriately averaged data as each dendrite is unique with a wide variation in solute profiles.

5.5) ADDITIONAL FACILITIES

5.5.1) Start-up Procedure

At the onset of solidification, the numerical procedure can only be invoked once sufficient nodes exist in the solid, i.e. a minimum of three composition points for determination of solute gradients. Either Scheil or lever rule equations are employed for this purpose. As to which is a better aproximation for a given solute depends on its diffusivity and the time and distance in question, as described by the Brody-Flemings back-diffusion parameter (Section 4.1). The diffusivity is calculated for the liquidus temperature, and the distance is defined by the cell size and the fraction of it in question determined by the numbers of nodes requested.

The time has to be estimated. For cooling rate control, the time is calculated from the distances, hence fraction solid, as a fraction of the total solidification time which would accrue for lever rule solidification. For heat extraction control, the time is estimated from the fraction solid and heat extraction rate, assuming no corresponding temperature change. The back-diffusion parameter, α, is then generated for each solute and the lever rule or Scheil equations are employed for the initial nodes depending on whether α is greater or less than 0.1. (The Brody-Flemings or Clyne-Kurz equations only give the residual liquid compositions, whereas the solute profile is required here.)

This procedure is performed automatically by the program.

A similar problem is encountered at the start of the peritectic reaction when there is too little austenite for the finite difference scheme to operate properly. The solution here, however, must operate simultaneously with the finite difference scheme continuing within the ferrite. Most substitutional solutes would be in closer agreement with the Scheil equation than the lever rule for austenite and this is achieved by operating the full peritectic solution scheme but with an artificial, zero diffusivity for all solutes in the austenite until sufficient nodes have been established for proper operation.

The absence of any flux into the austenite at the δ/γ interface can result in incorrect movement of the interface into the austenite, whereas the fact that the peritectic reaction has been invoked means that the austenite should encroach into both liquid and ferritic solid. Generally, carbon is present for which there is the option to consider it as uniform within each phase (three-phase Lever Rule) and such is its dominance that it tends to drive the interface into the prior ferrite even if the substitutional elements alone are baulked by their artificially curtailed diffusion. In the absence of carbon, the incorrect interface movement can persist for some time, sometimes right until sufficient nodes have developed for the full finite difference scheme to operate. Only seldom does the δ/γ interface outpace the γ/L interface such that the austenite is reduced, so this tends to be only a temporary problem for the overall program operation. Resultant, locally false composition profiles will tend to have a smaller effect the greater the elapsed time modelled thereafter and, of course, the greater the number of nodes employed.

A more common problem with the scheme appears when the peritectic is only reached at very high fractions solid. The temporarily curtailed austenitic diffusivites means that one is attempting to reach solidus while employing the equivalent of the Scheil equation. In response to the program prompt at arrival at the peritectic, it is advised that the array is regridded to create sufficient nodes such that this problem with the austenite start-up is passed safely prior to solidus.

Despite the logical preference to maintain the diffusivity in austenite less than that in ferrite, it is arguably preferable to adopt a lever rule type of austenite start-up to avoid such problems.

5.5.2) Secondary Dendrite Arm Coarsening Law

The computer model includes the effect of secondary dendrite arm coarsening in the manner discussed in Sections 2.4 and 4.2.3b. In summary, the curvatures which cause coarsening are not considered in the formulation, but coarsening is imposed upon the system, and this should therefore be done in a manner which approximates to practice. Any coarsening law could be imposed. One commonly observed relationship for the bulk of solidification is a third power law on time (Section 2.4). The direct application of this law still leaves a finite coarsening rate at solidus, which is unrealistic and, moreover, may encourage instability in operation of the computer progam. In practice, the arm coarsening during the initial stages of solidification is largely irrelevant to the residual liquid composition firstly because the resultant segregation is quite insensitive to size until later on, and secondly because the bulk of early solidification will be on the primary arms. At the end of solidification, the change in coarsening mechanism to one of coalescence is less likely to affect micro-segregation between secondary dendrite arms than are the earlier coarsening mechanisms, and also, the coarsening would be naturally curtailed.

The core composition of the secondary arms will be strongly dependent on the spacing in relatively early stages of solidification, once secondary arms have established a significant presence on the primary stem. It is not thought appropriate to start the conceptual model/ representative unit cell with spindley arms of zero spacing. (Furthermore, a mathematical problem with this start-up is that the zero unit cell begins with a fraction solid of unity!)

Currently, versions of the program exist with three arm coarsening treatments.

(i) The imposed coarsening law adopted in the computer model has an initial arm spacing and a subsequent coarsening rate proportional to the residual fraction liquid. This automatically reduces to zero towards the end of solidification as desired and, at intermediate stages, is found to be a reasonable approximation to a third power law, Fig.5.9 . The departure from this law noted in the very early stages coincides with where it does not matter as far as the residual liquid is concerned, and before the system has attained the form of the representative cell anyway. Although this could affect the core composition, it will be minimised by appropriate choice of initial spacing, λ_o, and subsequently elapsed modelled time.

The arm spacing can therefore be described as:-

$$\lambda = \lambda_o + \Sigma\ \alpha(1-f_s)\delta t \qquad (5.34$$

(ii) Arm coarsening may also proceed by any specified constants B and n in the equation $\lambda=Bt^n$. This is considered in detail in Section 5.6.3.

(iii) Very recently, a composition dependent arm coarsening equation due to Beaverstock (82) has been incorporated which is a multicomponent version of Kirkwood's theoretical treatment for binaries (73). The assessment of this alternative, however, lies beyond this thesis.

5.5.3) ReMeshing Procedure

Previous programs have employed the same node spacing, as established at the beginning of the computation, throughout the entire run. A fine node spacing with consequently small time steps and increased run time is often only required for very sensitive regions as when a phase disappears. Economies should therefore be obtained by a routine to regrid the representative cell with different node numbers as and when

desired. Moreover, the arm coarsening feature results in a non-integral node at solidus, and remeshing at this stage would facilitate continued calculation.

Crank and Gupta [150] suggested remeshing should be achieved by a third order equation (i.e. higher than the second order to which finite difference schemes operate) derived from the four points on the 'old' grid surrounding a target point on the 'new' grid, Fig.10a . This polynomial would be constructed so as to reproduce the four old values and the second-difference values on the old grid, as used in the diffusion calculation for 1D, either side of the new point. The origin is defined as the point on the old grid (ith node) immediately before the target point (jth node), which is a distance 'p' away in units of the old node spacing (not to be confused with the 'big P' used for locating the interface between nodes), whereupon:-

$$Zj = Zi + Ap + Bp^2 + Cp^3 \qquad (5.35$$

Derivation of the constants, A, B and C can be made in accordance with the desired polynomial stated above, whereupon:-

$$A = Z_{(i+1)} - Zi/2 - Z_{(i-1)}/3 - Z_{(i+2)}/6$$

$$B = \{Z_{(i+1)} - 2Zi + Z_{(i-1)}\}/2$$

$$C = \{Z_{(i+2)} - 3Z_{(i+1)} + 3Zi - Z_{(i-1)}\}/6 \qquad (5.36$$

In the present programs, the interfaces can exist between nodes, as indicated by a parameter, P, again in units of the old node spacing (Fig.10b). A remeshing interpolation procedure was derived in a similar manner for this situation near an interface, with the following resultant constants:-

$$A = Z_{(i+1)}[(1+2P)/3P] - Zi.[(2+P)/3(1+P)] - Z_{(i-1)}/3 - Z_I/[3P(1+P)]$$

$$B = \{Z_{(i+1)} - 2Zi + Z_{(i-1)}\}/2$$

$$C = \{Z_I.2 - Z_{(i+1)}(1+P)(2+P) + Zi.2P(2+P) - Z_{(i-1)}P(1+P)\}/[6P(1+P)] \quad (5.37$$

It can be seen that these reduce to the previous values (Equation 5.36) with P=1.

Resultant interpolation by this technique appears to give satisfactory results, e.g. Fig.5.11. Some idea of the flexibility available from such a procedure is given in Figure 5.12 which, for a specified test case, plots the difference in residual liquid concentration at solidus from the datum calculated with 100 nodes throughout solidification, for repeat runs regridded from 10 to 100 nodes at specified fractions solid. It can be seen that there is negligible loss of accuracy even if the remeshing is performed as late as 0.95 fraction solid. Similar results have been presented in Table 5.3.

5.5.4) Line Compound Precipitation

The main precipitate considered here is manganese sulphide which is deposited from the melt at the end of solidification of the majority of steels. (This is not strictly a "line compound" as some element substitution can occur, such as Fe if the Mn level in the steel is fairly low, Cr in stainless steels, and Ca in calcium-treated steels even with only a small fraction of a percent Ca present in the steel. Moreover, oxygen can substitute to a considerable extent for sulphur.) A routine was introduced into the original computer model [6] which removes Mn and S from the residual liquid in stoichiometric ratio, and such that a maximum solubility product, Y, is not exceeded. The contents, %Mn and %S, apparent from a program iteration are adjusted as follows:-

$$\%Mn \longrightarrow \%Mn-RZ, \qquad \%S \longrightarrow \%S-Z$$

where R is the atomic mass ratio of manganese to sulphur and:

$$Z=(1/2R).[(\%Mn-R.\%S)-((\%Mn+\%S)^2-4R(\%Mn.\%S-Y))^{0.5}] \qquad (5.38$$

Similar routines could be introduced for other precipitates although it could be problematic if they would represent a substantial fraction of the residual liquid volume. It is a not a rigorous approach, but should be superior to either terminating solidification as soon as the precipitate is stable, or ignoring the desire for precipitation and letting the sulphur, etcetera, plunge the solidus down to unrealistically cold values.

5.6) COMPUTED CHARACTERISTIC BEHAVIOUR

A major problem with this examination is the presence of "side-effects" whenever one wants to assess the influence of a given variable. If one changes the content of an element for example, to see what effect it has on peritectic reaction rates, how much is due to the increased content per se, as opposed to the associated decreased temperature of reaction and altered fraction solid range over which the reaction occurs? All too often, the net result of a single variable change is a balance of various knock-on effects and these have to be borne in mind.

5.6.1) Solute Profiles and Geometry

The normal profile encountered is a continuous increase from core to ID position. In practice, the ID peak should be eventually rounded from sub-solidus homogenisation, but at solidus the profile is expected to be continually steepening towards ID as predicted. Expanding from 1D to 2 and 3D (outward/convex growth) reduces the height of this peak as discussed previously (Section 4.1). Indeed, the whole profile can lie below the corresponding result from a lower dimension. Solute conservation is satisfied in both cases: the higher dimension has a greater proportion at larger radius, albeit of somewhat lower concentration. In Fig.5.13, example plots are presented from SOLVER 6 for 1%Mn, 50MJ/m^{3}S, 50μm static cell radius, for 1,2 and 3 dimensional cells. The peak Mn reduces dramatically from 1D to 2D, and less so for 2D to 3D. The core compositions are all very similar. The 1D plot lies above the other two for all distances r across the cell. The 2 and 3D plots, however, cross over.

Regarding the dendrite core, a given profile with respect to radius will lead to more rapid homogenisation with a higher dimensional basis. However, considering the concentrations originally laid down by the advancing solidification front, for a similar fraction-solid/concentration relationship the higher dimension will have a much shallower profile with respect to distance. Therefore, the core can be less homogenous with increasing dimension, as observed in Fig.5.13 between the 1 and 2D plots. The balance of these factors can only really be assessed by a numerical model.

Inclusion of the peritectic reaction can produce much more varied profiles. Austenite stabilisers will dip towards the core, whereas ferrite stabilisers will enrich, both being subject to subsequent diffusive homogenisation obscuring this effect. These peaks or troughs can be very steep upon the disappearance of ferrite (Fig.5.14), whereupon one wonders if practice obeys prediction. In particular, this could encourage a break-down of the austenite/ferrite interface from the dendritic scale to a much smaller scale, like the vermicular to lacey ferrite morphology change in stainless steels. (Constitutional supercooling could be applying on a smaller length-scale.) This same effect may well occur in other steels where the peritectic carries on, by hook or by crook, to completion, again obscuring evidence of such behaviour. In particular, this could be why these peaks are not generally noted for silicon, although it has been seen in this work, Section 3.4.4.

5.6.2) Diffusivity, Length and Time Scales

This and the following section [152] grew out of the experimental validation exercise on Turkeli's steels, Section 6.2. The sensitivity analysis was essentially restricted to one steel (0.4%C, 1.58%Mn) under two cooling rates (0.3 and 3.7oC/s).

a) Procedure

The partition coefficients and diffusivities were as listed in Tables 4.1 and 4.6. In Turkeli's work, secondary dendrite arm spacing measurements were plotted against time for each alloy and cooling rate. He derived different values for B and n in the generalised arm coarsening equation, $\lambda=Bt^n$, (where λ is dendrite arm spacing) for each case but as no systematic differences were evident, the simplest coarsening law which reasonably represented the entire data was employed as the basis here, namely $10t^{0.5}$. It was also evident that the final spacings within program runs, calculated with either Turkeli's values or the above general approximation, were inconsistent with the final spacings quoted from experiment. Moreover, the experimental results seemed mutually inconsistent in detail, with a trend but no full observance of slower cooling rates being associated with coarser spacings for a given alloy. Turkeli states how he had difficulty measuring the final arm spacings because they were associated with little segregation in his experiments (the majority being associated with the primary arms) so it was decided to use the coarsening laws unrestricted by such quoted final values, but free to reach whatever value resulted from the numerical calculation.

Control was transferred from cooling rate to heat extraction rate (at the current value of heat extraction still under cooling rate control apparent from the calculations at the start of the peritectic reaction, 17 and 200 MJm^{-3} respectively) for the duration of the peritectic reaction, as discussed previously (Section 5.4). A minimum of 40 nodes was employed for the numerical grid. This number would increase as coarsening progressed, but regridding (back to 40) was performed once the array had coarsened up to a maximum of 100 nodes. Numerical convergence (nodal sensitivity) thereupon seemed to be about $\pm$0.001%Mn for the inherently 'delicate' value of the final concentration of manganese in the liquid at solidus, which was considered quite acceptable. This value, termed Peak Mn, was employed as a test variable along with the value in the solid at the origin of the unit cell, i.e. on the dendrite spine, which was termed Core Mn. The streamlining option was employed for the calculations whereby carbon was

considered to be of uniform composition within a given phase.

The one dimensional morphology option was employed (apart from a couple of comparative test runs), as is considered reasonable for well developed secondary dendrite arms (2,5).

b) Background

It had been assumed that a back-diffusion term as employed in analytical treatments was only a first approximation for gauging whether or not more or less micro-segregation would be expected between two cases, as none of the associated assumptions are maintained in practice; viz single solutes, single phase solidification, fixed arm spacing, constant diffusivity, and a prescribed growth law. The computer model considers multicomponent alloys which can undergo the three-phase peritectic reaction, with dendrite arm coarsening, temperature-dependent diffusivity, and no prescribed growth law. It is advisable to consider first the much simpler case of single phase solid state diffusion.

It is evident from the finite difference formulation of diffusion by Fick's second law that if the (microscopic) diffusion modulus ($D\delta t/\delta x^2$) is constant, then the diffusion calculation will be the same. Macroscopically, if a given solute profile is scaled up, or "magnified", by a factor F, the subsequent diffusive adjustment of that profile will be identical if the time scale is increased by a factor F^2, or, if the diffusivity is increased by F^2, i.e. it will actually be the same calculation. If the temperature varies, thereby varying the diffusivity, this similarity will still be maintained if that variation is the same between each program iteration. This can be defined as a "macroscopic" version of the diffusion modulus, as mentioned above, viz:

$$M = D(T).t/X^2 \qquad (5.39$$

which will still describe similarity between cases when D is a function of temperature, D(T), although no actual numerical value for M could then be defined. There is thus a substantial basis to a term akin to the back-diffusion parameter, α, without invoking solidification and prescribed growth laws.

c) Numerical Investigation of the Influence of the Diffusion Modulus

For the example taken from the work of Turkeli (1), micro-segregation measurements were taken at the two cooling rates, W. Presupposing that a situation is sought whereby both yield the same micro-segregation, they will have the same temperature interval, ΔT, between liquidus and solidus, whereupon the local solidification time will be given by $\Delta T/W$. The macroscopic version of the diffusion modulus, Equation 5.39, can now be derived for each program run:

$$M = D(T).\ \Delta T\ /\ W.\ \lambda^2 \qquad (5.40$$

Dendrite arm spacings of about 40 and 140μm should compensate for the cooling rate difference from 3.7 to 0.3K/s. Examples of this are presented in Table 5.5 (static dendrite arms as considered thus far corresponding to the coarsening exponent n=0). Surprisingly, it can be seen that, like simple solid state diffusion, the same degree of micro-segregation is encountered if this modulus is the same. Unlike the Brody-Flemings or associated analytical treatments, however, this term M is not quantifiable in advance of the computer run and cannot be used to predict the level of microsegregation other than by comparison with results from a previous computer run.

Therefore, this investigation has found that M still applies with multicomponent systems, going through the three-phase peritectic reaction. There must be some mathematical reason for this equivalence as identified for simple solid state diffusion, within the "solute balance" formulation, i.e. the apportioning of solute around the interface as the interface advances.

The solute balance formulation employed within the SOLVER 6 micro-segregation program is very complicated (Section 5.4) but for a given species Z is based upon the following for the solid/liquid interface (Fig.1.2a, expanded in Section 5.4):

$$A = B + C + D \qquad (5.41$$

Component A is the solute change required by movement of the interface, B is the solute loss from the interface by diffusion into the bulk solid, C is the solute change in the residual liquid, and D is that associated with the expansion of the representative cell so as to mimic the arm coarsening process, in the manner proposed by Kirkwood [3,5]. For the one-dimensional unit cell, three out of these four groups of terms involve dimensionless fractions and would therefore yield the same results regardless of length and time scales, or diffusivity. Without diffusion, the micro-segregation behaviour is independent of length and timescales (as in the standard Scheil equation). Therefore it is the remaining term, B, which requires attention. (The schematic solute balance for the solid/solid interface is given in Fig.1.2a, where finite diffusion terms apply both sides of the interface, and for which $A=B_1+B_2$, the component formulations A and B being similar to those above.)

Diffusion within the solid varies according to the modulus as described. Therefore, there is some logic in the micro-segregation behaviour varying as a function of this modulus. However, the diffusive term, B, is not written expressly as a function purely of this modulus, and it has not proved possible to demonstrate its equivalence to such a function. The fact remains, however, that the numerical model demonstrates this result. Evidently it is an inherent result from the diffusion modulus employed in Fick's Law for diffusion within the instantaneous solute balance at the phase interfaces; it continually changes during solidification, and indeed sub-solidus, but these changes are occurring in parallel, yielding the same result at any stage.

5.6.3) Secondary Dendrite Arm Coarsening Parameters

a) Procedure

This was performed in the same investigation as for the previous section.

Coarsening laws determined from experiment are generally of the form:

$$\lambda = Bt^n \qquad (5.42$$

where B and n are constants whose values vary widely (n=0 to 1) between references. In particular, n=0 corresponds to a static, fixed arm spacing of B, reasonably valid for primary arms but admitted as an approximation in the absence of a more detailed treatment for secondary arms. The highest power reported from experiment is n=1, whereby the dendrite arm spacing increases with time linearly [4]. The most popular value, with some approximate theoretical backing, is around n=1/3, but reducing upon approach to solidus [3].

In the present exercise, the variation in the prediction of Core Mn and Peak Mn contents, as described before, has been studied as a function of B and n, pivoting around the values which yield the 40 and 140μm arm spacings for the experimental 3.7 and 0.3K/s cooling rates. Additionally, multiplying factors have been applied to the base temperature-dependent diffusivity employed.

b) Modulus Equivalence

For given 'n' values, values of B were determined which yielded 40μm at 3.7K/s or 140μm and 0.3K/s. It can be seen from the peak and core manganese contents, Table 5.5, resulting from the respective runs of the numerical model that these were the same for a given 'n' value, and the segregation decreased (both core and peak closer to the bulk value of 1.58%Mn) as 'n' increased.

This equivalence is specific to the arm-spacing/cooling rate combination, i.e. the level of segregation is not the same for a given 'n' regardless of the final arm spacing or the associated 'B' value in the coarsening law.

c) Peak Manganese Concentrations

The results for the peak manganese contents for various values of B are plotted in Figure 5.15 against the adopted value of n, the points representing Peak Mn taken from individual computer runs. Several issues can be raised from this figure, providing insights into the segregation response.

Considering first the results for the single cooling rate of 3.7K/s, for a given 'n', segregation increases as 'B' increases, i.e. as the length-scale increases. Results with static spacings (n=0, fixed arm spacing=B) show how the peak segregation increases dramatically with increasing B. This dramatic effect is soon lost, however, with the introduction of arm coarsening.

At low values of B, the peak value initially rises as n increases from zero. This simply reflects that the length-scale is increasing, accordingly. However, at high B values, the peak segregation decreases as n rises, and does so continuously. Furthermore, the results from low B values peak and then down-turn as n continues to increase, falling into line with the results from high B values. Indeed, at high n values, the sensitivity of the results to B effectively disappears.

Further understanding of this can be gained by considering Figure 5.16, where for B=10, the temperature-dependent diffusivity has been multiplied by various factors: 0.05,0.2,1.0 and 5.0. It can be seen that this behaves in identical fashion to Figure 5.15. There is evidently a limit, dependent on n, where the peak segregation becomes insensitive to length scale or diffusivity. In the static case (n=0) this

is infinite, as in the standard Scheil Equation (with no physical cut-off employed like a eutectic). This limit plummets, reciprocal fashion, as n increases. It can still be interpreted as a Scheil Equation (zero solid diffusivity) limit, but the process of solute redistribution accompanying dendrite arm coarsening means that, even with zero diffusivity, the peak segregation at solidus is actually finite. This is qualitatively consistent with analytical studies of mine (Section 4.1) and of Mortensen [80] and is examined further in the next sub-section.

The influence of coarsening will be critically dependent on n as, for low powers, the coarsening rate towards solidus will be small, but for high powers it will still be significant. This coarsening rate at solidus will be of much greater importance than any relative rates at earlier stages of solidification.

The family of curves therefore represents the balance between two "forces" influencing the extent of segregation: that whereby increasing n increases the length-scale and thereby reduces the effectiveness of diffusion, increasing segregation, and that whereby increasing n reduces segregation through the solute redistribution process accompanying arm coarsening. At high B (large length scales), where the influence of diffusivity is already small, the results soon approach this Scheil-style limit, whereas at low B, a much higher coarsening power is required before the effect of diffusivity and length-scale is overcome.

Similar behaviour is encountered with variation of the cooling rate. In Figure 5.15, the resultant curve for 0.3K/s has been added to those of the previous curves at 3.7K/s. At high B/high n, it has very little effect, but it has a marked effect at low B/low n where diffusivity is important. Here, a slower cooling rate results in less micro-segregation, as intuitively expected, i.e. closer to the equilibrium result. The drop-off of the slower cooled curve at low n is sufficient for it to cross over curves at the higher cooling rate but of

lower B value. Such cross-over points are those referred to earlier (Section 5.6.3b) where the arm-spacing/cooling rate combinations for a given n value yield the same "modulus" value, and as listed in Table 5.5.

Included in Table 5.5 are the Peak and Core Mn results from a comparative run with $\lambda=10t^{0.5}$ but for a two-dimensional (cylindrical) representative unit cell rather than the standard planar form. Again it can be seen that the results from both cooling rates are identical, within the accuracy of the numerical calculations, although different from the planar results. The Peak Mn is reduced relative to the planar case as expected from simple geometrical arguments, but the reduced Core Mn (i.e. more segregated) is a more subtle balance of opposing effects: a given solute gradient away from the core will lead to more rapid homogenistion in the cylindrical case, but for a similar fraction-solid/concentration relationship, the gradient in the cylindrical case is actually much shallower, Section 5.6.1.

d) Examination of Scheil Limit as Modified by Dendrite Coarsening

Reference was made above to the evident limiting segregation dependent only upon n, i.e. it appeared that even with zero diffusivity and regardless of length and time scales, a finite amount of segregation is encountered in the presence of dendrite arm coarsening, whereas this (mathematical) limit is infinite with a fixed arm spacing, as in the standard Scheil Equation.

Mortensen derived the following equation for this case assuming planar geometry and a constant cooling rate:

$$fs = \left(\frac{(1+n)}{(1-k)}\right) \frac{Z_1^{1/(k-1)}}{(Z1-Zo)^n} \int_{Zo}^{Z1} Z^{k/(1-k)} . (Z-Zo)^n . dZ \qquad (5.43$$

A value of Zl (liquid solute content) has to be found for which the equation integrates to the required fraction solid, i.e. unity in this case. This has to be done iteratively, and the results are plotted as a function of n against results from the numerical model in Figure 5.17. For this purpose, manganese as a sole solute was considered, in order to be directly comparable with Mortensen's binary, single solidification phase treatment, employing the partition coefficient for austenite/liquid (0.78). A low diffusivity of a twentieth of that otherwise adopted for manganese has been employed which, from comparison with Figure 5.16, should be reasonably close to the implied Scheil limit for n much above 0.25; the computer program cannot run with zero diffusivity. The coarsening law $\lambda=10t^{0.5}$ was employed, with a constant cooling rate of 1K/s.

It can be seen in Figure 5.17 that the numerical results are in excellent agreement. This should be the case, because Mortensen's treatment is a true analytical equation in that no approximations have been made. Therefore, if the computer model is restricted to mimic Mortensen's Scheil-style assumptions and constant cooling rate, one hopes it would agree, despite the totally different formulation and calculation procedure, because there can only be the one "right" answer.

The computer model allows for interactions between solutes on each others' partition coefficients and solvus slopes. However, no such effects were included in these program runs, and it was expected that the same Mortensen limit should apply in the target ternary Fe-C-Mn case (once the carbon content was increased such that a single solidification phase ensued, the peritectic reaction being beyond the scope of the analytical equation). In Figure 5.18 it can be seen that the results are broadly similar, although Mortensen's predictions fall below the numerical results at low n, i.e. for which greater diffusivity would be required according to the numerical results. It therefore appears that, even without interactions on partition coefficients and solvus slopes,

additional solutes can have significant effects on each others' behaviour, requiring a multicomponent model rather than considering the separate segregation behaviour of the component binaries.

This was also apparent in the enrichment of solutes during solidification: in a binary, the solute must enrich linearly with time under a constant cooling rate if the solvus slope is constant; in a multicomponent system only the net temperature depression must vary linearly, but the individual solutes need not do so (indeed it is unlikely that the respective solute balances would be satisfied simultaneously if each variation were linear).

The present computer program automatically handles such complications although quantitative theoretical/ mathematical validation is difficult beyond restrictive conditions where true analytical solutions are available, as with Mortensen's equation (Fig.5.17). The comparison with Mortensen's equation has, however, lent considerable confidence to formulation of the computer program.

e) Core Manganese Concentrations

Unlike the peak concentrations, the core manganese concentrations decrease continuously (i.e. segregate more strongly) as n increases for a given B, Figure 5.19: the accompanying increase in length scale reduces the diffusive homogenisation, but the actual coarsening rate towards solidus is largely irrelevant as the solid/liquid interface is sufficiently removed to have little influence on the dendrite core. (The Core Mn result from $\lambda=37.5*t^{\frac{1}{3}}$ suggests a possible drop-off in the curve, but it is thought more likely that this was an artefact of increased grid sensitivity with such a high coarsening rate at solidus.) As with the peak concentrations, the influence of diffusivity is equivalent to that of the B term in accord with the diffusion modulus, Figure 5.20.

The influence of cooling rate is critically dependent on n, Figure 5.19. At low n values, slower cooling results in less segregation (i.e. less depression of the core composition below the bulk value), but the effect crosses over at n=0.5 such that slower cooling would increase the level of segregation for high n values. (Indeed, the same is true of the Peak concentrations, but the cross-over at n=0.5 is hardly apparent in Figure 5.16 because all the values are tending to the coarsening-Scheil limit regardless of length or time-scale at high n.) This cross-over can again be understood in terms of the diffusion modulus. At n=0.5, the length and time scales are obliged to be in the square relationship employed in the modulus. At lower n values (the commonly quoted value being around 0.3 although 0 to 1 have been employed in the literature) the increase in time with slower cooling more than compensates for the increase in cell size from arm coarsening, and segregation is reduced. At higher n values, the opposite is true, and although the increase in time per se would tend to reduce segregation, the accompanying increase in cell size dominates and segregation consequently increases.

Therefore, if the coarsening law is truly of power n=0.5 as suggested as an average value from the work of Turkeli, the level of segregation will be the same regardless of cooling rate. (This is somewhat different from the constant back-diffusion parameter approach of Brody and Flemings, which scales the distance solidified with root time -and employing a constant dendrite arm spacing-, whereas here the dendrite arm spacing is scaled with root time.) This has been employed in the validation exercise reported in Section 6.2.

5.6.4) Diffusivity and Rates of the Peritectic Reaction

The main part of this exercise was conducted to try and separate out the influence of diffusivity alone. To avoid side-effects, the diffusivity was held temperature invariant, and the nominal solutes had the same partition coefficient and solvus slope (based around the simplified data set for

manganese). Furthermore, where more than one such solute was employed, the total amount of solute was kept the same (10%). Thereafter, a matrix of iron, carbon, silicon and manganese was analysed but again with temperature invariant diffusivity (set to the value for that solute at 1450°C from the simplified data set). Two additional runs were performed with nickel. The scheme is summarised in Table 5.6. The program was deployed with a static 50μm half-arm spacing and heat extraction of 10MJ/m^{3}s. The data set included silicon even when silicon was not present, and set accordingly to zero i.e. to equate the time steps which would be set by the relatively rapid diffusion of silicon. The only exceptions to this were the binary iron-carbon runs where, with carbon assumed to be uniform in a given phase, such fine steps were irrelevant. 60 nodes were employed.

a) Binary Fe-10%"Mn" with Various Diffusivities

The liquidus temperature will obviously be the same regardless of diffusivity, as solidification is deemed to start at the equilibrium value. Similarly, the temperature at the start of the peritectic reaction will be unaffected (as will the residual liquid concentration, necessarily) but the associated fraction solid will vary between the Scheil and lever rule limits. These, respectively, are for the adopted k of 0.74, f_s=0.585 (c.f. slowest diffusivity numerical result, $D_{Mn}/20$, f_s=0.594) and 0.776 (infinite diffusivity numerical "streamlined" result, f_s=0.776). The same limits are also true for the following section.

Firstly, it was encouraging to see that the program satisfied these limits, and did tend to the infinite diffusivity result (from employment of the streamlining option normally reserved for an interstitial like carbon) with increasing diffusivity. The fraction solid at the start of the peritectic and the temperature of the solidus varied with diffusivity in a simple and expected sense (Fig.5.21). (Fraction solid and temperature are plotted against the reciprocal of the multiplication factor, F, applied to the base diffusivity of Mn.) Similarly, other parameters like homogeneity and

solidification time varied progressively in the expected sense. However, the variation was not simple for several variables, like temperature or fraction solid, at the end of the peritectic reaction.

It appears that the end of the peritectic reaction is still susceptible to "side-effects" even in the current exercise where most have been accounted for. As diffusivity is reduced, the peritectic begins at smaller fractions solid. Precisely where the reaction ends depends on the balance of having less ferrite to remove, versus having a slower reaction rate to remove it. Even so, the average rate of ferrite removal does not vary in a particularly simple fashion, although it does at least always reduce with reducing diffusivity (Fig.5.22). It is not just a question of diffusivity, but the associated solute gradients, which will depend also on the fractions solid, etcetera. (If the reader is worried about the apparently precipitous fall from the infinite diffusivity result, i.e. zero on the reciprocal axis employed, the slope will be amazingly shallow on a non-reciprocal axis!)

For a solute of zero diffusivity, the Scheil equation solution is mimicked towards the core, tending to infinity or zero depending on whether k is less or greater than unity between ferrite and austenite. In the former case, this means the peritectic reaction is never completed. In the latter case, ferrite is lost at the critical temperature for pure iron (1392°C). Either way, there is no Scheil-style case where delta ferrite persists with austenite sub solidus unless the corresponding Scheil solution for the austenite/liquid interface is arbitrarily curtailed.

It is thought that the program is doing what it should, but is demonstrating how prone results are to interference from variables other than the one in question. The values which are not prone to such side-effects all show simple, logical variation consistent with known analytical limits or intuitive trends.

b) Ternary Fe-X%Mn-(10-X)%"Mn"

Ternary mixes with X=0,1,3,5,7,9,and 10% were computed, with "Mn" distinguished purely by diffusivity, for twice that of the base Mn and also infinite diffusivity, using the "streamlining" option of the SOLVER 6F program. Critical temperatures and associated fractions solid are presented in Fig.5.23. The end points of 0 and 10%"Mn" are as included in the previous sub-section. Although these end points (superimposed for reference in Figure 5.23) did not vary in a simple manner for variables pertaining to the end of the peritectic reaction (loss of ferrite), the variation between the base Mn origin and these end points was simple. Indeed, it appeared virtually linear, indicating that sufficient side-effects had been removed such that the behaviour essentially obeyed the simple law of mixtures.

In Figure 5.24 the rate of peritectic reaction is addressed by two variables, f_R and $\Delta f/\Delta t$ where:

$$f_R = \frac{\text{total gamma encroachment into delta}}{\text{total gamma encroachment into liquid}} \qquad (5.44$$

and

$$\Delta f/\Delta t = \frac{\text{total gamma encroachment into delta}}{\text{associated time taken}} \qquad (5.45$$

both calculated for the total period when all three phases are present. (Example rate comparisons at instantaneous points were more prone to side effects.) It can be seen that the equilibrium case has the highest gamma/delta reaction rate by both these measures (as might be expected, i.e. with no kinetic hindrances). The slower the diffusivity of a solute and the greater its content, the slower is the gamma/delta reaction rate both absolute and relative to the gamma/liquid reaction rate.

c) Fe-C/Si/Mn Matrix

The scheme, involving 0,0.1 and 0.3%C, 0 and 1%Si (a ferrite stabiliser) and 0 and 1%Mn (an austenite stabiliser) is depicted in Table 5.6. With no carbon present, no case reaches the peritectic, whereas with 0.3% carbon present, all cases attain this reaction and complete it prior to solidus. At 0.1%C, the straight binary reaches the peritectic shortly before solidus, continuing ferrite dissolution sub-solidus, as does the corresponding case with 1%Mn, whereas the cases with 1%Si, with or without Mn, do not, Table 5.7.

The addition of the austenite stabiliser increases the parameter f_R (as defined in the previous sub-section), whereas the ferrite stabiliser decreases it. However, both decrease the average rate of ferrite dissolution during the three-phase reaction, $\Delta f/\Delta t$, though Si much more so than Mn. These parameters are included in the table. (Remember that diffusivity is held constant, at the value for 1450oC, to avoid side effects on these rates due to different associated temperatures.)

d) Comparison with FeCNi

Two additional runs were performed, namely Fe-0.1%C,0.5%Ni and Fe-0.3%C,0.5%Ni, nickel being an alternative austenite stabiliser, for comparison, Table 5.7. The value of 0.5%Ni yielded peritectic reactions at very similar fractions solid to the corresponding ones with 1%Mn. Nickel, however, slows the delta/gamma reaction rate much more than manganese does and, unlike Mn, reduces rather than increases f_R. Therefore, it is not a simple case of austenite stabilisers increasing the relative rate of gamma/delta advance compared to gamma/liquid, but a balance of the "characters" of the elements, i.e. diffusivity, partition coefficients and solvus slopes. It is no doubt possible to find a ferrite stabiliser which reduces f_R less than does a certain austenite stabiliser. However, all finite-diffusivity solutes slow the overall rate of reaction, and ferrite stabilisers are more inclined to do so than are austenite stabilisers, as one would expect.

CHAPTER SIX

VALIDATION OF COMPUTED MICRO-SEGREGATION

"In fact in my own calculations, when I first pursued this line of thought, I was out by a factor of 10 to the power 10, to the power 123"

Roger Penrose, in "The Nature of Time" (ref.20)

6.1) COMPARISON WITH JERNKONTORET DATA

The Swedish Jernkontoret institute has produced a compilation of solidification data: "A Guide to the Solidification of Steels" [100], including liquidus, peritectic, and solidus temperatures, dendrite arm spacings and segregation ratios, with provision of cooling curves. It therefore represents an ideal source for comparison with the computer model.

6.1.1) Experimental Procedure

The Jernkontoret experiments were carried out on small ingots (35g) solidified in alumina crucibles within a furnace operating according to a preset cooling rate, and in an argon atmosphere (5ppm O_2). The furnace functioned by resistance heating of molybdenum wire within the alumina sleeve surrounding the crucible. A Pt/Pt-10% Rh thermocouple was centrally located within the specimen to record the actual

cooling curve as opposed to the furnace cooling rate, employing a digital microvolt meter. Calibration was performed on pure nickel melts, and the apparent precision was found to be +/- 2K.

The tubular furnace shell was double walled and water cooled, with the inside chromium plated to give good heat reflection. No insulation was used so that the furnace had a low thermal inertia, enabling cooling rates of up to 2K/s to be achieved down to 1000°C. The samples were quenched in brine within about three seconds from removal at the bottom of the furnace.

The plateaux on the cooling curves were taken as the liquidus temperatures, acknowledging the error due to growth undercooling but noting it to be of little practical significance. Some nucleation undercooling was usually observed before the plateaux were established. The degree of undercooling was generally larger and more varied at the start of the secondary (peritectic) reaction, when present. These temperatures are therefore less accurate. The solidus was defined as the temperature at which the temperature-time curve had its point of inflexion, i.e. with no further evidence of latent heat evolution. Comparative tests were made with determination of solidus upon heating, and (surprisingly) were found to be in reasonable agreement.

It was noted on some experiments that a small fraction of liquid was still present below the reported solidus, but this was not considered to be of practical significance.

All quoted temperatures were mean values of 2 to 5 measurements and are thus not necessarily those which could be evaluated from the reported cooling curves.

Fractions solid during solidification were back-calculated from the cooling curves by a heat balance on the differences between furnace and sample cooling rates. However, it was acknowledged that the liquidus plateaux include the

period of dendrite growth from the side walls before reaching the thermocouple, and the quoted low fractions solid, in particular, will not be strictly related to that of a local volume element.

Metallographic examination was performed with a variety of etches, as appropriate to the steel in question. For the carbon and low alloy steels used for the present comparisons, a saturated solution of picric acid, either in water or in a mixture of water and alcohol, was employed.

The secondary dendrite arm spacings were measured at low magnification, close to and parallel with the primary dendrite stems. At least four secondary arms were counted on each traverse, and at least ten such traverses were performed on each specimen.

Micro-segregation was studied by electron microprobe analysis of samples from the 0.5K/s furnace cooling rate, on two line scans from different areas of the specimens, mainly on secondary dendrite arm traverses. Mean solute analyses from dendritic ("D", arm core) and interdendritic ("ID",final region to solidify between the arms) regions were obtained for the quoted segregation ratios, "I":

$$I_i = Z_i(ID) \; / \; Z_i(D) \qquad (6.1$$

6.1.2) Computational Procedure

The computer program requires the steel composition, heat extraction or cooling rate, and dendrite arm spacing/ coarsening data specific to each test, and equilibrium and diffusion data relevant to the range of alloys in question.

In the absence of a usable MTDATA database for multicomponent steels until the very end of this project, validation of the computer program had to be performed with the simplified equilibrium data as described in Section 4.1, Table 4.1. The validation is therefore restricted to the carbon and low alloy series of 16 steels, for which departures from such non-interactive data should be minimised. The compositions are reproduced in Table 6.1.

For each steel, the elements considered were C,Si,Mn,P,Cr,Mo and Ni. The program version was chosen wherein interstitial, rapidly diffusing carbon was assumed to be of uniform concentration within a phase. This "streamlining" should introduce negligible error, whilst enabling run times to be reduced by orders of magnitude, Section 5.4.5. (Typical run times were around 20 minutes cpu on a VAX 8350.) The low concentrations present of other impurities were ignored. In particular, sulphur was not included, as manganese was always present in sufficient quantity to effectively remove it from the system as MnS at high fractions solid, and without noticeable effect on the Mn content.

The diffusion data were taken from Fridberg et al., wherein the diffusivities of the substitutional elements were related by constant factors to temperature dependent self diffusivities of iron in ferrite and austenite, Table 4.6.

The Jernkontoret results were quoted according to the set furnace cooling rate, but this bore little relationship to the cooling curves from within the sample and would therefore be inappropriate to use in the computer model. Instead, the apparent average heat extraction rate was employed. This was calculated from the quoted liquidus-solidus temperature interval and solidification time, employing 2000 MJ/m^3 for the latent heat and $5MJ/m^3/K$ for the specific heat (no differences assumed for different phases). Little difference in the rate was apparent for all 16 steels, and an average value of 10.25 $MJ/m^{3/s}$ was employed in the computer program, throughout. The comparisons were restricted to the intermediate furnace cooling rate samples, as cooling curves and segregation data were only provided for these, e.g. Fig.6.1.

Dendrite arm spacings at a specified temperature close to liquidus, and at the end of solidification, were quoted for each steel. The arm coarsening routine employed in the program used an initial spacing, and a constant coefficient for subsequent coarsening (Section 5.5.2) proportional to (1-fs), so could not be tied in advance to match the quoted near-liquidus and final values. By inspection, with use of a hand-calculator, an initial half-arm spacing of 15μm and coarsening coefficient of 0.4 were derived for input to the program. Considerable scatter was noted in the experimental values with no apparent explanation, but it was decided to use the same conditions for each steel, rather than to tailor them for each sample; indeed, the random scatter could be due to errors of experimental measurement rather than reality and, furthermore, it is desirable to see if the model is usable without such tailored data which cannot be known in advance of the experiment. The agreement with the Jernkontoret values could only be determined retrospectively. The mean, experimental near-liquidus value was 64μm, σ 8.5, whereas that evident from the computer runs (for the same temperature interval below liquidus as in the experiments) was 71μm, σ 11.5. The equivalent comparison for the final spacings is 114μm, σ 35 versus 117μm, σ 4.5. These differences are not significant, and there was no need to repeat the calculations with amended coarsening data. There was no correlation apparent within the scatter of the data.

The computer runs commenced with 10 nodes, and were regridded to 40 nodes either at a fraction solid of 0.9 or at the peritectic if it occurred late in solidification. All runs were regridded again to 40 nodes (some coarsening having occurred) at solidus, for subsequent sub-solidus computation down to the quoted quench temperature. If the computed solidus fell below the quench temperature, it was allowed to do so, and the computer run would then terminate at solidus. The steel of code J214 was computed to commence the peritectic reaction at a very early stage of solidification, for which a 10-node start was inadequate. This run commenced with 40 nodes. All runs employed a one-dimensional (secondary dendrite arm plate morphology) volume element.

The "D" and "ID" concentrations for the I ratios were averaged with adjacent nodes, taking some rough account of the electron micro-probe spot size as would be employed in their measurement.

6.1.3 Results and Discussion

a) Critical Temperatures

The calculated and experimental liquidus, solidus and peritectic temperatures are compared in Table 6.2. For the experimental liquidus and peritectic temperatures, the results from the intermediate furnace cooling rate in question are supplemented with those from the slowest cooling rate. As described earlier, the liquidus should be in close agreement with the equilibrium result, but any undercooling or inaccuracies in measurement will be least under the slowest cooling rate. For this reason, the graphical comparison in figure 6.2 is with the higher of two liquidus values (i.e. the slower cooling rate result apart from a 1 degree discrepency the other way for steel J202). Good agreement is observed, even though the liquidus calculation routine employs constant solvus gradients for each solute for a given phase interface.

Similarly, the graphical comparison for the maximum peritectic temperature is with the higher of the two results, and good agreement is again observed. Unlike liquidus, the peritectic does not equate to the equilibrium value of the bulk liquid. In the calculations, it corresponds to the equilibrium value of the residual liquid, and therefore it is affected by whatever segregation has occurred thus far during solidification. The main discrepency, however, will be the undercooling, being more marked for one solid phase on another than for liquid from solid; the free energy difference between ferrite and auatenite is very much smaller than that between the liquid and either solid phase. Therefore, if the non-

equilibrium solid phase is already present, there is relatively little driving force to encourage nucleation of the true equilibrium phase. Significant undercoolings are noted on the cooling curves, with no subsequent plateaux established to be sure that sufficiently fast and developed recalescence has occurred to indicate the equilibrium value for the residual liquid at that stage. The computer model assumes no such nucleation undercooling and, indeed, it is probably correct to do so for most applications where a pseudo steady state has occurred (at least in columnar structures) where there is no nucleation problem because austenite is already there from the adjacent, cooler volume element. The better estimate for the "real" temperature is therefore probably that from the slower cooling rate, even though the model considers the intermediate cooling rate. As before, the higher (non-undercooled) value was evident from the slower cooling rate in all but one case.

The corresponding results for values quoted specifically for the intermediate furnace cooling rate are plotted in figure 6.3. Similar trends are observed although the scatter and systematic shift is greater, presumably because of the difficulties with undercooling described above.

From the Table, and more clearly from the graphical comparison in figure 6.2, a systematic drift of computed solidus below the experimental result is observed with lower temperatures. However, the thermal solidus (i.e. determined by thermal analysis) is bound to be in error in the observed sense (i.e. overestimating the temperature at which all residual liquid disappears), so the model is at least qualitatively correct in this indication. The thermal solidus is where no further latent heat release is noted due to distortion of the cooling curve, but the richer alloys will have more persistent, highly segregated liquid films which are of too low a volume fraction to affect the cooling curves. Indeed, the Jernkontoret guide states that quenched liquid was sometimes observed in samples even though they were quenched from below their apparent, thermal solidus temperature.

Statistical correlation of computation against experiment was at 0.1% significance for liquidus (16 data pairs, correlation coefficient 0.990) and, despite the noted drift, for solidus also (16 data pairs, correlation coefficient 0.969 but with a noticeably skewed fit). Despite the low absolute errors in peritectic temperatures, the relatively low number and total temperature range of results led to 5% significance in this case (9 data pairs, correlation coefficient 0.745).

b) Extent of Peritectic Reaction

The computed extent of the peritectic reaction is not just a function of the micro-segregation model, but also of the adequacy of the simplified equilibrium data which it employs. Two obvious measures are the temperature interval between liquidus and the start of the peritectic, and the fraction solidified as ferrite prior to the peritectic. Excellent agreement on the former is displayed in Figure 6.4. In terms of the fraction ferrite, a partially systematic drift is observed, Figure 6.5. Qualitatively, this drift should be expected: the inclusion in the Jernkontoret study of encroachment of dendrites from the sample side-walls in the back-calculation of ferrite fraction (Section 6.1.1) will artificially increase the apparent ferrite fraction; moreover, nucleation undercooling will allow extra ferritic solidification to occur. Both these effects will increase the apparent, measured fraction solid, particularly of low values where there is still a marked temperature sensitivity. Therefore, as with solidus temperatures, departures are noted between experiment and prediction, but there are limitations in the experiment such that these departures are expected.

The temperature intervals and ferrite fractions are plotted against each other in Figure 6.6. These show good correlation, in a simple linear sense for the calculated ferrite fraction and stepped for the experimental ferrite fraction, in accordance with the preceding argument. Although the scatter

was small, even the calculated temperature interval versus calculated ferrite fraction relationship was not monotonic. This is not thought to indicate a lack of self consistency within the calculations, however, because of the multicomponent nature of the alloys. For a binary alloy, under the same heat extraction conditions, there should be a precise (though not necessarily straight) line between these variables, but where both are the net effect of varying proportions of varying species, disproportionate effects on these variables are likely, creating such apparent scatter.

One useful function of the simplified equilibrium data employed is that a peritectic equivalent can be defined, such that hypo-peritectic alloys have values less than unity, and hyper-peritectic alloys greater than unity, for the bulk composition (Section 4.1). The temperature intervals and ferrite fractions are compared with the bulk alloy composition's peritectic equivalent in Figure 6.7. It can be seen that this equivalent is a very satisfactory measure. The largest error is for steel J212, with 9K interval and 0.6 ferrite fraction with a peritectic equivalent value of 1.02. This is, of course, only marginally above the division at unity and, moreover, at the fastest of the three experimental furnace cooling rates, this composition did solidify directly to austenite. Therefore, despite the apparently large temperature interval and ferrite fraction, this steel was obviously borderline between peritectic and fully austenitic solidification.

There was one converse case of a predicted, hypo-peritectic alloy exhibiting no temperature interval or corresponding ferrite fraction (J214). Again, the equivalent was close to the division at unity (0.91). Furthermore, the computer model predicts that this case would have passed right through the peritectic reaction into fully austenitic solidification before the first test temperature was reached (1470°C, i.e. 13K below liquidus) from which the solidification mode could be confirmed.

It therefore appears that the simplified equilibrium data and their derived equivalents are remarkably successful for these carbon and low alloy steels.

One slightly unsatisfactory feature of the computer runs was apparent for steels J201 and J202 where, once the peritectic had been invoked, the peritectic equivalent of the residual liquid decreased, whereas for the other 14 compositions it continued to increase (albeit with a step change in rate). Therefore, one can ~~imply~~ infer from the computer model results that the first two steels should have reached a eutectic, rather than peritectic, reaction, i.e. with the solidification phase oscillating between ferrite and austenite rather than merely changing once only. This is not believed to be the case in practice, although divorced eutectic behaviour as with stainless alloys would be impossible to distinguish from a peritectic at the very late stages of solidification in question (~90-95% solid). Rather, this is thought to reflect incorrect equilibrium and/or diffusion data, with the most likely offending element being phosphorus; at low fractions solid, its content is too low to upset the net result, but at such late stages with marked enrichment of this element, such an effect is possible. Moreover, errors are more likely with enriched solute as the simplified data are based on dilute compositions, with no regard for changing partition or solvus slope coefficients (other than from ferrite -v-austenite). Phosphorus is a very potent ferrite stabiliser, and as such, an overestimation of its extent of segregation with the onset of austenite at these late stages of solidification may well be sufficient to convert the overall, residual liquid composition from a peritectic to a eutectic nature.

Regardless of such difficulties in appropriate data, it is interesting to note that the model is inherently capable of predicting whether a multicomponent alloy ought to be peritectic or eutectic under the applied conditions. Despite the availability of such a prediction, however, the model proceeds in both cases on the basis that a peritectic reaction has ensued.

c) Segregation Ratios

As with solidus, the segregation ratio is a difficult parameter to quantify. There will be some variability due to electron probe beam size and accuracy of its location in terms of measurement but, moreover, there will be tremendous variability in the sample. In relation to its computation, again like the apparent non-equilibrium solidus, it is a highly sensitive parameter and a very demanding test of the model.

The experimental and computed segregation ratios are included in Table 6.3, and are plotted in Figure 6.8. For the peritectic alloys, the minimum content of Cr and Mo does not occur along the dendrite spine. It is very likely that the quoted segregation ratios were maximum/ minimum rather than $Z_i(ID) / Z_i(D)$ as stated, and it is the ratios calculated on this basis (with Ni taken from the same places) which are plotted in Figure 6.8 for such alloys.

Correlation is observed, although three results for chromium and, particularly, molybdenum, are substantially removed from the ideal line of equality. The remaining 21 results are sufficiently close to this line such that it is expected that they fall within the experimental error.

The three unsatisfactory ratios for chromium occur exclusively with the high (>0.5%) carbon steels. It is well known that increasing carbon reduces the partition coefficient for chromium which, in turn, would increase its segregation ratio. The simplified equilibrium data, however, do not include this effect. (Modification of these data is, however, addressed in the following sub-section.) The observed discrepancy is in this sense and, therefore, at least qualitatively correct. The three unsatisfactory results for molybdenum are not, however, explicable from such an effect. They all occur under purely austenitic solidification, but the other three Mo results which are in good agreement with experiment would still have involved austenite at solidus. The experimental data were not available to see whether it is the "ID" or "D" composition in the ratio which is at fault.

In spite of these six unsatisfactory cases, the correlation coefficient between experiment and computation on all 27 data pairs was 0.727, which is significant at the 0.1% level (albeit with a somewhat skewed fit on account of the large Mo errors). Therefore, the overall agreement is found to be satisfactory.

d) Carbon/Chromium Interaction

The results so far are as reported to ECSC [9] and in the MCWASP-V conference [2]. Since then, the issue of the three rogue chromium segregation ratios referred to above has been addressed. The three steels in question are J214,215 and 216. All three were said to be hyperperitectic, although J214 was predicted to go through the peritectic reaction very early in the solidification sequence. Assuming all three were hyperperitectic, there is no need to employ self consistent data as described above (and detailed in Section 4.3) for the three phases. The program was therefore modified so as to employ the alternative austenite/liquid data described in Section 4.3, which do allow for the variation in partition coefficient. (The program was also modified to allow variable solvus slopes, but this was not actually required for these data.)

The modified program was run on a test case of 0.75%C,1%Cr with 1D static arms, and 10MJm^{3}s^{-1} heat extraction. Solute conservation was found to be very poor, and the chromium content at solidus tended to be very high, despite extensive debugging. The peak Cr was greater than would be encountered with the final, minimum partition coefficient active throughout solidification. There was no such problem evident with the program until the very final stages of solidification. This was became evident as a program property rather than a programming fault.

Increasing the number of nodes did not reduce the high final Cr content, but did improve solute conservation, i.e. the peak became sharper (Table 6.4). Coarsening the time step systematically reduced the peak Cr to levels more in line with

expectation, viz the result with the minimum K_{Cr} employed throughout solidification, and also improved solute conservation. The time step was increased up to half the diffusion modulus, i.e. half the limit for stable FD solution. The occasional convergence problem was encountered with the interface solution at this level with few nodes employed, so no coarser time step was attempted.

Basically, allowing solutes to affect each others' behaviour introduces another degree of freedom for the numerics to take liberties with. Normally, one would expect a numerical problem to be reduced by use of more nodes; the only virtue of coarser time steps is that there are fewer iterations for things to go wrong in, which is not particularly satisfactory.

Noting that the program behaviour was perfectly satisfactory until the final stages of solidification, the only question mark is over the sharpness of the peak, provided solute conservation is satisfactory. Given that the test data were segregation ratios substantially sub-solidus, differences in peak sharpness become less relevant because they are self compensating; the sharper the peak, the sooner it blunts with sub-solidus homogenisation. It was therefore decided to proceed to use the program for the rogue Cr Jernkontoret runs, checking that solute conservation was satisfactory rather than worrying particularly about the transient peak at solidus.

The Cr segregation ratios at the respective quench temperatures were, indeed, higher than before as expected from the modified equilibrium data based on MTDATA for the partition coefficients. (The partition coefficients based on Rickinson [145] gave <u>less</u> segregation than with the original data-set.) Also, one Ni ratio was reduced, more in line with experiment, and one rogue Mo result was rendered a little more out of line with experiment. Overall, the correlation with experiment was increased from 0.727 to 0.801 for the full 27 data pairs. The revised graph is presented in Figure 6.9.

6.2) COMPARISON WITH EXPERIMENTAL PERITECTIC Fe–C–Mn STEELS

6.2.1) Experimental Data

Experimental data were made available by Sheffield University from the PhD thesis of Altan Turkeli [78] on measured micro-segregation and the required information for its prediction (dendrite arm spacings and morphology, and thermal history), involving unidirectional solidification experiments on Fe–C–Mn compositions. The three compositions were chosen which effectively spanned the peritectic reaction, viz:

0.10%C, 1.57%Mn ("10C")
0.21%C, 1.60%Mn ("21C")
0.40%C, 1.58%Mn ("40C")

each with low residual contents (0.003%S, 0.005%P, <0.02%other). The 10C steel reaches the peritectic reaction close to solidus with subsequent sub-solidus ferrite dissolution. The 21C steel undergoes and completes the peritectic reaction in the second half of solidification, and the 40C steel does so in the first half of solidification. Samples of each steel were melted and resolidified in unidirectional solidification apparatus at a variety of furnace power settings and specimen withdrawal rates. Under each condition, cooling rates were quoted for both during solidification and between solidus and the final quench temperature. Pairs of primary and secondary dendrite arm spacings were quoted (of which the former were averaged for use in the model), as were EPMA manganese (minimum and maximum) contents, at various temperatures down to the "quench temperature": the coldest temperature reached by the specimen length under investigation, with positions higher up the temperature gradient assumed to represent this final position at earlier stages in its history. Single minimum/ maximum pairs were quoted from longitudinal sections along the temperature gradient, apart from at the quench temperature where a transverse section was analysed (i.e. all the same temperature) and up to five values were quoted. In view of the inherent variability in micro-segregation (up to 20%

relative noted amongst these alternative measurements at the quench temperature), only those values measured at the quench temperature were employed, where the repeat measurements were averaged.

Less variability was noted between these average values from different runs than present amongst repeat measurements in a given run, but useful comparison with prediction should still be possible in view of the amount of data available, i.e. there should be sufficient data to make the trends evident despite the inherent variability of the source values.

6.2.2 Modelling Procedure

Previous experience with the Jernkontoret data [100], and from the work of Kirkwood [3,5], indicated that a 1D coarsening basis was optimum for micro-segregation among secondary dendrite arms (Section 6.1). Turkeli, however, did not quote results for the secondary arms because, in his experiments, they were quite insubstantial and had all but homogenised come the quench temperature. In cross section, his dendrites resembled a "four-leaf clover", and it was felt that a 2D (cylindrical) static basis would be more appropriate for the peak micro-segregation, of half the primary arm spacing (Fig.6.10). The minimum Mn concentrations quoted by Turkeli corresponded to the primary arm cores for which, unfortunately, there was no fully appropriate length scale quoted for purposes of its calculation. Predicted core and peak concentrations were calculated according to three idealised geometries for comparison:

a) Cylindrical representative unit cell, diameter of primary arm spacing (Fig.2.23b)

b) Planar representative unit cell of coarsening secondary arm spacing (Fig.2.24a)

c) Cylindrical representative unit cell, diameter of half primary arm spacing ("clover-leaf", Fig.6.10)

As discussed in Section 5.6, a root-time coarsening law was employed (case b), consistent with the average coarsening behaviour as measured by Turkeli in his experiments. Moreover, this coarsening law renders the results wholly insensitive to cooling rate, whereupon a single run (distinguished only by quench temperature) could be employed per steel type.

The program option was employed as before whereby carbon is assumed to be of uniform composition within a given phase at any given time.

An issue previously identified (Section 5.4.5) was the inherent unsuitability of the computer model/representative cell for progressing through the peritectic reaction at a set cooling rate. With a typical dendrite morphology such that an implicit assumption of the representative unit cell is reasonable (Section 2.8) whereby the solute field is extremely flat in relation to the thermal field, a set cooling rate through the peritectic corresponds to gross step changes in heat extraction rate, causing program instabilities. Given the reasonably dendritic morphology evident in the experiments, it is suspected that the solute field was indeed fairly flat in relation to the thermal field, and that there therefore would have been transient deviations from the quoted cooling rates. Program control was switched from cooling rate to heat extraction rate during the reaction for the purposes of these calculations.

A minimum of 30 (50 at solidus) and maximum of 100 nodes were employed for the FD scheme, depending on the evident sensitivity of a given stage of the program operation; employing the regridding option -Section 5.5.3. The peak composition at solidus is generally still sensitive to the number of nodes within this range, but with the validation restricted to significantly lower quench temperatures very little residual effect would be expected in this exercise. Similarly, the core composition upon final dissolution of ferrite is nodally sensitive, particularly with the cylindrical basis. Runs were repeated with more nodes if evidently suspect core compositions coincided with the disappearance of ferrite, but there was

little incentive to examine the details of nodal sensitivity here because of the lack of a proper data for the alternative representative bases, as discussed above.

Run times varied considerably with cooling rate, liquidus/quench temperature interval, arm spacing, planar/cylindrical basis, and number of nodes but were typically of the order of 10-15 seconds cpu on the VAX 8350/6000. (If only the same could have been said about terminal connect time on our grossly time-shared computer facility.)

The equilibrium data and manganese diffusion coefficients employed were the same as for the Jernkontoret runs, c.f. Section 4.3.

6.2.3 Results and Discussion

The source data and results are provided in Table 6.5.

From the three model bases described above, condition (a) gave lower core and higher peak concentrations than from experiment. Condition (b) happened to give the closest agreement (slightly overestimated, Figure 6.11) with the quoted primary stem cores, but there is no good reason to presume that this was the relevant length scale. Condition (c) also gave a strong correlation (Table 6.5) with core compositions, but generally underestimating the concentration (i.e. overestimating the core segregation). Moreover, condition (c) gave the best agreement with the peak concentrations (which is generally the most important practically), as expected from the observed dendrite morphology.

The results from condition (c) are plotted against experiment in Figure 6.11, all values being ratioed with the albeit similar bulk manganese contents. Reasonable agreement is evident with the peak concentration noting the experimental scatter. The core compositions are noticeably skewed off the ideal 1:1 line in the direction of underestimating the concentration and, moreover, are highly stratified, such that

in practice a given steel tended to have the same core composition regardless of experimental conditions, whereas the calculated values remained sensitive to experimental conditions.

The model successfully predicts the higher peak and lower core manganese concentrations observed with higher carbon contents across the peritectic reaction. The higher peak concentrations would be expected because of the greater proportion of solidification as austenite with consequently much reduced solute diffusivity. A secondary compounded effect would be the marked lowering in solidus temperature from the higher carbon content, lowering the solute diffusivity within a given phase. The lower core concentrations with increasing carbon content are not so obviously expected, because the minimum manganese concentration is liable to occur upon ferrite dissolution which, to a first approximation, should be around the same temperature for all three carbon levels.

A further point demanding consideration is the evident lack of variability with experimental conditions for a given carbon content, apparent in experiment but not in the calculations. The approximate average coarsening law apparent from Turkeli's measurements exhibited an n value of 0.5 for the classic coarsening equation, $\lambda=bt^n$, whereupon the predicted results would be wholly insensitive to cooling rate (Section 5.6.3). Differences would only result in the solid state from quenching out the experiments at different temperatures, i.e. with different extents of sub-solidus homogenisation prior to measurement. It is satisfactory that, considering the mixed morphology with neither primary nor secondary morphology obviously dominant, the experimental results lie within the bounds of the primary and secondary dendrite arm bases. It is not immediately obvious, however, that the secondary arm bases should represent the primary core compositions so well. Perhaps, the secondary dendrite coasening process on four sides of the primary stem of this four-leaf clover morphology, is still dominant on the primary stem, but a non radially symmetric model would be required to confirm this.

Previously, an alternative suggestion [10] was that the ferrite/austenite phase interface could break down during the peritectic reaction, as often apparent in stainless steels. This could still be occurring but is not required to explain the observed stratification.

In view of the above, a single computer run for each steel is sufficient for the secondary arm basis, simply noting the different quench temperatures employed in individual cases: otherwise the results will be the same when the diffusion modulus is the same. A nominal cooling rate of 1K/s was employed, and the results are presented on a time base in Fig.6.13 (for which linear scaling would translate the results to other cooling rates) and on a temperature base in Fig.6.14. The development of manganese concentration on the dendrite cores is presented against temperature in Fig.6.15, where in particular its sharp but very temporary reduction upon the disappearance of ferrite at the core can be noted. (It has been argued [9] that in practice this extreme behaviour may sometimes cause and be limited by a break-down in the transformation morphology around the dendrite cores.) The predictions for each experiment can be read off purely according to the steel type and the quench temperature at which the experiment was terminated. Results thus obtained have been plotted against the experimental measurements, in ratio with the bulk compositions, in Fig.6.12. In comparison with the results previously calculated on the primary arm basis (Fig. 6.11) it can be seen that the agreement is improved (correlation coefficient 0.912 v 0.809). Furthermore, the results are now much less stratified, i.e. the calculated results are no longer more sensitive to the experimental conditions than were the experimental results. In general, these predictions on the secondary arm basis are a little higher than experiment (less segregated) whereas the opposite was true when calculated on the primary arm basis. Again, as stressed before, proper quantification would require a mixed primary/secondary arm basis, rather than one or the other as amenable to calculation at present.

It is interesting to note that the Peak Mn value is highest for the intermediate carbon content (Figs.6.13 and 6.14). No effect of carbon on the partition coefficient or solvus slope for manganese is included in these calculations, but the variation reflects the balance of "side-effects" which typically complicate examination of influences of specific variables on the extent of micro-segregation. As the carbon content is increased, the temperatures are depressed and diffusivities therefore reduced. Moreover, increasing carbon increases the extent of austenitic solidification prior to the peritectic. These effects will promote higher manganese segregation at solidus. Conversely, the solidification time will increase (at a given cooling rate) as carbon content increases, allowing more time for manganese diffusion to take place, and therefore promoting reduced manganese segregation. The balance of such opposing factors is impossible to predict other than by such a computer model.

This point was explored with further runs, one at each carbon level, but with all other factors being equal (constant diffusivity, 1.6%Mn). Critical results are presented in Table 6.6. The peritectic reaction starts at about the same temperature for each, but with a marked difference in fraction solid and, hence, "inherited" solute content. For the 0.21 and 0.4%C steels, it also ends at about the same temperature. The 0.1%C steel behaves differently in this respect because it reaches solidus prior to the loss of ferrite. So far, things are approximately in line with the Fe-C equilibrium response, as expected. The core Mn is relatively more depressed (90-v-93%) following the consumption of the greater amount of prior ferrite at the start of the peritectic, but the absolute Mn is still lower in the 0.4%C steel. These two then have the same temperature interval to solidus, in which the 0.4%C steel has the greater Mn recovery at core (19-v-16.6%) but is still lower. Therefore, the lower core Mn content in the 0.4%C steel is an effect of the lower inherited solute content at the start of the peritectic, due to its occurring at a lower fraction solid, despite relative recoveries thereafter.

Finally, it is worth noting that the increase of manganese content in the liquid with time is not linear (Fig.6.13); with the constant solvus slopes employed, linearity would be a necessary result in the component Fe-C or Fe-Mn binaries. The extra degree of freedom in a ternary case allows non-linear responses of both solutes, although these responses must be related such that the net sum of their temperature depressions must still vary linearly. Evidently, it is incorrect simply to sum individual binary results even when the solutes do not interact regarding partition coefficients or solvus slopes; a multicomponent model should be employed as in the present case.

CHAPTER SEVEN

DISCUSSION

"Well, that's two things I've learnt today...
Oh, I've forgotten them."
....Nigel Allcock, graduate trainee, British Steel

7.1) MODELLING FEATURES

The target computer model has been reached in all respects and, indeed, surpassed in several respects. The model can employ equilibrium data as supplied by the subcontract via separately constructed data files, i.e. MTDATA and the micro-segregation model are not linked computer codes at present. Moreover, due to time constraints, the quoted model results have been obtained from computer runs using much simplified data, with a consequent restriction for quantitative validation on carbon and low alloy steels. The micro-segregation model is already capable of application to high alloy and stainless steels, but the simplified equilibrium data would not be adequate for any meaningful predictions.

Peripheral to the model itself, important advances have also been provided regarding analytical treatments of micro-segregation and secondary dendrite arm coarsening.

Additional aspects for consideration were solidification contraction and undercooling prior to the development of secondary phases. If it is considered that the missing volume, following contraction of a solidification increment in the representative cell, will be automatically fed with liquid of the residual composition, then the net effect is the same as with zero contraction. Alternatively, if there is no compensatory liquid feeding but the material is relatively unconstrained, the dendritic mesh will naturally contract such that the effect need not be considered; minor reductions in scale are unlikely to affect calculation of the extent of diffusion to a significant extent. Otherwise, one has to consider interdendritic fluid flow which is beyond the range of quantification by a purely micro-segregation model, and cannot be considered separate from the macroscopic thermal conditions and physical properties of the mushy zone environment.

An attempt can be made at predicting the propensity for micro-porosity by assuming all the missing volume from solidification, or from beyond an artificially designated critical fraction solid, occurs as voidage at the dendrite root. It is, however, somewhat inconsistent to use a sophisticated micro-segregation model in conjunction with such arbitrary approximations.

Regarding undercooling, it has already been stated in Section 6.1 that even the undercooling of austenite nucleation on ferrite for the peritectic can be reasonably disregarded for steady state, columnar growth. The nucleation problem will occur at the extremities of the cast sections but, between these, there will generally be a seed available from previously deposited austenite in adjacent (cooler) regions. This is not likely to be the case, however, for the precipitation of primary carbides or manganese sulphide, which are not present as continuous phases during solidification. Moreover, this could also be problematic even for austenite in equiaxed growth.

The finite basis of the computer model is such that some very minor undercooling will occur before the onset of austenite. The formulation quickly removes these undercoolings. Tests with artificial, larger undercoolings indicate that the peritectic model code can generally cope with them and, when the difference is too large for it to accommodate, numerical errors are more likely than the numerical pseudo-equilibrium one is trying to represent in this case. For steels wherein the peritectic is reasonably well developed, the system would soon recover to a near equilibrium result (n.b. locally at the interface) and this should not be an important drawback for the computer model.

7.2 EQUILIBRIUM DATA

The ambitious target for the multicomponent equilibrium data to be provided by the NPL (MTDATA) has been met, even to the incorporation of O and N. This only became available as a working database system after the official end of the BST/ECSC project, and moreover, there were grave doubts as to its accuracy with high Si contents and high Cr and Ni contents (in the region of the 300-series austenitic stainless steels). This has not been linked in with the micro-segregation program.

The simplified equilibrium data which nevertheless exhibit a consistent peritectic, have proved remarkably successful for the carbon and low alloy steels (Section 6.1) and, therefore, useful results from the micro-segregation computer model could still be obtained.

7.3 VALIDATION OF INPUT DATA

As intended, comparison of calculated equilibrium liquidus data has been performed against an extensive series of experimental melts. Further comparisons with prediction were possible regarding the initial solidification phase. It was apparent that electron micro-probe evaluation of partition coefficients from dendrite core / bulk composition ratios were inadequate on these samples even for the slower diffusing elements. The data provided in this respect are therefore more limited than originally hoped, although some useful indications were apparent. Similarly, severe problems with the equilibration furnace have limited the usefulness of this aspect of the project. Considerable success has been obtained, however, with the available data.

The MTDATA system was shown to be of generally great practical value, although some points of disagreement were apparent.

7.4 VALIDATION OF MODEL

The acquisition of good experimental data suitable for the validation of the predicted micro-segregation is very hard to come by, and most of the validation peformed in this project has been against experimental data performed elsewhere (Section 6.1). The results have, however, been very encouraging, provided the solidification conditions were adequately known and the basis and statistical significance of the temperatures and profiles similarly sufficient. Certain departures from quoted experimental results were observed which were logically necessary, i.e. limitations of the experiment or source data were identified, for which the observed discrepency of the computed result was in the right sense.

7.5 COMPOSITION GUIDELINES

The micro-segregation model is sufficiently developed for use against various criteria, albeit with some limitation noted on account of the simplified input data currently employed. The question must be raised about the validity of the guidelines (e.g. on maximum tolerable segregation of a certain element$, minimum tolerable solidus, desired residual ferrite in stainless, etc.,) with which the model predictions are compared, unless on a purely qualitative basis.

7.6 ALLOY DESIGN

Investigation of the possibility of use of the equilibrium database for design of alloys with inherently low segregation has indicated that this can only proceed on a "trial and error" basis. As mentioned previously, the number of alloy combinations to investigate is phenomenal. It is also evident, however, that such a composition would have to be very highly alloyed for element interactions to be sufficiently evident, as with the minimum in Cr segregation around 15-20% Cr in the binary.

7.7 IMPLICATIONS FOR MACROSEGREGATION

The various processes of macrosegregation were summarised in Section 2.6. Micro-segregation was identified as a required feature in the majority of cases, but is not a sufficient analysis. The local and macroscopic thermo-physical condition has to be addressed unless a purely qualitative measure for macrosegregation propensity is acceptable. Indeed, with current technology, this is all that is available unless gross, simplifying assumptions are made regarding the mushy zone environment.

One relative indicator readily available from the micro-segregation model is the extent of the mushy zone in terms of temperature, overlaid on results from a macroscopic model of solidification which thereby can translate the extent into terms of distance. There is an obvious inconsistency here in that any available macroscopic model uses trivial micro-segregation formulations.

Indeed, there can be inconsistencies in the macroscopic model itself. If, for example, the Clyne-Kurz micro-segregation equation is employed as in the more sophisticated macroscopic models, this assumes advance knowledge of the solidification time and a parabolic growth law. Therefore, the fraction solid, residual liquid composition, and corresponding liquidus temperature profiles of the volume element, are determined by this equation. With fraction solid and temperature profiles thus defined, the heat extraction profile from the volume element is also, necessarily defined by a simple heat balance, whereas the macroscopic model is imposing a different (apart from any chance coincidence) heat extraction profile. Iteration on the set solidification time would be the easiest way to obtain consistency with such an approach.

Another ready application for a micro-segregation model to yield a relative measure of susceptibility to macro-segregation would be calculation of the residual liquid density (using, for example, the density coefficients as quoted by Poirier [153], noting the factor of 100 error in the quoted numbers). This would be applicable to volume segregation and A-segregation channeling within the dendritic mesh.

The calculation of subsequent micro-segregation within a macrosegregated liquid pool or channel would very much depend on the solidification morphology; particularly whether it adopted a dendritic form as often noted in A-segregate channels, or a microscopically smooth solidification front. The latter morphology would lead to extremely high segregation with a macroscopically concave morphology, as lines or, particularly, spots with inward 2D or 3D solidification, respectively (Section 3.2.3).

Attempts have been made to quantify other forms of macro-segregation using the criterion of a critical fraction solid beyond which the interdendritic liquid is too constrained to flow through the mesh. This assumption must be recognised to be somewhat arbitrary but it does at least allow progress to be made.

7.8 MODEL PROPERTIES

The flexibility of the computer model and its application to multicomponent systems presents a tremendous range of possibilties and effects which could be examined. Some of the properties apparent from its use so far, and some of which are mentioned elsewhere in the report, are summarised as follows:-

The model is inherently capable of predicting whether the system (compositional and physical) as described would undergo a three phase reaction and, if so, whether it would tend to be peritectic or eutectic. The model will, however, only continue calculation according to a peritectic reaction because no eutectic option has been programmed into it.

For a given system, the interdendritic micro-segregation decreases as the morphological basis is increased from 1 to 2 and 3D (convex growth).

The core composition need not exhibit a corresponding effect with increasing dimension even with a single solidification phase. A higher dimension will homogenise more quickly for a given composition profile, but the actual profile is liable to be fairly flat for a considerable distance from the core (a given fraction solid being a greater linear distance from the core as the dimensional basis increases from 1 to 2 to 3); the core segregation (i.e. extent ~below~ the bulk composition) can actually be greater.

Under the peritectic reaction, the core composition can exhibit marked segregation of either positive or negative character, depending on the ferrite/austenite partition coefficient. (A higher dimensional basis can increase this variability.) Twin-peak profiles can be generated; one where all elements segregate together (i.e. the region of final solidification), and the other (i.e. at the core) where peak compositions of some elements correspond to troughs of others.

With subsequent sub-solidus homogenisation and ferrite/ austenite phase boundary movement, it is possible for two elements in the same sample to exhibit directly opposed segregation profiles, i.e. one peaked at the final, interdendritic region and the other peaked at the core.

The apparently unlikely segregation features predicted by the model of twin peak profiles, and enrichment of certain elements within dendrite arms sufficient to promote localised, temporary remelting, have been borne out experimentally. It is probable, however, that such effects are less common in practice on account of degeneration of the austenite/ferrite encroachment to a finer scale morphology than that of the dendrite arms as during solidification.

Isothermal reaction in dual or three phase systems is readily computed, with variable interface compositions evident in multicomponent steels, whereas certain other models incorrectly assume all interface compositions to be constant under these conditions.

Program operation with carbon alone automatically produces the temperature plateau during the peritectic reaction, under heat extraction control. This case is not tenable under cooling rate control, which presumes instantaneous progress through a finite fraction solid, for the 'thermally flat' representative cell used here. (Such an assumption is fairly standard for micro-segregation calculations.)

Small additions of substitutional elements to a carbon steel do not markedly affect the progress of the peritectic reaction, whereas small additions of carbon have a disproportionate effect on that of an Fe-X system, where X is a substitutional element which exhibits a binary peritectic with iron. However, this is not a simple function of the different diffusivities, which alone produce a fairly linear response/ law-of-mixtures, but of the overall "character" of the element with carbon having a fairly low partition coefficient and steep solvus slope in iron.

Secondary dendrite arm coarsening according to a given imposed law can produce spurious results, such as a slower cooled sample having a lower solidus temperature than one which has been cooled at a faster rate (not accounting for any departures from local equilibrium at interfaces under rapid solidification). The slower cooling could lead to disproportionately coarser structure which requires excessive time for a comparable extent of back diffusion, highlighting the importance of accurate knowledge of arm spacing characteristics and interface morphology in general.

The influence of parameters within the coarsening equation, $\lambda=Bt^n$, has been examined in some detail. Of particular note, it was discovered that results with n=0.5 were insensitive to cooling rate, for both core and peak compositions. Peak compositions with high n were generally insensitive to cooling rate, because the results were dominated by the coarsening process, approaching the finite Scheil-style (zero back-diffusion result) limit experienced with such coarsening.

The absence of an effect of cooling rate with n=0.5 reflects the structure of the diffusion modulus. It is not explicit in the formulation that the equations collapse to the same values with n=0.5 but, arguably, the modulus is the relevant dimensionless number. As adjusted for coarsening, such a parameter arguably contains all the controlling variables for the effect (although others such as D and k will be needed to express its degree) and therefore, whether or not the problem is formulated in such a manner, the same answer should be yielded when this dimensionless number is constant, as with n=0.5.

7.9 PROSPECTS FOR FUTURE WORK

An enormous range of further work could be done with useful results, on:

a) Further validation-cum-use of the existing micro-segregation model.

b) Generation of improved input data (multicomponent equilibria, precipitation conditions, diffusion, secondary dendrite arm coarsening).

c) Developments of the model for consideration of other conditions (change of morphology in the solid state, as with the eutectoid reaction in carbon steels, or lacey ferrite transformation in stainless steels; and breakdown of the local equilibrium assumption at interfaces).

d) Incorporation into a macroscopic solidification model.

At present, Roger Beaverstock at BST has taken the program on (and translated it into FORTRAN) for use with British Steel's Scunthorpe plant, examining relative susceptibilities to segregation and solidification cracking in proposed grades new to their continuuous caster machines. He also intends to address the issue of linking the program with MTDATA once a satisfactory program/database are available, although the major effort in this respect is the translation to FORTRAN which has been achieved.

Prospects for incorporation into a macroscopic model are under discussion.

CHAPTER EIGHT

SUMMARY AND CONCLUSIONS

This segregation of the elements referred to gives a brittle, impure, and weak steel, which in the finished article may prove not merely objectionable but dangerous. Possibly this phenomenon is more marked in its harmful characteristics in iron and its combinations known as steel than in any other metallurgical product. This difficulty is intensified because of the peculiar behaviour of the elements present.

The author thought that if it were possible to find means of ascertaining how this segregation arises, useful information would be obtained and methods of investigation opened up by which the difficulty could be dealt with and overcome.

....Sir Robert Hadfield, sentences extracted from JISI Vol. LXXXVL, 1912 No.II

This project concerned the micro-segregation resulting from the casting process. The primary feature of this work is the mathematical modelling of this process, extending existing techniques of both analytical and numerical character. Ancilliary work comprised derivation of a simplified data set for multicomponent equilibrium which necessarily exhibits a self-consistent peritectic, with a sub-contract to the NPL for computed equilibrium data by the MTDATA package.

The emphasis of the work has been on the development of the numerical model as a tool for tackling micro-segregation phenomena, but experimental validation of both the model output and the equilibrium data input has been performed with promising results.

The basic concepts and computer model are fairly general to metallic alloys although the emphasis for application is naturally on steel.

8.1 EXPERIMENTAL

An extensive series of experimental melts has been produced for the measurement of liquidus temperature, for comparsion with equilibrium calculations by both binary summation and MTDATA. Both approaches can be used with considerable success, although certain strengths and weaknesses have been identified. The compositions have been chosen to complement earlier work, which is included in the assessment.

An equilibration furnace has been employed at Sheffield University but with little success in terms of generating useful, temperature/fraction solid and partition coefficient equilibrium data. The limited data thus obtained have revealed some deficiencies in the MTDATA predictions.

8.2 EQUILIBRIUM DATA

In addition to the sophisticated, multi-component equilibrium data obtained under sub-contract, a simple data set of partition and solvus slope coefficients has been constructed which is quick to use and which has proven highly successful for low alloy steels. These data are constructed such that, regardless of the composition in question, the liquid/ferrite, liquid/austenite and ferrite/austenite phase boundaries automatically agree on the onset of the peritectic, and with a corresponding peritectic equivalent of unity. Positive or negative peritectic-equivalent coefficients indicate austenite and ferrite stabilisers, respectively.

8.3 ANALYTICAL TREATMENTS

Analytical treatment of micro-segregation has been extended from planar morphology, linear or parabolic growth to planar, cylindrical or spherical morphology, and any chosen growth law, by simple modification to the back-diffusion coefficient within the standard (Clyne-Kurz) equation. Dendrite arm coarsening has also been incorporated, although a much more complicated final expression results.

8.4 THE MICRO-SEGREGATION COMPUTER MODEL

8.4.1 Features

The final numerical model can be summarised as follows:

a) Multicomponent compositions are treated on a proper, interactive basis.

b) Any reaction path through a peritectic region of the phase diagram is automatically catered for.

c) Operates under variable, set heat extraction or cooling rates, including sub-solidus thermal cycling for homogenisation.

d) A particular case of the above is isothermal homogenisation, where the ferrite/austenite phase boundary movement is allowed to occur with varying interface compositions. Certain other treatments assume these compositions to be constant, which is incorrect in a multi-component system.

e) Also unlike certain other treatments, no initial assumptions have to be made regarding growth rate or solidification time.

f) Finite, temperature dependent diffusion is employed in solid phases.

g) A static-grid finite-difference procedure is employed

h) Interfaces are allowed to progress smoothly across the grid, i.e. not restricted to nodes, and with second order interpolation for solute gradients at the interfaces.

i) Operates either on a static, primary arm basis or coarsening secondary arm basis according to any imposed coarsening law (currently with either coarsening rate proportional to the remaining fraction of liquid, by $\lambda=Bt^n$, or by a theoretical multicomponent arm coarsening equation derived for a constant cooling rate).

j) The assumed coarsening mode is of simple migration of arms in accord with the imposed law.

k) The model can consider planar, cylindrical or spherical representative cells.

l) The FD array can be remeshed (by third order interpolation) when desired, typically for deployment of a greater number of nodes only when such enhanced sensitivity is required, as at the approach to solidus.

m) A novel routine for the solid/solid interface movement allows local equilibrium for all solutes under diffusive control from both adjoining phases while mutually satisfying the same growth rate.

n) Optional "streamlining" of the program is available whereby an element such as carbon can be considered as being uniformly mixed within a given phase, requiring simultaneous solution of all the equations for both phase interfaces during the peritectic.

o) Equilibrium data have been provided by the National Physical Laboratory by free-energy minimisation calculation, although the micro-segregation program currently operates with simplified data (though still necessarily constructed so as to exhibit consistent, multi-component peritectics).

Examination of alternative finite difference schemes has shown that they do tend to the same answers if they can each address the same problem. The final, FD scheme employed in this project does, however, appear to be the only type which can be combined with the required, novel peritectic formulation.

8.4.2 Behaviour of the Computer Model

Computation of solidification with a single phase results in micro-segregation profiles which are qualitatively similar but differing in degree; i.e. a continuous increase in composition from the original dendrite arm core to the final, interdendritic region. If, however, the peritectic reaction is encountered, then a dramatic variation in segregation profiles can be encountered, with twin peaks or a peak and trough in concentration, or even (with extensive sub-solidus reaction) diametrically opposed profiles for different elements in the same sample. Twin peak profiles are self evident in standard austenitic stainless steels where vermicular ferrite remains at the dendrite cores. In this work, experimental evidence was obtained for twin peak silicon profiles in a simple, carbon-silicon-manganese steel, and enrichment of molybdenum (in Fe-C-Mo) within dendrite arms apparently sufficient to promote localised, temporary remelting.

If the ferrite/austenite phase transformation morphology should change to a finer scale towards the core, the more extreme effects predicted from the peritectic would not be apparent. For example, in austenitic stainless steels, the residual ferrite can be apparent as either vermicular or lacey; the former reflecting the original, dendritic scale as in the present model, and the latter breaking down to a finer

scale (thereby reducing required diffusion distances, and reducing the drawback of increased interfacial area by partially following crystallographic relationships with the parent austenite phase).

A function akin to the diffusion modulus or Fourier number, combining diffusivity, dendrite arm spacing and local solidification time, has been found to indicate similarity between micro-segregation results. This remains true even with diffusion as a function of temperature, in multicomponent alloys, without any artificially imposed growth law, undergoing the peritectic reaction, and with dendrite arm coarsening (for a given 'n' with $\lambda=Bt^n$). However, the actual degree of micro-segregation is not predictable on this basis.

The sensitivity of the computed micro-segregation to the constants B and n in the secondary dendrite arm coarsening equation, $\lambda=Bt^n$, has been assessed, for values between n=0 and 1 as have been quoted in the literature, on a peritectic Fe-C-Mn composition. With high B and n values, the peak manganese content (at solidus) tends to a single function of n equivalent to that for zero diffusivity (which would be mathematically infinite with static arms as in the Scheil equation, but with arm coarsening is finite) which decreases with increasing n. Evidently, if there is still significant coarsening at solidus, this dominates the micro-segregation development, rather than the overall dendrite arm spacing, cooling rate, or solute diffusivity. At low B and n values, the opposite is true and the degree of segregation increases with increasing n.

The manganese contents at solidus at the dendrite cores do not show a similar convergence at high B and n, and continuously decrease below the equilibrium (bulk) content as n increases. There is no sensitivity to cooling rate at n=0.5; with lower n values high cooling rates further depress the core content, and vice versa with higher n values. At n=0.5 the time obviously scales with the square of the length, as in the diffusion modulus.

For a given system, the interdendritic micro-segregation decreases as the morphological basis is increased from 1 to 2 to 3 dimensions, i.e. convex (outward) growth of planar, cylindrical and spherical representative cells. Concave growth, however, produces much more dramatic effects, drastically increasing the micro-segregation at solidus although, by similar virtue of the morphology, subsequent, sub-solidus homogenisation is relatively rapid.

For standard dendritic solidification, the simple, planar morphology appears to generate reasonable predictions.

Even running with the simplified peritectic data, the model can predict whether an alloy would solidify by a peritectic or eutectic reaction. However, how accurate its predictions are in this respect is difficult to determine, it being very difficult to tell in practice with undercoolings, divorced eutectics, etcetera, and, moreover, the current model only continues with a peritectic morphology.

A common difficulty with determining the influence of a given variable on the micro-segregation response is the occurrence of "side-effects". For example, by increasing an alloy content you are not simply investigating the effect of more alloy per se, but of the correspondingly lower temperatures, hence diffusivities, and different range of fraction solid over which the peritectic may be encountered. Mathematical attempts to assess individual variables have required examination of artificial systems, from which it appears that in a mixture of solutes identical apart from diffusivity, the effect on reaction rates, peritectic and solidus temperatures, etcetera, is essentially in proportion to the relative amounts of these solutes.

There is a tendency for ferrite stabilisers to slow the ferrite dissolution in the peritectic more than do austenite stabilisers, as might be expected, but this is not necessarily the case. Rather, it is a function of the overall character of the solute regarding its partition coefficients, solvus slopes and diffusivity, not just its peritectic-equivalent coefficient.

8.4.3 Validation

A general problem is the acquisition of appropriate, rigorous data for both the input to and validation of the model, although useful results have been obtained.

a) Mathematical

Some validation can be performed mathematically, i.e. for the nature of the model, certain bounding cases can be determined analytically, and the numerical model should generate the same results if restricted to these analytically soluble cases. For variation in diffusivity, it does indeed tend to the Scheil (zero diffusivity) and Lever Rule (infinite diffusivity) limits. The "streamlining" option whereby a solute is assumed to be completely mixed within a given phase does equate to the Lever Rule limit, and the standard FD solution tends to this same limit with increasing diffusivity. Furthermore, the model is in excellent agreement with Mortensen's analytical limit for Scheil-style micro-segregation but with dendrite arm coarsening (by $\lambda=Bt^n$).

b) Jernkontoret Data

This exercise employed the simplified peritectic equilibrium data set, restricting the validation to modestly alloyed steels from this reference. 27 data pairs (prediction-v-experiment) were available for maximum/minimum concentration ratio amongst the secondary dendrite arms at the quench temperatures, involving manganese, chromium, molybdenum and nickel. Correlation of 0.727 was obtained (0.1% significance), improved to 0.801 by expanding the equilibrium data to include carbon-chromium interaction on three of the 16 steels (possible because these did not undergo the peritectic reaction and so did not need the self-consistent peritectic data set). Three of the six results for molybdenum were significantly in error, damaging the albeit very high overall correlation, and no reason was immediately apparent for these few discrepencies. Otherwise, all the predictions were within experimental error of the measurements.

c) Turkeli's Data

Three peritectic Fe-C-Mn alloys investigated by Turkeli under a total of 29 conditions were assessed in terms of core and peak manganese contents at the quench temperatures. The observed morphology was akin to a four leaf clover in cross section, whereupon it is unclear whether a primary or secondary dendrite arm basis was the most appropriate for the model. On a primary basis the correlation with prediction by the model was 0.727 for the core compositions and 0.781 for the peaks, again both highly significant. On a secondary dendrite arm basis, the correlation with the cores was a remarkable 0.912.

8.4.4 Implications

The restrictive assumptions required for analytical solution of micro-segregation behaviour can lead to significant errors of prediction, and these should only be used as an initial "coarse filter" for deciding which alloys/conditions may require further attention. For example, the standard Clyne-Kurz equation is inappropriate for the secondary arm case because it does not consider arm coarsening, and to the primary case because it does not consider a cylindrical (conical) representative unit cell. Approximations can be made for these but even so the prescribed growth law and consequent micro-segregation uniquely define a heat extraction behaviour, such that this equation cannot be used consistently within treatments for which heat extraction is a variable defined separately by the external conditions.

Numerical treatments avoid these difficulties. It is evident that a multicomponent alloy requires a multicomponent model, as opposed to independent component binary calculations, even when the component solutes do not effect each others' equilibrium behaviour or diffusion coefficients. There are so many "side effects" associated with alteration of any one variable that it is quite likely that even qualitative prediction of the sense of a given alteration on the resultant micro-segregation could be in error.

Problems remain regarding source data: equilibrium, kinetic, and experimental micro-segregation for validation purposes. Within known territory, however, the present model appears to behave very well, lending confidence for its use in cases of "live" prediction rather than validation.

Semi-quantitative inferences can be made from this model regarding crack-susceptibility and macro-segregation, but combination of a non-trivial micro-segregation treatment with a non-trivial crack/macro treatment would still require considerable modelling effort. This issue is, however, being taken up by various establishments, for which the present model is under consideration.

ACKNOWLEDGEMENTS

This thesis is based upon work performed on behalf of British Steel,Technical (BST) with support from the European Coal and Steel Community (ECSC, Committee C6) [9]. Other BST staff were employed, primarily Mr.R.C. Beaverstock and Dr.G.J. Hassall, but also technical support from others on experimental work.

A significant component of the work comprised a sub-contract from BST-ECSC to the National Physical Laboratory (NPL[9]) for the computation of multicomponent composition and phase equilibria, employing the 'MTDATA' system [15] which, in turn, included data derived elsewhere within the SGTE [16] and CALPHAD [17] groups.

Other Sheffield students whose work has been particularly useful to this project were Mr.A. Turkeli [18] and Mrs.I. Kabymera [19]. The assistance of Messrs. Goddard and Parry on the equilibration furnace is also appreciated.

Special acknowledgement must be given to Dr.D.H. Kirkwood who, rather than functioning merely as 'supervisor' to this work has also been an active contributor. Such contributions have been duly identified within the text.

REFERENCES

1 "Solidification Processing 1987",Sheffield,21-24 Sept.'87, Institute of Metals, Book 421, Paper 1 and Session J.

2 Howe, A.A., "Micro-segregation in Peritectic Alloys", in "Modeling of Casting, Welding and Advanced Solidification Processes - V" Eds. Rappaz, Ozgu and Mahin, TMS publication of the conference held in Davos, Switzerland, Sept. 16-21, 1990

3 Kirkwood,D.H.,Mat.Sci.&Eng.1984,65(1),p101

4 Ogilvy,A.J.W.,PhD thesis, Sheffield University,1983

5 Ogilvy,A.J.W. and Kirkwood,D.H.,Appl.Sci.Res.1987,44,1/2,p43

6 Howe,A.A.,Appl.Sci.Res.1987,44,1/2,p51

7 Howe,A.A. and Kirkwood,D.H.,"Solidification Processing 1987", Sheffield,21-24 Sept.'87, Institute of Metals,Book 421,p63

8 Howe,A.A.,"Extension of Analytical Expressions for Micro-Segregation", Ironmkg.& Steelmkg.,18, No.4,1991,p284

9 Howe,A.A., "Segregation and Phase Distribution during Solidification of carbon, Alloy and Stainless Steels", ECSC final report EUR 13302 (7210.CF/801, S185)

10 Howe,A.A., "Effects of Element Interactions Upon Microsegregation", BSC internal report SH/PDN/3798/-/84/D

11 Howe,A.A., "Development of a Computer Model for Microsegregation", BSC internal report SH/PDN/3798/1/85/D

12 Howe,A.A., "Third Report on the Development of a Computer Model for Microsegregation", BSC internal report SH/PDN/3798/2/86/D

13 Howe,A.A., "An Examination of Microsegregation with back Diffusion and Dendrite Coarsening", BSC internal technical note PDN/833/85/A

14 Howe,A.A., Seminars on Segregation, BST Swinden Laboratories, 1985 and 1989.

15 MTDATA, National Physical Laboratory, Teddington, Middx.

16 SGTE, European organisation concerned with the computation of phase equilibria, which can be contacted via ref.15

17 CALPHAD (CALculation of PHAse Diagrams), International collaboration as above, to be contacted via ref.15 or the CALPHAD journal (Pergamon Press).

18 Turkeli,A.,PhD thesis, Sheffield University, 1989

19 Kabyemera,I.J.,MMet thesis, Sheffield University, 1987

20 Atkins,P.W.A.,"Time and Dispersal: The Second Law" from 'Nature of Time', Eds. R.Flood and M.Lockwood, Blackwell,1986

21 "Principles of Solidification",Chalmers,Wiley,1964

22 Crowley,A.B.,Howison,S.D. and Ockendon,J.R., ibid ref.1,p370

23 Hillert,M., "Solidification and Casting of Metals", I.of M.,p81

24 Mullins,W.W. and Sekerka,R.F.,J.of Appl.Phys.35,1964,p444

25 Sekerka,R.F.,J.of Cryst.Growth,3,1968,p71

26 Tiller,W.A., JISI 1959,p338

27 Hunt,J.D., Mat.Sci.&Eng.,65.1984,p75

28 Doherty,R.D. and Melford,D.A.,JISI 1966,p1131

29 Burden,M.H. and Hunt,J.D.,J.Cryst.Growth 1974,22,p99

30 Flood,S.C. and Hunt,J.D., "Columnar to Equiaxed Transition", Metals Handbook, 9th edition (1988) Vol.15, p130

31 Ohno,A., "The Solidification of Metals", ISI publ. 110, 1968, p349

32 Cornelissen,M.C.M., ibid ref.1, p218

33 Howe,A.A., "Estimation of Shell Thickness During Solidification", BSC internal technical note, PDN/750/82/D

34 Ameling,D.,Litterscheidt,H., and Schwerdtfeger,K.,Steelmkg. Proc. 1986,69,p387

35 Kurz,W.,ibid ref.1,p1

36 Hunt,J.D., ibid ref.1,p191

37 Trivedi,R., and Somboonsuk,K.,Acta Metall.,33,No.6,1985,p1061

38 Venugopalan,D.V. and Kirkaldy,K.S.,Acta Metall.,32,No.6,1984, p893

39 Laxmanan,V.,Acta Metall.,33,1985,No.6 p1023 &1037

40 Laxmanan,V.,Acta Metall.,33,1985,No.8 p1475

41 Lukas,H.L.,Henig,E-Th, and Zimmermann,B.,Calphad J.,1977,1,p225

42 Argent,B.B.,"Seminars on Phase Diagrams and Thermodynamics", Sheffield University, commenced 5/10/1987

43 Hayes,F.,"Thermodynamic Principles of Phase Diagram Calculations",UMIST monograph,1986

44 Hack,K.,"Thermodynamics of Alloys: Collection of Mathematical Tools", DMA internal report (C)10,June 1981

45 Ansara,I.,Int.Met.Rev. 1979,24,No.1,p20

46 Bale,C.W., and Pelton,A.D.,Met.Trans.B,14B,1983,p77

47 Zimmermann,B.,PhD thesis,Stuttgart University,1976

48 Redlich,O., and Kister,A.T.,Ind.& Eng.Chem.,40,1948,p345

49 Pelton,A.D.,and Thompson,W.T.,Prog.Solid State Chem.,10,No.3, 1975,p119

50 Pelton,A.D.,and Bale,C.W.,Calphad J.,1,No.3,1977,p253

51 Margules,M., S.B.Akad.Wiss.Wien,Math-Naturwiss.,Kl II,1895,104, p1243

52 Muggianu,Y.M.,Gambino,M., and Bros,J.P., J.Chim.Phys.,72,No.1, 1975,p83

53 Toop,G.W., Trans.AIME,233,1965,p850

54 Bonnier,E.,Caboz,R.,C.R. Hebd.Siances Acad.Sci.,250,1860,p527

55 Kohler,F., Monatsh.Chem.,S1,1960,p738

56 Colinet,C., DES, Fac.Sci.,Grenoble University,1967

57 A. Fick, Ann Phys Lpz,170 (1855) 59

58 J.B. Fourier, "Theorie analytique de la chaleur", Oeuvres de Fourier (1822)

59 J.Burke,"The Kinetics of Phase Transformations in Metals", Pergamon Press,(1965)

60 J.Crank, "The Mathematics of Diffusion",Clarendon Press (1956)

61 C.P.Flynn,"Point Defects and Diffusion",Clarendon Press (1972)

62 L.S.Darken,Trans.AIME,175(1948) p.184

63 A.C.Smigelskas and E.O.Kirkendall,Trans.AIME,171(1947) p130

64 Darken,L.S.,Trans.AIME,180(1949) p.430

65 Onsager,L., Ann.N.Y.Acad.Sci.,1945,46, p.241

66 Manning,J.R., Met.Trans.,1970,1, p.499

67 Haworth,C., Sheffield University, private communication

68 Papapetrou,A.,Z.Kristall.1935,92,p89

69 Klia,M.O.,Kristallografiya 1956,1(5),p576

70 Chernov,A.A., Kristallografiya 1956,1(5),p583

71 Kattamis,T.Z.,Coughlin,J.C. and Flemings,M.C.,Met.Trans.1967, 239,p1504

72 Kahlweit,M.,Scr.Metall.1968,2,p251

73 Kirkwood,D.H.,Mat.Sci. & Eng.1985,73,L1

74 Feurer,U.,and Wunderlin,R.,DGM Fachber.1977,38

75 Allen,D.J. and Hunt,J.D.,"Solidification and Casting of Metals",Sheffield University,1977,Met.Soc. Book 192,1979,p131

76 Battle,T.P., Int.Met.Rev. 1992,37,No.6, p249

77 Schurmann,E.,et al.,Steel Research 58,1987,11,p498

78 Turkeli,A.,PhD thesis, Sheffield University, 1989

79 Lalli,L.A.,"Modeling of Casting and Welding Processes", Met.Soc. of AIME,1981

80 Mortensen,A.,Met.Trans.A.1989,20A,p247

81 Brody,H.D. and Flemings,M.C.,Trans.AIME,1966,236,p615

82 Beaverstock,R.C., "Secondary Dendrite Arm Coarsening and Microsegregation in Alloy Steels", BST internal report, SL/PDN/R/S2223/1/92/A

83 Gulliver,G.H., "Metallic Alloys",Charles Griffen, London, 1922

84 Scheil,E., Z.Metallk.,1942,34,p70

85 Clyne,T.W. and Kurz,W.,Met.Trans.A.,1989,20A,p247

86 Ohnaka,I.,Trans.ISIJ,1986,26,p1045

87 Brimacombe,J.K. and Fujimura,T.,Trans.ISIJ 1986,26,p532

88 Fredriksson,H., "Solidification and Casting of Metals", Sheffield University,1977, Met.Soc. Book 192,1979,p131

89 Cornelissen,M.C.M., Ironmkg.and Steelmkg.,1986,13,(4),p204

90 Kirkwood,D.H. and Evans, 1968

91 Kobayashi,S.,Tetsu-to-Hagane 1985,71,S199 & S1066

92 Kobayashi,S.,et al.,Trans.ISIJ 1988,28,p214

93 Matsumiya,T.,et al.,Trans.ISIJ 1984,24,p873

94 Ueshima,Y.,et al.,Met.Trans.B 1986,17B,p845

95 Ueshima,Y.,et al.,Tetsu-to-Hagane 1987,73,p109

96 Subrumanian,S.V.,report,McMaster University,Canada,1985

97 Hillert,M.,and Staffanson,L.I.,Acta Chemica Scandinavica 1970, 24,p3618

98 Battle,T.P. and Pehlke,R.D.,Steelmaking Conference Proceedings, 1987,70,p121

99 Meittenen,J., "Solidification Processing 1987",Sheffield,21-24 Sept.'87, Institute of Metals, Book 421,p67

100 "Guide to the Solidification of Steels",Jernkontoret, Stockholm, 1977

101 Lalli,L.A.,"Modelling of Casting and Welding Processes", Met. Soc. of AIME,1981

102 Murray,W.D. and Landis,F.,J.Heat Transfer 1959,81,p106

103 Crank,J., and Nicolson,P.,Cambridge Phil.Soc.1947,43,p50

104 Roosz,A.,Halder,E.,and Exner,H.E.,Mat.Sci.1986,1,p1149

105 Roosz,A.,Cast Metals 1989,1(4),p223

106 Agren,J.,TRITA-MAC-0154,Royal Inst.of Tech,Stockholm,1979

107 Agren,J.,TRITA-MAC-0184,Royal Inst.of Tech,Stockholm,1981

108 Agren,J.,TRITA-MAC-0311,Royal Inst.of Tech,Stockholm,1986

109 Hultgren,A., K.V.A.Handlingar,1953,4(4),No.3

110 Hillert,M., ASM Seminar on Phase transformations, Metals Park,1970

111 Hillert,M., "The Mechanisms of Phase Transformations in Crystalline Solids", I.of M. Book 231,1969

112 Hillert,M., Proc. ICSTIS,Supple.Trans.ISIJ,1971,11,p1153

113 Kirkaldy,J.S. and Young,D.J., "Diffusion in the Condensed State" I.of M. Book 322,1985

114 Wunnenberg et al.,Stahl Eisen,1984,104,No.9,p23 (BISIT 24016)

115 Stefaniay,V., et al., Aluminium,59,1983,1,p8

116 Bulter,S.A., "Segregation Assessment of Concast Steels using an Automated SEM/EDS System", B.S.C. internal report, T/PP/1154/56/82/D

117 Brody,H., et al., Trans.AIME 1966,236,p624

118 Chuang,Y.K., Reinisch,D., and Schwerdtfeger,K., Met.Trans.A,6A, 1975,p235

119 Howe,A.A., "Prediction of Liquidus Temperatures of Stainless Steels", BSC internal technical note,PDN/726/82/E

120 Howe,A.A., "Re-Appraisal of Liquidus Temperatures of Stainless Steels", BSC internal report, SH/PDN/3471/-/83/D

121 Howe,A.A., "Estimation of Liquidus Temperatures for Steels", Ironmkg. & Steelmkg., 1988,15,No.3,p134

122 Land International, Wreakes Lane, Dronfield, Sheffield S18 6DJ

123 Andrews,K.W., note submitted to the Alloy Phase Diagram Data Committee of the Metals Society, 1981

124 Kubachewski,O., "Iron Binary Phase Diagrams", Berlin,Springer Verlag,1982

125 Wolf,M., Concast Metallurgical Seminar,Zurich,October 1982

126 Kagawa,A., and Okamoto,T.,Mater.Sci.Tech. 1986,2,p997

127 Rivlin,V.G. and Raynor,G.V.,Int.Met.Rev. 1980,25,p21

128 Chuang,Y-Y.,and Austin Chang,Y.,Met.Trans.A,18A,1987,p733

129 Allan,G.K.,ECSC final report 7210.CF/803, 1990

130 Morita,Z., and Tanaka,T., Trans.ISIJ,1983,23,p824

131 Geiger,G.H., and Poirier,D.R., "Transport Phenomena in Metallurgy", 1979, Addison Wesley, pp.256-263

132 Discussion at MIT on work of Brian Leibowitz, reported in: Howe,A.A., "Visit to the United States and Canada, 24th March-10th April 1987", BSB internal report PDN/V/10/-/87/D

133 Rickinson,B.A., PhD Thesis,Sheffield University,1975

134 Angus,H.T., "Cast iron",Butterworth,1976

135 Howe,A.A., "The Effect of Solidification Mode on Structure and Subsequent Processing of Austenitic Stainless Steels Produced at SMACC", BSC internal report SH/PDN/9586/-/81/D

136 Private communication, Dr.Bill Beech, Sheffield University

137 Sigworth,G.K and Elliott,J.F.,Metal Science,8,(1974),pp298-310

138 Bodsworth and Bell,"Physical Chemistry of Iron and Steel Manufacture",Longman,1972

139 Pelton,A.D. and Bale,C.W.,"A Modified Interaction Parameter Formalism for Non-Dilute Solutions", in CALPHAD XV, Fulmer Grange, July 7-11,1986

140 Schmidt,ibid ref.60

141 Crank,J., in "Moving Boundary Problems in Heat Flow and Diffusion" Proc.Conf. Oxford University,25-27th March 1974, eds. Ockendon and Hodgkins, Clarendon Press, 1975, p195

142 Beckett,S.J., and Howe,A.A., "Estimation of Liquidus Temperatures, Partition Coefficients and Peritectic Carbon Equivalents in Multicomponent Steels", BST internal report PDN/R/S1286/1/87/B

143 Cornelissen,M.C.M.,"Progress in Modelling of Solidification Processes", Sheffield University, 1986 (I.of M.)

144 Schmidtmann,E. and Rakoski,F., Stahl und Eisen 103, 18,p881

145 Rickinson,B.A. and Kirkwood,D.H., Metal Science, March 1978, p138

146 Ogilvy,A.J.W.,Ostrowski,A. and Kirkwood,D.H., Metal Science, April 1981,p168

147 Fridberg,J., Torndahl,L., and Hillert,M., Jernk.Ann.1969, 153, p263

148 Fox,L., in "Moving Boundary Problems in Heat Flow and Diffusion" Proc.Conf. Oxford University,25-27th March 1974, eds. Ockendon and Hodgkins, Clarendon Press, 1975

149 Beaverstock, R.C., private communication, BST Swinden Laboratories, Moorgate, Rotherham.

150 Crank,J. and Gupta,R.S., J.Inst.Math.App.,1972,10,3,p296

151 Post Graduate Lecture Series on Numerical Methods, Sheffield University, November 1987

152 Howe,A.A., "Computational Investigation of the Influence of Diffusivity, Length and Time Scales, and secondary Dendrite Arm Coarsening on Microsegregation in a C-Mn Steel", BST internal report, SL/PH/R/S2223/1/91/A

153 Fujii,T.,Poirier,D.R. and Flemings,M.C.,Met.Trans.B,1979, 10B,p331

TABLE 3.1
CAST COMPOSITION, WT.%

TABLE 3.1a PREVIOUS WORK

Low alloy and quasibinary steels

Sample No.	Grade	C	Si	Mn	P	S	Cr	Mo	Ni	N	Others
1	0.3%C	0.30	0.10	0.13	0.019	0.010	0.30	0.024	0.05	-	-
2	0.48%C	0.48	0.06	0.04	0.012	0.013	0.08	0.016	0.015	-	-
3	0.66%C	0.66	0.31	0.04	0.011	0.012	0.04	0.007	0.015	-	-
4	0.81%C	0.81	0.41	0.04	0.011	0.013	0.03	0.012	0.02	-	-
5	0.58%C	0.58	0.99	<0.02	0.016	0.011	0.03	<0.02	<0.02	0.018	-
6	0.89%C	0.89	0.43	<0.02	0.015	0.010	0.02	<0.02	<0.02	0.014	0.0110
7	1.2%C	1.20	0.53	<0.02	0.015	0.010	<0.02	<0.02	0.03	0.009	0.0160
8	1.48%C	1.48	0.55	<0.02	0.019	0.020	0.02	<0.02	0.04	0.009	0.0120
9	12.8%Mn, 0.026%C	0.026	0.44	12.80	-	-	-	-	-	-	-
10	12.9%Mn, 0.58%C	0.58	0.42	12.90	-	-	-	-	-	-	-
11	14.3%Mn, 0.73%C	0.73	0.43	14.30	-	-	-	-	-	-	-
12	13.8%Mn, 0.76%C	0.76	0.53	13.80	-	-	-	-	-	-	-
13	T409(1)	0.047	0.81	0.39	0.019	0.003	11.7	0.03	0.17	0.019	0.22Ti
14	T409(2)	0.038	0.81	0.50	0.024	0.003	11.7	0.05	0.25	0.032	0.02Ti
15	T409(3)	0.020	0.85	0.39	0.019	0.003	11.0	0.04	0.60	0.029	0.13Ti
16	T409(4)	0.020	1.05	0.39	0.015	0.003	11.8	0.04	0.15	0.023	0.29Ti
17	T430(1)	0.058	0.31	0.42	0.021	0.004	16.1	0.04	0.29	0.040	-
18	T430(2)	0.038	0.29	0.56	0.016	0.008	16.3	0.02	0.14	0.050	-
19	T430 FT	0.027	0.50	0.57	0.023	0.003	15.6	0.04	0.30	0.032	0.25Ti
20	9%Ni	0.052	0.09	0.18	0.008	0.003	0.46	0.06	9.0	0.027	-
21	33%Ni	0.040	0.20	0.15	0.009	0.010	0.70	<0.02	32.5	0.004	-
22	18%CrAl(1)	0.032	1.49	1.69	0.011	0.005	17.91	<0.02	<0.02	0.038	0.83Al
23	18%CrAl(2)	0.036	1.62	2.00	0.011	0.005	17.75	<0.02	<0.02	0.043	0.30Al
24	18% CrNiTi	0.029	1.70	1.44	0.020	0.004	18.8	0.24	1.39	0.045	0.17Ti
25	C14 low alloy cast	0.004	0.11	0.14	0.005	0.004	0.03	-	-	0.013	0.060
26	C44 low alloy cast	0.001	0.32	0.02	0.008	0.008	0.04	0.005	0.02	-	0.030
27	0.1%C	0.11	0.12	1.25	0.040	0.018	0.06	0.07	0.03	0.012	-
28	WERK 1.0566	0.12	0.27	1.53	0.010	0.005	0.02	<0.03	0.03	0.011	-
29	0.18%C	0.18	0.44	1.26	0.016	0.025	0.01	0.06	0.02	0.007	-
30	WERK 1.0580	0.19	0.40	1.42	0.012	0.007	0.07	0.02	0.13	0.005	-
31	T1034	0.36	0.27	0.58	0.015	0.012	0.08	0.02	0.05	0.007	-
32	T1070	0.69	0.23	0.72	0.022	0.024	0.02	0.01	0.02	0.002	-
33	T1095	1.01	0.25	0.46	0.012	0.009	0.02	0.02	0.03	0.002	-
34	T9310	0.10	0.28	0.57	0.008	0.009	0.14	0.14	3.30	0.009	-
35	0.2%CCrNi	0.20	0.25	0.90	0.014	0.039	0.81	0.06	1.05	0.009	-
36	0.3%CCrNiMo	0.27	0.02	0.32	0.006	0.008	1.66	0.42	3.50	0.007	-
37	T4130	0.29	0.21	0.62	0.012	0.006	1.11	0.21	0.15	0.004	-
38	0.3%CCrNiMo	0.29	0.22	0.52	0.009	0.010	1.02	0.25	3.2	0.005	-
39	T4135	0.35	0.24	0.67	0.010	0.020	0.92	0.19	0.05	0.008	-
40	T6150	0.52	0.22	0.85	0.010	0.006	1.07	0.07	0.07	0.008	-
41	WERK 1.2721	0.55	0.27	0.50	0.019	0.012	0.99	0.31	3.00	0.008	-
42	1.0%CCr	1.01	0.23	0.33	0.021	0.026	1.55	0.01	0.02	0.003	-
43	T501	0.13	0.36	0.37	0.003	0.007	5.00	0.58	0.01	0.006	-
44	M13	0.35	1.03	0.46	0.020	0.007	5.2	1.34	0.23	0.026	1.0V
45	0.5%CMoV, 5%Cr	0.50	1.00	0.48	0.025	0.010	5.1	1.36	0.18	0.036	1.2V
46	A2	0.96	0.29	0.67	0.020	0.015	5.2	1.19	0.13	0.024	0.21V
47	0.04%C, 5%Ni, 13%Cr	0.04	0.54	0.61	0.010	0.009	13.4	0.07	5.5	0.032	-
48	T410S	0.07	0.54	0.48	0.020	0.006	12.9	0.02	0.17	0.039	-
49	T414	0.14	0.19	0.68	0.009	0.014	12.0	0.01	1.20	0.040	-
50	T420	0.32	0.15	0.30	0.009	0.008	13.9	0.01	0.16	0.013	-

(Contd...)

TABLE 3.1
(Continued)

TABLE 3.1a (Continued)

High alloy steels

Sample No.	Grade	C	Si	Mn	P	S	Cr	Mo	Ni	N	Others
51	T201	0.044	0.40	6.9	0.013	0.005	17.8	0.29	4.25	0.204	
52	T201C	0.23	0.46	8.85	0.030	0.004	14.13	0.20	3.44	0.160	
53	T202	0.062	0.48	7.3	0.030	0.002	18.1	0.40	5.91	0.219	
54	T202(LN)	0.081	0.53	8.46	0.030	0.005	16.82	0.325	5.46	0.049	
55	T302	0.049	0.36	1.30	0.021	0.008	19.1	0.22	8.69	0.039	
56	T304	0.058	0.59	1.45	0.019	0.004	17.6	0.15	8.65	0.034	
57	T304(N)	0.032	0.51	1.63	0.021	0.003	18.8	0.08	9.43	0.0165	
58	T305	0.13	2.13	1.89	0.020	0.003	19.3	0.16	11.60	0.050	
59	T310(1)	0.046	0.24	1.86	0.007	0.003	25.0	0.33	20.70	0.074	
60	T310(2)	0.050	0.63	1.75	0.010	0.004	25.8	0.35	20.70	0.039	
61	T316	0.049	0.59	1.68	0.013	0.005	17.2	2.14	11.20	0.030	
62	T317 LM	0.022	0.70	1.74	0.026	0.007	18.4	4.46	15.20	0.052	
63	T317 LN	0.020	0.61	1.67	0.020	0.008	18.9	3.62	13.40	0.150	
64	T320(1)	0.063	0.55	1.55	0.023	0.003	17.3	2.15	12.0	0.028	
65	T320(2)	0.055	0.70	1.77	0.019	0.004	17.0	2.13	11.9	0.026	0.18Ti
66	T321	0.045	0.71	1.85	0.018	0.003	17.2	0.15	9.15	0.033	0.12Ti
67	T347(1)	0.063	0.29	1.45	0.022	0.003	17.9	0.18	9.29	0.060	0.47Nb
68	T347(2)	0.040	0.45	1.54	0.015	0.005	17.8	0.25	9.04	0.028	0.61Nb
69	552205(1)	0.028	0.40	1.14	0.020	0.006	22.2	3.11	5.61	0.188	
70	552205(2)	0.029	0.54	1.41	0.023	0.009	22.0	2.96	5.61	0.170	
71	T329	0.042	0.86	0.76	0.031	0.010	25.1	1.22	4.70	0.077	
72	T308L	0.012	0.31	1.76	0.006	0.008	19.8	0.10	9.9	0.031	
73	T304L	0.019	0.31	0.94	0.009	0.010	19.5	0.11	10.2	0.044	
74	T304	0.036	0.44	1.25	0.025	0.010	18.4	0.38	9.1	0.081	
75	T321	0.068	0.59	1.44	0.028	0.001	17.2	0.47	10.3	0.005	0.51Ti
76	T316Cb	0.052	0.44	1.71	0.013	0.007	17.2	2.80	12.6	0.010	0.54Nb
77	T316L	0.023	0.53	1.58	0.020	0.006	17.2	2.63	13.5	0.031	
78	T316	0.048	0.63	1.65	0.018	0.007	17.7	2.68	13.4	0.045	
79	T316N	0.024	0.58	1.79	0.009	0.011	17.4	2.77	12.8	0.20	
80	25%Cr,22%Ni,2%Mo	0.008	0.24	1.77	0.009	0.008	25.1	2.30	22.2	0.067	
81	T310S	0.055	1.20	1.75	0.011	0.008	24.2	0.08	20.4	0.051	
82	T310	0.13	0.52	1.67	0.009	0.003	24.3	0.11	20.5	0.053	
83	WERK 1.4539	0.013	0.48	1.74	0.007	0.003	19.2	4.44	25.1	0.035	1.51Cu
84	T310HC	0.41	1.00	1.34	0.007	0.010	25.2	0.08	20.6	0.022	
85	Alloy 800	0.07	0.62	0.56	0.007	0.003	21.1	0.06	30.9	0.019	
86	M2	0.88	0.30	0.32	0.030	0.017	3.9	4.9	0.36	0.036	1.9V, 6.1W
87	M7	1.0	0.38	0.38	0.010	0.037	3.8	9.2	0.14	0.036	2.0V, 1.5W

Nos. 27-50; 71-87 from Ref. 100

TABLE 3.1
(Continued)

TABLE 3.1b PRESENT WORK

Sample No.	C	Si	Mn	P	S	Cr	Mo	Ni	O	N
101	4.00	<0.01	0.037	0.002	0.006	-	-	-	0.0030	0.0005
102	3.10	<0.01	2.07	0.002	0.006	-	-	-	0.0060	0.0020
103	2.94	0.023	4.99	0.002	0.006	-	-	-	0.0020	0.0040
104	2.88	1.45	5.08	0.002	0.006	-	-	-	0.0055	0.0068
105	3.03	0.81	0.36	0.002	0.007	-	-	-	0.0130	0.0030
106	2.89	1.55	0.48	0.002	0.007	-	-	-	0.0077	0.0049
107	2.69	1.63	2.64	0.002	0.007	-	-	-	0.0045	0.0080
108	2.52	1.58	5.00	0.002	0.008	-	-	-	0.0100	0.0110
109	0.024	0.14	<0.1	<0.005	0.006	48.0	<0.04	45.0		
110	0.019	0.08	<0.1	<0.005	0.004	40.7	<0.04	48.6		
111	0.018	0.12	<0.1	<0.005	0.004	48.0	<0.04	40.4		
112	0.034	0.15	<0.1	<0.005	0.010	57.9	<0.04	30.5		
113	0.026	0.10	<0.1	<0.005	0.006	51.4	<0.04	29.6		
114	0.024	0.11	<0.1	<0.005	0.006	54.2	<0.04	25.1		
115	0.018	0.08	<0.1	<0.005	0.004	47.0	<0.04	32.5		
116	0.018	0.08	<0.1	<0.005	0.003	40.8	<0.04	29.8		
117	0.033	0.09	<0.1	<0.005	0.004	39.6	<0.04	21.2		
118	0.016	0.06	<0.1	<0.005	0.003	31.5	<0.04	19.7		
119	0.012	0.06	<0.1	<0.005	0.002	26.4	<0.04	15.4		
120*	0.006	1.35	0.05	<0.005	0.002	<0.02	<0.005	<0.02	(0.0125)	(0.0032)
120*	0.023	1.24	0.07	<0.005	0.003	<0.02	<0.005	<0.02	0.0125	0.0032
121*	0.007	4.88	0.10	<0.005	0.002	<0.02	<0.005	<0.02	(0.006)	(0.003)
122*	3.45	0.07	0.02	<0.005	0.005	0.07	<0.005	<0.02	(0.0062)	(0.0069)
122*	3.30	0.07	0.02	<0.005	0.004	0.07	<0.005	<0.02	0.0062	0.0069
123*	3.10	1.50	0.02	<0.005	0.005	0.06	<0.005	<0.02	(0.006)	(0.007)
124*	3.15	5.38	0.03	0.005	0.004	0.06	<0.005	<0.02	(0.006)	(0.007)
125*	3.15	1.81	0.50	<0.005	0.004	0.06	<0.005	<0.02	(0.006)	(0.007)
126*	3.10	1.55	2.71	<0.005	0.004	0.06	<0.005	<0.02	(0.006)	(0.007)
127*	0.058	0.06	0.08	<0.005	0.003	4.85	<0.02	6.97	(0.023)	(0.0046)
127*	0.096	0.06	0.08	<0.005	0.004	4.49	<0.02	6.84	0.023	0.0046
128*	0.015	0.06	0.08	<0.005	0.002	9.65	<0.02	9.84	(0.050)	(0.020)
129*	0.013	0.03	0.08	0.007	0.002	20.1	<0.02	15.0	(0.100)	(0.053)
130*	0.014	0.05	<0.05	<0.005	0.003	39.6	<0.02	19.9	(0.200)	(0.115)
131*	0.018	0.07	<0.05	0.006	0.003	54.0	<0.02	24.7	(0.276)	(0.160)
132*	0.017	0.03	<0.05	<0.005	0.002	53.7	<0.02	42.9	(0.273)	(0.157)
132*	0.029	0.20	<0.05	0.006	0.004	53.4	<0.02	43.5	0.273	0.157
133*	1.18	<0.05	<0.05	<0.005	0.003	66.0	<0.02	32.2	(0.153)	(0.093)
133*	1.23	0.06	<0.05	0.006	0.003	66.6	<0.02	31.5	0.153	0.093
134*	6.9	0.06	<0.05	0.006	0.006	62.5	<0.02	30.5		

* Analyses on test sample rather than actual pot sample

Brackets signify uncertainty: For O and N = interpolated values
For measured temperatures = inconclusive thermal analysis

(Contd...)

TABLE 3.1
(Continued)

TABLE3.1b (Continued)

Sample No.	C	Si	Mn	P	S	Cr	Mo	Ni	O	N
135	0.009	2.21	15.40	<0.005	0.003	<0.02	<0.005	<0.02		
136	0.011	0.60	15.60	<0.005	0.003	<0.02	<0.005	<0.02		
137	0.007	2.18	5.53	<0.005	0.002	<0.02	<0.005	<0.02		
138	0.010	2.11	0.10	0.005	0.002	10.20	<0.02	0.05		
139	0.011	0.55	0.04	0.005	0.002	10.20	<0.02	0.05		
140	0.008	2.07	0.03	0.004	0.002	5.37	<0.02	<0.02		
141	0.008	2.17	0.03	<0.005	0.001	<0.02	<0.02	9.07		
142	0.005	2.18	0.03	<0.005	0.001	<0.02	<0.02	6.13		
143	0.005	0.43	0.03	<0.005	0.001	<0.02	<0.02	6.04		
144	0.007	2.34	0.03	<0.005	0.008	<0.02	9.95	0.07		
145	0.007	0.46	0.03	<0.005	0.012	<0.02	10.05	0.07		
146	0.008	2.06	0.03	<0.005	0.005	<0.02	5.25	0.04		
147	0.020	0.98	0.30	0.012	0.013	0.08	<0.005	0.02		
148	0.011	0.06	0.05	<0.005	0.58	0.03	0.010	0.08		
149 a	0.005	0.23	<0.02	<0.005	0.11	<0.02	<0.005	<0.02		
b	0.009	0.18	0.03	<0.005	0.13	<0.02	<0.005	0.03		
150	0.006	0.24	0.09	0.46	0.003	<0.02	<0.005	0.02		
151	0.006	0.21	0.04	0.10	0.002	0.02	0.005	0.03		
152	0.28	0.30	0.06	0.54	0.003	<0.02	0.005	0.02		
153 a	0.31	0.30	0.04	0.10	0.002	<0.02	<0.005	<0.02		
c	0.25	0.30	0.04	0.11	0.002	<0.02	<0.005	<0.02		
154 b	0.67	0.73	0.08	0.51	0.002	<0.02	<0.005	<0.02		
c	0.64	0.76	0.08	0.54	0.002	<0.02	<0.005	<0.02		
155	0.72	0.36	0.07	0.11	0.002	<0.02	<0.005	<0.02		
156	0.51	0.39	0.11	<0.005	0.003	<0.02	<0.005	5.05		
157	0.27	0.36	0.05	<0.005	0.002	<0.02	<0.005	5.10		
158	0.27	0.24	0.04	<0.005	0.001	<0.02	<0.005	2.50		
159 a	0.99	0.36	0.12	<0.005	0.003	10.1	<0.02	<0.02		
b	0.98	0.36	0.13	<0.005	0.003	10.0	<0.02	<0.02		
160**	0.54	0.33	0.08	<0.005	0.003	10.0	<0.02	<0.02		
161 b	0.96	0.51	0.08	<0.01	0.013	0.25	9.8	0.03		
c	0.94	0.52	0.08	<0.01	0.015	0.25	10.1	0.03		
162	0.50	0.53	0.05	<0.01	0.013	0.02	9.7	0.02		

** +0.014% N, 0.017% O

TABLE 3.1
(Continued)

TABLE 3.1b RELATED WORK, REF. 129

Cast No.	C	Si	Mn	P	S	Cr	Mo	Ni	Co	Cu	N
201	0.036	2.13	1.59	0.005	0.003	19.1	<0.02	12.1	<0.02	<0.02	0.028
205	0.029	1.98	1.60	0.005	0.002	19.1	<0.02	16.1	<0.02	<0.02	0.031
206	0.027	0.58	1.56	0.006	0.002	22.1	<0.02	12.1	<0.02	<0.02	0.045
210	0.027	0.55	1.53	0.006	0.002	21.8	<0.02	16.0	<0.02	<0.02	0.041
211	0.028	0.58	1.63	0.006	0.002	25.3	<0.02	16.1	0.02	<0.02	0.057
214	0.025	0.62	1.56	0.006	0.002	25.3	<0.02	19.1	<0.02	<0.02	0.052
215	0.017	0.44	1.47	0.005	0.002	18.4	<0.02	9.5	<0.02	<0.02	0.033
218	0.024	0.43	1.42	0.007	0.003	18.7	<0.02	9.6	<0.02	<0.02	0.178
219	0.026	0.55	1.59	0.005	0.007	17.5	2.53	11.0	<0.02	0.03	0.034
222	0.014	0.60	1.54	0.008	0.004	17.7	2.34	11.1	<0.02	0.03	0.220

TABLE 3.2
LIQUIDUS AND PRIMARY PHASE PREDICTIONS

TABLE 3.2.1 LOW ALLOY AND QUASIBINARY STEELS

(a) Previous Work

No.	T_{Liq} (Measured) °C	T_{Liq} (Predicted) - T_{Liq} (Measured)			Primary Solidification Phase		
		Original	Modified	MTDATA	Actual	Peritectic Equivalent	MTDATA
1	1505	2.7	2.7	-4		0.54, δ	δ
2	1490	3.5	3.5	-3		0.89, δ	γ
3	1476	2.8	2.8	3		1.17, γ	γ
4	1464	3.3	3.3	1		1.43, γ	γ
5	1472	5.0	5.0	-6		0.86, δ	γ
6	1456	4.0	4.0	2		1.59, γ	γ
7	1437	-0.8	-0.8	-3		2.14, γ	γ
8	1408	6.4	6.4	3		2.67, γ	γ
9	1467	-0.2	0.3	-3		0.96, δ	δ
10	1424	-3.9	-3.2	-1		2.01, γ	γ
11	1413	-10.5	-7.5	2		2.41, γ	γ
12	1409	-7.0	-4.8	2		2.40, γ	γ
13	1502	-2.5	-2.5	-17		-1.01, δ	δ
14	1499	2.1	2.1	-14		-0.90, δ	δ
15	1500	1.0	1.0	-13		-0.89, δ	δ
16	1497	1.3	1.3	-16		-1.17, δ	δ
17	1501	-1.7	-1.7	-6		-1.04, δ	δ
18	1501	-0.4	-0.4	-12		-1.09, δ	δ
19	1501	-4.4	-4.4	-12		-1.22, δ	δ
20	1495	2.0	2.0	1		1.81, γ	γ
21	1454	-0.5	-0.5	4		6.24, γ	γ
22	1488	-3.3	-3.3	-43		-1.49, δ	δ
23	1483	2.1	-2.1	-43		-1.47, δ	δ
24	1478	-6.1	-6.2	-39		-1.48, δ	δ
25	1529	1.0	1.0	7		0.01, δ	δ
26	1530	1.3	1.3	3		-0.08, δ	δ
27	1513	3.6	3.6	6	δ	0.29, δ	δ
28	1514	0.9	0.9	1	δ	0.29, δ	δ
29	1507	1.6	1.5	-5	δ	0.33, δ	δ
30	1504	4.0	4.0	4	δ	0.39, δ	δ
31	1498	0.4	0.4	-1	δ	0.67, δ	δ
32	1471	2.0	2.0	4	γ	1.31, γ	γ
33	1457	-4.5	-4.5	-4	γ	1.88, γ	γ
34	1501	2.5	2.5	10	δ	0.70, δ	γ
35	1502	2.0	2.0	5	δ	0.53, δ	δ
36	1492	-2.6	-2.7	4	δ	1.01, γ	γ
37	1501	2.1	2.0	2	δ	0.46, δ	δ
38	1486	2.0	1.9	4	δ/γ	1.03, γ	γ
39	1494	3.3	3.3	-4	δ	0.57, δ	δ
40	1482	1.7	1.7	0	γ	0.92, δ	γ
41	1471	-4.7	-4.7	0	γ	1.47, γ	γ
42	1450	1.2	1.2	-3	γ	1.77, γ	γ
43	1506	4.1	4.0	-5	δ	-0.29, δ	δ
44	1470	4.1	3.6	-11	δ	-0.13, δ	δ
45	1460	0.3	-0.3	-9	δ	0.17, δ	δ
46	1436	2.3	2.0	2	γ	1.24, γ	γ
47	1476	2.2	2.2	-25	δ	0.07, δ	δ
48	1500	-0.3	-0.3	-10	δ	-0.86, δ	δ
49	1494	-2.2	-2.2	-4	δ	-0.35, δ	δ
50	1482	1.4	1.4	-6	δ	-0.41, δ	δ
Correlation coefficient		0.994	0.995	0.918	Successful predictions	22/24	22/24
Differences: Mean		0.54	0.49	-50.4			
Min.		-10.1	-7.5	-43.0			
Max.		7.4	6.4	10.0			
Std. Dev.		3.38	3.06	11.67			

Contd...

TABLE 3.2
(Continued)

TABLE 3.2.1 (Continued)

(b) Present Work

No.	T_{Liq} (Measured) °C	T_{Liq} (Predicted) - T_{Liq} (Measured)			Primary Solidification Phase		
		Original	Modified	MTDATA	Actual	Peritectic Equivalent	MTDATA
101	1170	9.2	9.2	21	γ	7.55, γ	γ
102	1285	-6.8	-6.8	-9	γ	6.02, γ	γ
103	1285	-4.7	-4.7	-3	γ	5.95, γ	γ
104	1270	1.6	1.6	-26	γ	5.47, γ	γ
105	1272.5	13.9	13.9	-6.5	γ	5.54, γ	γ
107	1285	15.0	15.1	-23	γ	4.88, γ	γ
108	1292.5	11.4	11.4	-17.5	γ	4.76, γ	γ
120	1520.7	0.9	0.9	-5.5	δ	-0.27, δ	δ
121	1467	1.3	1.3	-16	δ	-1.25, δ	δ
122	1277	-11.7	-11.7	-15	γ	6.22, γ	γ
127	1494	-0.3	-0.3	2	γ	1.16, γ	γ
128	1481	2.0	2.0	4	γ	1.20, γ	γ
135	1442	-6.9	-2.0	-14	δ*	0.67, δ	δ
136	1462	-10.0	-4.5	-12	γ	1.11, γ	δ
137	1485.5	-0.4	-0.4	-10.5	-	-0.11, δ	δ
138	1494.5	2.8	2.8	43.5	δ	-1.28, δ	δ
139	1511	4.0	4.0	4	-	-0.87, δ	δ
140	1501	6.1	6.1	-24	δ	-0.93, δ	δ
141	1477	4.8	4.8	-14	-	1.19, γ	γ
142	1483.5	4.0	4.0	10.5	-	0.62, δ	δ
143	1505	2.2	2.2	-6	γ*	1.06, γ	γ
144	1485.1	-17.0	-5.2	-39	δ*	-2.44, δ	δ
145	1501.5	-13.0	-0.3	-4.5	δ*	-1.97, δ	δ
146	1494	-3.1	-4.2	-14	δ*	-1.49, δ	δ
147	1521	2.9	2.9	-3	-	-0.19, δ	δ
148	1511.5	-0.2	0	4.5	-	0.14, δ	δ
149a	1525.5	4.4	4.4	4.5	-	-0.02, δ	δ
149b	1527	2.0	2.0	3	-	0, δ	δ
150	1513	5.0	5.0	8	δ*	-0.02, δ	δ
151	1526	4.8	4.7	5	-	-0.03, δ	δ
152	1489.5	1.5	1.5	3.5	-	0.49, δ	δ
153a	1503	0.6	0.6	1	-	0.52, δ	δ
153c	1509.5	-1.0	-1.0	-0.5	-	0.40, δ	δ
154b	1453	4.6	4.6	-3	δ*	1.11, γ	γ
154c	1456	2.4	2.4	-6	δ*	1.05, γ	γ
155	1470	1.1	1.1	0	-	1.28, γ	γ
156	1474.5	-8.7	-8.7	-3.5	γ*	1.84, γ	γ
157	1492	-5.5	-5.5	-3	-	1.40, γ	γ
158	1498	0.5	0.5	3	-	0.93, δ	δ
159a	1432.5	7.8	7.8	-1.5	γ*	1.03, γ	γ
159b	1435	6.1	6.1	-4	γ*	1.02, γ	γ
160	1471	1.5	1.5	-14	γ*	0.19, δ	δ
161b	1403	11.6	-	0	-	-0.16, δ	γ
161c	1408.5	6.2	-	-5.5	-	-0.25, δ	γ
162	1462	-14.6	-3.9	-18	δ*	-1.00, δ	δ
Correlation coefficient		0.997	0.997 (0.998)	0.985	Successful predictions	37/39	36/39
Differences: Mean		0.63	0.38 (0.97)	-6.01			
Min.		-17	-11.7 (-11.7)	-43.5			
Max.		15.1	22.8 (15.1)	21.0		10*/13*	10*/13*
Std. Dev.		5.44	5.17 (4.35)	11.89			

* Suggested primary phase, but possibly in error

TABLE 3.2
(Continued)

TABLE 3.2.2 HIGH CrNi ALLOYS

(a) Previous Work

No.	T_{Liq} (Measured) °C	T_{Liq} (Predicted) - T_{Liq} (Measured)			Primary Solidification Phase	
		FeCrNi Ref. 117	FeCrNi Ref. 128	MTDATA	Actual	MTDATA
51	1447	-17.60	-10.60	-16		δ
52	1431	-17.90	-12.90	-24		δ
53	1432	-14.10	-12.10	-20		δ
54	1441	-16.40	-12.40	-34		δ
55	1457	3.20	-5.80	-13		δ
56	1454	3.60	-4.40	-29		δ
57	1444	4	-8	-10		δ
58	1415	6.10	-4.90	-70		γ
59	1408	-3.90	6.10	-7		γ
60	1404	-1.80	6.20	-20		γ
61	1434	7	0	-33		γ
62	1411	-10.30	4.70	-30		γ
63	1417	-17.50	-0.50	-25		γ
64	1433	5.70	0.70	-30		γ
65	1431	3.50	-1.50	-30		γ
66	1449	2.90	-4.10	-27		γ
67	1445	7.50	-7.50	-4		δ
68	1449	4.40	-10.60	-10		δ
69	1458	-13.30	-10.30	-8		δ
70	1458	-14.20	-11.20	-8		δ
71	1469	-12.90	-3.90	-20	δ	δ
72	1449	8.30	-6.70	-6	δ	δ
73	1448	10.60	-3.40	-2	δ	δ
74	1452	1.70	-7.30	-11	δ	δ
75	1440	5.10	-2.90	-17	δ	δ
76	1423	10.80	3.80	-10	δ/γ	γ
77	1427	6	7	-13	γ	γ
78	1421	-12.60	4.40	-15	δ/γ	γ
79	1421	-5.10	-2.10	-12	γ	γ
80	1401	-4.10	7.90	-6	γ	γ
81	1400	-1.50	11.50	-32	γ	γ
82	1405	-6.90	3.10	-16	γ	γ
83	1391	-6.50	12.50	6	γ	γ
84	1385	-12.10	-3.10	-35	γ	γ
85	1400	7.80	26.80	12	γ	γ
86	1423	-10.30	-5.30	9	δ*	γ*
87	1400	-13.50	-8.50	1	δ*	γ*
Correlation coefficient		0.928	0.931	0.822	Successful predictions	15/15
Differences: Mean		-3.09	-1.77	-16.62		
Min.		-17.9	-12.9	-70.0		
Max.		10.8	26.8	12.0		
Std. Dev.		9.32	8.39	15.19		

Contd...

TABLE 3.2
(Continued)

TABLE 3.2.2 HIGH CrNi ALLOYS

(b) Present Work

No.	T_{Liq} (Measured) °C	T_{Liq} (Predicted) - T_{Liq} (Measured)			Primary Solidification Phase	
		FeCrNi Ref. 127	FeCrNi Ref. 128	MTDATA	Actual	MTDATA
109	1349	-14	19	-2	δ/γ	γ
110	1366	4	22	14	γ	γ
111	1372	-27	-7	-5	δ	δ
112	1472	-12	-17	19	δ	δ
113	1441	-11	-35	20	δ	δ
114	1467	-17	-6	45	δ	δ
115	1463	-68	-44	-48	δ	δ
116	1394	-9	-15	5	δ	δ
117	1432	-17	-38	13	δ	δ
118	1423	-8	-14	-2	δ	δ
119	1442	-17	-12	-2	δ	δ
127	1494	0	0	2	γ	γ
128	1481	2	2	4	γ	γ
129	1446	-22	-9	-4	γ	γ
130	1440	-35	-25	19	δ	δ
201	1426	-13	-3	-7	δ	δ
205	1416	-9	9	1	γ	γ
206	1442	-11	-13	-1	δ	δ
210	1428	-11	1	-7	γ	γ
211	1424	-15	-7	-6	δ	δ
214	1415	-8	2	-7	γ	γ
215	1457	4	-12	-1		δ
218	1449	1	-13	-4		δ
219	1441	1	-5	-8		δ
222	1433	-2	-8	-12		δ/γ
Combined, FeCrNi data						
Correlation coefficient		0.908	0.896	0.849	Successful predictions	36/36
Differences: Mean		-6.91	-4.73	-9.50		
Min.		-68.0	-44.0	-70.0		
Max.		10.8	26.8	45.0		
Std. Dev.		12.73	12.20	17.77		
All data						
Correlation coefficient		0.987		0.970		72/75
Differences: Mean		-2.18		-7.41		
Min.		-68.0		-70.0		
Max.		15.08		45.0		
Std. Dev.		9.51		14.57		

TABLE 3.3
"BS" CALCULATION SCHEMES (REF. 121)

	Liquidus	Solidus
	Datum 1537°C	Datum 1537°C
C	C<0.471: -87C 0.471 <C<1: -70C -8 1<C: -76C -2	C<0.09: -467C 0.09<C<0.17: -42 0.17<C: -177C -11.91
Si	Si<1: -9Si 1<Si: -Si² -9Si + 1	-18.85Si - 0.8Si² + 0.0366Si³
Mn	-5Mn	-7Mn
P	-34P	-450P + 370P² - 120P³
S	-40S	-170S
Cr	-0473Cr -0.208Cr²* + 0.0123Cr³ - 0.00018Cr⁴	Cr<20: -1.85Cr + 0.035Cr² 20<Cr: -0.95Cr + 0.035Cr² -18
Mo	Mo<1: -6 Mo 1<Mo: -4 Mo -2	-3.5Mo
Ni	Ni<4.4: -5Ni* 4.4<Ni: -1.92Ni - 13.54*	Ni<4.3: -5.3Ni 4.3<Ni<4.7 22.79 4.7<Ni: -3.2Ni + 0.0277Ni² -10.7
Al	0	0
Co	-2Co	-3Co
Cu	-5Cu	-8.5Cu
Sn	-8Sn	-30Sn
Ti	-15Ti	-46Ti + 2.7Ti²
V	V<1: -3V 1<V<2: -4V + 1 2<V: -3V - 1	-7V
Nb	-9Nb	-50Nb
W	-0.2W	-W
O	-630	
N	-72N	-186N -30 (cooling rate)

* For high Cr-Ni steels the datum should be the relevant Fe-Cr-Ni liquidus temperature

Current Amendments: Mn > 12.5, -(10Mn + 62.5)/3
Mo, -(19Mo - Mo²)/3

TABLE 3.4
THERMAL SOLIDUS PREDICTIONS

No.	Cooling Rate K s^{-1}	DTA Solidus, °C	Prediction - Measurement, K
27	0.824	1445	-9
27	0.271	1450	2.6
27	0.086	1455	3.1
28	0.714	1440	10.1
28	0.326	1440	21.7
28	0.079	1460	9.1
29	1.059	1415	16.2
29	0.357	1430	22.2
29	0.079	1460	0.6
30	1.000	1425	10.5
30	0.310	1440	16.2
30	0.075	1460	3.2
31	0.941	1415	-1.6
31	0.326	1425	6.8
31	0.071	1440	-0.5
32	1.286	1335	5.6
32	0.440	1355	10.9
32	0.103	1370	6.1
33	1.318	1310	-18.8
33	0.450	1320	-2.7
33	0.075	1340	-11.5
34	0.588	1450	-8.8
34	0.238	1450	1.7
34	0.055	1465	-7.8
35	0.842	1420	11.5
35	0.326	1425	22
35	0.080	1445	9.4
36	1.125	1395	17.5
36	0.325	1430	6.5
36	0.070	1445	-0.8
37	0.842	1420	9.5
37	0.295	1435	10.9
37	0.087	1450	2.1
38	0.875	1415	-1.7
38	0.273	1425	6.4
38	0.077	1435	2.2
39	1.059	1405	5.1
39	0.348	1415	16.4
39	0.104	1425	12.2
40	1.176	1380	-1.9
40	0.380	1385	16.9
40	0.115	1400	9.9
41	1.350	1335	12.8
41	0.385	1370	6.8
41	0.132	1375	9.4
42	1.059	1270	20.6
42	0.455	1300	8.7
42	0.107	1300	19.2
Correlation coefficient			0.983
Differences: Mean			6.66
Min.			-18.7
Max.			22.3
Std. Dev.			9.20

TABLE 3.5

EQUILIBRATION FURNACE SAMPLES

Sample	Composition C	Si	Mn	Cr	Mo	Ni	Liquidus oC	Test Temperature	Test Status
EF1	0.82	0.23	0.56				1466	1452	Good
EF2	"	"	"				"	1463	Good
EF3	"	"	"				"	1470	No Quench
EF4	"	"	"				"	1451	No Quench
EF5	"	"	"				"	(1450)	Good but loss of t/c signal
EF6 (156)	0.51	0.39	0.11	<0.02	<0.005	5.05	1474.5	1452	Good but too solid
EF7 (156)	"	"	"	"	"	"	"	1470	Good
EF8 (137)	0.007	2.18	5.53	<0.02	<0.005	<0.02	1485.5	1485	Good
EF9 (162)	0.50	0.53	0.05	0.02	9.7	0.02	1462	1461	No Quench

TABLE 3.6

THERMAL HISTORIES AND TEMPERATURE VARIABILITY

CASE	RAKE (mins. to temp)	SOAK mins. at temp.,		+/-	TEMP. @ Hmm above datum H=5	10	15	20
EF1	120	55	1452	2.5		+10		
EF2	70	50	1463	2	+7	+21		+35
2/2/89	55	20	650	0.5	+1.5	+1.5		-5
13/2/89	20	20	663	0.5	-1			
	+15	10	803	1.5		+1.5	+1.5	-2
EF3	60	30	1470	2.5		+1	-3	
				9*				
19/4/89	0	-	22	0	0	0	0	0
			168					-48
			303			-15		-50
			500			+6		-13
						-1	-4	-14
EF4	45	25	1451	2				
EF5	47	5	1452		0	-8	t/c failure	
EF6	65	35	1452	0.25	-5/+3			
EF7	40	30	1470	0				
EF8	80	30	1485	1	+3			
EF9	60	45	1461		-1			

*9oC increase upon accidentally jolting the furnace

TABLE 37
PARTITION COEFFICIENTS

Sample	Phase Pair	C			Si			Mn			Cr			Ni		
		(a)	(b)	(c)	(a)	(b)	(c)	(a)	(b)	(c)	(a)	(b)	(c)	(a)	(b)	(c)
4	γ/L	(0.69)	0.37	0.38		(>1.0)	1.26	0.77	0.75	0.70						
9	δ/L γ/L										1.19 0.94	1.26 0.79	1.16 0.90	0.81 1.05	0.77 1.30	0.85 1.08
19	δ/L δ/γ										1.06 -	1.12 1.23	1.09 1.28	0.79 -	0.74 0.67	0.78 0.68
29	γ/L										0.94	-	0.87	0.93	-	1.05
EF1	γ/L	-	-	0.37	-	0.88	0.75	-	0.78	0.69						

(a) Core/bulk (= k under Scheil condition)
(b) Dendrite/matrix (= k under Lever Rule condition)
(c) MTDATA prediction (ignoring minor changes with temperature)

Back diffusion should always result in (a) being nearer unity than in (b), with the actual k lying between the two)

TABLE 4.1
SIMPLIFIED PERITECTIC DATA

Solute	$m_{(\delta/L)}$	$m_{(\gamma/L)}$*	$m_{(\delta/\gamma)}$	$k_{(\delta/L)}$	$k_{(\gamma/L)}$*	$k_{(\delta/\gamma)}$	Ep*
C	-83	-62.3	+1122	0.17	0.32	1.88	1.898
Si	-9	-11.9	-67	0.70	0.60	0.85	-0.261
Mn	-5.1	-4.2	+8.75	0.74	0.78	1.05	0.080
P	-34	-33.4	-200	0.13	0.06	0.45	0.055
S	-40	-37.7	-200	0.05	0.02	0.40	0.207
Cr	-1	-1.8	-12.5	0.95	0.80	0.85	-0.075
Mo	-2.5	-4.6	-40	0.74	0.55	0.75	-0.187
Ni	-5	-2.9	+29	0.79	0.90	1.14	0.192
Ti	-18	-23	-167	0.50	0.25	0.50	-0.452
N	-72	-57.4	+480	0.25	0.47	1.88	1.324

* Derived from the other values m values in K/wt. %

TABLE 4.2

COMPARISON OF EXPERIMENTAL AND COMPUTED SOLIDIFICATION DATA:
Jernkontoret Steel 306 (Type 410S),
HISEG (non-peritectic) program

	Furnace Cooling Rate C/s	Heat Extraction Rate $MJ/m^3 s$	Liquidus C	Solidus* C	Solidification Time s	Final λ um
Exp^t	2	29	1497	1435	80	205
Calc^n			1498	1435	78	209
Exp^t	0.5	11	1500	1440	210	260
Calc^n			1498	1438	204	252

TABLE 4.3

ALTERNATIVE PERITECTIC CARBON EQUIVALENT FORMULAE

Source	C	Si	Mn	P	S	Cr	Mo	Ni
ref.126	1	-0.29	0.07	0.06	0.15	-0.11	-0.06	0.17
ref.142	1	-0.123	0.04		0.06	-0.018	-0.05	0.08
Ref.142	(Beckett & Howe) used in the PHASEG program							

TABLE 4.4

COMPARISON OF EXPERIMENTAL AND COMPUTED SOLIDIFICATION DATA:
Three examples from ref.100 (Jernkontoret) versus PHASEG program

Temperature,oC	Steel 202 (low C)		Steel 310 (low C,high Cr)		Steel 205 (medium C)	
	Exp.	Calc.	Exp.	Calc.	Exp.	Calc.
Liquidus	1515	1514	1500	1498	1498	1498
Peritectic (max)	1475	1471	n/a	n/a	1480	1482
Solidus*	1440	1447	1440	1438	1425	1392

The steel designations are those used in ref.100 and are not international specifications

* Tables refer to the non-equilibrium solidus

Table 4.5

Fe-Cr-C
Ternary Equilibrium Data used for Derivations of Solvus Slope and Partition Coefficient Equations (Rickinson/Ogilvy, ref.146)

Temp. K	Liquid Composition Chromium Lcr	Liquid Composition Carbon Lc	Partition Coeff. Chromium Kcr	Partition Coeff. Carbon Kc	
1767	5.20	0.49	0.86	0.20	*
1737	6.05	0.77	0.80	0.31	
1728	1.67	0.85	0.80	0.35	
1723	2.30	1.10	0.77	0.33	
1723	3.14	1.15	0.76	0.40	
1715	1.62	1.11	0.79	0.33	
1712	1.65	1.20	0.74	0.33	
1693	3.26	1.56	0.72	0.32	
1682	2.93	1.77	0.71	0.34	
1673	1.55	1.73	0.69	0.33	
1656	2.98	2.08	0.69	0.38	
1651	3.07	2.33	0.67	0.39	

* Ferrite solid phase (others austenite)

TABLE 4.6
DIFFUSIVITY DATA (REF. 147)

Self Diffusion of Iron D_{Fe}		Ferrite	Austenite
		1.6 × 10-4 Exp (-240000/RT)	0.7 × 10-4 Exp (-286000/RT)
Factors on D_{Fe} for the other elements	C	Assumed infinite	Assumed infinite
	Si	7	2
	Mn	1	2
	P	6	30
	Cr	2	3
	Mo	2	3
	Ni	1	0.5

TABLE 5.1

NUMERICAL STABILITY AND CONSISTENCY v MESH SIZE

Table 5.1a: Test Conditions

1 wt% "Z" with k=0.2, m_l=-10, 100um cell (200um arm spacing)
$D=10^{-11} m^2/s$

Cooling rate W=1oC/s, or heat extraction such as to give 90-100s solidification time.

Corresponding Clyne-Kurz result ca 15%Z with root-time growth

Programs: a) MISEG, binary with constant cooling rate.
b) MISEG1, binary with constant heat extraction.
c) PHASEG, multicomponent capability, constant heat extraction, reduced time steps towards solidus.
d) MISEG2, binary with root-time heat extraction.

Table 5.1b: Final Liquid Composition at Solidus, %

Nodes	(a)	(b)	(c)	(d)
10	10.3	127.7	23.6	21.6
12	11.0	-8.8		19.2
15	11.9	21.3	22.0	19.6
20	12.4	24.4		19.1
25	12.7	18.4		19.2
30	12.9	22.4	20.9	16.7
40	13.1	24.6		16.6
50		21.2		18.8
60	13.2	20.9		17.7
100	13.2			17.6

TABLE 5.2

NUMERICAL STABILITY AND CONSISTENCY v HEAT CAPACITY

Program MISEG2, conditions as Table 5.1

Nodes \ Cp	0	1	2	3	5	10
10	37.7	20.4	19.1	24.8	21.6	20.6
15	118.8		27.9		19.6	20.0
20	-115.2	29.7	19.9		19.1	16.6
30	53.1		23.0		16.7	

TABLE 5.3

EFFECT OF RE-MESHING ON NUMERICAL CONSISTENCY

Nickel binary case as described in text, comparing difference in final residual liquid content between text case and 100-node datum result.

Number of nodes and fraction solid at re-mesh operation			ΔNi
		10	2.57
20 to 0.9fs, then		10	2.45
10	0.9	20	1.30
10	0.8	20	1.27
		20	1.26
10	0.9	50	0.44
20	0.9	50	0.41
20	0.8	50	0.41
		50	0.40
10	0.9	100	0.04

TABLE 5.4

EXAMPLE COMPARISON OF STANDARD AND MOVING-GRID FORMULATIONS REGARDING NUMERICAL CONSISTENCY

Zo=1%, k=0.2, m=-10, 0=5, Q=300 /t

Peak Z% \ Nodes:	10	20	40	50	100
Standard	21.5	18.5	17.8	17.6	17.6
Moving grid	14.7	15.9	16.3	16.8	17.1

TABLE 5.5
CORE AND PEAK MANGANESE CONCENTRATIONS AT SOLIDUS FOR A GIVEN MODULUS, M

Conditions		n = 0	n = 0.25	n = 0.333	n = 0.5			n = 0.667	n = 0.75
λ_f = 40 μ, W = 3.7°C/s	Core Mn	1.240	1.284	1.298	1.323	1.323	1.305	1.346	1.357
	Peak Mn	3.902	2.833	2.679	2.484	2.484	2.245	2.371	2.332
	B	40	20	15.9	10	$2\sqrt{5}$	10	6.3	5
	f	1	1	1	1	0.2	1	1	1
	DIM	1	1	1	1	1	2	1	1
λ_f = 140 μ, W = 0.3°C/s	Core Mn	1.241	1.285	1.298	1.323	1.323	1.306	1.347	1.358
	Peak Mn	3.897	2.832	2.679	2.484	2.484	2.245	2.371	2.332
	B	140	37.5	24.16	10	$2\sqrt{5}$	10	4.14	2.66
	f	1	1	1	1	0.2	1	1	1
	DIM	1	1	1	1	1	2	1	1

B and n from the coarsening law, $\lambda = Bt^n$

f = factor multiplying the base diffusivity

DIM = dimensional basis of representative unit cell

TABLE 5.6

COMPUTER RUNS PERFORMED TO INVESTIGATE INFLUENCE OF DIFFUSIVITY ON MICROSEGREGATION IN BINARY AND TERNARY SYSTEMS

Base system:
Fe+10%Mn, D_{Mn} as @1450oC, $\lambda/2$=50um, Q=10mJ/m^3s, 80 nodes

Fe + 10%Mn
Fe + 5%Mn + 5%Mn (to check equivalence with the above)
Fe + 10%Z where $D_Z = D_{Mn}$ times 0.025,0.4,0.5,0.667,2,10,20,50, or infinite (Z otherwise equivalent to Mn)
For $D_z = 2D_{Mn}, 10D_{Mn}$ and infinity, Fe + 9%Mn + 1%Z Fe + 7%Mn + 7%Z Fe + 5%Mn + 5%Z Fe + 3%Mn + 7%Z Fe + 1%Mn + 9%Z
Fe + 0, 0.1 or 0.3%C with or without 1%Si and/or 1%Mn
Fe + 0.1 or 0.3%C, + 0.5%Ni

TABLE 5.7

COMPUTED RESULTS FROM Fe/C,Si,Mn,Ni TERNARIES

KEY: Liquidus, temp.
Peritectic-start, temp. and $fs^{p.s.}$
Peritectic-end, temp. and $fs^{p.e.}$
Solidus, temp. and $f\delta_{sol}$
Rates, f_R and $\Delta f/\Delta t$

%C	-		1%Si		1%Mn		1%Si+1%Mn		0.5%Ni	
0	1537		1528		1531.9		1522.9			
	-	-	-	-	-	-	-	-		
	-	-	-	-	-	-	-	-		
	1537	1	1523.8	1	1529	1	1515.8	1		
	-	-	-	-	-	-	-	-		
0.1	1528.7		1519.7		1523.6		1514.6		1526.2	
	1493	0.9774	-	-	1490.7	0.9474	-	-	1495.4	0.9437
	(1452.2	1)	-	-	(1459.6	1)	-	-		
	1493	0.8737	1475.1	1	1488.2	0.6870	1467.4	1	1494.1	0.7085
	4.589	0.0229	-	-	4.950	0.0221	-	-	4.175	0.0198
0.3	1512.1		1503.1		1507		1498		1509.6	
	1493	0.5225	1467	0.6925	1491.2	0.4540	1465.5	0.6491	1495	0.4410
	1493	0.6338	1451.5	0.9171	1490.8	0.5560	1450.8	0.8784	1494	0.5637
	1467.6	0	1418.9	0	1456.9	0	1408.6	0	1464.9	0
	4.695	0.0235	3.084	0.01315	5.450	0.0221	2.830	0.0122	3.593	0.0176

TABLE 6.1

JERNKONTORET STEELS USED FOR VALIDATION OF MICROSEGREGATION CALCULATIONS

(Full analyses in Table 3.1)

No.	C	Si	Mn	Cr	Mo	Ni
27	0.11	0.12	1.25	0.06	0.07	0.03
28	0.12	0.27	1.53	0.02	<0.03	0.03
29	0.18	0.44	1.26	0.01	0.06	0.02
30	0.19	0.40	1.42	0.07	0.02	0.13
31	0.36	0.27	0.58	0.08	0.02	0.05
32	0.69	0.23	0.72	0.02	0.01	0.02
33	1.01	0.25	0.46	0.02	0.02	0.03
34	0.10	0.28	0.57	0.14	0.14	3.30
35	0.20	0.25	0.90	0.81	0.06	1.05
36	0.27	0.02	0.32	1.66	0.42	3.50
37	0.29	0.21	0.62	1.11	0.21	0.15
38	0.29	0.22	0.52	1.02	0.25	3.20
39	0.35	0.24	0.67	0.92	0.19	0.05
40	0.52	0.22	0.85	1.07	0.07	0.07
41	0.55	0.27	0.50	0.99	0.31	3.00
42	1.01	0.23	0.33	1.55	0.01	0.02

TABLE 6.2
COMPARISON OF COMPUTED RESULTS WITH JERNKONTORET DATA
FOR CRITICAL TEMPERATURES AND EXTENT OF PERITECTIC REACTIONS

No.	Liquidus Temperature, °C			Maximum Peritectic Temperature, °C			Solidus		Prior Ferrite Fraction	
	Comp.	Exp./1.05	Exp./0.1	Comp.	Exp./1.05	Exp./0.1	Comp.	Exp./1.05	Comp.	Exp.
27	1518.5	1513	1515	1478.5	1476	1475	1424	1450	0.93	0.9
28	1516.5	1515	1514	1480.5	1475	1477	1455.5	1440	0.91	0.9
29	1510.0	1506	1507	1476.0	1470	1473	1419.0	1430	0.81	0.8
30	1509.0	1503	1506	1478.5	1477	1480	1423.0	1440	0.76	0.8
31	1501.0	1498	1501	1484.5	1480	1483	1380.0	1425	0.41	0.8
32	1476.5	1466	1474	-	-	-	1243.0	1355	0	0
33	1457.5	1457	1459	-	-	-	1183.0	1320	0	0
34	1505.0	1501	1502	1491.0	1485	1487	1442	1450	0.65	0.7
35	1507.0	1502	1503	1484.0	1474	1465	1417	1425	0.66	0.7
36	1492.0	1493	1492	-	1490	1490	1413.5	1430	0	0.4
37	1505.0	1501	1503	1478.5	1471	1475	1404.5	1435	0.61	0.8
38	1490.5	1486	1487	-	1474	1478	1393	1425	0	0.6/0
39	1500.5	1493	1495	1479.5	-	1480	1393	1415	0.49	0.6
40	1485.5	1482	1483	1481.5	-	-	1349	1385	0.10	0
41	1474.0	1471	1472	-	-	-	1271.5	1370	0	0
42	1455.5	1450	1451	-	-	-	(1212)	1300	0	0

TABLE 6.3
COMPARISON OF COMPUTED RESULTS WITH JERNKONTORET DATA FOR SEGREGATION RATIOS

No.	Mn		Cr			Mo			Ni		
	Comp.	Exp.	Comp.(a)	Comp.(b)	Exp.	Comp.(a)	Comp.(b)	Exp.	Comp.(a)	Comp.(b)	Exp.
27	1.4	1.3									
28	1.4	1.4									
29	1.6	1.4									
30	1.6	1.6									
31	1.9	1.6									
32	2.0	1.7									
33	2.1	2.1									
34			1.04	1.3	1.3	1.5	2.3	2.5	1.8	1.3	1.4
35			1.08	1.3	1.5				1.7	1.4	1.4
36			1.5		1.6	3.1		2.2	1.4		1.3
37			1.15	1.3	1.6	1.8	2.3	2.0			
38			1.6		1.7	3.4		2.2	1.4		1.4
39			1.3	1.4	1.5	2.2	2.6	2.4			
40			1.6		2.1						
41			1.7		2.1	4.2		2.5	1.5		1.2
42			1.8		2.6						

(a) Interdendritic/core ratio
(b) Maximum/minimum ratio, if different from (a)

TABLE 6.4

PEAK C and Cr, and Cr CONSERVATION with VARIABLE K_c and K_{cr}

Test case: 0.75%C,1%Cr, $\lambda/2$=100um, 1D static, Q=10mJ/m^{3}s and partition coefficient functions as in the text.
Datum conditions: program time step, δt=0.01*modulus up to fs=0.995, then 0.001*modulus

Time step factor	Nodal Grid	Peak Concentrations %C	%Cr	%Cr Conservation
(datum) 0.01/0.001	20 throughout	1.50	12.90	132
0.05/0.005	15	1.587	10.05	132
	20	1.586	10.06	124
	30	1.543	11.49	118
	15 →0.9fs, 30	1.568	10.63	117
	15 →0.9fs, 50	1.517	12.42	112
0.05/0.025	15	1.669	7.513	122
0.1/0.01	15	1.722	5.968	115
	15 →0.9fs, 20	1.707	6.361	112.5
	15 →0.9fs, 30	1.709	6.250	108
	15 →0.9fs, 50	1.683	6.997	105
0.1/0.1	15 →0.9fs, 30	1.729	5.693	107
	15 →0.9fs, 50	1.722	5.857	104
0.5/0.5	15 →0.9fs, 30	1.740	5.488	106
	15 →0.9fs, 50	1.767	4.624	102.5
	15 →0.9fs, 75	1.758	4.830	101.9
k_c const.	20	2.34	6.009	110
k_{cr} const.	20	1.684	6.898	115.5
both const.	20	2.34	4.12	106

TABLE 6.5

MICROSEGREGATION VALIDATION AGAINST TURKELI'S DATA

Code	Steel	Cooling Rate oC/s Liq.	Sol.	Quench Temp, oC	Arm Spacing um prim.	sec.	Core & Peak(ID) Compositions, wt%Mn Expt.	(a)	(b)	(c)
AT1a	0.1%C,	0.25	0.28	1445	312	110	1.43 - 1.83	1.285-2.021	1.457-1.708	1.363-1.697
AT1b	1.5%Mn	"	"	1370	"	"	1.44 - 1.71	1.313-1.869	1.50 -1.65	1.433-1.643
AT2	"	0.9	0.98	1260	252	92	1.445 - 1.75	1.206-1.980	1.528-1.616	1.388-1.725
AT3	"	1.85	2.02	1300	208	70	1.455 - 1.82	1.145-2.138	1.519-1.626	1.356-1.765
AT4	"	0.30	0.31	1220	258	100	1.465 - 1.74	1.368-1.725	1.536-1.608	1.488-1.605
AT5	"	1.05	1.11	1300	246	84	1.445 - 1.96	1.146-2.135	1.519-1.626	1.377-1.730
AT6	"	2.25	2.3	1240	186	42	1.465 - 1.85	1.146-2.084	1.532-1.612	1.364-1.745
AT7	"	0.39	0.4	1200	228	?	1.47 - 1.76	1.360-1.730	1.539-1.605	1.490-1.605
AT8	"	1.13	1.2	1250	208	?	1.455 - 1.71	1.201-1.979	1.53 -1.614	1.418-1.667
AT9	"	2.3	2.48	1270	160	?	1.455 - 1.82	1.189-2.016	1.526-1.618	1.392-1.695
AT10	0.21%C,	0.25	0.28	1225	350	115	1.44 - 2.02	1.23 -2.21	1.49 -1.72	1.35 -1.76
AT11	1.6%Mn	0.9	0.98	1285	292	83	1.44 - 2.08	1.22 -2.53	1.46 -1.75	1.28 -2.04
AT12	"	1.85	2.02	1260	248	55	1.45 - 2.01	1.16 -2.78	1.47 -1.73	1.24 -2.11
AT13	"	3.25	3.6	1330	221	60	1.42 - 2.11	1.18 -3.03	1.44 -1.78	1.23 -2.23
AT14	"	1.05	1.11	1275	225	65	1.41 - 2.17	1.20 -2.28	1.47 -1.74	1.30 -1.87
AT15	"	2.25	2.30	1270	200	45	1.41 - 2.07	1.18 -2.41	1.47 -1.74	1.26 -2.01
AT16	"	3.7	3.9	1320	180	32	1.42 - 2.18	1.11 -2.74	1.45 -1.77	1.23 -2.18
AT17	"	0.39	0.4	1120	225	65	1.41 - 1.95	1.27 -1.92	1.52 -1.68	1.50 -1.64
AT18	"	1.13	1.2	1200	220	50	1.42 - 2.10	1.18 -2.28	1.50 -1.71	1.31 -1.86
AT19	"	2.3	2.48	1290	180	35	1.41 - 2.07	1.17 -2.48	1.46 -1.75	1.29 -2.00
AT20	"	4.15	4.45	1270	170	25	1.41 - 2.09	1.15 -2.73	1.47 -1.74	1.28 -2.04
AT21	0.4%C,	0.30	0.31	1200	280	93	1.31 - 2.18	1.17 -2.14	1.41 -1.76	1.27 -1.77
AT22	1.58%Mn	1.05	1.11	1270	260	75	1.30 - 2.31	1.18 -2.59	1.39 -1.78	1.18 -2.07
AT23	"	2.25	2.3	1265	224	45	1.29 - 2.53	1.09 -2.85	1.39 -1.78	1.17 -2.17
AT24	"	3.7	3.9	1310	198	40	1.29 - 2.40	1.14 -3.22	1.38 -1.80	1.16 -2.36
AT25	"	0.39	0.4	1130	252	?	1.34 - 2.20	1.17 -1.99	1.43 -1.73	1.27 -1.76
AT26	"	1.13	1.2	1180	206	75	1.31 - 2.24	1.11 -2.18	1.42 -1.75	1.19 -1.92
AT27	"	2.3	2.48	1265	184	50	1.29 - 2.42	1.14 -2.43	1.39 -1.78	1.17 -2.03
AT28	"	4.15	4.45	1305	184	35	1.30 - 2.43	1.08 -2.99	1.38 -1.80	1.14 -2.36

TABLE 6.6

EXAMINATION OF THE ROLE OF CARBON
(All at 1.6%Mn, $\lambda/2$=50um, T=0.3)

	0.1%C	0.21%C	0.4%C
Liquidus	1520.5	1511.4	1495.6
Peritectic-start			
Temp.	1489.5	1489.9	1490.4
fs	0.93	0.64	0.155
%Mn, core	1.510	1.376	1.229
interface	1.634	1.446	1.234
liquid	2.208	1.955	1.668
Peritectic-finish			
Temp.	(1465.1)	1488.8	1490.1
fs	(1.00)	0.78	0.19
%Mn, core	1.373	1.245	1.143
liquid	-	2.158	1.684
ID	1.813	-	-
Solidus			
Temp.	1486.9	1470.5	1433.3
%Mn, core	1.532	1.347	1.289
interface	1.492	-	-
liquid	2.948	3.460	3.504
1300oC			
%Mn, core	1.546	1.452	1.360
ID	1.653	1.768	1.906

LIST of ETCHANTS EMPLOYED

NITAL (2% nitric acid in propanol)	Figs. 3.17 and 3.18
OBERHOFFERS 30g FeCl3, 1g CuCl2, 0.5g SnCl2 50ml HCl, 500ml ethanol, 500ml H_2O	Figs. 3.19 and 3.26a
"TED'S ETCH" 5% H_2SO_4 in H_2O, electrolytic at 2V	Figs. 3.21-3.25, and 3.26b
BERAHA FLUORIDE ETCH 20g ammonium bifluoride, 0.5g K_2SO_5 100ml H_2O	Fig. 3.27

Various others were employed during the course of the investigation, on the very wide range of ferrous alloys considered, e.g. 2g picric acid, 0.5g cupric chloride, 2ml Teepol, in 100ml water; an HF etch; and even electrolytic Cola as recommended for Fe-Cr-Ni alloys by fellow post graduates. Metallographic identification of primary solidification phase, where attempted, was by comparison of etching response with known cases, e.g. the primary ferrite remaining as backbones (vermicular intra-dendritic) or skeletons (lacey) in leaner Type 300 stainless series compositions, and other 'datum points' where compositions had been determined (e.g. Sample 109, Fig. 3.29). For various alloys (e.g. Sample 103/γ, or 121/δ), the composition was sufficiently far within a given primary phase field for there to be no reasonable doubt as to what the primary phase had been, even if no tell-tale morphologies and residual quantities were in the room-temperature structure.

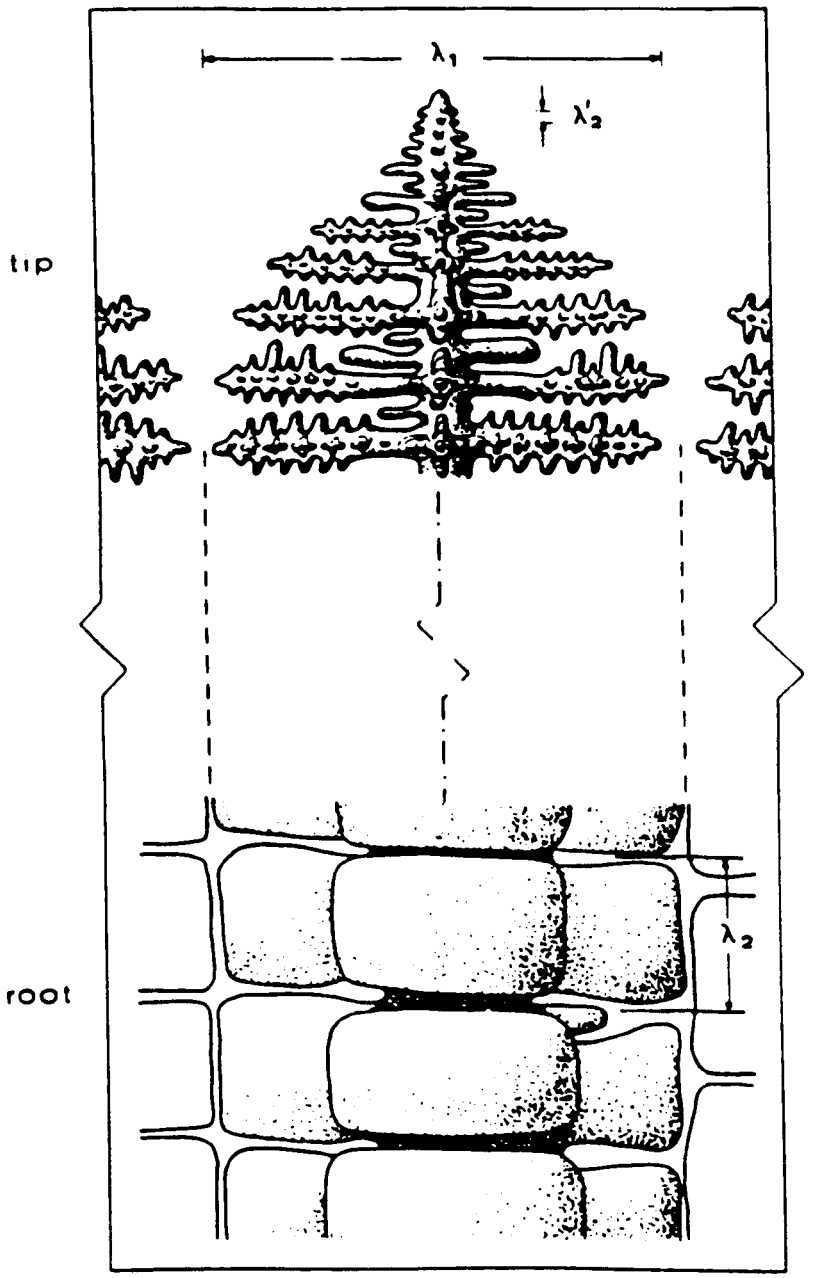

SCHEMATIC DENDRITE MORPHOLOGY AT TIP AND ROOT WITH EVIDENT COARSENING

FIG. 1.1a

(Kurz & Fisher)

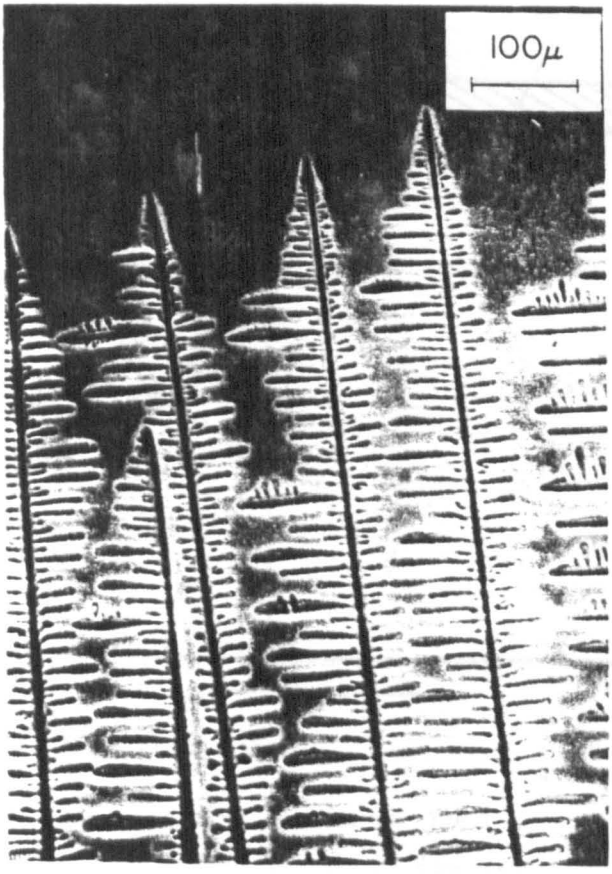

COMPETITIVE GROWTH FIG. 1.1b
(After K.A. Jackson, in 'Solidification', ASM 1971)

The dendrite arms terminate or grow and develop side branches, depending on the constraints of its surroundings. This mechanism is also implied in the tip region of Fig. 1.1a It is the dominant mechanism for the initial growth of each order of dendrite arm.

(a) Solid-Liquid Interface, $A = B + C + D$

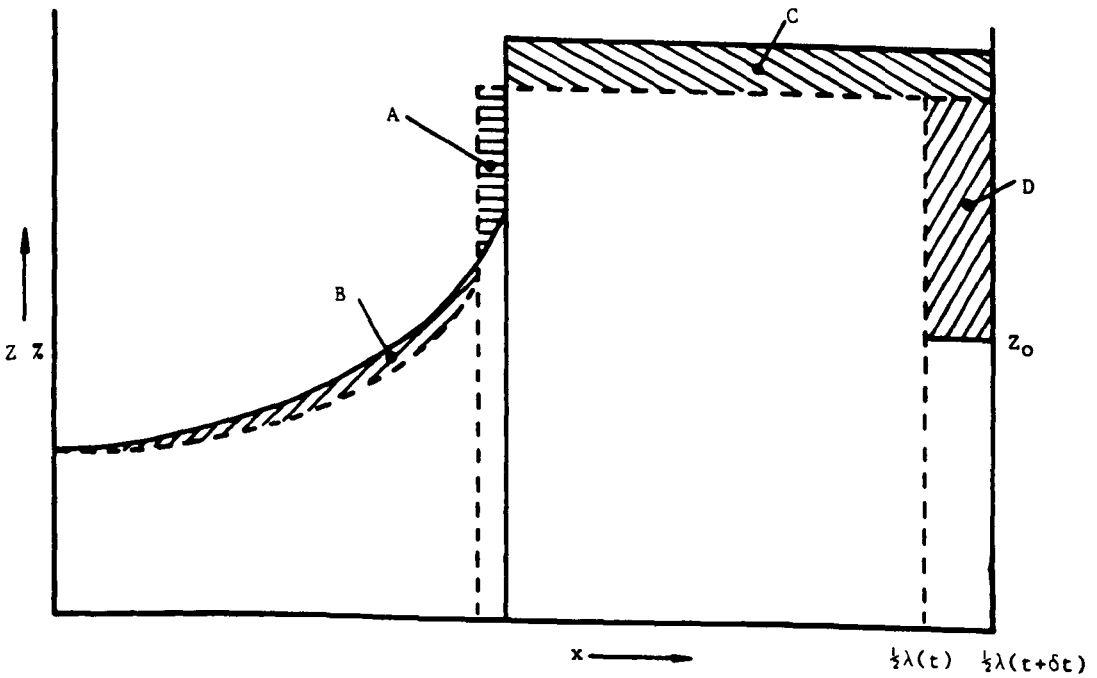

(b) Solid-Solid Interface, $A = B_1 + B_2$

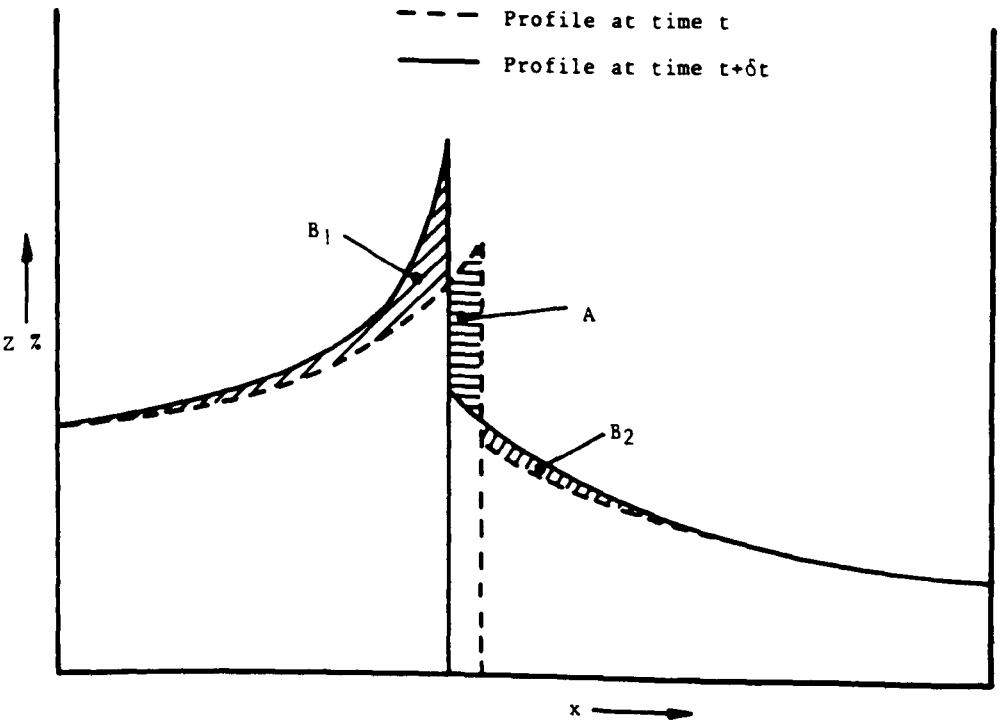

SCHEMATIC SOLUTE BALANCES

FIG. 1.2

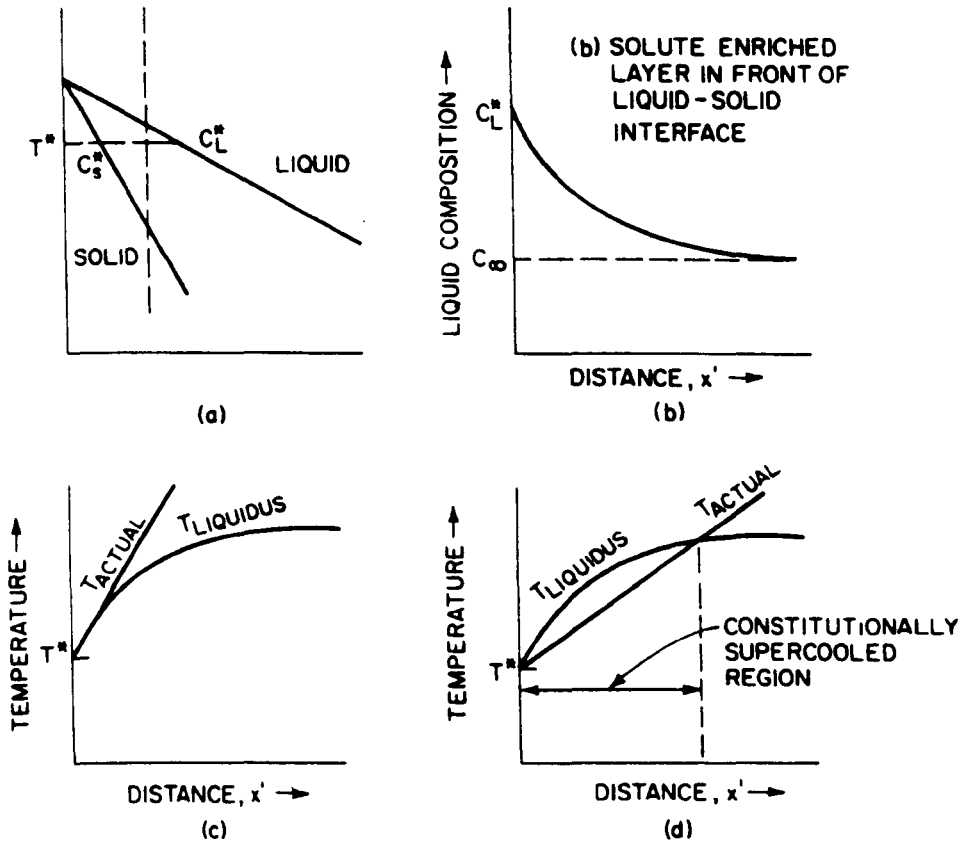

FIGURE 2-1
Constitutional supercooling in alloy solidification. (*a*) Phase diagram; (*b*) solute-enriched layer in front of liquid-solid interface; (*c*) stable interface; (*d*) unstable interface.

(Flemings)

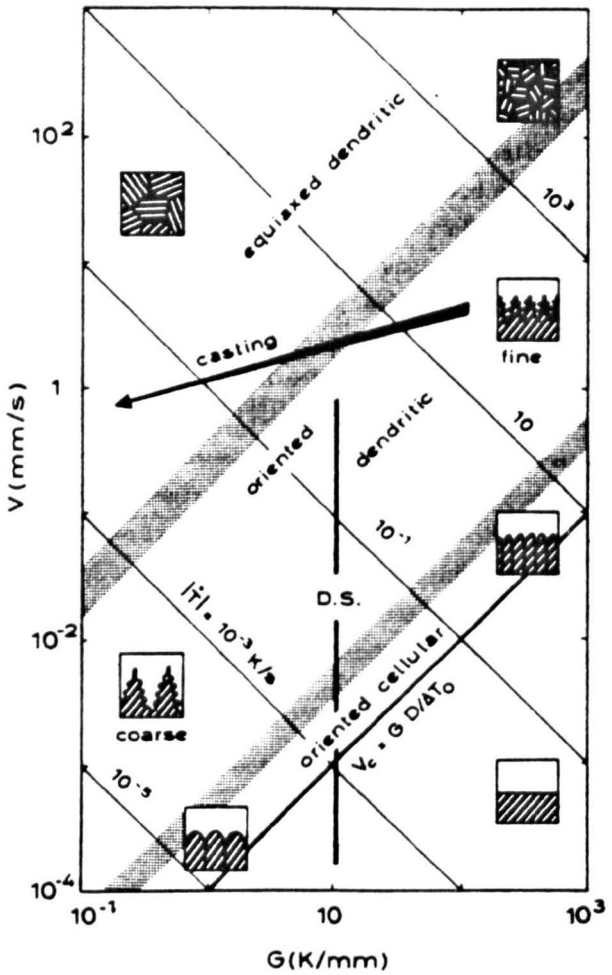

Figure 2·2 SCHEMATIC SUMMARY OF SINGLE-PHASE SOLIDIFICATION MORPHOLOGIES. This diagram summarises the various microstructures which can be obtained using a typical alloy, with a melting range (ΔT_o) of 50K, when the imposed temperature gradient, G, or growth rate, V, are varied. Provided that a unidirectional heat flow is imposed, the product, GV, is equivalent to the cooling rate, $\dot{T}$, which controls the scale of the microstructures formed. The ratio, G/V, largely determines the growth morphology. Moving from the lower left to the upper right along the lines at 45° leads to a refinement of the structure without changing the morphology (G/V = constant). Crossing these lines by passing from the lower right to the upper left leads to changes in morphology (from planar, to cellular, to dendritic growth), and the scale of the microstructure remains essentially the same ($\dot{T}$ = constant). The grey bands define the regions over which one structure changes into another. The conditions required to produce single-crystal turbine blades are those at the upper end of the thick vertical line (DS = directional solidification). Processes which produce perfect single crystals, such as those required for semiconductor-grade silicon preparation are found at the bottom of the same vertical line. (For single crystal growth, all but one of the crystals initially present must be eliminated.) In a conventional casting, the growth conditions at the solid/liquid interface change with time approximately in the manner indicated upon following the inclined arrow from right to left. Splat-cooling conditions are found in the far upper-right region. At these rates, k will begin to approach unity.

(Kurz & Fisher)

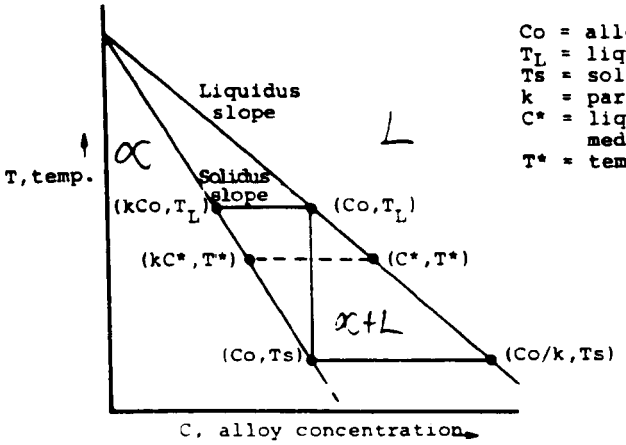

Co = alloy concentration
T_L = liquidus corresponding to Co
Ts = solidus corresponding to Co
k = partition coefficient (k<1)
C* = liquid concentration at an intermediate stage of solidification
T* = temperature corresponding to C*

REGION OF A BINARY EQUILIBRIUM PHASE DIAGRAM

(a) Dendrite tip exposed to liquid of the bulk composition

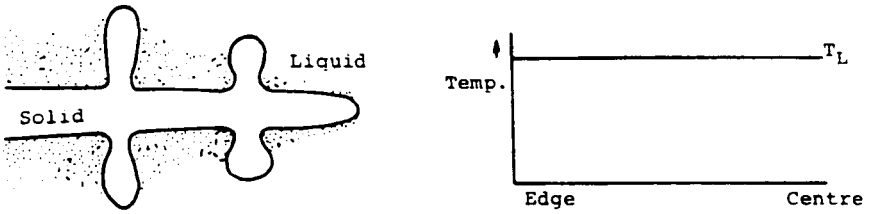

(b) Dendrite tip surrounded by segregated boundary layer

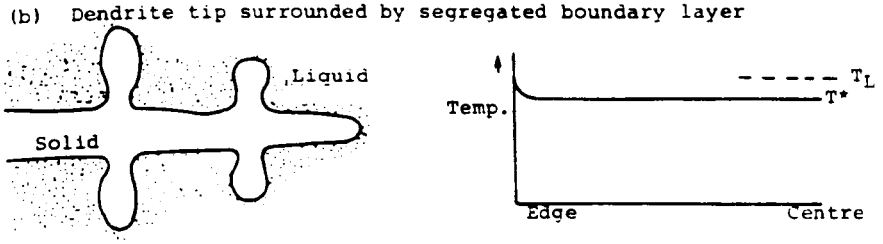

(c) Planar or cellular growth with mixing of segregate into bulk liquid

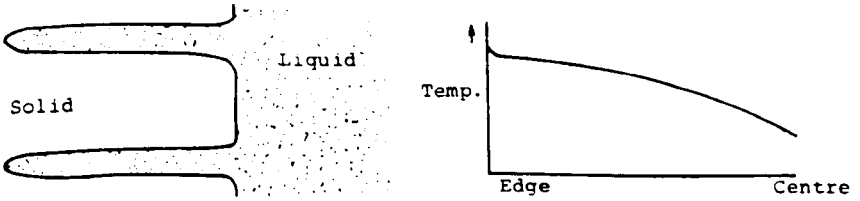

VARIATION IN TEMPERATURE AT THE GROWTH FRONT ACROSS A CASTING FIG. 2.3

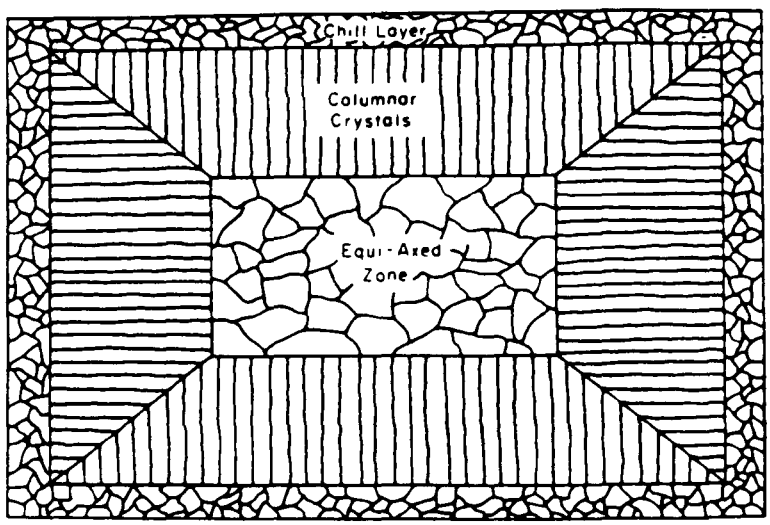

Transverse section of an as-cast structure showing the chill zone, columnar zone and equiaxed zone

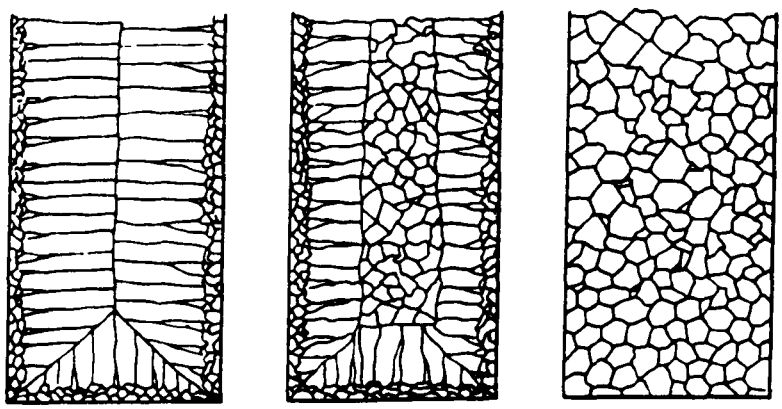

Possible casting structures: (a) wholly columnar except for chill zone; (b) partially columnar, partially equiaxed; (c) wholly equiaxed

Fig.2.4 Schematic As-Cast Macrostructures

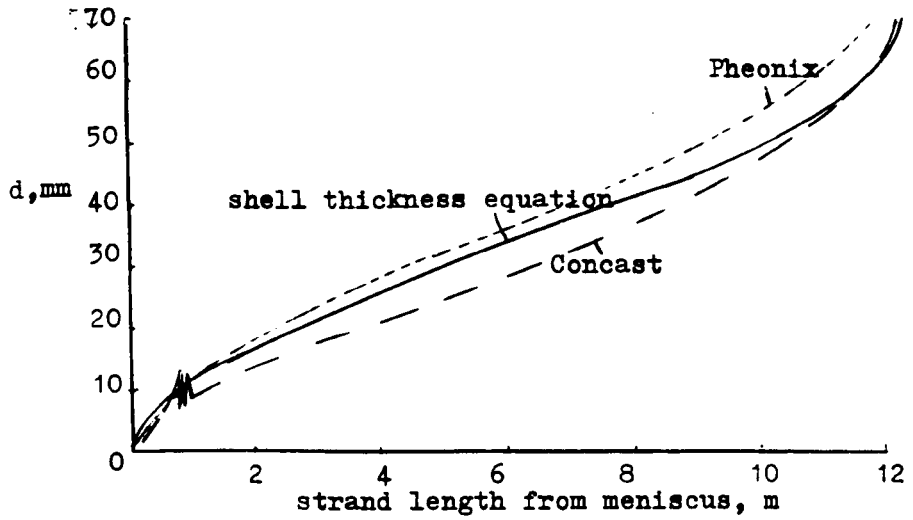

Fig. 2.5 COMPARISON OF SHELL THICKNESS EQUATION WITH ALTERNATIVE COMPUTER MODELS FOR 100mm BILLET

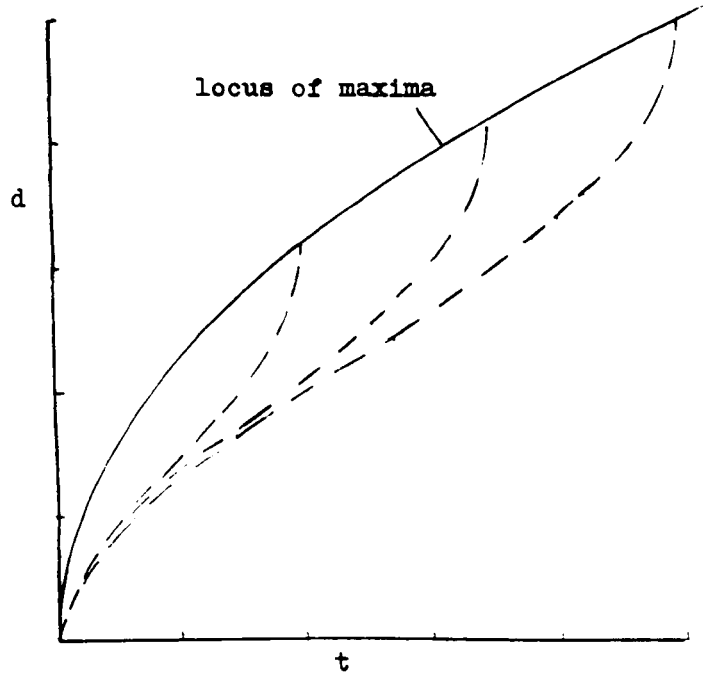

Fig. 2.6 ILLUSTRATION OF THE FAMILY OF SHELL THICKNESS EQUATION CURVES, WHEREBY THE FINAL VALUE TRACES A ROOT TIME (OR DISTANCE) CURVE

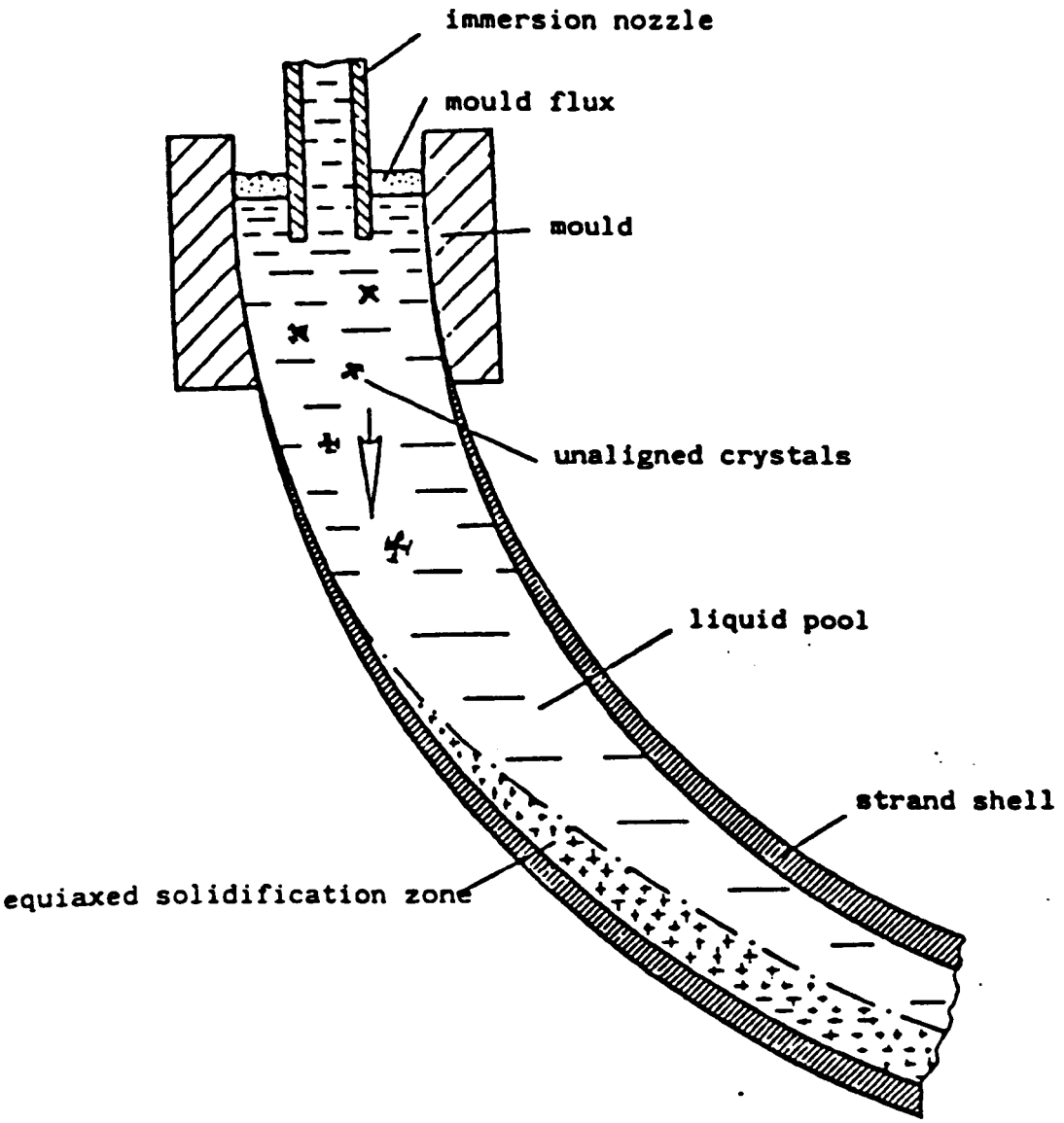

Fig 2.7 Sedimentation of equiaxed crystals in bow-type plants

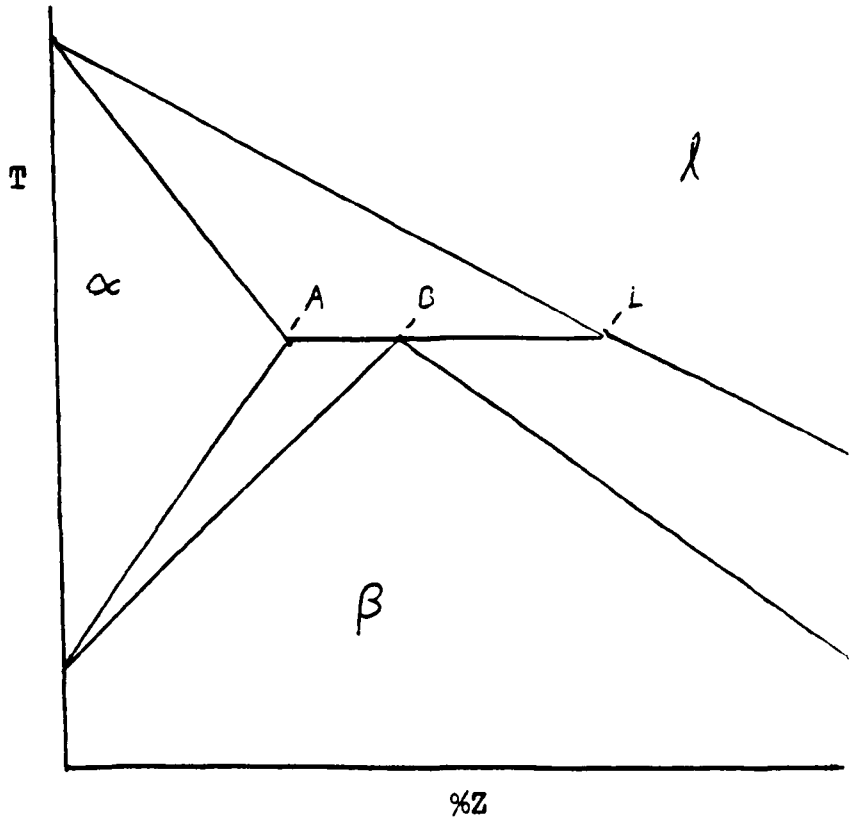

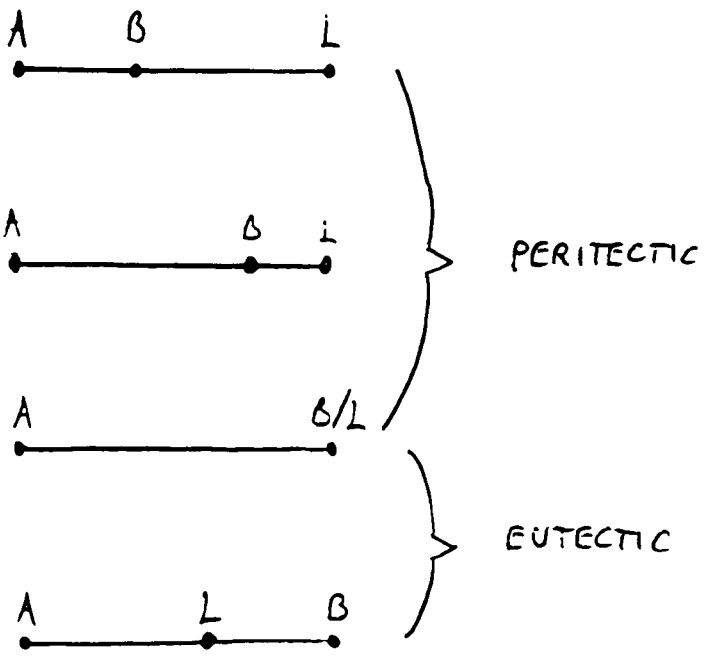

Fig.2.8 Schematic Peritectic Section of a Phase Diagram & Example 3-Phase Reaction Tie-Lines

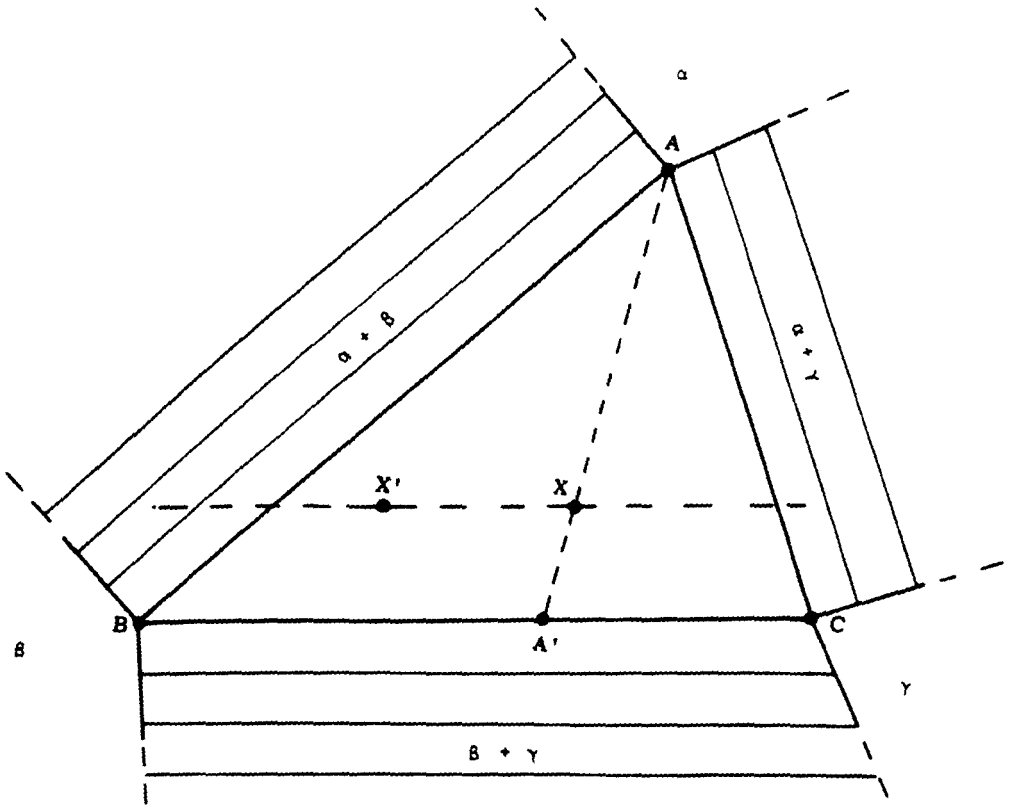

SCHEMATIC THREE-PHASE REACTION TRIANGLE ON A TERNARY ISOTHERM FIG. 2.9

For a bulk composition plotted at X, the proportion of phase α is given by XA'/AA', and will be the same value for any X' on a line parallel to BC

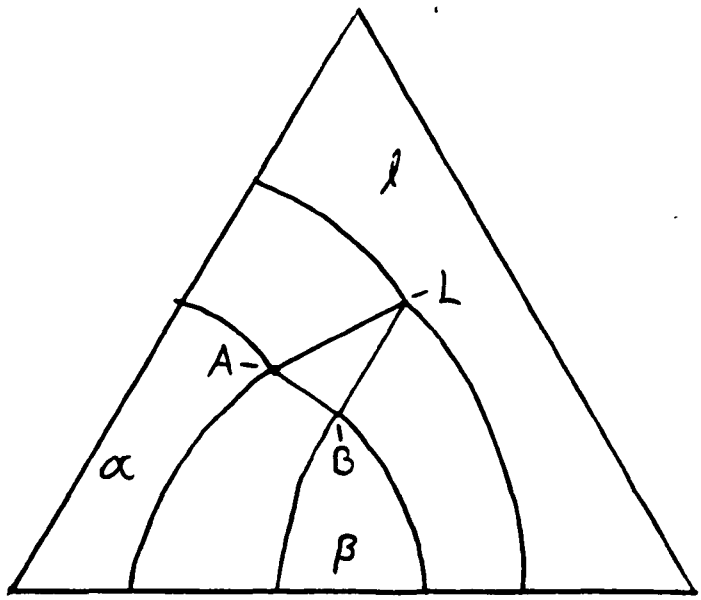

a) Isothermal Section

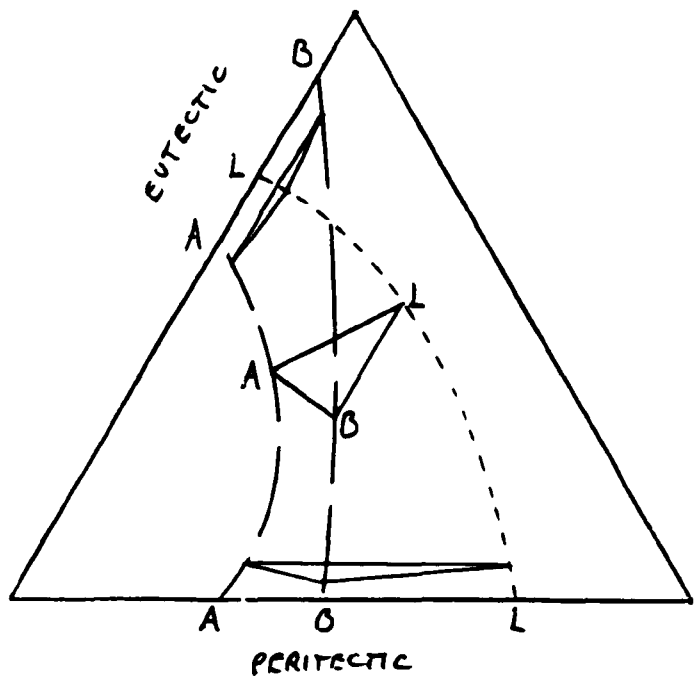

b) Tie-Triangle Traverse

Fig.2.10 Schematic Change From Peritectic to Eutectic 3-Phase Reactions

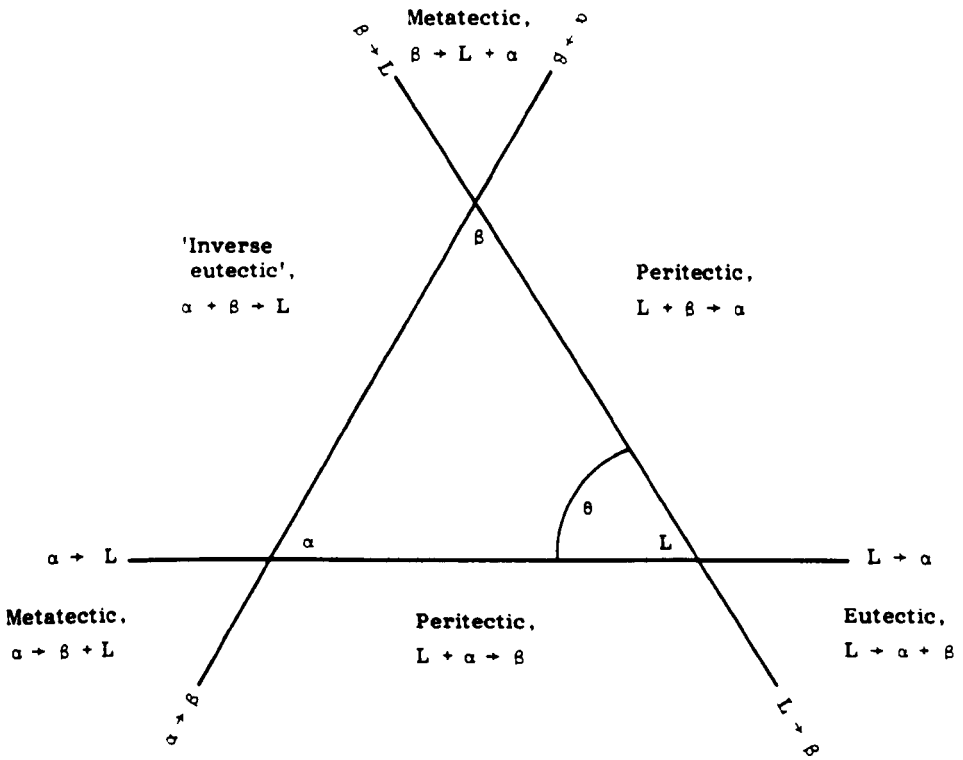

SCHEMATIC CLASSIFICATION OF α, β, L THREE-PHASE REACTION ACCORDING TO SENSE OF MOVEMENT OF THE THREE-PHASE TRIANGLE UPON A DECREASE IN TEMPERATURE

FIG. 2.11

The type of reaction is determined by which labelled zone the triangle encroaches into when the temperature is decreased, assuming no change in triangle shape occurs

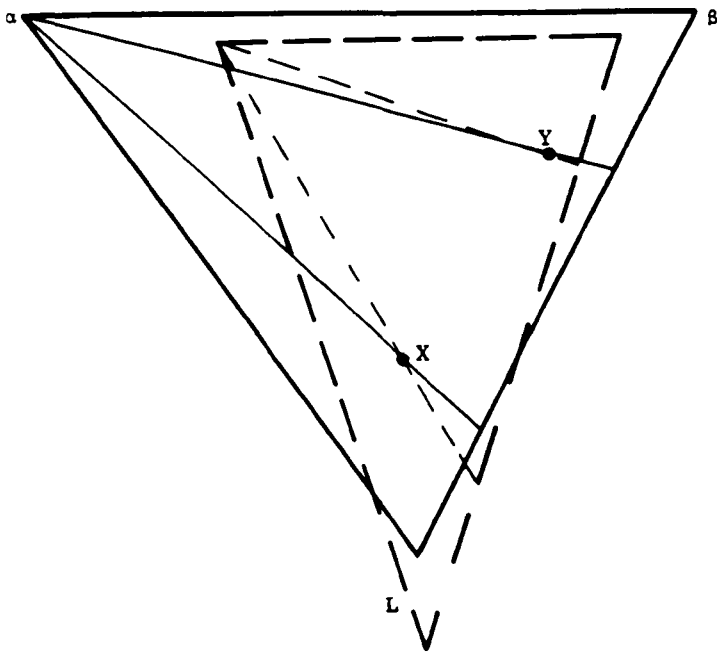

X and Y are alternative, bulk compositions

Triangle in solid lines is three-phase triangle at higher, and dotted lines lower, temperature

Thin lines are corresponding constructs to determine proportion of phase α, as in Fig. 2.9

SCHEMATIC EXAMPLE OF EUTECTIC AND PERITECTIC REACTIONS OCCURRING WITHIN THE SAME REACTION TRIANGLES

FIG. 2.12

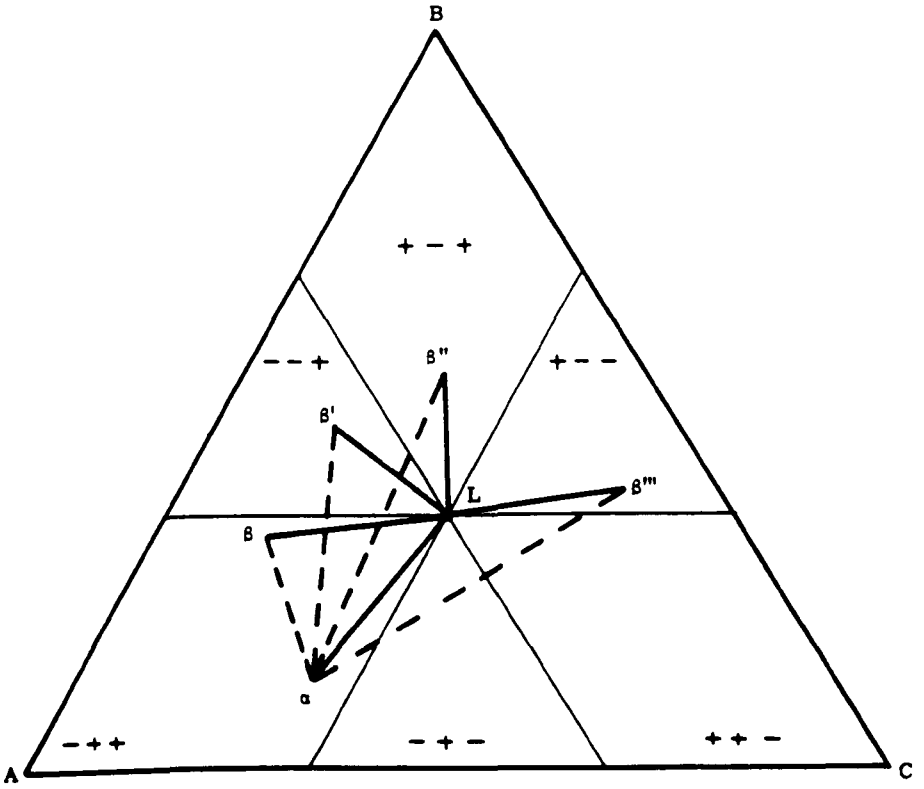

The ternary isotherm has been divided into 'sextants' through the arbitrary liquid composition, L. Within each, the senses of partition for any solid tie-line into that sextant are labelled in order for components A, B and C, a plus indicating that solute enriches in the liquid ($k < 1$), and vice-versa. For a given tie-line to phase α, alternative three-phase triangles with phase β could exist for which different components may have different senses of partition. For β, β', β'' and β''', it can be seen that 0, 1, 2 and 3 components have changed sense of partition, respectively, defined as the partition 'order' of the three-phase reaction, ^3O.

DEFINITION OF PARTITION ORDER IN A THREE-PHASE REACTION FIG. 2.13

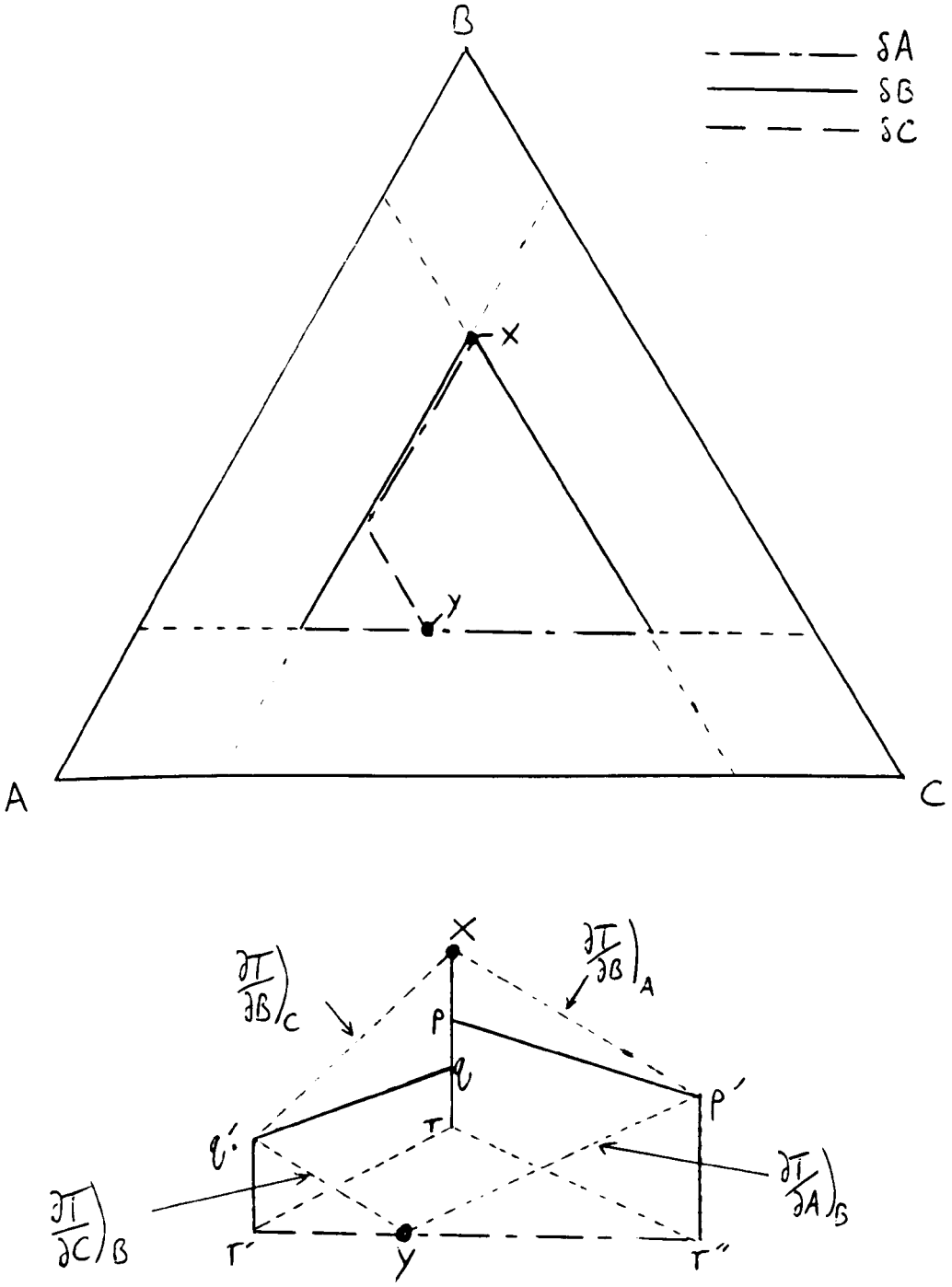

Fig.2.14 Illustrative Alternative "Routes" From Composition/ Temperature Point X to Point Y

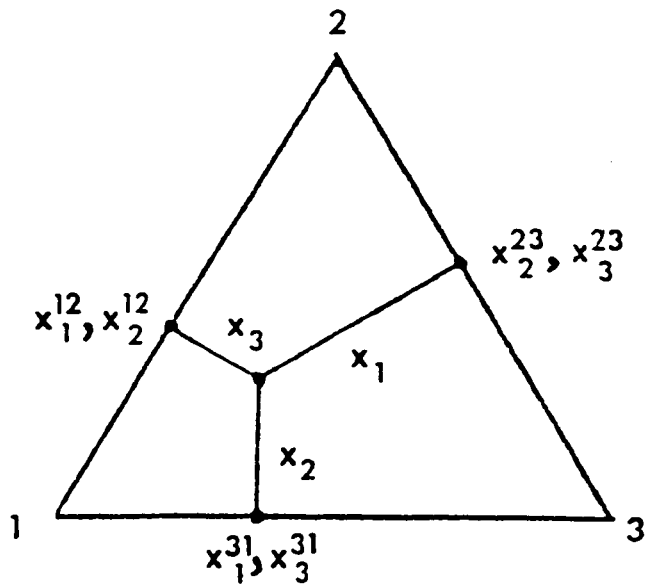

Fig 2.15 The ternary overall composition and the resulting binary compositions contributing to the Margules Equation

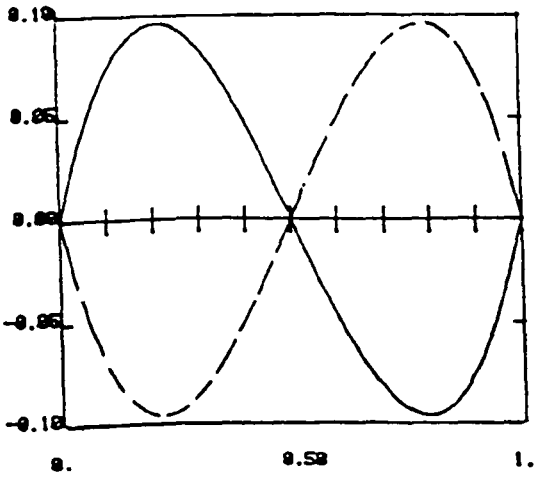

a) $\pm x_1 x_2 (x_1 - x_2)^1$

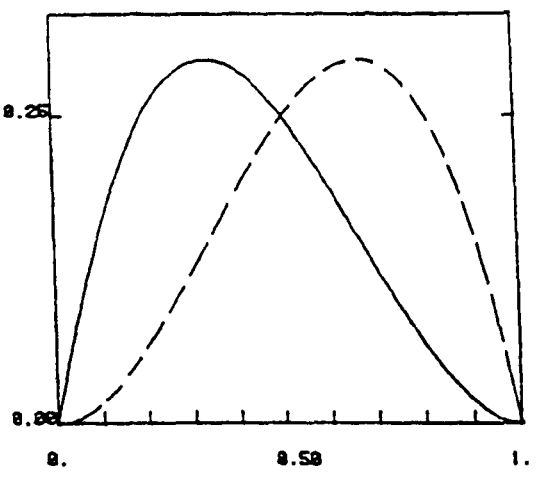

b) $x_1 x_2 ((x_1 - x_2)^0 \pm (x_1 - x_2)^1)$

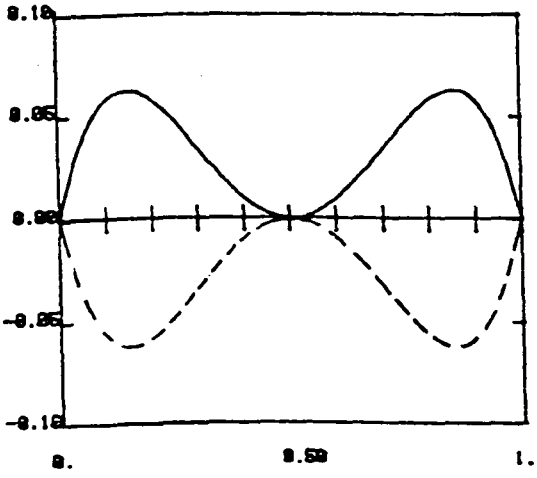

a) $\pm x_1 x_2 (x_1 - x_2)^2$

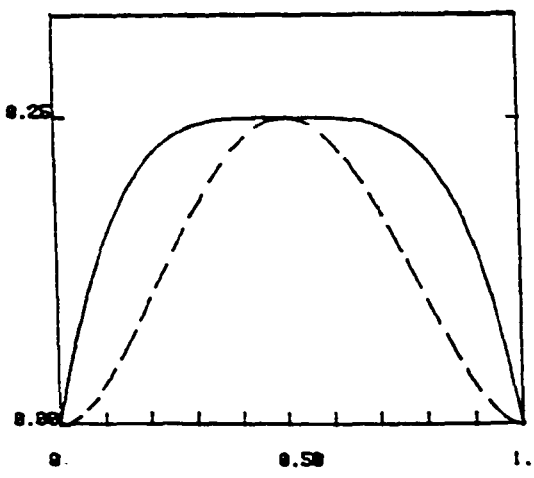

b) $x_1 x_2 ((x_1 - x_2)^0 \pm (x_1 - x_2)^2)$

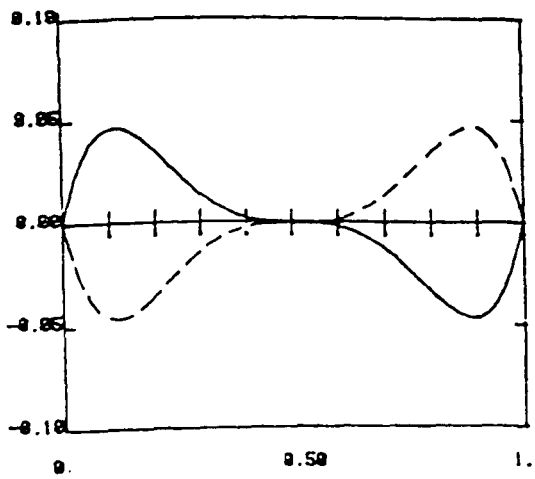

a) $\pm x_1 x_2 (x_1 - x_2)^3$

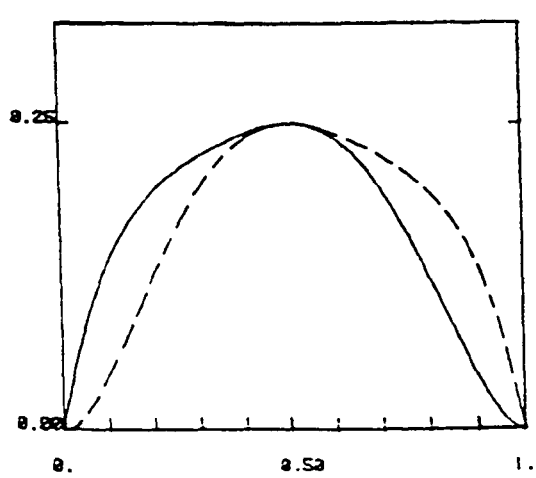

b) $x_1 x_2 ((x_1 - x_2)^0 \pm (x_1 - x_2)^3)$

Fig. 2.16 DIFFERENT ORDER COMPONENTS TO THE FREE ENERGY EXPRESSION

(Hack)

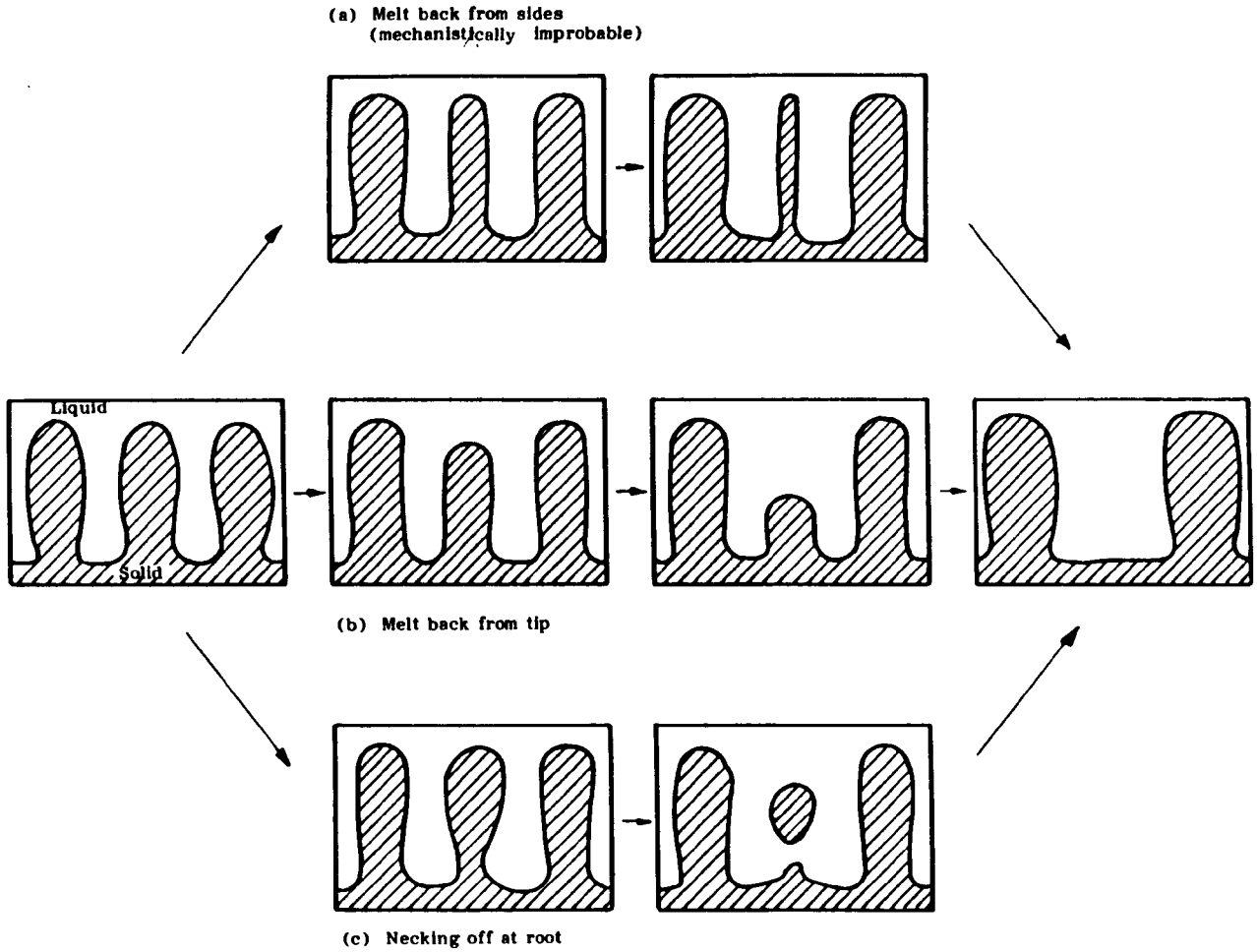

DENDRITE ARM RIPENING MECHANISMS FIG. 2.17

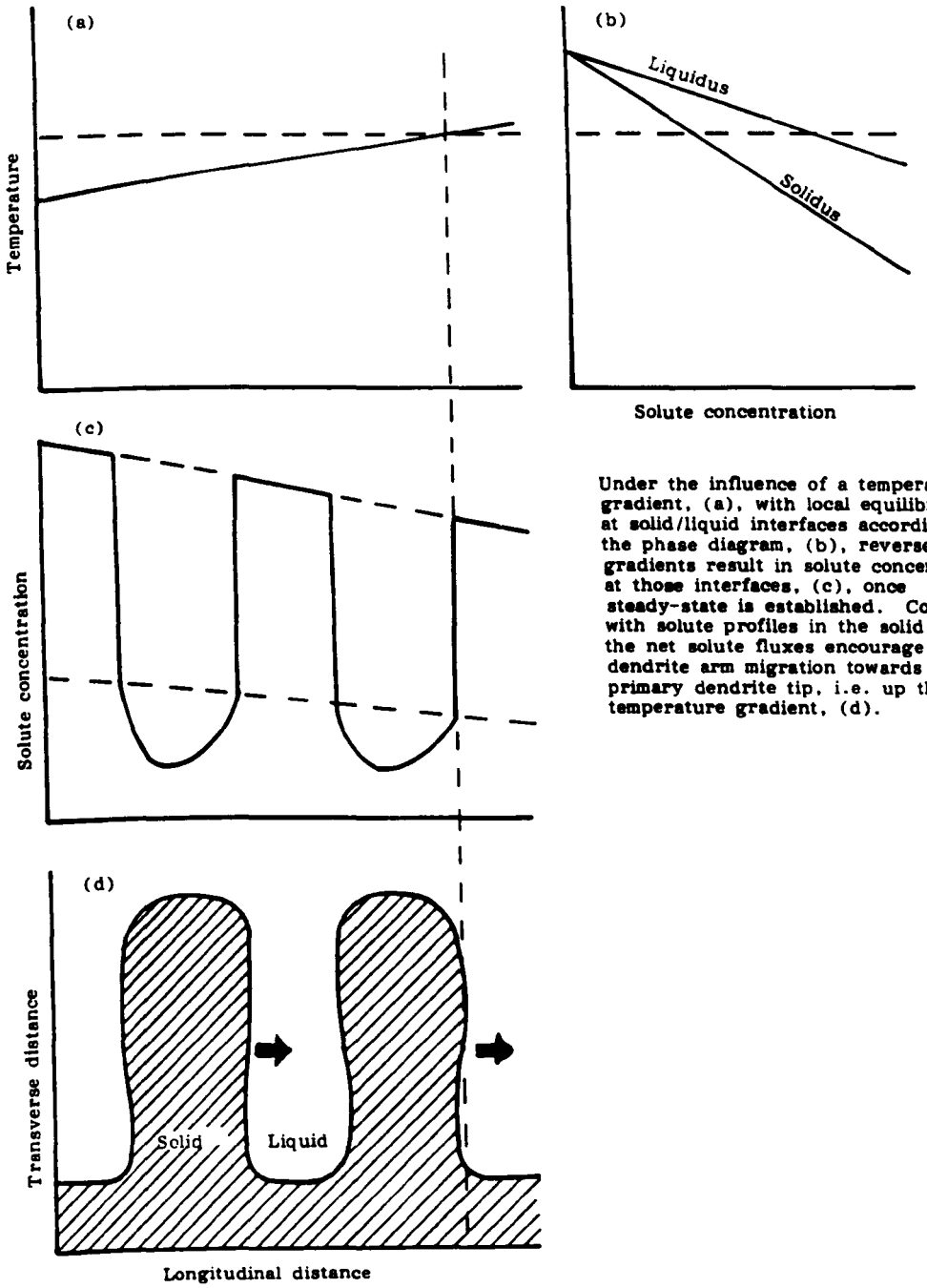

Under the influence of a temperature gradient, (a), with local equilibrium at solid/liquid interfaces according to the phase diagram, (b), reverse gradients result in solute concentration at those interfaces, (c), once steady-state is established. Coupled with solute profiles in the solid, (c), the net solute fluxes encourage dendrite arm migration towards the primary dendrite tip, i.e. up the temperature gradient, (d).

DENDRITE ARM MIGRATION (TGZM) FIG. 2·18

(a) Outward solidification from root

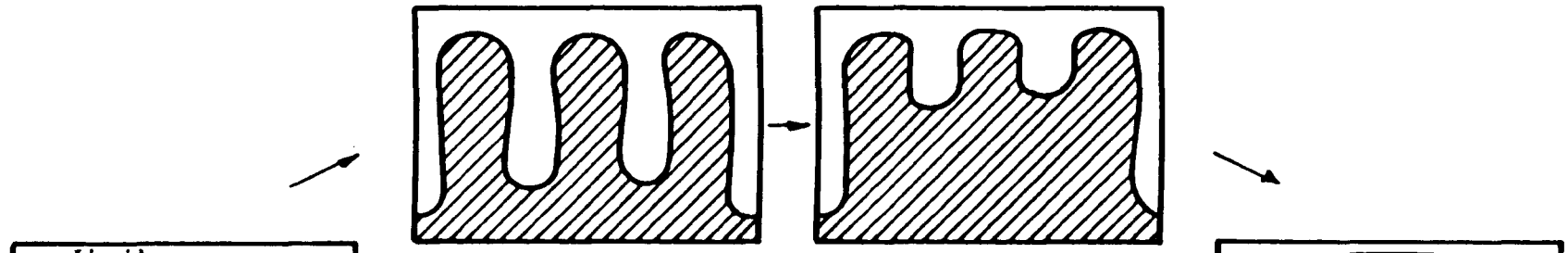

(b) Inward solidification from tip

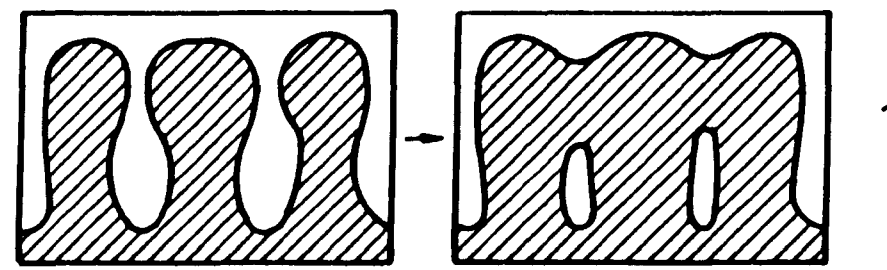

DENDRITE ARM COALESCENCE MECHANISMS FIG. 2-19

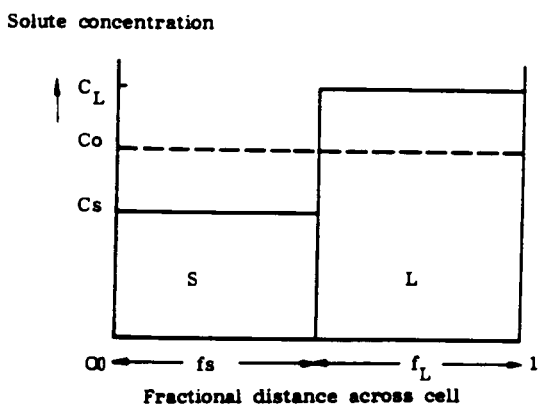

(a) Total solute balance

$f_s C_s + f_L C_L = C_o$

where $f_s + f_L = 1$,

$C_s = k\, C_L$

Various representation of the Lever Rule are obtained by direct manipulation of these equations

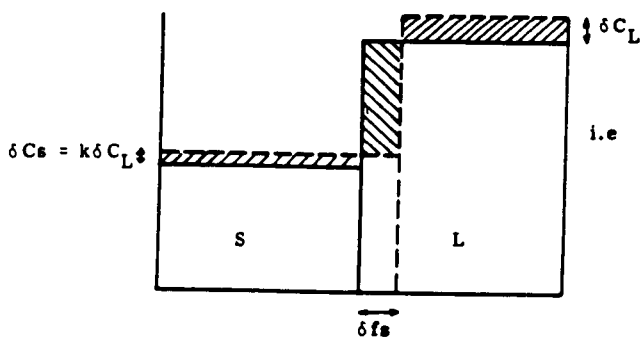

(b) Differential solute balance

If the sum of the differences of solute content is zero with an advance of fs, then solute must have been conserved

i.e $C_L(1 - k)\,\delta f_s = f_s k \delta C_L + (1 - f_s)\,\delta C_L$

This yields the same formulae as above upon integration

SCHEMATIC ORIGIN OF THE EQUILIBRIUM LEVER RULE FIG 2.20

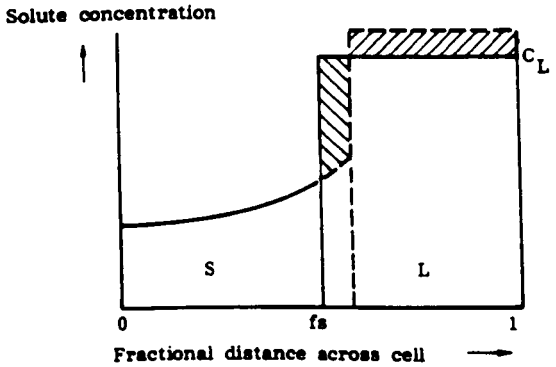

(c) Scheil (zero diffusion in solid)

Differential solute balance:-

$C_L (1 - k) \delta fs = (1 - fs) \delta C_L$

Integrates to the Scheil Equation

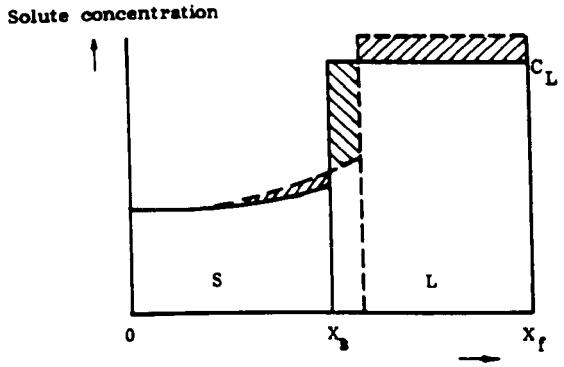

(d) Brody-Flemings (limited diffusion in solid)

$$C_L (1 - k) \delta Xs = \frac{Ddc}{dx} \cdot \delta t + (X_f - X_s) \delta C_L$$

Finite back-diffusion requires solute balance with actual distance and times, and simplifying assumptions are needed to enable integration.

These restrict it to limited diffusion in the solid

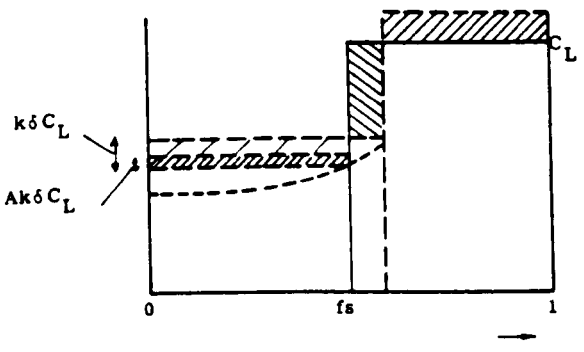

(e) Clyne-Kurz (unlimited diffusion in solid)

The region of back-diffused solute is treated as a fraction of that under equilibrium, determined by a parameter, 'A'

$C_L (1 - k) \delta fs = Afsk\delta C_L + (1 - k) \delta C_L$

Significance and choice of 'A' described in text

SCHEMATIC ORIGIN OF MICROSEGREGATION EQUATIONS FIG. 2.20 cont.

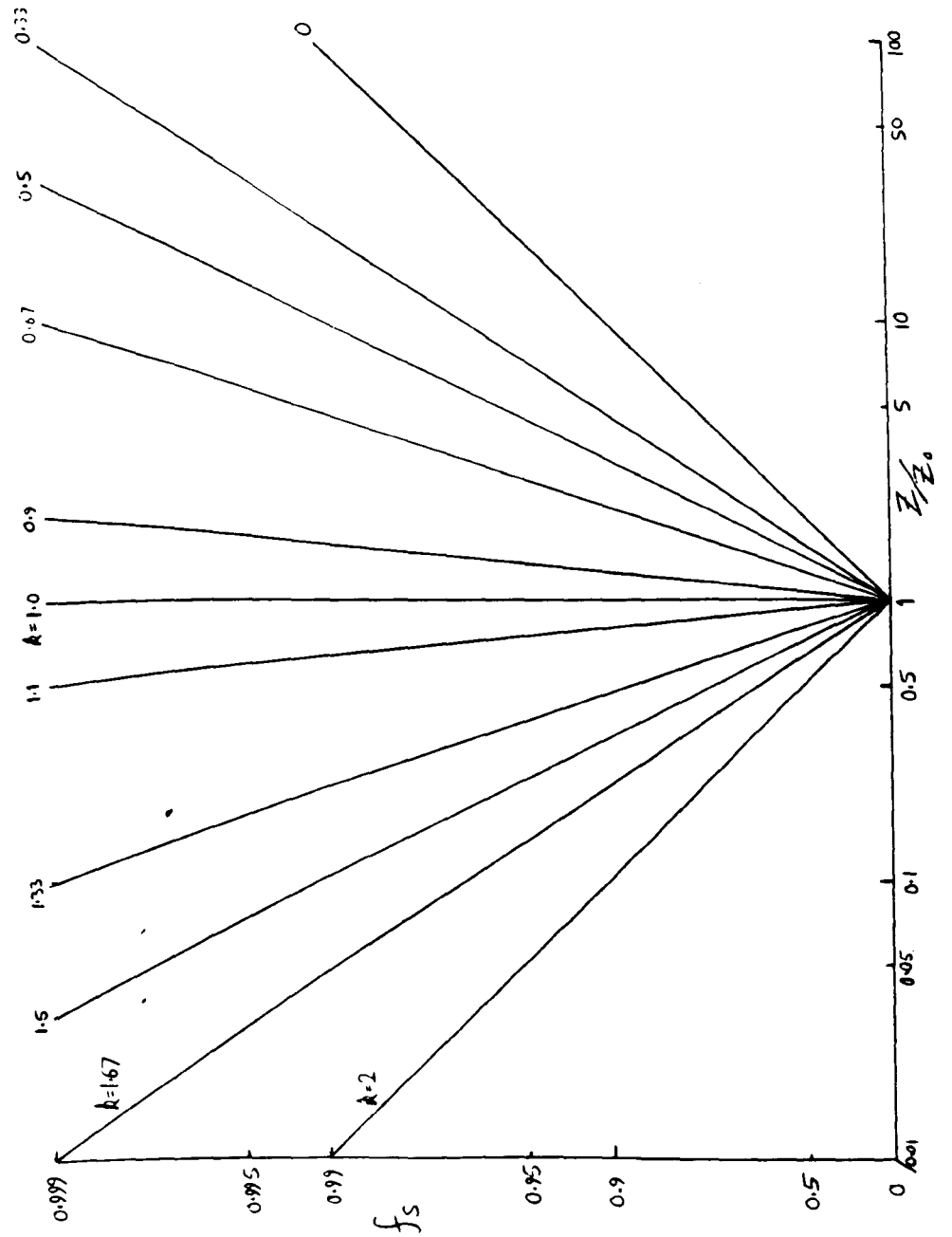

Fig. 2.21 REPRESENTATIONS OF THE SCHEIL EQUATION FOR MICROSEGREGATION

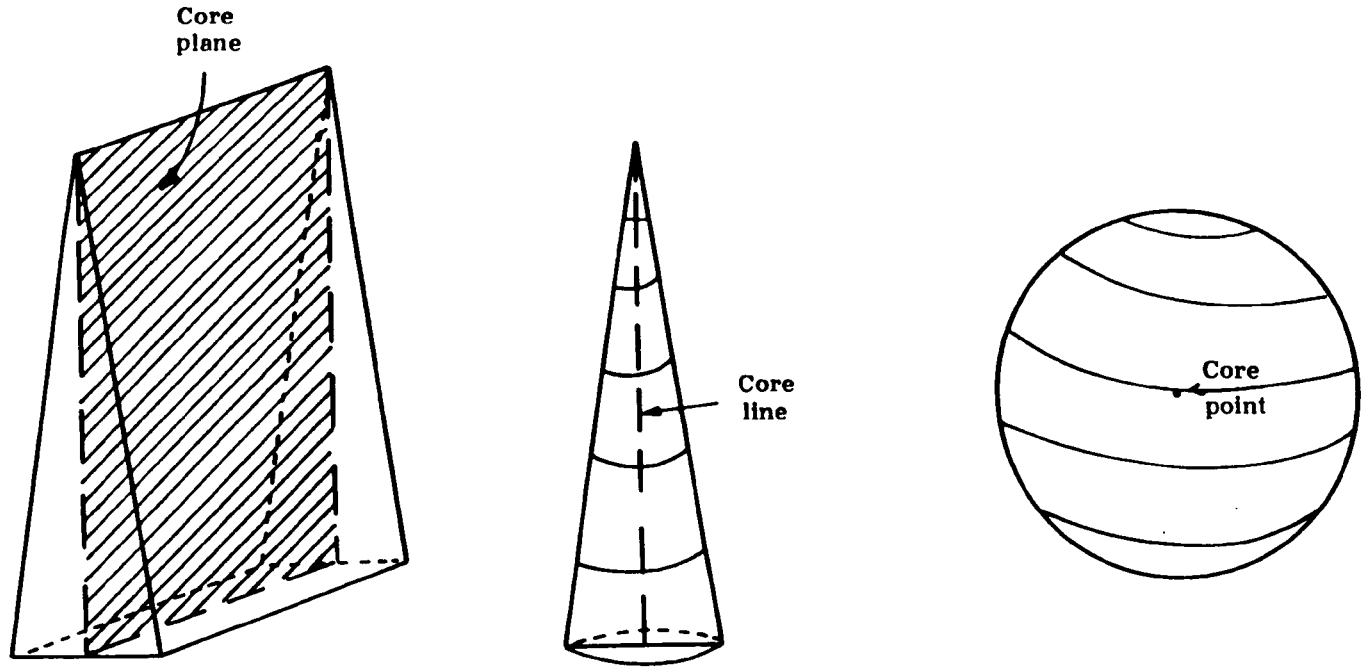

(a) 1D (b) 2D (c) 3D

In both the 1 and 2D cases, the assumed array of volume elements is depicted from dendrite tip (liquidus) to root (solidus), as in Fig. 2·28 In the 3D case, the volume element is the complete, solidifying globule, and only one instant can be represented.

SCHEMATIC PRIMARY DENDRITE ARM GROWTH MORPHOLOGY IMPLIED BY THE 1, 2 OR 3D VOLUME ELEMENTS

FIG. 2·22

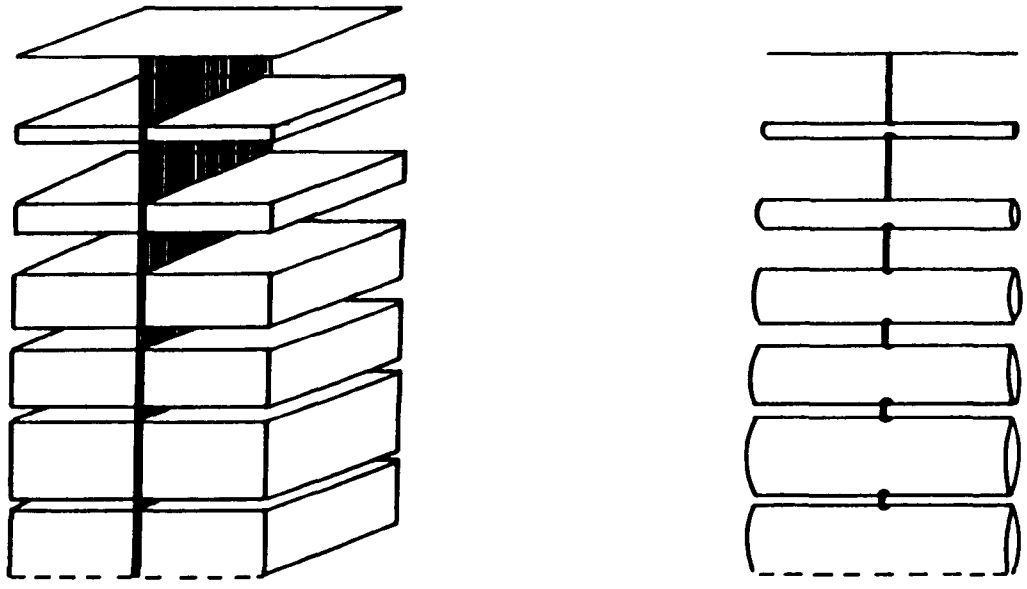

(a) 1D (b) 2D

The assumed array is depicted as in Fig.2-22. There is no corresponding interpretation for the 3D case

SCHEMATIC SECONDARY DENDRITE ARM GROWTH MORPHOLOGY IMPLIED BY THE 1 AND 2D VOLUME ELEMENTS FIG. 2-23

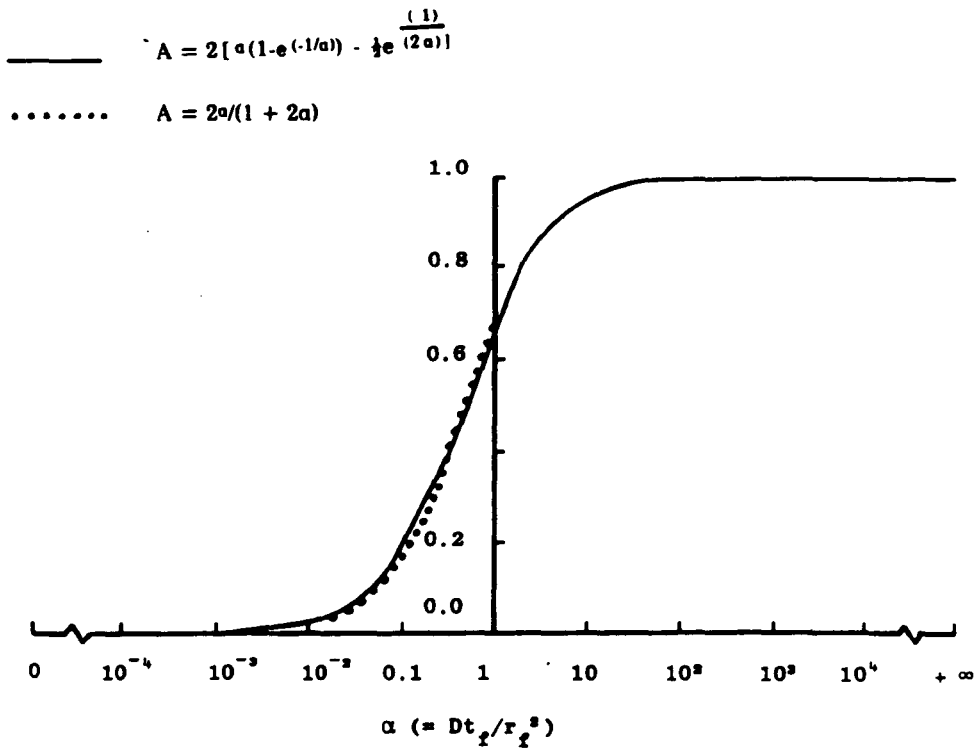

COMPARISON OF BACK-DIFFUSION PARAMETER CALCULATED BY ALTERNATIVE EQUATIONS FIG. 224

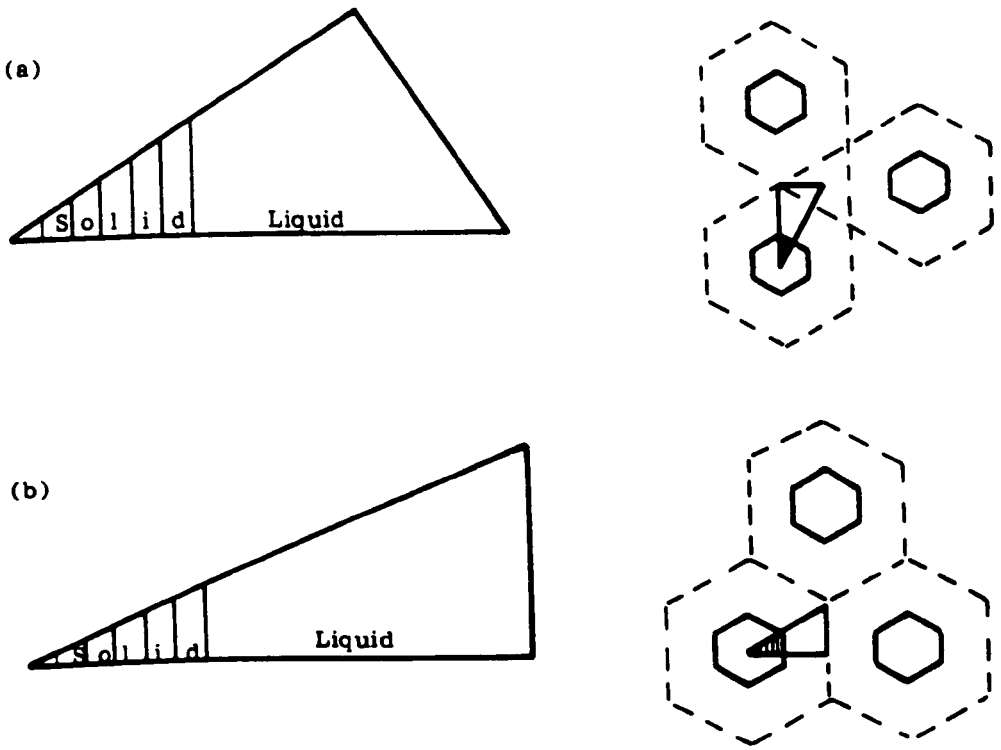

The final, concave solidification in case (a) leads to extreme microsegregation at solidus.

ALTERNATIVE REPRESENTATIVE 2D CELLS AND IMPLIED ARRAYS EMPLOYING HEXAGONAL MORPHOLOGIES FIG. 1-25

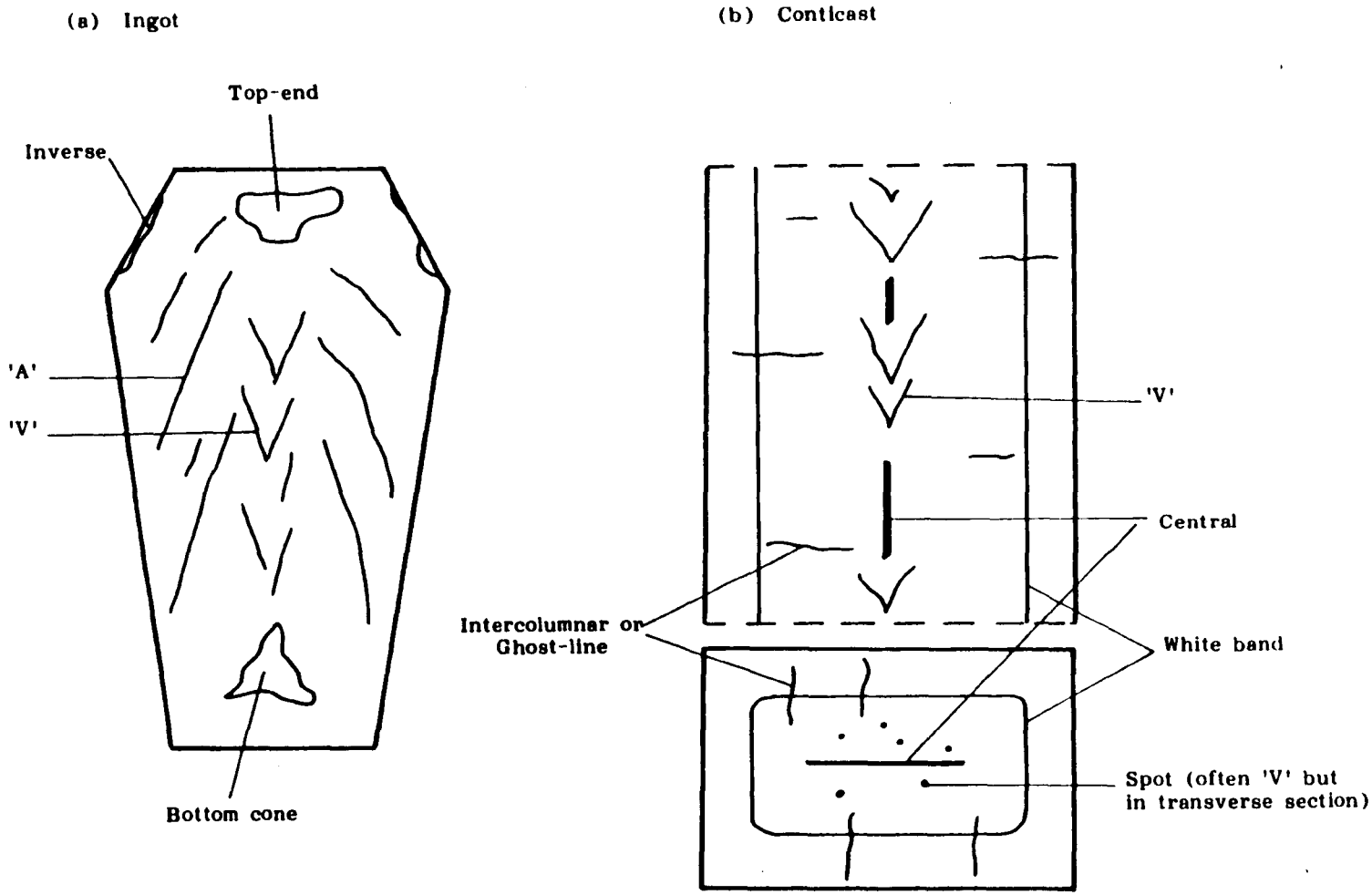

SCHEMATIC MACROSEGREGATION MODES FIG. 2-26

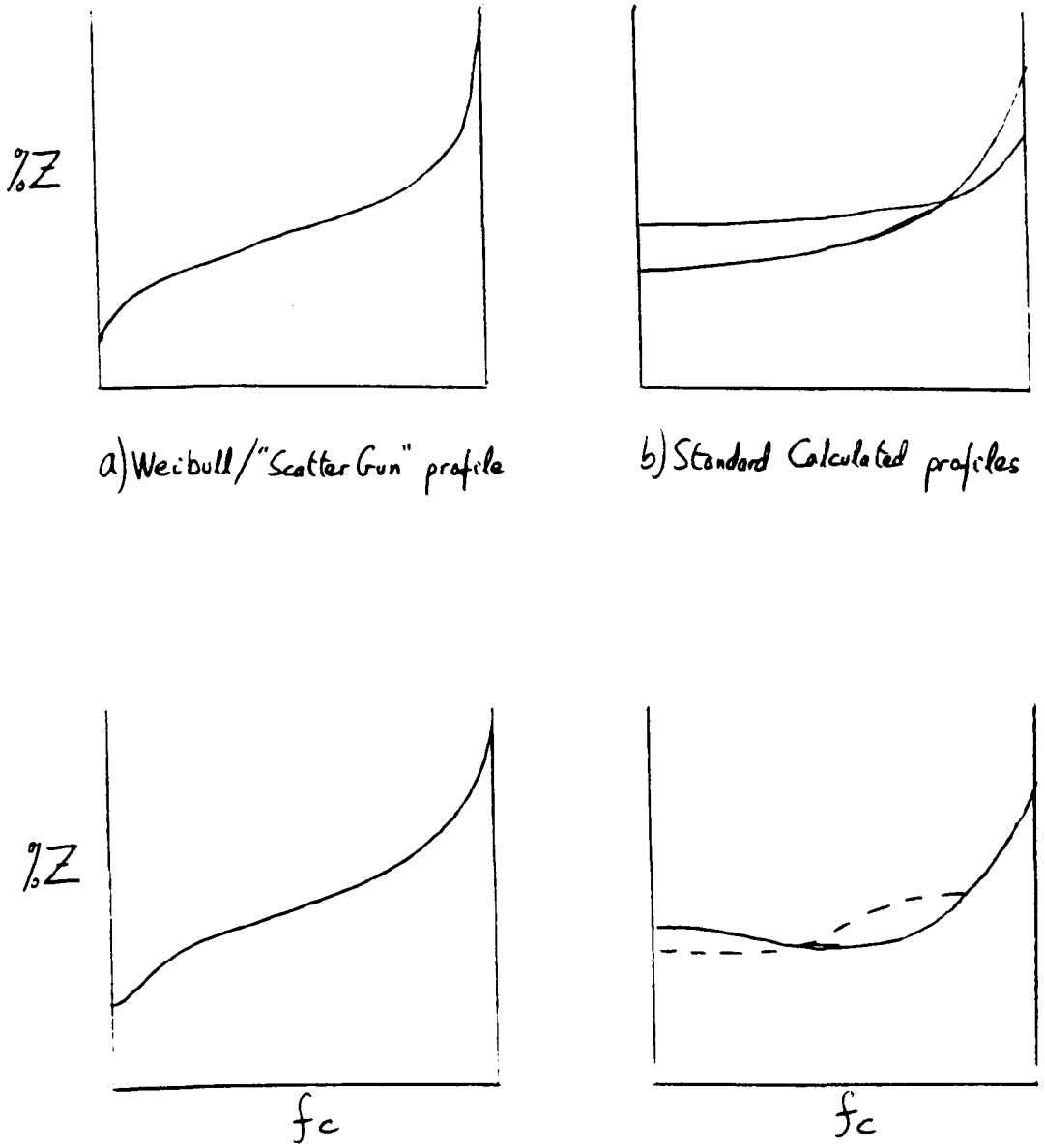

Fig.2.27 Illustrative Composition / Cumulative Fraction Microsegregation Representations (see text)

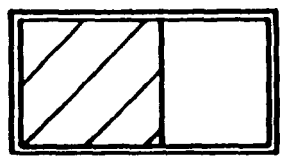

(a) Ideal, sealed volume element

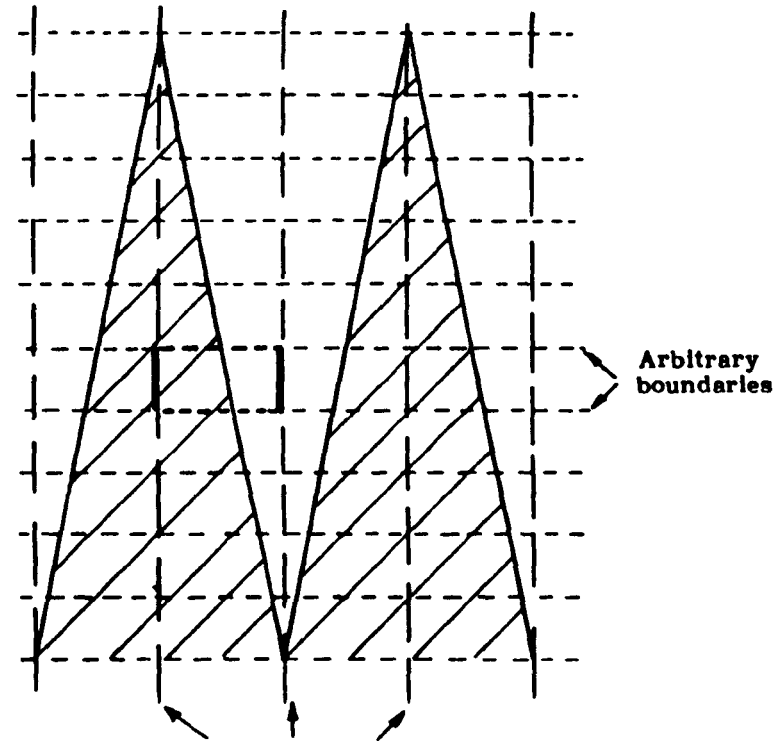

(b) Representative slice or volume element within an assumed array

THE VOLUME ELEMENT CONCEPT EMPLOYED IN THE CALCULATION OF MICROSEGREGATION FIG. 2·28

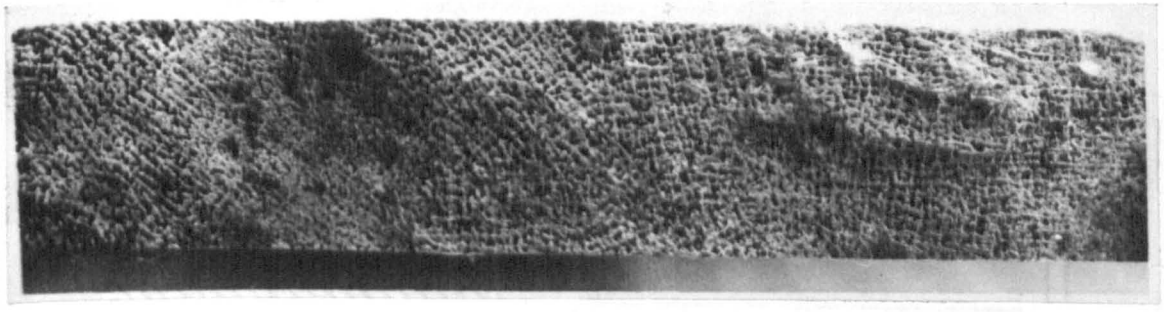

x 2

(a) Deep etched section, transverse to growth direction of directionally solidifed node steel

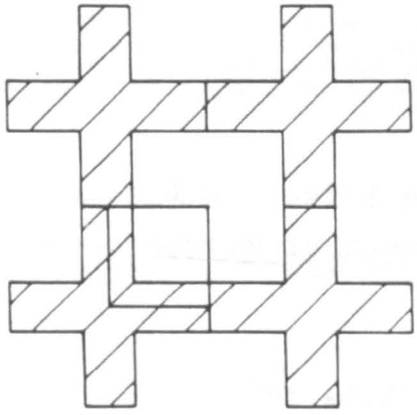

(b) Schematic representation, including the 'quarter cell' considered by the SQUARE program

METALLOGRAPHIC AND SCHEMATIC REPRESENTATIONS OF THE SQUARE GEOMETRY TRANSVERSE TO THE GROWTH DIRECTION

FIG. 2.29

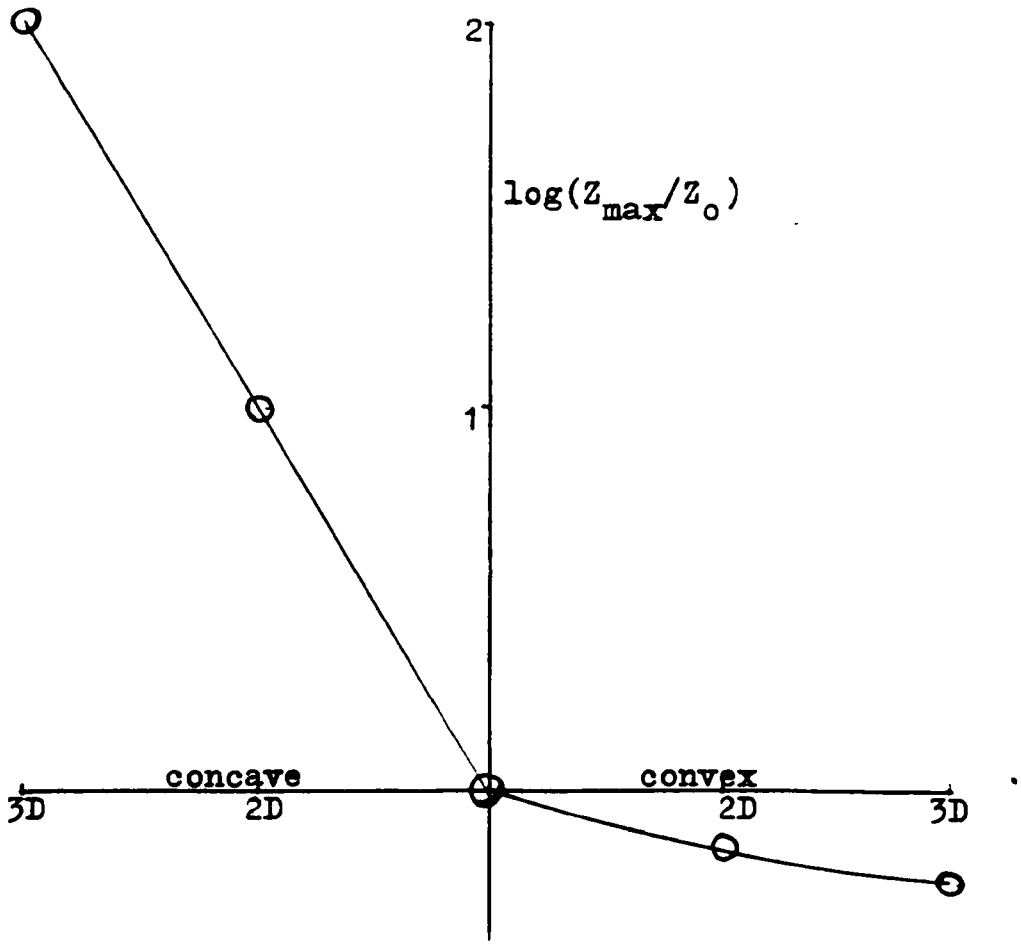

Fig.2.30 The Effect of Dimensional Basis on the Extent of Microsegregation

(Scheil Equation, k=0.5, curtailed at 0.99x radial distance, with Z_o defined as Z_{max} from 1D result)

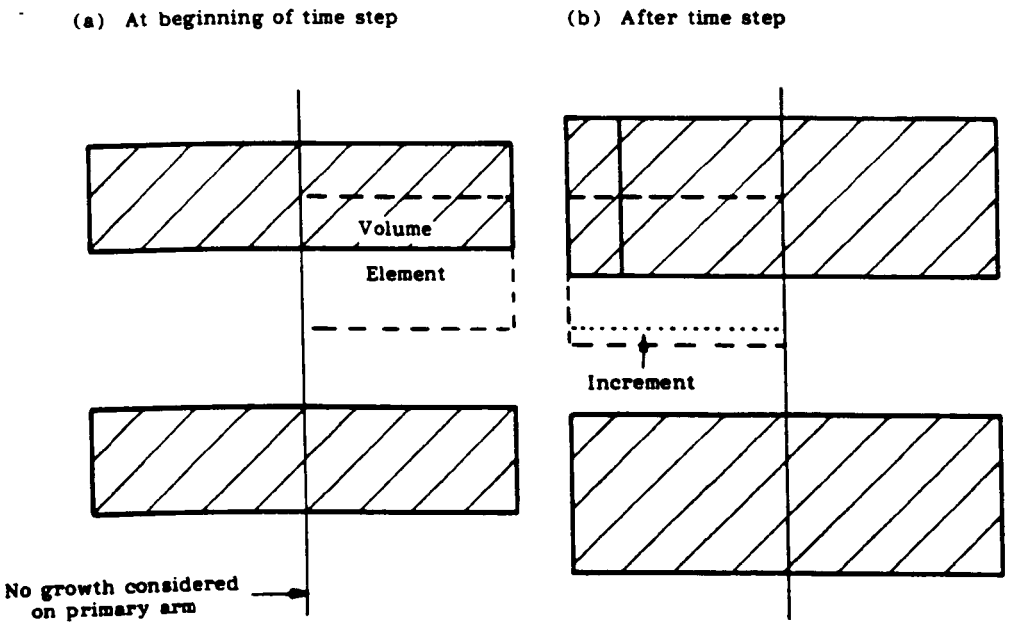

From (a) to (b), further solidification has occurred on the secondary arms, and the volume element has expanded, i.e. the half distance between cores of adjacent arms has increased, as if the primary stem has been stretched. The net fraction solid should still increase despite the expansion.

SCHEMATIC SECONDARY DENDRITE ARM COARSENING PROCESS IMPLIED BY KIRKWOOD'S MICROSEGREGATION MODEL FIG. 2.31

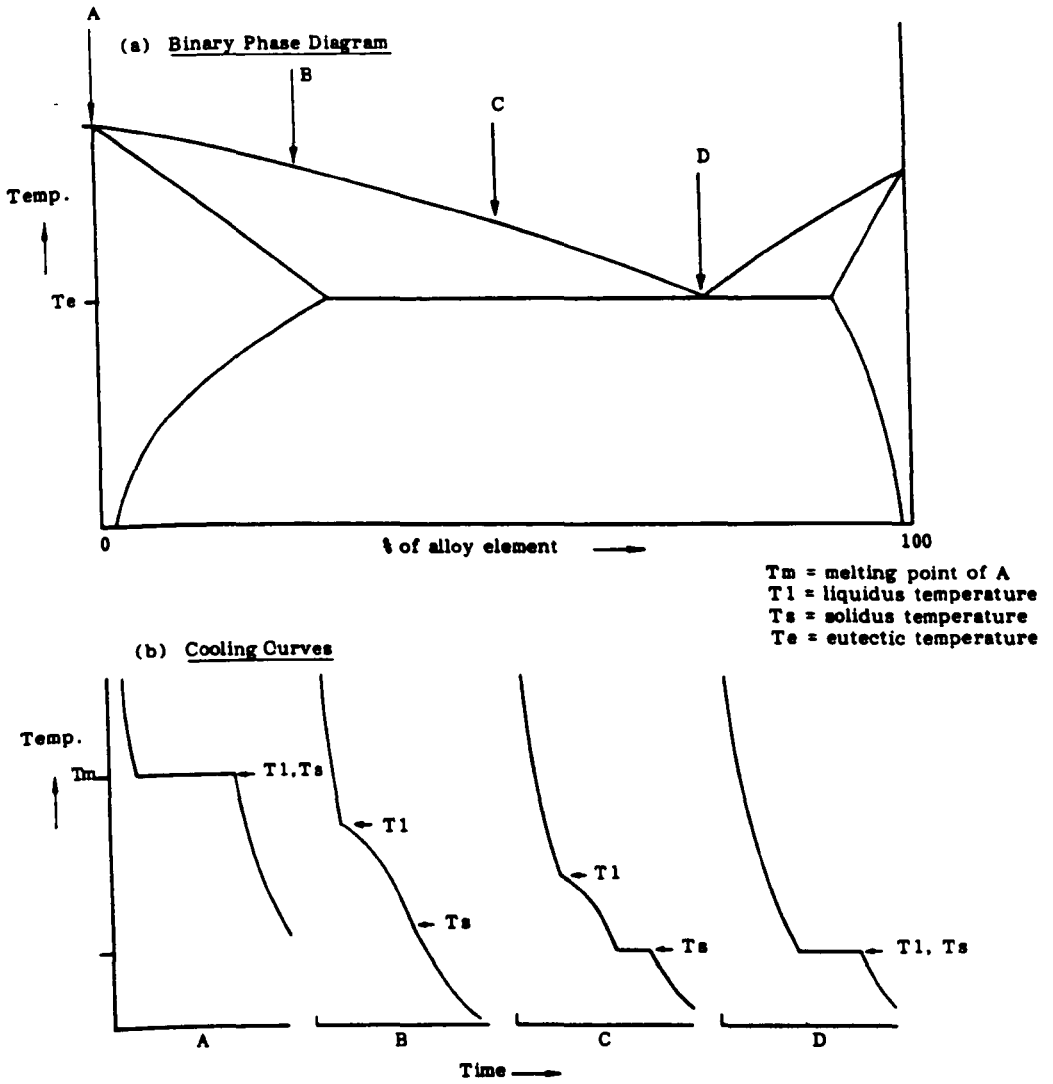

COOLING CURVES CORRESPONDING TO FOUR COMPOSITIONS ON A BINARY PHASE DIAGRAM FIG. 3.1

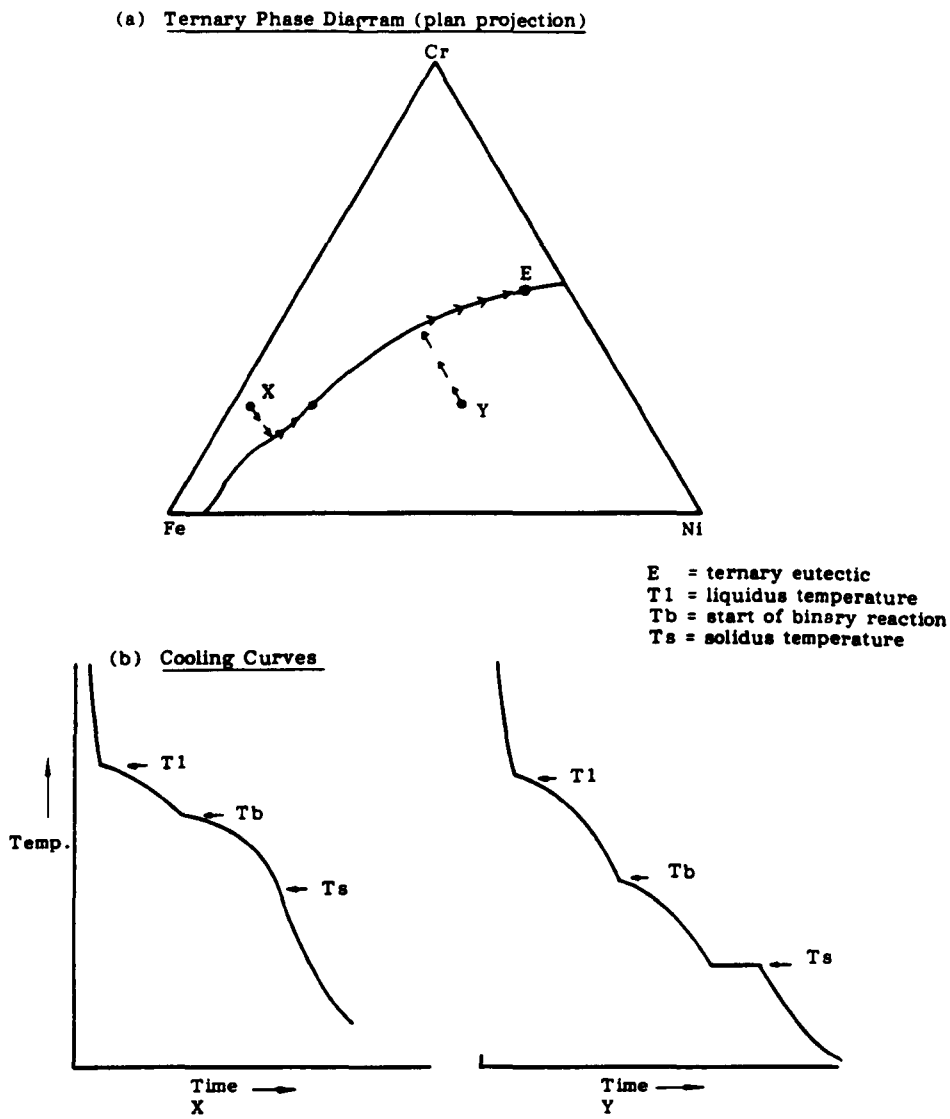

COOLING CURVES CORRESPONDING TO TWO COMPOSITIONS ON A TERNARY PHASE DIAGRAM FIG. 3·2

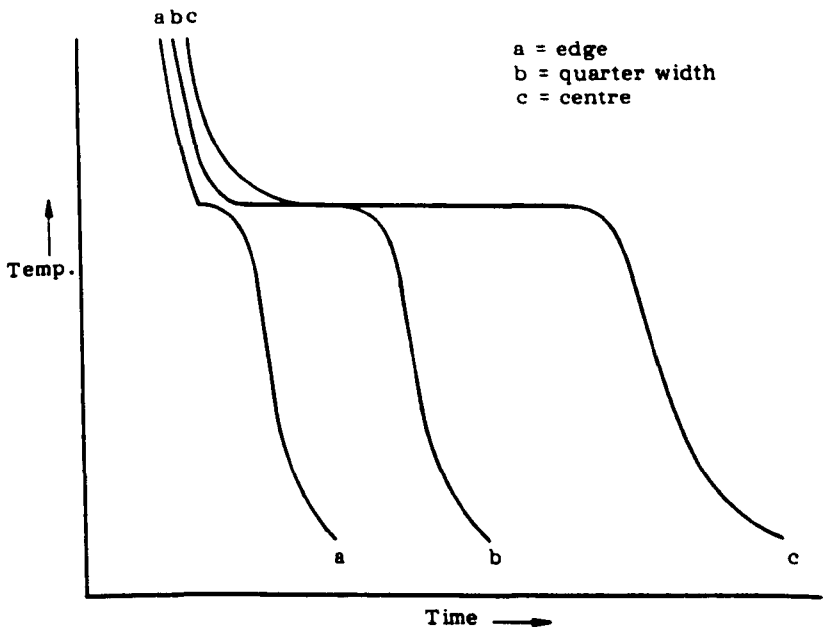

COOLING CURVES CORRESPONDING TO THREE THERMOCOUPLE LOCATIONS FIG. 3.3

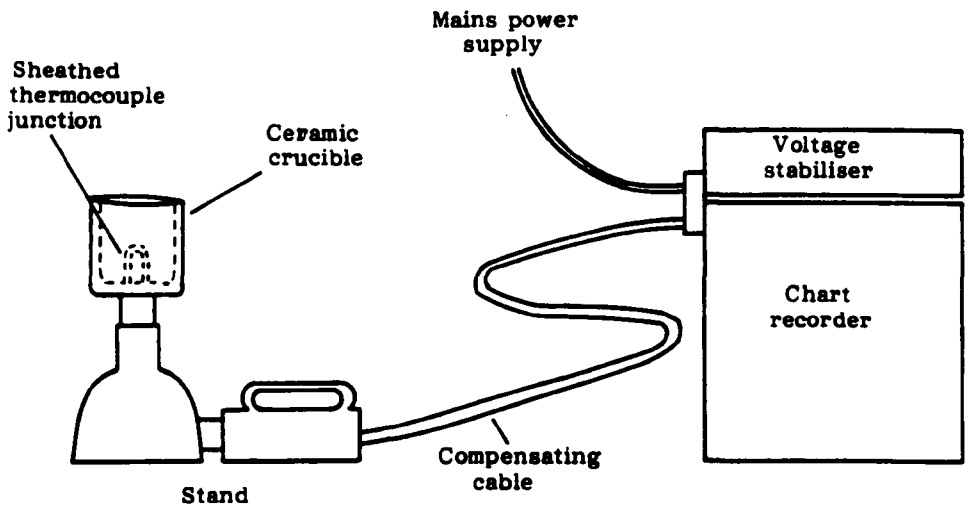

SCHEMATIC DIAGRAM OF 'CHECKPOINT' SYSTEM FIG. 3·4

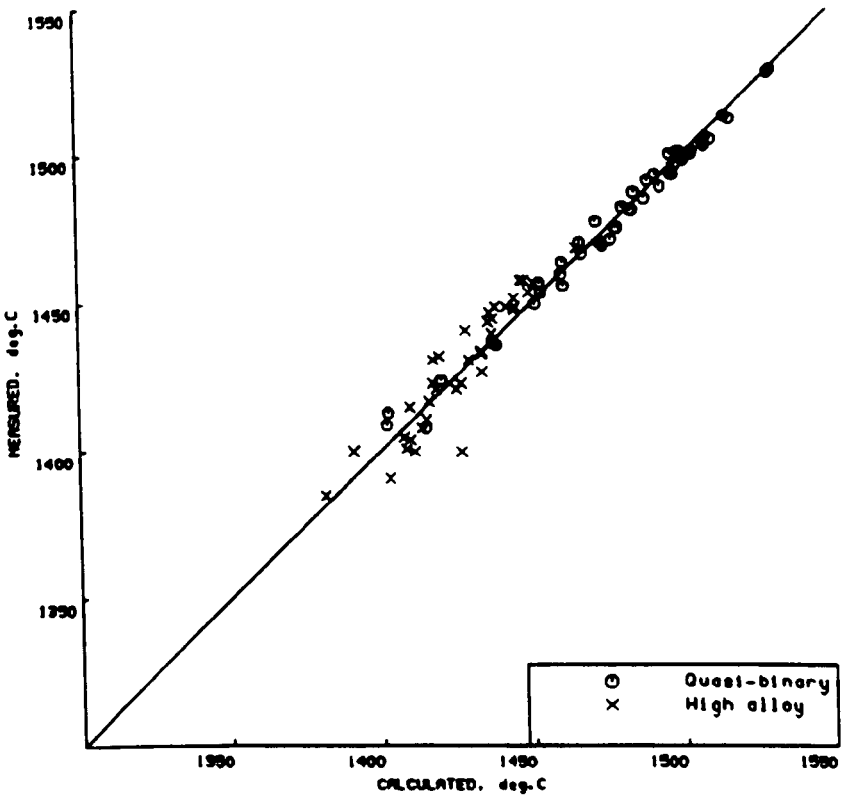

MEASURED v "BS" LIQUIDUS, REF.111 FIG 3·5

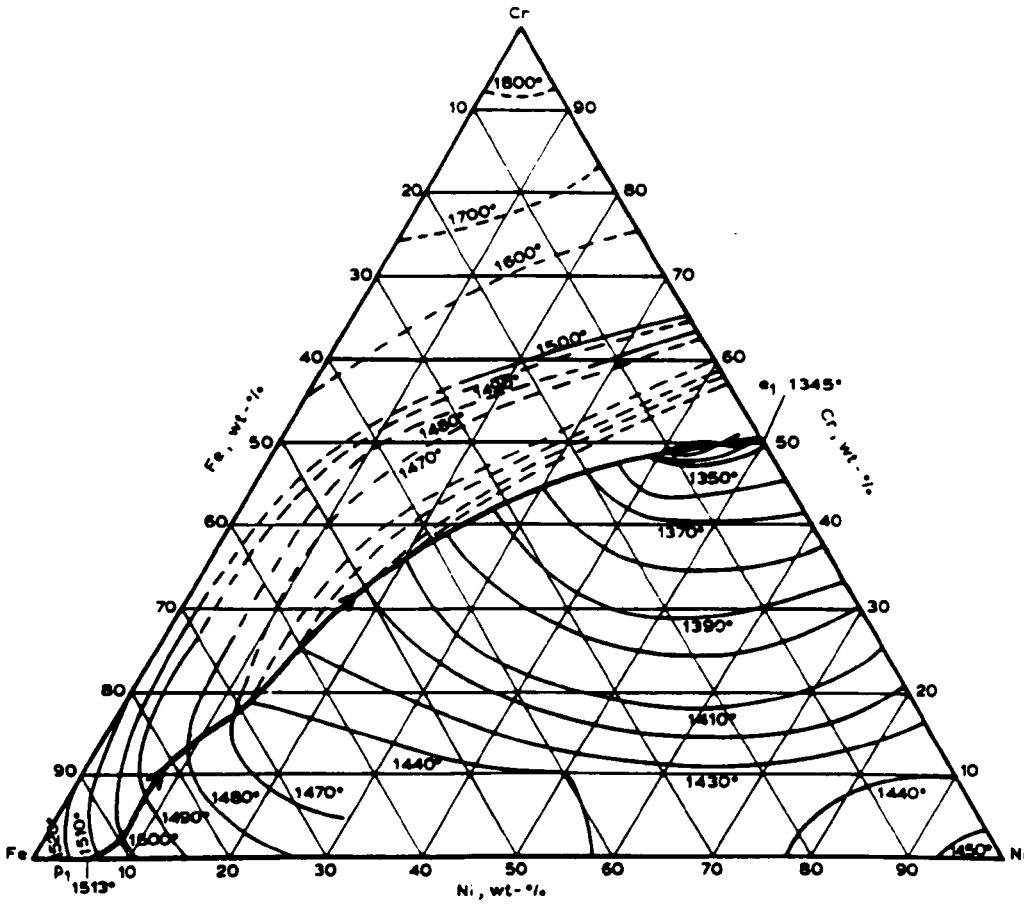

FeCrNi LIQUIDUS PROJECTION AFTER REF.127 FIG. 3.6

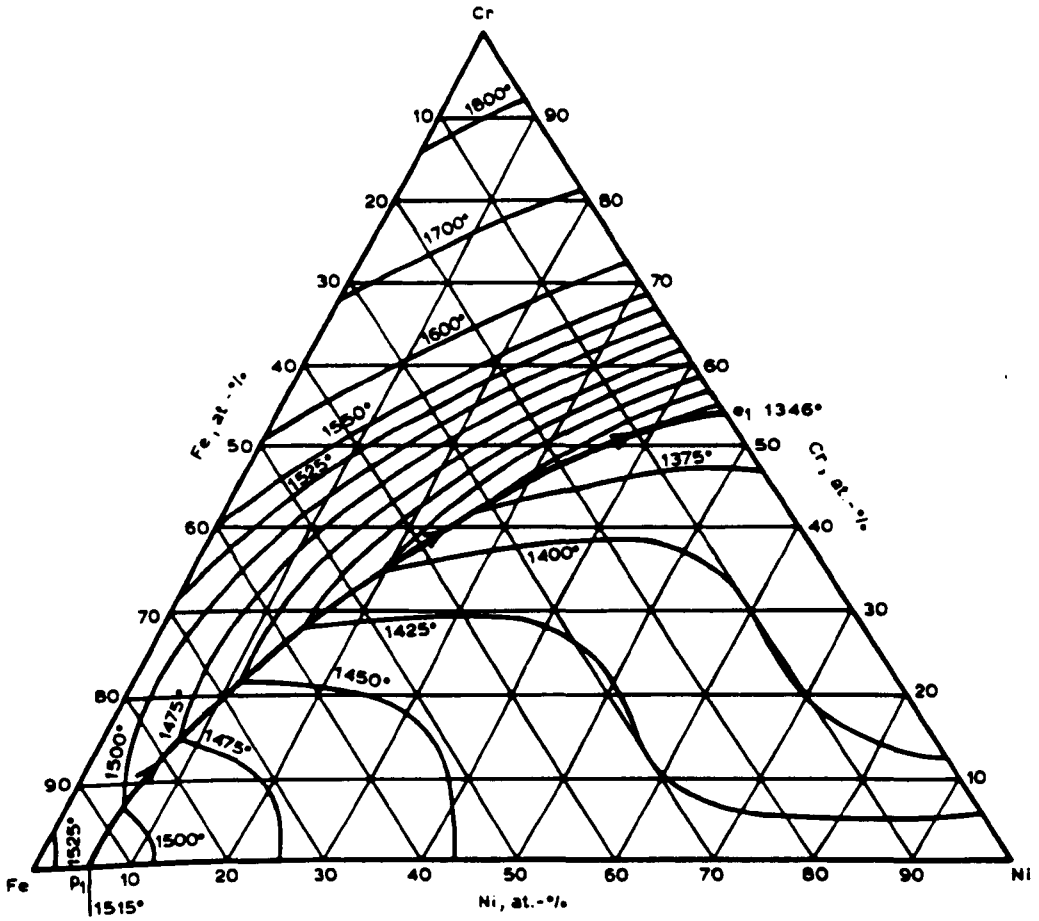

FeCrNi LIQUIDUS PROJECTION AFTER REF. 128 FIG. 3.7

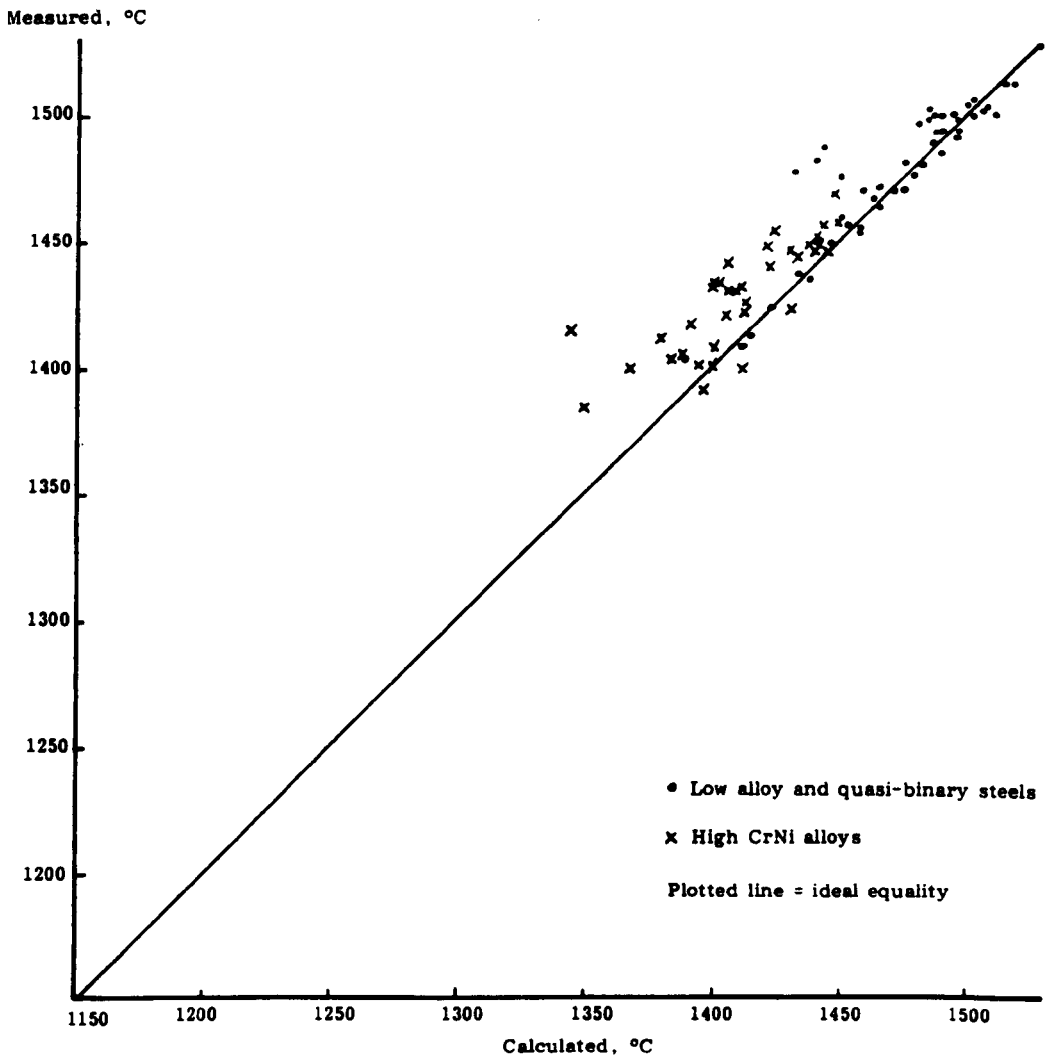

MEASURED v MTDATA LIQUIDUS, PREVIOUS DATA FIG. 3.8

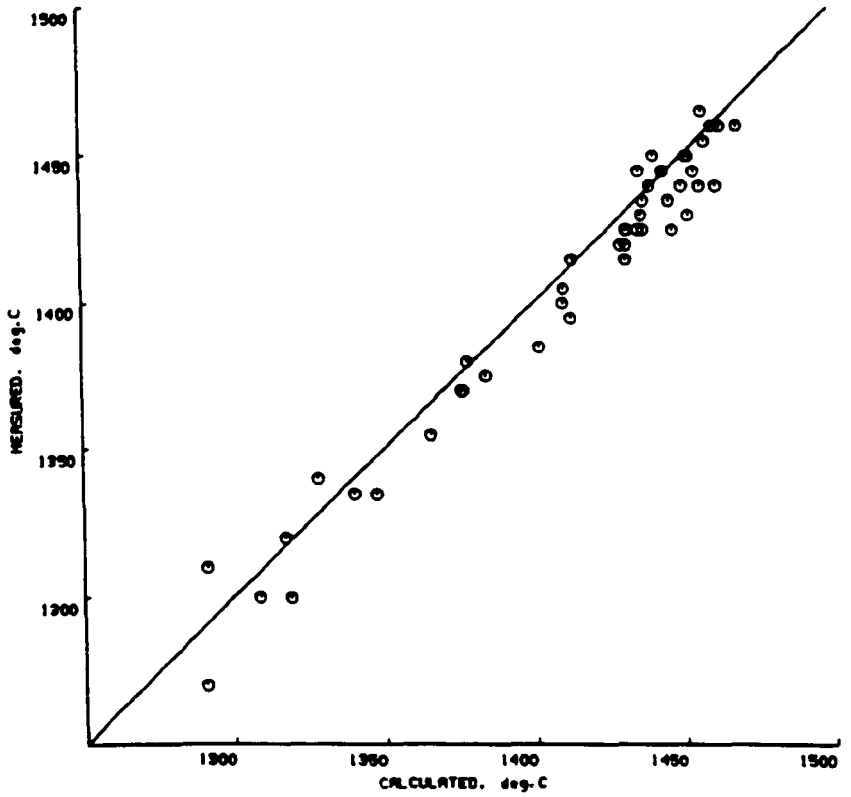

MEASURED v CALCULATED SOLIDUS, REF.121 FIG.3·9

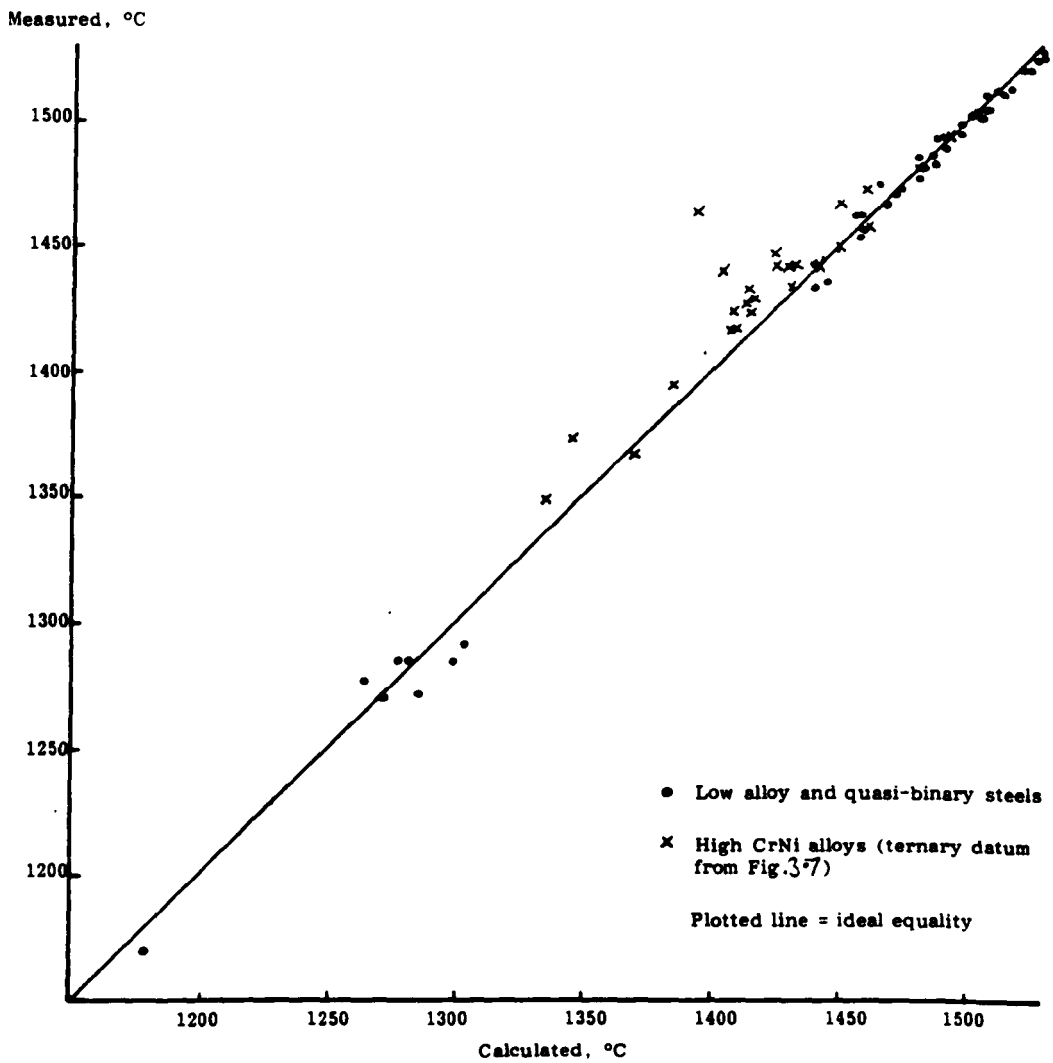

MEASURED v BS LIQUIDUS, PRESENT DATA FIG. 3·10

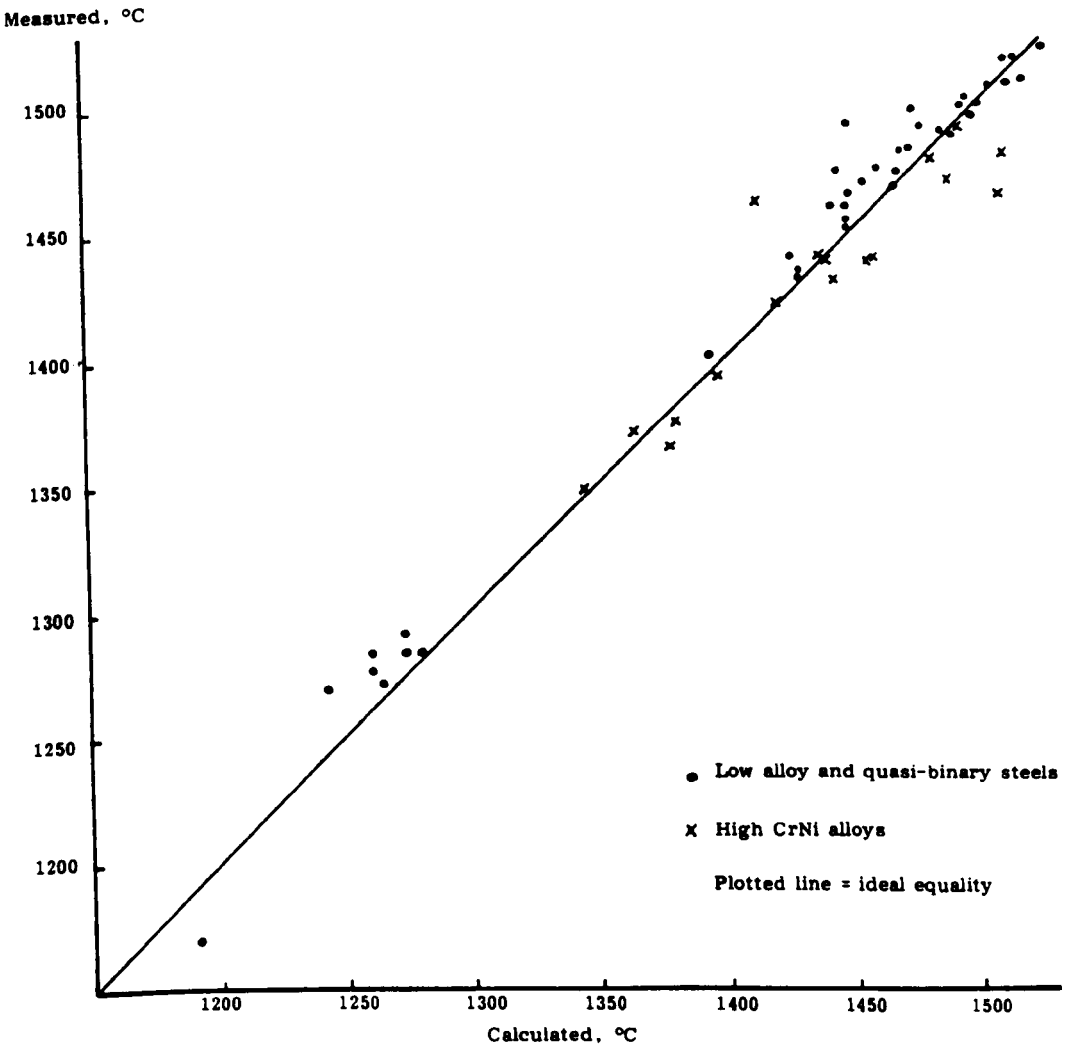

MEASURED v MTDATA LIQUIDUS, PRESENT DATA FIG. 3.11

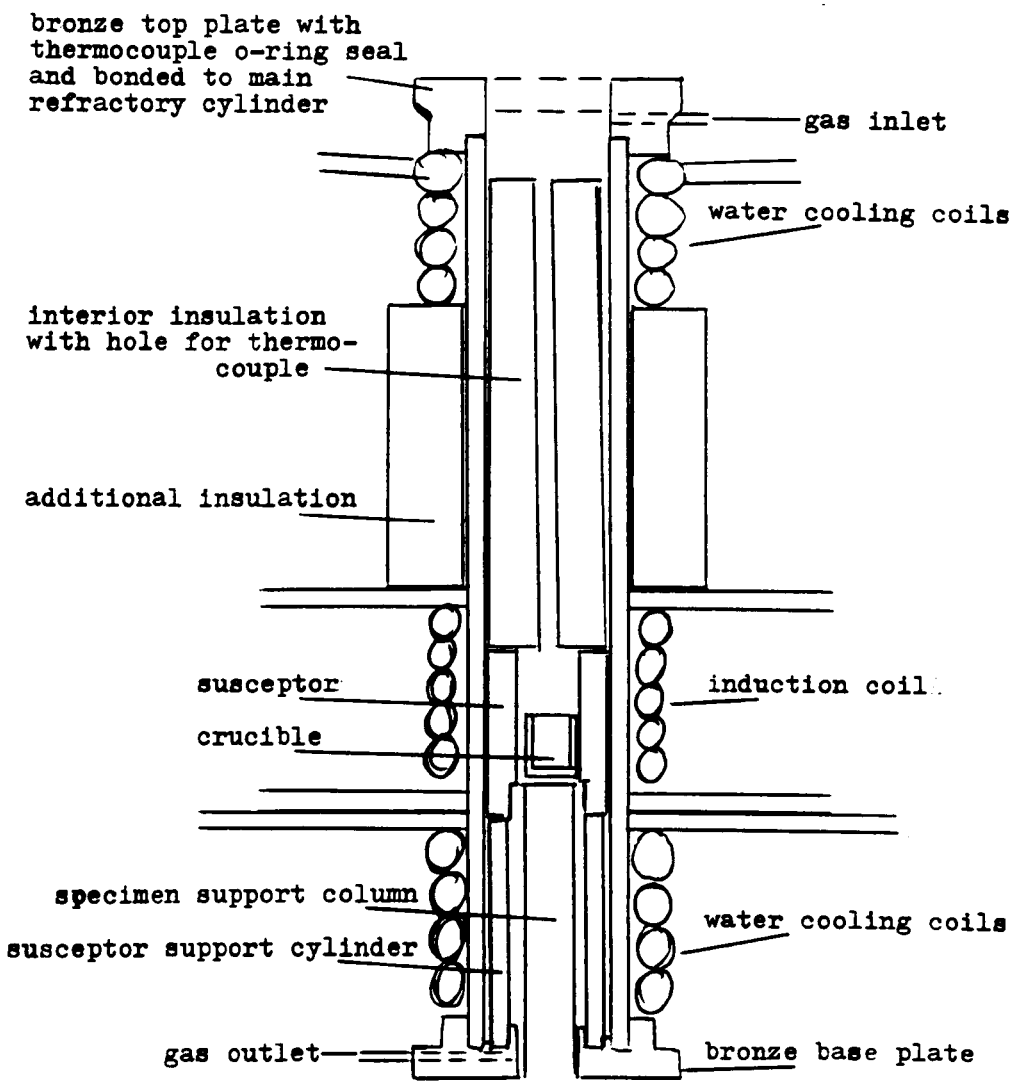

Fig.3.12 APPARATUS AS ACQUIRED

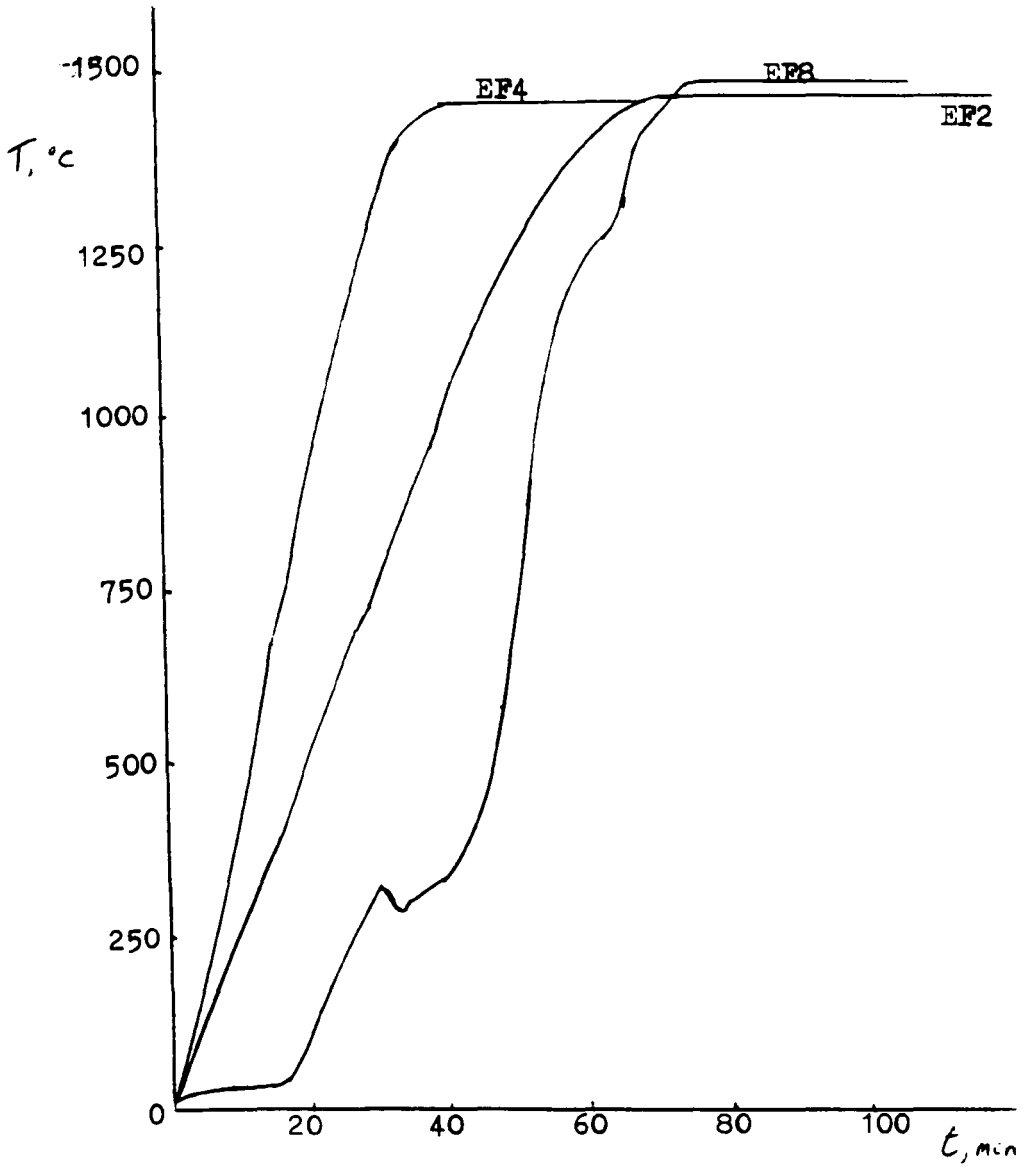

Fig. 3.13 EXAMPLE THERMAL HISTORIES FROM EQUILIBRATION FURNACE EXPERIMENTS

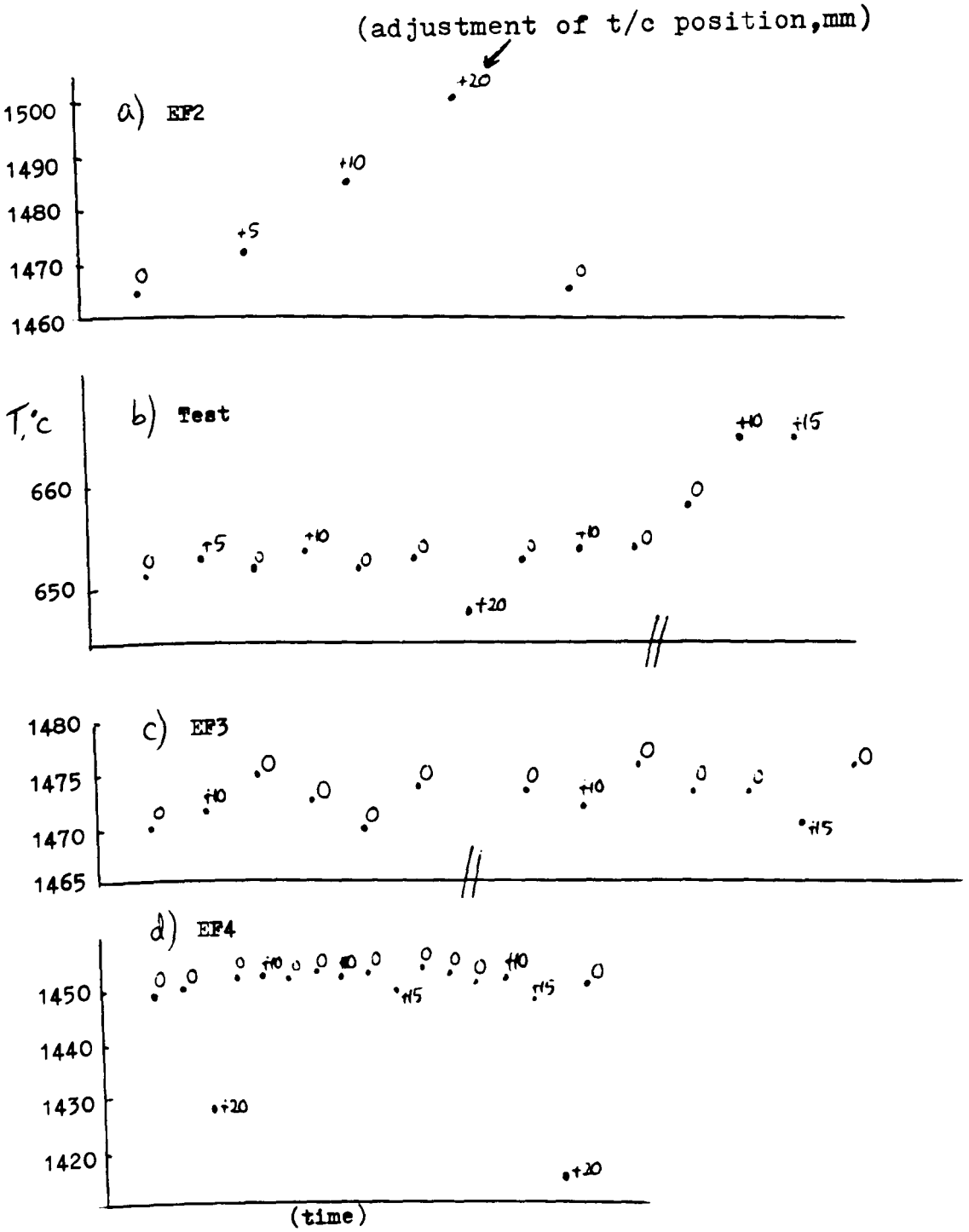

Fig. 3.14 EXAMPLES OF TEMPERATURE VARIABILITY AND GRADIENTS EXPERIENCED WITH THE EQUILIBRATION FURNACE (contd..)

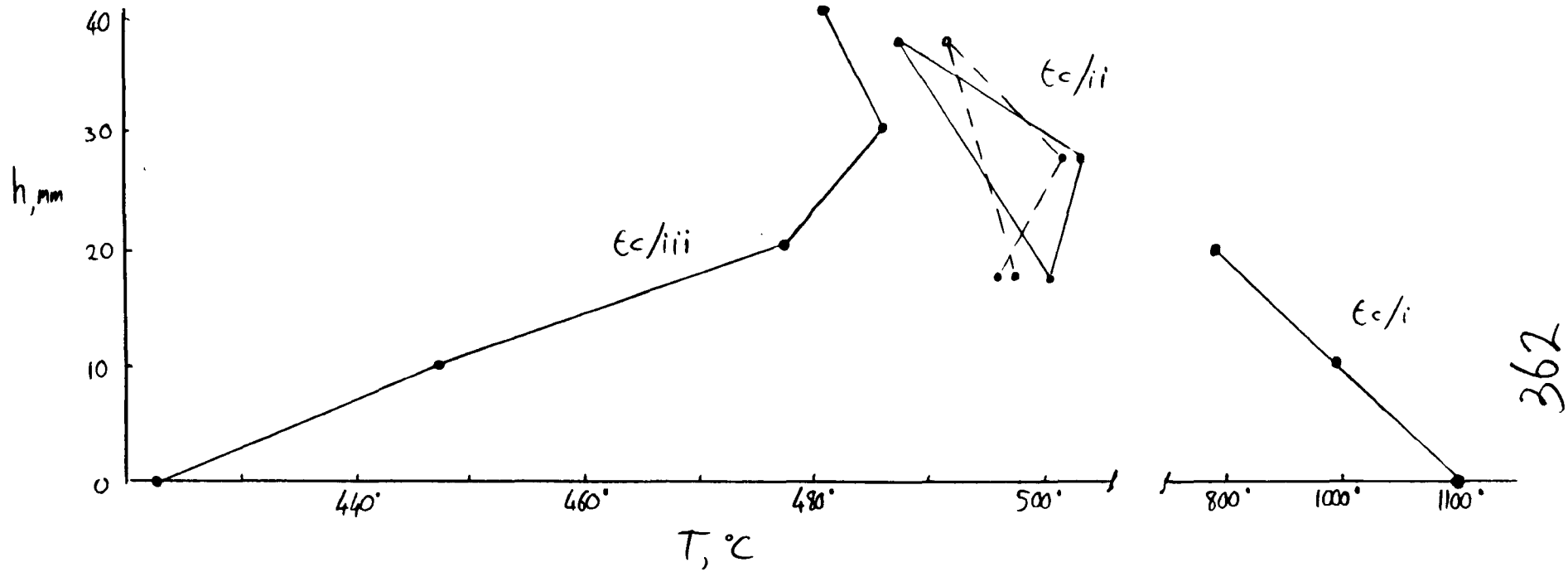

Fig. 3.14 continued

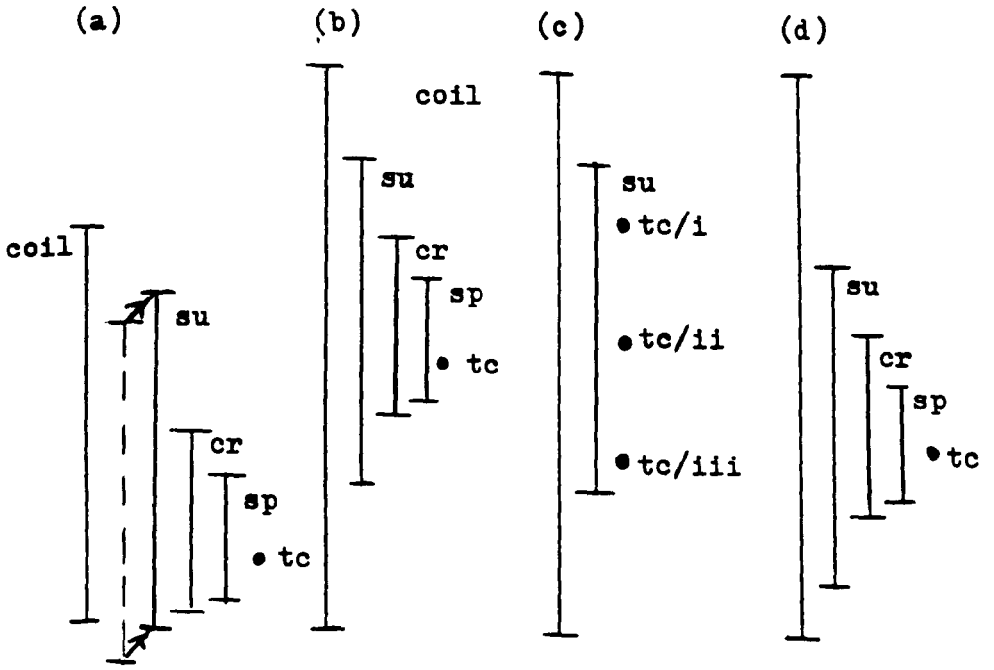

Fig. 3.15 ALTERNATIVE RELATIVE POSITIONS WITHIN THE EQUILIBRATION FURNACE (×0·85)

Case (a), apparatus as acquired, susceptor pushed up upon insertion of specimen
Case (b), assumed ideal but unable to release specimen
Case (c), test case, see Fig.3.14
Case (d), configuration as from EF4

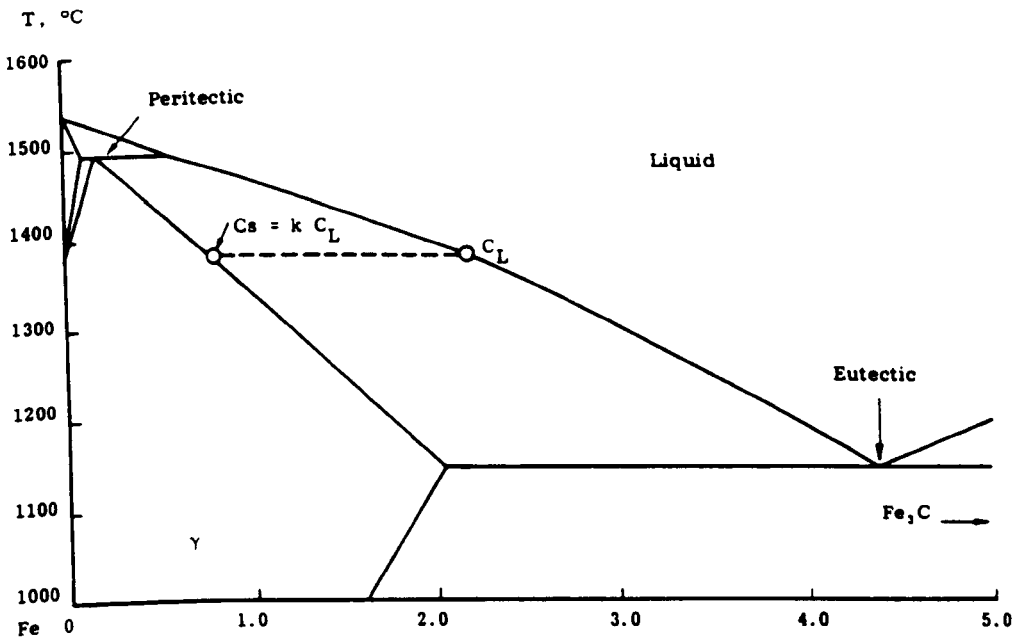

PART OF THE Fe-C (C AS CEMENTITE, Fe_3C) PHASE DIAGRAM FIG.3.16

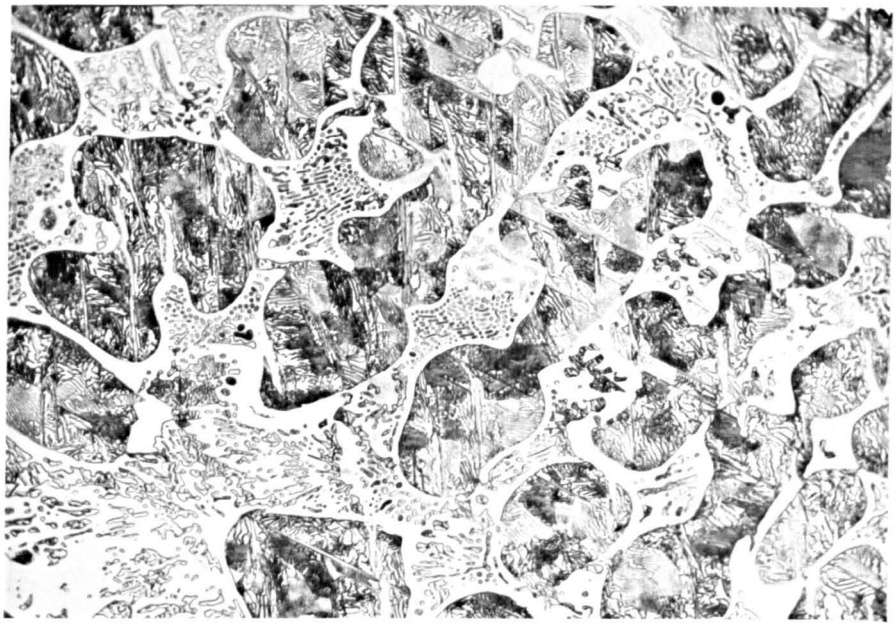

PRIOR AUSTENITE DENDRITES (NOW PEARLITIC) IN LEDEBURITE

x 200 SAMPLE 122 FIG. 3.17

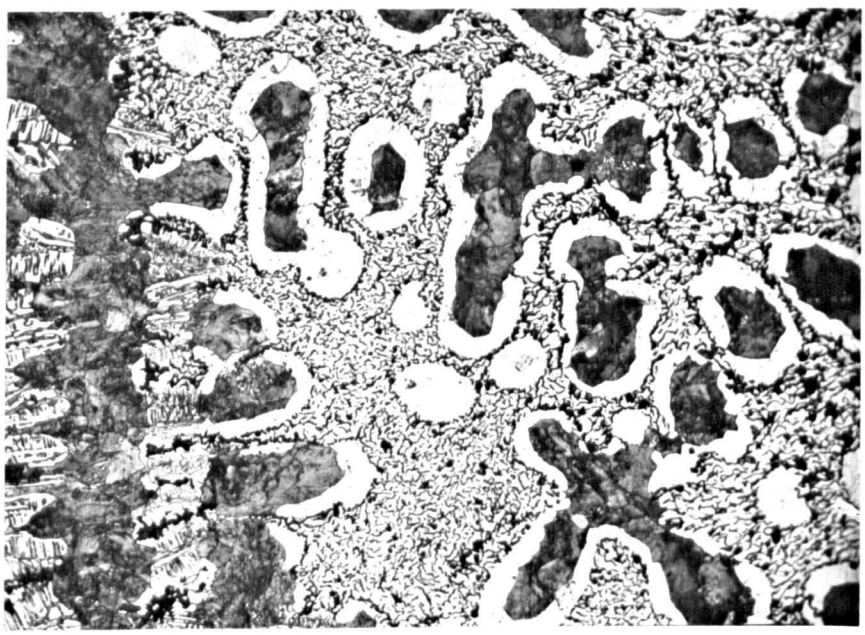

PRIOR AUSTENITE DENDRITES (NOW PEARLITIC WITH FERRITE 'HALOS') IN LARGELY GRAPHITIC EUTECTIC

x 200 SAMPLE 123 FIG. 3.18

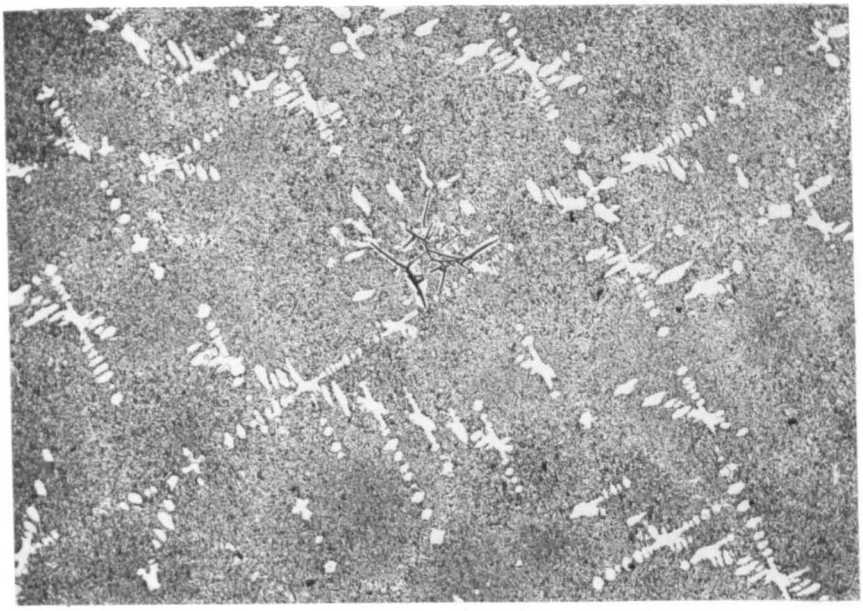

Primary, ASTM Type C (kish) graphite with (a) non-equilibrium secondary austenite growth and Type D (undercooled) graphite

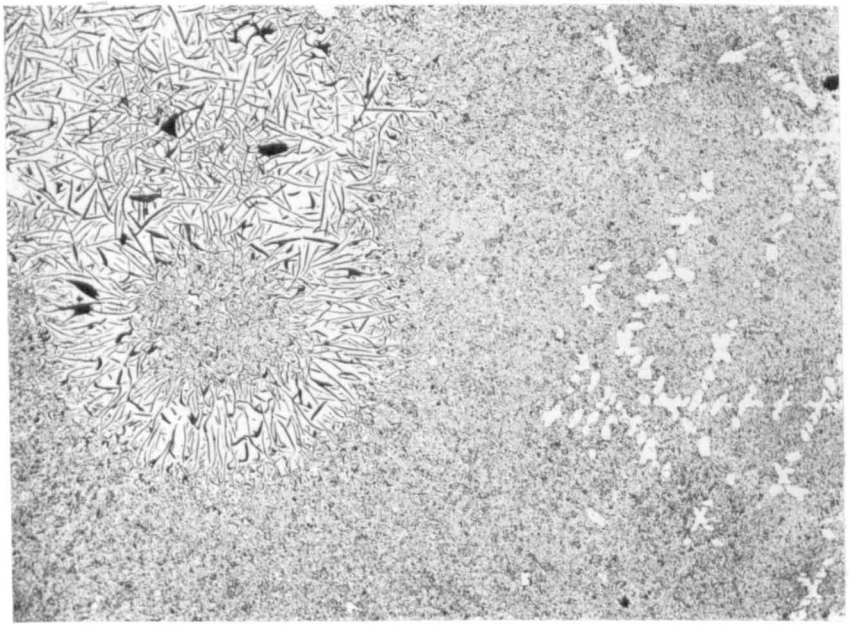

Eutectic cell Type B (rosette) graphite (b) and Type D, as in (a)

SAMPLE 124
x 50

FIG. 3.19

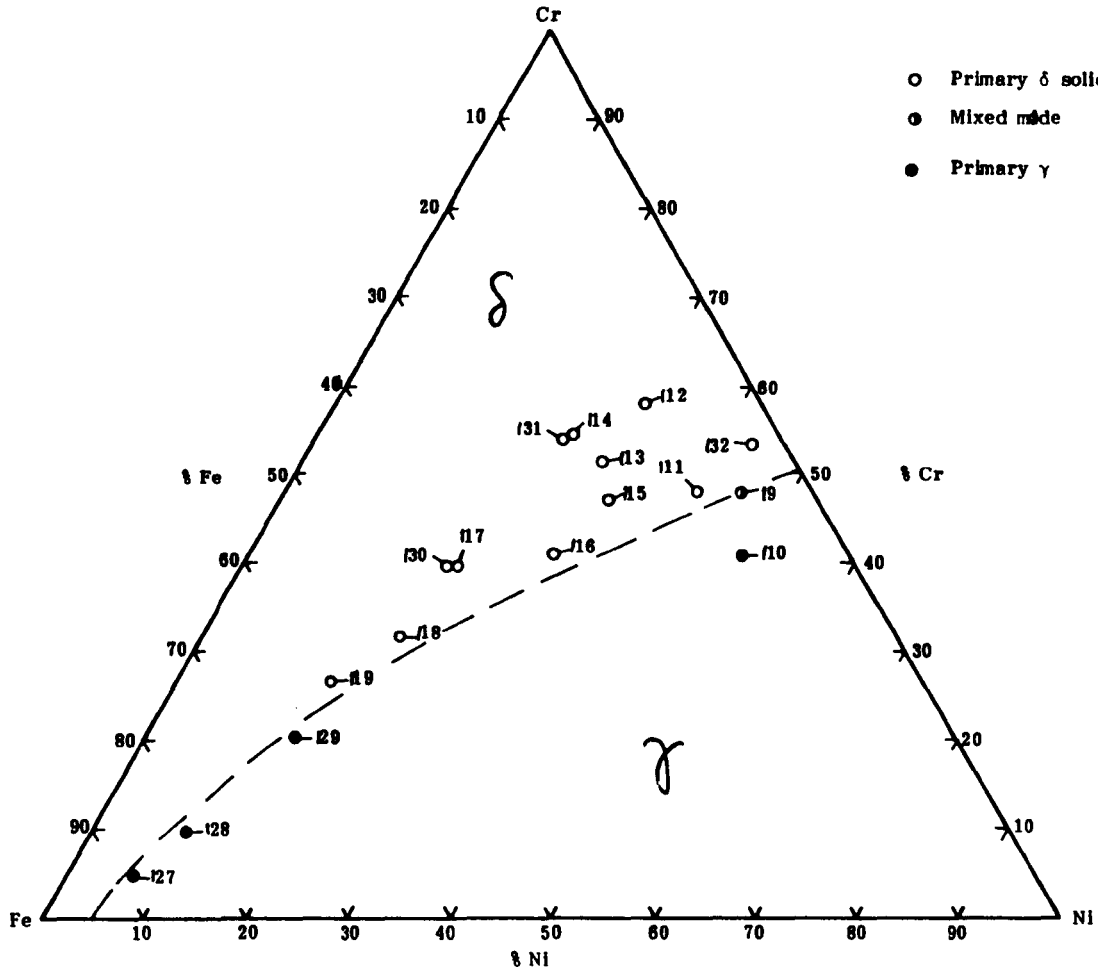

TERNARY PLOT OF FeCrNi TEST CAST COMPOSITIONS

FIG. 3-20

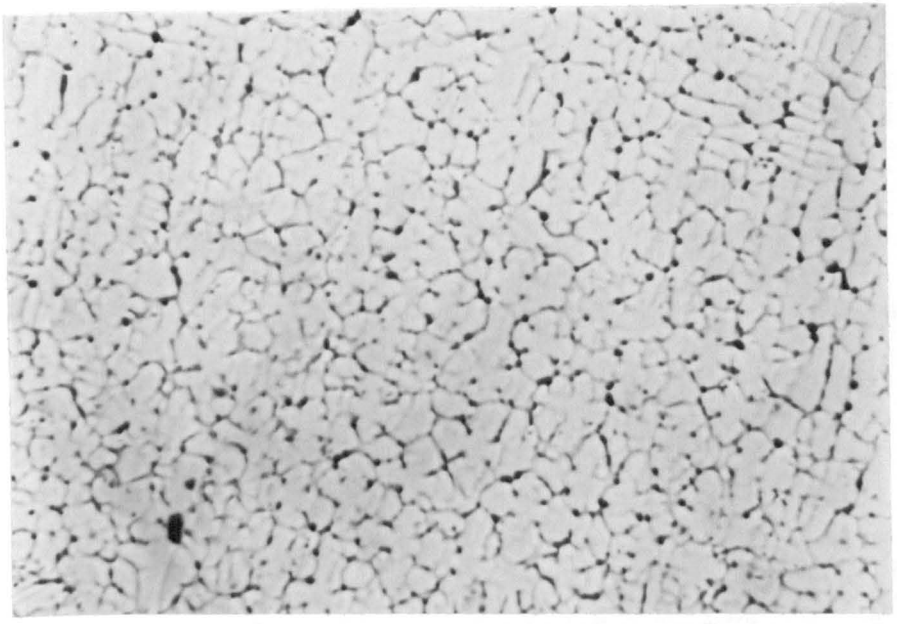

Transverse to dendrite axes (a)
Evidence of second, interdendritic phase

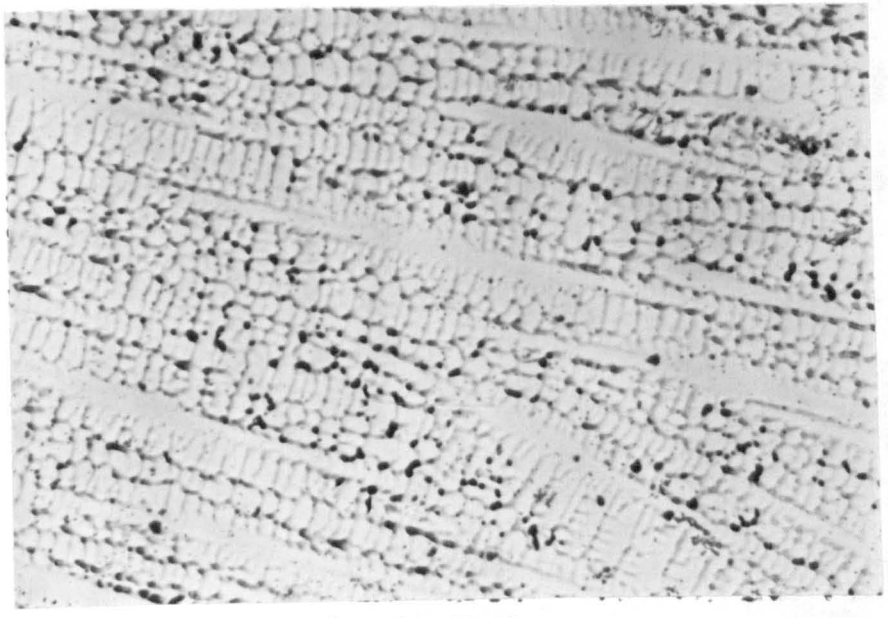

Longitudinal (b)

FeCrNi SERIES, SAMPLE 129
x 50 FIG. 3.21

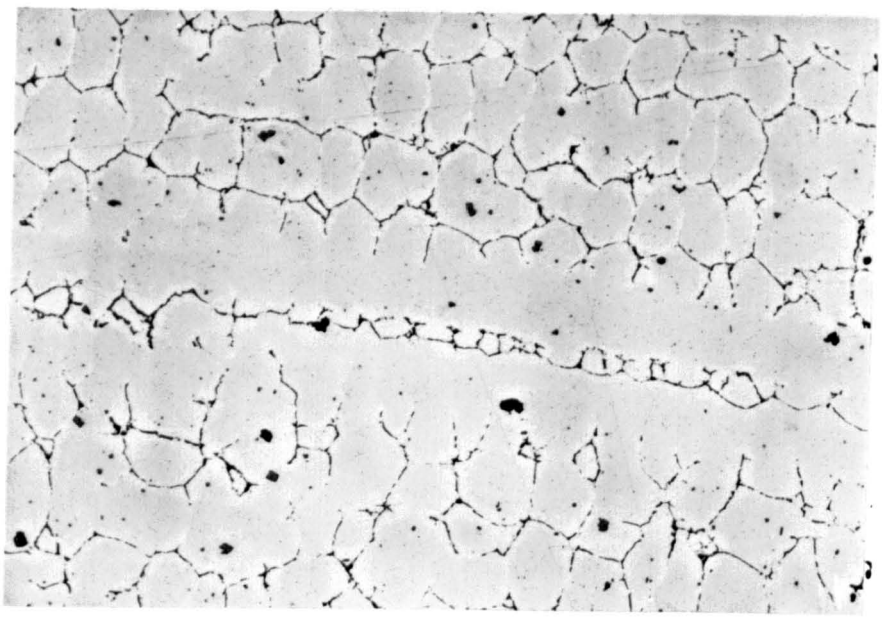

FeCrNi SERIES, SAMPLE 110
AUSTENITE DENDRITES WITH INTERDENDRITIC FERRITE
x 100 FIG. 3.22

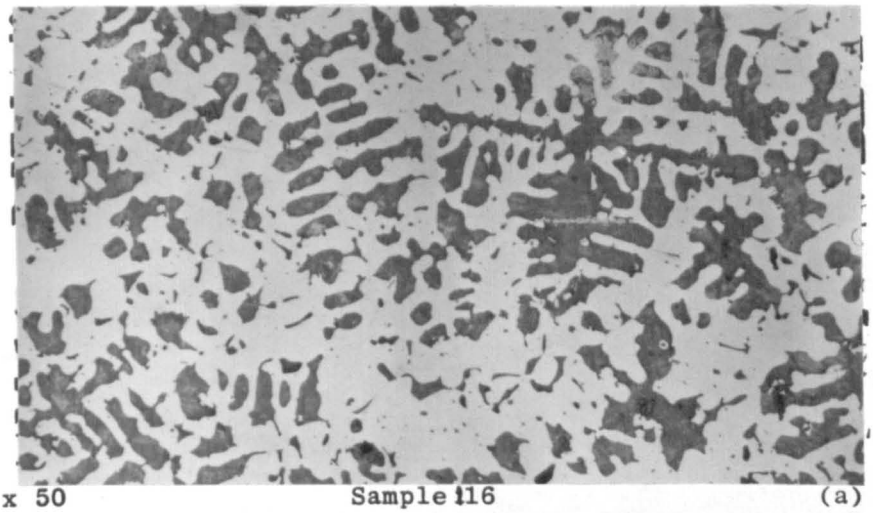

x 50 Sample 116 (a)

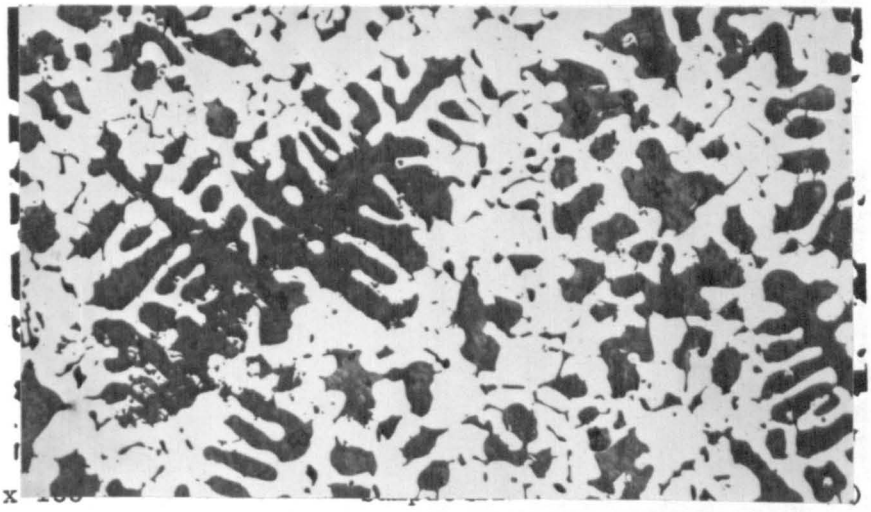

x

FeCrNi SERIES, PRIMARY FERRITIC SOLIDIFICATION NEAR THE EUTECTIC TROUGH FIG. 3.23

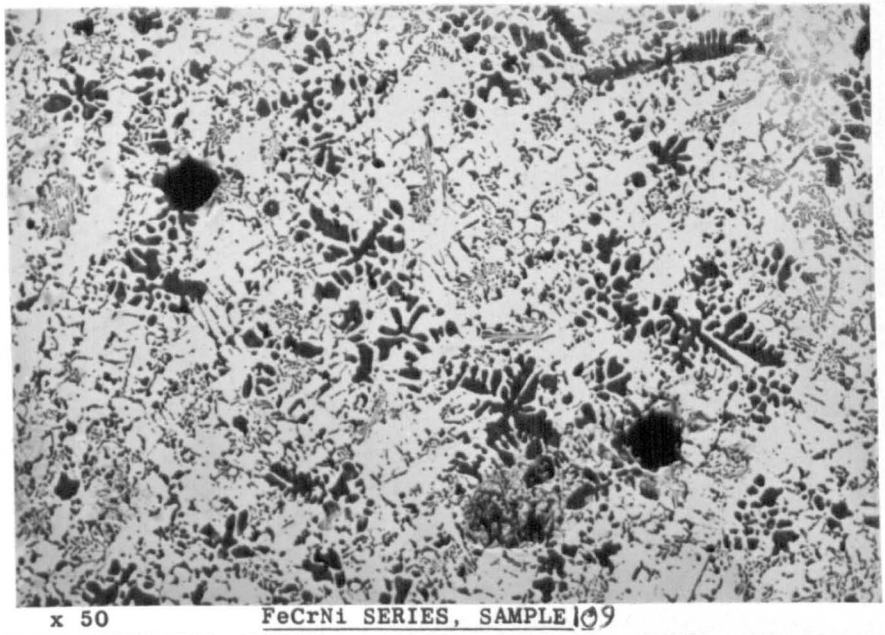

a) x 50 FeCrNi SERIES, SAMPLE 109
AUSTENITE DENDRITES (LIGHT), FERRITE DENDRITES (DARK), AND EUTECTIC

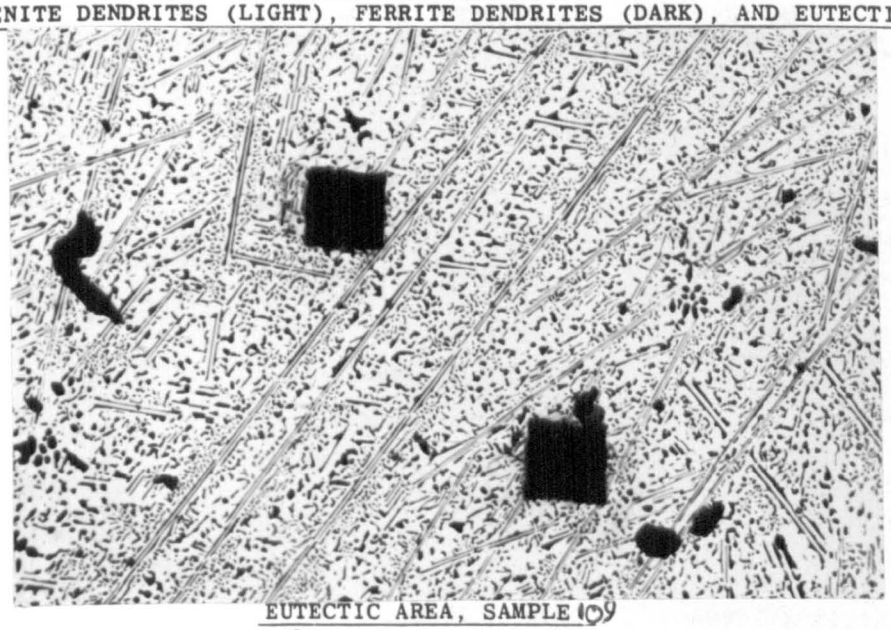

b) EUTECTIC AREA, SAMPLE 109
x 100

FIG. 3.24) ALTERNATIVE SOLIDIFICATION MODES WITHIN THE SAME SAMPLE (109)

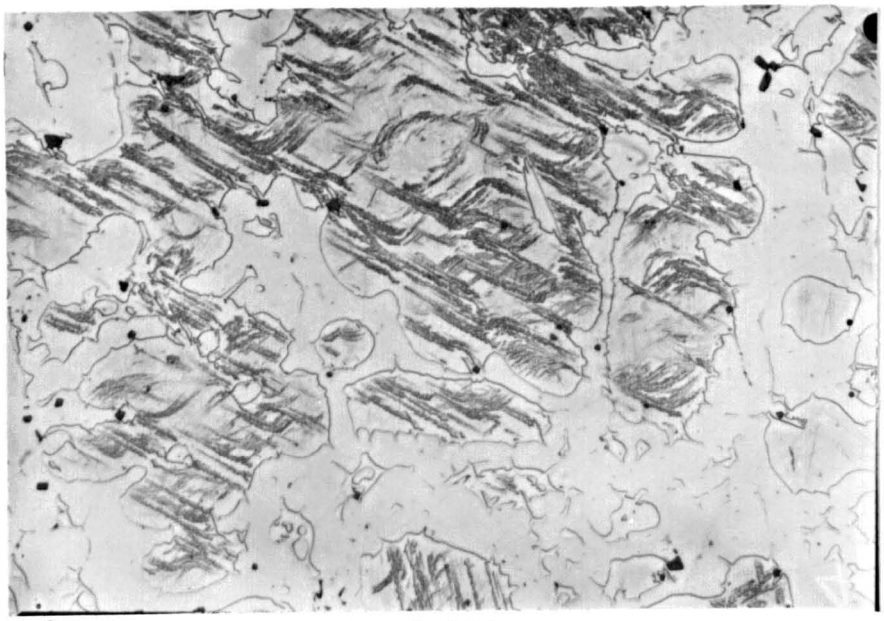

x 300 Sample 117 (a)

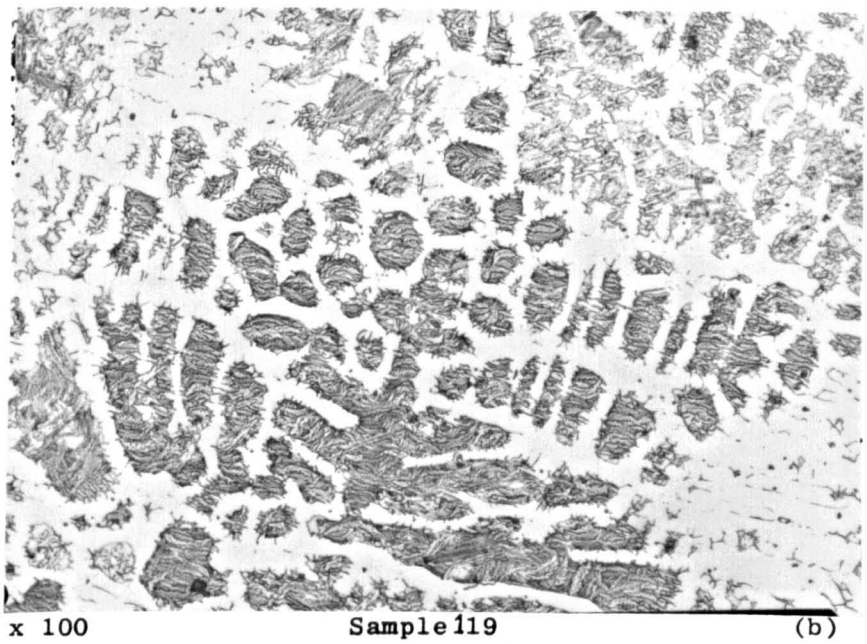

x 100 Sample 119 (b)

EXAMPLES OF 'WOOLLY' FERRITE TRANSFORMATION

FIG. 3.25
(Contd..)

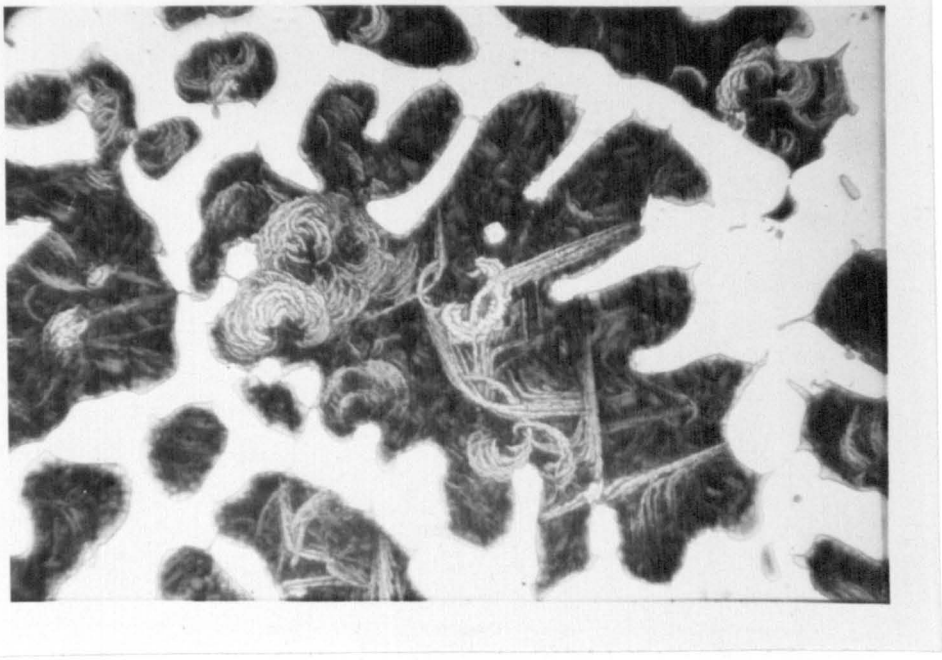

x 200 Sample 116 (c)

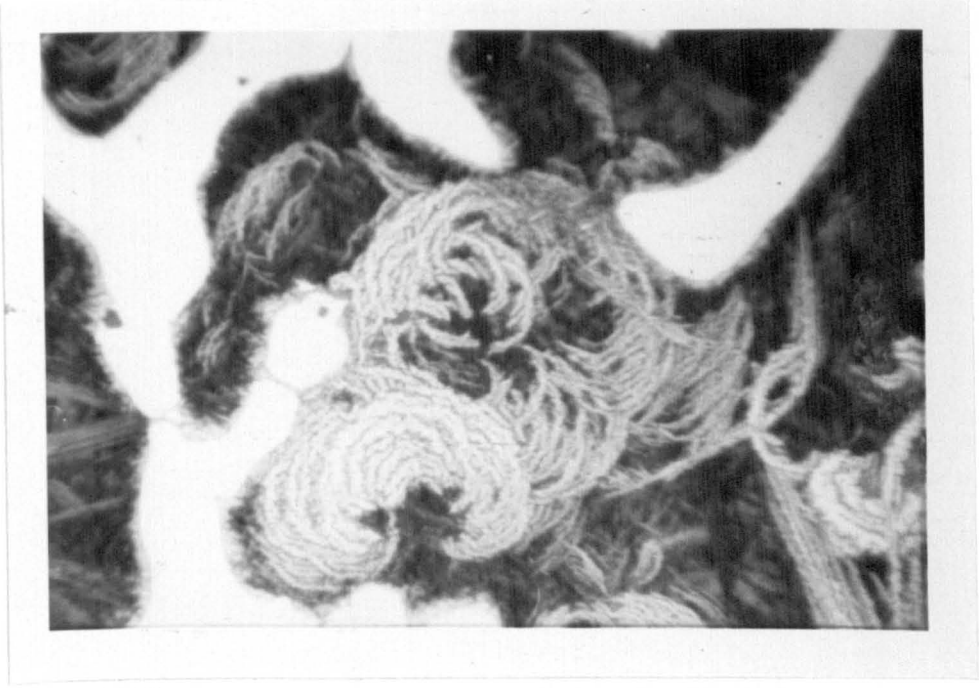

x1000

EXAMPLES OF 'WOOLLY' FERRITE TRANSFORMATION

FIG. 3.25

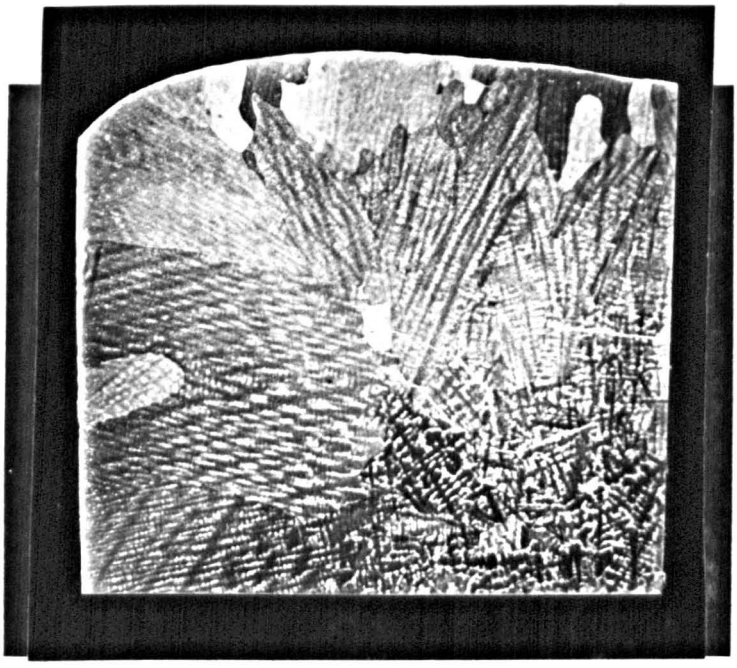

DENDRITE AND GRAIN STRUCTURES
x 4 SAMPLE 121 FIG. 3.26a

REGIONS OF FINE SCALE DENDRITIC, FACETTED AND EUTECTIC STRUCTURE BETWEEN PRIMARY DENDRITES
x 200 SAMPLE 133 FIG. 3.26b

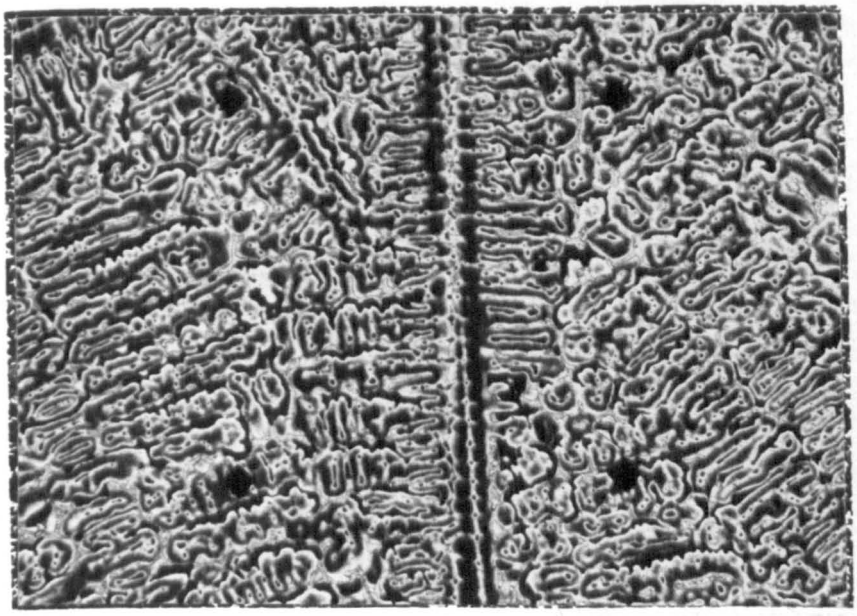

x 100 (a)

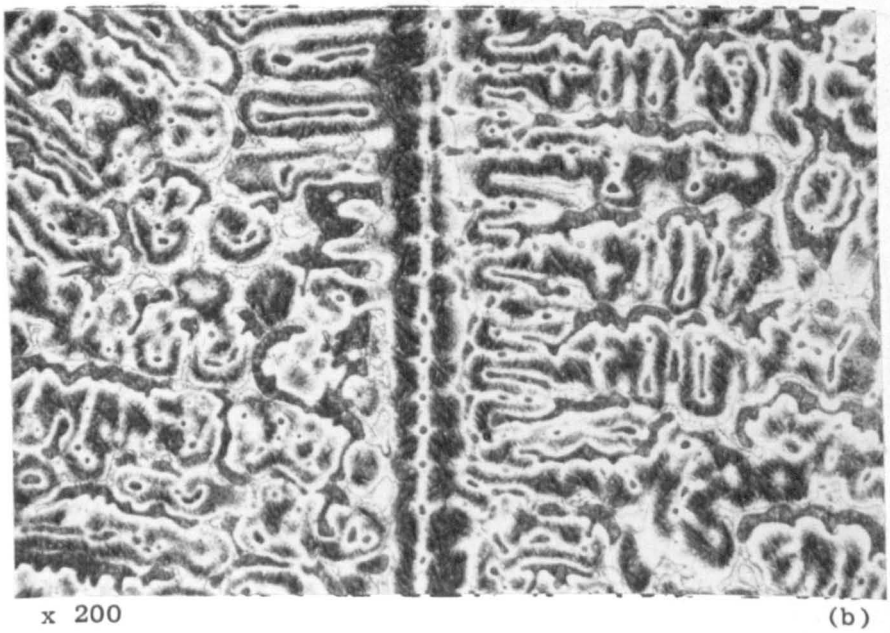

x 200 (b)

APPARENT POSITIVE SEGREGATION WITH POSSIBLE RE-LIQUATION WITHIN DENDRITE CORES
SAMPLE 162

FIG. 3.27

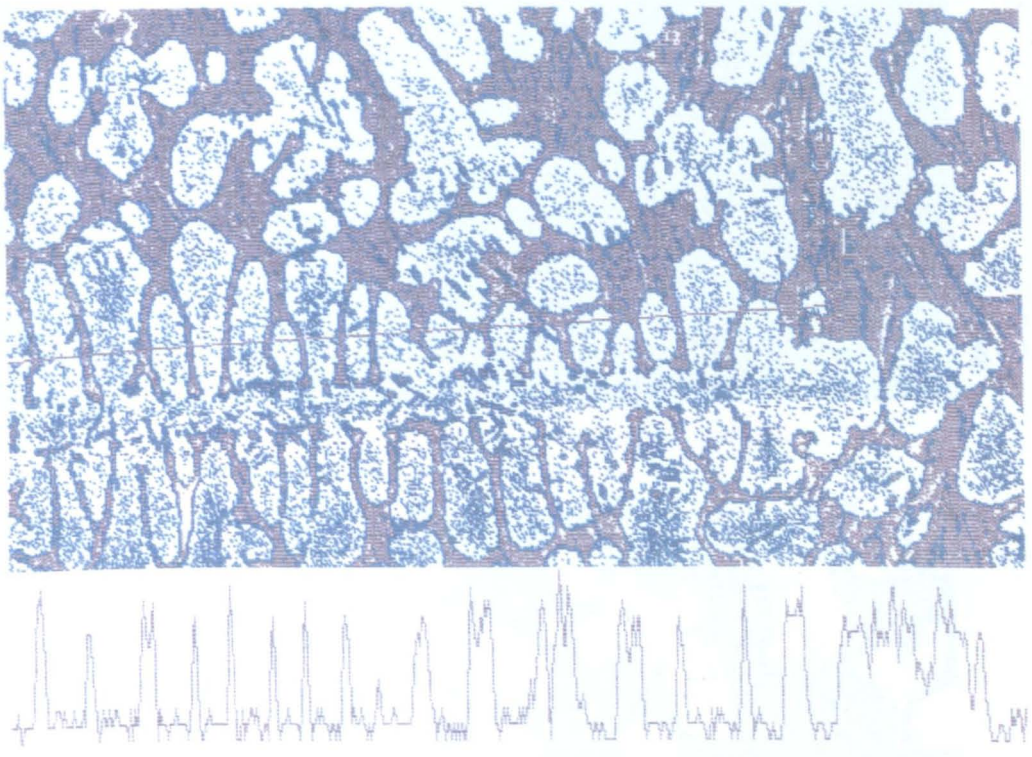

a) 04951 4B 6D135B T CARBON X-RAY IMAGE

Fig. 3.28 EPMA COMPOSITION MAPS (EP.MAPS) OF SAMPLE 104 (2.88%C,1.45%Si,5.08%Mn)

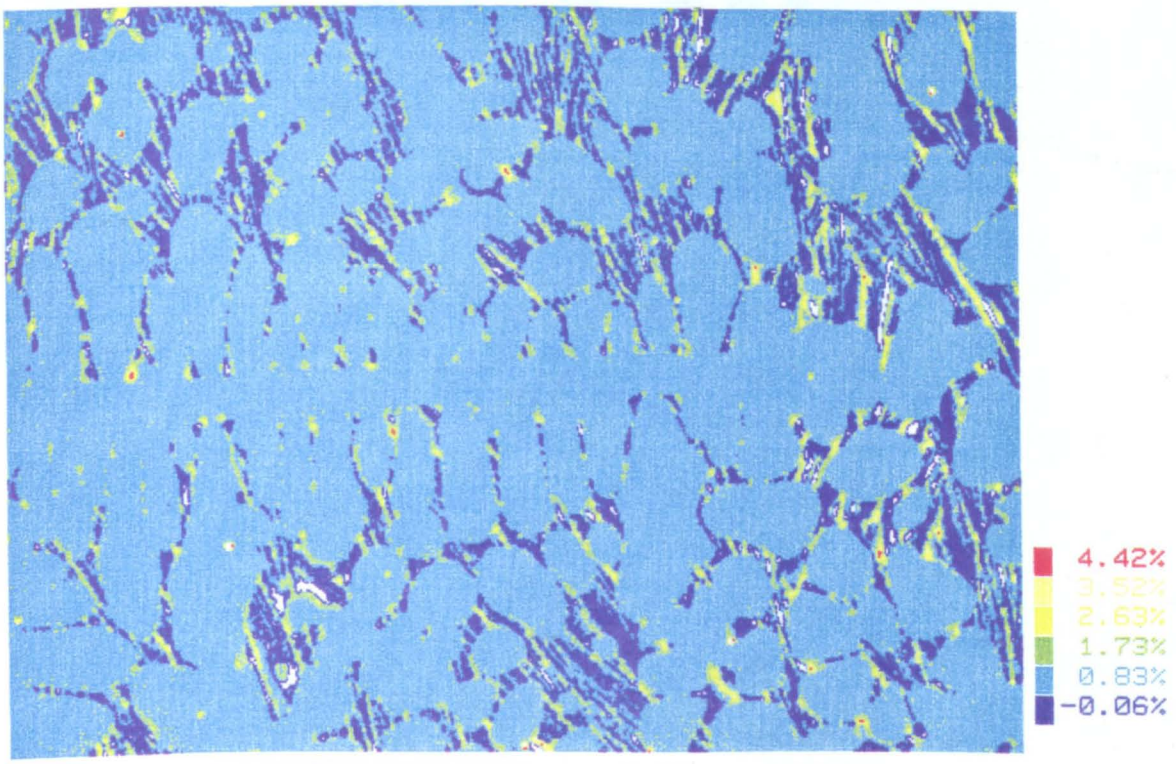

b) Q4951 4B 6D13SB T SILICON X-RAY IMAGE 1.024mm x 0.768mm

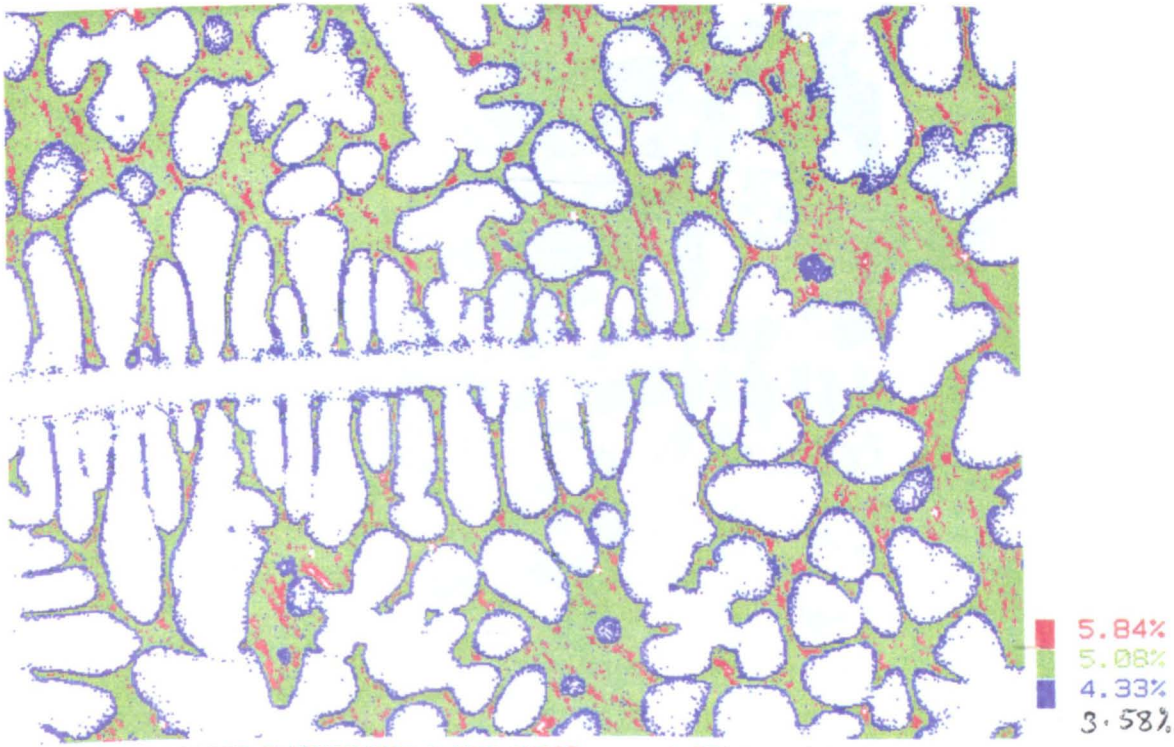

c) Q4951 4B 6D13SB T MANGANESE X-RAY IMAGE 1.024mm x 0.768mm

Fig. 3.28 continued

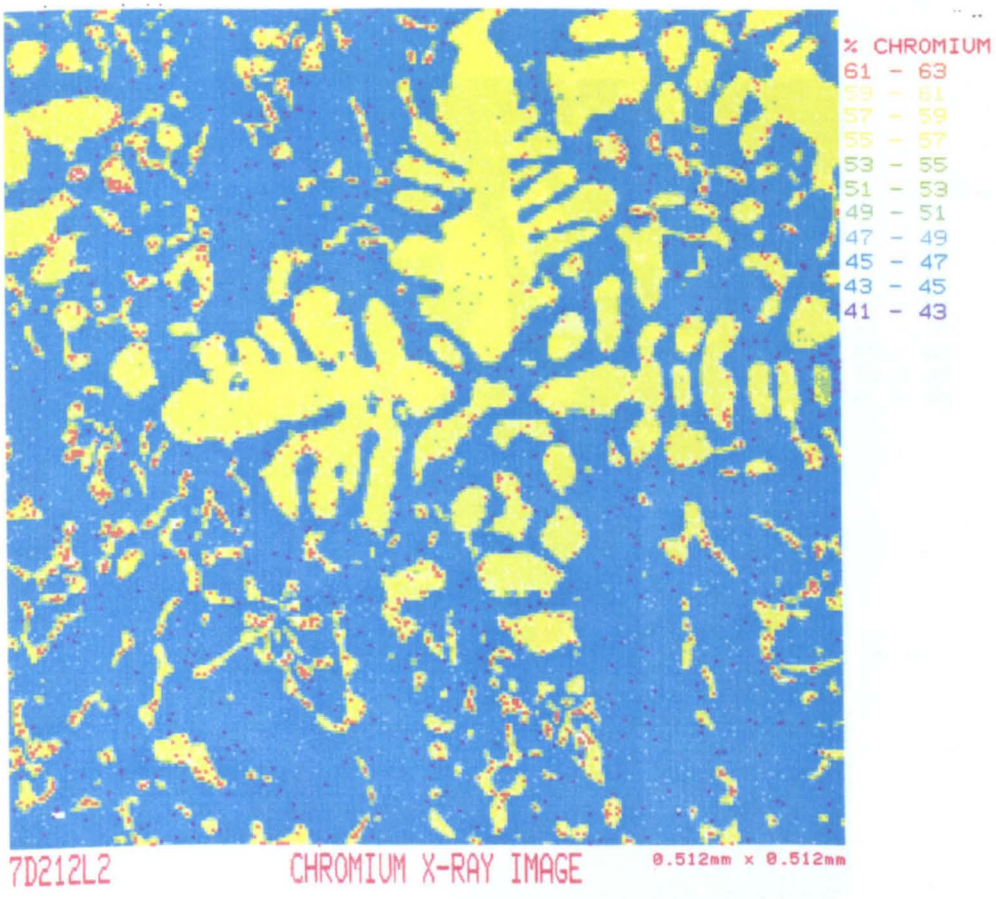

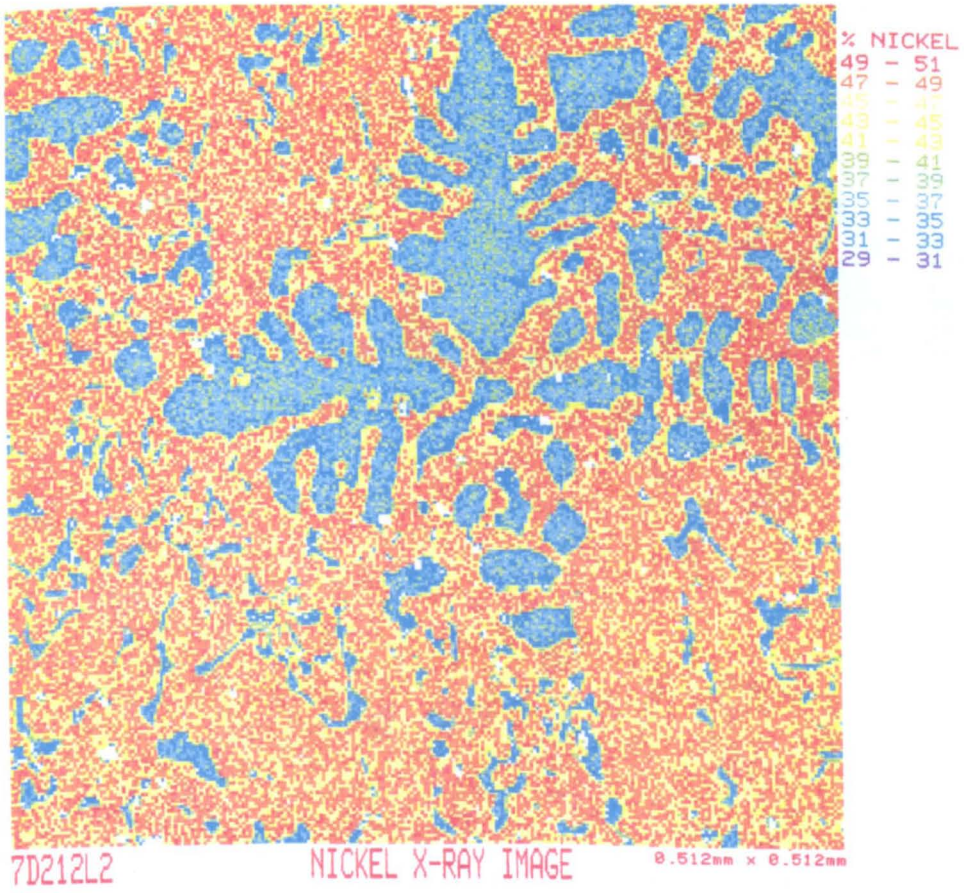

a) Ferrite Dendrite

Fig. 3.29 EP.MAPS OF SAMPLE 109 (48%Cr, 45%Ni)

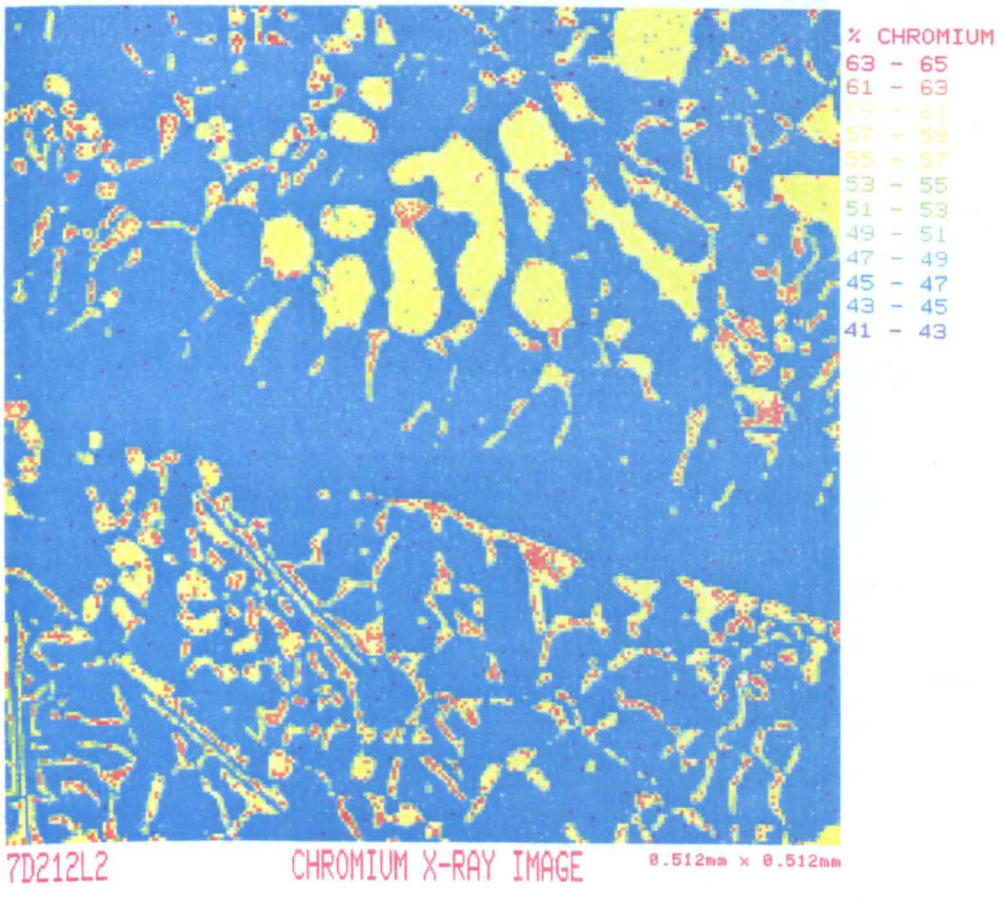

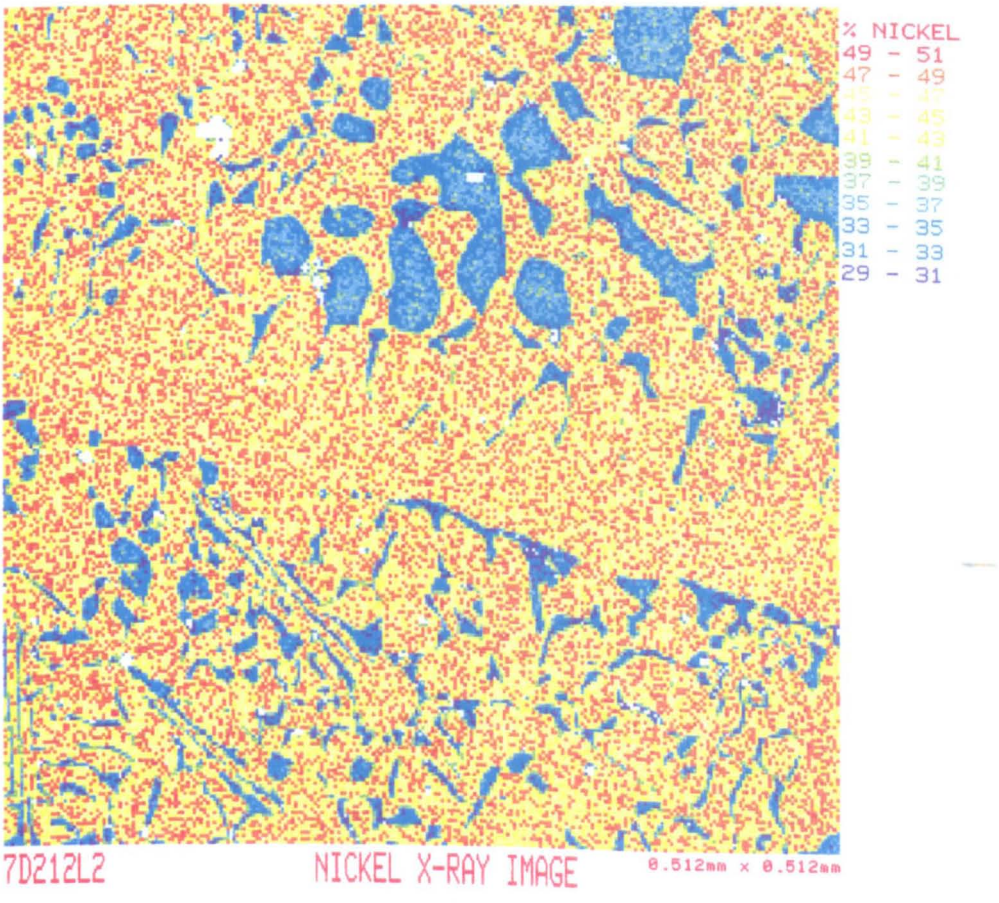

b) Austenite Dendrite

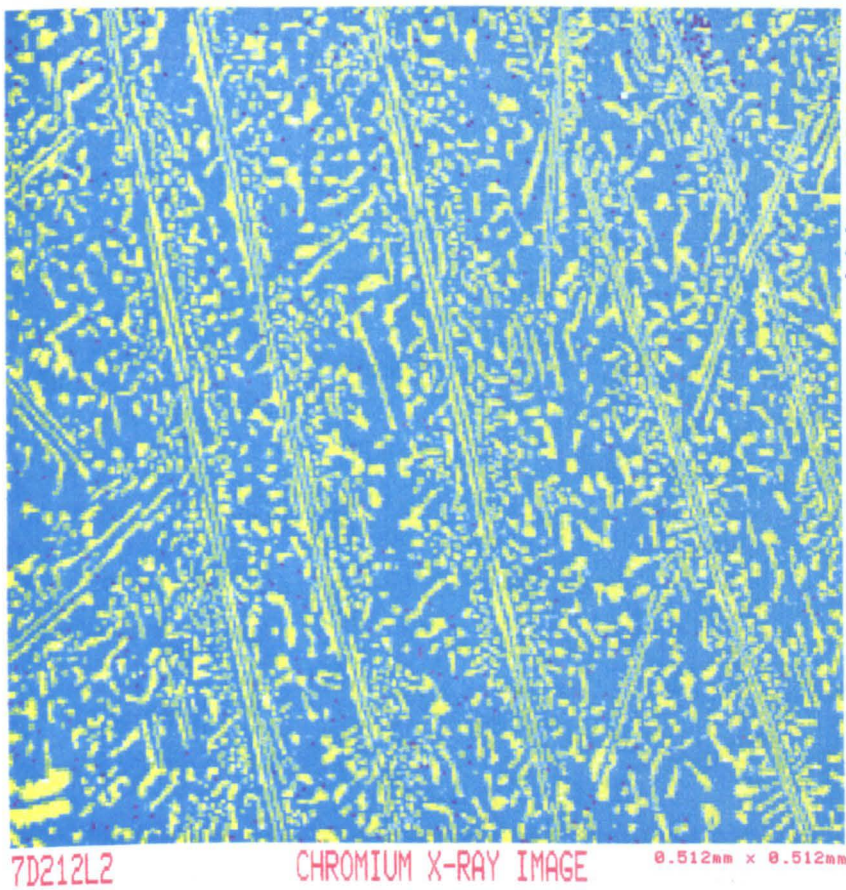
% CHROMIUM
59 - 61
57 - 59
55 - 57
53 - 55
51 - 53
49 - 51
47 - 49
45 - 47
43 - 45
41 - 43
7D212L2
CHROMIUM X-RAY IMAGE
0.512mm x 0.512mm

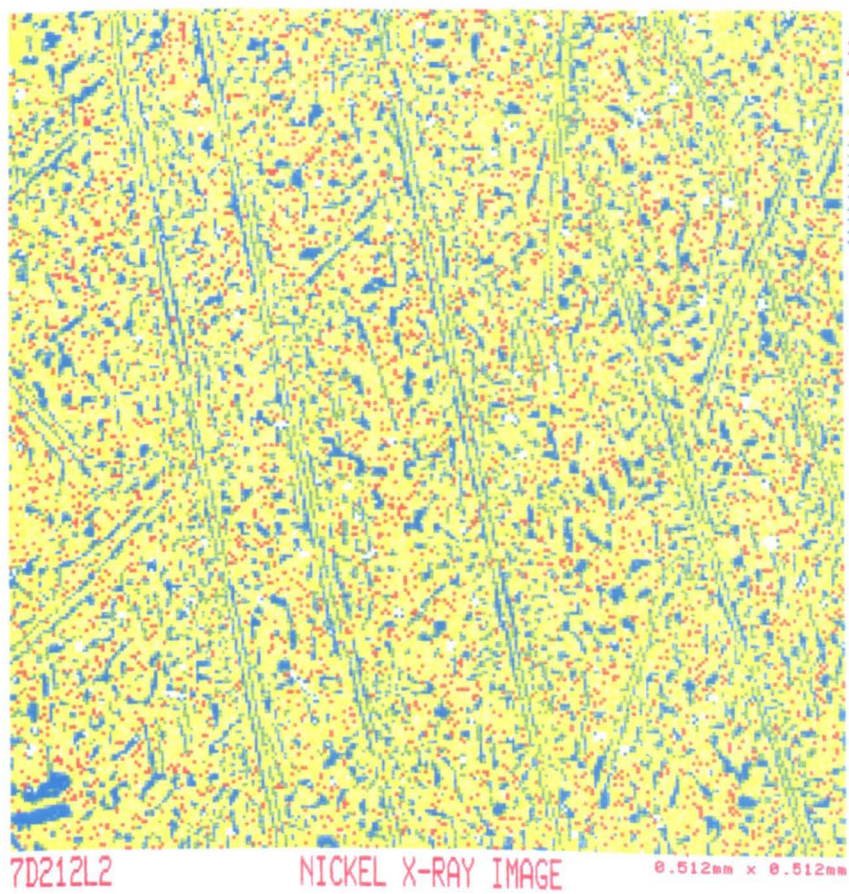
% NICKEL
47 - 49
45 - 47
43 - 45
41 - 43
39 - 41
37 - 39
35 - 37
33 - 35
31 - 33
7D212L2
NICKEL X-RAY IMAGE
0.512mm x 0.512mm

c) Eutectic

Key to Figures 3.30 and 3.33

EF8: Mn wt%

	- 4.3
4.3	- 5.1
5.1	- 6.0
6.0	- 6.5
6.5	- 7.1
7.1	-

Si wt%

	- 1.60
1.60	- 1.95
1.95	- 2.20
2.20	- 2.33
2.33	- 2.55
2.55	-

Fe wt%

	- 91
91	- 92
92	- 93
93	- 94
94	- 95
95	-

EF9: Si wt%

	- 0.20
0.20	- 0.36
0.36	- 0.44
0.44	- 0.52
0.52	- 0.70
0.70	-

Mo wt%

	- 7.0
7.0	- 8.5
8.5	-10.5
10.5	-12.0
12.0	-18.0
18.0	-

Fe wt%

	- 15
15	- 77
77	- 87
87	- 90
90	- 95
95	-

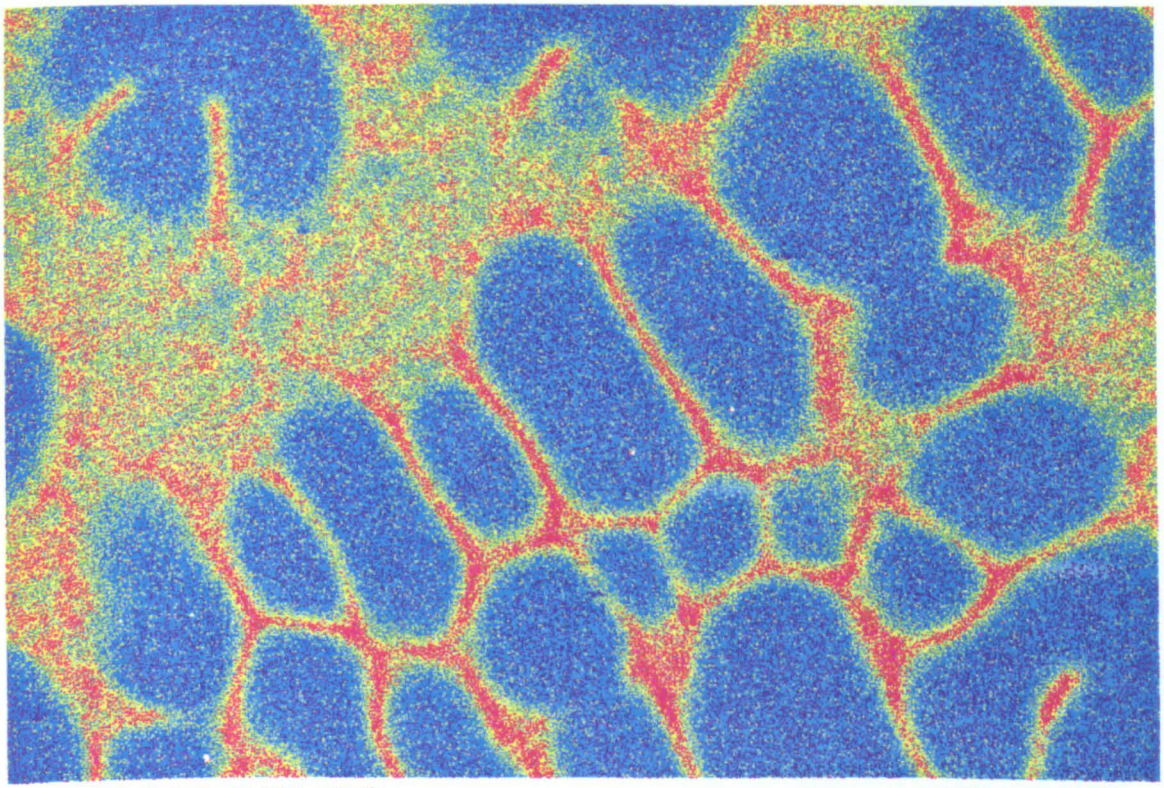

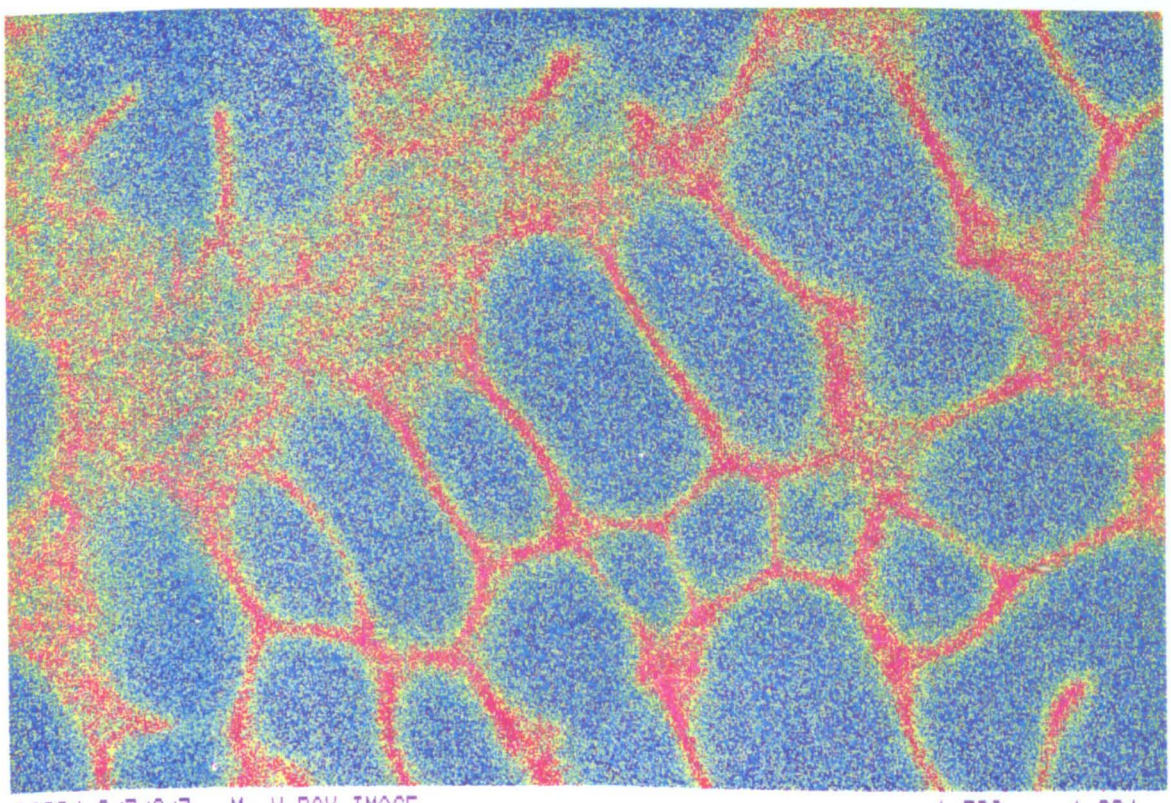

Fig. 3.30 EP.MAPS OF SAMPLE EP8 (2.18%Si, 5.53%Mn)

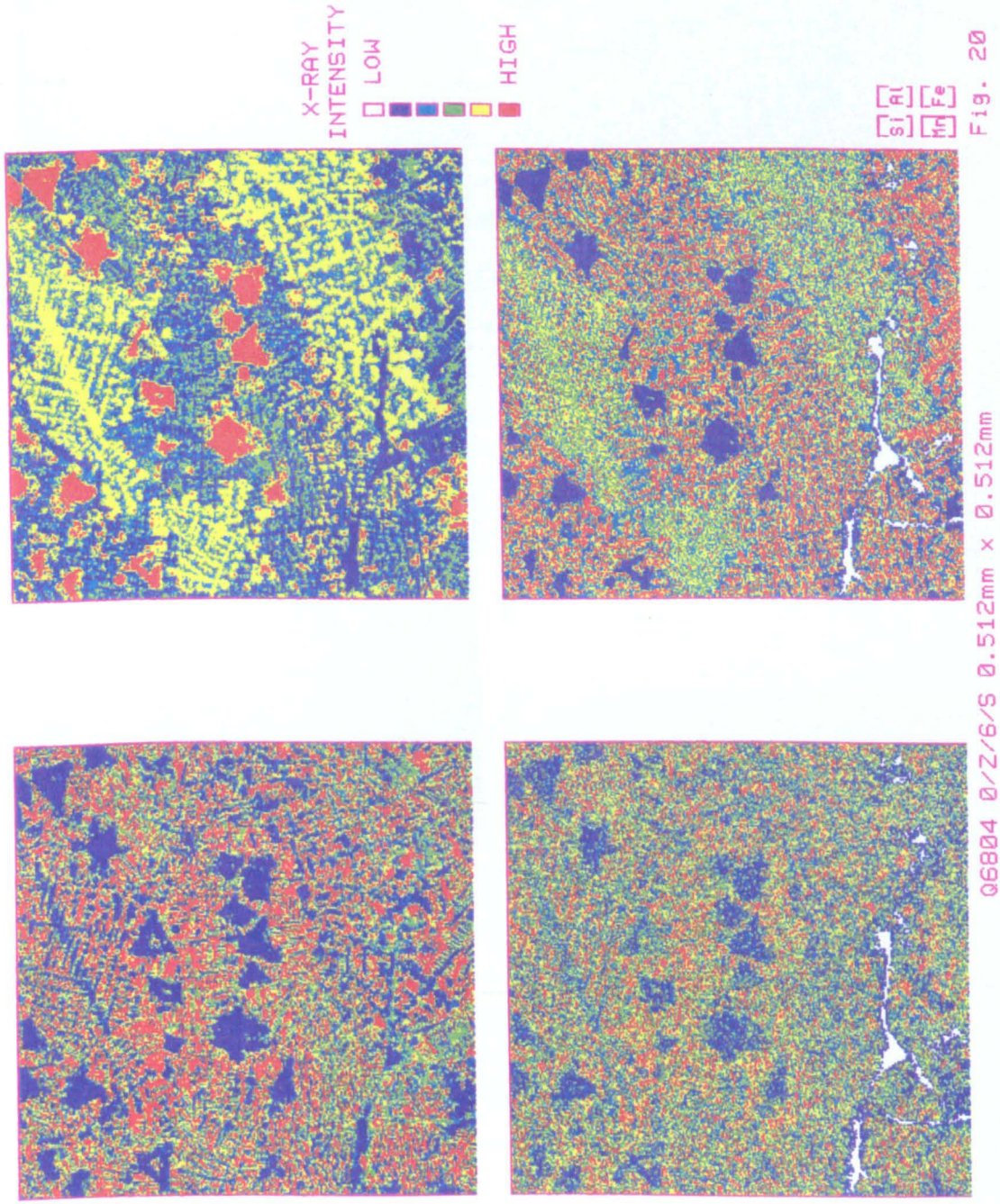

Fig. 3.31 EP.MAPS OF SOLIDIFIED OXIDE POOL WITHIN EF8

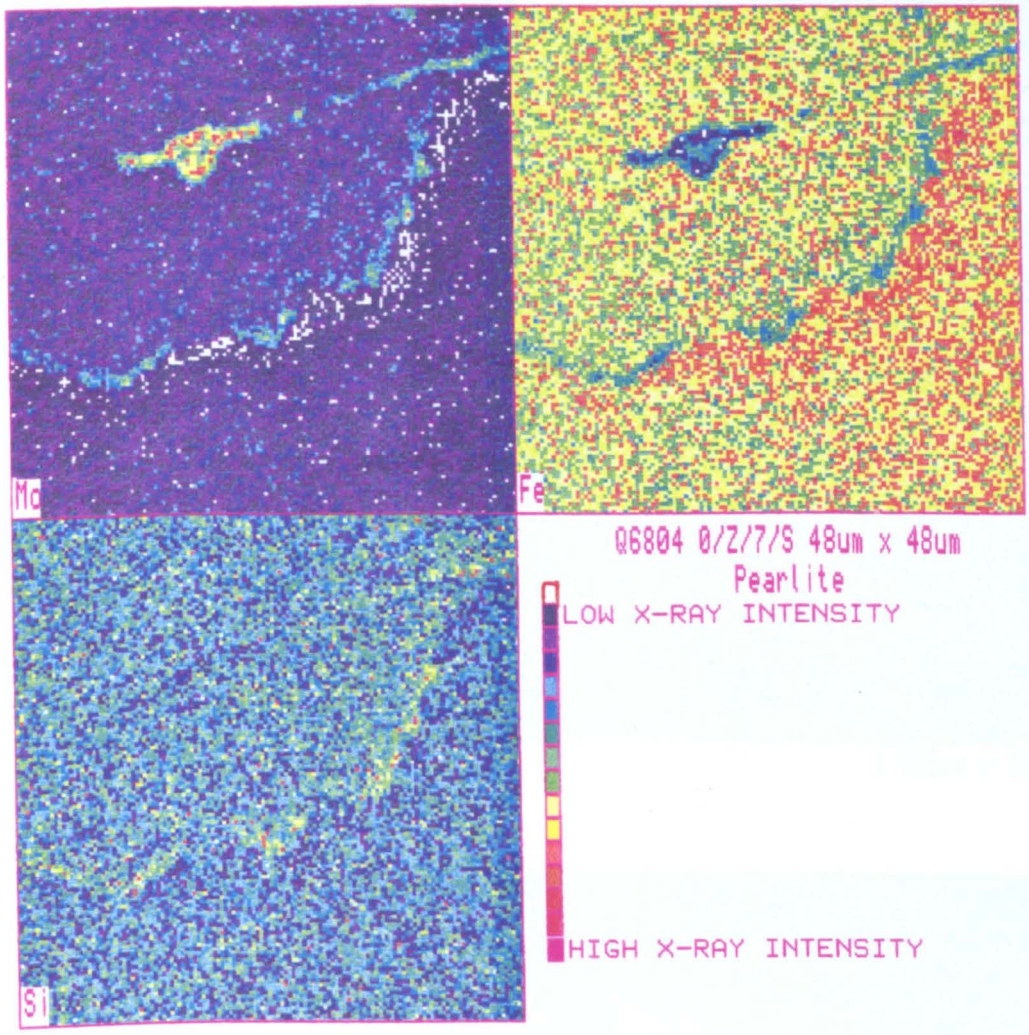

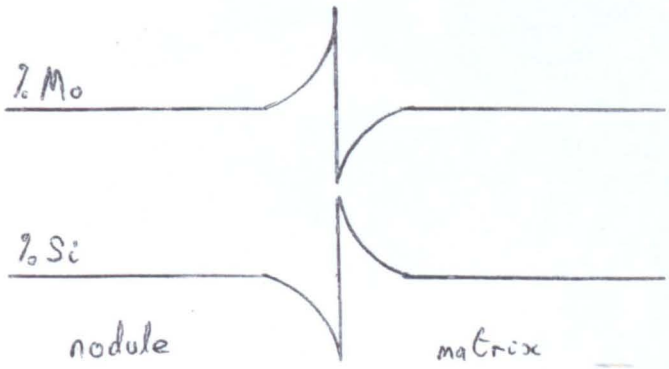

Fig. 3.32 EP.MAPS OF A PEARLITE NODULE IN EF9 AND SCHEMATIC COMPOSITION PROFILES ACROSS NODULE PERIPHERY

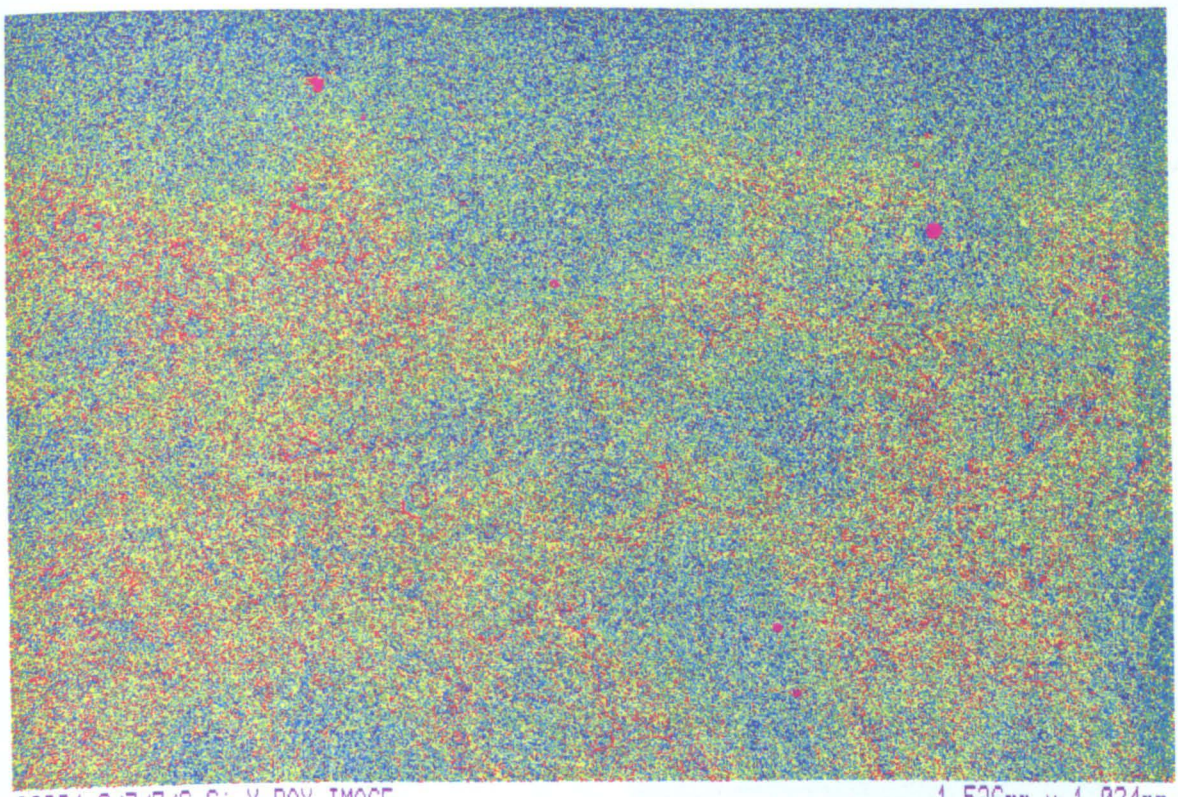

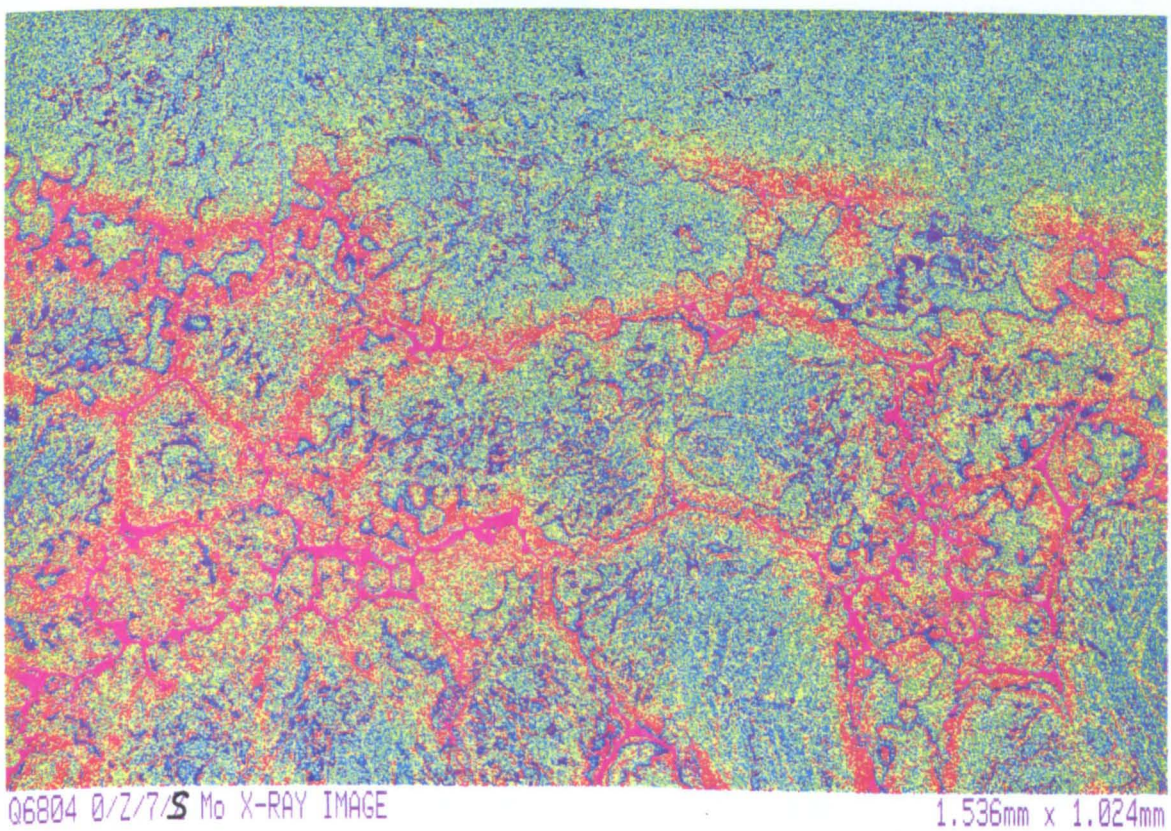

a) General

Fig. 3.33 EP.MAPS OF EF9 (0.5%C, 0.53%Si, 9.7%Mo)

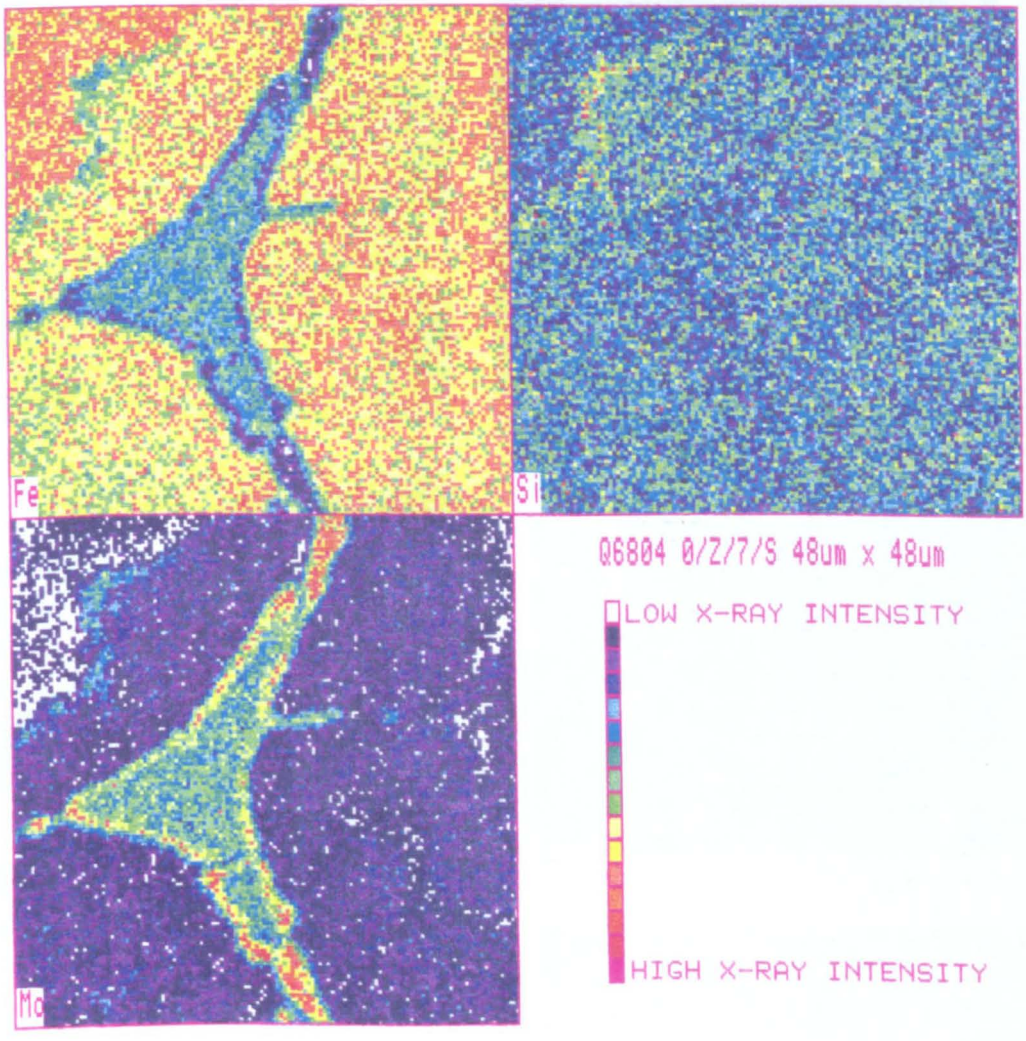

b) Detail of a Grain Boundary Carbide

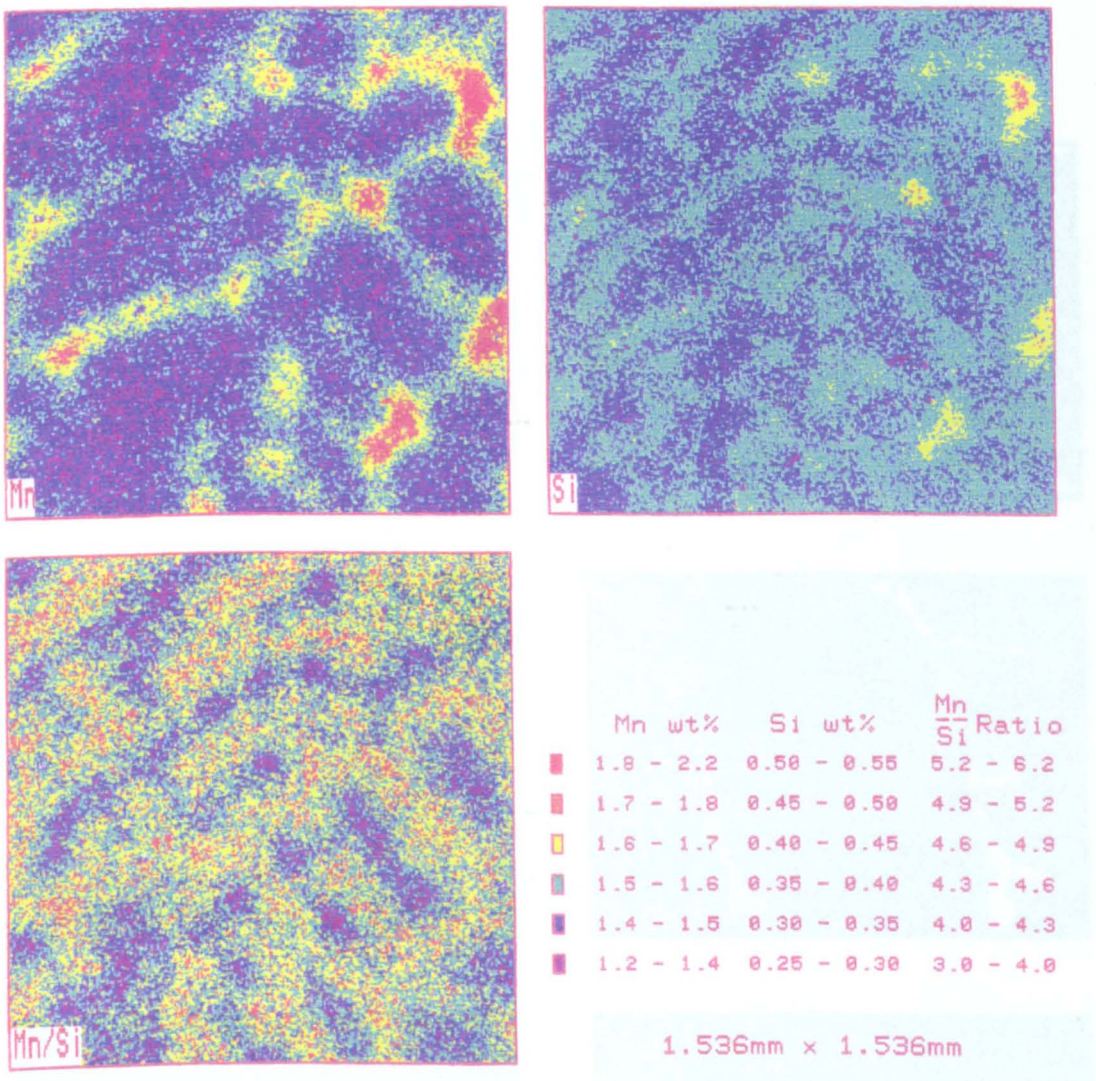

Fig. 3.34 EP.MAPS OF UDS SAMPLE EXHIBITING SECONDARY SILICON PEAKS AT DENDRITE CORES

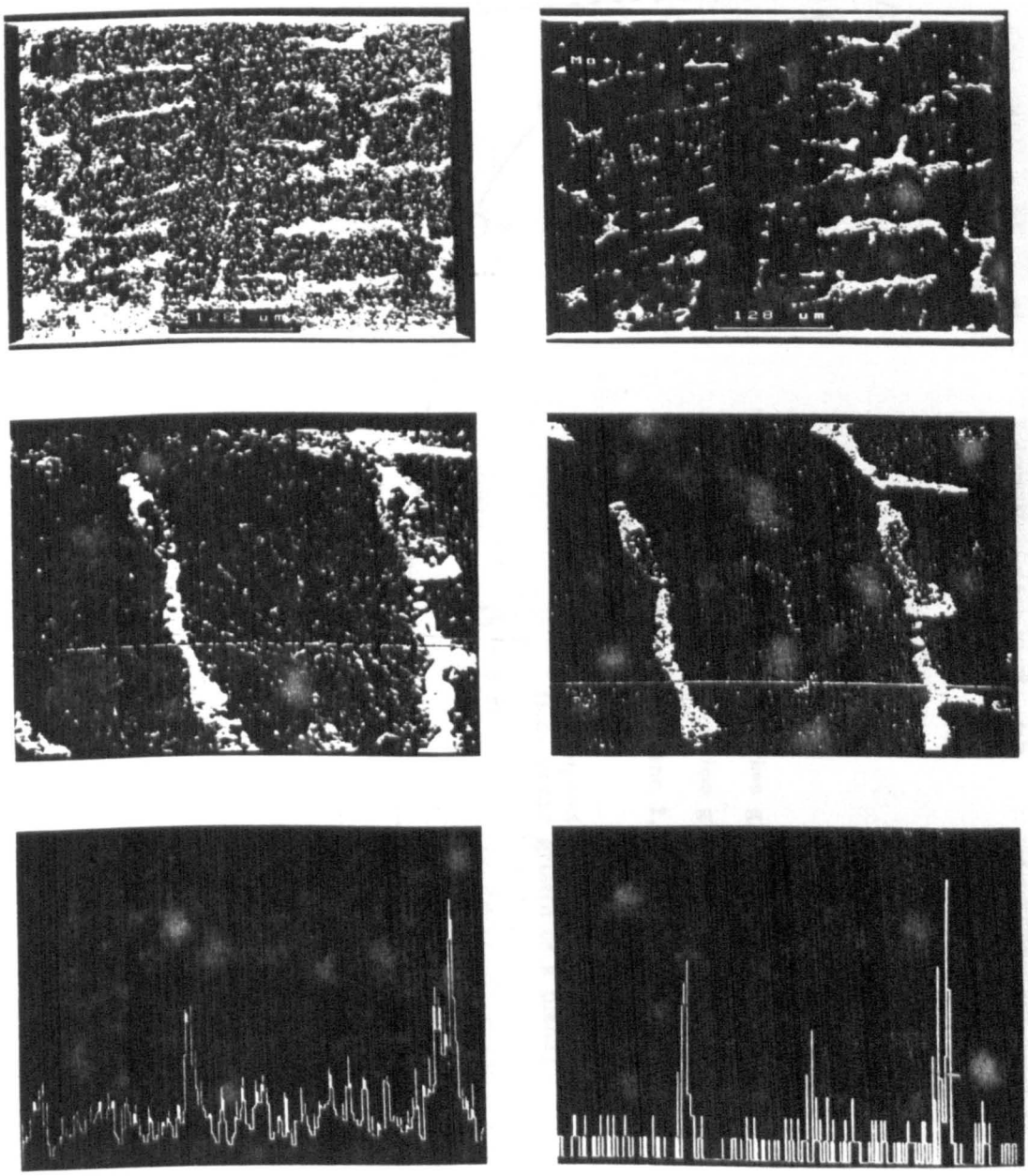

Carbon (a) Molybdenum (b)

SEGREGATION MAPS, DETAILS AND 128 um LINE PROFILES BY SIMS
SAMPLE 162 FIG. 3.35
(cf. FIG 3.27)

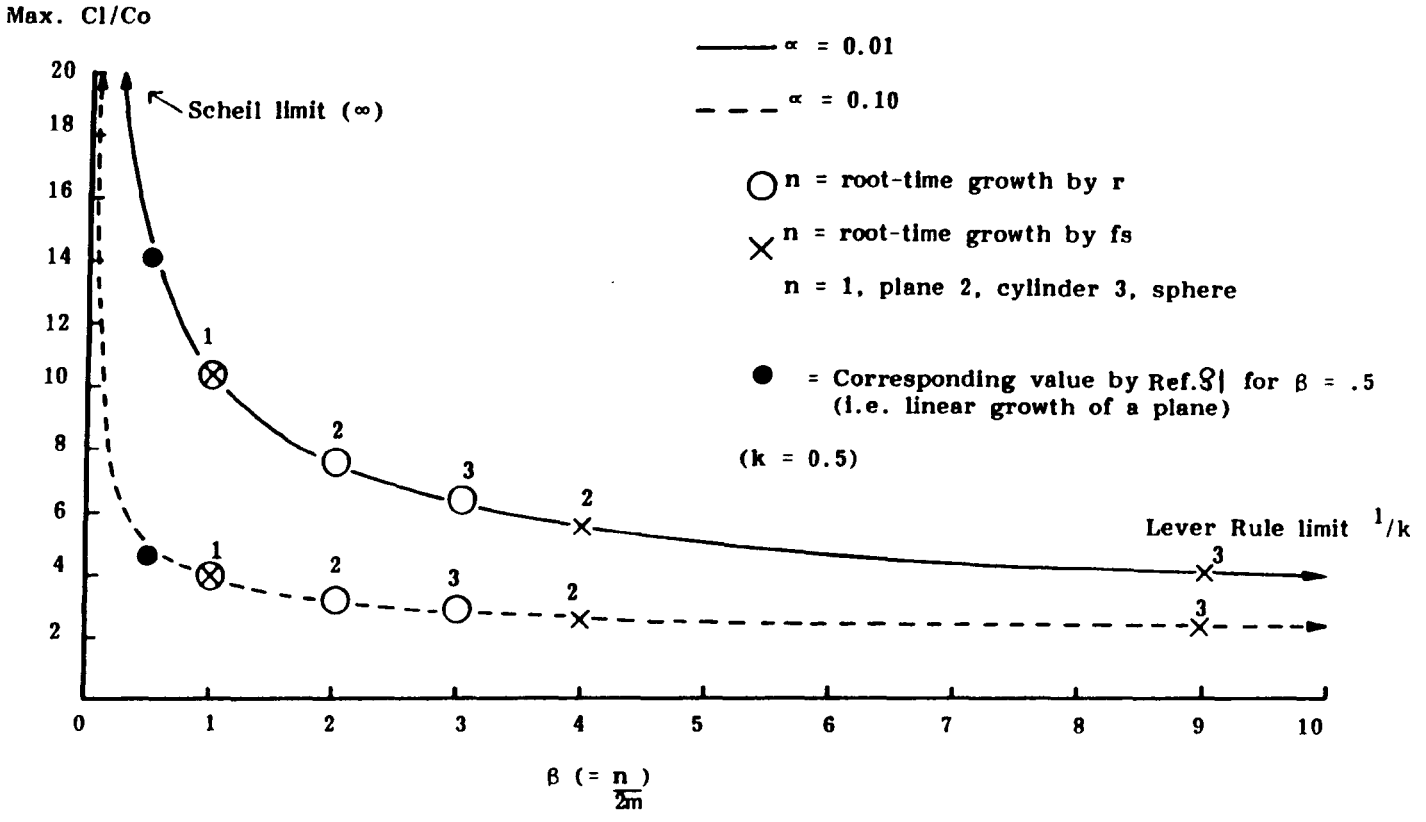

EFFECT OF β PARAMETER ON MAXIMUM SEGREGATION RATIO WITH CONVEX GROWTH FIG. 4.1

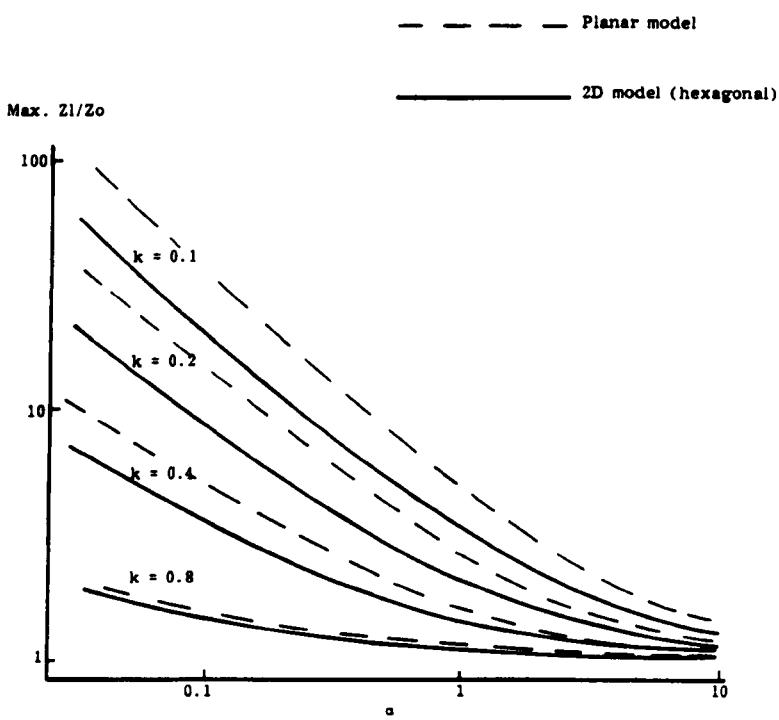

MAXIMUM MICROSEGREGATION AS A FUNCTION OF PARTITION (k) AND BACK-DIFFUSION (α) COEFFICIENTS FOR 1 AND 2D CELLS. AFTER KOBOYASHI

4.2

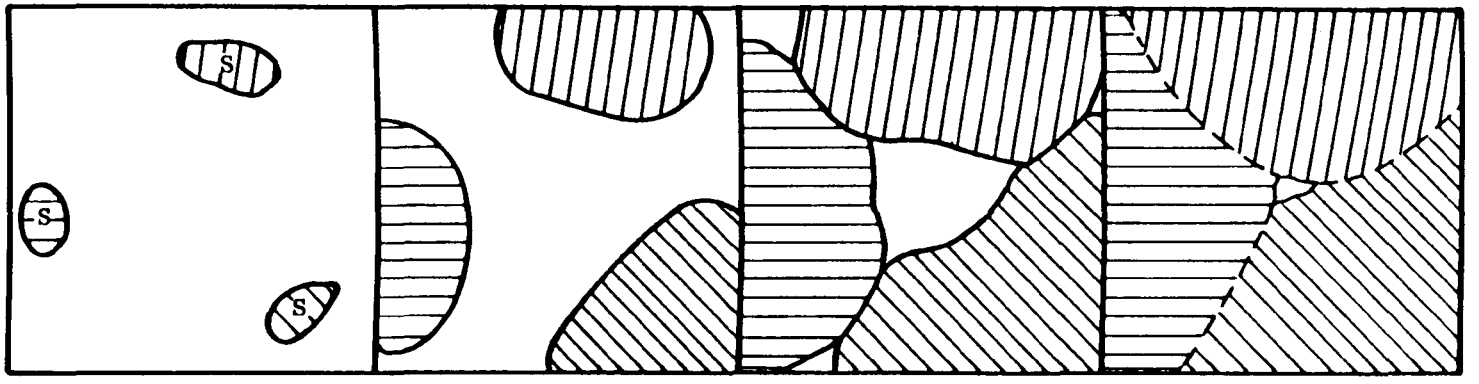

(a) Region with solid nuclei in liquid

(b) Convex growth of solid grains

(c) Abutting grains with intergranular channels and pools

(d) Concave growth of solid into residual liquid.

(e) Coring pattern (segregation contour) resulting from sequence (a) to (d), rising to central, intense peak.

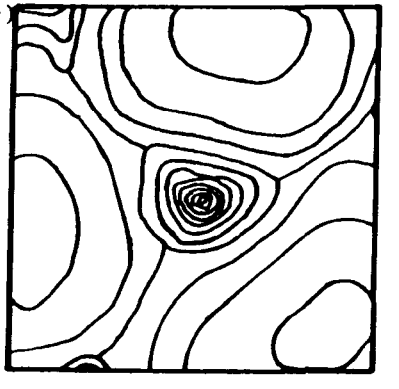

IMPINGEMENT AND SEGREGATION WITH GLOBULITIC SOLIDIFICATION

FIG. 43

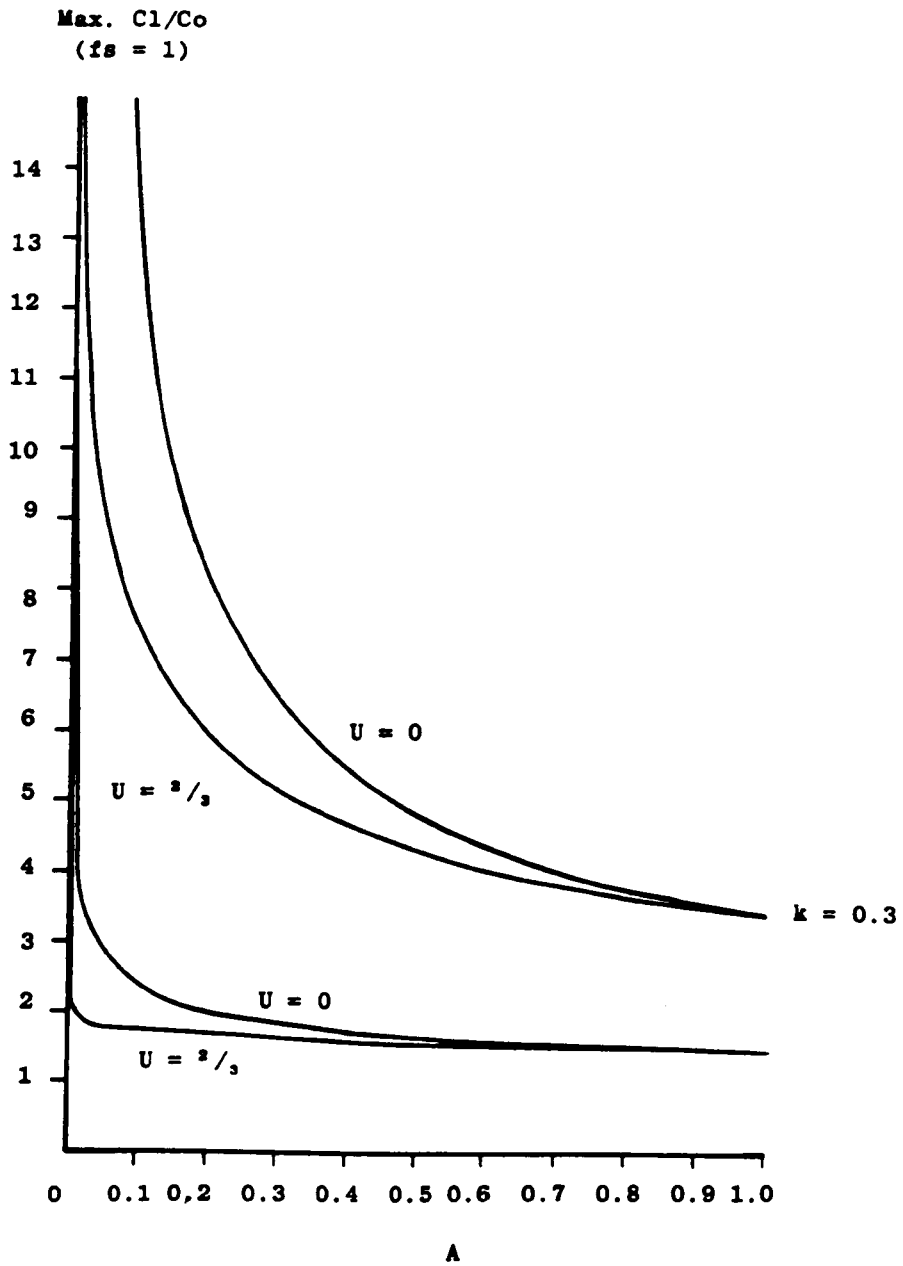

EFFECT OF BACK-DIFFUSION (A), PARTITION (k) AND ARM-COARSENING (U) COEFFICIENTS ON MAXIMUM MICROSEGREGATION

FIG. 4.4

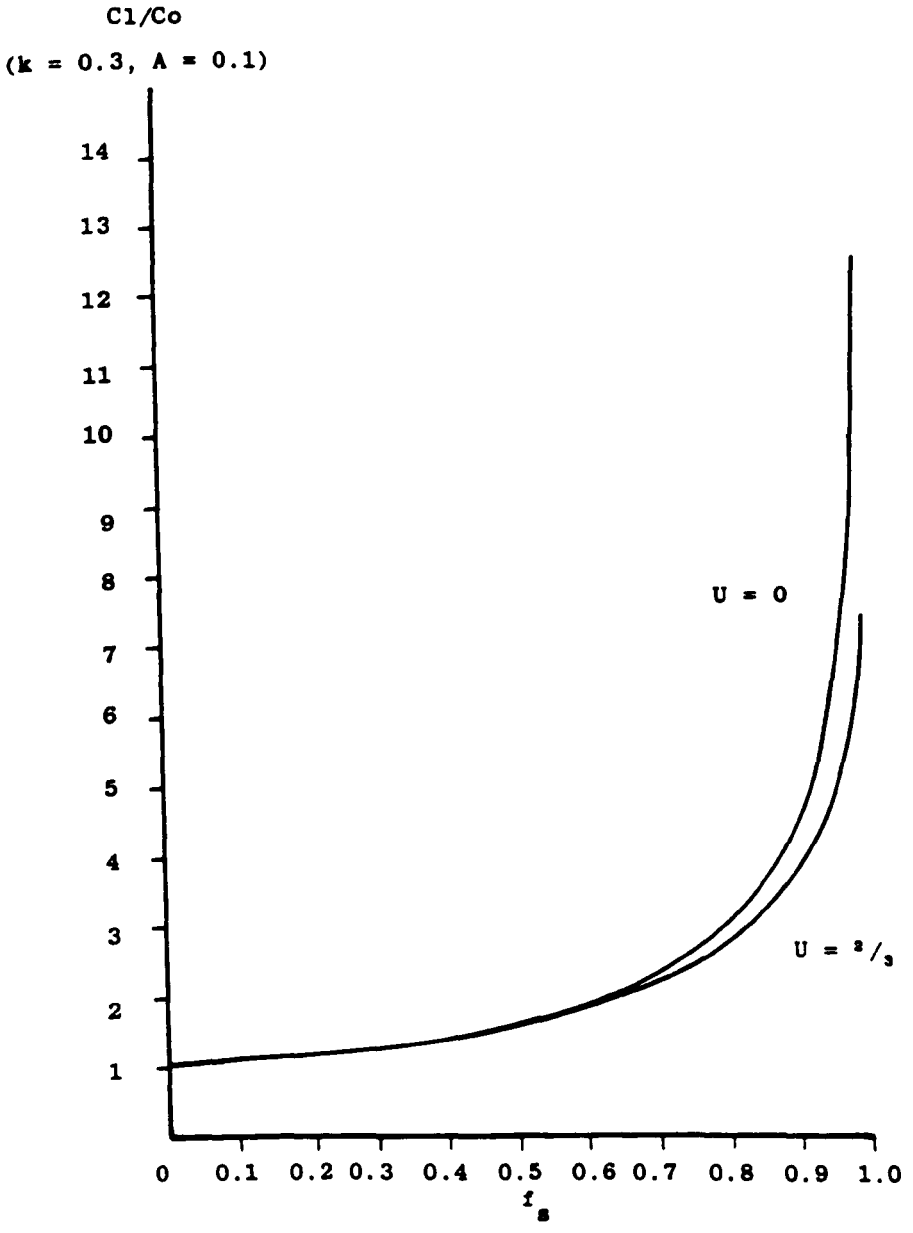

EFFECT OF DENDRITE ARM COARSENING ON THE DEVELOPMENT OF MICROSEGREGATION DURING SOLIDIFICATION

FIG. 4.5

(a) Austenite Stabiliser

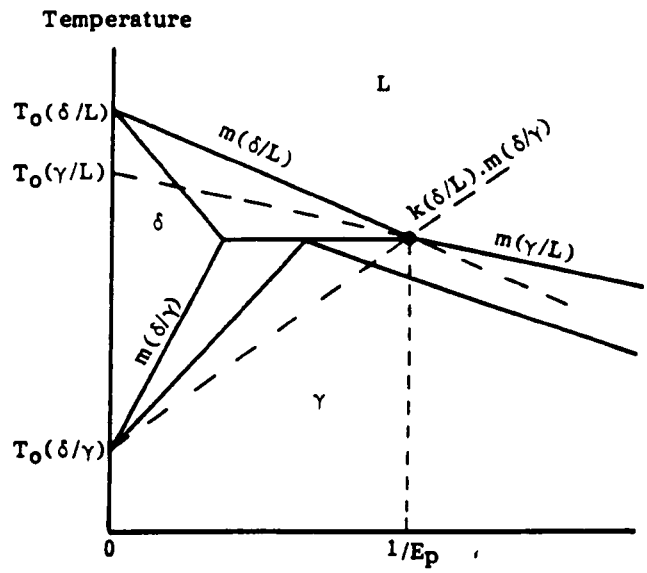

(b) Ferrite Stabiliser

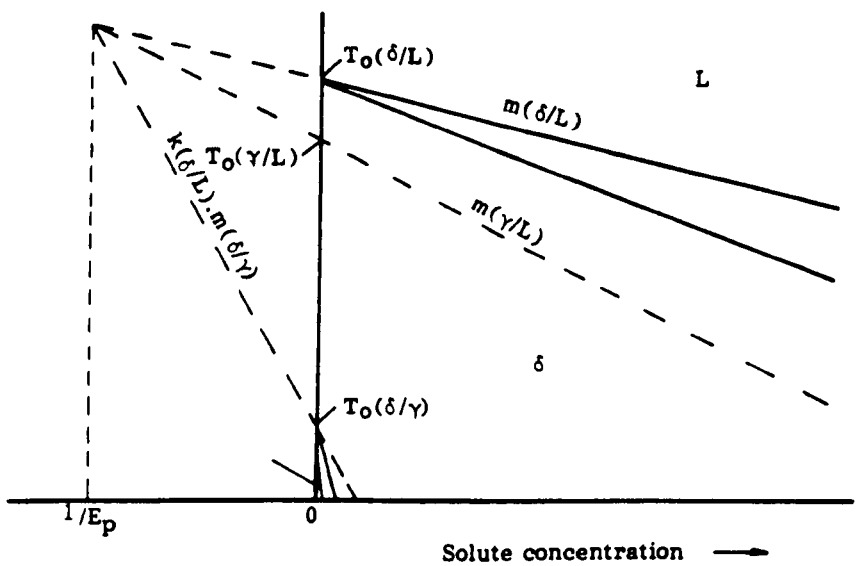

DERIVATION OF PERITECTIC EQUIVALENT COEFFICIENTS, E_p, FROM LINEAR, BINARY PHASE DIAGRAMS FIG. 4.6

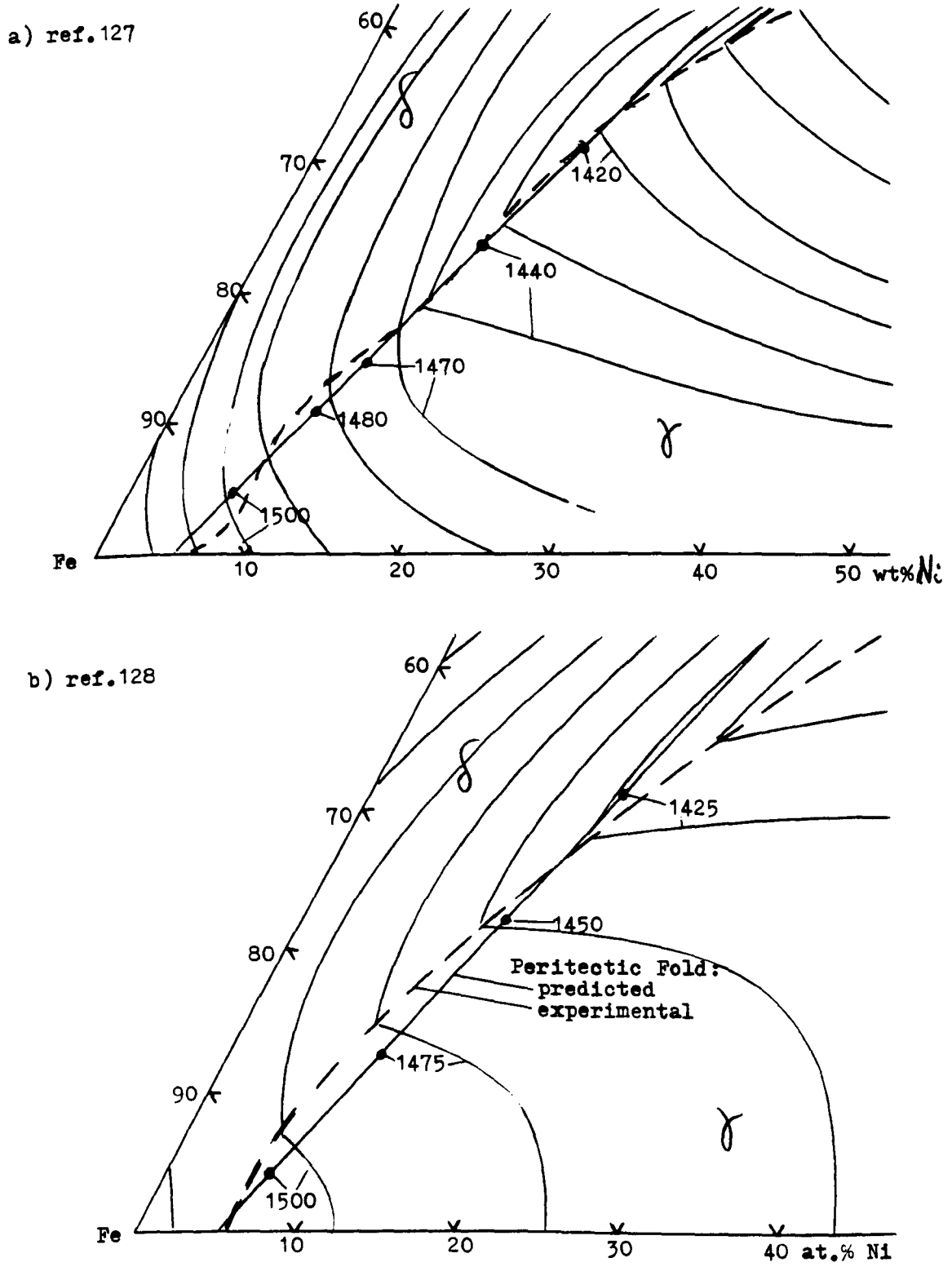

Fig.4.7 COMPARISON OF PREDICTIONS FROM THE SIMPLIFIED DATA-SET with PUBLISHED PHASE DIAGRAMS for Fe-Cr-Ni

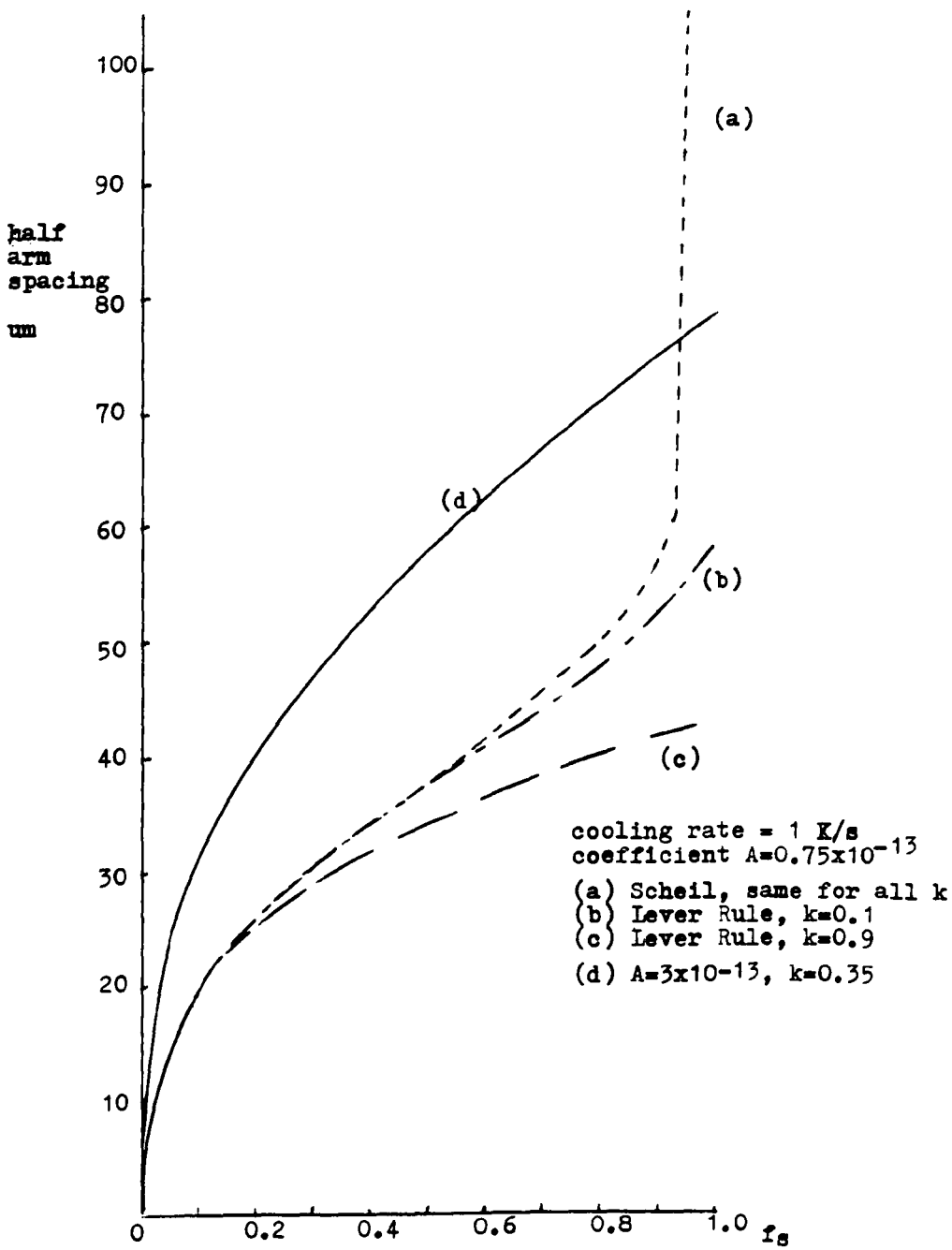

Fig. 4.8 CALCULATED VARIATION OF ARM SPACING DURTNG SOLIDIFICATION

——— Position/concentration before solidification increment

— — — — Position/concentration after solidification increment

Effective back diffusion term in time δt comprised the three labelled areas, 1 + 2 + 3:-

$$\delta C1' \cdot (K^{bcc} \cdot f^{bcc}) + \delta C1 \cdot (K^{fcc} \cdot f^{fcc}) + \delta f^{bcc} \cdot C1 \cdot (K^{fcc} - K^{bcc})$$

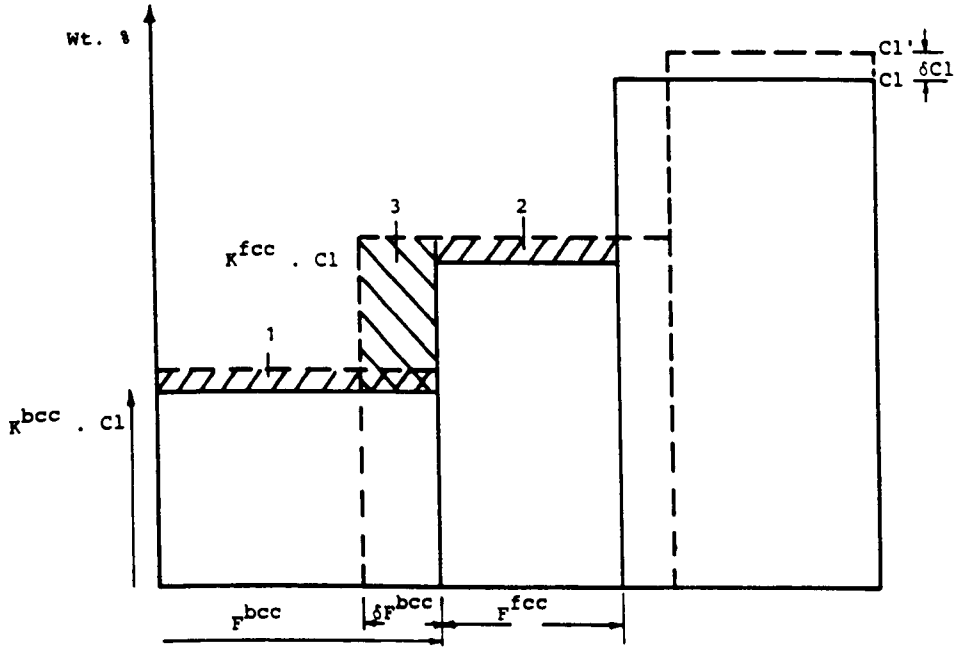

SCHEMATIC REPRESENTATION OF SOLUTE BALANCE FOR INTERSTITIAL ELEMENTS DURING THE PERITECTIC REACTION

FIG. 4·9

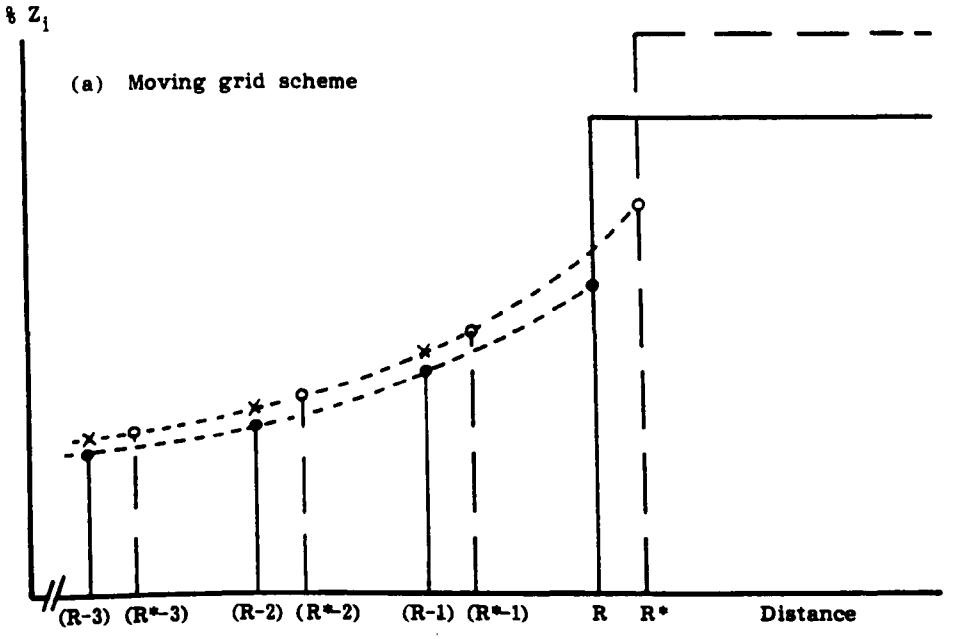

Compositions, ● , updated to, × , by explicit forward difference, from which compositions, o , and the new grid are interpolated, the grid moving with the interface.

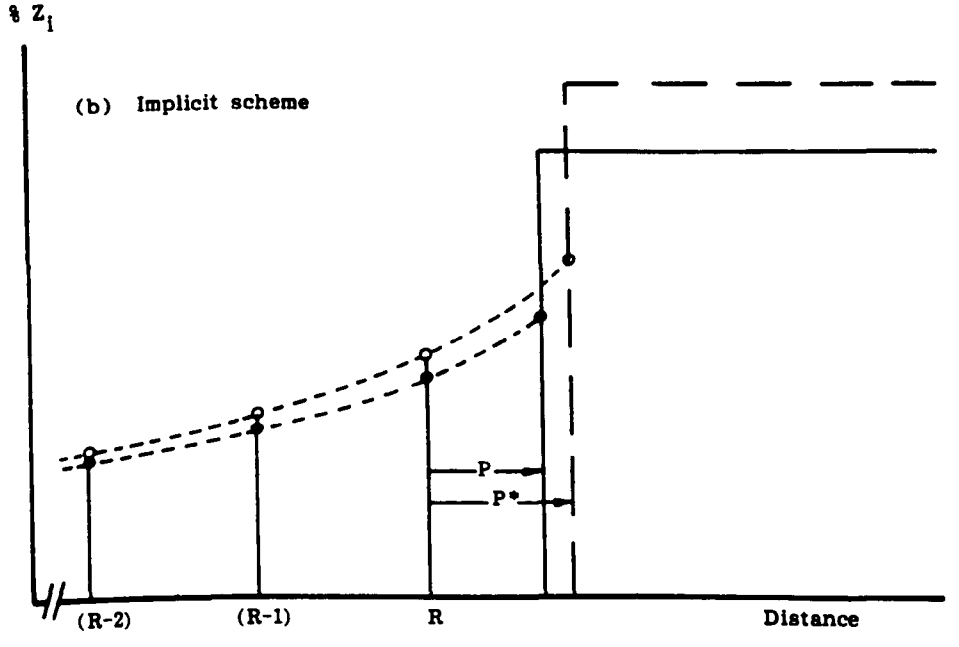

Complete new profile, o , obtained simultaneously by Crank-Nicolson scheme, with the addition of 'lopsided' terms for the changing part node, P, to the interface.

SCHEMATIC DESCRIPTION OF ALTERNATIVE FD ROUTINES FIG. 5.1

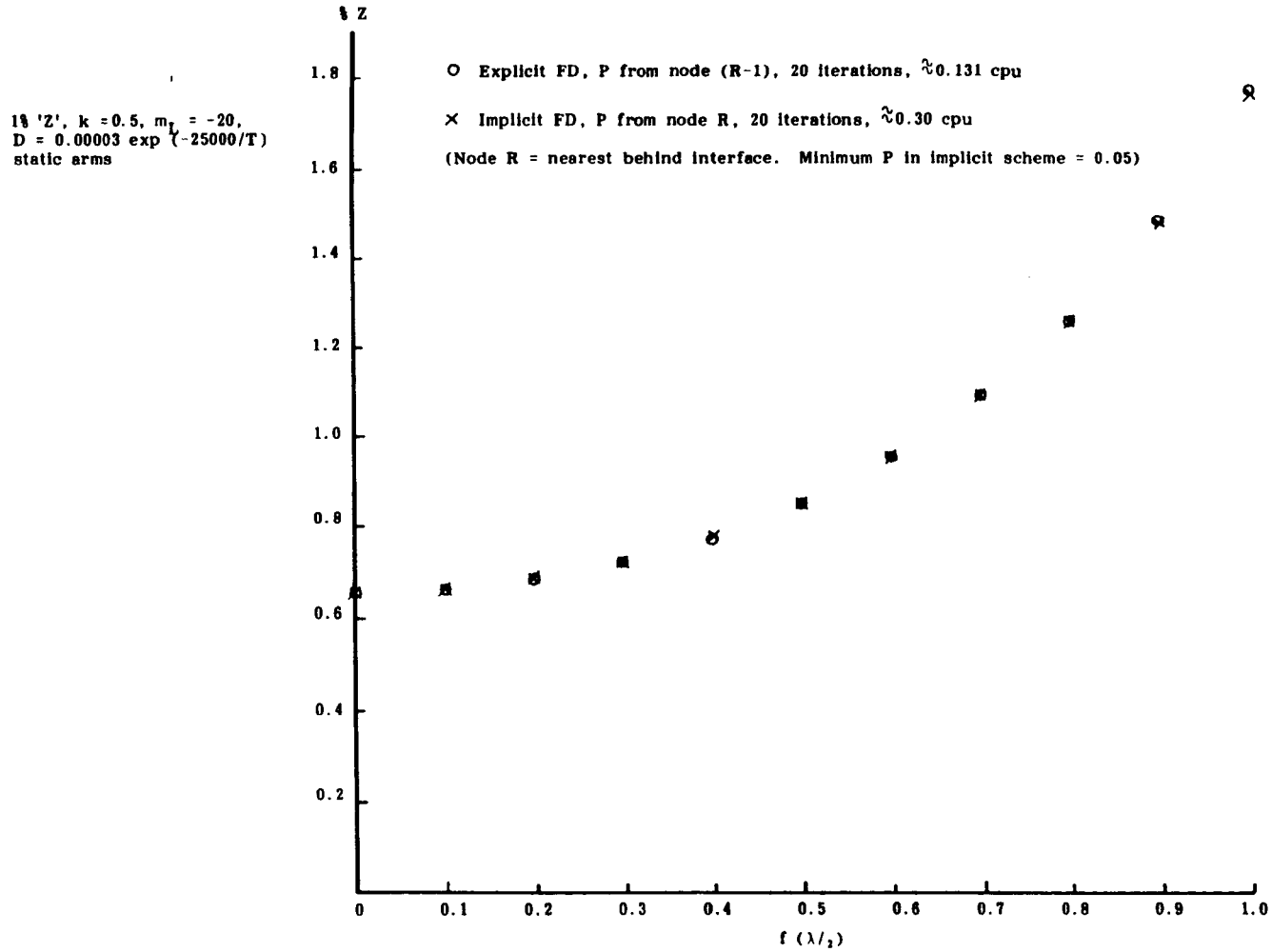

COMPARISON OF MICROSEGREGATION PROFILES AT SOLIDUS CALCULATED BY EXPLICIT AND IMPLICIT SCHEMES

FIG. 5.2

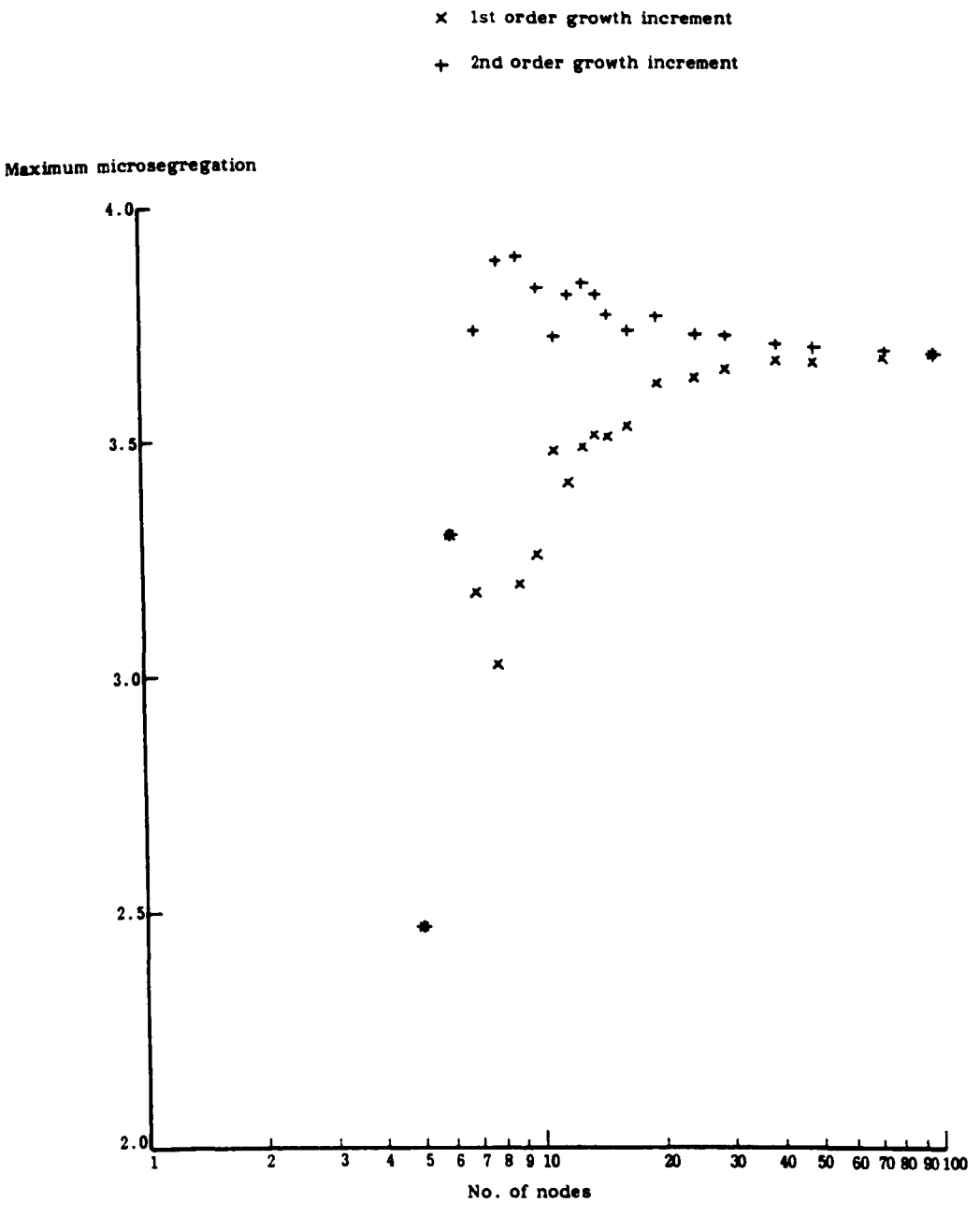

TEST CASE COMPARISON OF COMPUTED, MAXIMUM MICROSEGREGATION FOR DIFFERENT NUMBERS OF NODES, WITH AND WITHOUT A SECOND ORDER GROWTH INCREMENT

FIG. 53

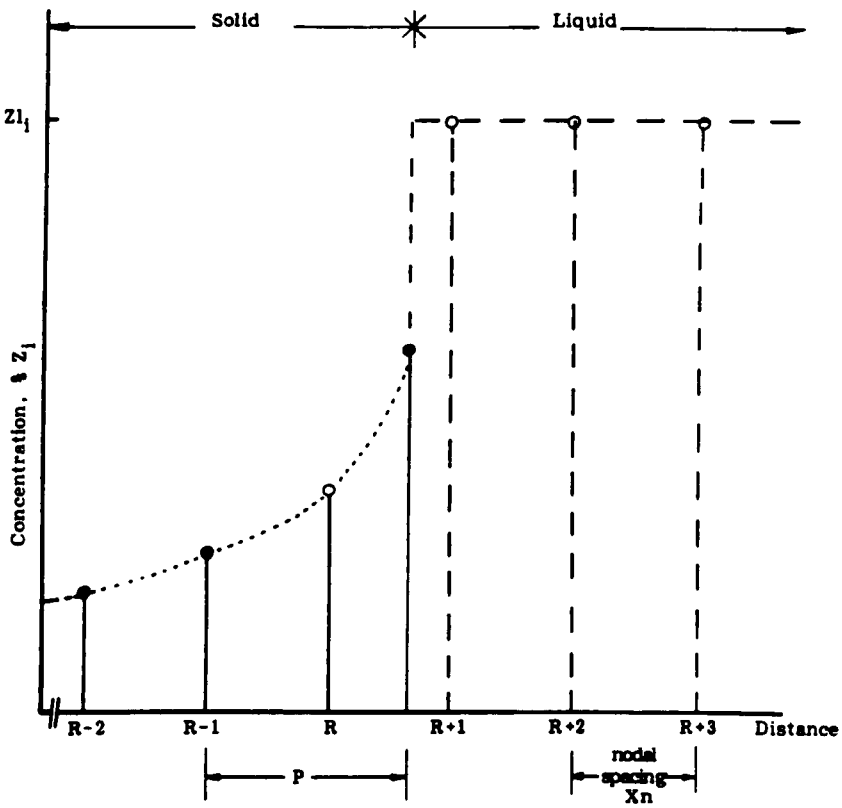

Composition gradient at interface:-

$$\frac{dZ}{dx} = \frac{1}{Xn}\left(k Z_l \frac{(1+2P)}{P(1+P)} - Z_{(R-1)} \frac{(1+P)}{P} + Z_{(R-2)} \frac{P}{(1+P)}\right)$$

Second derivative for calculation of diffusion near the interface:-

$$\frac{d^2Z}{dx^2} = \frac{2}{Xn^2}\left(\frac{k Z_l}{P(1+P)} - \frac{Z_{(R-1)}}{P} + \frac{Z_{(R-2)}}{(1+P)}\right)$$

SCHEMATIC DESCRIPTION OF SECOND ORDER TREATMENT FOR THE SOLID/LIQUID INTERFACE BETWEEN NODES FIG. 5.4

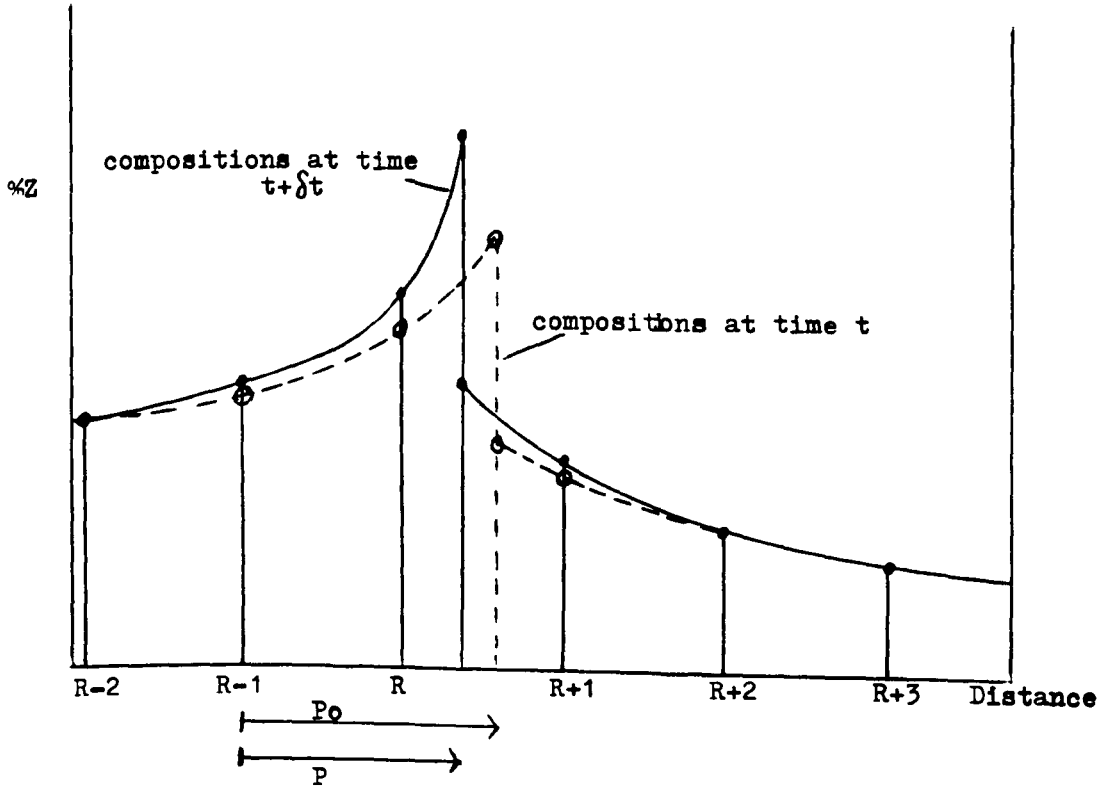

Fig. 5.5 SCHEMATIC DESCRIPTION OF SOLID/SOLID PHASE INTERFACE TREATMENT

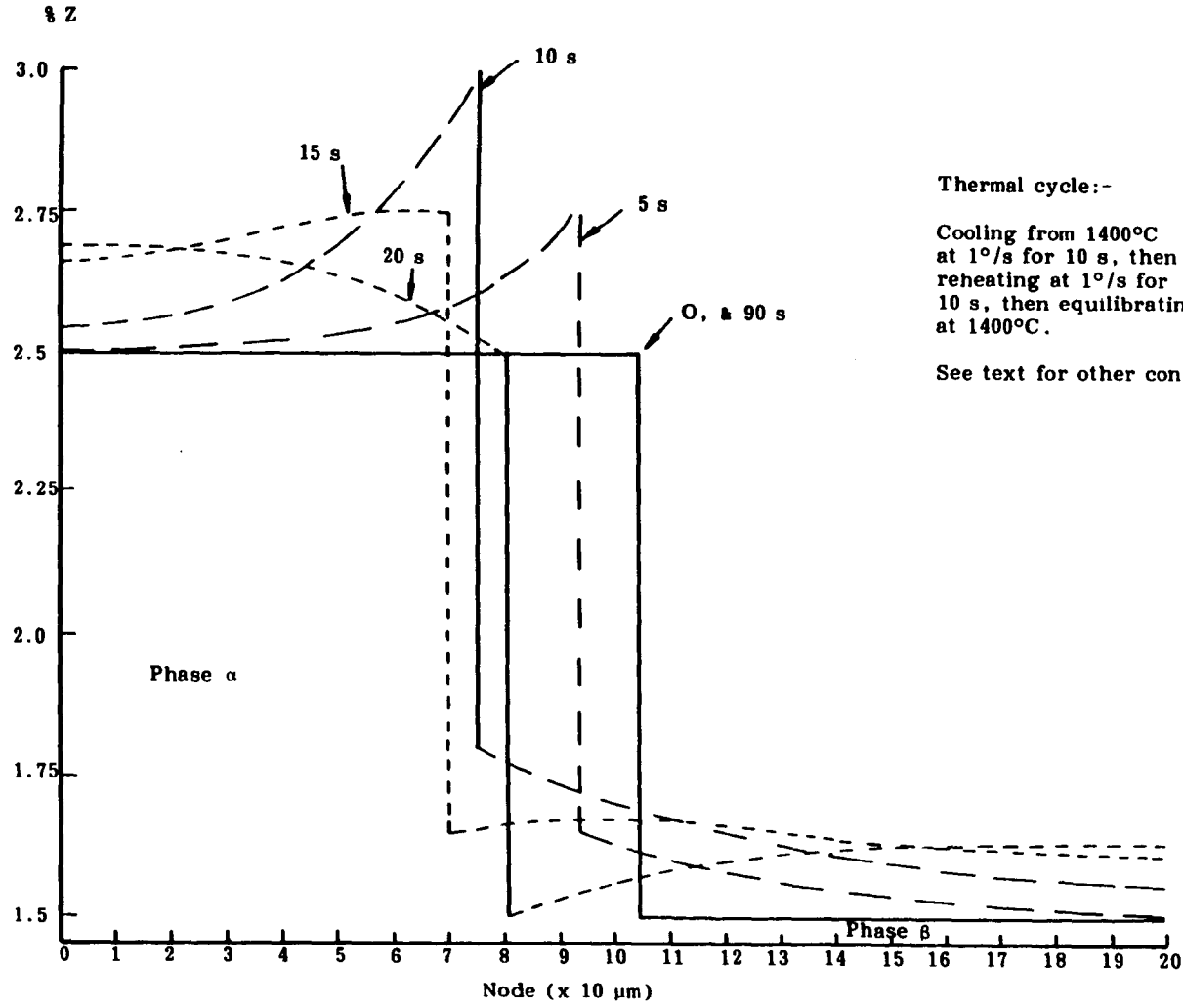

Thermal cycle:-

Cooling from 1400°C at 1°/s for 10 s, then reheating at 1°/s for 10 s, then equilibrating at 1400°C.

See text for other conditions

EXAMPLE PLOTS OF COMPUTED COMPOSITION PROFILES FOR A TEST CASE UNDER AN IMPOSED THERMAL CYCLE

FIG. 5·6

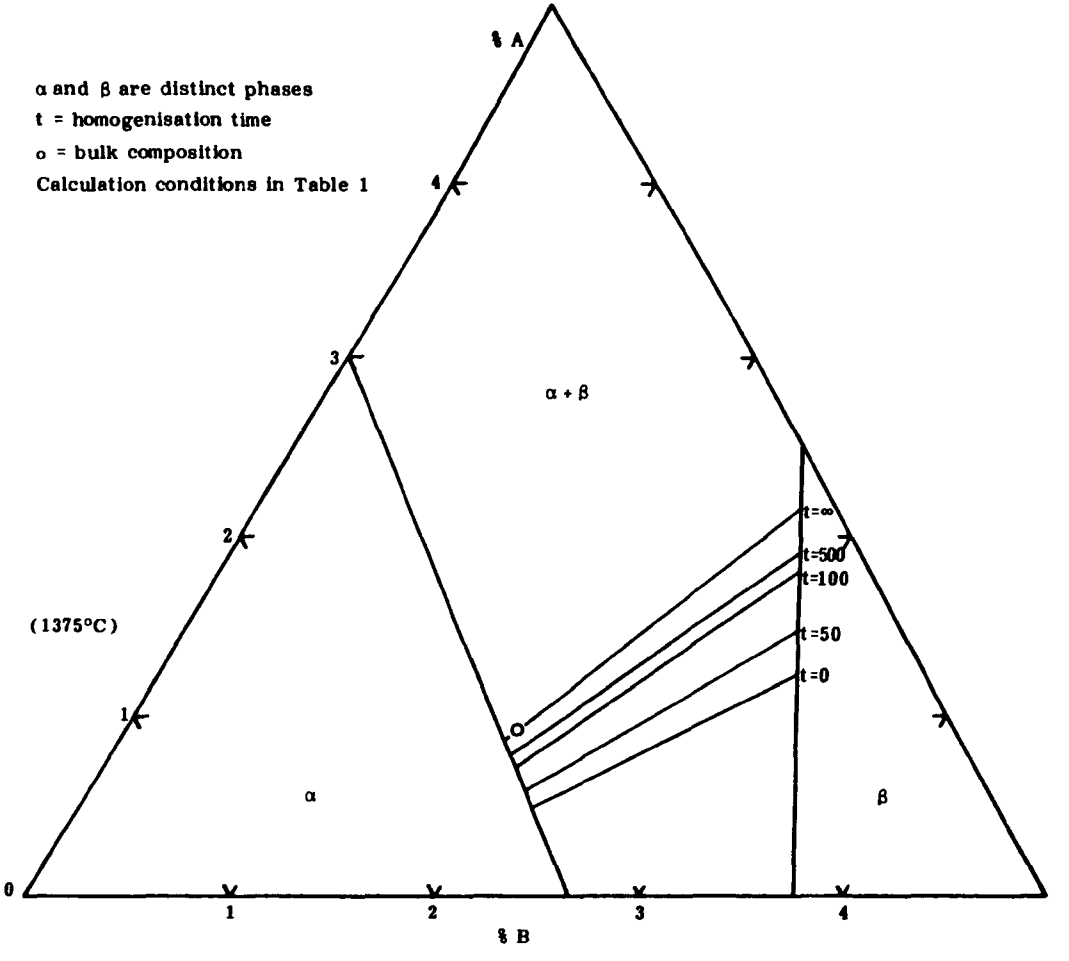

SOLVENT-RICH CORNER OF A HYPOTHETICAL TERNARY PHASE DIAGRAM DEMONSTRATING CALCULATED VARIATION OF TIE-LINES ACROSS THE PHASE BOUNDARY DURING ISOTHERMAL HOMOGENISATION

FIG. 5·7

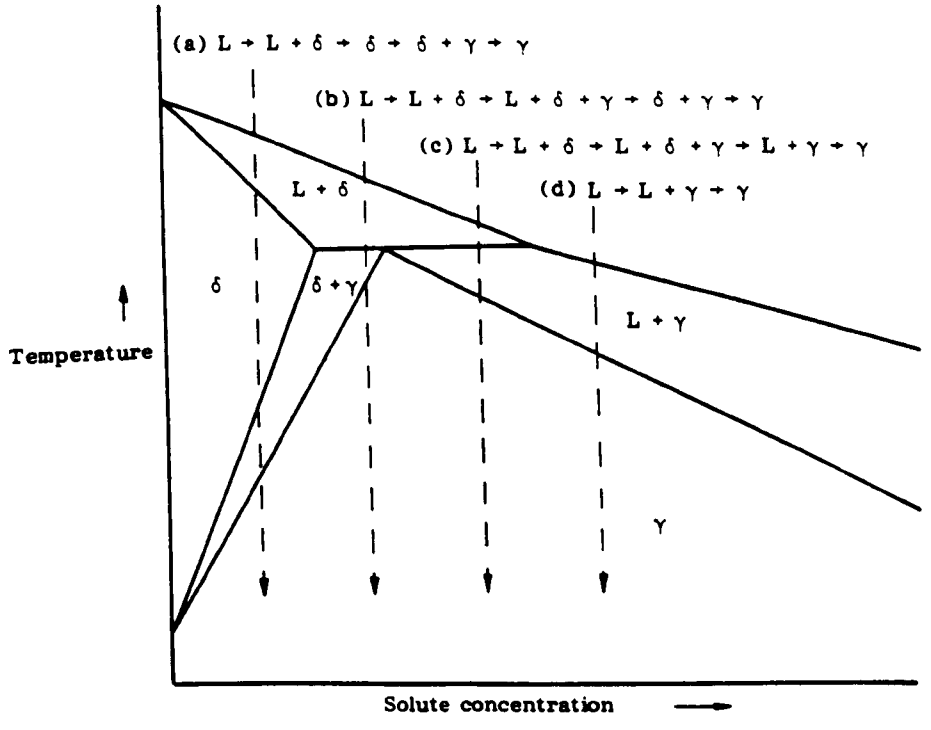

ALTERNATIVE PHASE SEQUENCES ADDRESSED BY THE COMPUTER MODEL (SCHEMATIC)

FIG. 5.8

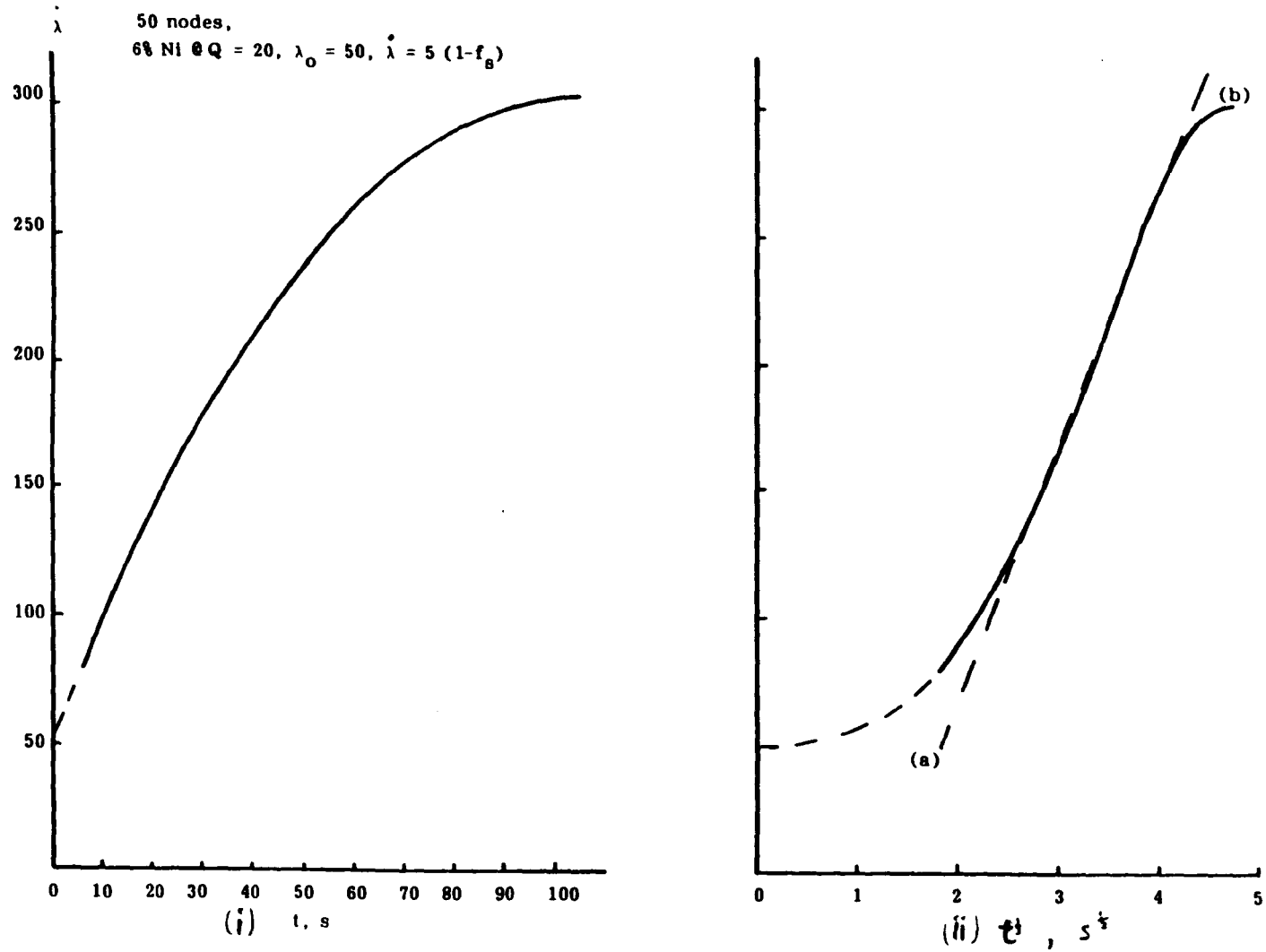

EXAMPLE OF COMPUTED ARM COARSENING BEHAVIOUR FIG. 5.9

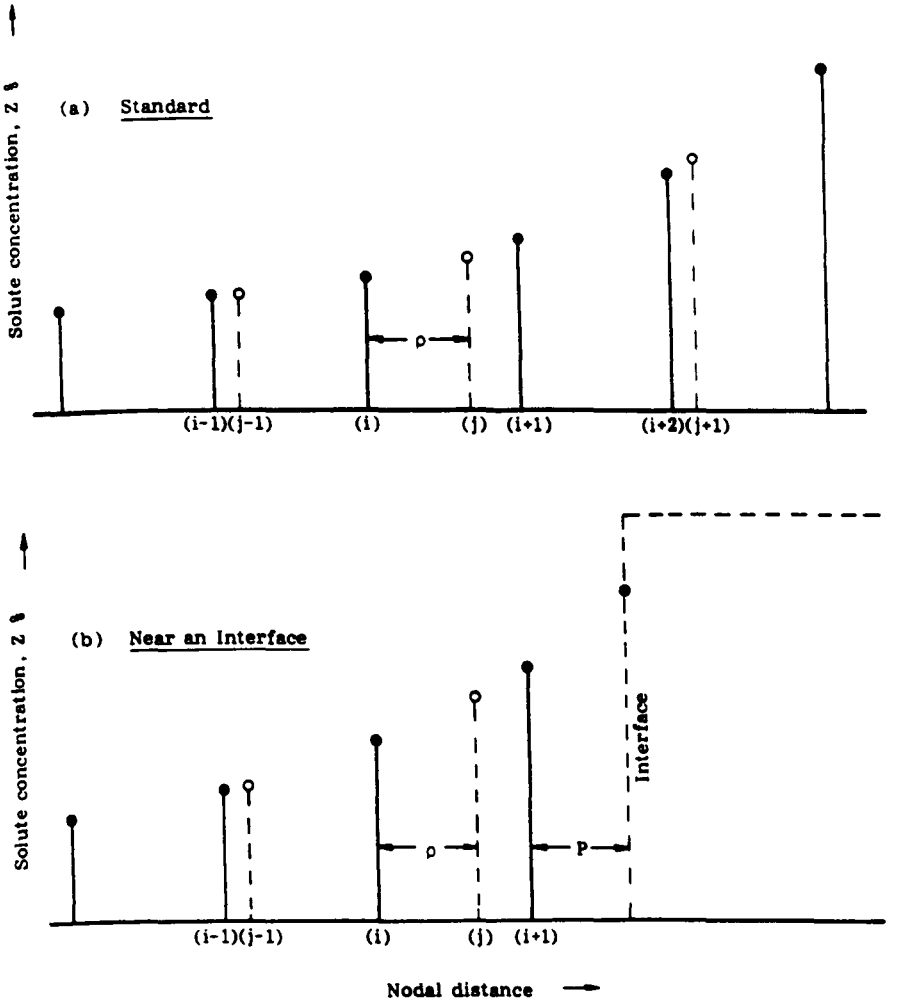

RE-MESHING FOR THE jTH NODE OF THE NEW GRID FIG 5.10

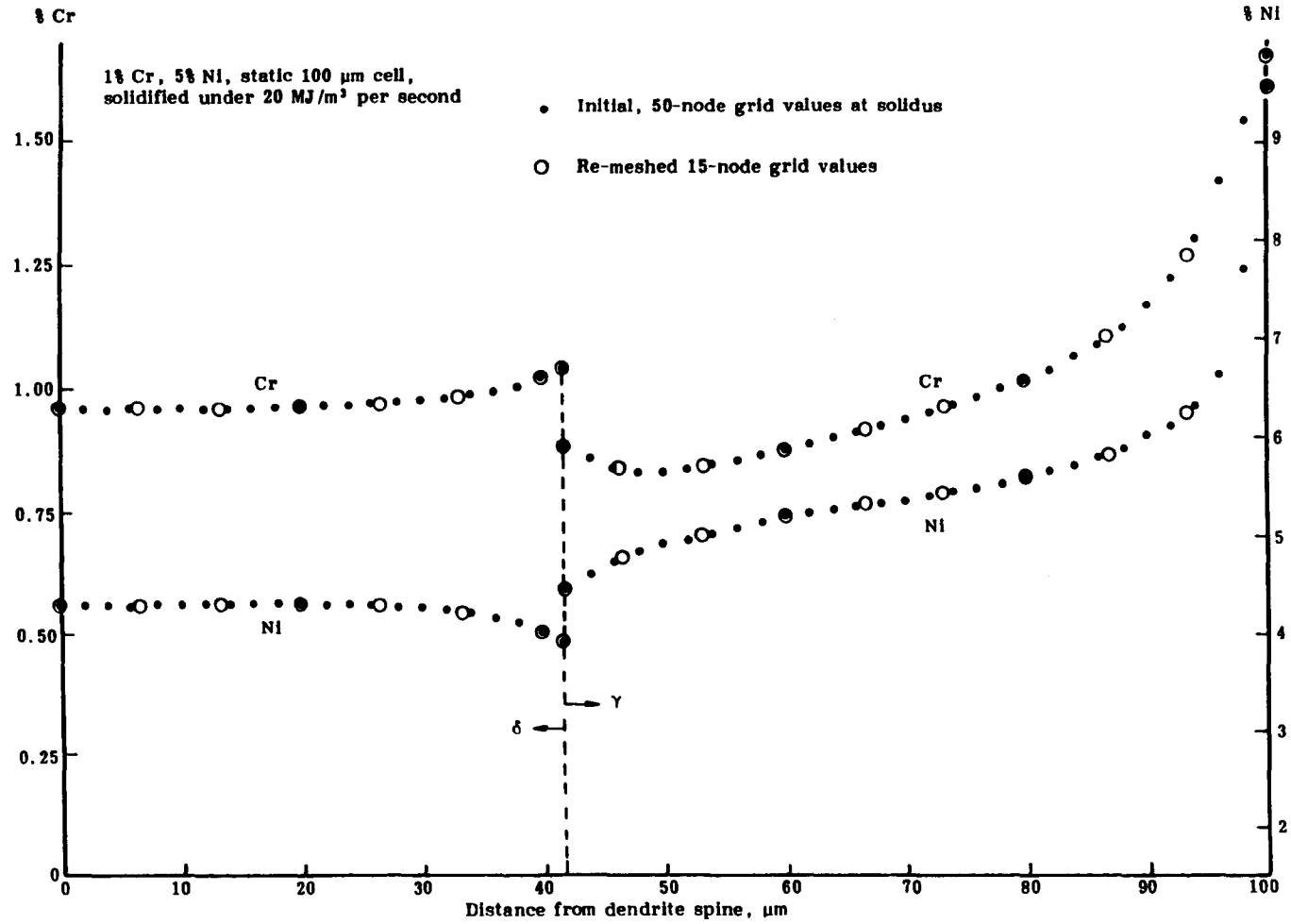

EXAMPLE RESULT OF RE-MESHING PROCEDURE

FIG. 5-11

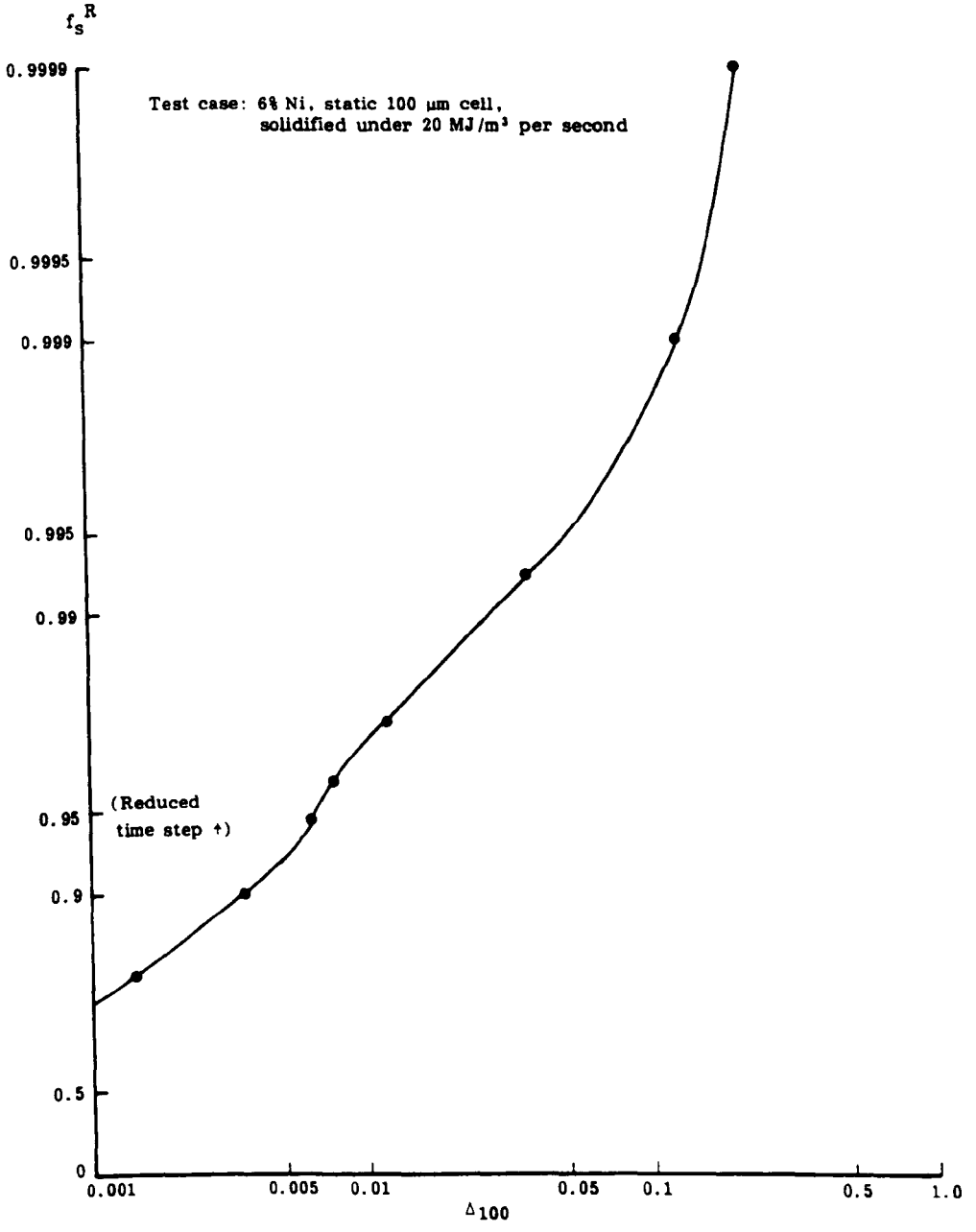

f_s^R = fraction solid when cell is re-meshed from 10 to 100 nodes
Δ_{100} = fractional error in final liquid composition from that calculated with a 100-node cell throughout

EXAMPLE PLOT OF COMPUTED PRECISION v FRACTION SOLID FOR MESH REFINEMENT FIG. 5·12

Fig. 5.13 ILLUSTRATIVE EXAMPLES OF THE EFFECT OF GEOMETRY ON COMPUTED MICROSEGREGATION PROFILE

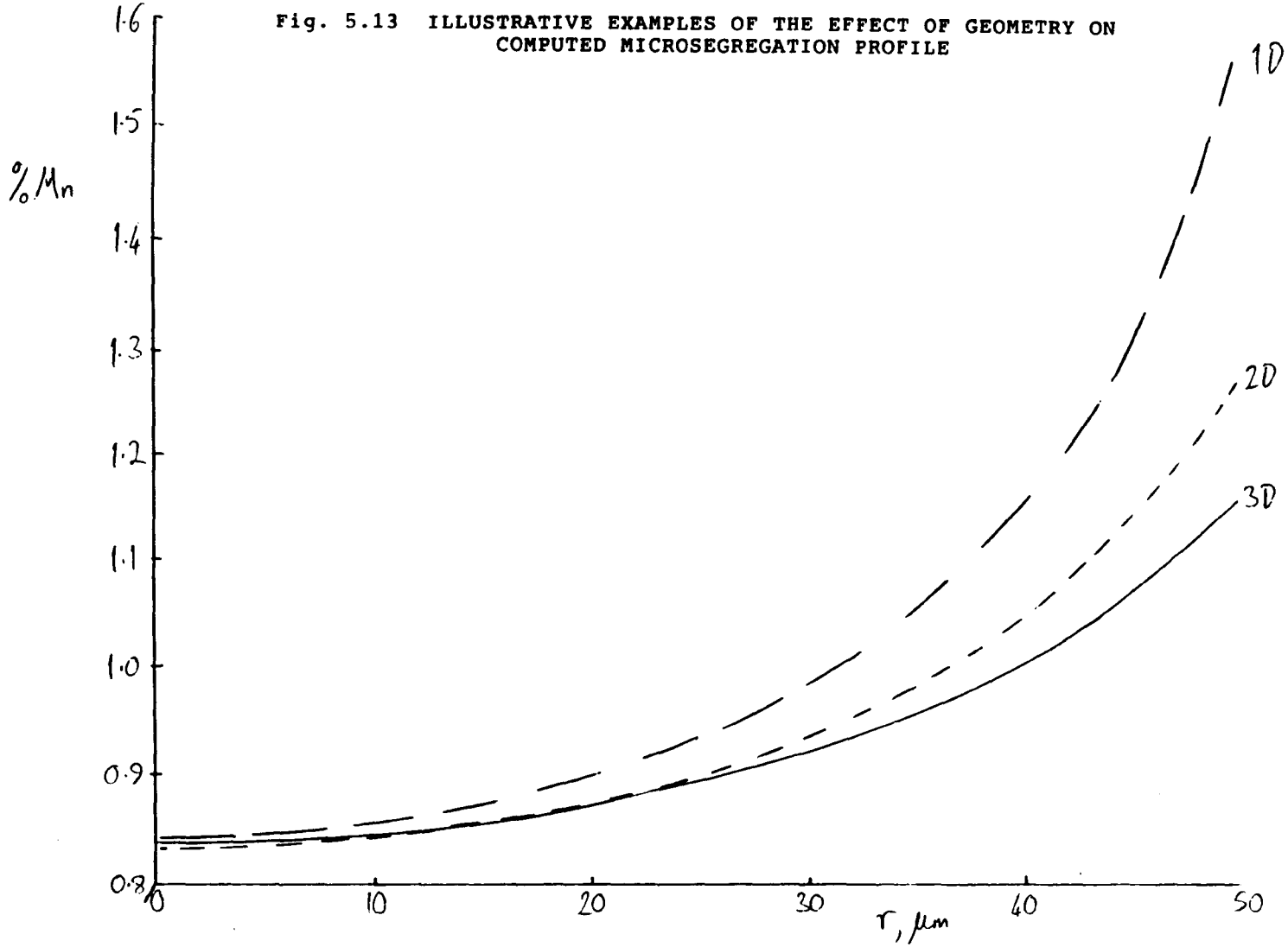

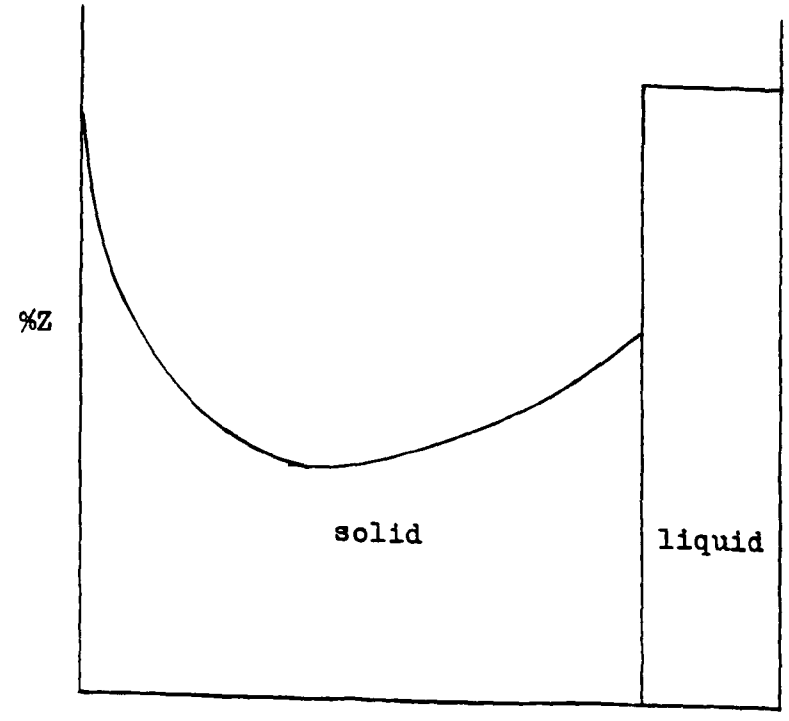

a) Where Z is a ferrite stabiliser

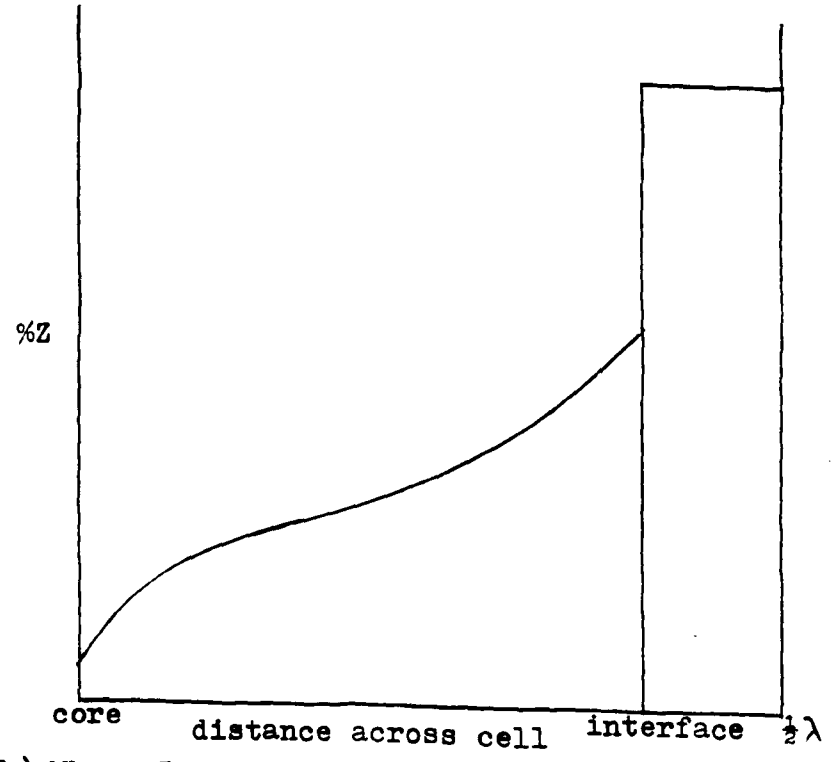

b) Where Z is an austenite stabiliser

Fig.5.14 SCHEMATIC SOLUTE PROFILES UPON THE DISAPPEARANCE OF FERRITE

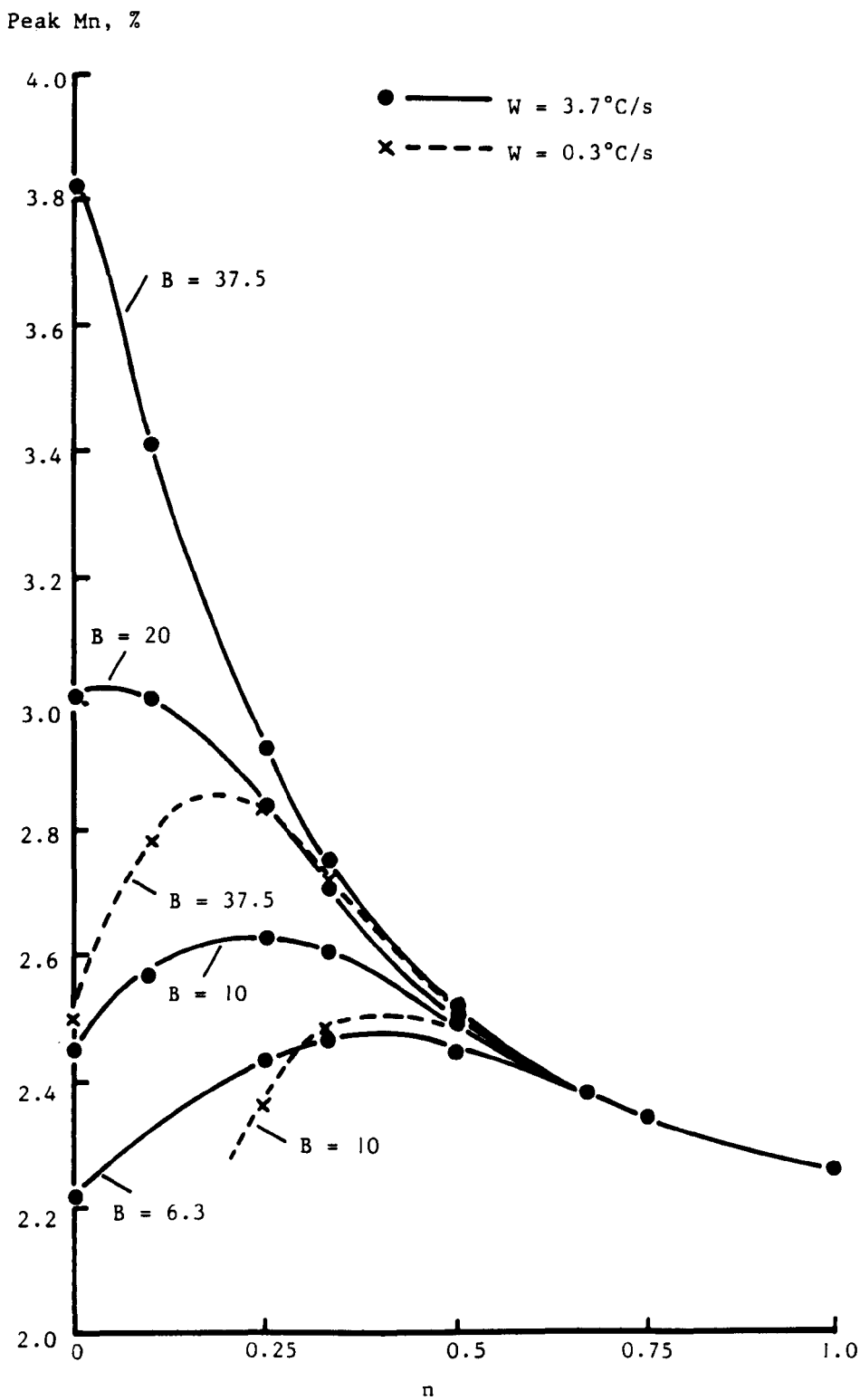

SENSITIVITY OF PEAK Mn (AT SOLIDUS) TO n, B AND W FOR $\lambda = Bt^n$

FIG. 5.15

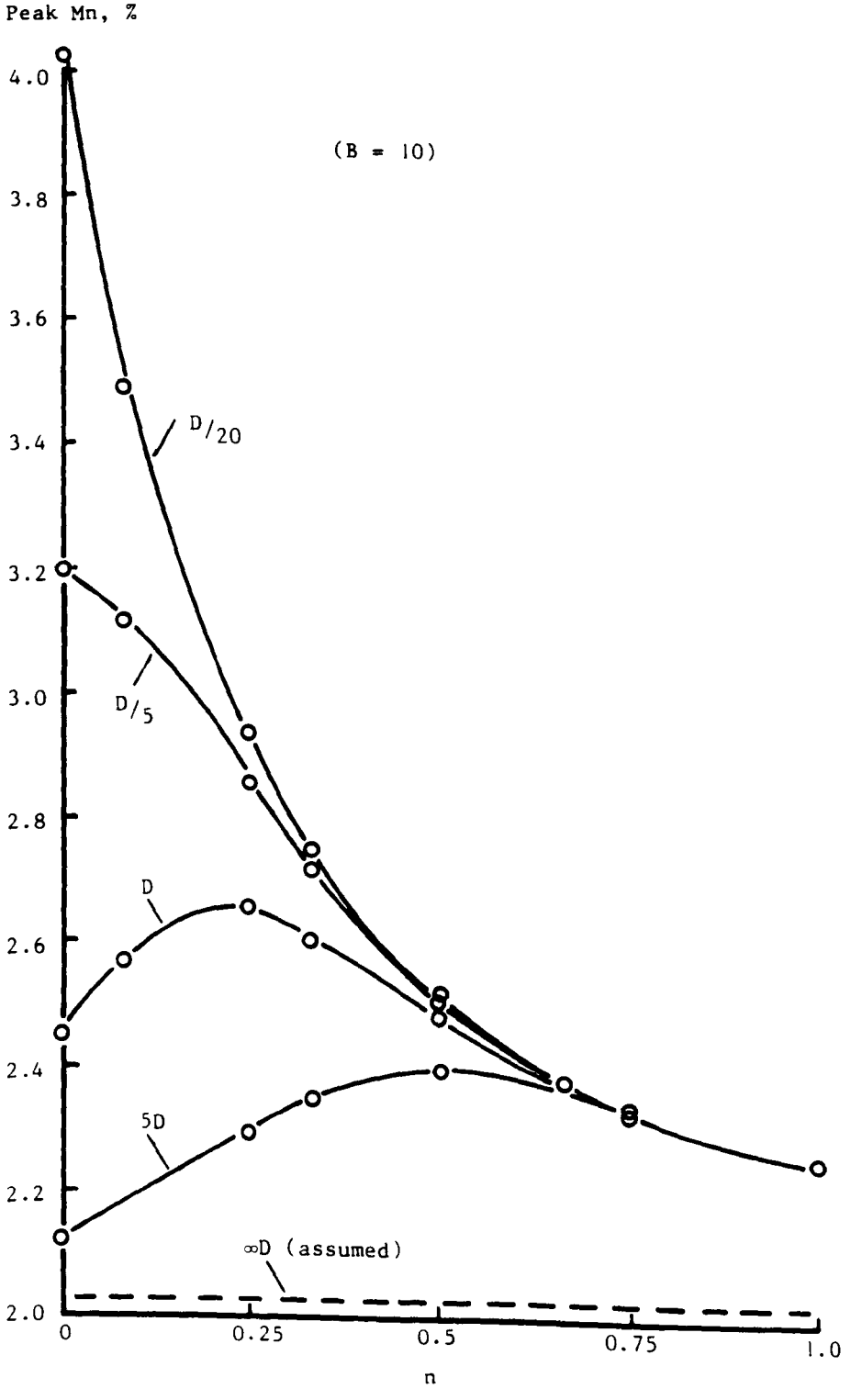

SENSITIVITY OF PEAK Mn TO n AND D_{Mn} for $\lambda = Bt^n$

FIG. 5.16

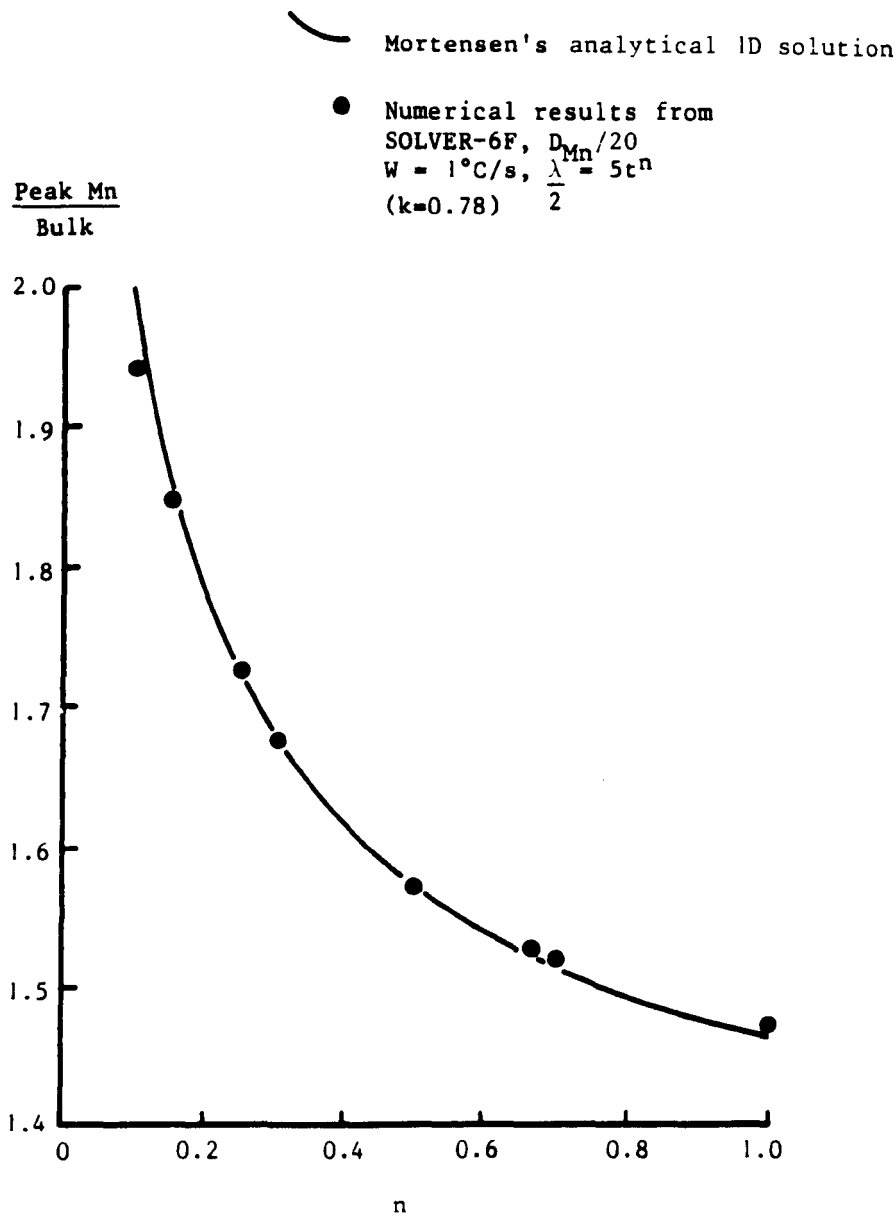

SCHEIL LIMIT UNDER DENDRITE ARM COARSENING, Fe-Mn BINARY: COMPARISON OF ANALYTICAL SOLUTION WITH NUMERICAL PREDICTION

FIG. 5.17

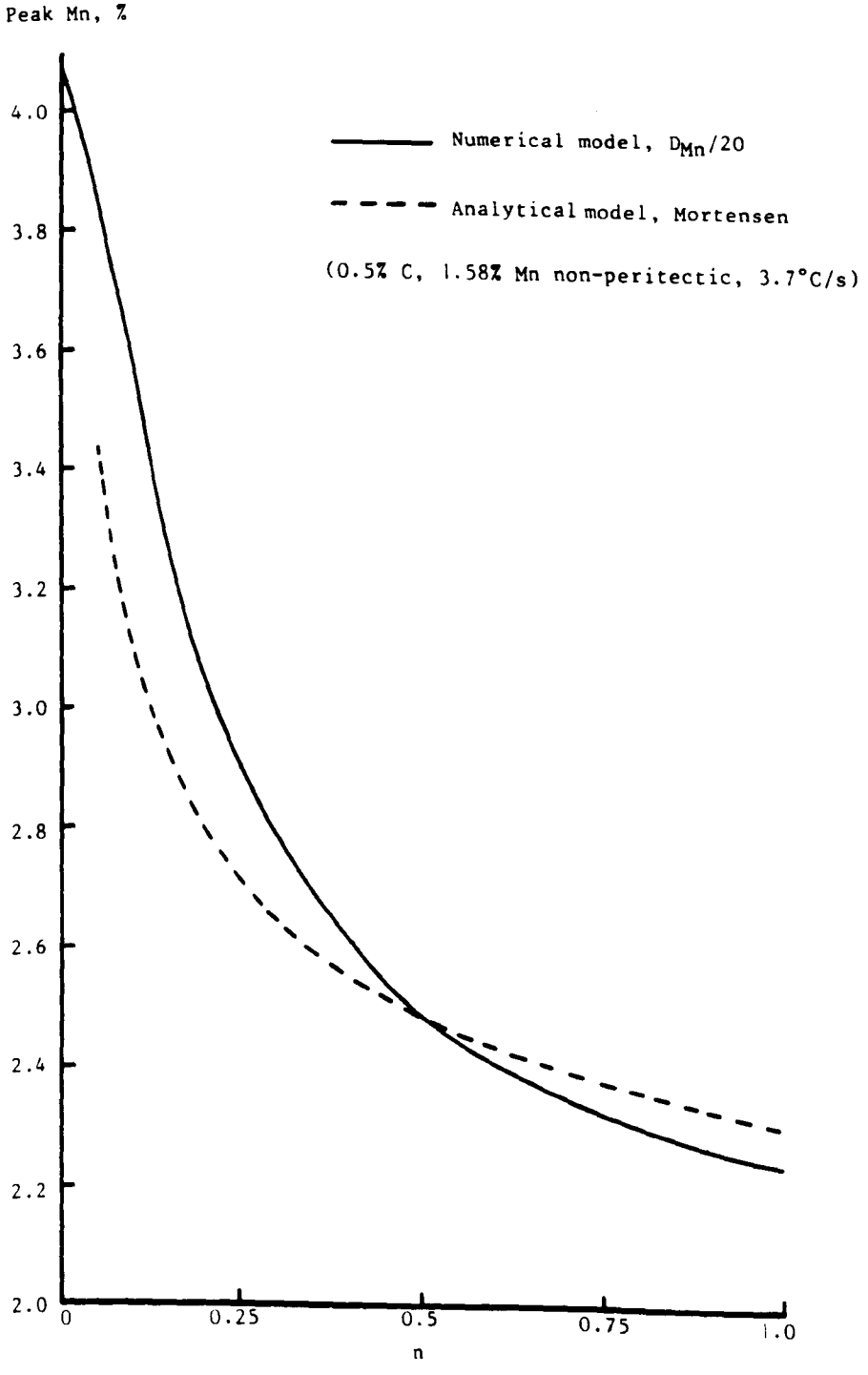

COMPARISON OF TERNARY (Fe-C-Mn) NUMERICAL MODEL WITH BINARY (Fe-Mn) ANALYTICAL MODEL OF THE "SCHEIL" ZERO-DIFFUSIVITY LIMIT AS A FUNCTION OF n

FIG. 5.18

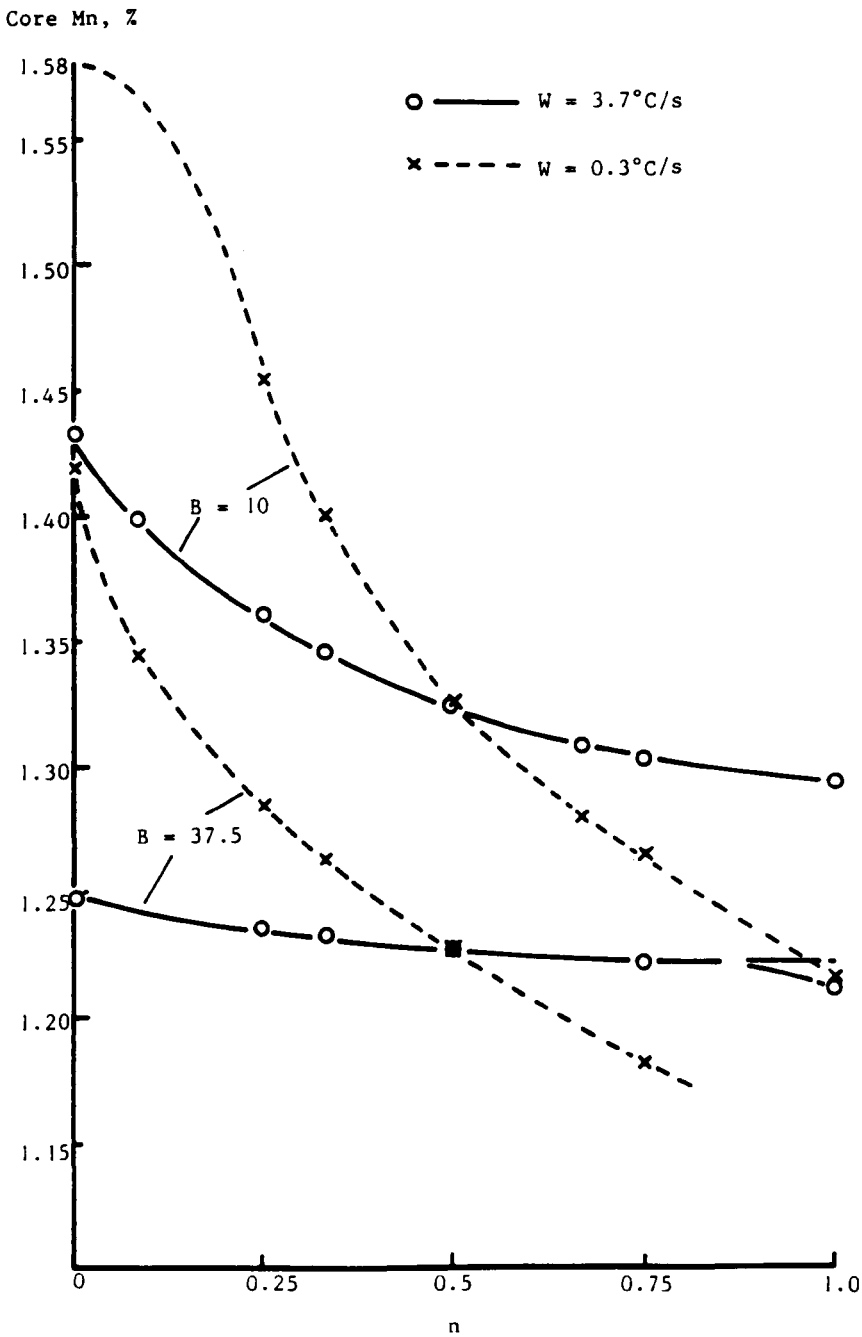

SENSITIVITY OF CORE Mn TO n, B AND W FOR $\lambda = Bt^n$ FIG. 5.19

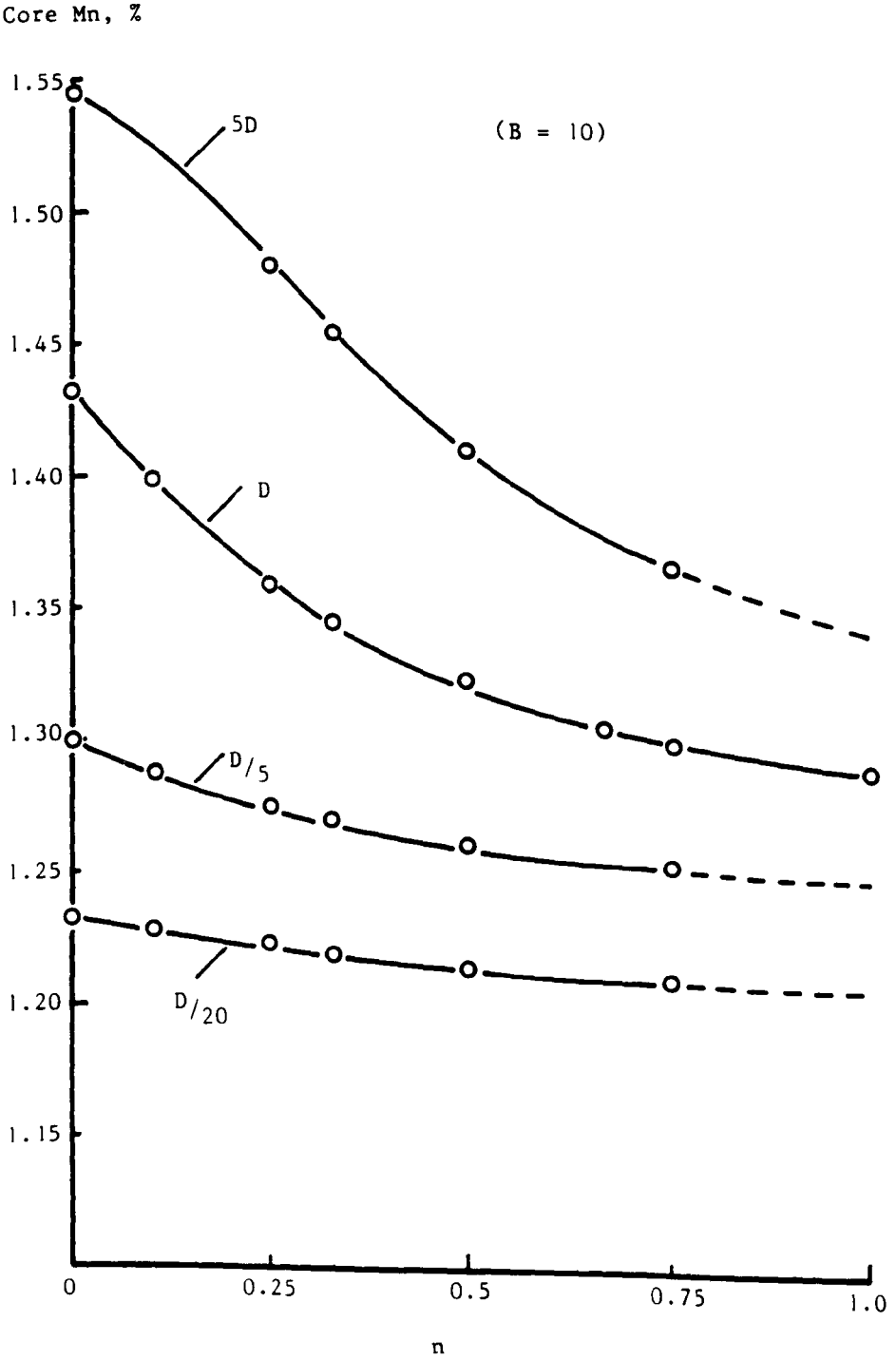

SENSITIVITY OF CORE Mn TO n AND D_{Mn} FOR $\lambda = Bt^n$

FIG. 5.20

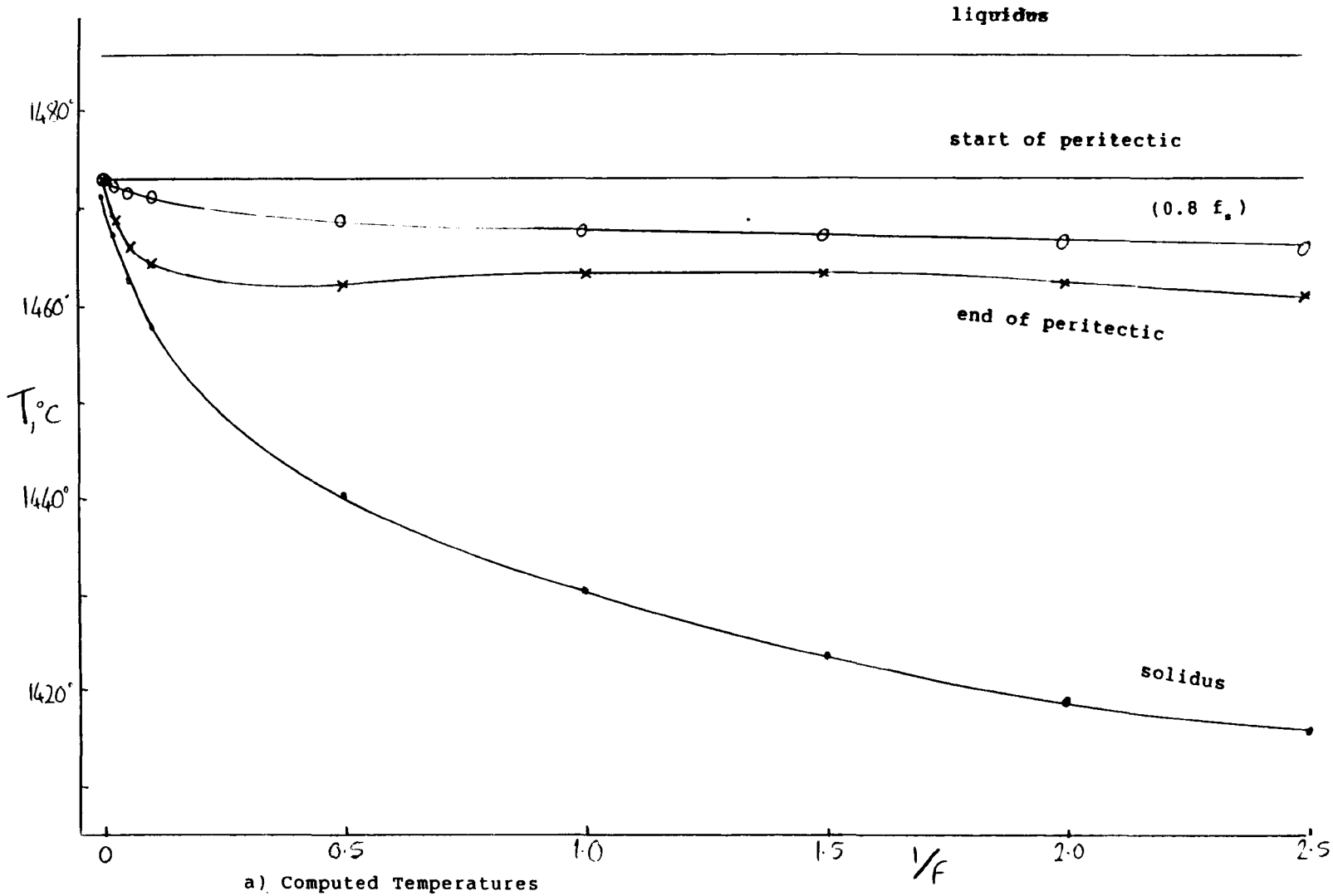

a) Computed Temperatures

Fig. 5.21 INFLUENCE OF DIFFUSIVITY ($F*D_{Mn(1450oC)}$) ON THE PERITECTIC REACTION

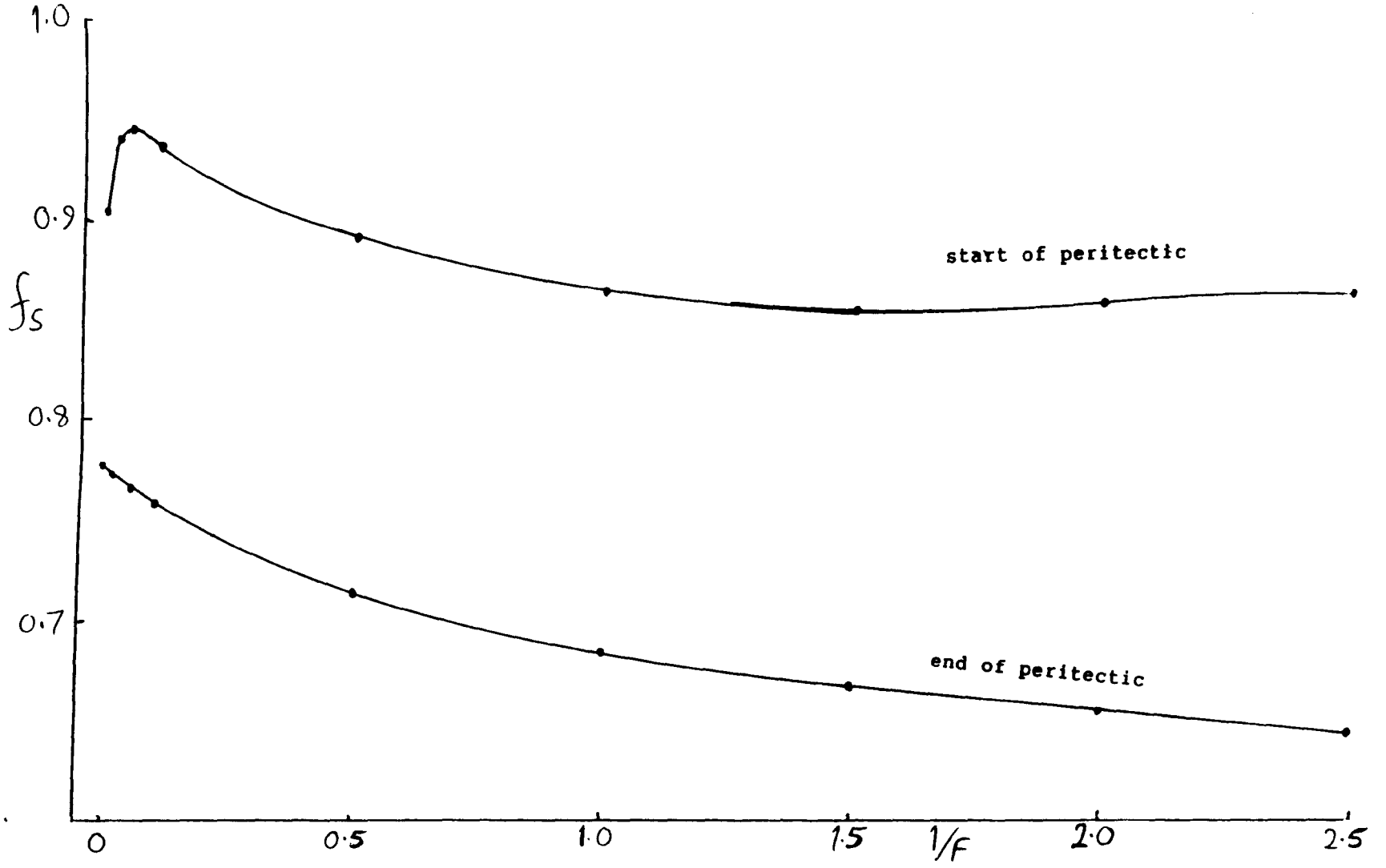

Fig. 5.21 b) Computed Fractions Solid

Fig. 5.22 INFLUENCE OF DIFFUSIVITY ($F^{*}D_{Mn(1450^{o}C)}$) ON FERRITE DISSOLUTION

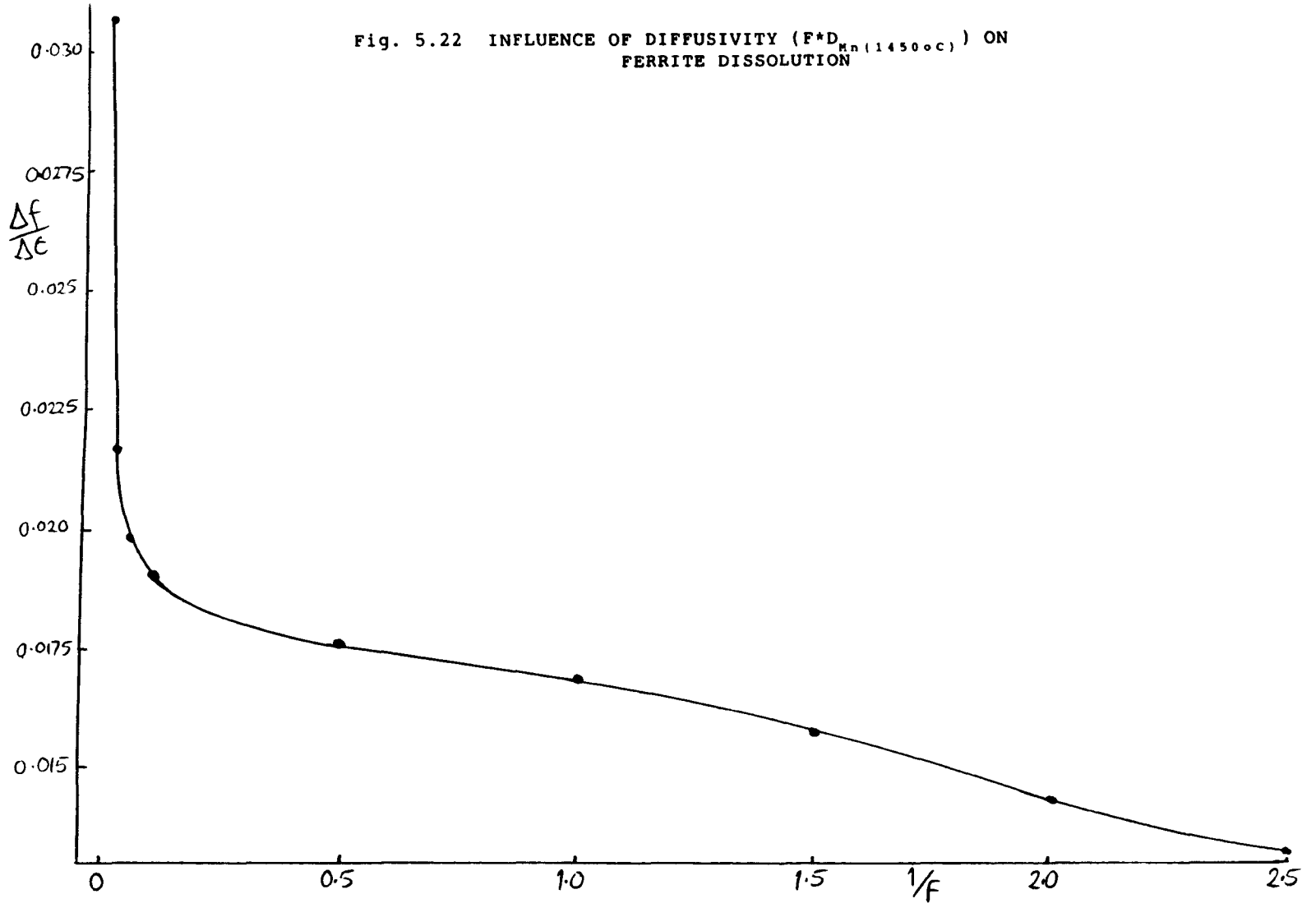

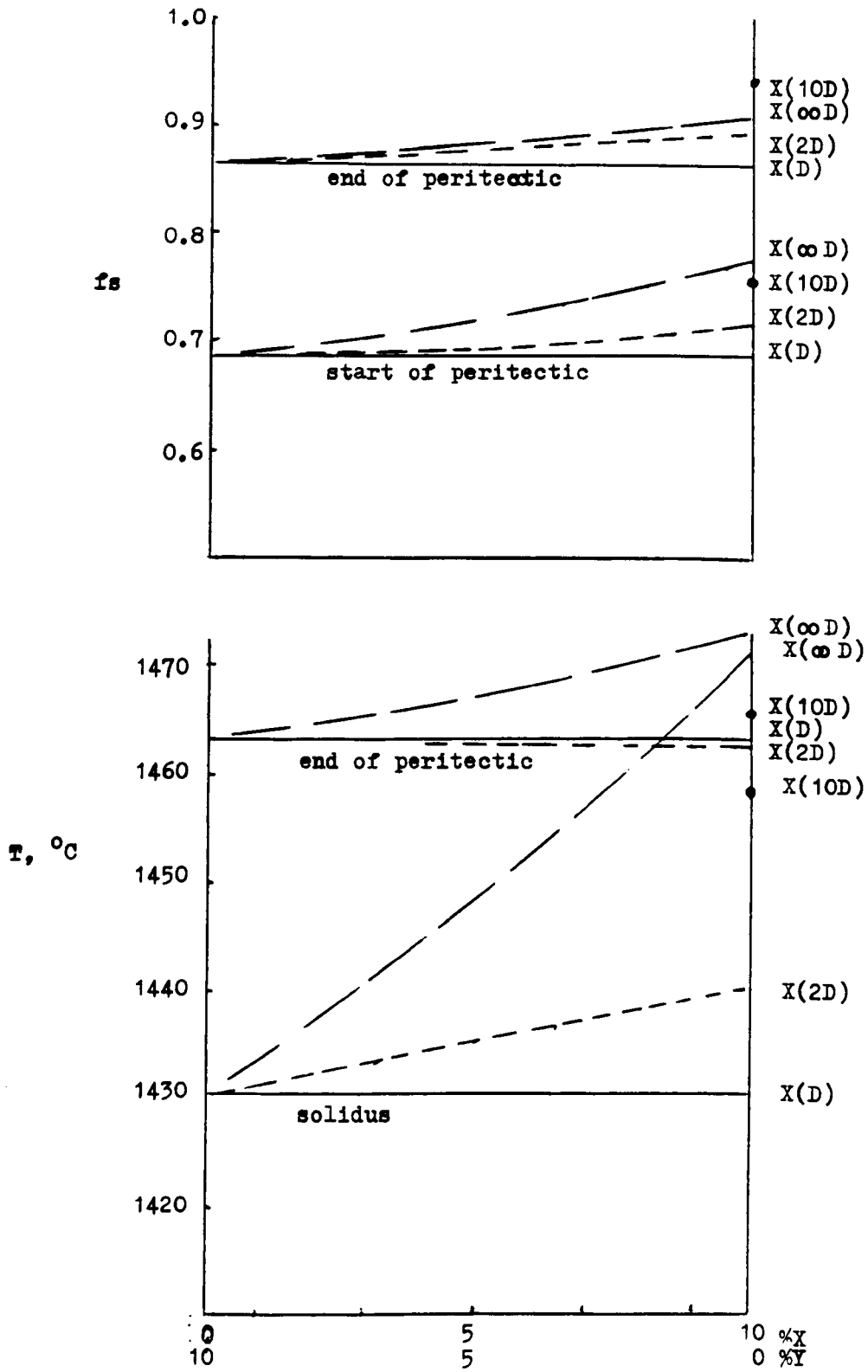

Fig.5.23 CRITICAL FRACTIONS SOLID AND TEMPERATURES WITH VARYING PROPORTIONS OF SOLUTES IDENTICAL APART FROM DIFFUSIVITY (X+Y=10%, Y at base diffusivity D)

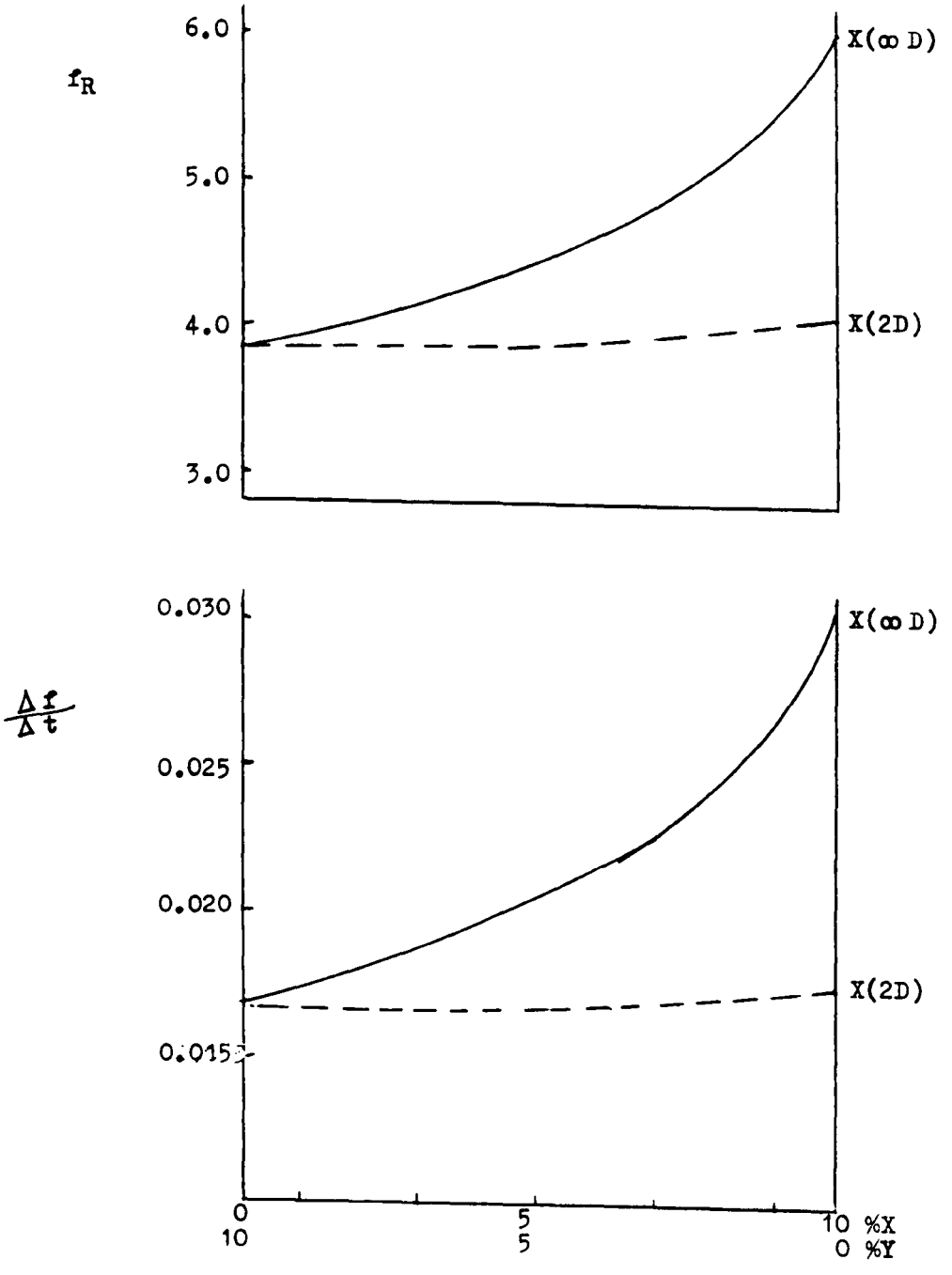

Fig.5.24 RATES OF PERITECTIC REACTION WITH VARYING PROPORTIONS OF SOLUTES IDENTICAL APART FROM DIFFUSIVITY

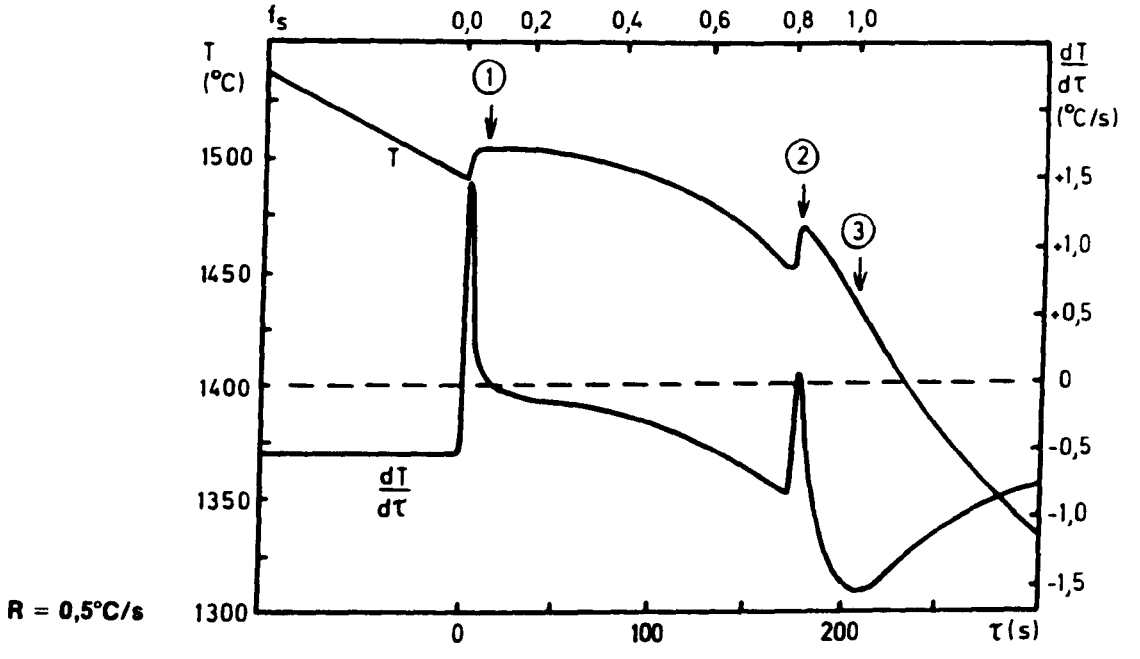

EXAMPLE THERMAL ANALYSIS RESULT FROM JERNKONTORET DATA FIG. 6.1

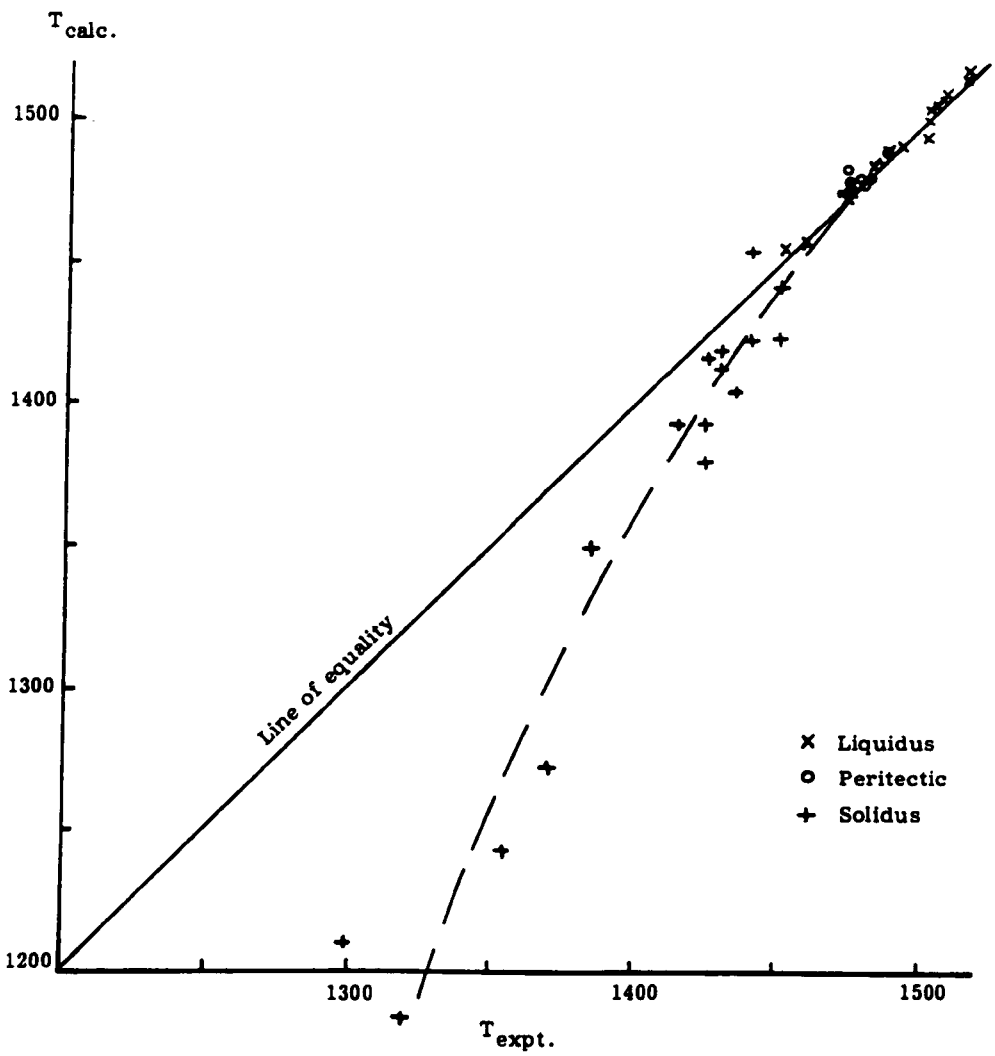

CALCULATED v EXPERIMENTAL CRITICAL TEMPERATURES, °C FIG. 6.2

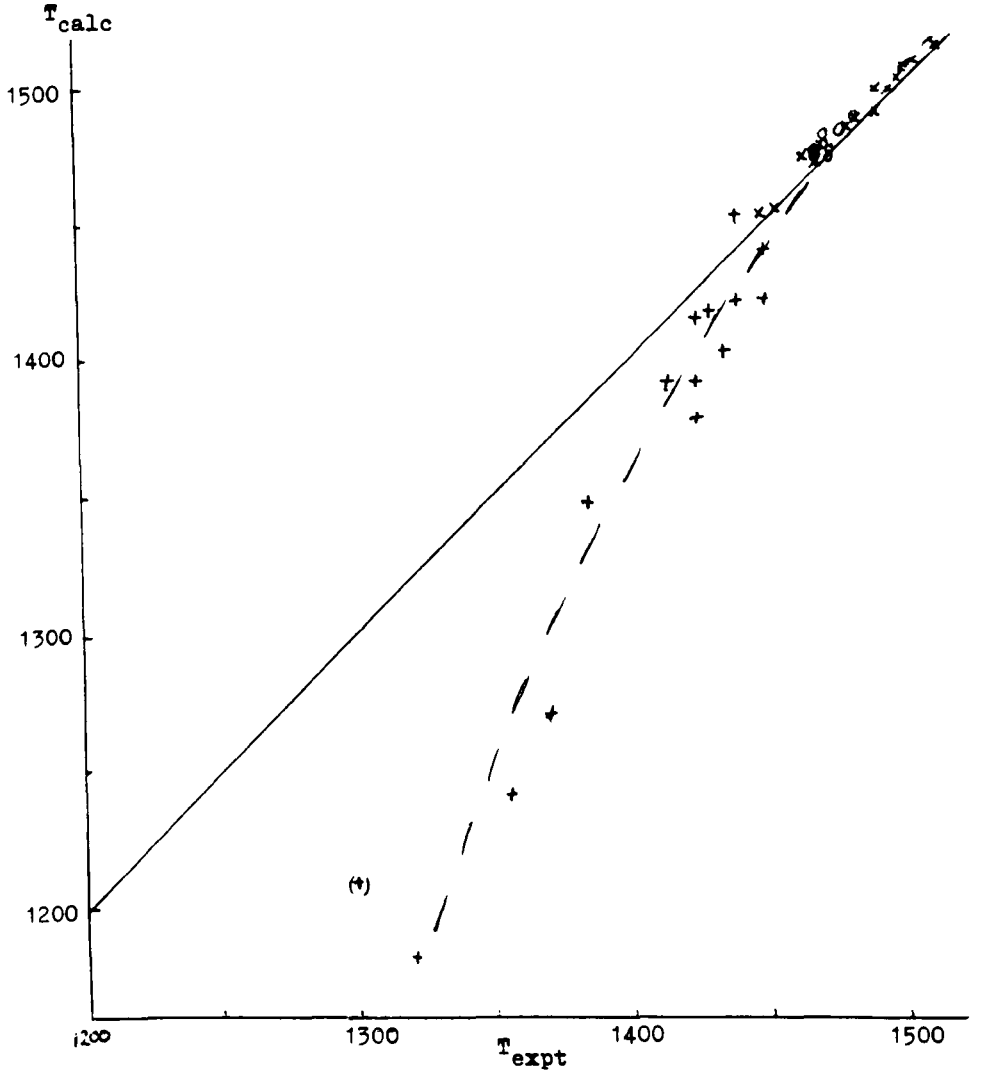

Fig.6.3 As Fig. 6.2 But Restricted to Results From The 0.5K/s Furnace Cooling Rate

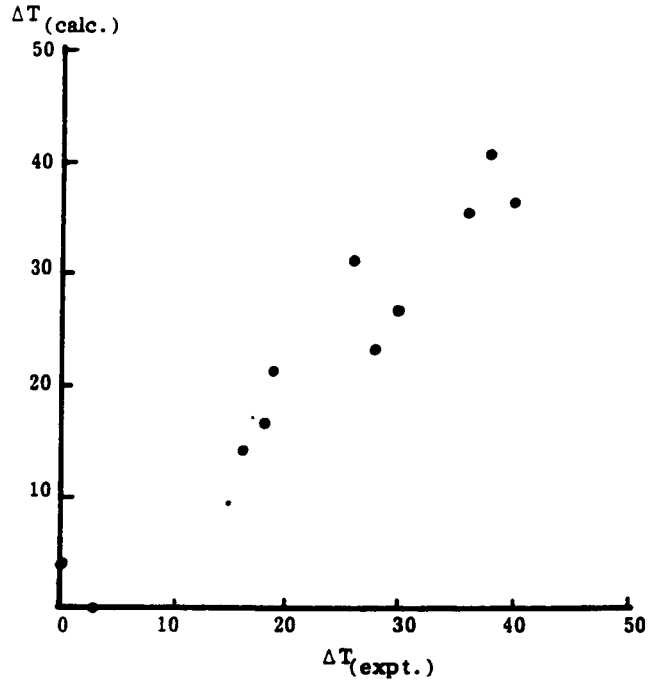

CALCULATED v EXPERIMENTAL LIQUIDUS-PERITECTIC TEMPERATURE INTERVALS FIG. 6.4

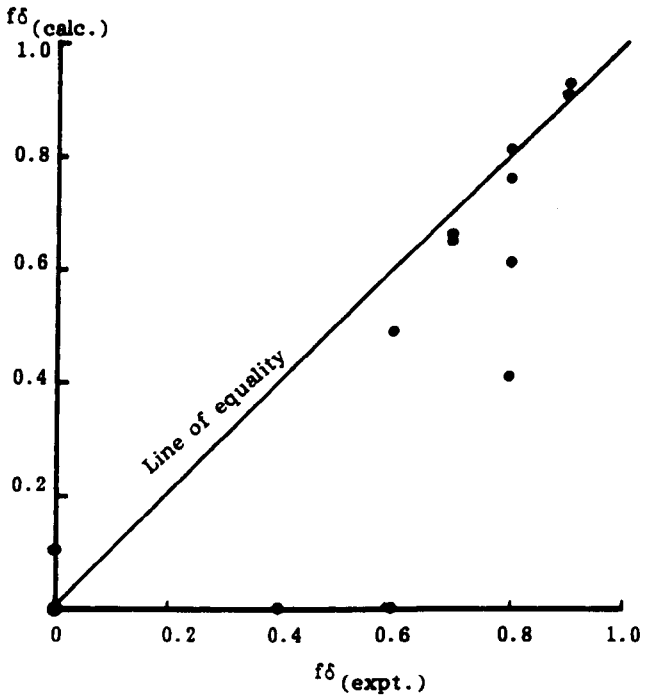

CALCULATED v EXPERIMENTAL FRACTIONAL SOLIDIFICATION AS FERRITE FIG 6.5

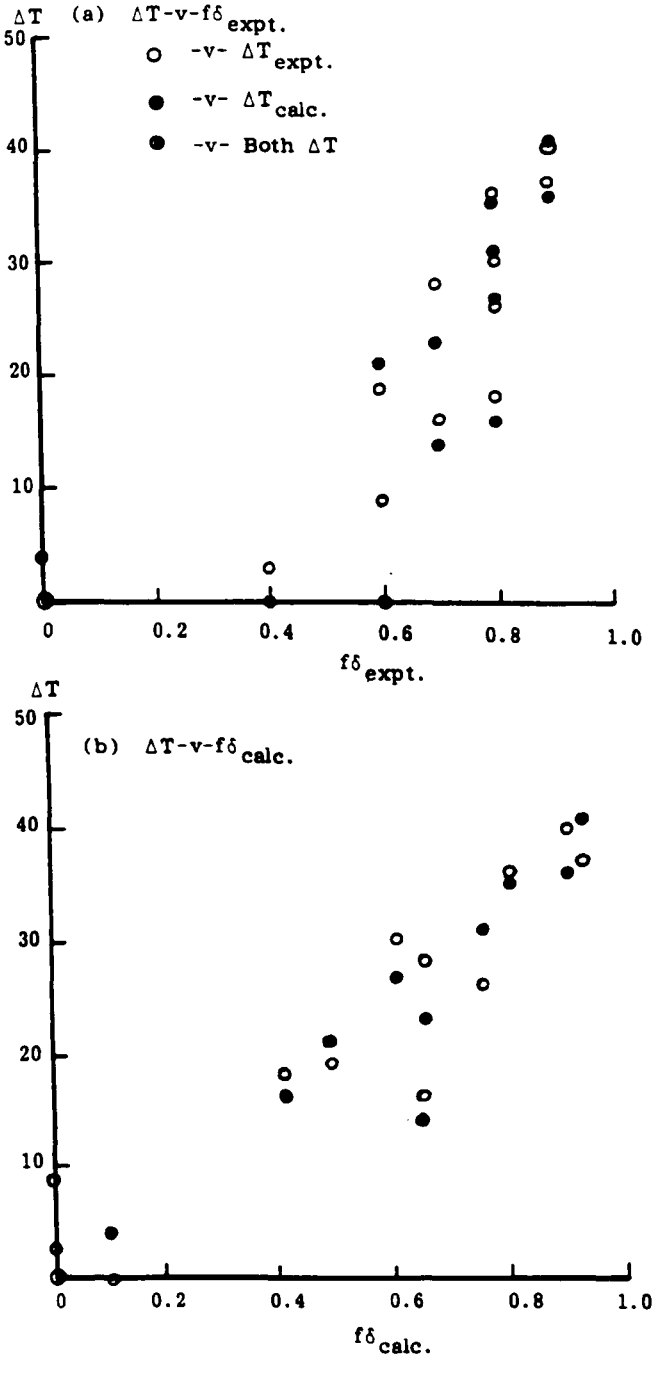

LIQUIDUS-PERITECTIC INTERVAL v FRACTIONAL SOLIDIFICATION AS FERRITE

FIG. 6.6

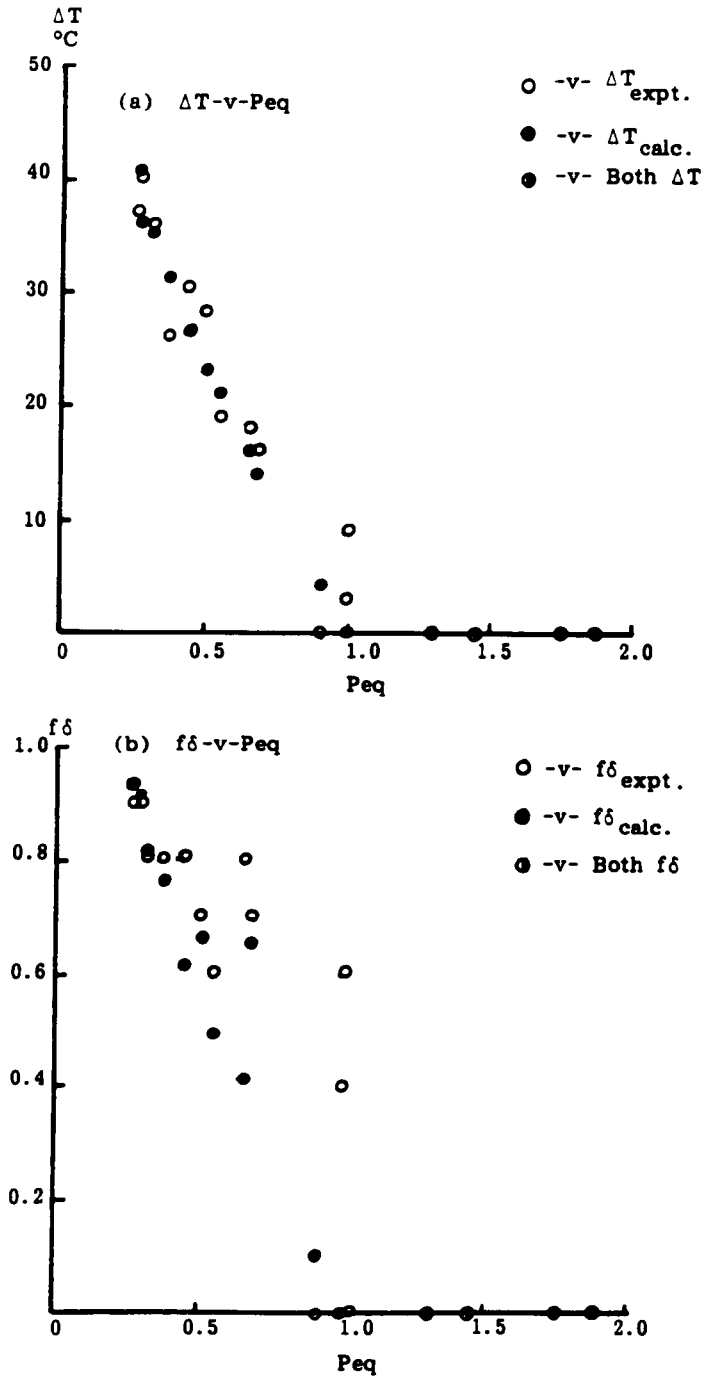

LIQUIDUS-PERITECTIC INTERVAL AND FRACTIONAL SOLIDIFICATION AS FERRITE v PERITECTIC EQUIVALENT OF BULK COMPOSITION

FIG. 6.7

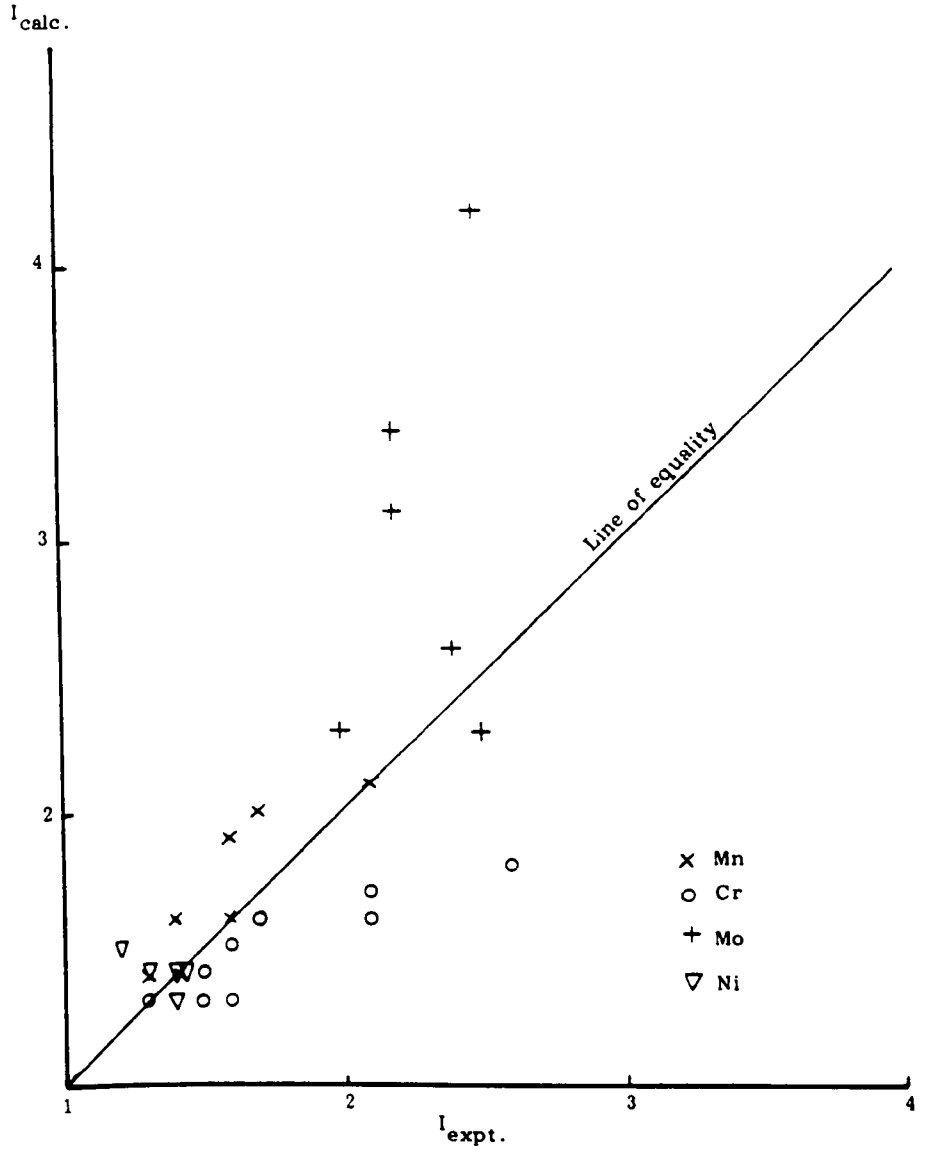

CALCULATED v EXPERIMENTAL SEGREGATION RATIOS FIG. 6.8

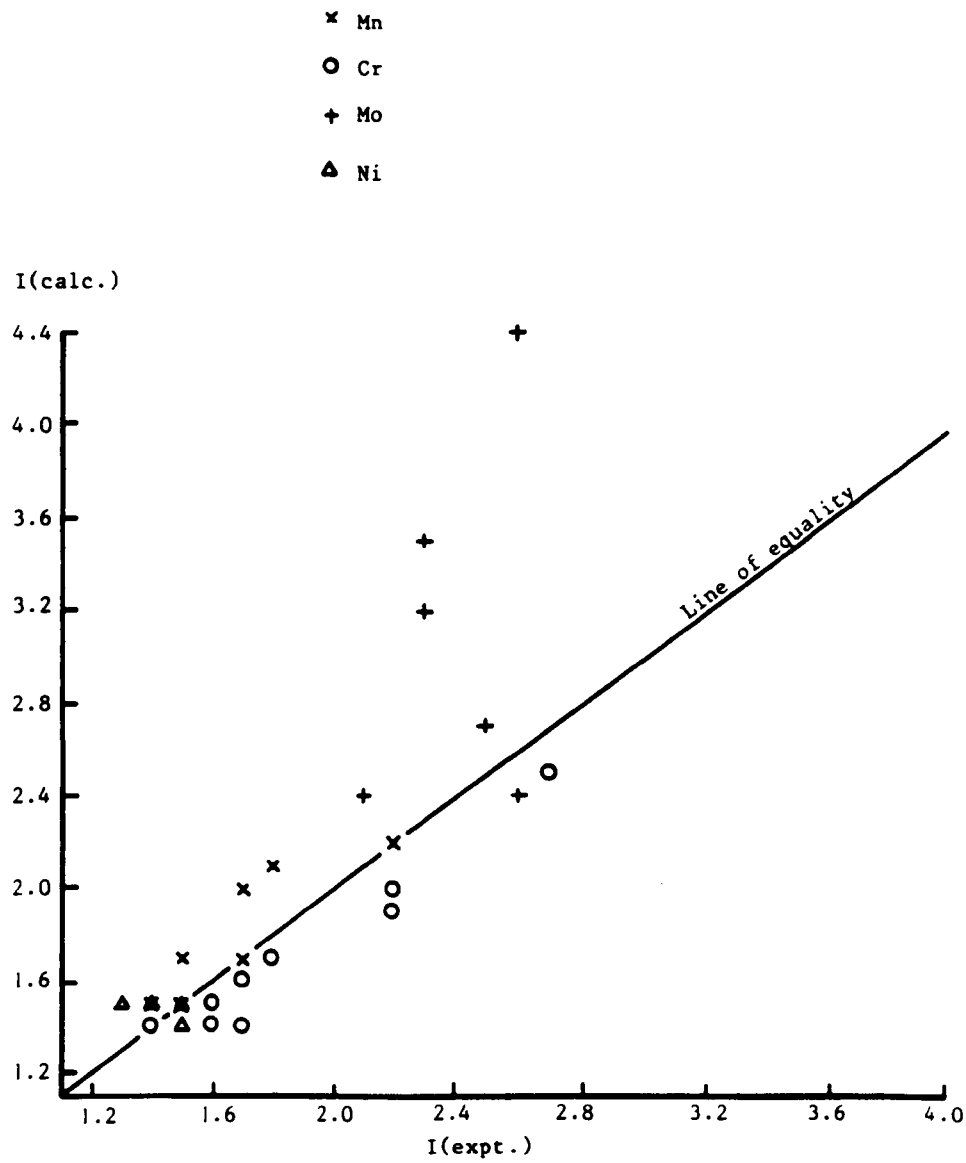

I = maximum/minimum solute content at quench temperature
Experimental data from Ref.

CALCULATED v EXPERIMENTAL SEGREGATION RATIOS, I FIG. 6.9

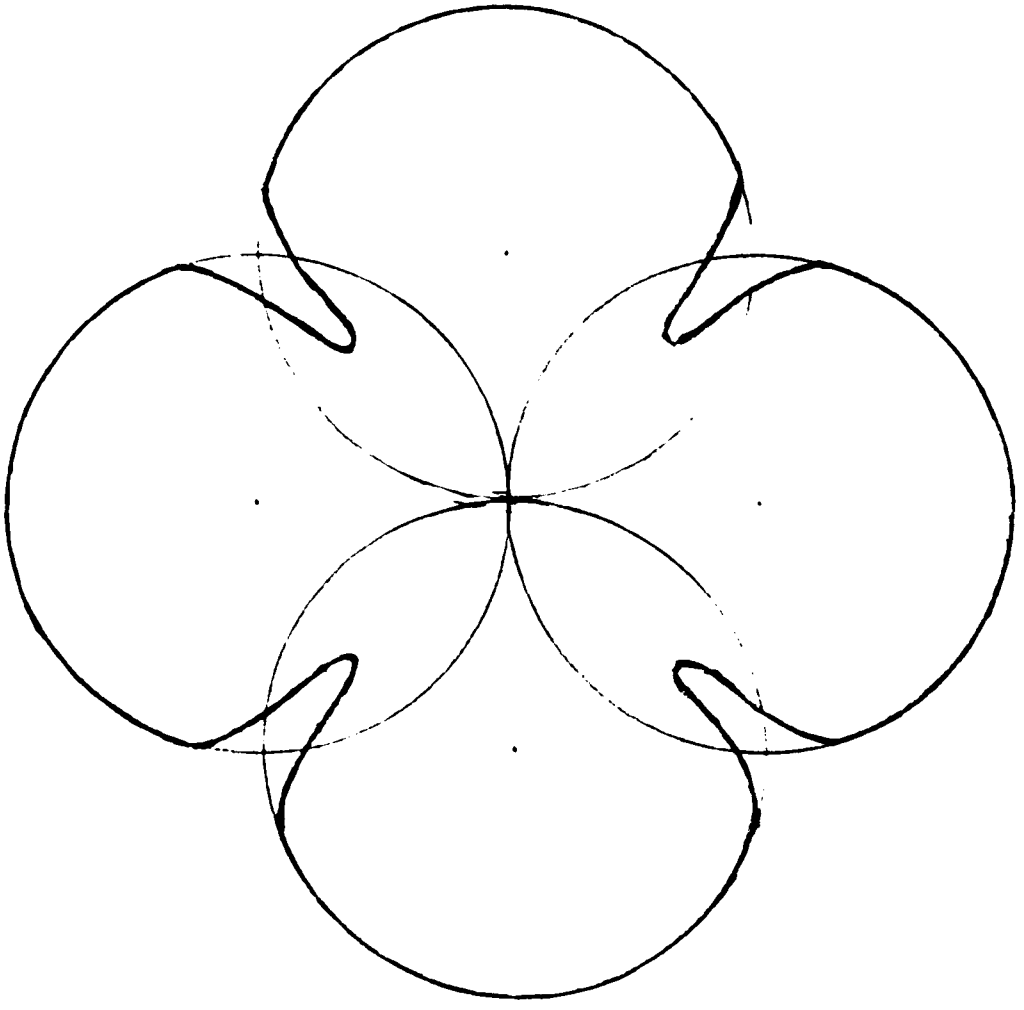

Fig.6.10 SCHEMATIC SECTION THROUGH A "CLOVER LEAF" DENDRITE (TYPICAL OF TURKELI'S EXPERIMENTS) AND ITS REPRESENTATION BY 2D, $\frac{1}{2}\lambda$ CELL SIZE

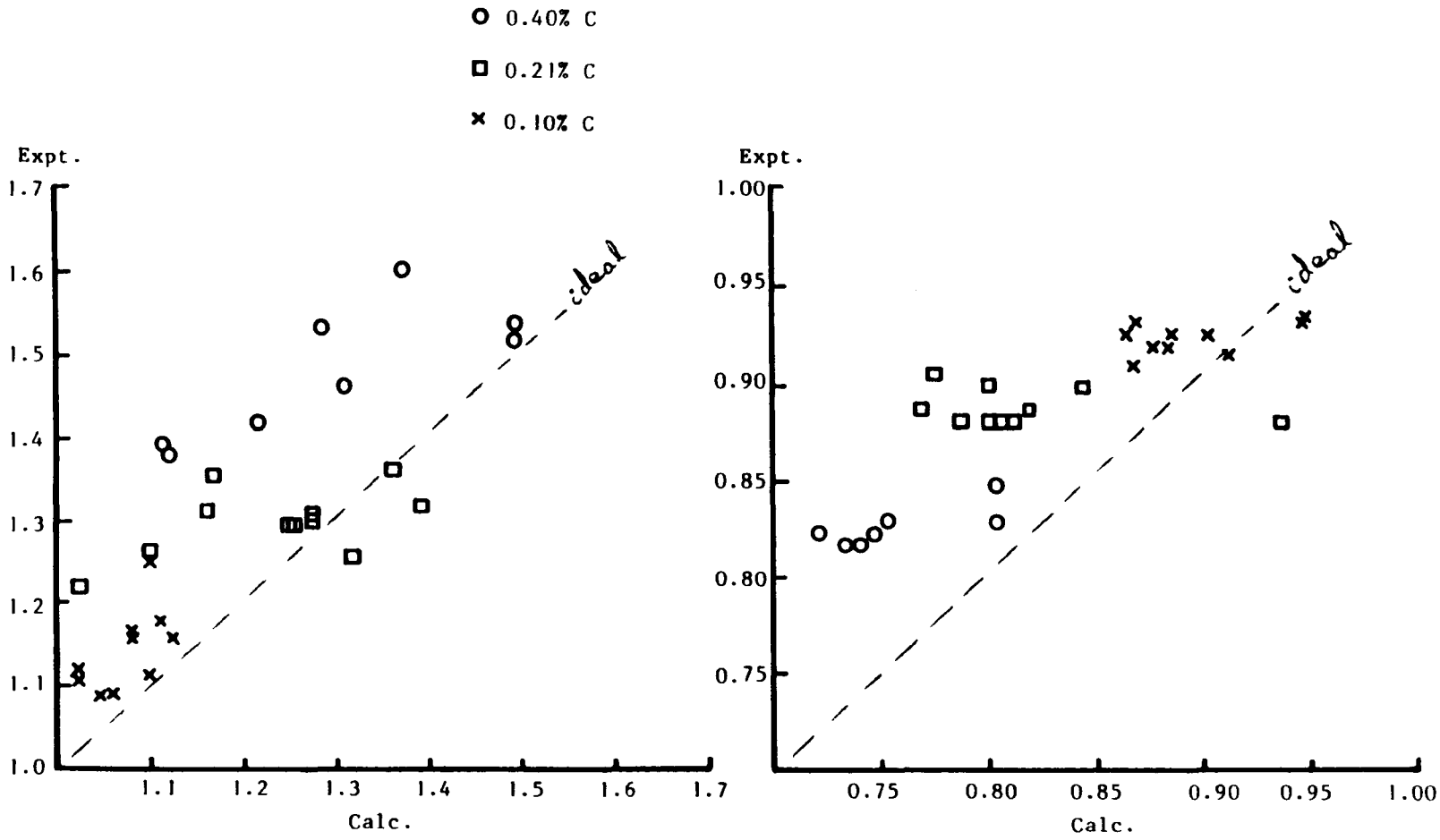

(a) Peak Mn Ratios

(b) Core Mn Ratios

COMPARISON OF CALCULATED AND EXPERIMENTAL MICROSEGREGATION

FIG. 6·11

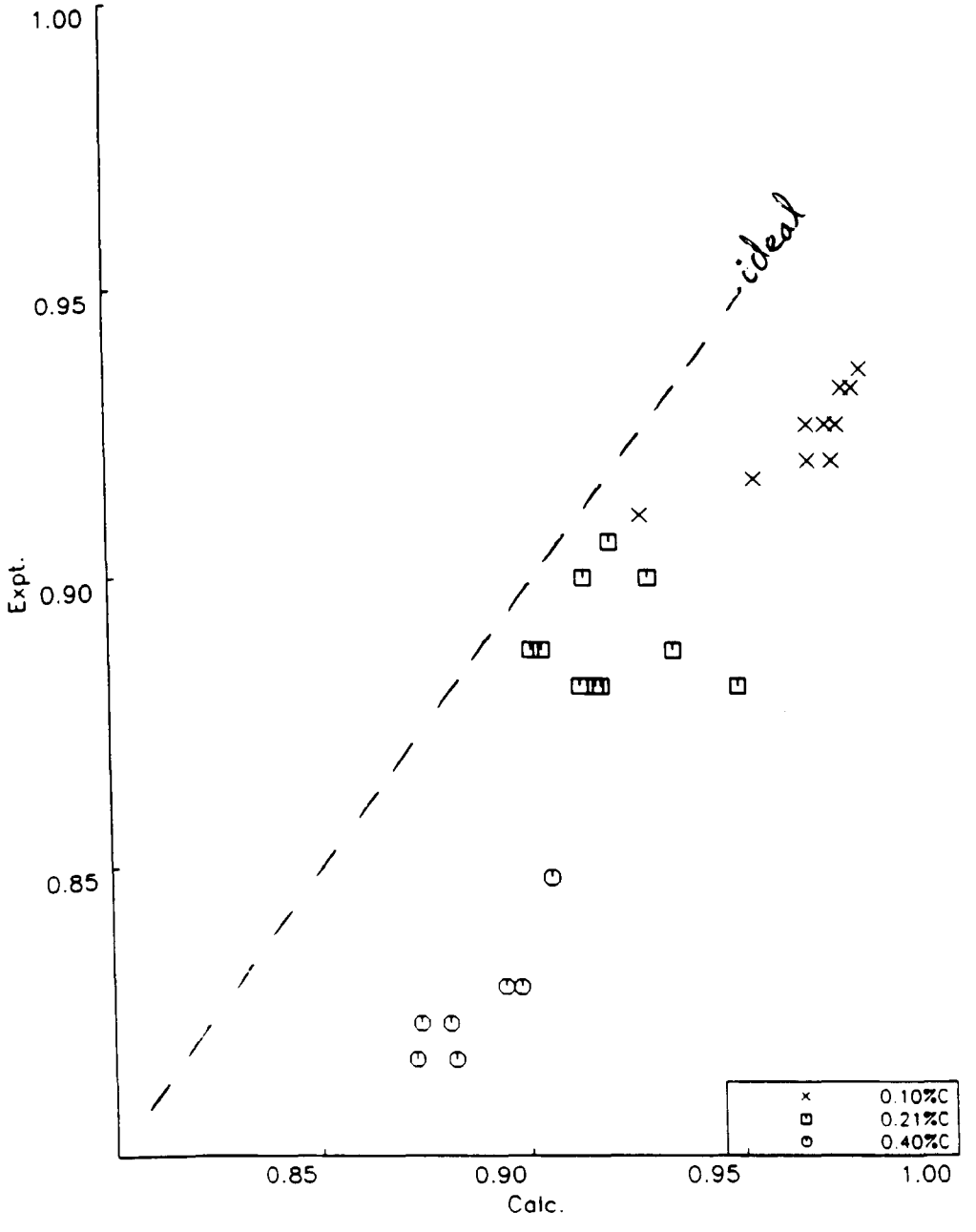

CORE Mn RATIOS RE-CALCULATED ON A SECONDARY DENDRITE ARM BASIS, WITH $\lambda = 10\sqrt{t}$ (cf. Fig. 6.11)

FIG. 6.12

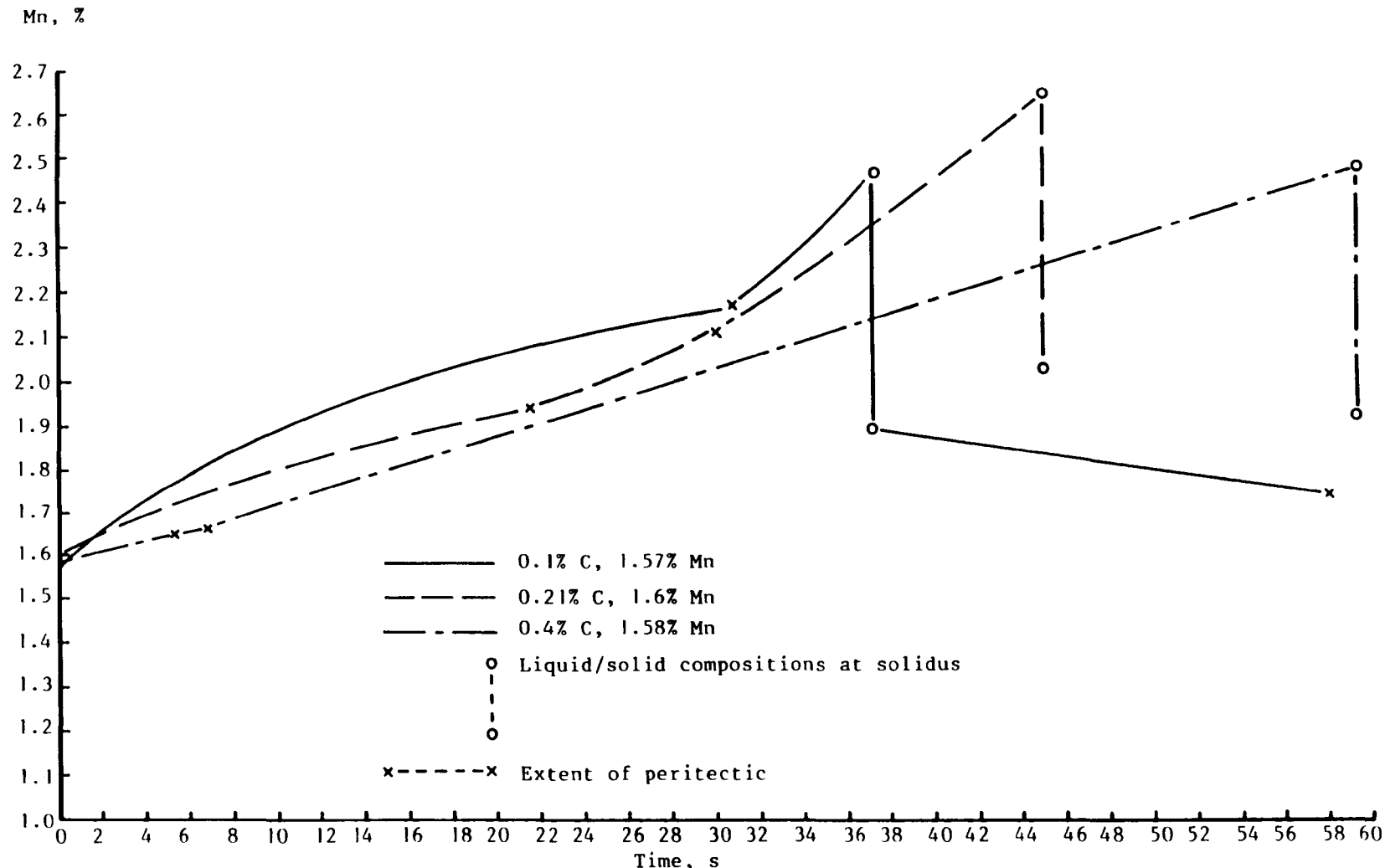

454

VARIATION OF MAXIMUM MANGANESE CONCENTRATION WITH TIME FOR TURKELI's STEELS, $\lambda_2 = 10\sqrt{t}$ DURING SOLIDIFICATION

FIG. 6·13(a)

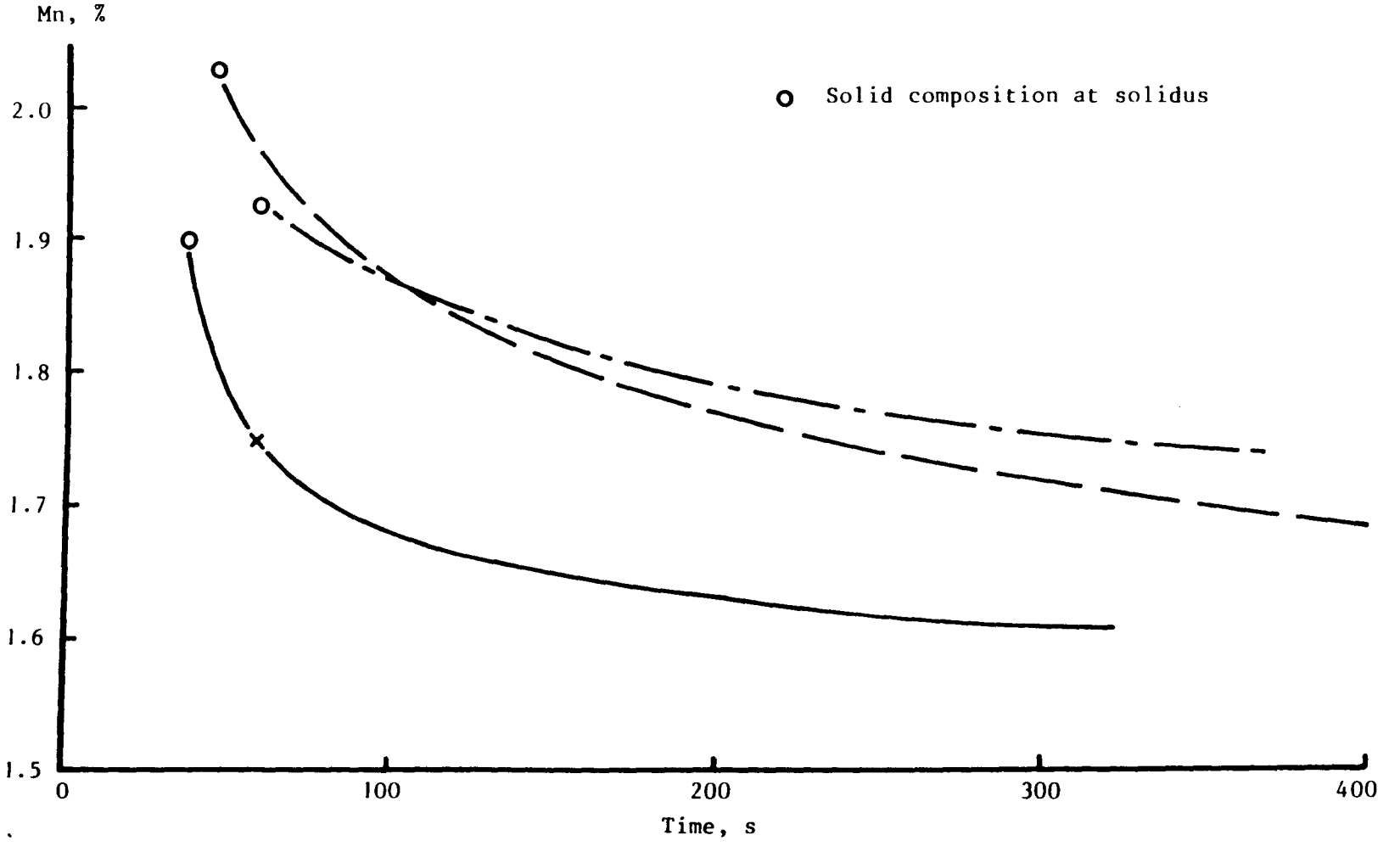

VARIATION OF MAXIMUM MANGANESE CONCENTRATION WITH TIME FOR TURKELI's STEELS SUB-SOLIDUS

FIG. 6.13(b)

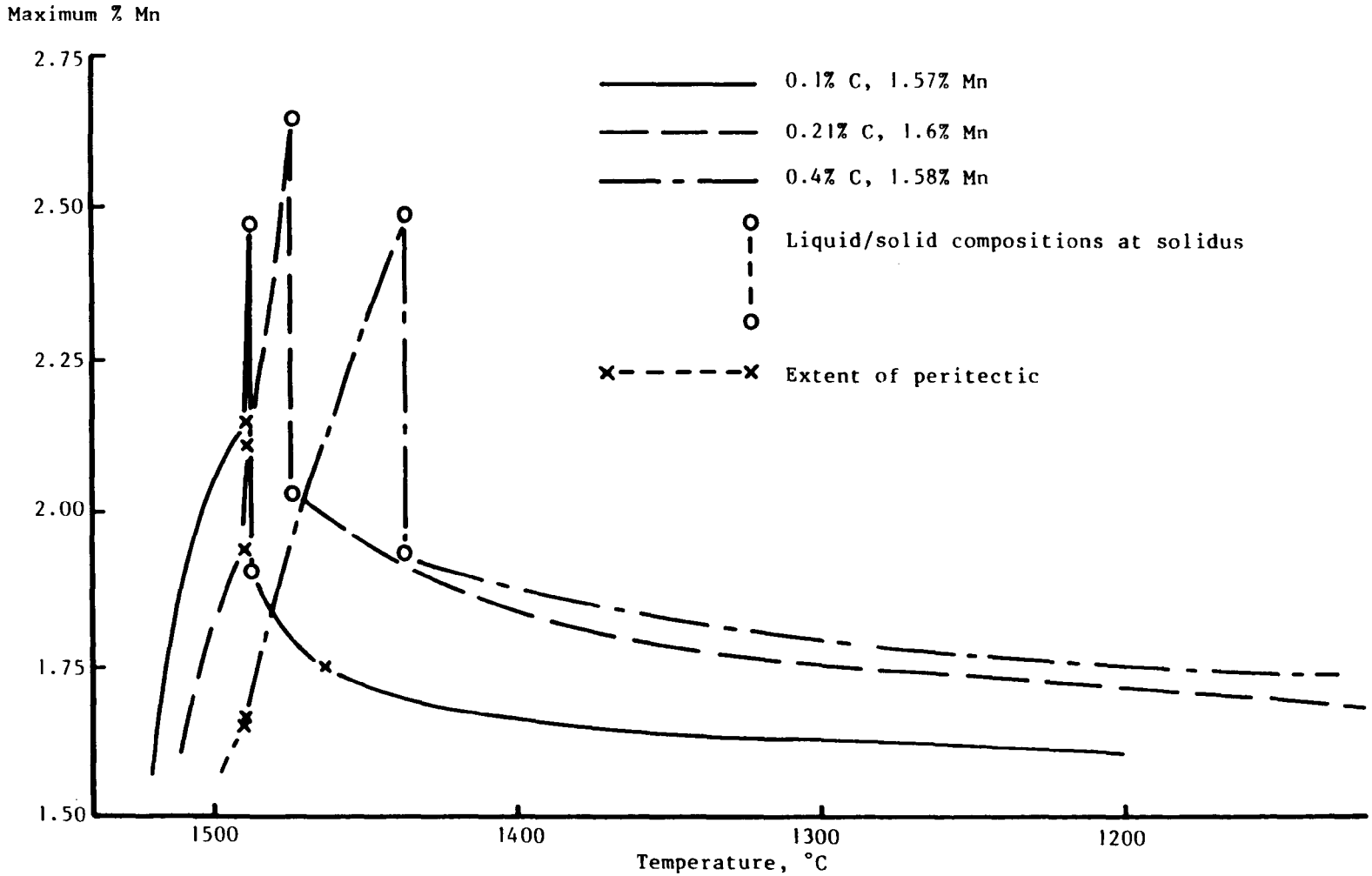

VARIATION OF MAXIMUM MANGANESE CONCENTRATION WITH TEMPERATURE FOR TURKELI's STEELS FIG. 6.14

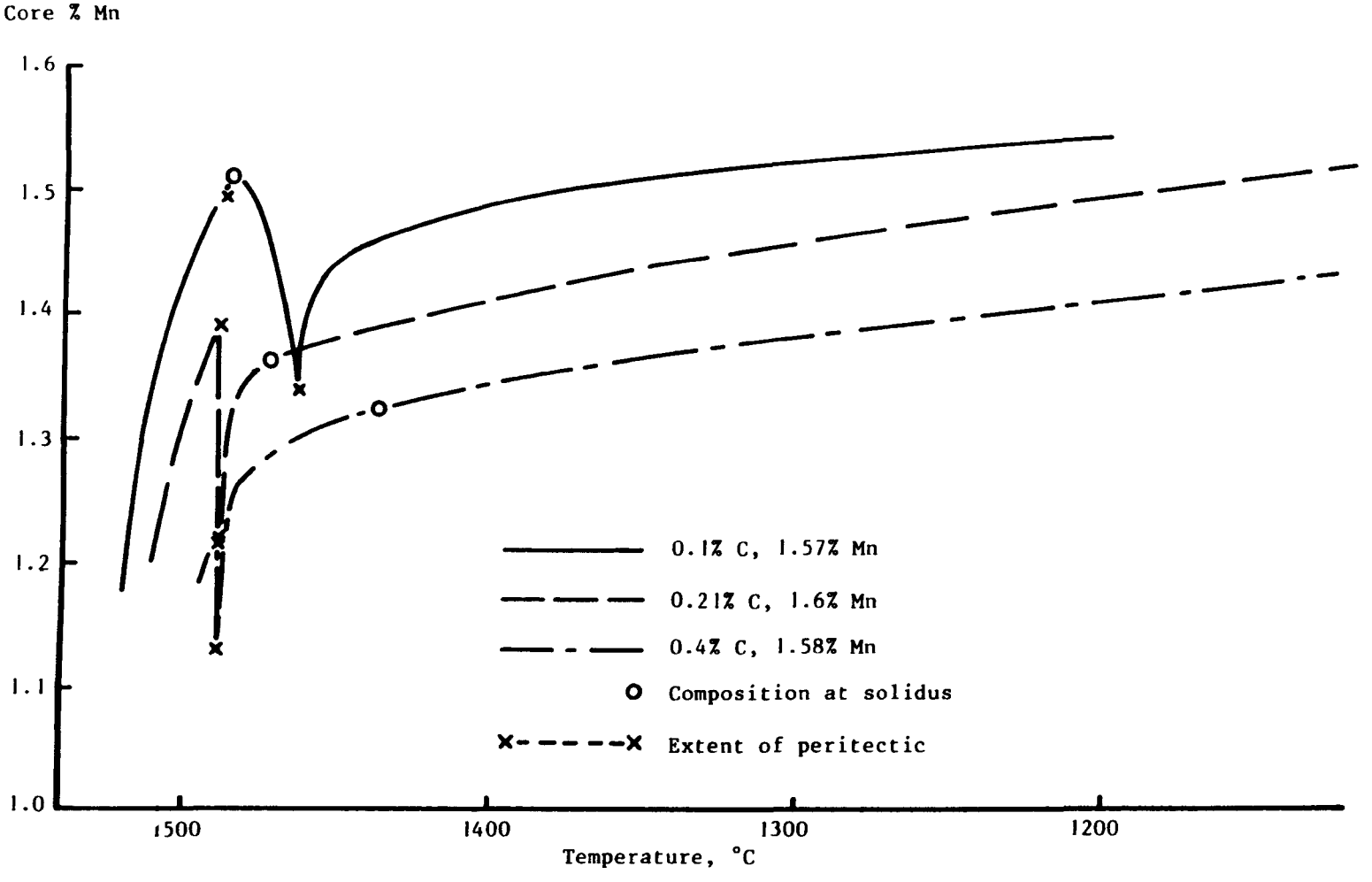

VARIATION OF CORE MANGANESE CONCENTRATION WITH TEMPERATURE FOR TURKELI's STEELS FIG. 6.15

APPENDIX

ANNOTATED PROGRAM LISTINGS

A) Program EQUIL

This program employs the peritectic equivalent concept and the consistent peritectic data set, progressing up to the onset of the peritectic reaction under equilibrium solidification.

Data employed:

File "EQUIL.DAT"

Critical temperatures for pure iron datum,
Liquidus slope, δ/γ solvus, δ/L partition coefficient, γ/δ partition coefficient, for C,Si,Mn,P,S,Cr,Mo,Ni,Ti,N,B

```
1537,   1526,   1392,
-83,    1122,   0.17,   1.88
-9,     -67,    0.7,    0.85
-5.1,   8.75,   0.74,   1.05
-34,    -200,   0.13,   0.45
-40,    -200,   0.05,   0.4
-1,     -12.5,  0.95,   0.85
-2.5,   -40,    0.74,   0.75
-5,     29,     0.79,   1.14
-18,    -167,   0.5,    0.5
-72,    480,    0.25,   1.88
-104,   -115,   0.064,  0.6
```

Program "EQUIL.BAS"

```
10      PRINT:PRINT "CONSTANT k AND m EQUILIBRIUM CALCULATIONS"
        PRINT 'for SOLIDIFICATION up to the PERITECTIC':PRINT
        DIM M1(20),M2(20),M3(20),K1(20),K2(20),K3(20)
        DIM Z0(20),ZL(20),PEQ(20),ZP(20)

        OPEN "EQUIL.DAT" FOR INPUT AS FILE #1, RECORDSIZE 255

        INPUT #1, T1,T2,T3
        FOR I%=1 TO 11
        INPUT #1, M1(I%),M3(I%),K1(I%),K3(I%)
        K2(I%)=K1(I%)*K3(I%)
        M2(I%)=((T2-T3)*M1(I%)+(T1-T2)*K1(I%)*M3(I%))/(T1-T3)
        ZP(I%)=(T1-T3)/(K1(I%)*M3(I%)-M1(I%))
        PEQ(I%)=1/ZP(I%)
        PRINT I%,PEQ(I%)
        NEXT I%
```

```
20      INPUT 'Weight% C';Z0(1)
        INPUT '%Si';Z0(2)
        INPUT '%Mn';Z0(3)
        INPUT '%P';Z0(4)
        INPUT '%S';Z0(5)
        INPUT '%Cr';Z0(6)
        INPUT '%Mo';Z0(7)
        INPUT '%Ni';Z0(8)
        INPUT '%Ti';Z0(9)
        INPUT '%N';Z0(10)
        INPUT '%B';Z0(11)

        INPUT 'Fraction-solid interval for printout';DFS
        FS=-DFS

50      ! CALCULATION
        GOTO 200 IF FS>=1
        FS=FS+DFS
        TT1=T1  : TT2=T2        : TT3=T3        : PEQ=0
        FOR I%=1 TO 11
        ZL(I%)=Z0(I%)/(1-(1-K1(I%))*FS)
        TT1=TT1+M1(I%)*ZL(I%)
        TT2=TT2+M2(I%)*ZL(I%)
        TT3=TT3+M3(I%)*K1(I%)*ZL(I%)
        PEQ=PEQ+PEQ(I%)*ZL(I%)
        NEXT I%

        PRINT:PRINT 'Fraction solid';FS
        PRINT ZL(I%);'  '; FOR I%=1 TO 11
        PRINT
        PRINT 'TT1';TT1,'TT2';TT2,'TT3';TT3,'Pe';PEQ
        GOTO 100 IF TT3>TT1
        GOTO 50

100     PRINT:PRINT 'Peritectic reached'        : GOTO 300
200     PRINT:PRINT 'Fully solidified as delta-ferrite'
300     PRINT:INPUT 'Any more';Y$
        GOTO 20 IF LEFT(Y$,1)<>'N'
        END
```

(When PEQ=1, the solvus temperatures TT1=TT2=TT3, i.e. onset of peritectic three phase equilibrium.)

B) FLOWCHART OF "SOLVER" MAIN PROGRAM ROUTINES

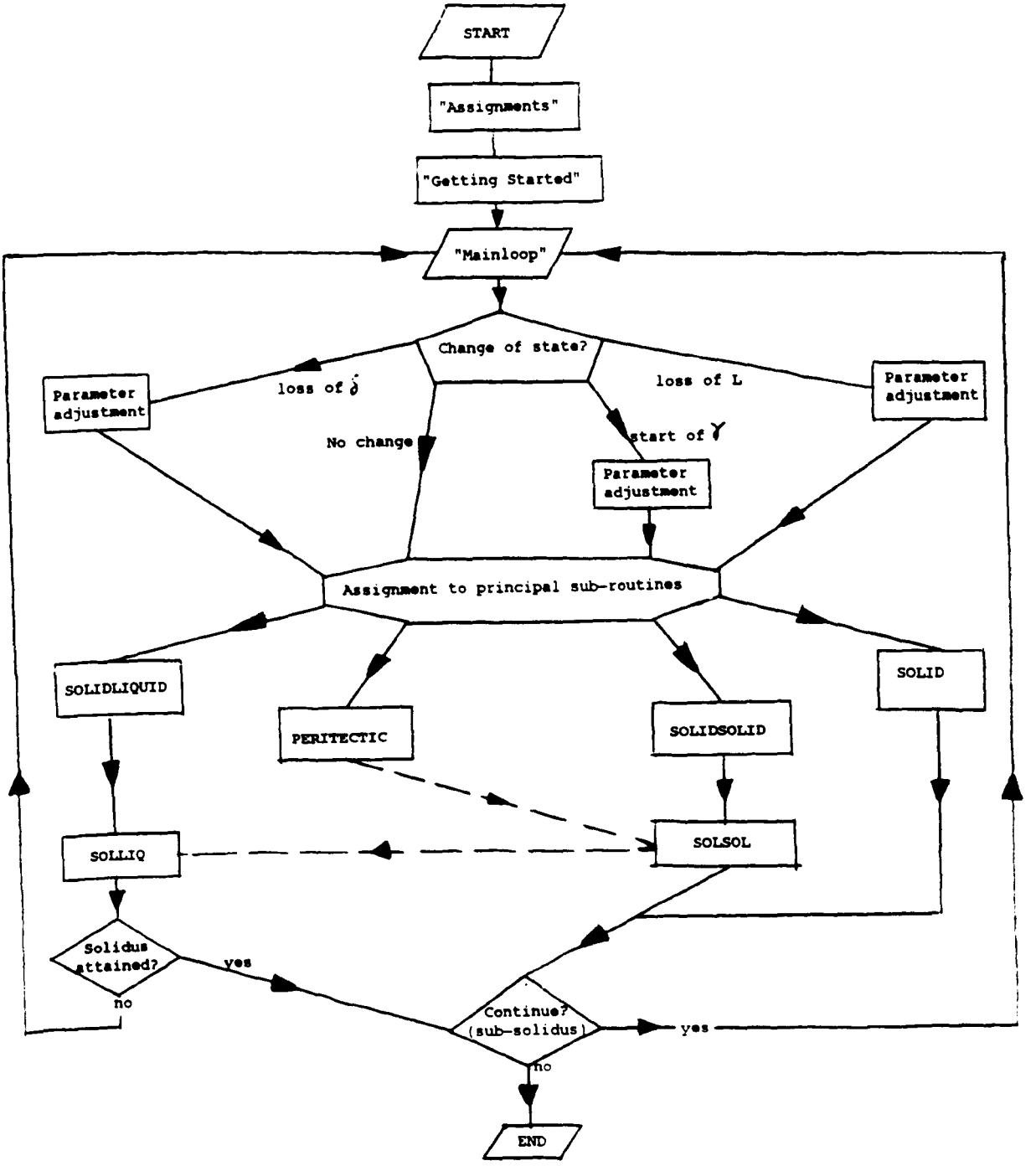

Annotated program listing follows

"SOLVER" program, $\lambda=Bt^n$ option

LINE 10

Introductory on-screen text
Dimensions of arrays

Selection of dimensional basis
Static or coarsening option
Parameters for coarsening option

LINE 15

Spacing for static arm option
"Killing" coarsening parameters

LINE 20

Selection of data file for element data
Reading of file: Name of solvent, its critical temperatures, latent and specific heats, number of solutes, base diffusivity parameters of solvent
Name of interstitial solute, and two of its solvus slopes and partition coefficients
Calculation of third solvus slope and partition coefficient for interstitial ("streamlined") solute
Reading of above data for other solutes, with also their factors on solvent self-diffusivities
Calculation of third solvus slope and partition coefficient
Identification of most rapid finite diffuser for control of FD time stepping
Input of contents of selected elements (can be zero)
Assumed ferritic solidification, setting up of active parameters for solid/liquid interface
Peritectic equivalent test for above assumption and resetting of parameters if false
(PHASE% is additive of 1 for liquid, 2 for ferrite, and 4 for austenite, any total being unique to a particular phase mixture)
GOSUB HEAT for thermal control parameters, see later

```
10  PRINT\PRINT
    PRINT "'S O L V E R _ PhD' "
    PRINT '-----------------'
    PRINT 'Multicomponent micro-segregation model for 1, 2 or 3D peritectic solidification,'
    PRINT '          working either by heat-extraction  or cooling rate control,'
    PRINT '     **> streamlined by complete mixing of interstitial within a phase <**'
    PRINT '                          Re-gridding routine.'
    PRINT\PRINT '    (Be careful not to re-grid when it would leave a solid phase short on nodes)'
    PRINT\  PRINT ' VERSION WITH L=B*T^n ARM COARSENING'                    \ PRINT
    DIM NAME$(20),M1(20),M2(20),M3(20),K1(20),K2(20),K3(20),KL(20),CEP(20)
    DIM Z0(20),ZL(20),ZI(20),ZIOLD(20),XD1(20),XD2(20),DA(20),DB(20),DL(20)
    DIM Z(20,100),ZT(20,100),Y(100),MODA(20),MODB(20),GRAD(20),ZP(20)
    DIM GZ0(20),GZ(20),ZIT(20),ZLI(20),ZLT(20)

    INPUT 'Dimensional basis, plane(1),cylinder(2) or sphere(3)';NDIM%
    Y(I%)=(NDIM%-1.)/(2*I%) FOR I%=1 TO 100
    INPUT 'Primary/static(0) or secondary/coarsening(1) dendrite arm basis';NDEN%
    IF NDEN%=1 THEN INPUT 'B and n for L=Bt^n';BDEN,NDEN
    INPUT 'Maximum arm spacing (or very high if not wanted to be invoked)';LMAX
    BDEN=BDEN/1000000                       \ LMAX=LMAX/1000000
    PRINT
    GOTO 20

15  INPUT 'What static arm spacing (um)';L  \ L=L/1000000   \ LNDIM=L^NDIM%
    LDEN=L          \ ADEN=0        \ MDEN=0        \ RDEN=0        \ LNEW=L        \ LMAX=L
    PRINT

20  PRINT\INPUT 'Solute data-file number';NDAT$
    F$='SOLVE_' + NDAT$ + '.DAT'
    PRINT ' - reading from ';F$;'  ...',
    OPEN F$ FOR INPUT AS FILE £1, RECORDSIZE 255

    INPUT £1, SOLVENT$,T1,T2,T3,HL,HD,CPL,CPD,CPA,NZ%
    INPUT £1, D01,DQ1,D02,DQ2
    INPUT £1, INT$,MC1,MC3,KC1,KC3
    KC2=KC1*KC3
    MC2=((T2-T3)*MC1+(T1-T2)*KC1*MC3)/(T1-T3)
    ZPC=(T1-T3)/(KC1*MC3-MC1)
    CEPC=1./ZPC
    FOR I%=1 TO NZ%
    INPUT £1, NAME$(I%),M1(I%),M3(I%),K1(I%),K3(I%),XD1(I%),XD2(I%)
    IF XD1(I%)>XFAST THEN XFAST=XD1(I%)          \ D%=I%              \ END IF
    K2(I%)=K1(I%)*K3(I%)
    M2(I%)=((T2-T3)*M1(I%)+(T1-T2)*K1(I%)*M3(I%))/(T1-T3)
    ZP(I%)=(T1-T3)/(K1(I%)*M3(I%)-M1(I%))
    CEP(I%)=1./ZP(I%)                    ! *.53 for carbon equivalent
    NEXT I%
    PRINT "Diffusion time step by ";NAME$(D%)
    CLOSE 1%

    ! INITIAL COMPOSITION
    PRINT 'Initial content of ';INT$;'  plus available ';NZ%;' elements in ';SOLVENT$
    PRINT INT$;                                          \ INPUT C0
    CL=C0
    FOR I%=1 TO NZ%
    PRINT NAME$(I%);                     \ INPUT Z0(I%)
    ZL(I%)=Z0(I%)
    NEXT I%

    PHASE%=3
    CEP=CEPC*CL
    KCL=KC1                                  \ MCL=MC1
    FOR I%=1 TO NZ%
    CEP=CEP+CEP(I%)*ZL(I%)
    KL(I%)=K1(I%)
    ML(I%)=M1(I%)
    TLL=T1
    NEXT I%
    X=1.E-10 ! Nominal value

    PRINT\PRINT 'Peritectic equivalent of bulk composition = ';CEP
    IF CEP>1 THEN PRINT 'This steel is already hyper-peritectic.'
                  PHASE%=5      \ ONSET%=1      \ HP%=1       \ X=0
                  KCL=KC2                       \ MCL=MC2
                  FOR I%=1 TO NZ%
                  KL(I%)=K2(I%)
                  ML(I%)=M2(I%)
                  NEXT I%
                  TLL=T2
                  X=0
    END IF

    GOSUB HEAT
```

LINE 30

Selection of number of nodes to traverse initial representative cell (arbitrary max of 100)
Determine liquidus for start of model run
Select initial number of nodes across solid, compositions to be determined by Scheil or lever depending on each element's diffusivity within a Brody-Fleming style α parameter, using estimated times and size if coarsening
These compositions are then calculated

GOSUB TEMPERATURE to determine resultant operating temperature, which is the liquidus of the residual liquid
Time and size corrected retrospectively after compositions have beeen determined by Scheil and lever
Actual distances determined, across solid and nodal spacing, and associated parameters
GOSUB DIFFUSERS for temperature dependent diffusivity of solutes for subsequent FD code
PRINTOUT stage

If peritectic equivalent now greater than unity, program flag suggests re-run with more nodes to avoid this occurrence within this start-up routine

```
30   PRINT\INPUT 'How many nodes to start the problem';N%
     N%=5 IF N%<5
     IF N%>100 THEN PRINT 'Maximum currently allowed = 100' \ GOTO 30
     END IF

     ! FINDING LIQUIDUS
     GOSUB TEMPERATURE
     PRINT\PRINT "Program to start at t=0 at liquidus of";TL;' deg.C'
     TW=TL          \ TLIQ=TL       \ TOLD=TL       \ TK=TL+273     \ LIQUID%=1
     GOSUB PRINTOUT

     ! GETTING STARTED_____________________________________________
     !
     PRINT\PRINT\INPUT 'Scheil/Lever start-up till node <3>';RL%
     RL%=3 IF RL%<3
     CL=C0/(1-(1-KCL)*((1.*RL%/N%)^NDIM%))
     W=MCL*(CL-C0)
     ! Sorting out which is Scheil and which is Lever start-up
     DSELF1=D01*EXP(-DQ1/(8.314*TK))
     DSELF2=D02*EXP(-DQ2/(8.314*TK))
     IF CEP<1 THEN DL(I%)=XD1(I%)*DSELF1 FOR I%=1 TO NZ%                    &
      ELSE DL(I%)=XD2(I%)*DSELF2        FOR I%=1 TO NZ%
     END IF
     FS0=(1.*RL%/N%)^NDIM%
     IF Q=0 THEN TGUESS=MCL*(CL-C0)
     TGUESS=TGUESS+FS0*ML(I%)*Z0(I%)*(1/KL(I%)-1) FOR I%=1 TO NZ%
     TGUESS=TGUESS/QTH
     END IF
     TGUESS=HL*FS0/Q IF Q>0
     IF NDEN%=1 THEN                  LGUESS=BDEN*TGUESS^NDEN ELSE LGUESS=L
     END IF
     XGUESS=FS0*LGUESS
     TX2=TGUESS/XGUESS^2
     PRINT 'Guess T,X,L';TGUESS,XGUESS,LGUESS
     PRINT\PRINT 'Start-up bases'
     FOR I%=1 TO NZ%
     AGUESS(I%)=DL(I%)*TX2
     PRINT NAME$(I%);' ';INT(100*AGUESS(I%)+.5)/100;
     IF AGUESS(I%)<.1 THEN PRINT ': Scheil', ELSE PRINT ': Lever',          \ END IF
     IF I%=5% THEN PRINT                    \ END IF
     NEXT I%
     IF AGUESS(D%)<10 THEN SLOW=10 ELSE SLOW=2                              \ END IF
     ! The assignments, as suggested above
     FOR I%=1 TO NZ%
     IF AGUESS(I%)<0.1 THEN Z(I%,J%)=KL(I%)*Z0(I%)*(1-(1.*J%/N%)^NDIM%)^(KL(I%)-1) FOR J%=0 TO RL%   &
        ELSE Z(I%,J%)=KL(I%)*Z0(I%)/(1-(1-KL(I%))*FS0) FOR J%=0 TO RL%      \ END IF
     ZL(I%)=Z(I%,J%)/KL(I%)
     W=W+ML(I%)*(ZL(I%)-Z0(I%))
     NEXT I%
     FSP=.1*INT(10*FS0)

     GOSUB TEMPERATURE
     TS=(HTH*FS0+(TL-TLIQ))/QTH             \ TTOT=TS               \ TW=TL
     L=BDEN*TS^NDEN IF NDEN%=1
     LNDIM=L^NDIM%
     XN=L/N%                \ XN2=XN*XN     \ XL=RL%*XN             \ FS=(XL/L)^NDIM%
     FSOLD=FS0                      \ TOLD=TL
     X=XL IF ONSET%=0
     W=-W/TS
     QTEST=(HL*FS+CPL*(TL-TLIQ))/TS
     GOSUB DIFFUSERS
     GOSUB PRINTOUT

     PL=1                   \ P=1                   \ FP=0
     IF CEP>1 AND PHASE%<5 THEN PRINT\PRINT '*** Early change of solidification phase'
     PRINT 'Please repeat with different nodes or on single solidification phase program'
     PRINT
```

LINE 50

Core routine loop of program, calling upon appropriate subroutines.
Default printout every 10000 loops
Average heat capacity determined

System check on phases present
Loss of ferrite flag and variable reassignments

LINE 55

Continued check, with start of austenite flag and variable reassignments

LINE 60–69

If ferrite alone, killing austenite diffusivity terms by equation with ferrite terms
Resetting control variables if γ or γ+L

LINE 70

Scheil-style start-up of austenite (standard code but with control variables reducing austenite diffusivity to zero)

LINE 72–90

Sufficient nodes established for diffusive handling of austenite

Build up of variables required in PERITECTIC routine

LINE 99

Determining new fraction ferrite

```
50    ! ____________________________________________________
      !

MAINLOOP:                    !
                             !
      KOUNT%=KOUNT%+1
      IF KOUNT%=10000 THEN GOSUB PRINTOUT                    \ KOUNT%=0
      END IF

      CP=CPL*(1-FS)+CPA*(FS-FSD)+CPD*FSD
      IF Q$<>'W' THEN              QTH=Q/CP
      HTH=HL/CP                    \ HDTH=HD/CP
      END IF

      ! System characterisation
      LIQUID%=0                    \ PHASE%=0
      IF XL<L THEN PHASE%=1                                          ! Liquid
      LIQUID%=1                    \ END IF
      IF X>0 THEN PHASE%=PHASE%+2                                    ! Ferrite
      IF X<XN THEN X=-0                  \ PRINT\PRINT "LOSS OF FERRITE"
      ONSET10%=1                   \ R%=0                 \ PHASE%=PHASE%-2
      ZT(I%,0)=K2(I%)*ZI(I%) FOR I%=1 TO NZ%
55    PHASE%=PHASE%+4 IF XL>X OR CEP>1                               ! Austenite
      IF ONSET10%=1 THEN GOSUB PRINTOUT    \ ONSET10%=0              \ END IF

      GOSUB 4700 !IF PHASE%>5

      IF PHASE%>4 AND ONSET%=0 THEN ONSET%=1
      PRINT\PRINT '**AUSTENITE**'\PRINT
      FSD=FS
      KCL=KC2                              \ MCL=MC2
      FOR I%=1 TO NZ%
       ZI(I%)=K1(I%)*ZL(I%)
       ZIOLD(I%)=ZI(I%)
       KL(I%)=K2(I%)
       ML(I%)=M2(I%)
       TLL=T2
      NEXT I%
      GOSUB PRINTOUT
      GOTO 69

60    IF PHASE%=2 AND ONSET2%=0 THEN ONSET2%=1
      XD2(I%)=XD1(I%) FOR I%=1 TO NZ%
      GOSUB PRINTOUT
      GOTO 69
      END IF

      IF ABS(PHASE%-4.5)<.6 AND ONSET3%=0 THEN ONSET3%=1
      P=1                    \ R%=0                  \ V=0
      GOSUB PRINTOUT
      END IF

69    COL=CL
      IF LIQUID%<>1% THEN GOTO 99

70    IF RL%-R%<4 AND PHASE%>5 THEN ONSET8%=1
      IF ONSET8A%=0 THEN PRINT\PRINT\PRINT 'Scheil-style start-up of austenite'
      ONSET8A%=1
      END IF
      GOTO 74
72    IF ONSET7%=0 AND PHASE%>4 THEN PRINT\PRINT
      PRINT 'Full, diffusive continuation of austenite growth';KOUNT%,FSNEW
      ONSET7%=1                    \ ONSET8%=0
74    R0L%=RL%                     \ X0L=XL
      GOSUB DIFFUSERS
      QTH2=QTH*DTS+HTH*FS+HDTH*FSD

      ! Build up of variables for PERITECTIC
      LNEW=BDEN*(TTOT+DTS)^NDEN IF NDEN%=1
      IF LNEW>LMAX AND LMAX%=0 THEN PRINT\PRINT "MAXIMUM ARM SPACING REACHED" \ GOSUB PRINTOUT
      LMAX%=1
      END IF
      LNEW=LMAX IF LMAX%=1
      ALPHA1=0                     \ ALPHA2=0
      A=(XL/LNEW)^NDIM%
      BB=A*DTS*NDIM%/XL
      CC=1-(L/LNEW)^NDIM%

      FOR I%=1 TO NZ%
      IF ONSET8%=1 THEN GRAD(I%)=0                   \ GOTO 90
80    GRAD(I%)=(Z(I%,RL%-2)*PL/(1+PL)-Z(I%,RL%-1)*(1+PL)/PL+KL(I%)*ZL(I%)*(1+2*PL)/(PL*(1+PL)))/XN
90    ALPHA1=ALPHA1+ML(I%)*ZL(I%)*(1-KL(I%))
      ALPHA2=ALPHA2+ML(I%)*(BB*DL(I%)*GRAD(I%)+CC*(ZL(I%)-Z0(I%)))
      NEXT I%

99    AD=(X/LNEW)^NDIM%
```

LINE 100

Calling major subroutines according to control variable PHASE% (2-7 valid, 1 would be liquid alone prior to model run onset)

LINE 120

Composition array equated to temporary ones from within subroutines

Updates on size, fractions solid

Error flag if fraction solid decreasing

FD grid control variable updates

Temperature update

For sub-solidus operation, check and request for continued operation

LINE 130-250

Checks for attainment of solidus and associated control variables

Regridding for sub-solidus continuation without a non-integral node inherited from arm coarsening

Sub-solidus continuation by modelled time, including printout interval

SOLID: Homogenisation within a single phase system (PHASE%=2 or 4)

SOLIDLIQUID:

Solid compositions and interfacial advance in solid/liquid system (PHASE%=3 or 5)

Newton-Raphson solution for new fraction solid, employing variables established in main loop, including solute gradients from explicitly predicted concentrations

LINE 1100

Call to subroutine shared with PERITECTIC routine

```
100     ! Assignment to principal subroutines
        ON PHASE% GOSUB FAIL,SOLID,SOLIDLIQUID,SOLID,SOLIDLIQUID,SOLIDSOLID,PERITECTIC,FAIL

120     ! Leftover updates
        Z(I%,J%)=ZT(I%,J%) FOR J%=0 TO N% FOR I%=1 TO NZ%
        TTOT=TTOT+DTS
        IF NDEN%=1 THEN L=LNEW                    \ LNDIM=L^NDIM%                    \ N%=INT(L/XN)
        END IF
        IF N%>99 THEN PRINT\PRINT 'Maximum currently allowed = 100 nodes. Re-grid or bust.'\ GOSUB PRINTOUT
        END IF

        FSOLD=FS          \ FSDOLD=FSD
        FSD=(X/L)^NDIM%
        IF XL<L THEN FS=(XL/L)^NDIM%
        PRINT '**NET REMELTING**',FS IF FS<FSOLD
        PL=PL-AL%         \ RL%=RL%+AL%
        FP=L/XN-N%        \ FP=0 IF FP<1E-10
        END IF

        IF PHASE%<4 THEN R%=RL%
        ZI(I%)=K1(I%)*ZL(I%) FOR I%=1 TO NZ%
        X=XL     \        P=PL
        END IF

        GOSUB TEMPERATURE

        IF ONSET6%>0 AND TTOT>TMOR THEN GOTO 250                    \ END IF
        IF TIMINT>0 AND TPRINT<TTOT THEN TPRINT=TTOT+TIMINT
        GOSUB PRINTOUT
130     IF FS>FSP THEN FSP=FSP+.1
        IF FS>FS0 THEN GOSUB PRINTOUT
200     GOTO 50 IF XL<L OR ONSET6%=1
        ONSET6%=1         \ PL=1   \ RL%=N%          \ AL%=0          \ VL=0
        XL=L*(1+1E-6)     \ FS=1   \ HTH=0           \ W=-QTH         \ NDEN%=0
210     PRINT\PRINT 'END OF SOLIDIFICATION'
        ZLI(I%)=KL(I%)*ZL(I%) FOR I%=1 TO NZ%
250     IF FP+1==1 THEN GOSUB PRINTOUT ELSE PRINT 'FP,L,L/XN,N%=';FP,L,L/XN,N%
        PRINT '**RE-GRIDDING REQUIRED FOR CONTINUATION**'        \ GOSUB REGRID  \ GOSUB 9350
        END IF
        FP=0
        PRINT\INPUT 'Additional run time (sec)';TIMEX
        GOTO 20000 IF TIMEX<=0
        TMOR=TTOT+TIMEX
        INPUT 'Printout interval<1 sec>';TIMINT                  \ TIMINT=1 IF TIMINT=0
        TPRINT=TTOT+TIMINT

300     GOTO 50

        ! MAJOR SUB-ROUTINES_____________________________________________________

SOLID:                          !
                                !
        FOR I%=1 TO NZ%
        ZT(I%,0)=Z(I%,0)+2*MODB(I%)*NDIM%*(Z(I%,1)-Z(I%,0))
        ZT(I%,J%)=Z(I%,J%)+MODB(I%)*(Z(I%,J%-1)*(1-Y(J%))-2*Z(I%,J%)+Z(I%,J%+1)*(1+Y(J%))) FOR J%=1 TO N%-1
        ZT(I%,N%)=Z(I%,N%)+2*MODB(I%)*(Z(I%,N%-1)-Z(I%,N%))
        NEXT I%
        RETURN

SOLIDLIQUID:                    !
                                !
        FOR I%=1 TO NZ%
        ZT(I%,0)=Z(I%,0)+2*MODB(I%)*NDIM%*(Z(I%,1)-Z(I%,0))
        ZT(I%,J%)=Z(I%,J%)+MODB(I%)*(Z(I%,J%-1)*(1-Y(J%))-2*Z(I%,J%)+Z(I%,J%+1)*(1+Y(J%))) FOR J%=1 TO RL%-1
        NEXT I%

        ! Netwon-Raphson for Fs
        FSOLD=((XL-(XL/TS)*DTS)/L)^NDIM% IF KOUNT%<2
        FSG=2*FS-FSOLD

                                FOR NEWT%=1 TO 10
        ZLFS=(ALPHA1*(FSG-A)-ALPHA2)/(1-FSG)
        F=-QTH*DTS+HTH*(FSG-FS)+MCL*(C0/(1-(1-KCL)*FSG)-COL)+ZLFS
        THINGUMMY=-QTH*DTS+HTH*(FSG-FS)
        FD=HTH+MCL*C0*(1-KCL)/(1-(1-KCL)*FSG)^2+(ALPHA1*(1-A)-ALPHA2)/(1-FSG)^2
        FSNEW=FSG-F/FD
        DELF=FSNEW-FSG
        FSG=FSNEW
        NEWT%=10 IF ABS(DELF)<1.E-15
                                NEXT NEWT%
        PRINT 'Poor convergence in S/L';DELF IF ABS(DELF)>1.E-13
        CL=C0/(1-(1-KCL)*FSNEW)

1100    GOSUB SOLLIQ
        RETURN
```

SOLIDSOLID

Solid compositions and interfacial advance in solid/solid system (PHASE%=6)

Newton-Raphson scheme for nodal position P parameter with implicit-style simultaneous solution for new interfacial compositions

Poor convergence flags, largely obsolete after extensive debugging

GOSUB SOLSOL shared with PERITECTIC routine

PERITECTIC

Composition update in ferrite and austenite and simultaneous advance of δ/γ and γ/L interfaces

Build up of variables for Newton-Raphson scheme for δ/γ nodal position parameter P, central to solution for both interfaces with implicit-style simultaneous solution for new solid interfacial compositions (see pages 164-7)

```
SOLIDSOLID:                          !
                                     !
        FOR I%=1 TO NZ%
        IF R%>0 THEN ZT(I%,0)=Z(I%,0)+2*MODA(I%)*NDIM%*(Z(I%,1)-Z(I%,0))
        ZT(I%,J%)=Z(I%,J%)+MODA(I%)*(Z(I%,J%-1)*(1-Y(J%))-2*Z(I%,J%)+Z(I%,J%+1)*(1+Y(J%))) FOR J%=1 TO R1%
        END IF
        ZT(I%,J%)=Z(I%,J%)+MODB(I%)*(Z(I%,J%-1)*(1-Y(J%))-2*Z(I%,J%)+Z(I%,J%+1)*(1+Y(J%))) FOR J%=R4% TO N%-1
        ZT(I%,N%)=Z(I%,N%)+2*MODB(I%)*(Z(I%,N%-1)-Z(I%,N%))
        NEXT I%

        ! SIMULTANEOUS SOLUTION SCHEME FOR INTERFACE
        HP%=1 IF RL%-R%>4
        DD=AD*DTS*NDIM%/(X*XN)
        PG=P+2*CHAP-OLDCHAP                          \ PG1=PG
        POLD=P
        NEWTSS%=5 IF NEWTSS%=0
2050    FOR NEWT%=1 TO NEWTSS%+(A1%+A2%)*5
2051    FSDNEW=((X+(PG-POLD)*XN)/L)^NDIM%
        FSDD=(XN*NDIM%/(L^NDIM%))*(X+(PG-POLD)*XN)^(NDIM%-1)
        KFD=KC3+(1-KC3)*FSDNEW
        F=-QTH*DTS +HDTH*(FSDNEW-FSD) +MC3*(C0/KFD-CI)
        FD=FSDD*(HDTH+C0*MC3*(KC3-1)/(KFD*KFD))
         FOR I%=1 TO NZ%
        F=F+M3(I%)*( FNG(PG)/FNH(PG)-ZI(I%) )
        FD=FD+M3(I%)*( FNH(PG)*FNGD(PG)-FNG(PG)*FNHD(PG) )/(FNH(PG))^2
         NEXT I%
        PT=PG-F/FD                          ! Newton-Raphson approximation for next guess
        DELP=PT-PG
        NEWT%=NEWTSS%+(A1%+A2%)*5  IF ABS(DELP)<1.E-15
        PG=PT
                                 NEXT NEWT%
        OLDCHAP=CHAP                         \ CHAP=PG-P

        IF ABS(DELP)>1.E-6 AND SSC%=0 THEN PRINT\PRINT
        PRINT 'Poor SOLIDSOLID Convergence, ';NEWTSS%;' iterations'
        PRINT "POLD,P,PG,DELP,A1%,A2%,F,FD,TESTFD";POLD,P,PG,DELP,A1%,A2%,F,FD,TESTFD
        NEWTSS%=NEWTSS%+5 IF NEWTSS%<100
        GOSUB PRINTOUT
        IF NEWTSS%=100 THEN INPUT "Continue CONVERGENCE flags (0 for Yes, 1 for No)";SSC%

2100    GOSUB SOLSOL

        RETURN


PERITECTIC:                          !
                                     !
        FOR I%=1 TO NZ%
        IF R%>0 THEN ZT(I%,0)=Z(I%,0)+2*MODA(I%)*NDIM%*(Z(I%,1)-Z(I%,0))
        ZT(I%,J%)=Z(I%,J%)+MODA(I%)*(Z(I%,J%-1)*(1-Y(J%))-2*Z(I%,J%)+Z(I%,J%+1)*(1+Y(J%))) FOR J%=1 TO R1%
        END IF
        ZT(I%,J%)=Z(I%,J%)+MODB(I%)*(Z(I%,J%-1)*(1-Y(J%))-2*Z(I%,J%)+Z(I%,J%+1)*(1+Y(J%))) FOR J%=R4% TO RL%-1%
        NEXT I%

        ! General variables
        ALPHA4=KC1*MC3/(MC2-KC1*MC3)
        DD=AD*DTS*NDIM%/(X*XN)
        ALPHA1=ALPHA1*ALPHA4                     \ ALPHA2=ALPHA2*ALPHA4
        BQUAD=ALPHA1-QTH2-HTH
        CQUAD=QTH2-ALPHA1*A-ALPHA2

        ! Newton-Raphson for P
        HP%=1 IF RL%-R%>4
        ! IF PG=0 THEN PG=P ELSE PG=2*PG-POLD-A1%+A2% \ END IF
        PG=P+2*CHAP-OLDCHAP                      \ PG1=PG
        POLD=P
        COL=CL
        NEWTPERI%=10 IF NEWTPERI%=0

                                 FOR NEWT%=1 TO NEWTPERI%
        ZIP=0                    \ ZIPD=0
        FSDNEW=((X+(PG-POLD)*XN)/LNEW)^NDIM%
        FSDD=(XN*NDIM%/(LNEW^NDIM%))*(X+(PG-POLD)*XN)^(NDIM%-1)

        FOR I%=1 TO NZ%
        ZIP=ZIP+M3(I%)*(FNG(PG)/FNH(PG)-ZI(I%))
        ZIPD=ZIPD+M3(I%)*(FNH(PG)*FNGD(PG)-FNHD(PG)*FNG(PG))/(FNH(PG)^2)
        NEXT I%
        BQUAD1=BQUAD+HDTH*FSDNEW+(1+ALPHA4)*ZIP
        CQUAD1=CQUAD-HDTH*FSDNEW-(1+ALPHA4)*ZIP
        BQUADD=(1+ALPHA4)*ZIPD+HDTH*FSDD
```

Continuation of central peritectic solution scheme

LINE 2550

Call to 'slave' subroutines shared with other major routines

SOLLIQ

The first of these slave subroutines, shared by SOLIDLIQUID and PERITECTIC

Various updates, including new residual liquid compositions, and testing for attainment of solidus

Error flags for decreasing residual liquid compositions (very common towards solidus when the system is dominated by one or two strong segregants)

Automatic attempt at remedial action, curtailing arm coarsening which increases prospects for this reduction

LINE 3105

Determining apparent cooling rate, for information under heat extraction control, or to test consistency under cooling rate control

Updating nodal compositions within the span of the Lagrangian system around the interface

LINE 3500

Handling procedure for fraction solid exceeding unity (solidus)

Time step adjusted for current growth rate to make system equal unit fraction solid rather than exceed it

Final compositions appropriately modified

```
        IF HTH=0 THEN FSNEW=-CQUAD1/BQUAD1
        FSNEWD=(BQUADD/BQUAD1)*(1+FSNEW)
        GOTO 2500
        END IF
        FSNEW=(-BQUAD1+SQR(BQUAD1*BQUAD1-4*HTH*CQUAD1))/(2*HTH)
        FSNEWD=(BQUADD/(2*HTH))*(-1+(BQUAD1+2*HTH)/SQR(BQUAD1*BQUAD1-4*HTH*CQUAD1))
2500    CL=C0/(1-(1-KC2)*FSNEW-(KC2-KC1)*FSDNEW)
        CLD=((1-KC2)*FSNEWD+(KC2-KC1)*FSDD)*C0/((1-(1-KC2)*FSNEW-(KC2-KC1)*FSDNEW)^2)

        F=-QTH2+HTH*FSNEW+HDTH*FSDNEW+ZIP+KC1*MC3*(CL-COL)
        THINGUMMY=-QTH2+HTH*FSNEW+HDTH*FSDNEW
        FD=HTH*FSNEWD+HDTH*FSDD+ZIPD+KC1*MC3*CLD

        PT=PG-F/FD      \ DELP=PT-PG
        NEWT%=NEWTPERI% IF ABS(DELP)<1.E-15
        PG=PT
                                NEXT NEWT%
        OLDCHAP=CHAP                    \ CHAP=PG-P

        IF ABS(DELP)>1.E-6 THEN PRINT 'Poor PERITECTIC convergence, ';NEWTPERI%;' iterations    '
        NEWTPERI%=NEWTPERI%+5 IF NEWTPERI%<100
        GOSUB PRINTOUT

2550    GOSUB SOLSOL
        GOSUB SOLLIQ
        RETURN

        ! INTERFACE SLAVE SUB-ROUTINES ____________________________________________________

SOLLIQ:                         !
                                !
        XLOLD=XL        \ XL=LNEW*FSNEW^(1/NDIM%)       \ VL=(XL-X0L)/DTS
        GOTO 3500 IF FSNEW>=1
        FOR I%=1 TO NZ%
        Z0L(I%)=ZL(I%)
        ZLT(I%)=Z0L(I%)+(Z0L(I%)*(1-KL(I%))*(FSNEW-A)-BB*DL(I%)*GRAD(I%)-CC*(Z0L(I%)-Z0(I%)))/(1-FSNEW)
        IF KOUNT%<3 THEN GOTO 3104                      \ END IF
        IF ZLT(I%)<Z0L(I%) AND GZ0(I%)=0 THEN GZ0(I%)=1
        PRINT W,-Q/CPL+HL*(FS-FSOLD)/(CPL*DTS),MCL*(CL-COL)+ZLFS
        PRINT\PRINT '***Peak ';NAME$(I%);'~';Z0L(I%);'@';FSNEW;',  LOOP ';KOUNT%,'VL';VL,'L.dot';CORS
        GOTO 3105 IF LLRN=1
        LLRN=1          \ ADEN=0        \ CORS=0        \ NDEN%=0       \ CC=0
        PRINT\PRINT '**THROWING A WOBBLER!  Remedial action: ARM-COARSENING CURTAILED'
        GOSUB PRINTOUT
        I%=0
        END IF
3104    NEXT I%
3105    W=-MCL*(CL-COL)
        FOR I%=1 TO NZ%
        ZL(I%)=ZLT(I%)
        W=W-ML(I%)*(ZL(I%)-Z0L(I%))
        NEXT I%
        W=W/DTS
        PL=PL+VL*DTS/XN
        AL%=INT(PL-1)
                FOR I%=1 TO NZ%
                FOR J%=0 TO AL%
        IF ONSET%=0 THEN ZT(I%,RL%+J%)=ZT(I%,RL%-2)*(1+J%)*(1+J%-PL)/(1+PL) +                  &
        ZT(I%,RL%-1)*(2+J%)*(PL-J%-1)/PL+KL(I%)*ZL(I%)*(2+J%)*(1+J%)/(PL*(1+PL))               &
        ELSE IF XLOLD<XN*(RL%+J%) THEN                                                          &
        ZT(I%,RL%+J%)=KL(I%)*Z0L(I%)*((1-(XN*(RL%+J%)/LNEW)^NDIM%)/(1-A))^(KL(I%)-1)
3110            NEXT J%
                NEXT I%
        GOTO 3999

3500    ! Attainment of solidus
        PRINT\PRINT 'APPROACHING SOLIDUS'       \ GOSUB PRINTOUT
        DTSV=(LNEW-XLOLD)/VL
        PRINT 'PL=';PL;'  --> ';
        PL=LNEW/XN-RL%+1                        \ PRINT PL
        PRINT 'Predicted DTS=';DTS;' --> ';DTSV
        CL=CL+(CL-COL)*DTSV/DTS
        CI=KC1*CL
        FOR I%=1 TO NZ%
        ZL(I%)=ZL(I%)+(ZL(I%)-Z0L(I%))*DTSV/DTS
        ZT(I%,N%)=KL(I%)*ZL(I%) IF FP+1==1
        NEXT I%

        FSNEW=1 \ LLRN=1        \ CORS=0        \ CSOL=0        \ BSOL=0        \ W=0   \ NDEN%=0
        XL=LNEW \ FSOLD=FS      \ FS=1

3999    RETURN
```

SOLSOL

Slave subroutine shared by SOLIDSOLID and PERITECTIC

Updating various variables including interfacial compositions

LINE 4210–4650

Interpolation from new values for near-interface and missed nodes within the span of the Lagrangian scheme. This has to cope with interfacial movement in either direction, hence the relative complexity of the logic

LINE 4700

Reassignment of subscript identities for when too few nodes of ferrite exist for the standard FD formulation, i.e. R%–X lying beyond the representative cell

TEMPERATURE

Subroutine summoned from various parts of main code, determining the (local) equilibrium temperature for the interfacial compositions, and the peritectic equivalent

```
SOLSOL:                          !Setting the acceptable values
                                 !
        P=PG
        V=(P-POLD)*XN/DTS
        X=X+V*DTS
        ! Calculation of new compositions
        IF LIQUID%=0 THEN CINEW=C0/KFD
        WTEST=-MC3*(CINEW-CI)
        CI=CINEW
        END IF
        IF LIQUID%=1 THEN WTEST=-KC1*MC3*(CL-COL)                    \ END IF
        FOR I%=1 TO NZ%
        ZI(I%)=FNG(PG)/FNH(PG)
        WTEST=WTEST-M3(I%)*(ZI(I%)-ZIOLD(I%))
        ZIOLD(I%)=ZI(I%)
        NEXT I%
        WTEST=WTEST/DTS

        ! Interpolation from new values for near-interface and missed nodes
        A1%=0                    \ A2%=0
        IF V<0 THEN GOTO 4300
4210            A1%=INT(P-1)
        IF ONSET4%=0 THEN ONSET4%=1                  \ ONSET5%=0
        PRINT\PRINT 'DELTA encroaching into GAMMA ','LOOP';KOUNT%,FSNEW
4250    GOSUB 4600
        GOSUB 4500 \ GOTO 4400
4300    IF ONSET5%=0 THEN ONSET5%=1                  \ ONSET4%=0
        PRINT\PRINT 'GAMMA encroaching into DELTA','LOOP';KOUNT%,FSNEW
4350    A2%=INT(2-P)                                  \ GOSUB 4500 \ GOSUB 4600

4400    R%=R%+A1%-A2%                                 \ GOSUB 4700
        P=P-A1%+A2%
        Z(I%,J%)=ZT(I%,J%) FOR J%=0 TO N%  FOR I%=1 TO NZ%
        IF R%<0 THEN R%=0                             \ P=1
4499    RETURN

4500    ! Interpolations for left-hand phase
        FOR I%=1 TO NZ%
        ZT(I%,R%+J%)=ZT(I%,R2%)*(1+J%)*(1+J%-P)/(1+P) +                          &
        ZT(I%,R1%)*(2+J%)*(P-J%-1)/P + ZI(I%)*(2+J%)*(1+J%)/(P*(1+P)) FOR J%=0 TO A1%
        NEXT I%
        RETURN

4600    ! Interpolations for right-hand phase
        GOTO 4650 IF RL%-R%<4
        FOR I%=1 TO NZ%
        ZT(I%,R%+1-J%)=ZT(I%,R3%)*(1+J%)*(P+J%-2)/(4-P) +                        &
        ZT(I%,R4%)*(2+J%)*(2-J%-P)/(3-P) + K3(I%)*ZI(I%)*(2+J%)*(1+J%)/((3-P)*(4-P)) FOR J%=0 TO A2%
        NEXT I%
        GOTO 4699

4650    GOTO 4699 IF A2%=0
        ! Coping with an otherwise un-reassigned node passed by the interface
        IF POLD=P OR ZIOLD(1)=0 THEN ZT(I%,R%)=K3(I%)*ZI(I%) FOR I%=1 TO NZ% &
        ELSE ZT(I%,R%)=K3(I%)*(((1-P)*ZIOLD(I%)-(1-POLD)*ZI(I%))/(POLD-P))   &
        FOR I%=1 TO NZ%

4699    RETURN

4700    ! Subscript assignment
        R1%=R%-1                         \ R2%=R%-2 \ R3%=R%+3 \ R4%=R%+2
        R1%=R% IF R%<1
        R2%=R% IF R%<2
        R3%=R% IF R%>N%-2
        R4%=R% IF R%=N%-1
        RETURN


        ! BREAD 'n BUTTER SUB-ROUTINES

TEMPERATURE:                     !
                                 !
        TL=TLL+MCL*CL                    \ TDG=T3+KC1*MC3*CL                  \ CEP=CEPC*CL
        TDG=T3+MC3*CI IF FS=1                    !ADDED 15/5/91
        FOR I%=1 TO NZ%
        TL=TL+ML(I%)*ZL(I%)
        TDG=TDG+M3(I%)*ZI(I%)
        CEP=CEP+CEP(I%)*ZL(I%)
        NEXT I%
        TOLD=TW
        TW=TW-W*DTS
        TK=TW+273
        RETURN
```

DIFFUSERS

Diffusivity calculation, currently by factors on iron's self diffusivity

Warning flag for very low diffusivity/Scheil trap

Austenite and ferrite set as A and B, the latter set to zero by HP% during Scheil-style austenite start-up

Modulus terms calculated, MODB reset to that for whichever phase is adjacent to the liquid

FAIL

Flag for erroneous PHASE% control variable value

REGRID

FD array re-meshing (see pages 172-4)

Alternative codes for bulk nodes (straight Crank & Gupta) and those up to liquid interface and either side of δ/γ interface, adjusted according to partial node parameters

```
DIFFUSERS:                          !
                                    !
        DSELF1=D01*EXP(-DQ1/(8.314*1723))
        DSELF2=D02*EXP(-DQ2/(8.314*1723))
        MAYDAY=(DSELF1*XD1(D%)*4*NDIM%)
         IF MAYDAY==0 THEN PRINT 'MAYDAY! Diffusivity gone to zero';DSELF1      \ GOSUB PRINTOUT
         MAYDAY=XN2
         END IF
        DTS=XN2/MAYDAY
        DTS=DTS/SLOW IF FS>.995 AND LIQUID%=1
        IF X<XN AND X>0 AND FS<.995 THEN DTS=DTS/SLOW
        END IF
        DTS=1 IF DTS>1              \ XNT=XN2/DTS
        FOR I%=1 TO NZ%
        DA(I%)=DSELF1*XD1(I%)       \ DB(I%)=HP%*DSELF2*XD2(I%)
        IF PHASE%<4 THEN DL(I%)=DA(I%) ELSE DL(I%)=DB(I%)
        END IF
        MODA(I%)=DA(I%)/XNT         \ MODB(I%)=DL(I%)/XNT
        NEXT I%
        RETURN

FAIL:   PRINT 'ERROR, PHASE%=';PHASE%
        GOSUB PRINTOUT
        RETURN

REGRID:                             !
                                    !
        GOSUB 9350
        INPUT 'How many new nodes across the cell';NRX%
        NRX%=RL% IF NRX%=0          \ XNRX=L/(1.*NRX%)      \ RX=XNRX/XN \  KRX%=INT(XL/XNRX)
        ! Extreme nodes
        FOR I%=1 TO NZ%
        ZT(I%,0)=Z(I%,0)
        IF FS<1 THEN ZLI(I%)=KL(I%)*ZL(I%) ELSE ZLI(I%)=Z(I%,N%)
        END IF
        NEXT I%

        FOR K%=1 TO KRX%
        RXK=1.*RX*K%                \ J%=INT(RXK)
        PRX=RXK-J%                  \ PRXL=RXK-RL%+1                \ PRXS=RXK-R1%
        IF PRX==0 THEN ZT(I%,K%)=Z(I%,J%) FOR I%=1 TO NZ%
        GOTO 8510
        END IF
        ! Near-core nodes
        IF J%<1 THEN ZT(I%,K%)=Z(I%,0)+(Z(I%,1)-Z(I%,0))*PRX*PRX FOR I%=1 TO NZ%
        GOTO 8510
        END IF
        FOR I%=1 TO NZ%
        ! Near-end nodes
        IF J%>RL%-2 THEN BRX=(Z(I%,RL%)-2*Z(I%,RL%-1)+Z(I%,RL%-2))/2
        ARX=Z(I%,RL%)*(1+2*PL)/(3*PL)-Z(I%,RL%-1)*(2+PL)/(3*(1+PL))-Z(I%,RL%-2)/3-ZLI(I%)/(3*PL*(1+PL))
        CRX=(2*ZLI(I%)-Z(I%,RL%)*(1+PL)*(2+PL)+Z(I%,RL%-1)*2*PL*(2+PL)-Z(I%,RL%-2)*PL*(1+PL))/(6*PL*(1+PL))
        ZT(I%,K%)=Z(I%,RL%-1%)+ARX*PRXL+BRX*PRXL*PRXL+CRX*PRXL^3
        GOTO 8500
8100    ! Bulk nodes
        ARX=Z(I%,J%+1)-Z(I%,J%)/2-Z(I%,J%-1)/3-Z(I%,J%+2)/6
        BRX=(Z(I%,J%+1)-2*Z(I%,J%)+Z(I%,J%-1))/2
        CRX=(Z(I%,J%+2)-3*Z(I%,J%+1)+3*Z(I%,J%)-Z(I%,J%-1))/6
        ZT(I%,K%)=Z(I%,J%)+ARX*PRX+BRX*PRX*PRX+CRX*PRX^3
        GOTO 8500 IF PHASE%<6
        ! Near delta/gamma interface nodes
        IF K%<X/XNRX AND K%>1.*(R1%)/RX THEN BRX=(Z(I%,R%)-2*Z(I%,R1%)+Z(I%,R2%))/2
        ARX=Z(I%,R%)*(1+2*P)/(3*P)-Z(I%,R1%)*(2+P)/(3*(1+P))-Z(I%,R2%)/3-ZI(I%)/(3*P*(1+P))
        CRX=(2*ZI(I%)-Z(I%,R%)*(1+P)*(2+P)+Z(I%,R1%)*2*P*(2+P)-Z(I%,R2%)*P*(1+P))/(6*P*(1+P))
        ZT(I%,K%)=Z(I%,R1%)+ARX*PRXS+BRX*PRXS*PRXS+CRX*PRXS^3
        END IF
        IF K%>X/XNRX AND K%<1.*R4%/RX THEN BRX=(Z(I%,R%+1)-2*Z(I%,R4%)+Z(I%,R3%))/2
        P3=3-P                      \ PRX3=3-PRXS
        ARX=Z(I%,R%+1)*(1+2*P3)/(3*P3)-Z(I%,R4%)*(2+P3)/(3*(1+P3))-Z(I%,R3%)/3-K3(I%)*ZI(I%)/(3*P3*(1+P3))
        CRX=(2*K3(I%)*ZI(I%)-Z(I%,R%+1)*(1+P3)*(2+P3)+Z(I%,R4%)*2*P3*(2+P3)-Z(I%,R3%)*P3*(1+P3))/(6*P3*(1+P3))
        ZT(I%,K%)=Z(I%,R4%)+ARX*PRX3+BRX*PRX3*PRX3+CRX*PRX3^3
        END IF
8500    NEXT I%
8510    NEXT K%
        Z(I%,K%)=ZT(I%,K%) FOR K%=0 TO KRX% FOR I%=1 TO NZ%
        IF ONSET6%=1 AND ONSET6A%=0 THEN Z(I%,NRX%)=ZLI(I%) FOR I%=1 TO NZ% \ ONSET6A%=1       \ END IF
        PL=1+XL/XNRX-KRX%                   \ FP=0
        XN2=XNRX*XNRX               \ XN=XNRX
        N%=NRX%                                 \ RL%=KRX%
        R%=INT(X/XN)                \ P=1+X/XN-R%                   \ PG=0
        PRINT '---->N%,R%,P,RL%,PL';N%,R%,P,RL%,PL                  \ PRINT
        GOSUB DIFFUSERS
        RETURN
```

HEAT

Summoned as an option within PRINTOUT, to alter the cooling rate or heat extraction rate control

PRINTOUT

Various parameters listed by default, others optional from interactive prompts

Opportunity presented for regridding or changing thermal control

LINE 9700

Check for solute conservation

```
HEAT:                           ! Alter heat extraction or cooling rate
                                !
        PRINT\INPUT 'Cooling rate (W) or heat extraction (Q) control';Q$
        IF LEFT(Q$,1)='W' THEN INPUT 'What cooling rate';W
        QTH=-W                  \ HTH=0
        GOTO 8700

8600    INPUT 'What heat extraction rate';Q
        IF KOUNT%=0 THEN QTH=Q/CPL
        HTH=HL/CPL
        END IF

8700    RETURN


PRINTOUT:                       !
                                !
        PRINT\PRINT
        QTEST=( HL*(FS-FSOLD) +HD*(FSD-FSDOLD)+CP*(TW-TOLD))/DTS IF KOUNT%>0
        PRINT 'TIME';TTOT,'Peri';CEP,'System';PHASE%;':';R%;'~';RL%;'~';N%;', ';VL;'~';CORS;'~';V,'Loop';KOUNT%
        PRINT 'TEMPS,';TW;'* -liq';TL;'* -d/g';TDG,'SIZE';L*1E6,'Fs';FS,'W';W,'Q';QTEST
        PRINT\PRINT , \ PRINT INT$, \ PRINT NAME$(I%), FOR I%=1 TO NZ%
        PRINT\PRINT 'Core:',
        !                       CARBON OPTIONS  (IF X>0 THEN PRINT KC1*CL, ELSE PRINT KC2*CL,)
        ON PHASE% GOTO 9011,9011,9012,9011,9013,9014,9012,9010
9010                    PRINT "ERROR: PHASE%=";PHASE%                   \ GOTO 9020
9011                    PRINT C0,                       \ GOTO 9020
9012                    PRINT KC1*CL,                   \ GOTO 9020
9013                    PRINT KC2*CL,                   \ GOTO 9020
9014                    PRINT CI,
9020                    !                       OTHER ELEMENTS, CORE
        PRINT Z(I%,0), FOR I%=1 TO NZ%
        IF PHASE%>5 THEN PRINT\PRINT 'Int.:',
        IF PHASE%==6 THEN PRINT CI, ELSE PRINT KC1*CL,                  \ END IF
        FOR I%=1 TO NZ%
        PRINT ZI(I%),
        NEXT I%
        END IF
        IF LIQUID%=1 THEN PRINT\PRINT 'Liquid:',
        PRINT CL,
        PRINT ZL(I%), FOR I%=1 TO NZ%
        PRINT
        GOTO 9300
9100    PRINT\PRINT 'End:',
        IF PHASE%==6 THEN PRINT KC3*CI, ELSE PRINT C0,                  \ END IF
        GOTO 9200 IF FP>0
        PRINT Z(I%,N%), FOR I%=1 TO NZ%
        PRINT
        GOTO 9300
9200    PRINT ZLI(I%), FOR I%=1 TO NZ%
        PRINT
9300    GOTO 9999 IF KOUNT%=0
        INPUT'Solute profiles(Y), re-grid (R), change Q/W (C), or <proceed>';SPRO$
        GOTO 9350 IF LEFT(SPRO$,1)='Y'
        GOSUB HEAT IF LEFT(SPRO$,1)='C'
        IF LEFT(SPRO$,1)='R' THEN GOSUB REGRID ELSE GOTO 9999
9350    PRINT '(Delta from 0 to ';X/XN;
        PRINT ',liquid from ';RL%-1+PL;' to ';N%+FP; IF LIQUID%=1
        PRINT ')'
        IF RL%<N% THEN Z(I%,J%)=ZL(I%) FOR J%=RL%+1 TO N% FOR I%=1 TO NZ%
9600    FOR J%=0 TO N%
        PRINT J%,,
        PRINT Z(I%,J%), FOR I%=1 TO NZ%
        PRINT
        NEXT J%
        IF FP>0 THEN PRINT N%+FP,,
        PRINT ZL(I%), FOR I%=1 TO NZ%
        PRINT 'FP=';FP
        PRINT

9700    ! SOLUTE BALANCE CHECK
        FOR I%=1 TO NZ%
        SUM(I%)=Z(I%,0)/(2^NDIM%) +(.5*NDIM%)*(N%^(NDIM%-1))*(Z(I%,N%)+FP*ZL(I%))
        SUM(I%)=SUM(I%)+1.*NDIM%*(J%^(NDIM%-1))*Z(I%,J%) FOR J%=1 TO N%-1
        SUM(I%)=SUM(I%)/(1.*(N%+FP))^NDIM%
        NEXT I%
        PRINT 'Mean solute in ';NDIM%;'-D volume:-'                     \ PRINT ,
        FSD=FS IF ONSET%=0
        IF PHASE%==6 THEN PRINT CI*(FSD+KC3*(1-FSD)),                   \ GOTO 9750
9710    IF LIQUID%=1 THEN PRINT CL*(1-(1-KC2)*FS-(KC2-KC1)*FSD),        ELSE PRINT '*';C0,
9750    PRINT SUM(I%), FOR I%=1 TO NZ%
        PRINT\PRINT
9999    RETURN
```

LINE 10000–10043

Setting up defined functions for Newton-Raphson solution for δ/γ nodal position parameter, P

LINE 20000–30000

End flag

Opportunity for a final printout

Solute conservation requoted as percentages

Other versions exist, e.g. with alternative arm coarsening laws embedded such as Beaverstock's multicomponent extension of Kirkwood's equation (149). Beaverstock has also produced a FORTRAN translation of this code.

```
10000   ! DEFINED FUNCTIONS_____________________________________________
        ! G,H, and their derivatives, GD,HD, are for Newton-Raphson for P


10001   DEF FNG(X)
10002   FNG=DD*( DA(I%)*(ZT(I%,R2%)*X/(1+X) -ZT(I%,R1%)*(1+X)/X) -                    &
            DB(I%)*(-ZT(I%,R3%)*(3-X)/(4-X) + ZT(I%,R4%)*(4-X)/(3-X)) )
10003   FNEND

10011   DEF FNH(X)
10012   FNH=(K3(I%)-1)*(FSDNEW-AD) -DD*(DA(I%)*(1+2*X)/(X*(1+X)) +                    &
            K3(I%)*DB(I%)*(7-2*X)/((3-X)*(4-X)) )
10013   FNEND

10021   DEF FNGD(X)
10022   FNGD=DD*( DA(I%)*(ZT(I%,R2%)/((1+X)*(1+X)) + ZT(I%,R1%)/(X*X)) -               &
             DB(I%)*(ZT(I%,R3%)/((4-X)*(4-X)) + ZT(I%,R4%)/((3-X)*(3-X))) )
10023   FNEND

10031   DEF FNHD(X)
10032   FNHD=(K3(I%)-1)*FSDD +DD*(DA(I%)*(1+2*X+2*X*X)/(X*(1+X))^2 -                  &
             K3(I%)*DB(I%)*(25-14*X+2*X*X)/((3-X)*(4-X))^2)
10033   FNEND

10041   DEF FND(X)
10042   FND=DL(I%)*( Z(I%,3)*X/(1+X)-Z(I%,2)*(1+X)/X + K3(I%)*ZI(I%)*(1+2*X)/(X*(1+X)) )/XN
10043   FNEND


20000   ! WRAPPING THINGS UP_____________________________________________
        !
        PRINT\PRINT 'END OF COMPUTATION'
        GOSUB PRINTOUT
        GOSUB 9700
        PRINT ,'%-CONS.',
        FOR I%=1 TO NZ%
        IF Z0(I%)>0 THEN PRINT 100*SUM(I%)/Z0(I%), ELSE PRINT ' - ',
20010   NEXT I%
        PRINT\PRINT\PRINT
30000   END
```

One thing I have learned in a long life: that all our science, measured against reality, is primative and childlike - and yet it is the most precious thing we have ....Albert Einstein

And you can do a whole PhD on that?
....Christine Jamieson, neighbour